

**Mechanism of Assembly of the Tyrosyl Radical-Diiron(III) Cofactor
of *E. coli* Ribonucleotide Reductase**

by

Wing Hang Tong

Submitted to the Department of Chemistry
in Partial Fulfillment of the Requirements
for the Degree of

Doctor of Philosophy
in Biochemistry

at the
Massachusetts Institute of Technology

February 1996

© 1996 Massachusetts Institute of Technology
All rights reserved

Signature of Author

Department of Chemistry
January 30, 1996

Certified by

Professor JoAnne Stubbe
Thesis Supervisor

Accepted by

Professor Dietmar Seyferth

MASSACHUSETTS INSTITUTE
OF TECHNOLOGY

Chairman, Departmental Committee on Graduate Students

MAR 04 1996

ARCHIVES

LIBRARIES

This doctoral thesis has been examined by a Committee of the Department of Chemistry as follows:

Professor James R. Williamson

Chairperson

Professor JoAnne Stubbe

Thesis Supervisor

Professor Lawrence J. Stern

To my parents, for their love and patience

Mechanism of Assembly of the Tyrosyl Radical-Diiron(III)
Cofactor of *E. coli* Ribonucleotide Reductase

Wing Hang Tong

Submitted to the Department of Chemistry on January 30, 1996
in partial fulfillment of the requirements for the degree of
Doctor of Philosophy in Biochemistry

Abstract

The R2 subunit of *E. coli* ribonucleotide reductase contains a tyrosyl radical-diiron(III) cluster cofactor that is essential for its catalytic activity. The *in vitro* assembly of this cofactor involves reductive activation of O₂ by the diferrous form of the iron cluster, to effect a one-electron reduction of an endogenous tyrosine residue Y122. Previous study have shown that, when iron-free R2 (apo R2) is mixed at 5 °C with Fe²⁺ and O₂, the kinetic and spectroscopic characteristics of the assembly process depend markedly on the initial Fe²⁺/R2 ratio. When the reaction is carried out with excess Fe²⁺ (Fe²⁺/R2 ≥ 5), it was proposed that an iron cluster X accumulates and oxidizes Y122 to form •Y122 and the product diferric cluster. When the reaction is carried out with limiting Fe²⁺ (Fe²⁺/R2 = 2.0 -2.4), it was proposed that a second intermediate characterized by a broad absorption band near 560 nm generates •Y122. In this study, the complementary kinetic and spectroscopic methods of stopped-flow absorption, rapid freeze-quench EPR, and rapid freeze-quench Mössbauer spectroscopies, together with site-directed mutagenesis studies, have been used to characterize the assembly reaction when pre-formed ferrous-R2 complex is mixed with O₂. When the reaction of Fe(II)-R2 with O₂ is carried out with excess Fe²⁺, the time-courses of X, •Y122 and the diferric cluster are consistent with the proposal that X generates •Y122. These results have also offered evidence for a conformational change in apo R2 to allow for entry of Fe²⁺ into the cofactor-binding site. Furthermore, the Mössbauer kinetic data suggest that a peroxo-diiron(III) intermediate forms before X. In the case of the reaction carried out with limiting Fe²⁺, the data indicate that the 560 nm absorbing species is not responsible for generation of •Y122. Furthermore, the data indicate, in contrast to the previous hypothesis, that the 560-absorbing species is not a tryptophan radical cation. It is proposed that X generates •Y122 in the reaction of Fe(II)-R2 with O₂ under limiting Fe²⁺ conditions.

Thesis Supervisor: Prof. JoAnne Stubbe
Title: John C. Sheehan Professor of Chemistry and Biology

Acknowledgments

At this final hour, it is not easy to write this acknowledgment adequately. But, throughout my graduate school years, I have had many valuable and enjoyable interactions with my very interesting coworkers and I owe a debt of gratitude to these people for many reasons. Many of them have made important scientific contributions to this work. Others provided me with friendship and moral support which are essential to keep me going. These debts I acknowledge with pleasure.

First, I would like to thank my advisor, Prof. JoAnne Stubbe for her support and guidance. Joanne's unflagging enthusiasm and dedication constantly inspire me. Her attention to details and precision always challenges me to reevaluate and refine my scientific approach. I thank her for providing me with many invaluable opportunities and for constantly pushing me to do a little more.

Our collaboration with Prof. Boi Hanh (Vincent) Huynh and Prof. Dale Edmondson has been one of the most valuable of my graduate school experiences. My several visits to Emory University yielded many interesting results, and I thank them for sharing with me their expertise in rapid freeze-quench methodology. Shuxian Chen in Prof. Huynh's lab made valuable contributions to this thesis. Shuxian carried out most of the quantitative Mössbauer analysis in Chapter 2, as well as the simulation of the Mössbauer spectrum of the putative peroxo diiron (III) intermediate. In addition to these estimable contributions, I am grateful to Shuxian for patiently answering my questions concerning Mössbauer spectroscopy.

By far the best aspect of my graduate school experience are the interactions with my coworkers. Most current and former members of the Stubbe lab have contributed to the work in this thesis. Our scientific discussions, frequently conducted on one of the chalk boards in the lab or on a piece of scrap paper, have yielded many new ideas. And our discussions on the scientific process also

constantly force me to reevaluate and refine my own scientific approach. For these I am truly grateful.

Dr. Douglas Burdi made very valuable contributions to this thesis. He is the driving force behind the ENDOR characterization of X, and these results have provided us with a better simulation of X, which plays a crucial part in the quantitative analysis in Chapter 2. In addition to these contributions, Doug has been a pleasure to work with. Our different approaches to science strike for a nice balance for the overall project. I am grateful to him for all of his help and I also thank him for constantly challenging me to take bolder steps.

In my first two years, I worked closely with Marty Bollinger. Marty taught me the various techniques that are crucial to the work in this thesis. Even more valuable than these contributions was his friendship and moral support. Our discussions through the years have been among the most productive and the most enjoyable of my graduate school experience.

Many of the current and former members of the Stubbe lab deserve thanks. Every Alice needs a White Knight. Someone who will stop for a moment in their own long hard quest and give direction to the little pawn. During my first years in the Stubbe lab, Ernie Mueller offered help and steady friendship, for which I am deeply grateful. I also thank Squire Booker and Mike Absalon for the good times and for sharing with me their keen insight on scientific and other matters. On various occasion, Stuart Licht has provided me with wise counsel on many topics. I thank him for his help and for the many interesting "scientific" discussions we shared. I also thank other members of the Stubbe lab who have helped me look forward to coming to work every morning.

I owe my friend Alaine a debt of gratitude for many reasons. Alaine wrote the computer program for analyzing the statistical problem in Chapter 4 and our many discussion of the problem have greatly facilitated the analysis and the

interpretation of the data. During the final stages in the preparation of this manuscript, Alaine helped me extensively with proofreading and paperwork. I am very grateful for all her help and for the fruitful discussions we shared.

Lastly, and most importantly, I thank my family and my friends. Their kindness and patience are what kept me working through the toughest times.

"Would you tell me please, which way I ought to go from here?"

"That depends a good deal on where you want to get to," said the Cat.

"I don't much care where," said Alice.

"Then it doesn't matter which way you go," said the Cat.

"-so long as I get somewhere," Alice added as an explanation.

"Oh, you're sure to do that," said the Cat, "if you only walk long enough."

Alice felt that this could not be denied...

Contents

Abstract	6
Acknowledgments	7
Table of Contents	11
List of Figures	17
List of Schemes	26
List of Tables	30
Chapter 1: The R2 Subunit of <i>E. coli</i> Ribonucleotide Reductase: Structure, Function, and Reactivity	
Introduction	35
<i>E. coli</i> Ribonucleotide Reductase	42
Assembly of the Tyrosyl Radical-Diferric Cofactor of <i>E. coli</i> R2	
Reaction Stoichiometry	50
Mechanisms Proposed for the R2 Reaction Prior to This Work	52
Current Study of the R2 Reconstitution Mechanism	61
Structure and Physical Properties of R2 and its Cofactor.	63
Native R2.	64
Reduced (or Diferrous) R2.	72
R2 with Divalent Metal Ions Other than Fe ²⁺	80
Apo R2.	80
Intermediate Iron Cluster X	81
Structural Considerations for the Cofactor Assembly	87
Reactivity of R2 and its Cofactor	92
Reactions of Other Diiron(II) Complexes with O ₂	
Methane Monooxygenase Mechanism	99
A Synthetic S = 1/2 complex with Localized High-Spin Fe(IV) and Fe(III) sites	104
References	107
Chapter 2: Reconstitution of Native R2 from Ferrous R2 and O₂ under Excess Fe²⁺ Conditions	117
Experimental Procedures	
Materials and Methods	121
Purification of <i>E. coli</i> R2	122

Stopped-flow Absorption Spectroscopy	124
EPR Spectroscopy	125
Mössbauer Spectroscopy	125
Reaction of Fe(II)-R2 ($\text{Fe}^{2+}/\text{R2} = 5$) with O_2 as Monitored by SF-Abs Spectroscopy	127
Calibration of Rapid Freeze-Quench Apparatus	128
Reaction of Fe(II)-R2 ($\text{Fe}^{2+}/\text{R2} = 5$) with O_2 as Monitored by RFQ-EPR and RFQ-Möss Spectroscopies	131
Determination of the Packing Factor for the RFQ-EPR Experiments	132
Results	
Reaction of Fe(II)-R2-wt with O_2 as Monitored by SF-Abs Spectroscopy	134
Reaction of Fe(II)-R2-Y122F with O_2 as Monitored by SF-Abs Spectroscopy	145
Reaction of Fe(II)-R2-wt with O_2 as Monitored by RFQ-EPR Spectroscopy	151
Reaction of Fe(II)-R2-Y122F with O_2 as Monitored by RFQ-EPR Spectroscopy	159
Mössbauer Time course of the Reaction of Fe(II)-R2-wt with O_2	168
Quantitation of X and the Diferric Cluster as Functions of Time	169
Quantitation of the Fast-Relaxing Ferric Species	177
Analysis of the Mössbauer Time-Course for Additional Components	181
Discussions	191
New Features of Current R2 Reconstitution Mechanism	200
Implications for Mechanism of Delivery of the "Fourth Electron"	203
References	209

Chapter 3: Reconstitution of Native R2 under Limiting Fe^{2+}

Conditions	213
Experimental Procedures	
Materials	217
Reaction of Fe(II)-R2 ($\text{Fe}^{2+}/\text{R2} = 2.3$) with O_2 as Monitored by SF-Abs, RFQ-EPR, and RFQ-Mössbauer Spectroscopy	217
Is the Species Trapped by the Rapid Freeze-quench Method	

Chemically Competent to Generate the Native Cofactor?	217
Time-Course of the Reaction of Apo R2 with 2.3 Fe ²⁺ and O ₂ as Monitored by SF-Abs, RFQ-EPR	218
Time-Course of the Reaction of Apo R2 with Fe ²⁺ and O ₂ in ² H ₂ O as Monitored by SF-Abs , RFQ-EPR and RFQ-Möss Spectroscopies	218
Results	
Reaction of Fe(II)-R2-wt (Fe ²⁺ /R2 = 2.3) with O ₂ as Monitored by SF-Abs spectroscopy	219
Reaction of Fe(II)-R2-wt (Fe ²⁺ /R2 = 2.3) with O ₂ as Monitored by RFQ-EPR spectroscopy	230
Control for Rapid Freeze-Quenching of R2	231
Reaction of Fe(II)-R2-wt with O ₂ in the Presence of Ascorbate as Monitored by SF-Abs and RFQ-EPR Spectroscopies	236
Quantitative Analysis of the Reaction of Apo R2 with Limiting Fe ²⁺	237
Reaction of Apo R2 with Limiting Fe ²⁺ in ² H ₂ O as Monitored by SF-Abs Spectroscopy	246
Reaction of Apo R2 with Fe ²⁺ in ² H ₂ O as Monitored by RFQ-EPR Spectroscopy	250
Temperature Dependence of the Reaction of Apo R2-wt with Limiting Fe ²⁺ as Monitored by SF-Abs Spectroscopy	270
Discussion	
Mechanism of Reconstitution Reaction under Limiting Fe ²⁺ Conditions.	282
Identity of the Broad EPR g ~ 2 Features	284
Identity of the 560 nm-Absorbing Species	287
References	289
Chapter 4: Probing the Binding Interactions between R2 and Fe²⁺	291
Theory	299
Experimental Procedures	
Materials	309
Reaction of Fe(II)-R2-wt (Fe ²⁺ /R2 = 1) with O ₂ as Monitored by SF-Abs Spectroscopy	309
Dissociation of Fe ²⁺ from Fe(II)-R2 Complex	310

Reaction of Fe(II)-R2 with O ₂ in the Presence of Mn ²⁺ or EDTA	310
Mn ²⁺ Pulse/chase Experiment	311
Results	
Reaction of Fe(II)-R2 (Fe ²⁺ /R2 = 1) with O ₂ as Monitored by SF-Abs Spectroscopy	311
Dissociation of Fe ²⁺ from Fe(II)-R2 Complex	312
Reaction of Fe(II)-R2 with O ₂ in the Presence of Mn ²⁺ and EDTA	329
Mn ²⁺ Pulse/chase Experiment	340
Discussion	
Implications for the Binding of Fe ²⁺ by Apo R2	344
Implications for Mechanism of the R2 Reconstitution Reaction	345
The Sequence of Events Leading to Formation of the Intermediate Iron Cluster, X	364
References	371

Appendix 1: Reconstitution of R2-Y122F from Apo R2, Fe²⁺ and O₂ Monitored by SF-Abs, RFQ-EPR, and RFQ-Möss Spectroscopies	373
Experimental Procedures	
Materials	377
Reaction of apo R2-Y122F with Fe ²⁺ and O ₂ as Monitored by SF-Abs, RFQ-EPR, and RFQ-Möss spectroscopies	377
Results	
Reaction of apo R2-Y122F with Excess Fe ²⁺ and O ₂ as Monitored by SF-Abs Spectroscopy.	379
Quantitation of X and the Diferric Cluster in the Excess Fe ²⁺ Reaction by Mössbauer Spectroscopy.	384
Analysis of the Mössbauer Time-course for Additional Components	395
Reaction of Apo R2-Y122F with Excess Fe ²⁺ and O ₂ at 25 °C as Monitored by SF-Abs Spectroscopy	402
Reaction of Apo R2-Y122F with limiting Fe ²⁺ and O ₂ as Monitored by RFQ-EPR Spectroscopy	407
EPR Time-course of the Reaction Apo R2-Y122F with	

Limiting Fe ²⁺	410
Quantitative Analysis of the Reaction of Apo R2 -Y122F with Limiting Fe ²⁺	415
Reaction of apo R2-Y122F with limiting Fe ²⁺ is Accompanied by Cross-linking of the Protein.	417
Discussion	
Mechanism for the Reaction of Apo R2-Y122F with Excess Fe ²⁺ and O ₂	420
Implications on Electron Transfer Pathway during Cofactor Assembly and Catalytic Turnover.	424
Reaction of Apo R2-Y122F with Limiting Fe ²⁺ and O ₂	427
References	431

Appendix 2: Characterizations of Two Mutant Proteins, R2-W48F and R2-W48Y	435
Experimental Procedures	
Materials.	438
Construction and Expression of R2-W48 Mutants by the Eckstein Method	438
Purification of R2-W48F and R2-W48Y.	441
Circular Dichroism Spectra of R2-W48F and R2-W48Y	443
Effects of R2-W48F and R2-W48Y on the Catalytic Activity of R2-wt	443
Iron Binding Properties of R2-W48F and R2-W48Y	
Results	
Preparation of R2-W48 Mutants.	445
Characterizations of R2-W48 Mutants.	446
Reaction of R2-W48 Mutants with Fe ²⁺ and O ₂	460
Effects of the Mutant Proteins on Catalytic Activity of R2-wt	455
Discussion	455
References	457

Appendix 3: Simulation of the Statistical Distribution of Fe²⁺ Bound to R2	461.
--	-------------

List of Figures

Figure		Page
1.1:	Schematic representation of <i>E. coli</i> ribonucleotide reductase.	44
1.2:	Schematic representation of the tyrosyl radical-diiron(III) cofactor of <i>E. coli</i> ribonucleotide reductase.	46
1.3:	UV-Visible absorption spectra of the tyrosyl radical-diiron(III) cofactor in <i>E. coli</i> ribonucleotide reductase	54
1.4:	X-band EPR spectrum of the tyrosyl radical of <i>E. coli</i> R2.	56
1.5:	Schematic representation of the cofactor site in met R2.	70
1.6:	Schematic representation of the cofactor site in diferrous R2.	74
1.7:	Schematic representation of the cofactor site in Mn(II)-R2.	82
1.8:	Proposed hydrogen-bonding network in the cofactor site in apo R2.	84
1.9:	Schematic representation of the possible structures of X based on recent Mössbauer and Q-band ENDOR studies.	88
2.1:	Development of the absorption spectrum of the cofactor upon mixing Fe(II)-R2-wt with O ₂ under excess Fe ²⁺ conditions.	136
2.2:	A ₃₆₅ -versus-time trace in the reaction of Fe(II)-R2-wt with O ₂ compared to that in the reaction of apo R2-wt with Fe ²⁺ and O ₂ .	138
2.3:	Formation of •Y122 in the reaction of Fe(II)-R2-wt with O ₂ compared to that in the reaction of apo R2-wt with Fe ²⁺ and O ₂ .	140

2.4:	Least-squares analysis of A₄₁₀, dropline-versus-time trace from the reaction of Fe(II)-R2-wt with O₂ under excess Fe²⁺ conditions.	142
2.5:	Least-squares analysis of A₃₆₅-versus-time trace from the reaction of Fe(II)-R2-wt with O₂ under excess Fe²⁺ conditions.	146
2.6:	Least-squares analysis of A₃₆₅-versus-time trace from the reaction of Fe(II)-R2-Y122F with O₂ under excess Fe²⁺ conditions.	148
2.7:	Time-course of the reaction of Fe(II)-R2-wt with O₂ under excess Fe²⁺ conditions as monitored by EPR spectroscopy.	152
2.8:	EPR spectra of the reaction of Fe(II)-R2-wt (⁵⁷Fe²⁺/R2 = 5) with O₂ quenched at 0.044 s.	154
2.9:	Kinetics of formation of X and •Y122 in the reaction of Fe(II)-R2-wt with O₂ under excess Fe²⁺ conditions.	156
2.10:	Least-squares fitting of the measured quantity of •Y122 as a function of time in the reaction of Fe(II)-R2-wt with O₂ under excess Fe²⁺ conditions.	160
2.11:	Least-squares fitting of the measured quantity of X as a function of time in the reaction of Fe(II)-R2-wt with O₂ under excess Fe²⁺ conditions.	162
2.12:	Least-squares fitting of the measured quantities of X as a function of time to two sequential, first-order processes.	164
2.13:	Measured quantity of X as a function of time in the reaction of Fe(II)-R2-Y122F with O₂ under excess Fe²⁺ conditions as monitored by EPR spectroscopy.	166

2.14:	Reference spectra for ferrous-R2, the diferric cluster, and the diiron intermediate X.	170
2.15:	Time-course of the reaction of Fe(II)-R2-wt with O ₂ under excess Fe ²⁺ conditions as monitored by Mössbauer spectroscopy.	172
2.16:	Time-course of X in the reaction of Fe(II)-R2-wt with O ₂ under excess Fe ²⁺ conditions as monitored by RFQ-Mössbauer spectroscopy.	174
2.17	Time-course of the diferric cluster in the reaction of Fe(II)-R2-wt with O ₂ as monitored by RFQ-Mössbauer spectroscopy.	178
2.18:	Quantitation of the putative fast-relaxing ferric species in the reaction of Fe(II)-R2 with O ₂ under excess Fe ²⁺ conditions.	182
2.19:	Least-squares fitting of the quantity of the fast-relaxing ferric species as a function of time.	184
2.20:	Mössbauer spectrum showing a partially resolved peak at approximately 1.2 mm/s in the 0.028 s time-point of the reaction of Fe(II)-R2 with O ₂ under excess Fe ²⁺ conditions.	186
2.21:	Mössbauer spectrum showing a partially resolved peak at approximately 0.02 mm/s in the 0.028 s time-point of the reaction of Fe(II)-R2 with O ₂ under excess Fe ²⁺ conditions.	188
2.22:	Mössbauer spectra showing features of the possible "ferric" species which accumulate in the reaction of Fe(II)-R2-wt with O ₂ under excess Fe ²⁺ conditions.	192
2.23	Mössbauer spectrum demonstrating the goodness of fit of the most current analysis.	194

2.24	A₆₀₅-versus-time trace in the reaction of Fe(II)-R2-wt with O₂ under excess Fe²⁺ conditions.	204
3.1:	Formation of •Y122 in the reaction of Fe(II)-R2-wt with O₂ under limiting Fe²⁺ conditions as monitored by SF-Abs spectroscopy.	220
3.2:	A₅₆₀-versus-time traces in the reaction of Fe(II)-R2-wt with O₂ under limiting Fe²⁺ conditions in the presence and in the absence of ascorbate.	224
3.3:	Least-squares fitting of A₅₆₀-versus-time trace in the reaction of Fe(II)-R2-wt with O₂ under limiting Fe²⁺ conditions.	226
3.4:	Least-squares fitting of the formation of •Y122 in the reaction of Fe(II)-R2-wt with O₂ under limiting Fe²⁺ conditions to three sequential, first-order processes.	228
3.5:	Time-course of the reaction of Fe(II)-R2-wt with O₂ as monitored by EPR spectroscopy.	232
3.6:	EPR spectra of the reaction of Fe(II)-R2-wt (Fe²⁺/R2 = 2.3) with O₂ quenched at 0.059 s before and after the sample was thawed.	234
3.7:	Formation of •Y122 in the reaction of Fe(II)-R2 (Fe²⁺/R2 = 3) with O₂ in the presence of ascorbate as monitored by SF-Abs spectroscopy.	238
3.8:	Time-course of the reaction of Fe(II)-R2 (Fe²⁺/R2 = 3) with O₂ in the presence of ascorbate as monitored by EPR spectroscopy.	240
3.9:	Demonstration of how the amount of the 560 nm-absorbing transient species is estimated from the A₅₆₀-versus-time trace of the reaction of apo R2-wt with limiting Fe²⁺ and O₂.	242

3.10:	Comparison of the measured quantities of X and •Y122 with the measured quantity of EPR-active species in the g = 2 region in the reaction of apo R2-wt with limiting Fe ²⁺ .	244
3.11:	A ₄₁₀ , dropline-versus-time trace in the reaction of apo R2-wt with limiting Fe ²⁺ in ² H ₂ O compared to that in ¹ H ₂ O.	248
3.12:	Non-linear regression analysis of A ₄₁₀ , dropline-versus-time trace in the reaction of apo R2-wt with limiting Fe ²⁺ in ² H ₂ O.	252
3.13:	A ₅₆₀ -versus-time trace in the reaction of apo R2-wt with limiting Fe ²⁺ in ² H ₂ O compared to that in ¹ H ₂ O.	254
3.14:	Formation of •Y122 in the reaction of apo R2-wt with excess Fe ²⁺ in ² H ₂ O compared to that in ¹ H ₂ O.	256
3.15:	Time-course of the reaction of apo R2-wt with limiting Fe ²⁺ in ² H ₂ O as monitored by EPR spectroscopy.	258
3.16:	Time-course of the reaction of apo R2-wt with O ₂ in ¹ H ₂ O as monitored by EPR spectroscopy.	260
3.17:	An example of the deconvolution of the EPR spectrum from the reaction of apo R2-wt with limiting Fe ²⁺ in ² H ₂ O.	262
3.18:	Hypothetical spectrum for the broad EPR features which accumulate in the reaction of apo R2 with limiting Fe ²⁺ .	266
3.19:	Analysis of the experiment depicted in Fig. 3.15 to show that no significant amount of the broad EPR features accumulates in the reaction of apo R2-wt with limiting Fe ²⁺ in ² H ₂ O.	268
3.20:	Effect of temperature on the A ₅₆₀ -versus-time trace in the reaction of apo R2-wt with limiting Fe ²⁺ .	272

3.21:	Effect of temperature on the A ₅₆₀ -versus-time trace in the reaction of apo R2-Y122F with limiting Fe ²⁺ .	274
3.22:	A ₅₆₀ -versus-time trace in the reaction of apo R2-wt with limiting Fe ²⁺ at 15 °C.	276
3.23:	A ₅₆₀ -versus-time trace in the reaction of apo R2-Y122F with limiting Fe ²⁺ at 15 °C.	278
3.24:	A ₄₁₀ , dropline-versus-time trace in the reaction of apo R2-wt with limiting Fe ²⁺ at 25 °C.	280
4.1:	Experimental design for the Mn ²⁺ -quench experiment.	306
4.2:	Experimental design for the Mn ²⁺ pulse/chase experiment.	307
4.3:	A ₄₁₀ , dropline-versus-time trace of the reaction of Fe(II)-R2 (1 Fe ²⁺ /R2) with O ₂ compared to that of the reaction of Fe(II)-R2 (2.3 Fe ²⁺ /R2) with O ₂ .	314
4.4:	Formation of •Y122 in the reaction of Fe(II)-R2 with O ₂ when Fe ²⁺ /R2 = 1	316
4.5:	A ₄₁₀ , dropline-versus-time trace of the reaction of Fe(II)-R2 (2.3 Fe ²⁺ /R2) with O ₂ compared to that of the reaction of Fe(II)-R2 (1 Fe ²⁺ /R2) with O ₂ in the presence of ascorbate.	318
4.6:	Least-squares fitting of the equation for a first-order growth to A ₅₆₂ -versus-time trace upon mixing Fe(II)-R2-wt with ferrozine when Fe ²⁺ /R2 = 1.	320
4.7:	Least-squares fitting of the equation for two exponentials to A ₅₆₂ -versus-time trace in the reaction of Fe(II)-R2-wt with ferrozine when Fe ²⁺ /R2 = 1.	322

4.8:	Least-squares fitting of the equation for three exponentials to A_{562} -versus-time trace in the reaction of Fe(II)-R2-wt with ferrozine when $Fe^{2+} / R2 = 2.3$.	324
4.9:	Least-squares fitting of the equation for three exponentials to A_{562} -versus-time trace in the reaction of Fe(II)-R2-wt with ferrozine when $Fe^{2+} / R2 = 3.4$.	326
4.10:	Least-squares fitting of the equation for a first-order growth to A_{410} , dropline-versus-time trace in the reaction of Fe(II)-R2-wt with O_2 when $Fe^{2+} / R2 = 2.3$ and in the presence of Mn^{2+} .	332
4.11:	Least-squares fitting of the equation for a first-order growth to A_{410} , dropline-versus-time trace in the reaction of Fe(II)-R2-wt with O_2 when $Fe^{2+} / R2 = 3.4$ and in the presence of Mn^{2+} .	334
4.12	Least-squares fitting of the equation for a first-order growth to A_{410} , dropline-versus-time trace in the reaction of Fe(II)-R2-wt with O_2 when $Fe^{2+} / R2 = 2.3$ and in the presence of EDTA.	336
4.13	Least-squares fitting of the equation for a first-order growth to A_{410} , dropline-versus-time trace in the reaction of Fe(II)-R2-wt with O_2 when $Fe^{2+} / R2 = 3.4$ and in the presence of EDTA.	338
4.14:	•Y122 yield as a function of delay time in the pulse/chase experiment.	342
4.15:	Extrapolation of the data in Fig. 4.14 to show the "burst" of •Y122 formation in the pulse/chase experiment.	346
4.16:	Theoretical plots of •Y122/R2 ratio at completion of reaction versus $Fe^{2+} / R2$ ratio for the different scenarios in Scheme 4.6 (A), Scheme 4.7 (B) and Scheme 4.8 (C).	360
4.17:	A_{410} , dropline-versus-time trace when Mn^{2+} is added 45 ms after the reaction of apo R2 with excess Fe^{2+} is initiated.	368

A.1.1	Development of the absorption spectrum of the diferric cluster upon mixing apo R2-Y122F with O ₂ and excess Fe ²⁺ .	380
A.1.2	A ₃₆₅ -versus-time trace in the reaction of apo R2-Y122F with excess Fe ²⁺ .	382
A.1.3	Mössbauer time-course of the reaction of apo R2-Y122F with excess Fe ²⁺ .	386
A.1.4	Formation of the diferric cluster in the reaction of apo R2-Y122F with excess Fe ²⁺ as monitored by RFQ-Möss spectroscopy.	388
A.1.5	Decay of X in the reaction of apo R2-Y122F with excess Fe ²⁺ as monitored by RFQ-Möss spectroscopy.	390
A.1.6	Non-linear least square fitting of the kinetic model of Scheme A.1.1 to the measured quantities of X and the diferric cluster as functions of time.	392
A.1.7	EPR spectrum of the reaction of apo R2-Y122F with excess Fe ²⁺ quenched at 60 s.	396
A.1.8	Mössbauer time-course of X in the reaction of apo R2-Y122F with excess Fe ²⁺ compared with that of apo R2-wt under the same conditions.	398
A.1.9	Mössbauer time-course of the diferric cluster in the reaction of apo R2-Y122F with excess Fe ²⁺ compared with that of apo R2-wt under the same conditions.	400
A.1.10	Formation of the fast-relaxing ferric species in the reaction of apo R2-Y122F with excess Fe ²⁺ compared with that of apo R2-wt under the same conditions.	403

A.1.11	Mössbauer spectrum showing the accumulation of X in the reaction of apo R2-Y122F with excess Fe ²⁺ at 25 °C.	405
A.1.12	A ₅₆₀ -versus-time trace in the reaction of apo R2-Y122F with limiting Fe ²⁺ .	408
A.1.13	A ₄₁₀ , dropline-versus-time trace used to assess the formation of tyrosyl radical in the reaction of apo R2-Y122F with limiting Fe ²⁺ .	411
A.1.14	EPR time-course of the reaction of apo R2-Y122F with limiting Fe ²⁺ .	413
A.1.15	The products of the reaction of apo R2-Y122F with Fe ²⁺ as analyzed by SDS gel electrophoresis.	418
A.2.1	Schematic representation of the plasmid pTB2 that contains the coding sequence of R2 (<i>nrdB</i>).	440
A.2.2	SDS gel showing heat-induced expression of R2-W48Y in K38/pTB2-W48Y.	447
A.2.3	CD spectra of R2-W48F, R2-W48Y and R2-wt at 5 °C.	448
A.2.4	Development of the absorption spectrum of R2-W48F upon mixing with an aliquot of Fe ²⁺ in 10 mM H ₂ SO ₄ .	451
A.2.5	Development of the absorption spectrum of R2-W48F upon mixing with Fe ²⁺ and ascorbate.	453

List of Schemes

Scheme		Page
1.1:	Reaction catalyzed by ribonucleotide reductases.	36
1.2:	Ribonucleotide reductases use a diverse array of cofactors.	38
1.3:	Mechanism proposed in our previous work for assembly of the R2 cofactor	41
1.4:	Current working hypothesis for the catalytic mechanism of <i>E. coli</i> ribonucleotide reductase.	48
1.5:	Overall reaction of apo R2 with Fe ²⁺ and O ₂ .	51
1.6:	Early elaboration of the mechanism for the R2 reconstitution reaction which involves high-valent iron-oxo intermediate.	53
1.7:	Schematic representation of the R2 diferrous cluster and its interaction with azide proposed by Elgren <i>et al.</i> (1993).	77
1.8:	Schematic representation of the R2 diferrous cluster and its interaction with azide proposed by Pulver <i>et al.</i> (1995).	78
1.9:	Schematic representation of the possible nuclear reorganizations involved in the R2 reconstitution reaction.	93
1.10:	Different states of R2 and their interconversions.	96
1.11:	Schematic representation of the mechanism proposed for the hydroxylation reaction catalyzed by MMO based on analogy to P-450 chemistry.	100

1.12:	Schematic representation of the mechanism proposed by Liu <i>et al.</i> (1995b) for the hydroxylation reaction catalyzed by MMO from <i>M. capsulatus</i> (Bath).	102
1.13	Reaction of a diiron(III) complex, $\text{Fe}_2(\mu\text{-O})(5\text{-Me-TPA})_2\text{-}(\text{OH})(\text{H}_2\text{O})](\text{ClO}_4)_3$ (where TPA = tris(2-pyridylmethyl)amine) (2), with H_2O_2 at $-40\text{ }^\circ\text{C}$ in CH_3CN .	106
2.1:	Proposed minimal mechanism for the reaction at $5\text{ }^\circ\text{C}$ of apo R2, O_2 , and excess Fe^{2+} .	119
2.2:	Kinetic model for two sequential, first-order processes used in analysis of the SF-Abs, RFQ-EPR, and RFQ-Möss kinetic data.	144
2.3:	Schematic mechanism for the excess Fe^{2+} reaction elaborated to reflect the conformational change which occurs prior to formation of diferrous-R2.	196
3.1:	Schematic representation for the mechanism proposed in our previous work for the reaction of apo R2-wt at $5\text{ }^\circ\text{C}$ with O_2 and limiting Fe^{2+} (Bollinger <i>et al.</i> , 1994a).	215
3.2:	Kinetic model for two sequential, first-order processes used in analysis of the SF-Abs, RFQ-EPR, and RFQ-Möss kinetic data.	222
3.3:	Kinetic model for three sequential, first-order processes.	230
3.4:	Mechanism for the limiting Fe^{2+} reaction expanded to reflect the possibility that R2 cofactor assembly is preceded by an equilibrium between two different forms of X.	286
4.1:	Schematic representation of the Fe^{2+} -R2 complexes which might be present in the equilibrium mixture of apo R2 and Fe^{2+} under anaerobic conditions for the case of two metal-binding sites in each R2 monomer.	294

4.2:	Schematic representation of the Fe ²⁺ -R2 complexes which might be in the equilibrium mixture of apo R2 and Fe ²⁺ under anaerobic conditions for the case of three metal-binding sites in each R2 monomer.	296
4.3:	Concept of using Mn ²⁺ to trap the non-competent Fe ²⁺ -R2 complexes.	302
4.4:	Concept of using EDTA to trap the non-competent Fe ²⁺ -R2 complexes.	304
4.5:	Our current working hypothesis for the mechanism of the reaction of Fe(II)-R2 with O ₂ .	350
4.6:	The scenario in which any R2 with a diferrous cluster in the cofactor site would not be affected by addition of Mn ²⁺ or EDTA and would proceed to generate •Y122.	352
4.7:	The scenario in which there are two Fe ²⁺ -binding sites on each R2 monomer and that only R2 dimer with at least three Fe ²⁺ bound can form •Y122 in the presence of Mn ²⁺ or EDTA.	354
4.8:	The scenario in which each R2 monomer contains three Fe ²⁺ -binding sites. In this scenario, only R2 with all three Fe ²⁺ -binding sites filled will react to form •Y122 in the presence of Mn ²⁺ or EDTA.	356
4.9:	Illustration of the manners in which a number of different Fe ³⁺ products may be generated in the delivery of the fourth electron for cofactor assembly.	362
4.10:	Different possible sequences of event that lead to formation of X in the reaction of apo R2 with O ₂ and Fe ²⁺ .	366

A.1.1:	Kinetic model for two sequential, first-order processes used in analysis of the SF-Abs, RFQ-EPR, and RFQ-Möss kinetic data.	379
A.1.2:	Kinetic model for two sequential, first-order processes used in analysis of the A₅₆₀-versus-time trace.	410
A.1.3:	Proposed minimal mechanism for the reaction at 5 °C of apo R2, O₂, and excess Fe²⁺.	421

List of Tables

Table		Page
1.1:	Summary of selected physical properties of native R2 from <i>E. coli</i> .	66
1.2:	Summary of selected physical properties of intermediate X.	90
1.3:	Spectroscopic and kinetic parameters (at 4 °C) for intermediates in the reaction of MMOH _{red} with O ₂ .	104
2.1:	Measured volumes of the rapid freeze-quench aging hoses and the corresponding reaction times for a ram velocity of 1 cm/s.	130
2.2:	Summary of least-squares fits of a first-order process to the region between 0.05 - 5.0 s of the A ₄₁₀ , dropline-versus-time traces of the reaction of Fe(II)-R2-wt with O ₂ under excess Fe ²⁺ conditions.	135
2.3:	Summary of least-squares fit to Scheme 2.2 of the A ₃₆₅ -versus-time traces from the reaction of Fe(II)-R2-wt with O ₂ under excess Fe ²⁺ conditions.	150
2.4:	Summary of the analysis for the EPR spectra from the reaction of Fe(II)-R2-wt with O ₂ under excess Fe ²⁺ conditions.	158
2.5:	Quantitation of X in the time-resolved EPR spectra of the reaction of Fe(II)-R2-Y122F with O ₂ under excess Fe ²⁺ conditions. Total spin was calculated assuming a packing factor of 0.67.	168
2.6:	Parameters for the reference spectra used in the quantitative analysis of the Mössbauer spectra of the time-course samples.	169

2.7:	Quantitative analysis of the Mössbauer spectra of the reaction of Fe(II)-R2 (5 Fe²⁺/R2) with O₂ under excess Fe²⁺ condition.	176
2.8:	Electron counting for the reaction of Fe(II)-R2-wt with O₂ under excess Fe²⁺ conditions.	206
3.1:	Summary of least-squares fits to Eq. 3.1 of the A₅₆₀-versus-time traces from the reaction of Fe(II)-R2-wt (Fe²⁺/R2 = 2.3 - 2.4) with O₂.	223
3.2:	Summary of analysis of the EPR spectra from the reaction of Fe(II)-R2-wt (2.3 Fe²⁺/R2) with O₂.	231
3.3:	Summary of analysis of the EPR spectra from the reaction of Fe(II)-R2-wt (3 Fe²⁺/R2) with O₂ in the presence of ascorbate.	246
3.4:	Summary of total spin quantitation at various time-points in the reaction of apo R2-wt with limiting Fe²⁺.	247
3.5:	Summary of total spin quantitation at various time-points in the reaction of apo R2-wt with limiting Fe²⁺ in ²H₂O.	264
3.6:	Summary of analysis of the A₅₆₀-versus-time traces from the reaction of apo R2 with limiting Fe²⁺ at different temperatures.	271
4.1:	Summary of least-squares fits to Eq. 4.1 of the A₅₆₂-versus-time traces from the reaction of Fe(II)-R2 with ferrozine.	328
4.2:	Summary of quantitation of Fe²⁺ bound by R2 in the Fe(II)-R2 sample.	329
4.3:	Summary of •Y122/R2 ratio at completion in the reaction Fe(II)-R2 with O₂ in the presence of EDTA or Mn²⁺.	331

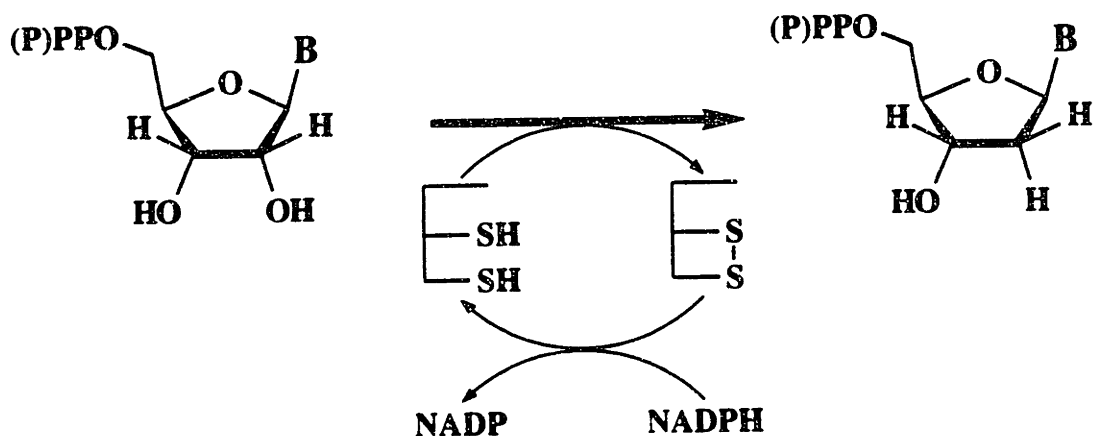
4.4:	Summary of least-squares fits of A_{410} , dropline-versus-time traces to a first-order process from the reaction of Fe(II)-R2 with O_2 in the presence of Mn^{2+} or EDTA.	331
4.5:	Summary of $^{51}Y122/R2$ ratio at completion in the pulse/chase experiment.	341
A.1.1:	Summary of analysis of the Mössbauer spectra from the reaction of apo R2-Y122F with excess Fe^{2+} at 5 °C.	385
A.1.2:	Measured quantities of X in the reaction of apo R2-Y122F with excess Fe^{2+} compared to those in the reaction of apo R2-wt with excess Fe^{2+} at 5 °C.	395
A.1.3:	Summary of analysis of the Mössbauer spectra from the reaction of apo R2-Y122F with excess Fe^{2+} at 25 °C.	407
A.1.4:	Summary of the analysis of the EPR and the Mössbauer spectra from the reaction of apo R2-Y122F with limiting Fe^{2+} .	416
A.2.1:	Oligonucleotide primers used for mutagenesis by the Eckstein method.	441
A.2.2:	Summary of the effect of different forms of R2 on the interaction between R1 and R2-wt.	456

**Chapter 1: The R2 Subunit of *E. coli* Ribonucleotide Reductase:
Structure, Function, and Reactivity**

Introduction

The ribonucleotide reductases (RNRs) constitute a unique class of metalloenzymes that catalyze the reduction of all four ribonucleotides to the corresponding 2'-deoxyribonucleotides (Scheme 1.1) (Thelander & Reichard, 1979; Eriksson & Sjöberg, 1989; Stubbe, 1990b). This transformation is the first committed step in DNA biosynthesis, providing the only means by which all known organisms obtain the deoxynucleotide precursors for DNA biosynthesis. As a consequence of being at such a critical juncture in metabolism, and as a consequence of their universal importance to cell replication and DNA repair, RNRs are considered to be attractive targets for the rational design of anti-cancer and anti-viral drugs. For these reasons, the structures and catalytic mechanisms of RNRs have been under intense investigation.

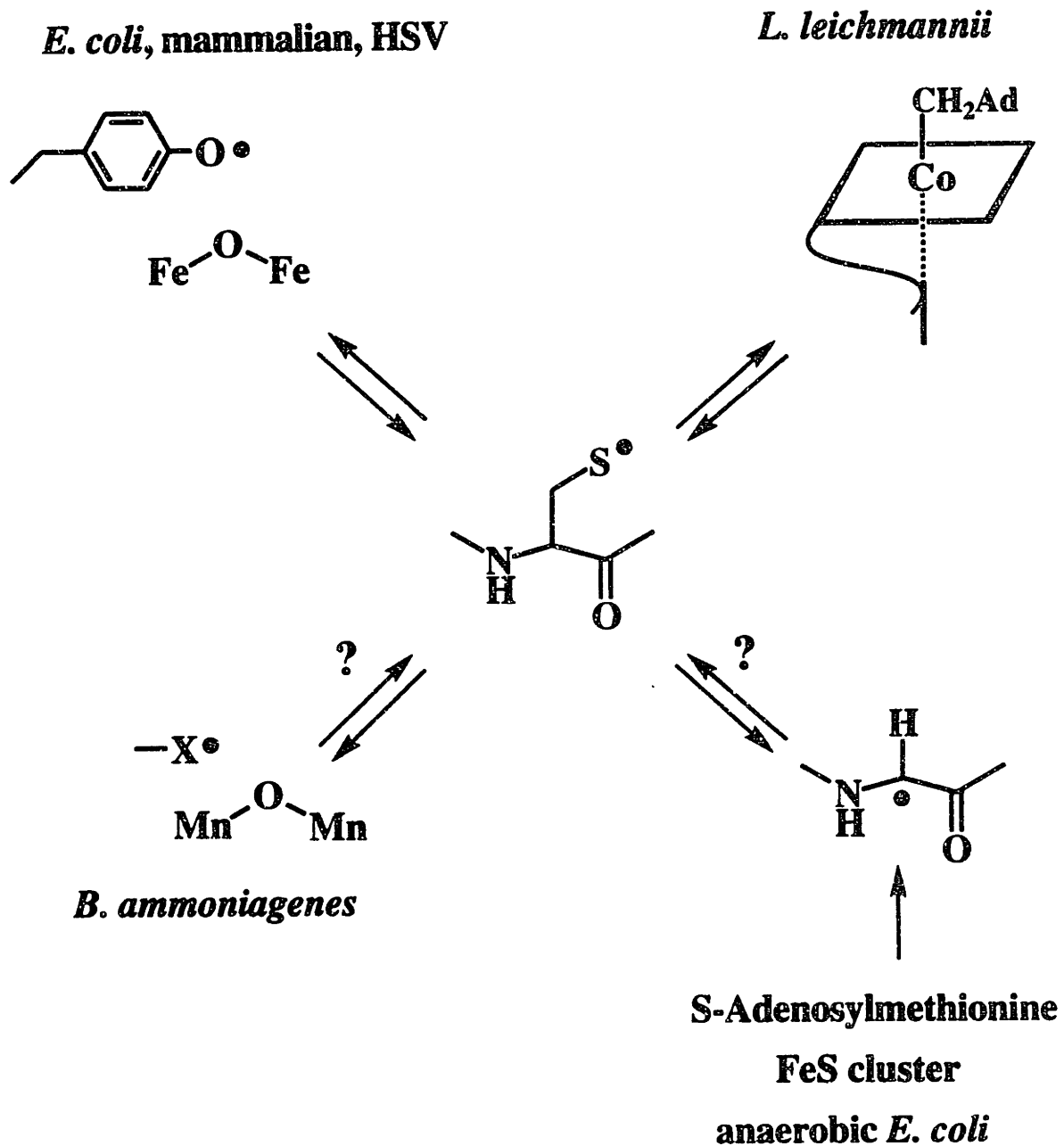
Scheme 1.1: Reaction catalyzed by ribonucleotide reductases.



Studies in the past two decades have revealed many interesting and unusual aspects of this enzyme (Eriksson & Sjöberg, 1989; Stubbe, 1990b; Fontecave *et al.*, 1992; Reichard, 1993; Thelander & Gräslund, 1994). In contrast to most other

enzymes that govern key metabolic processes, the RNRs are surprisingly diverse, both in terms of primary sequence, quaternary structure, as well as the cofactors involved in effecting substrate turnover (Stubbe, 1990b; Reichard, 1993). Biochemical studies in the last decade have indicated that the first step in the catalytic mechanism of all known RNRs thus far investigated is the homolytic scission of the 3'C-H bond of the nucleotide substrate (Stubbe *et al.*, 1981; Stubbe *et al.*, 1983) which is effected by a protein radical (Stubbe, 1990a). As shown in Scheme 1.2, nature has evolved at least four different classes of RNRs which have distinctly different quaternary structures and cofactor requirements (Reichard, 1993). Despite the differences in these reductases, the cofactors share a capability for the generation and stabilization of a protein radical. The RNR isolated from *E. coli* (EC 1.17.4.1) is by far the best characterized of all the reductases. As will be discussed in detail subsequently, this enzyme contains a novel tyrosyl radical-diferric cluster cofactor, and is prototypical of all known mammalian and viral RNRs (Thelander & Reichard, 1979; Lammers & Follmann, 1983; Stubbe, 1990b). Extensive biochemical and spectroscopic studies have led to the advancement of the hypothesis that the tyrosyl radical-diferric cluster cofactor in the R2 subunit generates, via long-range electron transfer process, a thiyl radical in the active site in the R1 subunit which initiates turnover by abstracting the 3'-H atom from the substrate (Mao *et al.*, 1992b). The enzyme isolated from *Lactobacillus leichmannii* represents the best studied of the second class of RNRs that use an organometallic cofactor, 5'-deoxyadenosylcobalamin (AdoCbl) (Blakey, 1978). Recent studies have indicated that the function of AdoCbl is to generate a thiyl radical essential for catalytic turnover (Booker *et al.*, 1994; Licht *et al.*, 1996). In addition, a ribonucleotide reductase has been isolated from *E. coli* grown under anaerobic conditions that is distinct from the *E. coli* reductase discussed above (Eliasson *et al.*, 1990; Eliasson *et al.*, 1992). This enzyme contains an essential glycy radical that is generated by an

Scheme 1.2: Ribonucleotide reductases use a diverse array of cofactors. The cofactors used by the four major classes of RNRs are shown.



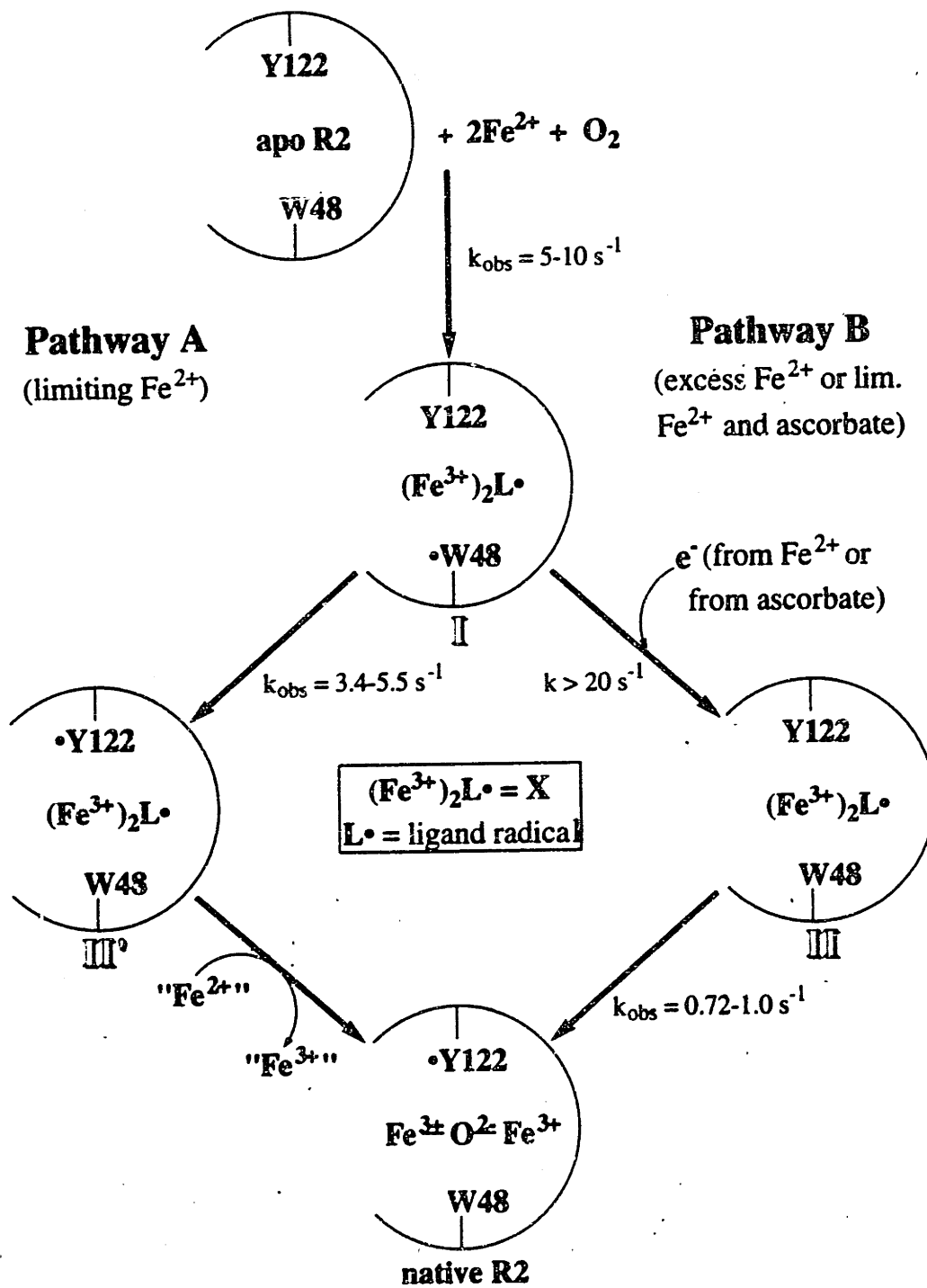
"activating enzyme" (Bianchi *et al.*, 1993; Mulliez *et al.*, 1993; Sun *et al.*, 1995) via a novel mechanism involving the use of S-adenosylmethionine (AdoMet), and a [4Fe-4S] cluster (Harder *et al.*, 1992). Finally, recent studies by Follmann and coworkers have shown that the RNR isolated from *Brevibacterium ammoniagenes* requires Mn³⁺ for catalytic activity (Willing *et al.*, 1988). The UV/vis spectrum of the *B. Ammoniagenes* RDPR is similar to model compounds that contain two Mn³⁺ atoms coupled through a μ -oxo bridge (Sheats *et al.*, 1987). Whether this enzyme contains a tyrosyl radical or perhaps some other organic radical remains to be established, but preliminary biochemical studies have shown a number of similarities between this enzyme and the enzyme from *E. coli*, suggesting that they may catalyze nucleotide reduction via similar mechanisms (Willing *et al.*, 1988).

Since the discovery of a stable tyrosyl radical in R2, much effort has been directed towards elucidating its role in nucleotide reduction and the manner by which this tyrosyl radical is generated. Studies from many laboratories have shown that the function of the iron cluster involves the reaction of its reduced state with O₂ to effect the one-electron oxidation of an endogenous tyrosine residue (Brown *et al.*, 1969; Atkin *et al.*, 1973; Sahlin *et al.*, 1989; Bollinger *et al.*, 1991a). The reaction of O₂ at a diiron(II) center is not unique to R2. The prevalence and biological importance of proteins that contain oxo- or hydroxo-bridged dinuclear iron clusters are now widely recognized (Lippard, 1988; Sanders-Loehr *et al.*, 1989; Kurtz, 1990; Vincent *et al.*, 1990; Stubbe, 1991; Feig & Lippard, 1994; Andersson & Gräslund, 1995). A growing list of proteins that contain oxo- or hydroxo-bridged diiron clusters includes hemerythrin (Wilkins & Wilkins, 1987), purple acid phosphatase (Antanaitis & Aisen, 1983; Doi *et al.*, 1988; True *et al.*, 1993), ribonucleotide reductase (Lammers & Follmann, 1983; Sjöberg & Gräslund, 1983; Thelander *et al.*, 1985; Reichard, 1988), protein A of methane monooxygenase (Woodland *et al.*, 1986; Ericson *et al.*, 1988; Fox *et al.*, 1988; DeWitt *et al.*, 1991), rubrerythrin (LeGall *et al.*,

1988; Ravi *et al.*, 1993; Moura *et al.*, 1994; Gupta *et al.*, 1995), stearyl-ACP desaturases (Sanders-Loehr, 1989; Que & True, 1990; Fox *et al.*, 1993; Fox *et al.*, 1994), nigerythrin (Pierik *et al.*, 1993). Several of these dinuclear iron proteins perform critical functions in the organisms in which they are found: hemerythrin is the O₂-carrier in marine invertebrates including sipunculids, annelids, priapulids and brachiopods (Wilkins & Wilkins, 1987); ribonucleotide reductase (RNR) catalyzes the first committed and rate limiting step in DNA biosynthesis, converting ribonucleotides into deoxyribonucleotides (Thelander & Reichard, 1979); and methane monooxygenase converts methane to methanol, thereby allowing methanotrophic bacteria to use methane as their sole carbon source (Dalton, 1980; Anthony, 1982). Because of the importance of the tyrosyl radical-diiron(III) cofactor to the function of *E. coli* RNR, and because of the general biochemical significance of reactions between O₂ and diiron clusters, much effort has been directed towards investigating the mechanisms by which *E. coli* self-assembles its cofactor from Fe²⁺ and O₂.

Extensive studies of the reaction of the apo form of R2 with Fe²⁺ and O₂ have been carried out previously in our laboratory, and these studies have provided a coherent mechanism for R2 cofactor assembly at 5 °C in the reaction of apo R2 with O₂ and Fe²⁺ at 5 °C (Scheme 1.3) (Bollinger *et al.*, 1994a; Bollinger *et al.*, 1994b). The major focus of this thesis is directed towards investigating the mechanism of cofactor assembly when the diferrous form of R2 reacts with O₂. The experiments described in this thesis were carried out with the expectation that they may verify the proposed mechanism (Scheme 1.3) and provide further insight into the reconstitution reaction. This chapter seeks to provide an overview of the *E. coli* ribonucleotide reductase, and presents a platform for which to discuss the R2 cofactor assembly process. It will focus primarily on the structural and mechanistic aspects of the unique tyrosyl radical-diiron (III) cluster cofactor, describing the various oxidation states of the iron cluster, the initial characterization of the cofactor

Scheme 1.3: Mechanism proposed in our previous work for assembly of the R2 cofactor. The broken circle represents only one of the two monomers of apo R2. The broken circle represents only one of the two monomers of apo R2.



assembly process, as well as recent studies of another diiron protein, methane monooxygenase.

***E. coli* Ribonucleotide Reductase**

The RNR isolated from *E. coli* (Thelander & Reichard, 1979; Lammers & Follmann, 1983; Stubbe, 1990b) acts on nucleoside substrates that are diphosphorylated, and the dNDP products are then phosphorylated to the corresponding dNTP by nucleoside diphosphate kinase before being incorporated into DNA. The *E. coli* enzyme is prototypical of all known mammalian and viral RNRs (Stubbe, 1990b; Conner *et al.*, 1994; Thelander & Gräslund, 1994). As a result, this enzyme has been widely and intensively studied as a model for rational design of anticancer and anti-viral drugs. The *E. coli* RNR is composed of two homodimeric subunits (Fig. 1.1). In the holoenzyme both of these subunits are dimeric, yielding a putative overall tetrameric $\alpha_2\beta_2$ quaternary structure (Thelander, 1973). The R1 subunit contains the binding site for NDP substrates, as well as binding sites for NTP and dNTP allosteric effectors. This subunit also contains catalytically important cysteine residues which become oxidized concomitant with substrate reduction (Mao *et al.*, 1992b). During turnover, cysteines 225 and 462 are oxidized to a disulfide, thereby providing the reducing equivalents required for nucleotide reduction (Mao *et al.*, 1992a; Mao *et al.*, 1992b). Cysteines 754 and 759 function to shuttle reducing equivalents into and out of the active site via disulfide interchange with the *in vivo* reductants, such as thioredoxin (Mao *et al.*, 1992b). The fifth essential cysteine residue, C439, is proposed to function as a thiyl radical which initiates nucleotide reduction by abstracting the 3'-H atom in the substrate (Mao *et al.*, 1992c).

The small subunit, R2, contains a stable tyrosyl radical (at Y122) adjacent to an μ -oxo bridged diferric cluster (Fig. 1.2), both essential for activity of the holoenzyme

(Atkin *et al.*, 1973; Sjöberg *et al.*, 1977). Early spectroscopic studies - optical spectroscopy, magnetic susceptibility measurements, Mössbauer spectroscopy, and Raman spectroscopy - suggested that the protein contains two high-spin Fe³⁺ atoms that are antiferromagnetically-coupled through a μ -oxo bridge (Sanders-Loehr, 1989; Que & True, 1990; Feig & Lippard, 1994). The dinuclear iron cluster is necessary for the generation and maintenance of the tyrosyl radical, which in turn is essential for catalysis (Atkin *et al.*, 1973). This tyrosyl radical is exceptionally stable, having a half-life that is on the order of hours at room temperature, and years at -80 °C. Reduction of the tyrosyl radical to tyrosine results in complete loss of catalytic activity (Atkin *et al.*, 1973). Until the X-ray crystallographic data revealed that the cofactor of *E. coli* R2 is situated deep within the protein (Nordlund, 1990; Nordlund *et al.*, 1990; Nordlund & Eklund, 1993), •Y122 was considered to be the best candidate for the 3'H abstracting species. However, since there is no evidence thus far for a large-scale conformational change to bring the •Y122 into proximity of the 3'-H of the substrate bound in R1 (Ehrenberg, 1988), it was proposed that the R2 radical initiates 3'-C-H bond homolysis by generating, via long-range electron transfer, a reactive radical on the R1 subunit (Nordlund, 1990; Stubbe, 1990b; Mao *et al.*, 1992b; Mao *et al.*, 1992c). Very recent work by Uhlin, *et al.* revealed that the substrate binding site is also buried deep within R1 (Uhlin & Eklund, 1994). Docking experiment suggested a distance of 35 Å between the R2 tyrosyl radical and the active site cysteine C439 of R1. This observation further underscores the possible functional importance of electron transfer between the cofactor in R2 and the active site in R1.

Despite the differences in the reductases, extensive biochemical studies have indicated that these reductases have evolved to catalyze nucleotide reduction via a similar, radical-based mechanism. The available evidence supports the working hypothesis shown in Scheme 1.4 (Stubbe & van der Donk, 1995). An essential

Fig. 1.1: Schematic representation of *E. coli* ribonucleotide reductase.

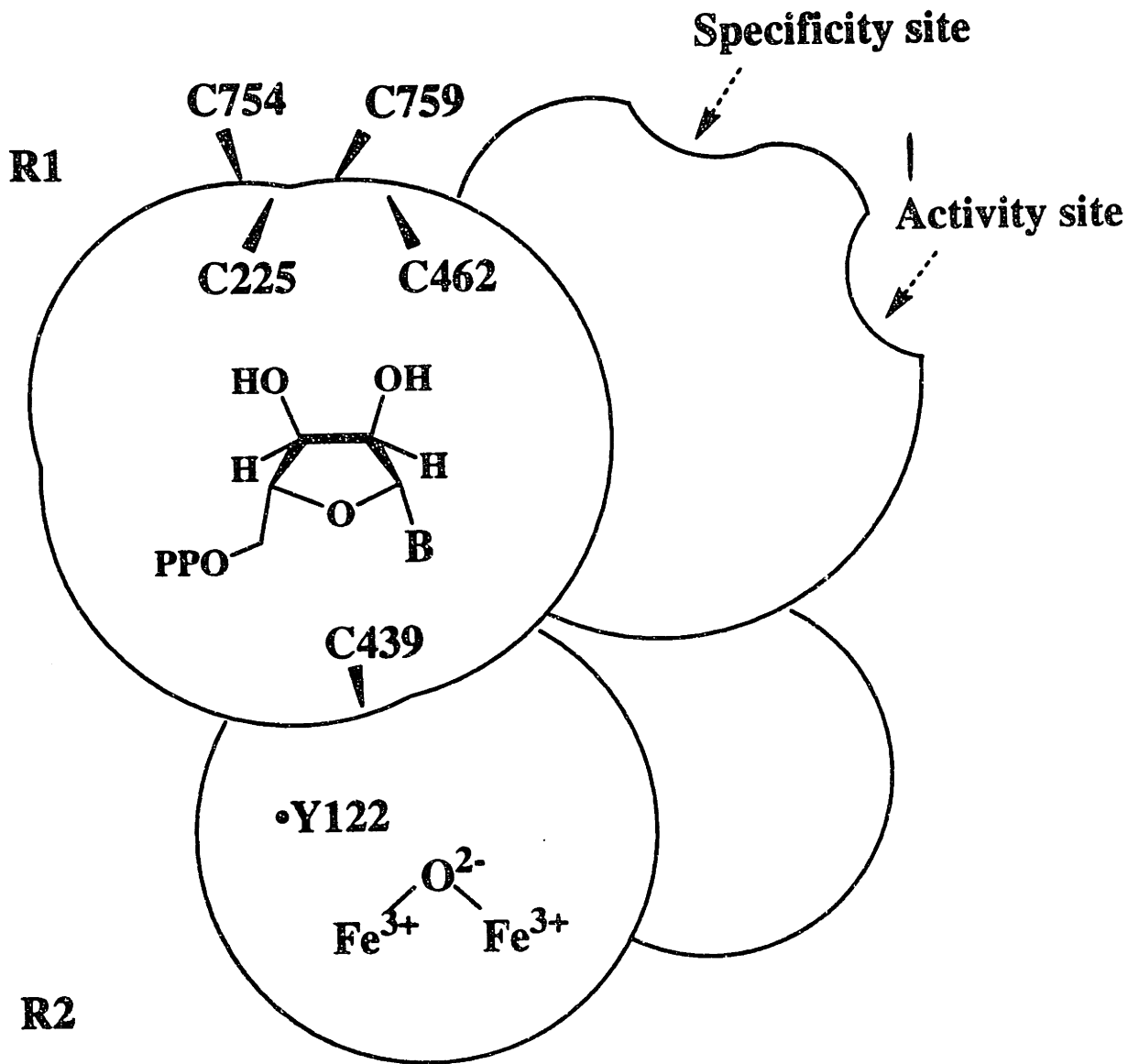
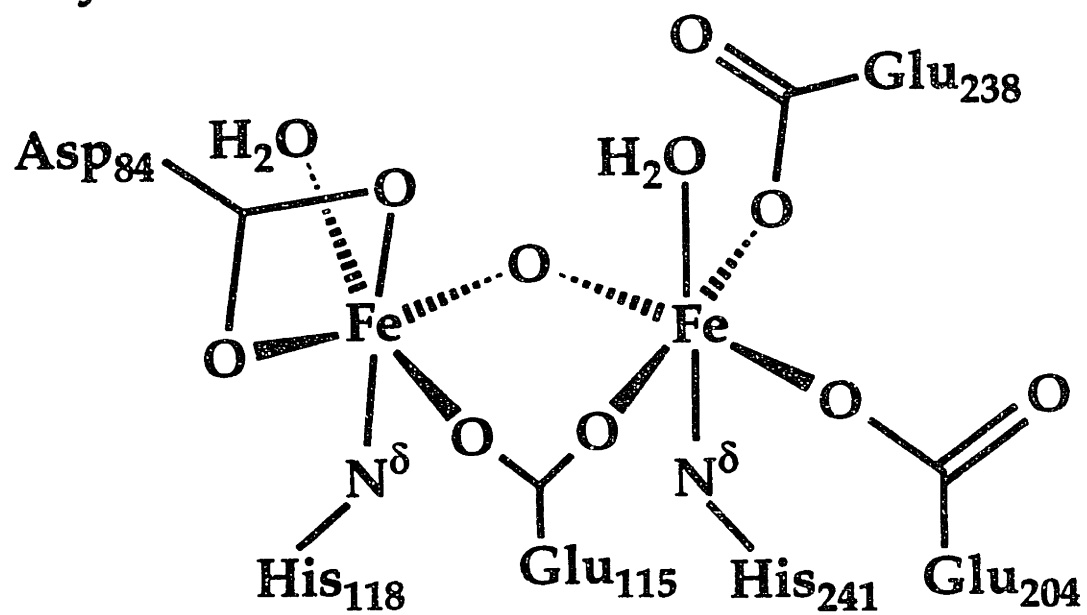
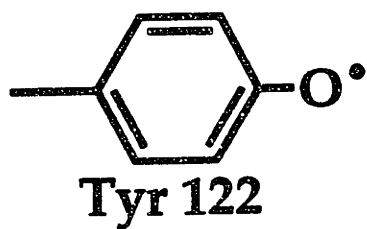
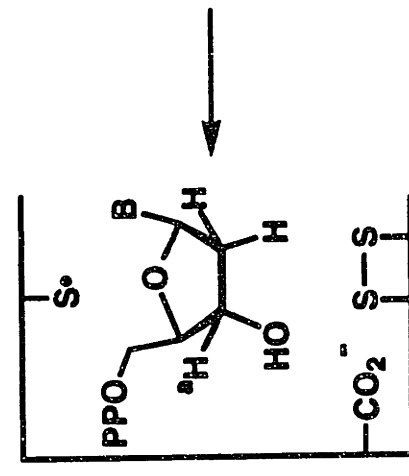
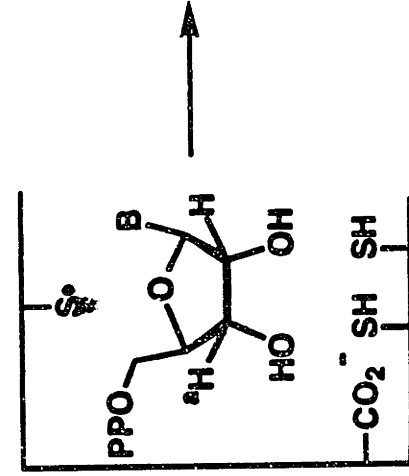
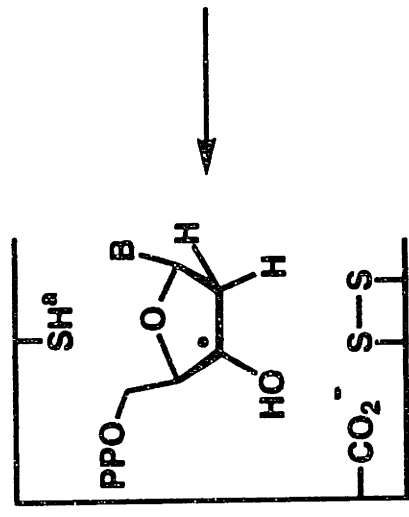
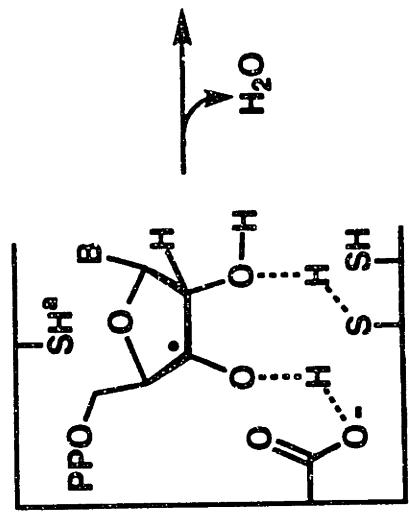
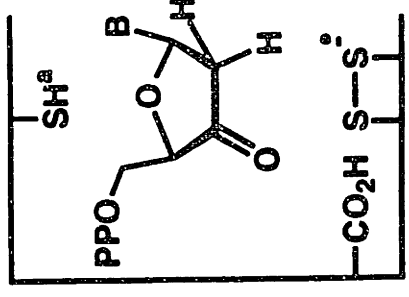
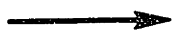
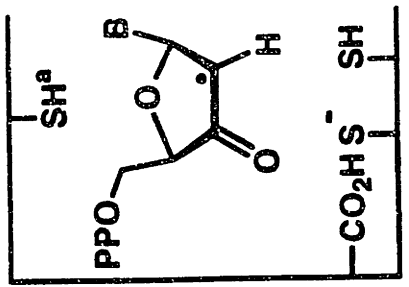


Fig. 1.2: Schematic representation of the tyrosyl radical-diiron(III) cofactor of *E. coli* ribonucleotide reductase (Nordlund *et al.*, 1990; Nordlund & Eklund, 1993).



Scheme 1.4: Current working hypothesis for the catalytic mechanism of *E. coli* ribonucleotide reductase.



feature of the proposed mechanism is the cofactor-mediated formation of a transient thiyl radical which initiates the nucleotide reduction process by abstracting the 3'-H atom of the ribonucleotide substrate. Subsequent to the loss of the 2'-OH group (probably as H₂O), the two cysteines on the α -face of the ribonucleotide reduce the 2'-deoxynucleotide radical intermediate to generate a 3'-ketodeoxynucleotide and a disulfide radical anion. Further reduction of this intermediate by the disulfide radical anion gives 2'-deoxynucleotide radical intermediate and a disulfide. Finally, return of the 3'-H atom produces the deoxynucleotide product and regenerates the thiyl radical. In order to achieve multiple turnovers, the resulting disulfide bond must be re-reduced. This can be achieved *in vitro* with high concentrations (25 - 30 mM) of small thiols such as dithiothreitol (DTT) or dihydrolipoic acid (DHL). *In vivo*, these cysteines are reduced by the protein thioredoxin (TR), which ultimately derives its reducing equivalents from NADPH via a second protein, thioredoxin reductase (TRR) (Laurent *et al.*, 1964; Moore *et al.*, 1964). In the case of *E. coli* RNR, glutaredoxin can also serve as the hydrogen donor for *E. coli* RNR via a system coupled to glutathione reductase, glutathione and NADPH (Aslund *et al.*, 1994).

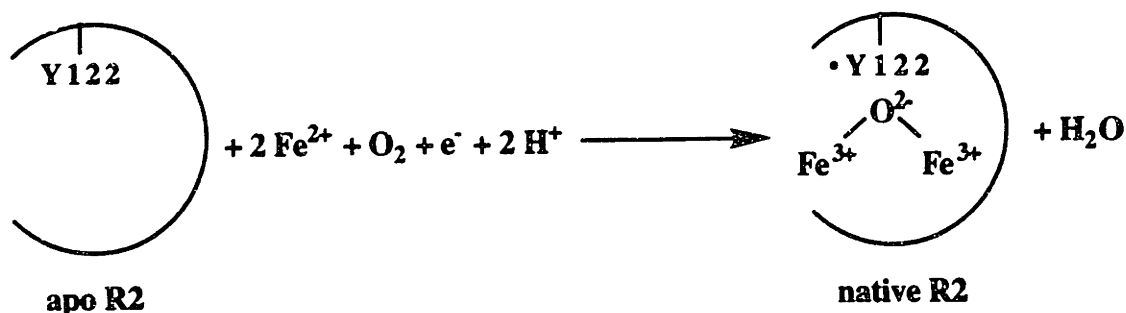
Assembly of the Tyrosyl Radical-Diferric Cluster Cofactor of *E. coli* R2

Reaction Stoichiometry

Initial studies of the cofactor assembly process in R2 were focused on defining the stoichiometry of the reaction (Ochiai *et al.*, 1990; Elgren *et al.*, 1991; Bollinger *et al.*, 1991a; Bollinger *et al.*, 1994a). The results of these studies are all consistent with the net reaction that is summarized by Scheme 1.5.

In this reaction, three of the four electrons required for reduction of O₂ are provided in the conversion of two ferrous ions into the diferric cluster and the oxidation of Y122 to •Y122. As indicated, an additional electron is required for the

Scheme 1.5: Overall reaction of apo R2 with Fe²⁺ and O₂



four-electron reduction of O₂, and several studies have indicated that both Fe²⁺ and ascorbate are capable of providing this fourth electron (Ochiai *et al.*, 1990; Elgren *et al.*, 1991; Bollinger *et al.*, 1991a; Bollinger *et al.*, 1994a). Using a combination of oxygraph, EPR and Mössbauer spectroscopies, Elgren *et al.* determined a Fe²⁺/•Y122 ratio of 3.9 ± 0.5 and an O₂/•Y122 ratio of 1.3 ± 0.2 for reconstitution of R2 from *E. coli* at 25 °C (Elgren *et al.*, 1991). In contrast, Bollinger *et al.* measured a Fe²⁺/•Y122 ratio of 3.3 ± 0.3 and a •Y122/R2 of 1.2 ± 0.1 for the reconstitution of R2 from *E. coli* at 5 °C (Bollinger *et al.*, 1991a; Bollinger *et al.*, 1994a). In the study of the reconstitution of mouse R2, Ochiai *et al.* measured a Fe²⁺/•Y ratio of 3.4 ± 0.3 (Ochiai *et al.*, 1990). The observation of a Fe²⁺/•Y ratio in excess of 3 in all three studies strongly suggests that oxidation of a third Fe²⁺ ion can provide the fourth electron required for cofactor assembly.

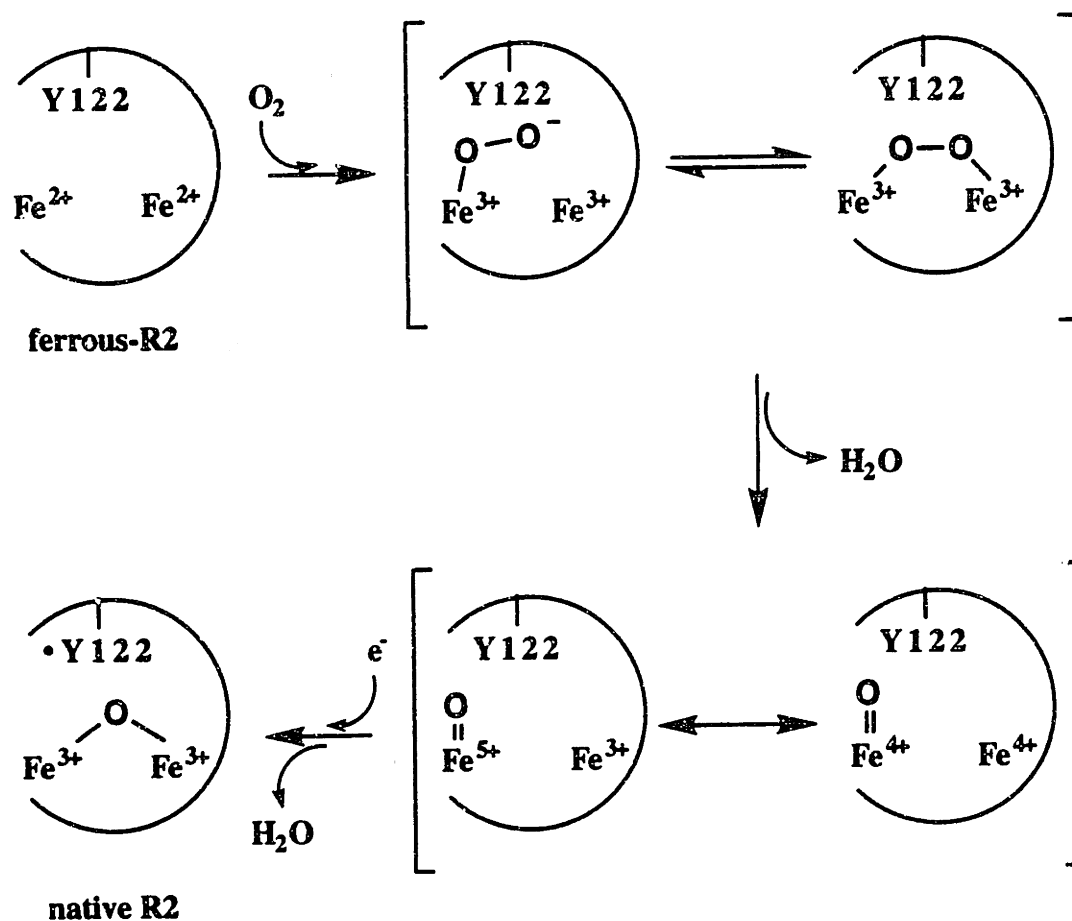
While all of these studies indicated that Fe²⁺ is capable of providing the fourth electron required for cofactor assembly, the state of this "third" Fe²⁺ remains controversial. The EPR studies by Ochiai *et al.* suggested that a substantial amount of mononuclear Fe³⁺ ion is generated in the reconstitution reaction. Based on this result, these researchers reasoned that an additional (lower affinity) Fe²⁺ binding site exists in R2 to facilitate delivery of the fourth electron required for cofactor assembly

(Ochiai *et al.*, 1990). This hypothesis is supported by the results of Bollinger *et al.* (1994a). In their study of the R2 reconstitution reaction under excess Fe^{2+} conditions, Bollinger *et al.* showed by RFQ-Möss spectroscopy that a significant quantity (0.5 equiv. Fe^{3+} relative to the quantity of diferric cluster produced) of a fast-relaxing ferric species is produced concomitantly with the formation of the intermediate iron cluster, X (Bollinger *et al.*, 1994a). In contrast, using Mössbauer spectroscopy, Elgren *et al.* showed that > 92 % of the added Fe^{2+} is incorporated into dinuclear clusters at completion of the reaction (Elgren *et al.*, 1991). On the basis of these results, Elgren *et al.* concluded that electron transfer between R2 monomers must occur, allowing Fe^{2+} bound in one monomer to supply the fourth electron to a different R2 monomer without producing mononuclear Fe^{3+} .

Mechanisms Proposed for the R2 Reaction Prior to This Work

On the basis of functional analogy to heme-iron dependent peroxidases (Marnett *et al.*, 1986; McMurry & Groves, 1986; Ortiz de Montellano, 1986), early elaboration of the mechanism of the R2 reaction with O_2 often invokes high valent (Fe(IV) or Fe(V)) iron intermediates (Scheme 1.6). In these mechanisms, reaction of the reduced form of R2 with O_2 results in formation of a peroxo-diferric intermediate. Heterolytic O-O bond cleavage of the peroxo-diferric intermediate leads to formation of a perferryl (Fe(V)) species (Ochiai *et al.*, 1990; Sahlin *et al.*, 1990; Fontecave *et al.*, 1990a). This putative high-valent iron intermediate then accepts one electron from Y122 and a second electron from an unspecified source to generate the product, native R2. Support for this mechanism was drawn from the observation that peroxides and other oxygen donors can activate met R2 to generate tyrosyl radical, even though this reaction is extremely slow, and the yield of tyrosyl radical is poor (Fontecave *et al.*, 1990a). However, it is possible that hydrogen peroxide activates met R2 by reducing the diferric cluster to form diferrous R2.

Scheme 1.6: Early elaboration of the mechanism for the R2 reconstitution reaction which involves high-valent iron-oxo intermediate.



Subsequent reaction of the reduced cluster with O₂ can then generate •Y122.

Recently, the assembly of the tyrosyl radical-diferric cluster cofactor in R2 has been examined in our laboratory using stopped-flow absorption (SF-Abs), rapid freeze-quench EPR (RFQ-EPR) and rapid-freeze quench Mössbauer (RFQ-Möss) spectroscopies (Ravi *et al.*, 1994; Bollinger *et al.*, 1994a; Bollinger *et al.*, 1994b). The distinctive UV/vis absorption of the R2 cofactor (Fig. 1.3) and the EPR spectra of the tyrosyl radical (Fig. 1.4) make the assembly of the R2 cofactor ideally amenable to

Fig. 1.3: UV-Visible absorption spectra of the diferric cluster (**A**) and the tyrosyl radical (**B**) in *E. coli* ribonucleotide reductase (Bollinger *et al.*, 1991a). Spectrum **C** is the sum of **A** and **B**.

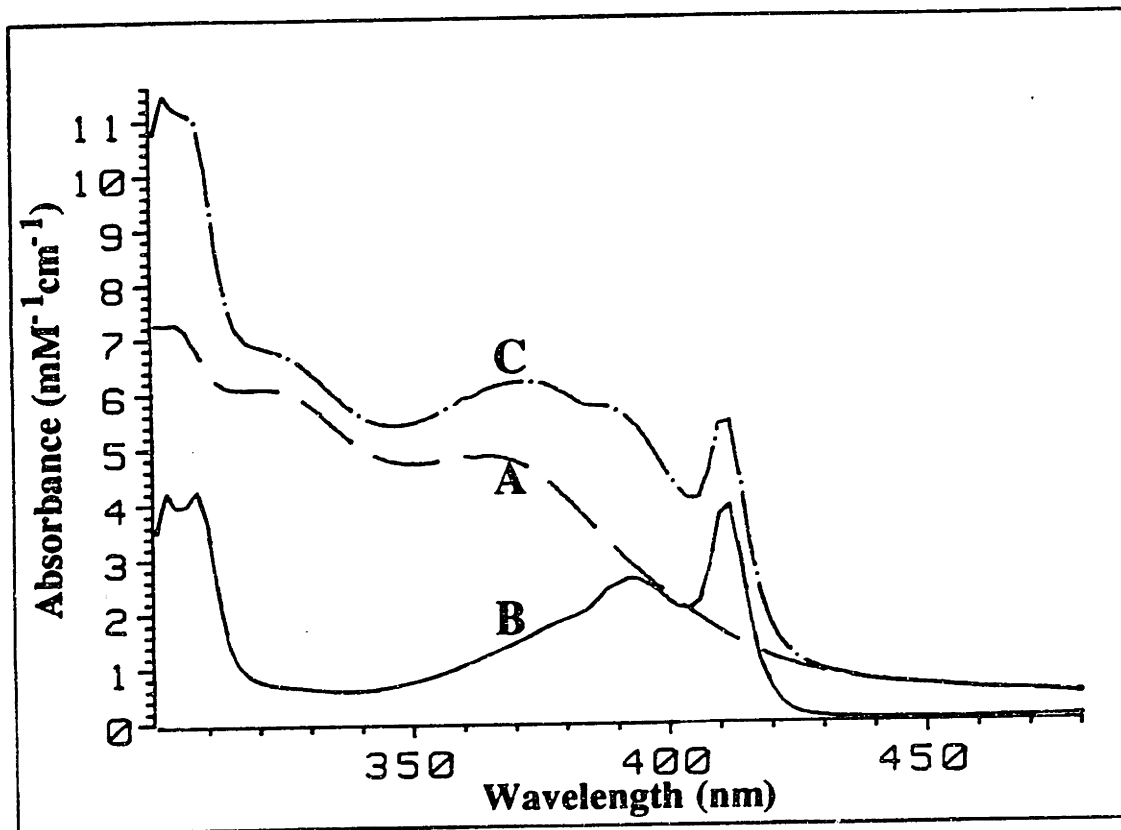
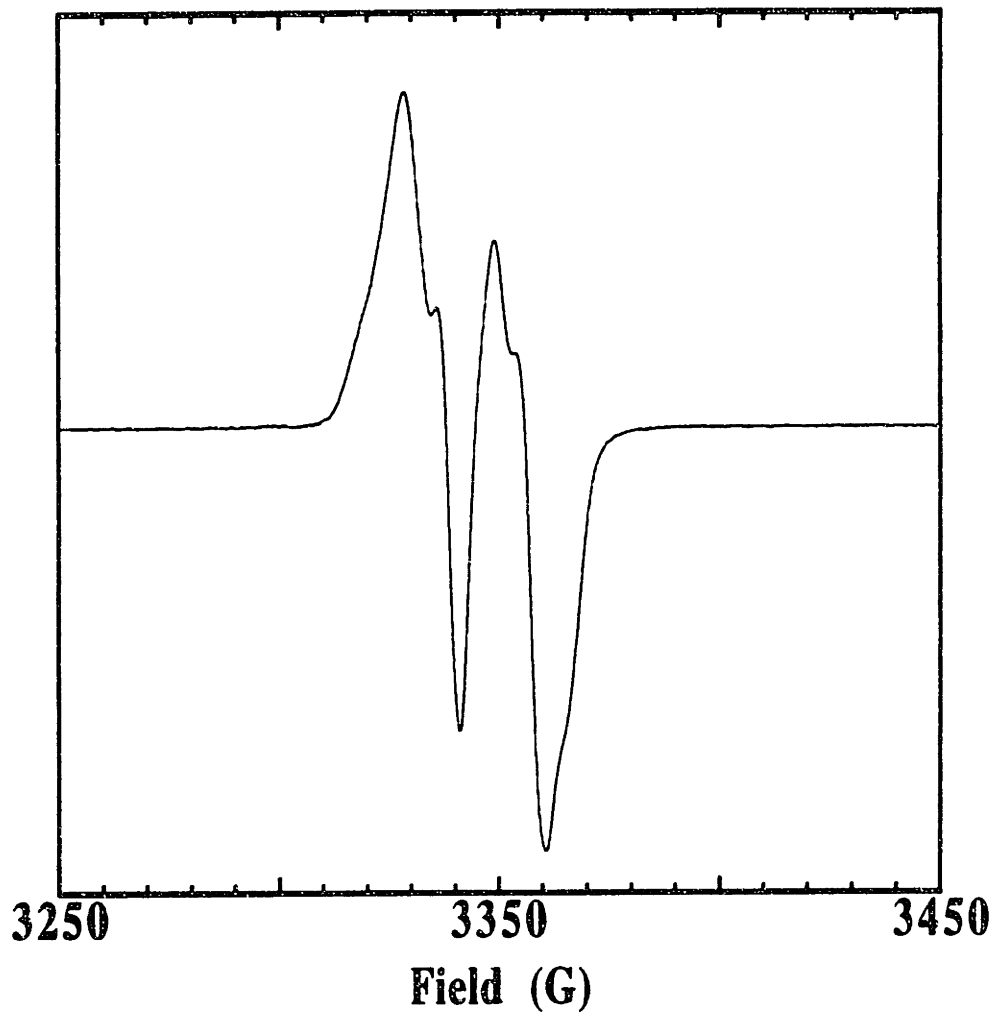


Fig. 1.4: X-band EPR spectrum of the tyrosyl radical of *E. coli* R2. The spectrum was acquired at 20 K with a microwave power of 1 μ W, a frequency of 9.43 GHz, a modulation amplitude of 4 G, a sweep time of 200 s, a time constant of 200 ms, and a receiver gain of 1×10^4 .



studies by SF-Abs and RFQ-EPR spectroscopy, as the formation of the cofactor can readily be monitored. As demonstrated by Bollinger *et al.*, the SF-Abs study of the R2 reconstitution has allowed kinetic characterization of the \bullet Y122 production, and suggested that more than one species can generate the tyrosyl radical (Bollinger *et al.*, 1991a). Since an essential step in the cofactor assembly involves oxidation of Y122 to \bullet Y122, it is reasonable to expect that EPR-active intermediates might accumulate during the reaction. Indeed, using RFQ-EPR spectroscopy, Bollinger *et al.* identified multiple transient EPR-active species in the reaction (Bollinger *et al.*, 1991a; Bollinger *et al.*, 1991b). On the basis of the EPR and Mössbauer spectroscopic results, one of the EPR-active species, X, was proposed to consist of two high-spin ferric ions coupled to a ligand radical (Ravi *et al.*, 1994). Successful adaptation of the rapid freeze-quench methodology to Mössbauer study has also provided a third method to monitor the entire time-course of cofactor assembly, as the concentration at any time of the iron-containing reactants, intermediates, and product can be determined. Finally, the consistency of the SF-Abs, RFQ-EPR, and RFQ-Möss data in these studies demonstrates that the results of these very different methods can be directly compared. These studies have provided the technical basis for the mechanistic study of the R2 cofactor assembly reported in this thesis.

Using a combination of SF-Abs, RFQ-EPR and RFQ-Möss spectroscopies, Bollinger *et al.* have characterized the reaction at 5 °C of apo R2 with Fe^{2+} and O_2 and proposed a coherent mechanism for the reaction (Scheme 1.3) (Ravi *et al.*, 1994; Bollinger *et al.*, 1994a; Bollinger *et al.*, 1994b). Early study of the reaction of apo R2 at 5 °C with Fe^{2+} and O_2 indicated that the development of the optical and the EPR spectra of the R2 cofactor depends markedly on the initial $\text{Fe}^{2+}/\text{R2}$ ratio (Bollinger *et al.*, 1991a). When apo R2-wt is mixed with Fe^{2+} and O_2 , an intermediate I (which contains X and the putative \bullet W48⁺) accumulates with a k_{obs} of 5 - 10 s^{-1} . When reducing equivalent is readily available (as in the case of the reaction carried out

with excess Fe^{2+} and ascorbate), I is rapidly reduced by one electron to give a second intermediate II. In a subsequent step, II oxidizes Y122 by one electron to give $\bullet\text{Y122}$ and the diferric cluster in native R2. Because conversion of I to II is significantly faster than formation of I, I is kinetically invisible and pathway B in Scheme 1.3 can be described by two sequential first-order processes, in which X accumulates ($k_{\text{obs}} = 5 - 10 \text{ s}^{-1}$), and decays concomitantly with formation of $\bullet\text{Y122}$ and the diferric cluster ($k_{\text{obs}} = 0.7 - 1 \text{ s}^{-1}$).

In the case of the reaction carried out with limiting Fe^{2+} ($\text{Fe}^{2+}/\text{R2} = 2.2 - 2.4$), development of the cofactor appears to differ markedly from the excess Fe^{2+} reaction, and the kinetics are much more complicated (Bollinger *et al.*, 1994b). Stopped-flow data indicates that formation of $\bullet\text{Y122}$ is initially faster in the limiting Fe^{2+} reaction than in the excess Fe^{2+} reaction (Bollinger *et al.*, 1991a). In spite of this fact, the limiting Fe^{2+} reaction requires >120 s to reach completion, compared to less than 30 s for the excess Fe^{2+} reaction. Moreover, a broad, transient absorption band centered near 560 nm rapidly develops in the limiting Fe^{2+} reaction, and appears to decay concomitantly with the initial fast phase of $\bullet\text{Y122}$ (Bollinger *et al.*, 1991a). The observation that the presence of either excess Fe^{2+} or a reductant such as ascorbate prevents development of the 560 nm absorption transient, and the observation that suppression of the transient in both cases correlates with suppression of the initial fast phase of $\bullet\text{Y122}$ production led to the proposal that the 560 nm absorbing species is the $\bullet\text{Y122}$ -generating intermediate in the rapid phase of the limiting Fe^{2+} reaction (Bollinger *et al.*, 1991a). Furthermore, comparison of the SF-Abs and the Mössbauer data indicates that $\bullet\text{Y122}$ formation precedes diferric cluster formation in the limiting Fe^{2+} reaction (Bollinger *et al.*, 1994b). Thus, data from each of the three methods suggested that $\bullet\text{Y122}$ generation proceeds by a different mechanism under limiting Fe^{2+} conditions (Bollinger *et al.*, 1994b). These observations also imply a

partition of pathways, with the partition ratio determined by the availability of the extra reducing equivalent (Scheme. 1.3).

On the basis of its light absorption characteristics (Menage *et al.*, 1990) and chemical precedent (Brennan *et al.*, 1991), the 560 nm-absorbing species was initially proposed to be a μ -peroxodiferric cluster (Bollinger *et al.*, 1991a). Subsequent study, however, demonstrated that no Mössbauer features can be discerned which correlate temporally with the 560 nm absorption transient (Bollinger *et al.*, 1994b). This result suggests that the 560 nm absorbing species is not iron-based. It was proposed, then, that the species is a protein radical. Time-resolved EPR spectra of the reaction of apo R2 with limiting Fe^{2+} provided support for this assertion. In addition to the spectra of X and $\bullet\text{Y122}$, transient broad features are discernible in the time-resolved spectra of the limiting Fe^{2+} reaction. The observation that these broad EPR features develop only in the limiting Fe^{2+} reaction, and not in the presence of excess Fe^{2+} or ascorbate led to the proposal that these features are correlated with the 560 nm absorption band. Drawing on the structural and functional analogy between R2 and a heme-dependent protein, cytochrome c peroxidase (CCP), it was proposed that a tryptophan cation radical ($\bullet\text{WH}^+$) is produced by one-electron oxidation of W48, and that $\bullet\text{W48}^+$ can generate $\bullet\text{Y122}$ in the limiting Fe^{2+} reaction (Bollinger *et al.*, 1994b).

With the tentative assignment of the 560 nm absorbing species as $\bullet\text{W48}^+$, Bollinger *et al.* proposed the following mechanism for the limiting Fe^{2+} reaction (Bollinger *et al.*, 1994b). When reducing equivalent is not readily available ($\text{Fe}^{2+}/\text{R2} = 2.2 - 2.4$), two intermediates were proposed to accumulate (Pathway A in Scheme 1.3). The first intermediate I was proposed to contain the intermediate X and a $\bullet\text{W48}^+$. One-electron oxidation of Y122 by $\bullet\text{W48}^+$ generates the second intermediate (II') which was proposed to contain $\bullet\text{Y122}$ and the intermediate X. Finally, reduction of X by Fe^{2+} yields the product cofactor (Bollinger *et al.*, 1994b).

Current study of the R2 Reconstitution Mechanism

As mentioned above, previous studies of the R2 reaction in this laboratory have led to the identification of two species that are kinetically competent to effect Y122 oxidation and allowed proposal of a working hypothesis for the cofactor assembly shown in Scheme 1.3 (Ravi *et al.*, 1994; Bollinger *et al.*, 1994a; Bollinger *et al.*, 1994b). In the chapters that follow, we have used a combination of SF-Abs, RFQ-EPR, and RFQ-Möss spectroscopies to examine the kinetics of the reaction at 5 °C of diferrous R2 with O₂. As shown in Scheme 1.3, the proposed mechanism for the reconstitution of R2 represents the least complex mechanism that can accommodate the data. Clearly the first process in this model - formation of intermediate X from apo R2 - is composed of multiple steps. Since it might be expected that, at least two of these steps - binding of Fe²⁺ to apo R2, and binding of O₂ to the diferrous R2 complex - would exhibit a dependence on reactant concentrations, it was therefore somewhat surprising that the *k*_{obs} for formation of X is invariant, over a R2 concentration range of 25 - 300 μM (Bollinger *et al.*, 1994a). On the basis of this observation, it was proposed that a conformational change in apo R2 limits the rate of formation of X (Bollinger *et al.*, 1994a). This hypothesis raises the possibility that formation of X upon reaction of the pre-formed Fe(II)-R2 complex with O₂ might be significantly faster. It also raises the interesting possibility of observing intermediates that are formed prior to X. For these reasons, the reaction of the pre-formed Fe(II)-R2 with O₂ is studied and the results are the major focus of this thesis.

Many of the experiments presented herein are intended to address similar questions concerning the cofactor assembly. The particular issues that will be addressed concern: 1) the identity of the •Y122 generating species; 2) the source of the fourth electron required for cofactor assembly, and the manner by which it is delivered into the cofactor site; 3) the possible involvement of a tryptophan cation radical in the reaction; 4) the nature and the order of the events which lead to the

formation of the intermediate X, and; 5) the factors which govern the kinetics and reaction mechanism of cofactor assembly.

The results of Chapter 2 demonstrate that, as with the reconstitution of native R2 from apo R2, reconstitution of native R2 from Fe(II)-R2 also proceeds through the intermediate X. The stopped-flow UV/vis absorption experiments have provided indication for accumulation of X and suggested that formation of intermediate X in the reaction of Fe(II)-R2 with O₂ is much faster than in the reaction of apo R2 with Fe²⁺ and O₂. The rapid freeze-quench EPR and Mössbauer experiments further confirm the formation of X, and demonstrate that X is the precursor of •Y122 and the diferric cluster. The kinetic data also show that X accumulates in the Fe(II)-R2 reaction with a rate constant which is significantly greater than that in the apo R2 reaction. These results are consistent with the idea put forth previously that the rate-limiting conformational change in apo R2 is required to allow for entry of Fe²⁺ into the cluster binding site (Bollinger *et al.*, 1994a).

Chapter 3 discusses the reaction of Fe(II)-R2 with O₂ under limiting Fe²⁺ conditions as monitored by SF-Abs, RFQ-EPR and RFQ-Möss spectroscopies. The stopped-flow data of Chapter 3 indicates that the 560 nm absorption transient is not responsible for generation of •Y122 in this reaction. Furthermore, comparison of the SF-Abs and the RFQ-EPR data indicates that the broad g = 2.0 EPR signal is not temporally correlated with the 560 nm-absorbing species. This observation is ultimately taken as evidence against the previous assignment of the 560 nm-absorbing species as a tryptophan cation radical. In addition, when the reaction of apo R2 with limiting Fe²⁺ is carried out in ²H₂O, the broad EPR features are not detected, even though the 560 nm transient absorption is still observable. This observation also provides a strong argument against the previous hypothesis that the 560 nm-absorbing species is associated with the broad g = 2 EPR species (Bollinger

et al., 1994b). The observation that the 560 nm-absorbing species is not correlated with any of the EPR signals observed thus far is also inconsistent with a role for it in generating $\bullet Y122$. Although the identity of the $\bullet Y122$ -generating species cannot be determined by the experiments in Chapter 3 due to the poor resolution of the EPR spectra and the complexity of the kinetics of the limiting Fe^{2+} reaction, speculation regarding its identity is presented.

In addition, several experiments were designed to probe the binding interactions between Fe^{2+} and apo R2, with the expectation that these experiments may facilitate the interpretation of the kinetic data and provide insight to the reaction mechanism. The results of these experiments were presented in Chapter 4. These results provide arguments against the hypothesis that binding of Fe^{2+} to apo R2 is "highly cooperative" (Fontecave *et al.*, 1990b; Elgren *et al.*, 1991; Atta *et al.*, 1992a). The results of Chapter 4 also demonstrate that the fourth electron required for electron balance is supplied by a Fe^{2+} ion bound by R2, and suggest that this electron may be, at least in part, delivered via intramolecular electron transfer from the opposite monomer of R2, as was proposed by Elgren *et al.* (1991). Finally, the Mn- and EDTA-quench experiments have provided kinetic evidence that production of $\bullet Y122$ in the reaction of Fe(II)-R2 with O_2 under limiting Fe^{2+} can proceed through the intermediate, X. The simplest mechanism for the R2 reconstitution from Fe(II)-R2 which is consistent with the data related in Chapters 2 - 4 will be discussed.

Structure and Physical Properties of R2 and its Cofactor

Over the past two decades, extensive studies have been directed towards characterization of the structural and biophysical properties of the tyrosyl radical-diiron(III) cluster of R2. These studies have demonstrated several different forms of R2 with various oxidation state and metal-ions occupancy. As demonstrated by the

previous work of Bollinger *et al.* (Bollinger *et al.*, 1994a; Bollinger *et al.*, 1994b) and by the experiments described in this thesis, the ability to convert native R2 into various states and to reconstitute the native protein forms the technical basis for the *in vitro* study of cofactor assembly reaction. In order to understand the R2 cofactor assembly process, a knowledge of the structure of the protein and its iron cluster and the chemical reactivity of the cofactor are required. Early studies have been focused on the characterization of the native cofactor, but recent efforts have begun to yield information on the other forms of R2. A brief discussion of the different forms of R2 and their reactivities is presented here.

Native R2

The presence of a oxo-bridged diiron(III) center was initially suggested from optical (Atkin *et al.*, 1973), Mössbauer (Atkin *et al.*, 1973; Lynch *et al.*, 1989), EXAFS, resonance Raman (Sjöberg *et al.*, 1980; Sjöberg *et al.*, 1982; Backes *et al.*, 1989), and magnetic studies. Interpretation of the spectroscopic data for the iron center of *E. coli* R2 has been greatly facilitated by the extensive structural and spectroscopic investigation of another μ -oxo-bridged diiron protein, hemerythrin and its synthetic analogues (Lippard, 1988; Sanders-Loehr, 1989; Que & True, 1990; Feig & Lippard, 1994). The absorption spectrum of R2 (Fig. 1.3) has a broad band at 365 nm and a shoulder at 320 nm which are assigned as the oxo-to-iron charge transfer transitions in the iron cluster (Atkin *et al.*, 1973; Sanders-Loehr *et al.*, 1989). The Mössbauer spectrum of native R2 reveals two quadrupole doublets of equal intensity with isomer shifts (δ) of 0.45 and 0.55 mm/s, and quadrupole splitting (ΔE_Q) of 1.64 ± 0.06 and 2.41 ± 0.06 mm/s that are indicative of an diiron(III) complexes (Atkin *et al.*, 1973; Lynch *et al.*, 1989). The Mössbauer spectra of R2 at 4.2 K in strong applied fields indicates that the two iron centers in the dinuclear unit are coupled antiferromagnetically. Variable temperature magnetic susceptibility measurements

yielded a J of $-108 \pm 25 \text{ cm}^{-1}$ ($H = -2JS_1 \cdot S_2$) (Pettersson *et al.*, 1980), while studies using saturation-recovery EPR spectroscopy reported a J of -92 cm^{-1} (Hirsh *et al.*, 1992).

The presence of a μ -oxo-bridged diferric cluster in R2 was further supported by the results of resonance Raman studies (Sjöberg *et al.*, 1980; Sjöberg *et al.*, 1982; Backes *et al.*, 1989). These studies revealed features at 496 and 756 cm^{-1} which were assigned to the $\nu_s(\text{Fe-O-Fe})$ and the $\nu_{as}(\text{Fe-O-Fe})$ based on analogy to the resonance Raman study of hemerythrin. These data also allowed estimation of the Fe-O-Fe angle as 130° and of the Fe-O distance as 1.78 Å, giving an Fe-Fe distance of 3.2 Å. Recent studies by Ling *et al.* using $^{18}\text{O}_2$ and a R2-Y122F mutant protein have provided convincing evidence that dioxygen is the source of the μ -oxo bridge in *E. coli* R2 (Ling *et al.*, 1994).

The occurrence of a μ -oxo-bridge in R2 was also supported by the EXAFS studies carried out by Scarrow *et al.*, (Scarrow *et al.*, 1986; Scarrow *et al.*, 1987) and those by Bunker *et al.* (Bunker *et al.*, 1987). The EXAFS analysis by Scarrow, *et al.* showed an Fe-Fe distance of 3.22 Å and provided evidence for a short μ -oxo bridge (Fe-O bonds of 1.8 Å) (Scarrow *et al.*, 1986; Scarrow *et al.*, 1987). An independent study by Bunker, *et al.* calculated an Fe-Fe distance of 3.24 - 3.48 Å (Bunker *et al.*, 1987). The angle is smaller than what has been observed in complexes with only one μ -oxo bridge and suggests at least one additional bridge (Bunker *et al.*, 1987; Scarrow *et al.*, 1987). The EXAFS data also revealed a first shell distance in R2 (2.06 Å) shorter than that in hemerythrin (2.13 Å), suggesting that more oxygen and fewer nitrogen ligands are coordinated to the metal center in R2 (Bunker *et al.*, 1987; Scarrow *et al.*, 1987). NMR studies have provided evidence for histidine(s) coordination to the metal cluster (Sahlin *et al.*, 1986). The observed contact-shifted resonances and their solvent exchange behaviors are as expected for N-H groups of imidazoles coordinated to μ -oxo diiron(III) complexes (Gómez-Romero *et al.*, 1988). Selected data concerning the μ -oxo diiron(III) cluster are listed in Table 1.1.

Table 1.1: Summary of selected physical properties of native R2 from *E. coli*.

		Native R2		Reduced R2
		Fe ³⁺ -O-Fe ³⁺	•Y122	
Optical	λ_{\max} , nm	325 (9400)	412 (4100)	-
	(ϵ , M ⁻¹ cm ⁻¹)	370 (7200)		
Magnetic Susceptibility ($H = -2 JS_1 \cdot S_2$)	J , cm ⁻¹	-108 ± 25		10
Mössbauer site 1	δ , mm/s	0.54 ± 0.03		1.26
	ΔE_Q , mm/s	1.64 ± 0.06		3.13
site 2	$A/g_n\beta_n$ (T)			
	δ , mm/s	0.45 ± 0.03		
EPR	ΔE_Q , mm/s	2.41 ± 0.06		
	$A/g_n\beta_n$ (T)			
EPR	g_{11}		2.009	
	g_{22}		2.004	
	g_{33}		2.002	
	g_{avg}		2.005	
	J , cm ⁻¹	-108 ± 7		
Resonance Raman	ν_s , cm ⁻¹	496	1498	
	ν_{as} , cm ⁻¹	756		
EXAFS	Fe-Fe, Å	3.22-3.48		

The discovery of the tyrosyl radical was facilitated by its UV-visible absorption features (Brown *et al.*, 1969; Atkin *et al.*, 1973) and by its EPR signal (Ehrenberg & Reichard, 1972). Early X band EPR and ENDOR studies in conjunction with specific deuteration of the tyrosine residues in the protein demonstrated that the radical arises from a tyrosine residue (Sjöberg *et al.*, 1977). Alignment of R2 sequences from different organisms showed conservation of the Y122 residue in *E. coli* R2 (Sjöberg *et al.*, 1985), and subsequent site-directed mutagenesis studies showed that replacing

R2-Y122 with a less oxidizable residue, F, gives a protein that has no EPR signal and no catalytic activity (Larsson & Sjöberg, 1986). These results, together, provided convincing evidence that the Y122 residue is the site of the free radical. The low temperature EPR spectrum of the tyrosyl radical of R2 (Fig. 1.4) exhibits a large doublet hyperfine coupling ($A = 19$ G), which is due to one of the β -hydrogens, and a smaller triplet splitting ($A = 7$ G), which arises from the ring hydrogens in positions 3 and 5 (Sjöberg *et al.*, 1977; Bender *et al.*, 1989). The X-band ENDOR experiments by Bender *et al.* also suggested that the radical is deprotonated, a conclusion supported by the latter resonance Raman studies by Sander-Loehr and coworkers (Backes *et al.*, 1989). Additional EPR experiments demonstrated that electronic relaxation of the radical is enhanced by magnetic interaction with the iron cluster (Ehrenberg & Reichard, 1972; Sahlin *et al.*, 1987; Hirsh *et al.*, 1992), indicating that the tyrosyl radical is within 10 Å of the diiron cluster. Very recently, using high-frequency (139.5 GHz) EPR spectroscopy, Gerfen *et al.* provided a detailed characterization of the principle g -values ($g_{11} = 2.0091$, $g_{22} = 2.0046$, $g_{33} = 2.0053$) of \bullet Y122 of R2 (Gerfen *et al.*, 1993). The hyperfine coupling values obtained in this study were also in good agreement with those determined in the earlier ENDOR study (Bender *et al.*, 1989). Selected data concerning the tyrosyl radical are listed in Table 1.1.

An issue which remains somewhat controversial is the stoichiometry of the \bullet Y122 and the diferric cluster in R2. As originally isolated, R2 was found by a colorimetric iron assay to contain 2 Fe^{3+} ions per dimer subunit (Brown *et al.*, 1969; Thelander, 1973). This led to the proposal of a single iron cluster and a single tyrosyl radical at the interface of the two monomers of R2. This hypothesis, however, is inconsistent with the Mössbauer data which indicate that the two ferric ions are inequivalent (Atkin *et al.*, 1973). Subsequent studies by several laboratories led to the cloning and overproduction of R2 (Eriksson *et al.*, 1977; Platz & Sjöberg, 1980; Carlson *et al.*, 1984; Salowe & Stubbe, 1986) which markedly affected the observed

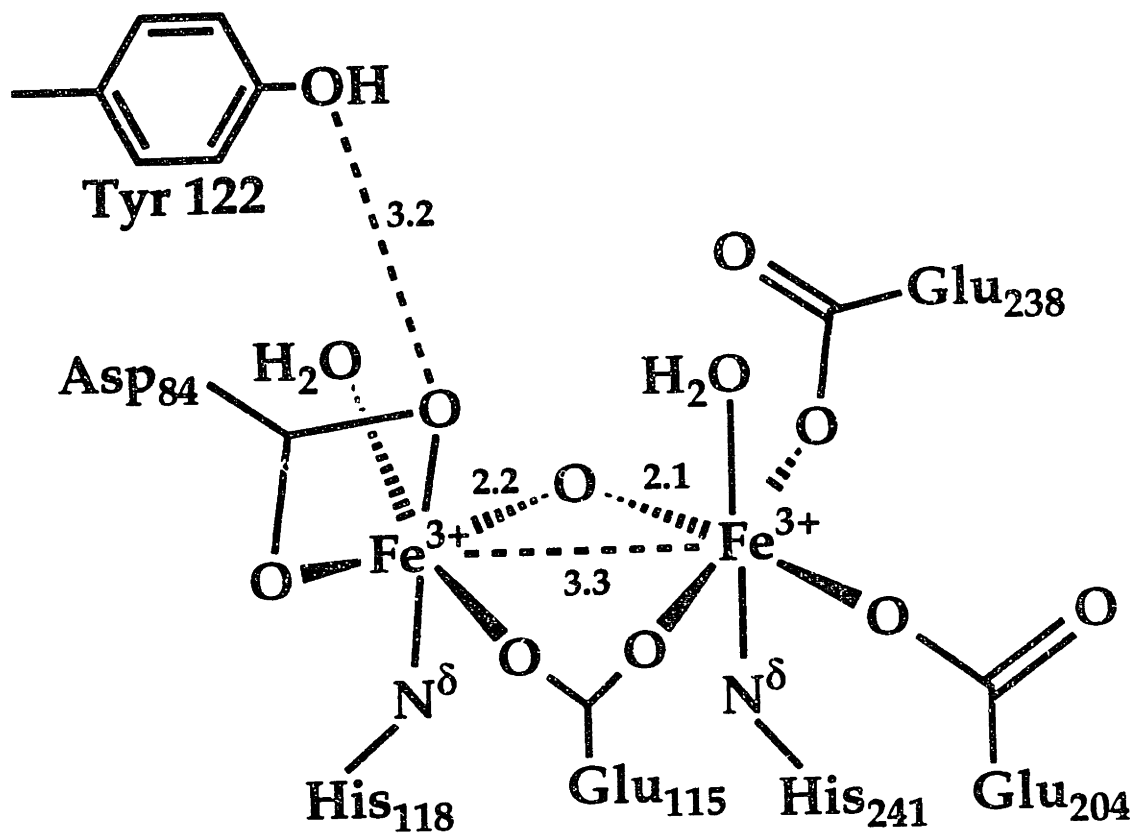
Fe³⁺ and tyrosyl radical stoichiometries (Sjöberg *et al.*, 1987; Lynch *et al.*, 1989; Bollinger, 1992), and greatly facilitated the study of the cofactor assembly process (Bollinger *et al.*, 1994a; Bollinger *et al.*, 1994b). On the basis of the sequence information of *nrdB*, the gene which encodes R2, the molecular weight of the protein was corrected from the previously reported value of 78 kD (Thelander, 1973) to a value of 87 kD (Carlson *et al.*, 1984). This correction led to a correction of the molar absorptivity at 280 nm (ϵ_{280}) to 131,000 M⁻¹ cm⁻¹, which in turn increased the calculated Fe³⁺ and tyrosyl radical content of R2. The overproduction of R2 also greatly simplifies its purification, thereby minimizing loss of Fe³⁺ and tyrosyl radical. As a result, the recombinant R2 after purification was found to contain 2.7 ± 0.3 Fe³⁺ and 1.1 ± 0.1 tyrosyl radicals per R2 (Sjöberg *et al.*, 1987).

The observation of a Fe³⁺/R2 ratio in excess of the theoretical value of 2 (assuming one diiron cluster bound between the two monomers) prompted several other groups to reevaluate this quantity. Isolating R2 (specific activity 4700-5700 U/mg) from an overproducing strain N6405/pSPS2 (Salowe & Stubbe, 1986), Lynch *et al.* determined an ϵ_{280} for the protein of 141,000 M⁻¹cm⁻¹ (Lynch *et al.*, 1989). In addition, using a combination of inductively coupled plasma emission, EPR and Mössbauer spectroscopy, these investigators determined a Fe²⁺/R2 ratio of 3.9 and a •Y122/R2 ratio of 1.4 in the protein as isolated. On the basis of these results, they concluded that R2 must contain one diferric cluster and potentially one tyrosyl radical in each monomer. Meanwhile, Bollinger *et al.* obtained quite different results in studying R2 isolated from the same overproducing strain (specific activity of 5800 - 8000 U/mg) (Bollinger, 1992). In agreement with the results of Lynch *et al.* (1989), Bollinger *et al.* found less than two tyrosyl radicals per R2 (Bollinger, 1992). Assuming an ϵ_{280} of 131,000 M⁻¹ cm⁻¹, a •Y122/R2 ratio of 1.2 ± 0.1 was calculated. However, in contrast to the results of Lynch *et al.* (1989), Bollinger *et al.* consistently found significantly less Fe³⁺ (Bollinger, 1992). Several methods of extraction of Fe

from R2 and several methods for quantitation of the extracted Fe were compared. In all these cases, the Fe/R2 ratio was found to be 3.0 ± 0.2 . At present, the reason for these discrepancies remain unclear.

Recent work by Nordlund and Eklund has resulted in the determination of the crystal structure of the met form of the R2 protein (which contains the diferric cluster and a normal Y122 residue) at 2.2 Å resolution (Nordlund, 1990; Nordlund & Eklund, 1993), confirming the structure that had been proposed based on spectroscopic and other biophysical studies (Table 1.1). The two β protomers are related by a molecular two-fold rotation axis and are associated, through both hydrophobic and charged interactions, to produce a heart-shaped molecule. Each monomeric subunit contains one iron center and potentially one tyrosyl radical, which are both situated deep within each protomer, such that the two cofactors are separated by a distance of 25 Å, and each cofactor is at least 10 Å away from the nearest surface of the R2 protein. Within each dinuclear cluster, the Fe-Fe distance is 3.3 Å, in agreement with the results of the EXAFS studies (Fig. 1.5) (Bunker *et al.*, 1987; Scarrow *et al.*, 1987). In addition to an oxo-bridge, the two iron atoms are bridged by a glutamate residue, E115. The coordination sphere of one Fe^{3+} ion is completed by one histidine (H241), two monodentate carboxylate residues (E238 and E204) and a water molecule. The other Fe^{3+} ion is coordinated by one histidine residue (H118), one bidentate carboxylate residue (D84), and a water ligand. The tyrosyl radical, $\bullet\text{Y122}$, is 5.3 Å from the nearest Fe^{3+} atom. The observation that the met R2 in the crystal can be reactivated by reduction of the ferric ions in the presence of O_2 suggest that the crystal structure of R2 is similar to native R2. It is, however, important to note that the crystals of R2 were obtained in the presence of ethyl mercuric thiosalicylate at pH 6.0. Reichard *et al.* have shown an optimal pH range of 7.5 - 8.1 for R2 activity (Reichard *et al.*, 1961), and Atkin *et al.* have reported loss of iron and activity in R2 at pH below 6.5 (Atkin *et al.*, 1973). It is therefore important

Fig. 1.5: Schematic representation of the cofactor site in met R2 (Nordlund *et al.*, 1990; Nordlund & Eklund, 1993).



to establish whether the crystal structure reflects the physiologically relevant form of R2.

Reduced (or Diferrous) R2

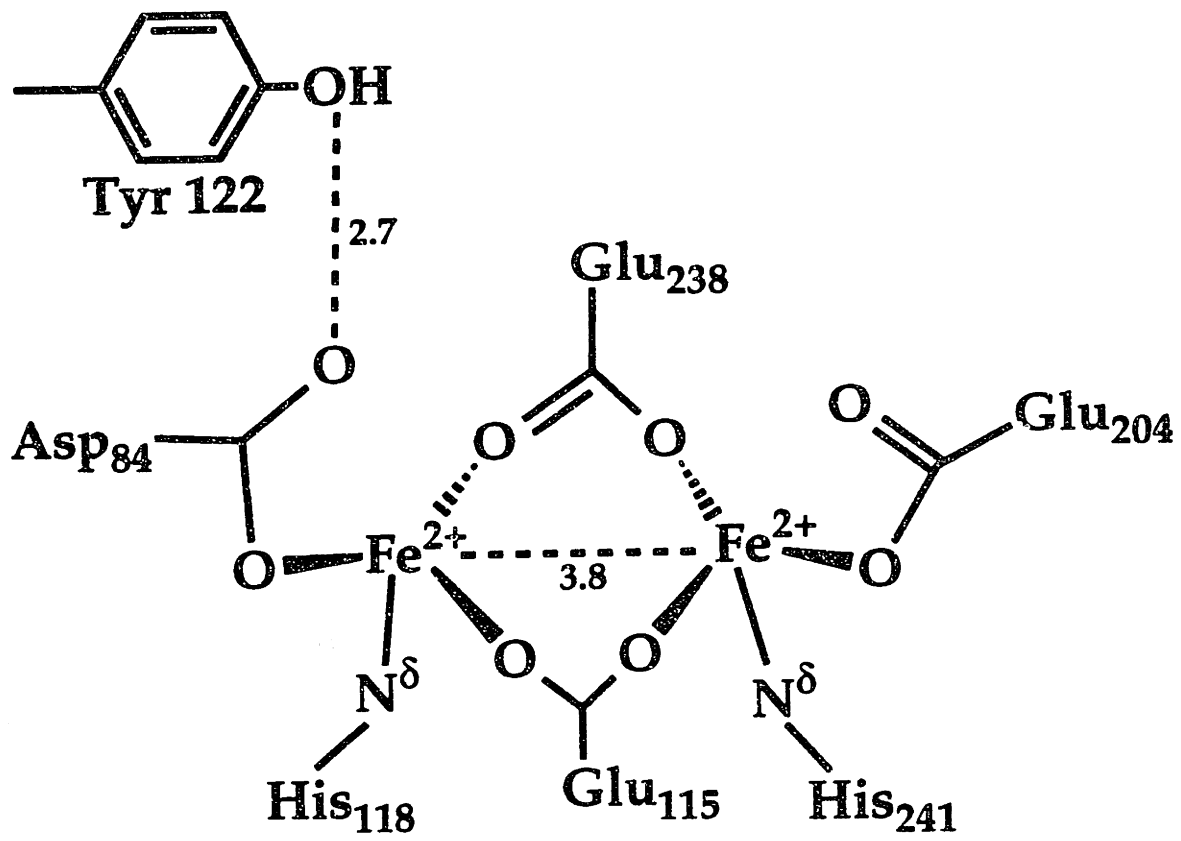
The three-electron reduction of the native form of R2 yields the O₂-sensitive diferrous form of the protein, which is characterized by a normal non-radical Y122 residue and a dinuclear ferrous cluster (Fig. 1.6). At present, the ligand environment of the fully reduced R2 is not fully understood. In contrast with the native R2, only a limited number of spectroscopic studies have been directed toward defining the geometric and electronic structure of the diferrous cluster. Several studies have shown that the strong antiferromagnetic coupling of the diferric cluster (Pettersson *et al.*, 1980; Sahlin *et al.*, 1989; Atta *et al.*, 1992b) is significantly decreased upon reduction, but there is some disagreement on the nature of the metal-metal interaction and the coordination environment of diferrous R2. From their NMR studies, Sahlin and coworkers concluded that the two ferrous ions in reduced R2 are weakly antiferromagnetically coupled (Sahlin *et al.*, 1989). Temperature dependence of a 57-ppm resonance, which was assigned to imidazole N-H protons of the coordinated histidines, suggested a J of -10 cm^{-1} ($H = -JS_1S_2$). A multi-field saturation magnetization study of reduced R2 also suggest that the diferrous cluster is very weakly coupled, with a $J = 0.6 \text{ cm}^{-1}$ (Atta *et al.*, 1992b). Recognizing that the exchange interaction ($J = 0.6 \text{ cm}^{-1}$) in reduced R2 is much smaller than that in reduced hemerythrin ($J = 12 - 38 \text{ cm}^{-1}$) which has a hydroxo bridge, it was suggested that the ferrous ions are bridged by carboxylate group only (Reem & Solomon, 1987; Atta *et al.*, 1992b).

Preliminary crystallographic data on the reduced iron cluster have been reported (Nordlund *et al.*, 1995). Structural studies of the diferrous R2 complex were initially carried out on a mutant protein, R2-S211A (Aberg, 1993). The diferrous

form of the protein was obtained by reduction of met R2-S211A by dithionite in the presence of a mediator phenosafranin. The structure of reduced R2-S211A has been determined to 2.5 Å and refined to an R-value of 18 %. Interpretation of the x-ray data, however, was complicated by the observation that one of the R2 monomers in the resolved structure resembles the met R2 structure, while the other monomer resembles the Mn(II)-R2 structure (as discussed below), suggesting that there might be a mixture of reduced R2 and met R2 in the crystals. Nevertheless, these data may provide some interesting information on the reduced form of the protein. Except for some considerable movements in the carboxylate ligands, the overall structure of reduced R2-S211A is similar to those of apo R2-wt and met R2-wt. The Fe²⁺ ions in the diferrous cluster are 3.8 Å apart and are bridged by E115. In contrast to the diferric cluster, no oxo-bridge is present. Instead, in the reduced form, E238 changes from a monodentate ligand in the diferric cluster into a bridging ligand between the two ferrous ions. Another carboxylate ligand, D84, also undergoes a considerable carboxylate shift, changing from bidentate to monodentate coordination of one of the Fe²⁺ ions. As in the met R2 structure, each ferrous ion is also coordinated to one histidine ligand (H118 and H241). Another significant difference between the diferrous R2 and the met R2 structures is that the two water ligands in the met R2 structure are absent in the reduced protein (Nordlund *et al.*, 1995). The overall effect is two essentially equivalent, four-coordinate, carboxylate-bridged ferrous ions. These x-ray crystallographic data are, however, inconsistent with expectations based on the Mössbauer (Lynch *et al.*, 1989) and CD (McCormick *et al.*, 1991) studies which suggest that the two ferrous ions are in different coordination environments.

Small molecule binding interactions with reduced R2 have been studied by several groups with the expectation that these experiments may reflect O₂ interaction with the diiron site (Elgren *et al.*, 1993; Pulver *et al.*, 1995). Integer spin EPR studies on reduced R2 by Elgren and coworkers revealed the presence of a low-

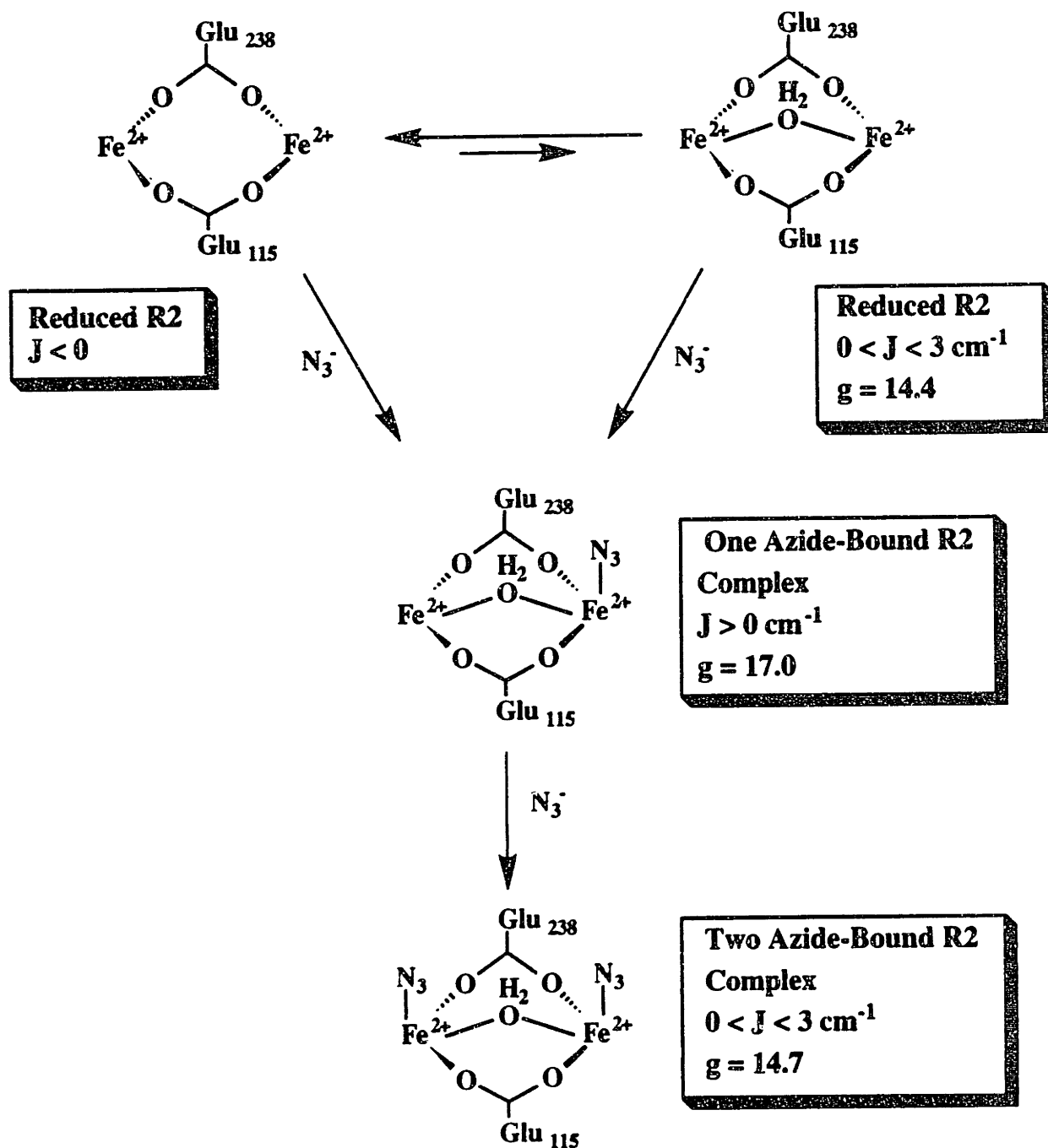
Fig. 1.6: Schematic representation of the cofactor site in diferrous R2 (Aberg, 1993; Nordlund *et al.*, 1995).



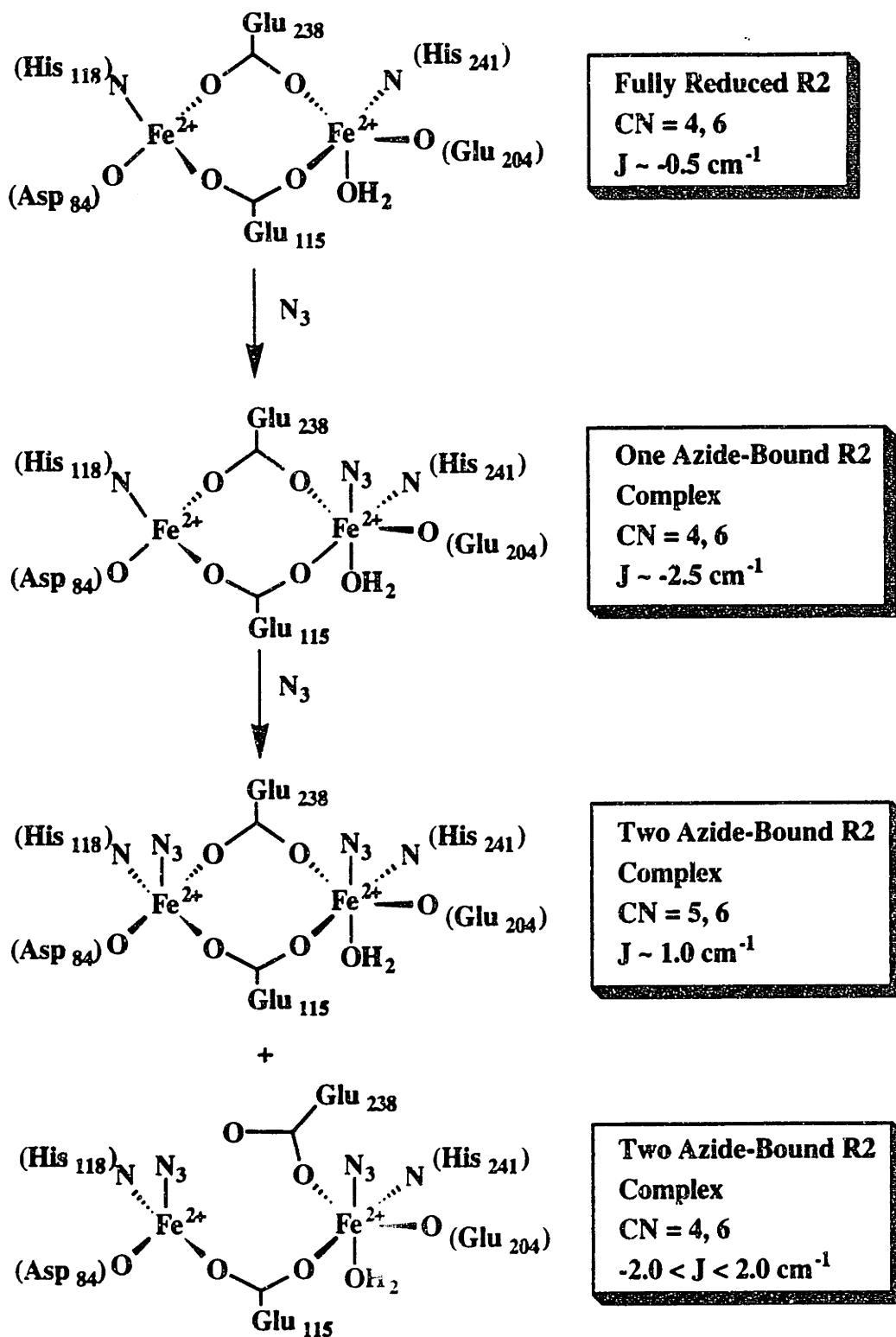
field EPR signal at $g = 14.4$ (Elgren *et al.*, 1993). Interpreting the signal position and the temperature-dependence of this signal, these researchers proposed that it arises from a ground state and that it originates from a small fraction ($\sim 10\%$) of diferrous R2 with a ferromagnetically coupled diiron site. Anaerobic addition of 40-70 mM NaN_3 to reduced R2 elicited a new and more intense EPR signal at $g = 17.0$, suggesting azide binding to the diferrous cluster. Increasing the concentration of azide to 500 mM resulted in a shift of the signal to $g = 14.7$. A model for azide-binding was proposed to account for these observations (Scheme 1.7). In this interpretation, an aqua bridge in a small fraction of reduced R2 was proposed to account for the $g = 14.4$ signal and the observed small, ferromagnetic coupling ($0 < J < 3 \text{ cm}^{-1}$). The binding of one azide converts most of the diiron clusters to ferromagnetically coupled sites with a $g = 17.0$ resonance. The signal shift from $g = 17.0$ at low azide concentration to $g = 14.7$ at high azide concentrations was interpreted as indication of binding of a second azide ion. Taken together, these results suggested the presence of a μ -aqua bridge and open coordination site(s) in the diferrous cluster (Elgren *et al.*, 1993).

More recently, Pulver *et al.* obtained somewhat different results using a combination of circular dichroism (CD) and magnetic circular dichroism (MCD) spectroscopies (Pulver *et al.*, 1995). The results of these studies indicated that the fully reduced R2 iron cluster is best described with one five- and one four-coordinate Fe^{2+} ions that are weakly antiferromagnetically coupled with a J of $\sim -0.5 \text{ cm}^{-1}$ (Scheme 1.8). Azide-binding experiments provided further support for this hypothesis. The data suggested that the one azide-bound R2 complex consists of one four- and one six-coordinate $\text{Fe}(\text{II})$ ions that are antiferromagnetically coupled with a J of $\sim -2.5 \text{ cm}^{-1}$. Increasing the azide concentration resulted in formation of two distinct two-azide-bound complexes. One of these complexes consists of one five-

Scheme 1.7: Schematic representation of the R2 diferrous cluster and its interaction with azide proposed by Elgren *et al.* (Elgren *et al.*, 1993).



Scheme 1.8: Schematic representation of the R2 diferrous cluster and its interaction with azide proposed by Pulver *et al.* (Pulver *et al.*, 1995).



and one six-coordinate Fe^{2+} ions that are ferromagnetically coupled with a J of $\sim 1.0 \text{ cm}^{-1}$. The second complex is weakly coupled, $-2.0 < J < 2.0 \text{ cm}^{-1}$, and consists of one four- and one six-coordinate Fe^{2+} ions. A model for the diferrous cluster based on the CD and MCD results is shown in Scheme 1.8. These results also suggested that there are open coordination sites in diferrous R2 for binding of small molecules like O_2 , and azide. The results of Pulver *et al.*, however, argued against the presence of a μ -aqua bridge in the azide-bound R2 complex as suggested by Elgren *et al.* (Elgren *et al.*, 1993). If the model proposed by Elgren *et al.* is correct, it might imply an increase in coordination number for the diferrous cluster (Scheme 1.7). The CD and MCD data suggested that binding of one azide results in relatively minor changes in the iron cluster (Pulver *et al.*, 1995). The data are consistent with a simple scenario in which the first azide binds to an open coordination position on the five-coordinate iron in diferrous R2, resulting in hexacoordination, while the second Fe^{2+} remains four-coordinate (Scheme 1.8)

Despite some apparent discrepancy, the results of both of these studies suggest that there is an open coordination position on each ferrous ion in the reduced form of R2 and suggest the possibility of a O_2 molecule bridging the two iron atoms (Elgren *et al.*, 1993; Pulver *et al.*, 1995). However, caution has to be taken in interpreting these results, as extremely high concentrations of azide were required for these experiments. Nevertheless, it might be relevant to consider the possibility of a hydroxyl or aqua-bridge in the diferrous R2-azide complex. As will be discussed later, the very recent ENDOR study of X suggests that this intermediate may contain a oxo- or hydroxyl-bridge derived from solvent. It is tempting to speculate that a hydroxyl or aqua- bridge also exists in the diferrous R2- O_2 complex.

R2 with Divalent Metal ions Other than Fe²⁺

Until recent report of the reduced R2 structure (Aberg, 1993; Nordlund *et al.*, 1995), the Mn²⁺-substituted R2 (Mn(II)-R2) has been used as a structural model for the reduced form of R2. EPR and x-ray diffraction data indicate that Mn(II)-R2 contains two dinuclear manganese clusters at the cofactor sites (Fig. 1.7) (Atta *et al.*, 1992a). The coordination environment of the dimanganese site differs markedly from that of the diferric cluster in the met R2 structure (Nordlund & Eklund, 1993). Residue E238, which is monodentate in met R2, bridges the two metal ions in Mn(II)-R2 (Atta *et al.*, 1992a). The bidentate mode of D84 in the diferric structure changes to monodentate in the Mn(II)-R2 form. These carboxylate shifts are very similar to those observed in the reduced R2 structure. As with reduced R2-S211A, the dimanganese cluster is bridged by two carboxylate (E115 and E238) and contains no O²⁻, OH⁻ or aqua bridge. EPR studies of the Mn(II)-R2 indicates that the coupling between the two Mn²⁺ ions is very weak, and is consistent with the presence of only carboxylate bridges between the two ions. Unlike the O₂-sensitive diferrous R2, Mn(II)-R2 is very stable in the divalent state.

A Co(II)-substituted of R2 has also been prepared by anaerobic addition of 4 equivalents of Co(II) to apo R2 (Elgren *et al.*, 1994). The absorption, CD and EPR spectra of this Co(II)-R2 indicates that the Co²⁺ ions are in a five-coordinate environment consisting of N or O ligands, and that the Co²⁺ ions are not magnetically coupled. Unlike the very O₂-sensitive diferrous R2 protein, the Co(II)-R2 complex ~~does~~ not readily bind or reduce O₂.

Apo R2

Iron-free R2, or apo R2, can be obtained by treating native protein with strong chelators under slightly denaturing conditions (Atkin *et al.*, 1973). Early studies showed that mixing apo R2 with Fe²⁺ and O₂ results in formation of the native

cofactor. Because the ligand residues are highly hydrophilic, removal of iron from R2 might be expected to lead to a conformational change to expose the ligand residues to the solvent and to allow entrance of ferrous ions. It is thus somewhat surprising that, during its purification apo R2 shows stability and chromatographic characteristics very similar to that of the native R2, suggesting that apo R2 can fold into a stable protein which resembles native R2. X-ray diffraction data of the apo form of R2 indicates that the overall structure of apo R2 is very similar to the met R2 structure (Aberg, 1993; Aberg *et al.*, 1993). The only significant differences occur at the metal binding sites. All carboxylate ligand residues in the metal-binding site change their conformation and fill the vacancies created by the removal of the iron ions (Fig. 1.8). The net effect of this is an unusual clustering of four carboxylate side chains in the interior of the R2 subunit. It was proposed that the charges of the four carboxylate ligand residues are partly compensated for by protonation of the two nearby histidine residues (H118 and H241) and protonation of two of the carboxyl groups. Nordlund reasoned that the folded state is stabilized by extensive van der Waals interactions and hydrogen bonds between the unusually long helices of R2. Hydrogen-bonding to polar side chains in the vicinity also helps to reduce the effect of the energetically unfavorable clustering of internal carboxyl residues.

Intermediate Iron Cluster X

Previous studies by Bollinger *et al.* on the cofactor assembly reaction revealed a $S = 1/2$ species, **X**, that is kinetically competent to oxidize Y122 (Ravi *et al.*, 1994; Bollinger *et al.*, 1991a; Bollinger *et al.*, 1991b). Interpretation of the EPR and Mössbauer data led to the proposal that **X** is a spin coupled system involving two high-spin ferric ions and a free radical (Ravi *et al.*, 1994; Ravi & Bominaar, 1995). The initial analysis of the Mössbauer data, which assumed isotropic magnetic hyperfine coupling tensors, yielded isomer shifts of 0.55 and 0.36

Fig. 1.7: Schematic representation of the cofactor site in dimanganese(II) R2 (Atta *et al.*, 1992).

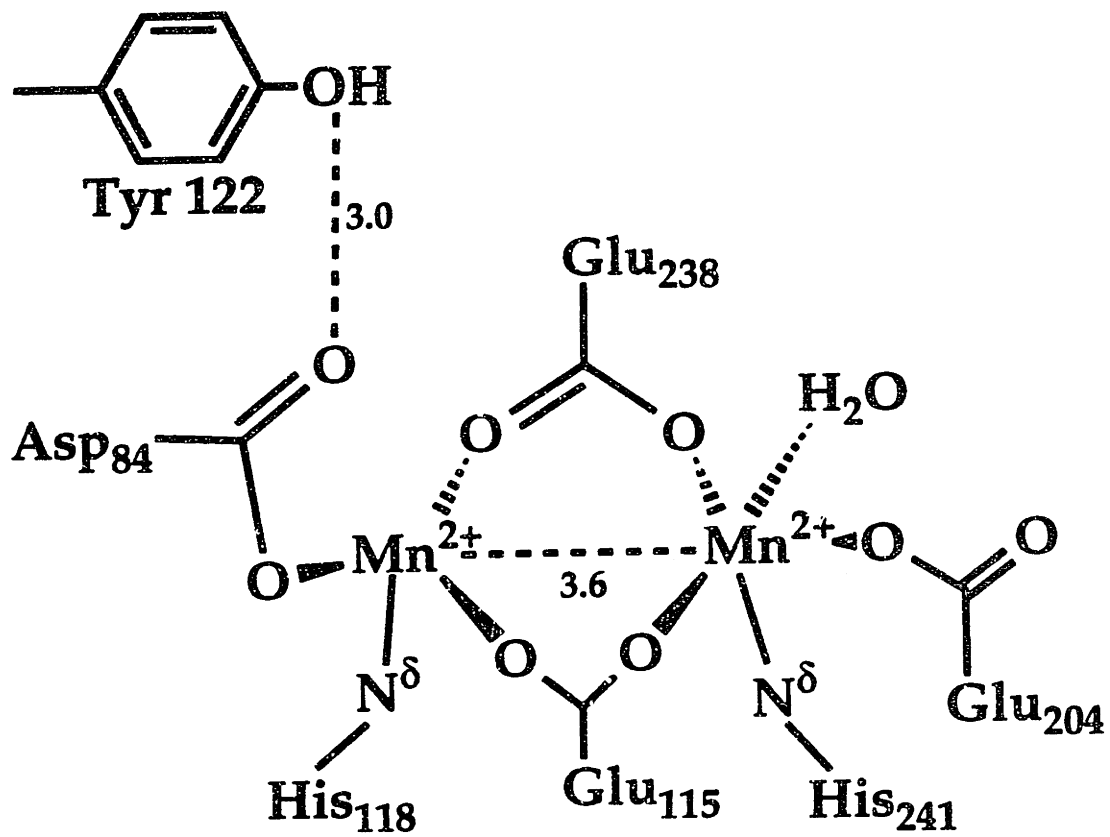
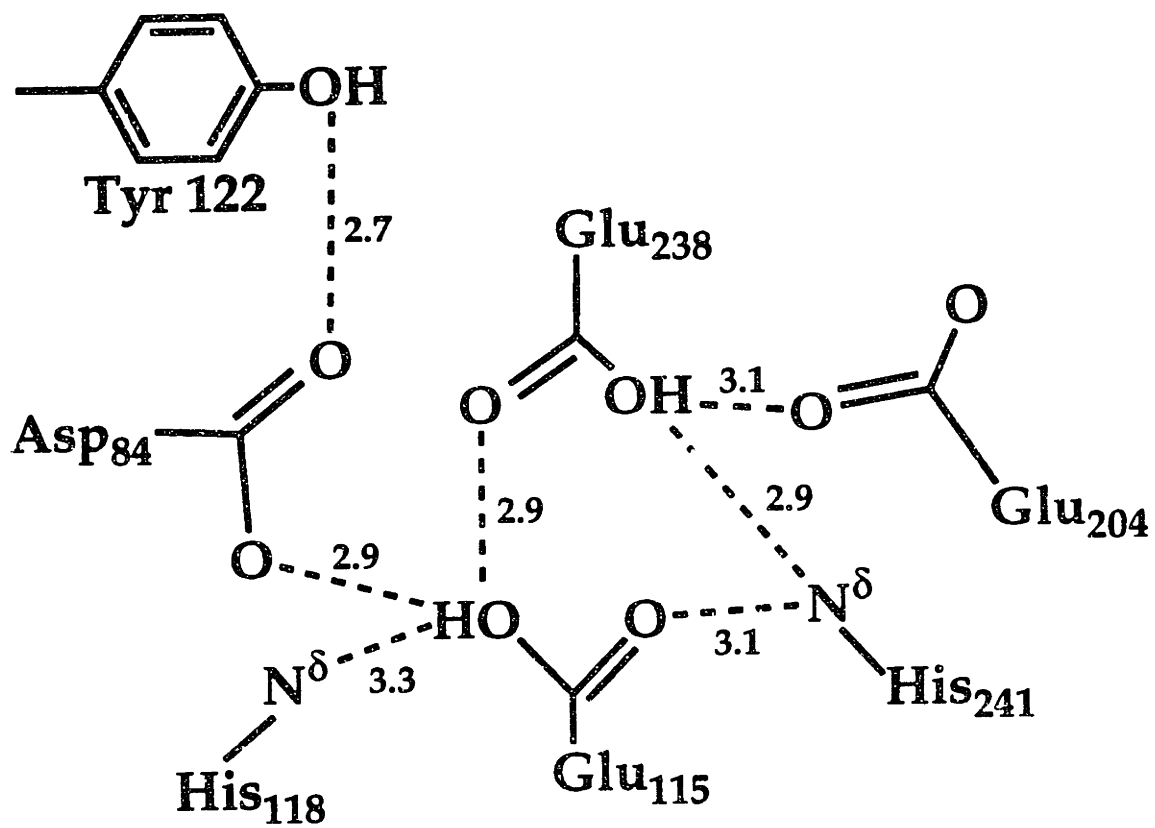


Fig. 1.8: Proposed hydrogen-bonding network in the cofactor site in apo R2 (Aberg, 1993).



mm s⁻¹ for iron site 1 and 2 respectively. These isomer shifts and the quadrupole splittings of ~ 1 mm/s are consistent with high-spin ferric ions. By using a three-spin coupling model ($S_1 = 5/2$ and $S_2 = 5/2$ for the two iron sites, and $S_3 = 1/2$ for the radical), both the signs and the magnitudes of the observed A values for the iron sites could be explained.

Recently, successful adaptation of the rapid freeze-quench methodology to Q-band ENDOR study have allowed further characterization of the intermediate X (Burdi *et al.*, 1996). The Q-band EPR spectrum of X at Q-band (35 GHz) showed resolved g -anisotropy with $g_1 \sim 2.007$, $g_2 \sim 1.999$, and $g_3 \sim 1.994$. When X was prepared with ¹⁷O₂ (32 % enriched), two new signals appeared, suggesting that both atoms of O₂ are present in X. ENDOR spectra collected across the whole EPR envelop indicated one strongly-coupled oxygen atom ($A(^{17}\text{O}) = [26, 26, 31]$ MHz), and one weakly-coupled oxygen atom ($A(^{17}\text{O}) \sim 4$ MHz). When X was prepared with H₂¹⁷O (32 % enriched), a signal from a single strongly-coupled ¹⁷O was observed, with $A(^{17}\text{O})$ very similar to those of the strongly-coupled ¹⁷O species derived from molecular oxygen (Burdi *et al.*, 1996). One possible interpretation is that H₂¹⁷O exchanged into a site that is initially derived from C₂. However, previous resonance Raman study on the cofactor assembly of R2-Y122F suggested that the oxo-bridge of the diferric cluster is derived from O₂ (Ling *et al.*, 1994), and that solvent exchange of the μ -oxo bridge in native or met R2 is relatively slow ($t_{1/2} \sim 15$ min at 5 °C) (Sjöberg *et al.*, 1982). At present, these data have been interpreted as an indication of **three** exogenous O atoms associated with X: two derived from O₂, one derived from solvent. Furthermore, the ¹H data show strongly-coupled, anisotropic, exchangeable proton(s) associated with one or more of these sites, suggesting the possibility of bridging or terminal hydroxide ligands in X.

In addition, ⁵⁷Fe ENDOR spectroscopy has also been extended to the characterization of the intermediate X (Sturgeon *et al.*, 1996). These results showed

that iron site 1 has a very nearly isotropic hyperfine tensor ($A/g_n\beta_n(\text{site 1}) = -[53.0, 51.6, 52.3]\text{T}$), while iron site 2 shows considerable degree of anisotropy ($A/g_n\beta_n(\text{site 2}) = +[19.6, 26.3, 26.3]\text{T}$). Using the more precise hyperfine tensors determined by ENDOR spectroscopy, the Mössbauer spectrum of X were reanalyzed. These analysis indicated that, while the isomer shift of iron site 1 (0.56 mm/s) remains unchanged, the isomer shift of iron site 2 is reduced to 0.26 mm/s. The observation of the lower isomer shift and substantial magnetic hyperfine anisotropy for iron site 2 suggested the possibility that X contains Fe(IV). On the other hand, while the value of 0.26 mm/s is significantly smaller than the 0.36 mm/s reported previously for iron site 2, this value is notably different from the reported isomer shifts for ferryl (Fe(IV)) ions (Schulz *et al.*, 1984; Leising *et al.*, 1991). Presently, two models for X are being considered (Fig. 1.9). In the first case, X might be discussed in terms of the model proposed previously by Ravi *et al.*, which involves a diferric center coupled to an O radical (Ravi *et al.*, 1994). The exiting data are also consistent with an oxo- or hydroxo-bridged Fe^{3+} ($S = 5/2$) - Fe^{4+} ($S = 2$) center, with considerable delocalization of unpaired spin density onto a O ligand(s). Fig. 1.9 shows two configurations of X which are consistent with the available data. Addition experiments are required to distinguish between these possibilities and to provide a more definitive description of X. Selected biophysical data on X are listed in Table 1.2.

Structural Considerations for the Cofactor Assembly

Although there are conflicting results from the different studies of the reduced form of R2, some general features about the cofactor assembly process can be made through the comparison of the existing structural and biophysical data on apo R2, reduced R2, X, and native R2. One of the most notable differences between these structures are found in the carboxylate ligand residues, suggesting that the

Fig. 1.9: Schematic representation of the possible structures of **X** based on recent Mössbauer and Q-band ENDOR studies (Burdi *et al.*, 1996; Sturgeon *et al.*, 1996)

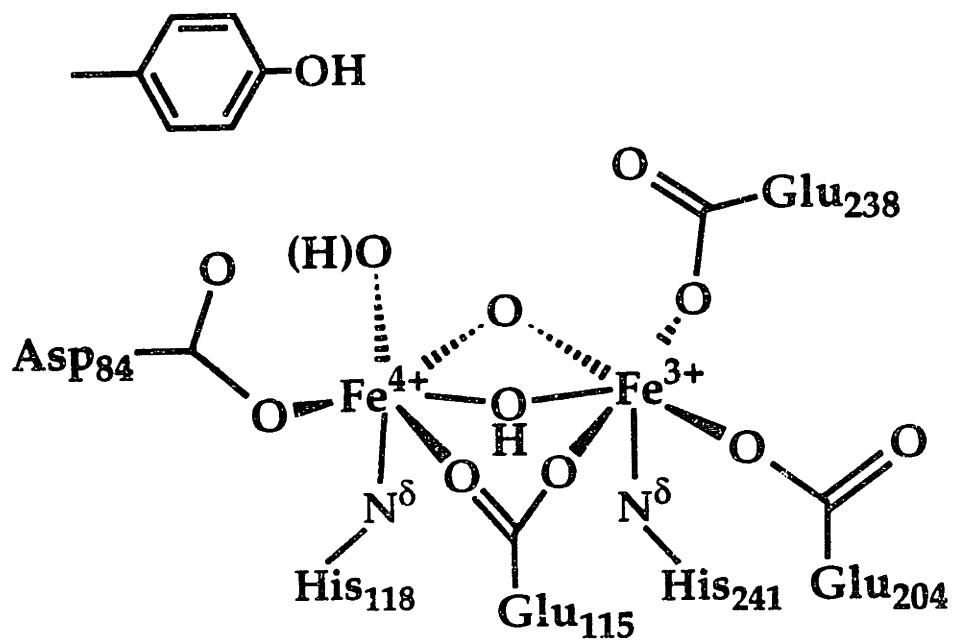
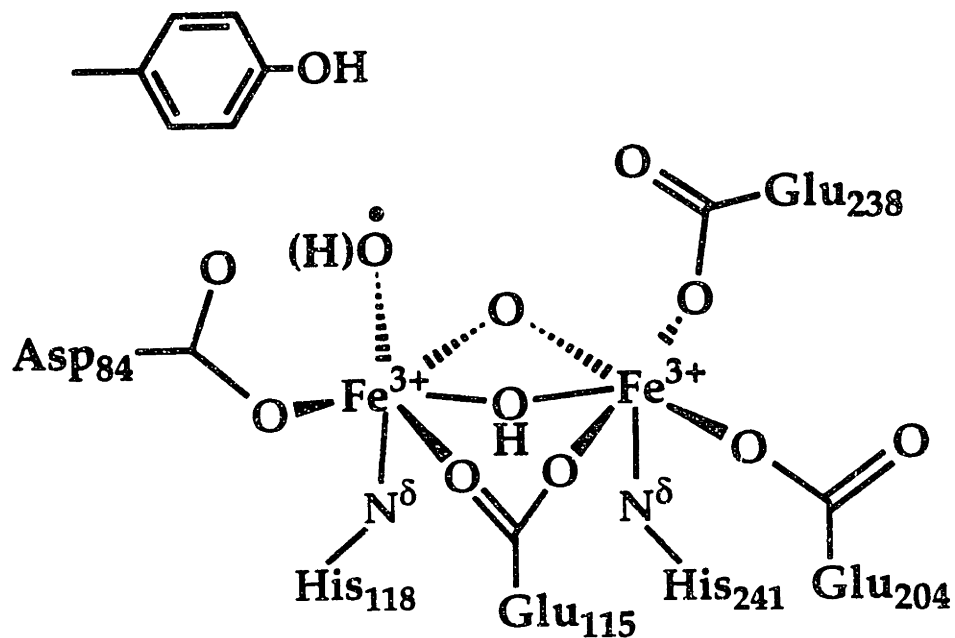


Table 1.2: Summary of selected physical properties of the intermediate X.

		X
Optical	λ_{\max} , nm	365
Mössbauer		
site 1	δ , mm/s	0.56 ± 0.03
	ΔE_Q , mm/s	-0.9 ± 0.1
	η	0.5 ± 0.2
site 2	δ , mm/s	0.26 ± 0.04
	ΔE_Q , mm/s	-0.6 ± 0.1
	η	2.7 ± 0.3
EPR	g_{11}	2.007
	g_{22}	1.999
	g_{33}	1.994
	g_{avg}	2.000
Q-band ENDOR		
site 1	$A_1/g_n\beta_n$ (T)	-53.0 ± 0.1
	$A_2/g_n\beta_n$ (T)	-51.6 ± 0.1
	$A_3/g_n\beta_n$ (T)	-52.3 ± 0.1
site 2	$A_1/g_n\beta_n$ (T)	$+19.6 \pm 0.1$
	$A_2/g_n\beta_n$ (T)	$+26.3 \pm 0.1$
	$A_3/g_n\beta_n$ (T)	$+26.3 \pm 0.1$

reconstitution process must be accompanied by considerable carboxylate ligand shifts. Binding of Fe^{2+} to apo R2 is achieved by conformational changes in all the carboxylate ligand residues in the apo R2 form (Fig. 1.8) to achieve the di-carboxylate-bridged diferrous R2 structure (Fig. 1.6). Comparison of the apo R2, reduced R2, and met R2 shows that the structure of reduced R2 shows an expansion of the carboxylate cluster in the cofactor site (Aberg, 1993). This is also accompanied by a considerable movement of a Y209 residue (Aberg, 1993). X-ray diffraction data of

reduced R2 indicates that the hydroxyl group of Y209 moves by 2 Å. The net effect of these conformational changes is to open up a channel from the protein surface to the cofactor-binding site in the reduced R2 structure which is absent in the apo R2 and met R2 structure (Aberg, 1993; Nordlund & Eklund, 1993). This might be of relevance since this channel may represent the pathway by which Fe^{2+} and O_2 enter the cofactor-binding site. These observations also provide a structural basis for the proposal by Bollinger *et al.* that a conformational change occurs in the formation of diferrous R2 (Bollinger *et al.*, 1994a).

As shown in Chapter 2, reaction of diferrous R2 with O_2 results in formation of the intermediate X. Very recent ENDOR studies suggested that this intermediate may contain two oxo- or hydroxyl-bridges: one derived from O_2 and the second one from solvent (Burdi *et al.*, 1996). Steric consideration suggests that at least one of the carboxylate bridge in the diferrous form changes to monodentate coordination in X. Considering that the ions in both the diferrous and the diferric cluster are bridged by E115, it is possible that the metal ions in X are also bridged by this carboxylate ligand. If this interpretation is correct, it would imply that the bridging ligand E258 in diferrous R2 changes from a bridging position in diferrous R2 to monodentate coordination during the conversion to the intermediate X. Finally, conversion of X to diferric cluster might be accompanied by carboxylate shift of D84 from monodentate to bidentate, and conversion of a bridging oxo- or hydroxyl bridge to monodentate at one of the ferric ions in the diferric cluster. A schematic representation of the nuclear reorganizations that might be involved in the reconstitution process is presented in Scheme 1.9.

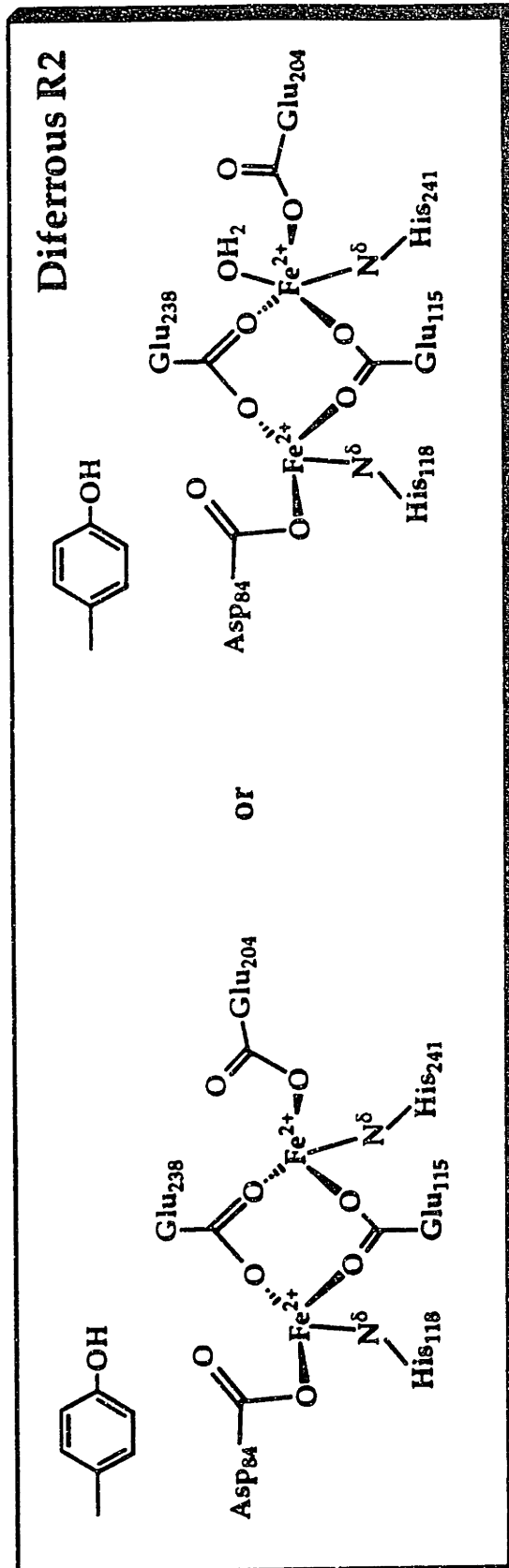
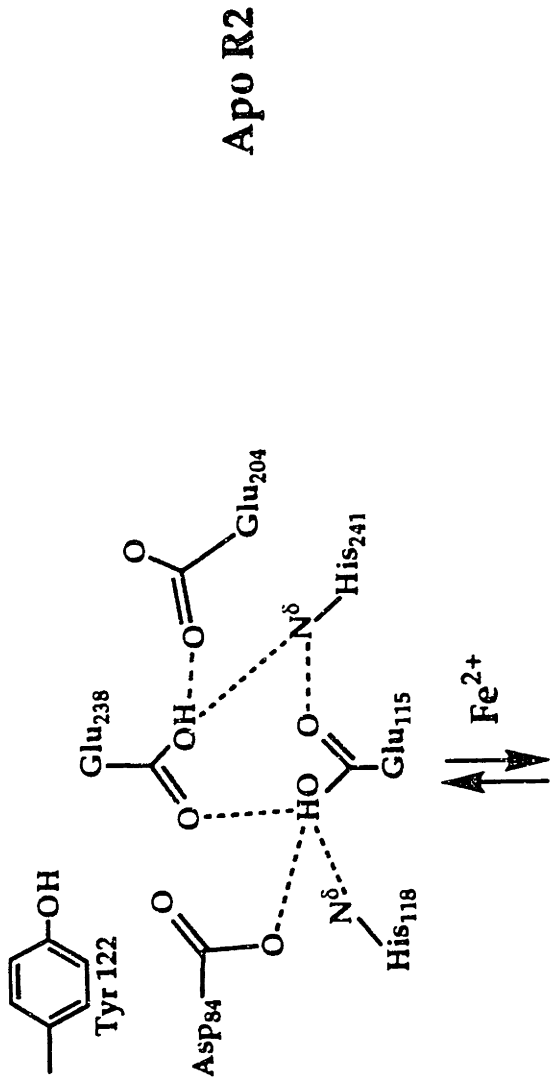
In addition to ligand movements, the structural information as well as chemical considerations also point to the involvement of proton transfers in the cofactor assembly process. Aberg *et al.*, proposed that the cofactor is neutral in the three structurally determined R2 proteins (Aberg, 1993; Aberg *et al.*, 1993). In apo R2,

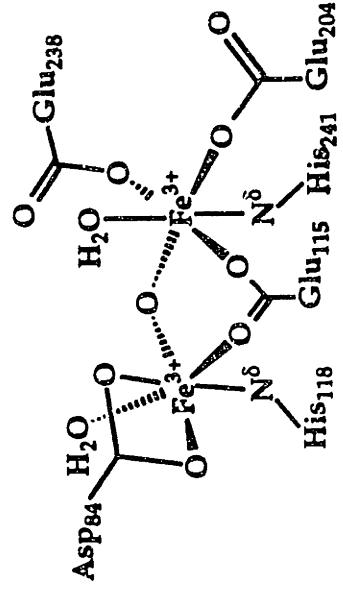
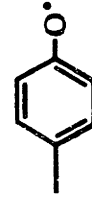
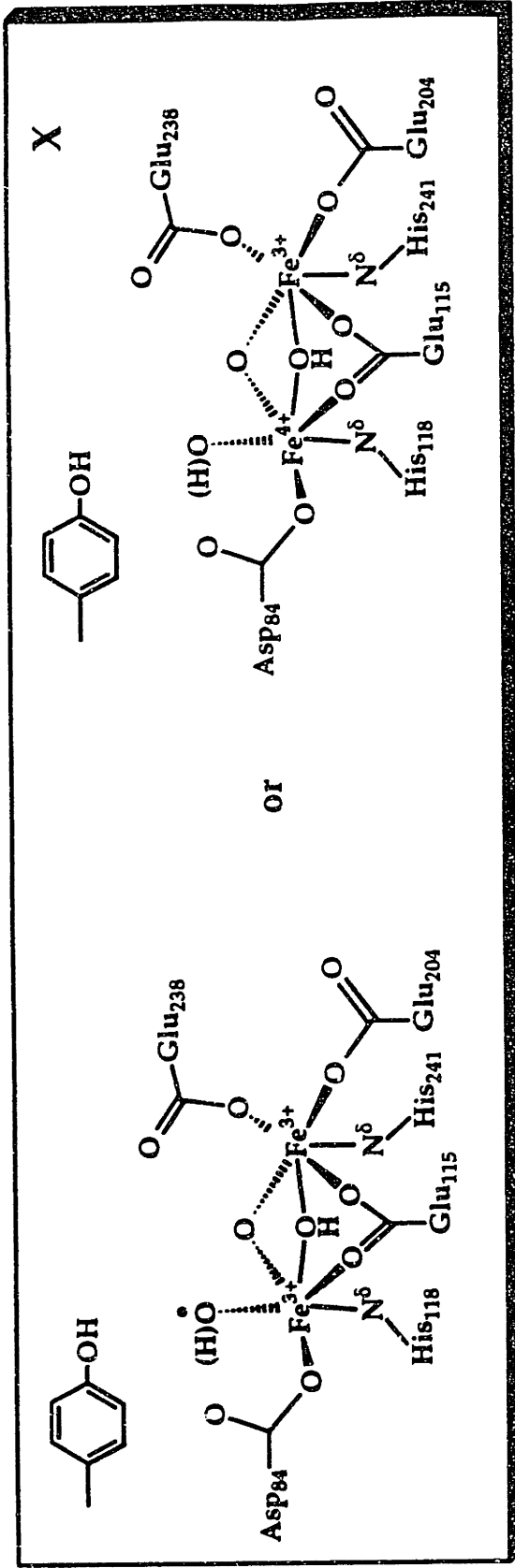
this is achieved by protonation of the two histidines and two of the carboxylate groups (Aberg, 1993; Aberg *et al.*, 1993). Binding of two Fe^{2+} ions to apo R2 is accompanied by release of four protons in cofactor binding site. In the reduced R2, the four positive charges from the two Fe^{2+} ions are neutralized by the four negatively-charged carboxylate ligands (Aberg, 1993). Subsequent oxidation of the diferrous cluster and the nearby Y122 residue results in native R2. ENDOR (Bender *et al.*, 1989) and resonance Raman (Backes *et al.*, 1989) studies on R2 indicate that $\bullet\text{Y122}$ is a neutral radical. During cofactor assembly, deprotonation of Y122 must occur. These hypotheses further underscore the likely functional importance of proton transfer in the cofactor assembly process. That the hydrogen bonding network and the proton transfer process(es) may play important roles in the overall kinetic mechanism is also supported by the results of Chapter 3 which show that multiple steps in the reconstitution reaction are sensitive to deuterium substitution of the solvent-exchangeable protons.

Reactivity of *E. coli* R2 and its Cofactor

In addition to its structure and physical properties, the chemical reactivity of *E. coli* R2 has also been an intensive field of research (Fontecave *et al.*, 1992). Investigations of the redox properties of the diiron center in R2 reveal four accessible oxidation states (Scheme 1.10). As isolated, the enzyme is in the fully oxidized, catalytically active form, with a μ -oxo-diiron(III) cluster adjacent to a tyrosyl radical, $\bullet\text{Y122}$. One-electron reduction of native R2, by radical scavengers such as hydroxyurea, hydroxylamine and reduced flavin, reduces the $\bullet\text{Y122}$ without affecting the diferric cluster to form the inactive met R2 (Brown *et al.*, 1969; Fontecave *et al.*, 1992; Swarts *et al.*, 1995). Reduction of native R2 or met R2 with dithionite in the presence of viologen mediator generates the fully reduced R2, or diferrous R2 (Sahlin *et al.*, 1989). Reduced R2 can also be generated by treatment of

Scheme 1.9: Schematic representation of the possible nuclear reorganizations involved in the R2 reconstitution reaction.

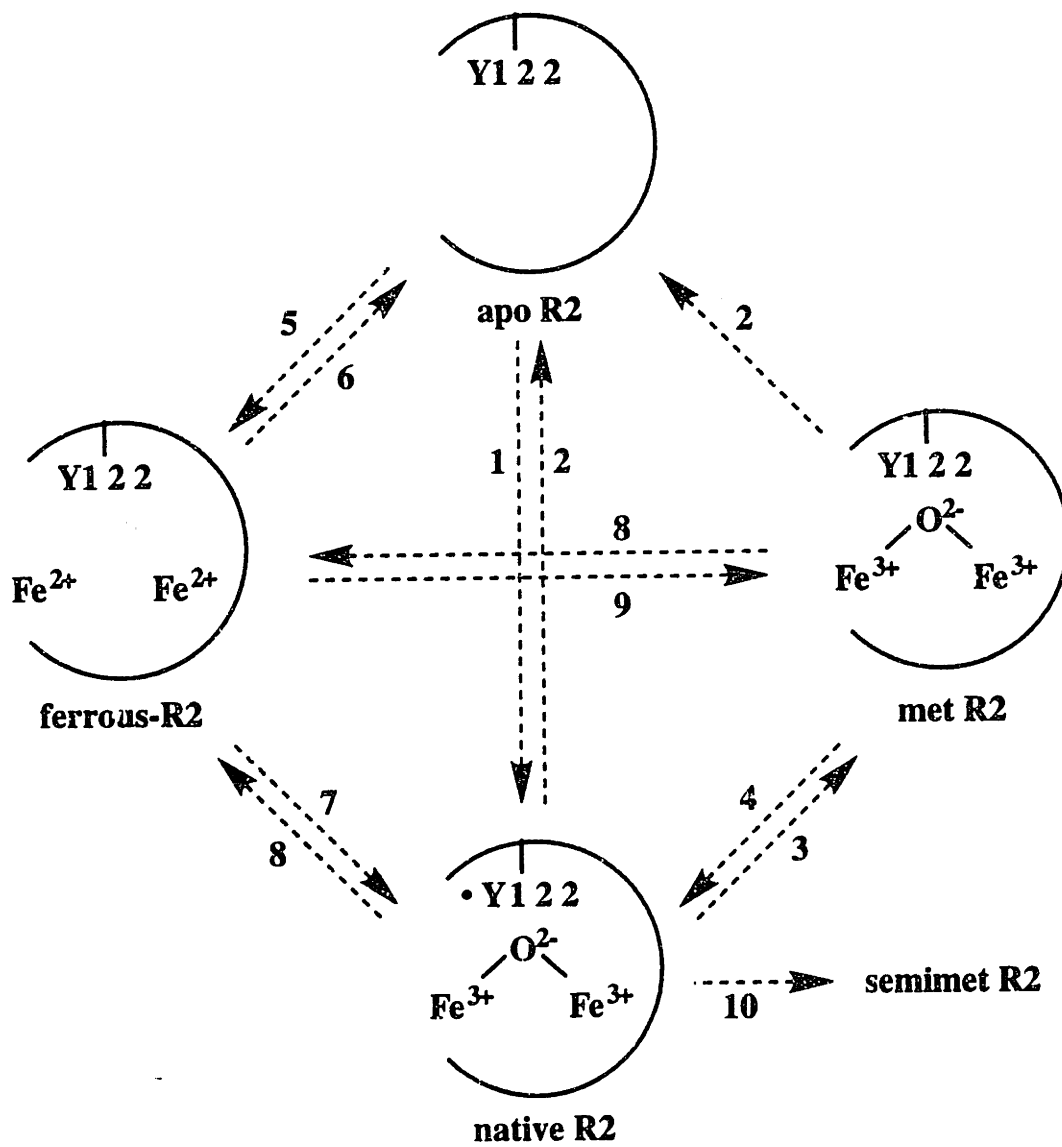




Native R2

Scheme 1.10: Different states of R2 and their interconversions. The broken circle represents only one of the two monomers of apo R2.

1. Fe^{2+} , O_2 (Brown *et al.*, 1969; Atkin *et al.*, 1973)
2. chelator (e.g. 8-hydroxyquinoline-5-sulfonic acid) and mild denaturant (e.g. 1 M imidazole) (Atkin *et al.*, 1973)
3. one-electron donors (e.g. hydroxyurea, hydroxylamine, reduced flavin, phenols) (Brown *et al.*, 1969; Fontecave *et al.*, 1992; Atta *et al.*, 1993)
4. oxo-donors (e.g. H_2O_2 , iodosobenzoate) (Sahlin *et al.*, 1990; Fontecave *et al.*, 1990a)
5. Fe^{2+} (Sahlin *et al.*, 1989)
6. chelator (e.g. 8-hydroxyquinoline-5-sulfonic acid, EDTA) (Atkin *et al.*, 1973; Salowe, 1987)
7. O_2 (Sahlin *et al.*, 1989)
8. anaerobic incubation with dithionite and methyl- or benzylviologen (Sahlin *et al.*, 1989), reduced flavins and Fe^{2+} (Fontecave *et al.*, 1989), DTT at $\text{pH} > 8$ (Fontecave *et al.*, 1990b), or diimide (Gerez *et al.*, 1991)
9. H_2O_2 (Gerez & Fontecave, 1992)
10. chemical reduction by diimide or hydrazine (Gerez *et al.*, 1991; Gerez & Fontecave, 1992), x-ray irradiation followed by annealing (Hendrich *et al.*, 1991), or γ -irradiation followed by annealing (Davydoc *et al.*, 1994)



native R2 with reduced flavins and Fe^{2+} (Fontecave *et al.*, 1989), with DTT at $\text{pH} > 8$ (Fontecave *et al.*, 1990b), or with diimide (Gerez *et al.*, 1991).

Apo R2, which lacks both iron and radical, can be generated by treatment of met R2 or of the native R2 with a ferric ion chelator (e.g. 8-hydroxyquinoline-5-sulfonic acid) in the presence of a mild denaturant (e.g. 1 M imidazole) (Atkin *et al.*, 1973). Treatment of met R2 with H_2O_2 (Sahlin *et al.*, 1990) or with oxygen atom donors such as 2-iodoxobenzoate (Fontecave *et al.*, 1990a) can also regenerate the native protein, although the reaction is extremely slow and the yield of tyrosyl radical from this process is poor. Incubation of the apo R2 with Fe^{2+} gives ferrous R2 (Sahlin *et al.*, 1989), which reacts upon mixing with O_2 to give the native protein.

In addition, a semi-met form, which contains no tyrosyl radical and a mixed-valence (Fe^{2+} , Fe^{3+}) cluster, has been proposed as a possible intermediate in the redox reactions of the iron center in R2 (Elgren *et al.*, 1991). In one study, Gerez *et al.* observed an unstable (Fe^{2+} , Fe^{3+}) antiferromagnetically coupled form of R2 with $S = 1/2$ upon reduction of native R2 by diimide or hydrazine (Gerez *et al.*, 1991; Gerez & Fontecave, 1992). On the other hand, Hendrich *et al.* characterized an (Fe^{2+} , Fe^{3+}) form of R2 by irradiation of a frozen aqueous solution of met R2 with X-rays at 77 K (Hendrich *et al.*, 1991), which contains ferromagnetically coupled iron ions ($S = 9/2$). Very recent EPR studies by Davydov *et al.* suggests that the antiferromagnetically coupled cluster represents a non-equilibrium (Fe^{2+} , Fe^{3+}) cluster with a hydroxo-bridge (Davydov *et al.*, 1994). Upon annealing, this cluster is transformed into a ferromagnetically coupled (Fe^{2+} , Fe^{3+}) form with a hydroxo or aqua bridge. However, whether this mixed-valence cluster is physiologically relevant remains to be established.

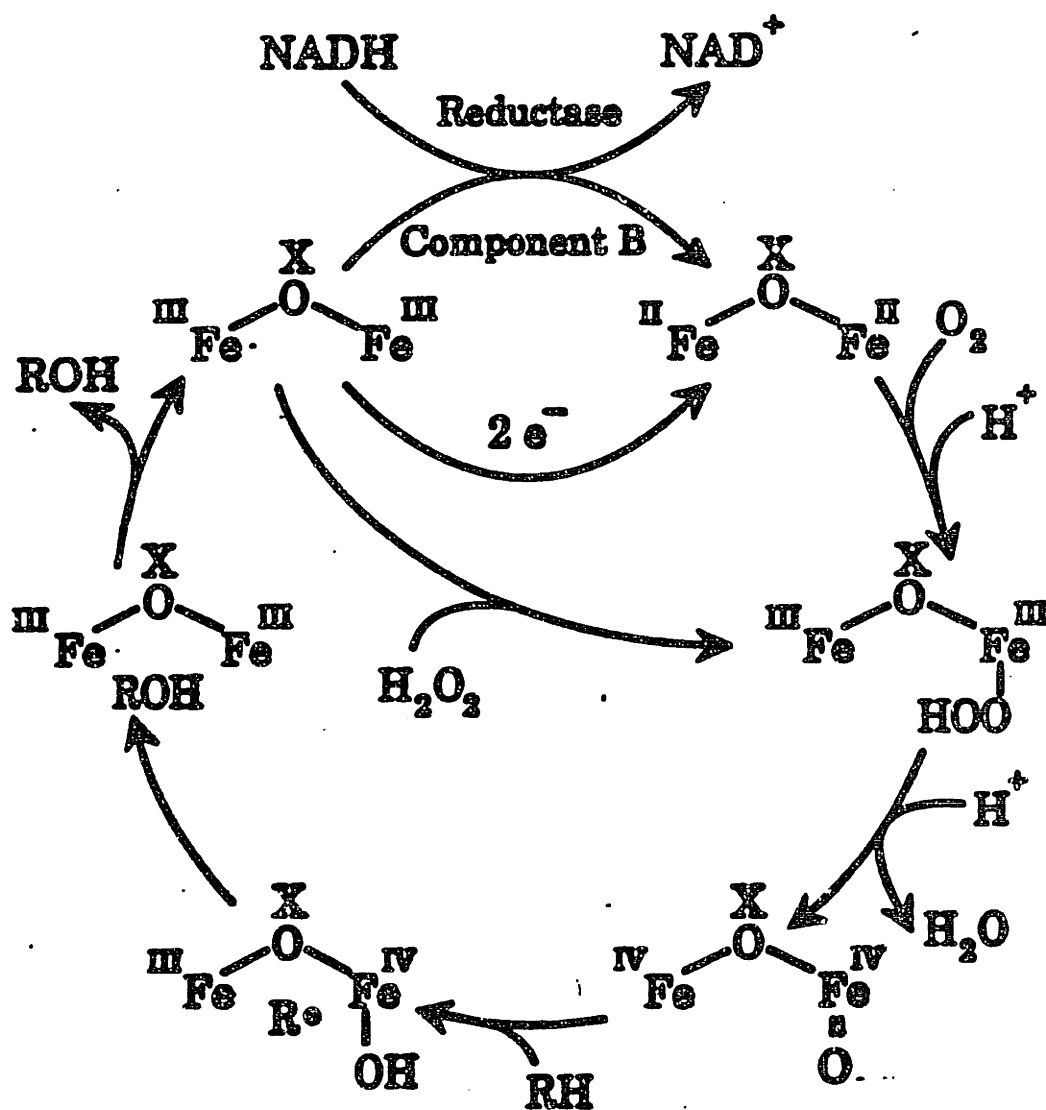
Reaction of Other Diiron(II) Complexes with O₂

Methane Monooxygenase

Methane monooxygenase (MMO) is a multi-component enzymatic system which catalyzes the conversion of methane to methanol (Colby *et al.*, 1979). The hydrolase component (MMOH) of soluble MMO contains two oxygen-bridged dinuclear iron clusters that can be stabilized in three redox states: oxidized (Fe³⁺, Fe³⁺), mixed valent (Fe²⁺, Fe³⁺), and reduced (Fe²⁺, Fe²⁺). It was proposed that the diiron(II) state of MMOH_{red} in the presence of protein B (MMOB) activates O₂ for substrate hydroxylation. The accumulated data of MMO suggest a catalytic mechanism for MMO similar to that of cytochrome P-450 (Scheme 1.11). One of the central features of this mechanism is the proposal of a high valent iron-oxene intermediate species.

Most studies on MMOs have focused on the proteins isolated from *Methylosinus trichosporium* (OB3b) or *Methylcoccus capsulatus* (Bath). The active-site structures and the hydroxylation mechanisms of the MMOs from these two different organisms share many common features, but there are also considerable differences between these proteins, particularly in terms of the optimal temperature at which these proteins function. Recently Lee *et al.* have reported their study of the catalytic cycle of the soluble form of MMOH isolated from *Methylosinus trichosporium* (OB3b) using stopped-flow absorption spectroscopy, chemical-quench and rapid freeze-quench EPR experiments (Lee *et al.*, 1993a; Lee *et al.*, 1993b). Rapid mixing of O₂ with diferrous MMOH in the presence of MMOB resulted in loss of the $g = 16$ EPR signal characteristic of the diferrous cluster at a k_{obs} of $22 \pm 5 \text{ s}^{-1}$. In a subsequent step, a second intermediate, compound Q, accumulates with a k_{obs} of $1 \pm 0.1 \text{ s}^{-1}$ and then decays at $0.05 \pm 0.01 \text{ s}^{-1}$. Mössbauer study revealed a diamagnetic species with $\Delta E_{\text{Q}} = 0.53 \text{ mm/s}$ and $\delta = 0.17 \pm 0.02 \text{ mm/s}$ which led to the assignment of compound Q as a diiron (IV) complex. Furthermore, the observation that the

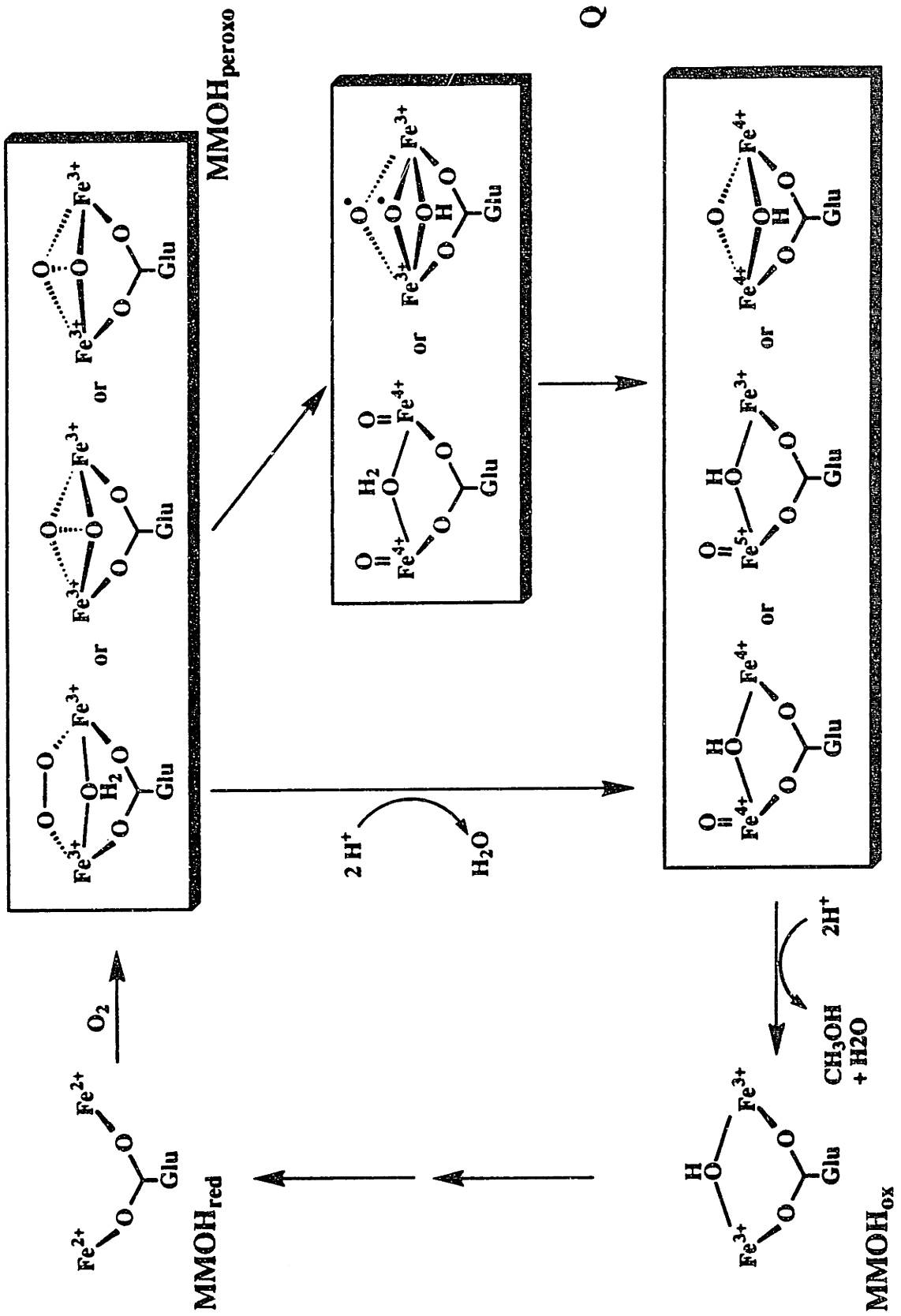
Scheme 1.11: Schematic representation of the mechanism proposed for the hydroxylation reaction catalyzed by MMO based on analogy to P-450 chemistry. For clarity, only the iron center and the hydroxide bridge are shown.



Mössbauer spectra of the two iron sites of Compound Q are indistinguishable suggested that the activated oxygen is bound to the cluster symmetrically. The rate of decay of Q depends on both the concentration and the type of substrate present and agrees with the rate of formation of product, suggesting that compound Q may be the activated form of the enzyme that leads directly to substrate hydroxylation or an immediate precursor.

While these experiments were in progress, Liu and coworkers were studying the reaction of O₂ with the diferrous MMOH from *Methylococcus capsulatus* (Bath) (Liu *et al.*, 1994; Liu *et al.*, 1995a; Liu *et al.*, 1995b). Stopped-flow absorption and rapid freeze-quench Mössbauer spectroscopies provide evidence for two reaction intermediates (Liu *et al.*, 1994). On the basis of chemical considerations, the kinetic data, and a resonance Raman study reporting an oxygen-isotope sensitive band at 905 cm⁻¹, the first intermediate was proposed to be a diiron (III) peroxide complex (MMOH_{peroxo}) (Liu *et al.*, 1994; Liu *et al.*, 1995a). This intermediate exhibits a doublet with $\delta = 0.66$ mm/s and $\Delta E_Q = 1.51$ mm/s (Liu *et al.*, 1994). Kinetic studies revealed that MMOH_{peroxo} formed with a k_{obs} of ~ 25 s⁻¹, a rate which is in good agreement with that (22 s⁻¹) reported for the disappearance of $g = 16$ EPR signal of MMOH_{red} (Liu *et al.*, 1995b). The second intermediate (Q) has kinetic and spectroscopic properties ($\lambda_{max} \sim 350$ and 420 nm) similar to compound Q in *M. trichosporium* OB3b. However, Mössbauer study revealed that the two irons are inequivalent, with $\delta = 0.21$ mm/s and $\Delta E_Q = 0.68$ mm/s for one site and $\delta = 0.14$ mm/s; $\Delta E_Q = 0.55$ mm/s for the other (Liu *et al.*, 1994). On the basis of these kinetic and spectroscopic data, Liu *et al.* proposed a mechanism for the reaction cycle of MMOH from *M. capsulatus* (Bath) shown in Scheme 1.12 . Selected data concerning the diiron center in MMOH are listed in Table 1.3.

Scheme 1.12: Schematic representation of the mechanism proposed by Liu *et al.* for the hydroxylation reaction catalyzed by MMO from *M. capsulatus* (Bath). For clarity, only the iron center and the hydroxide bridge are shown.



Q

Table 1.3: Spectroscopic and kinetic parameters (at 4 °C) for intermediates in the reaction of MMOH_{red} with O₂.

		<i>M. capsulatus</i> (Bath) ^a		<i>M. trichosporium</i> OB3b ^b
		MMOH _{peroxo}	Q	Q
optical	λ_{\max} (nm)	625-650	350	330
			420	430
	k _{form} (s ⁻¹)	22.	0.5	1
	k _{decay} (s ⁻¹)		0.07	0.05
Mössbauer (4K)	site 1:			
	δ (mm/s)	0.66	0.21	0.17
	ΔE_Q (mm/s)	1.51	0.68	0.53
	site 2:			
	δ (mm/s)		0.14	
	ΔE_Q (mm/s)		0.55	
	k _{form} (s ⁻¹)	28	0.4	
k _{decay} (s ⁻¹)	0.4	0.03		
Raman	ν_{O-O} (cm ⁻¹)	905		

^a data from Liu et al. (1995b)

^b data from Lee et al. (1993)

A Synthetic S = 1/2 complex with Localized High-Spin Fe(IV) and Fe(III) sites

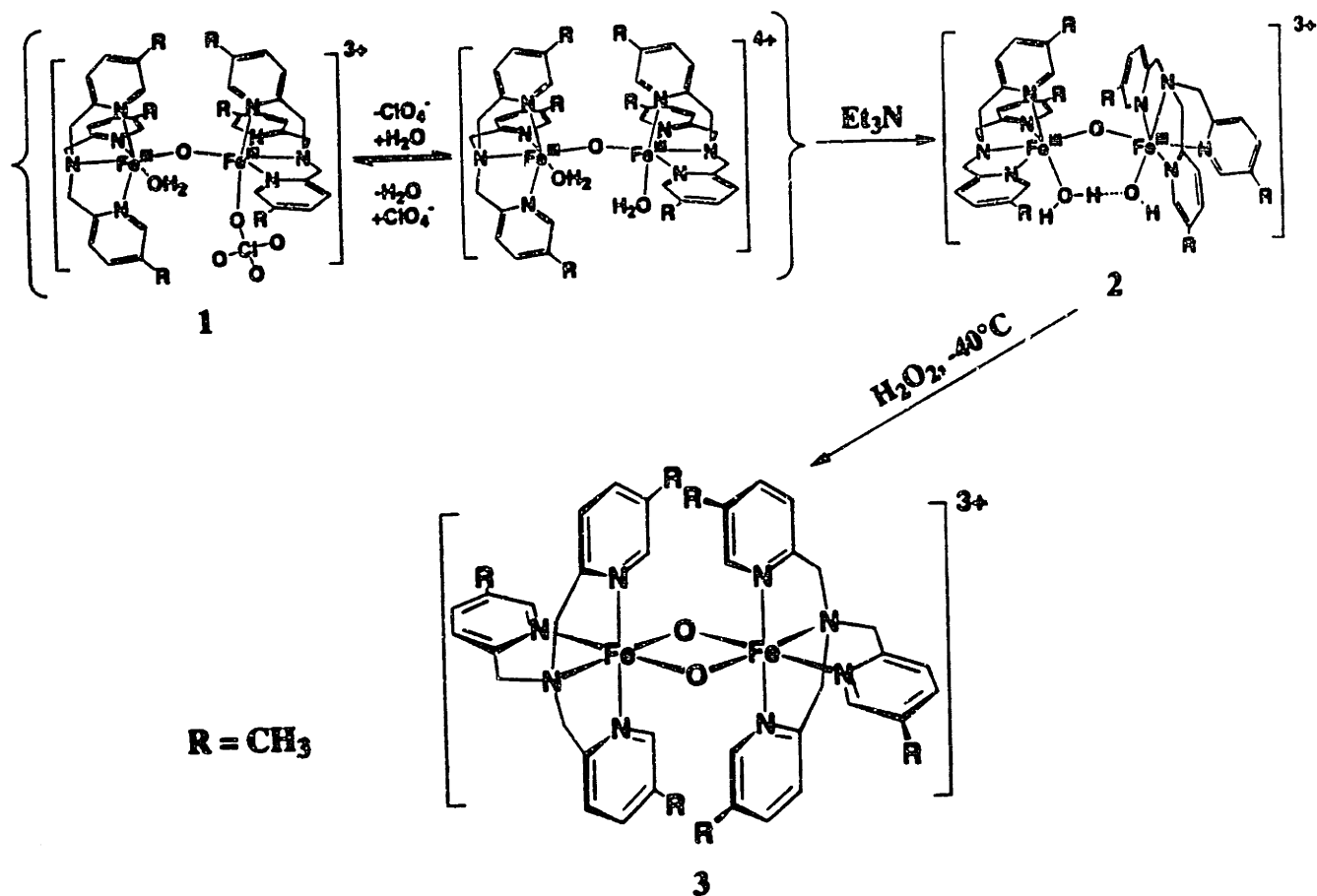
Although the initial characterization of X by EPR and Mössbauer spectroscopies provided strong support for the diferric radical formulation of X, other investigators have suggested by analogy with the heme-iron peroxidases that the generation of •Y122 may involve one or more high-valent iron-oxo intermediates (Sahlin *et al.*, 1990; Fontecave *et al.*, 1990a; Que, 1991; Lam *et al.*, 1993; Ling *et al.*, 1994). Recent characterization of a synthetic S = 1/2 model complex with

an exchange-coupled Fe^{3+} ($S = 1/2$) - Fe^{4+} ($S = 2$) pair had further fueled the debate of the involvement of a high-spin iron-oxo intermediate in the generation of $\bullet\text{Y122}$ in the R2 reconstitution reaction (Dong *et al.*, 1995).

Earlier study of the reaction of a diiron(III) complex (**2**), $\text{Fe}_2(\mu\text{-O})(5\text{-Me-TPA})_2\text{(OH)(H}_2\text{O)](ClO}_4)_3$ (TPA = tris(2-pyridylmethyl)amine), with H_2O_2 at -40°C in CH_3CN results in formation of a $S = 3/2$ species which has been characterized as a novel bis(μ -oxo)diiron(III, IV) complex with a valence-delocalized Fe^{3+} ($S = 1/2$) - Fe^{4+} ($S = 1$) pair (Scheme 1.13). Very recently, Dong *et al.* reported that introduction of a 6-methyl substituent on one of the pyridines of the TPA ligand of **2** resulted in a new model complex, which reacts with H_2O_2 to form an $S = 1/2$ complex with EPR properties very similar to intermediate X in R2 reconstitution reaction (Dong *et al.*, 1995). On the basis of the electrospray ionization mass data, EPR studies in conjunction with isotopic labeling with ^{57}Fe and ^{17}O (from H_2^{17}O), as well as by analogy to the $S = 3/2$ complex, Dong *et al.* proposed that the new $S = 1/2$ species also has a $\text{Fe}_2(\mu\text{-O})_2$ core (Dong *et al.*, 1995).

However, in contrast to the $S = 3/2$ complex, Mössbauer data suggested that the $S = 1/2$ complex is an exchange-coupled pair with localized high-spin Fe(IV) and Fe(III) sites. The observed isomer shifts (0.48 mm/s for iron site and 0.08 mm/s for site 2), quadrupole splittings (1.6 mm/s for site 1 and 0.5 mm/s for site 2), together with analysis of the Mössbauer data collected over a range of applied fields are most consistent with an antiferromagnetically coupled Fe^{3+} ($S = 1/2$) - Fe^{4+} ($S = 2$) pair. Recognizing the similarity between the EPR spectrum of X and that of the $S = 1/2$ model complex, these investigators proposed that an (Fe^{3+} , Fe^{4+}) model should also be considered in describing the electron structure of X. It should be noted that, while the isomer shift for the the Fe(III) site of the $S = 1/2$ model complex (0.48 mm/s) compares well with iron site 1 in X (0.56 mm/s), the isomer shift for the Fe(IV) site of the model complex (0.08 mm/s) is significantly lower than that of iron site 2 of X

Scheme 1.13: Reaction of a diiron(III) complex, $\text{Fe}_2(\mu\text{-O})(5\text{-Me-TPA})_2(\text{OH})(\text{H}_2\text{O})(\text{ClO}_4)_3$ (where TPA = tris(2-pyridylmethyl)amine) (2), with H_2O_2 at -40°C in CH_3CN .



(0.26 mm/s). At present, it is not entirely clear whether the difference in isomer shifts is due to the more nitrogen-rich ligand environment of the model compound compared to **X**, or whether it is a reflection of differences in oxidation state of the iron site. Spectroscopic studies designed to address these issues are in progress.

References

- Aberg, A. (1993) Ph. D. Thesis, Stockholm University.
- Aberg, A., Nordlund, P. & Eklund, H. (1993) *Nature* 361, 276-278.
- Andersson, K. K. & Gräslund, A. (1995) *Adv. Inorg. Chem.* 43, 359-408.
- Antanaitis, B. C. & Aisen, P. (1983) *Adv. Inorg. Biochem.* 5, 111-136.
- Anthony, C. (1982) *The Biochemistry of the Methyloprotoplasts*. Academic Press, Orlando, FL.
- Aslund, F., Ehn, B., Marandavizueté, A., Pueyo, C. & Holmgren, A. (1994) *Proc. Natl. Acad. Sci. USA* 91, 9813-9817.
- Atkin, C. L., Thelander, L., Reichard, P. & Lang, G. (1973) *J. Biol. Chem.* 248, 7464-7472.
- Atta, M., Nordlund, P., Åberg, A., Eklund, H. & Fontecave, M. (1992a) *J. Biol. Chem.* 267, 20682-20688.
- Atta, M., Scheer, C., Fries, P. H., Fontecave, M. & Latour, J.-M. (1992b) *Angew. Chem., Int. Ed. Engl.* 31, 1513.
- Backes, G., Loehr, T. M., Sjöberg, B.-M., Sahlin, M. & Sanders-Loehr, J. (1989) *Biochemistry* 28, 1923-1929.
- Bender, C. J., Sahlin, M., Babcock, G. T., Barry, B. A., Chandrashekar, T. K., Salowe, S. P., Stubbe, J., Lindström, B., Petersson, L., Ehrenberg, A. & Sjöberg, B.-M. (1989) *J. Am. Chem. Soc.* 111, 8076-8083.

- Bianchi, V., Eliasson, R., Fontecave, M., Mullieq, E., Hoover, D. M., Matthews, R. G. & Reichard, P. (1993) *Biochem. Biophys. Research Comm.* 197, 792-797.
- Blakey, R. C. (1978) *Methods Enzymol.* 51, 246-259.
- Bollinger, J. M., Jr. (1992) Ph. D. Thesis, Massachusetts Institute of Technology.
- Bollinger, J. M., Jr., Edmondson, D. E., Huynh, B. H., Filley, J., Norton, J. R. & Stubbe, J. (1991a) *Science* 253, 292-298.
- Bollinger, J. M., Jr., Stubbe, J., Huynh, B. H. & Edmondson, D. E. (1991b) *J. Am. Chem. Soc.* 113, 6289-6291.
- Bollinger, J. M., Jr., Tong, W. H., Ravi, N., B. H., Edmondson, D. E. & Stubbe, J. (1994a) *J. Am. Chem. Soc.* 116, 8015-8023.
- Bollinger, J. M., Jr., Tong, W. H., Ravi, N., Huynh, B. H., Edmondson, D. E. & Stubbe, J. (1994b) *J. Am. Chem. Soc.* 116, 8024-8032.
- Booker, S., Licht, S., Broderick, J. & Stubbe, J. (1994) *Biochemistry* 33, 12676-12685.
- Brennan, B. A., Chen, Q., Juarez-Garcia, C., True, A. E., O'Connor, C. J. & Que, L., Jr. (1991) *Inorg. Chem.* 30, 1937-1943, and references cited therein.
- Brown, N. C., Eliasson, R., Reichard, P. & Thelander, L. (1969) *Eur. J. Biochem.* 9, 512-518.
- Bunker, G., Peterson, L., Sjöberg, B.-M., Sahlin, M., Chance, M., Chance, B. & Ehrenberg, A. (1987) *Biochemistry* 26, 4708-4716.
- Burdi, D., Sturgeon, B. E., Tong, W. H., Stubbe, J. & Hoffman, B. M. (1996) *J. Am. Chem. Soc.* In press,
- Carlson, J., Fuchs, J. A. & Messing, J. (1984) *Proc. Natl. Acad. Sci. U.S.A.* 81, 4294-4297.
- Colby, J., Dalton, H. & Whittenbury, R. (1979) *Annu. Rev. Microbiol.* 33, 481-517.
- Conner, J., Marsden, H. & Clements, J. B. (1994) *Reviews in Medical Virology* 4, 25-34.
- Dalton, H. (1980) *Adv. Appl. Microbiol.* 26, 71-87.

- Davydoc, R., Kuprin, S., Gräslund, A. & Ehrenberg, A. (1994) *J. Am. Chem. Soc.* 116, 11120-11128.
- DeWitt, J. G., Bentsen, J. G., Rosenzweig, A. C., Hedman, B., Green, J., Pilkington, S., Papaefthymiou, G. C., Dalton, H., Hodgson, K. O. & Lippard, S. J. (1991) *J. Am. Chem. Soc.* 113, 9219-9235.
- Doi, K., Antanaitis, B. C. & Aisen, P. (1988) *Struct. Bonding (Berlin)* 70, 1-26.
- Dong, Y., Que, L., Jr., Kauffmann, K. & Münck, E. (1995) *J. Am. Chem. Soc.* 117, 11377-11378.
- Ehrenberg, A. (1988) *Chemica Scripta* 28A, 27-31.
- Ehrenberg, A. & Reichard, P. (1972) *J. Biol. Chem.* 247, 3485-3488.
- Elgren, T. E., Hendrich, M. P. & Que, L. (1993) *J. Amer. Chem. Soc.* 115, 9291-9292.
- Elgren, T. E., Lynch, J. B., Juarez-Garcia, C., Münck, E., Sjöberg, B.-M. & Que, L., Jr. (1991) *J. Biol. Chem.* 266, 19265-19268.
- Elgren, T. E., Ming, L. J. & Que, L. (1994) *Inorg. Chem.* 33, 891-894.
- Eliasson, R., Fontcave, M., Jörnvall, H., Krook, M., Pontis, E. & Reichard, P. (1990) *Proc. Natl. Acad. Sci. USA* 87,
- Eliasson, R., Pontis, E., Fontcave, M., Gerez, C., Harder, J., Jörnvall, J., Krook, M. & Reichard, P. (1992) *J. Biol. Chem.* 267, 25541-25547.
- Ericson, A., Hedman, B., Hodgson, K. O., Green, J., Dalton, H., Bentsen, J. G., Beer, R. H. & Lippard, S. J. (1988) *J. Am. Chem. Soc.* 110, 2330-2332.
- Eriksson, S. & Sjöberg, B.-M. (1989) "Ribonucleotide Reductase" in *Allosteric Enzymes* (Hervé, ed.) CRC Press, Boca Raton, FL, 189-215.
- Eriksson, S., Sjöberg, B.-M., Hahne, S. & Karlstrom, O. (1977) *J. Biol. Chem.* 252, 6132-6138.
- Feig, A. L. & Lippard, S. J. (1994) *Chem. Review* 94, 759-805.
- Fontcave, M., Eliasson, R. & Reichard, P. (1989) *J. Biol. Chem.* 264, 9164-9170.

- Fontecave, M., Gerez, C., Atta, M. & Jeunet, A. (1990a) *Biochem. Biophys. Res. Comm.* 168, 659-664.
- Fontecave, M., Gerez, C., Mansuy, D. & Reichard, P. (1990b) *J. Biol. Chem.* 265, 10919-10924.
- Fontecave, M., Nordlund, P., Eklund, H. & Reichard, P. (1992) *Adv. Enzymol. Relat. Areas Mol. Biol.* 65, 147-183.
- Fox, B. G., Shanklin, J., Ai, J., Loehr, T. M. & Sanders-Loehr, J. (1994) *Biochemistry* 33, 12776-12786.
- Fox, B. G., Shanklin, J., Somerville, C. & Münck, E. (1993) *Proc. Natl. Acad. Sci. U.S.A.* 90, 2486.
- Fox, B. G., Surerus, K. K., Münck, E. & Lipscomb, J. B. (1988) *J. Biol. Chem.* 263, 10553-10556.
- Gerez, C. & Fontecave, M. (1992) *Biochemistry* 31, 780-786.
- Gerez, C., Gailard, J., Latour, J. M. & Fontecave, M. (1991) *Angew. Chem., Int. Ed. Engl.* 30, 1135-1136.
- Gerfen, G., Bellew, B. F., Un, S., Bolliner, J. M. & Stubbe, J. (1993) *J. Am. Chem. Soc.* 115, 6420-6421.
- Gómez-Romero, P., Casan-Pastor, N., Ben-Hussein, A. & Jameson, G. B. (1988) *J. Am. Chem. Soc.* 110, 1988-1990.
- Gupta, N., Bonomi, F., Kurtz, D. M., Jr., Ravi, N., Wang, D. L. & Huynh, B. H. (1995) *Biochemistry* 34, 3310-3318.
- Harder, J., Eliasson, R., Pontis, E., Ballinger, M. & Reichard, P. (1992) *J. Biol. Chem.* 267, 25548-25552.
- Hendrich, M. P., Elgren, T. E. & Que, L., Jr. (1991) *Biochem. Biophys. Res. Comm.* 176, 705-710.
- Hirsh, D. J., Beck, W. F., Lynch, J. B., Que, L., Jr. & Brudvig, G. W. (1992) *J. Am. Chem. Soc.* 114, 7475-7481.

- Kurtz, D. M., Jr. (1990) *Chem. Rev.* 90, 585-606.
- Lam, K.-Y., Govindaraju, K., Han, J.-Y., Salmon, G. A. & Sykes, A. G. (1993) *J. Chem. Soc. Dalton Tans.* 2797-2801.
- Lammers, M. & Follmann, H. (1983) *Struct. Bonding (Berlin)* 54, 27-91.
- Larsson, A. & Sjöberg, B.-M. (1986) *EMBO J.* 5, 2037-2040.
- Laurent, R. C., Moore, E. C. & Reichard, P. (1964) *J. Biol. Chem.* 239, 3436-3444.
- Lee, S.-K., C., N. J. & Lipscomb, J. D. (1993a) *J. Biol. Chem.* 268, 21569-21577.
- Lee, S.-K., Fox, B. G., Froland, W. A., Lipscomb, J. D. & Münck, E. (1993b) *J. Am. Chem. Soc.* 115,
- LeGall, J., Prickril, B. C., Moura, I., Xavier, A. V., Moura, J. J. G. & Huynh, B.-H. (1988) *Biochemistry* 27, 1636-1642.
- Leising, R. A., Brennan, B. A., Que, L., Jr., Fox, B. G. & Münck, E. (1991) *J. Am. Chem. Soc.* 113, 3988-3990.
- Licht, S., Gerfen, G. J. & Stubbe, J. (1996) *Science* in press,
- Ling, J., Sahlins, M., Sjöberg, B.-M., Loehr, T. M. & Sanders-Loehr, J. (1994) *J. Biol. Chem.* 269, 5595-5601.
- Lippard, S. J. (1988) *Angew. Chem. Int. Ed. Engl.* 27, 344-361.
- Liu, K. E., Valentine, A. M., Wang, D., Huynh, B. H., Edmondson, D. E., Salifoglou, A. & Lippard, S. J. (1995b) *J. Am. Chem. Soc.* 117, 10174-10185.
- Liu, K. E., Valentine, A. M., Qiu, D., Edmondson, D. E., Appelman, E. H., Spiro, T. G. & Lippard, S. J. (1995a) *J. Am. Chem. Soc.* 117, 4997-4998.
- Liu, K. E., Wang, D., Huynh, B. H., Edmondson, D. E., Salifoglou, A. & Lippard, S. J. (1994) *J. Am. Chem. Soc.* 116, 7465-7466.
- Lynch, J. B., Juárez-García, C., Münck, E. & Que, L., Jr. (1989) *J. Biol. Chem.* 264, 8091-8096.

- Mao, S. S., Holler, T. P., Bollinger, J. M., Yu, G. X., Johnston, M. I. & Stubbe, J. (1992a) *Biochem.* 31, 9744-9751.
- Mao, S. S., Holler, T. P., Yu, G.-X., Bollinger, J. M., Jr., Booker, S., Johnston, M. I. & Stubbe, J. (1992b) *Biochemistry* 31, 9733-9743.
- Mao, S. S., Yu, G. X., Chalfoun, D. & Stubbe, J. (1992c) *Biochemistry* 31, 9752-9759.
- Marnett, L. J., Weller, P. & Battista, J. R. (1986) "Comparison of the Peroxidase Activity of Hemoproteins and Cytochrome P-450" in *Cytochrome P-450 Structure, Function and Biochemistry* (Ortiz de Montellano, ed.) Plenum Publishing Corp., London, 29-76.
- Massey, V. (1957) *J. Biol. Chem.* 229, 763-770.
- McCormick, J. E., Reem, R. C., Foroughi, J., Bollinger, J. M., Jensen, G. M., Stephens, P. J., Stubbe, J. & Solomon, E. I. (1991) *New J. Chem.* 6, 439.
- McMurry, T. J. & Groves, J. T. (1986) in *Cytochrome P-450 Structure, Function and Biochemistry* (Montellano, ed.) Plenum Publishing, Corp., London, 1-28.
- Menage, S., Brennan, B. A., Juarez-Garcia, C., Münck, E. & Lawrence Que, J. (1990) *J. Am. Chem. Soc.* 112, 6423-6425.
- Moore, E. C., Reichard, P. & Thelander, L. (1964) *J. Biol. Chem.* 239, 3445-3452.
- Moura, I., Tavares, P. & Ravi, N. (1994) *Method Enzymol.* 243, 216-240.
- Mulliez, E., Fontecave, M., Gaillard, J. & Reichard, P. (1993) *J. Biol. Chem.* 268, 2296-2299.
- Nordlund, P. (1990) Ph.D. Thesis, Swedish University of Agricultural Sciences.
- Nordlund, P. & Eklund, H. (1993) *J. Mol. Biol.* 232, 123-164.
- Nordlund, F., Eklund, H., Åberg, A. & deMare, D. (1995) "Abstracts of Papers." 209th National Meeting of the American Chemical Society.
- Nordlund, P., Sjöberg, B. M. & Eklund, H. (1990) *Nature* 345, 593-598.

- Ochiai, E.-I., Mann, G. J., Gräslund, A. & Thelander, L. (1990) *J. Biol. Chem.* 265, 15758-15761.
- Ortiz de Montellano, P. R. (1986) in *Cytochrome P-450 Structure, Function and Biochemistry* (Montellano, ed.) Plenum Publishing Corp., London,
- Petersson, L., Gräslund, A., Ehrenberg, A., Sjöberg, B.-M. & Reichard, P. (1980) *J. Biol. Chem.* 255, 6706-6712.
- Pierik, A. J., Wolbert, R. B. G., Portier, G. L., Verhagen, M. F. J. M. & Hagen, W. R. (1993) *Eur. J. Biochem.* 212, 237-245.
- Platz, A. & Sjöberg, B.-M. (1980) *J. Bacteriol.* 143, 561-568.
- Pulver, S. C., Tong, W. H., Bollinger, J. M., Jr., Stubbe, J. & Solomon, E. I. (1995) *J. Am. Chem. Soc.* 117, 12664-12678.
- Que, L., Jr. (1991) *Science* 253, 273.
- Que, L., Jr. & True, A. E. (1990) "Dinuclear Iron- and Manganese-Oxo Sites in Biology." *Prog. Inorg. Chem. Bioinorg. Chem.* 38, 97-200.
- Ravi, N., Bollinger, J. M., Jr., Tong, W. H., Ravi, N., B. H., Edmondson, D. E. & Stubbe, J. (1994) *J. Am. Chem. Soc.* 116, 8007-8014.
- Ravi, N. & Bominaar, E. L. (1995) *Inorg. Chem.* 34, 1040-1043.
- Ravi, N., Prickrel, B. C., Kurtz, D. M., Jr. & Huynh, B. H. (1993) *Biochemistry* 32, 8487.
- Reem, R. C. & Solomon, E. I. (1987) *J. Am. Chem. Soc.* 109, 1216-1226.
- Reichard, P. (1988) *Annu. Rev. Biochem.* 57, 349-374.
- Reichard, P. (1993) *Science* 260, 1773-1777.
- Reichard, P., Baldesten, A. & Rutberg, L. (1961) *J. Biol. Chem.* 236, 1961.
- Sahlin, M., Ehrenberg, A., Gräslund, A. & Sjöberg, B.-M. (1986) *J. Biol. Chem.* 261, 2778-2780.

- Sahlin, M., Gräslund, A., Petersson, L., Ehrenberg, A. & Sjöberg, B.-M. (1989) *Biochemistry* 28, 2618-2625.
- Sahlin, M., Petersson, L., Gräslund, A., Ehrenberg, A., Sjöberg, B.-M. & Thelander, L. (1987) *Biochemistry* 26, 5541-5548.
- Sahlin, M., Sjöberg, B.-M., Backes, G., Loehr, T. & Sanders-Loehr, J. (1990) *Biochem. Biophys. Res. Comm.* 167, 813-818.
- Salowe, S. P. (1987) Ph. D. Thesis, University of Wisconsin.
- Salowe, S. P. & Stubbe, J. (1986) *J. Bacteriol.* 165, 363-366.
- Sanders-Loehr, J. (1989) "Binuclear Iron Proteins" in *Iron Carriers and Iron Proteins* (Loehr, ed.) VHC Publishers Inc., 375-466.
- Sanders-Loehr, J., Wheeler, W. D., Shiemke, A. K., Averill, B. A. & Loehr, T. M. (1989) *J. Am. Chem. Soc.* 111, 8084-8093.
- Scarrow, R. C., Maroney, M. J., Palmer, S. M., Que, L., Jr., Roe, A. L., Salowe, S. P. & Stubbe, J. (1987) *J. Am. Chem. Soc.* 109, 7857-7864.
- Scarrow, R. C., Maroney, M. J., Palmer, S. M., Que, L., Jr., Salowe, S. P. & Stubbe, J. (1986) *J. Am. Chem. Soc.* 108, 6832-6834.
- Schulz, C. E., Rutter, R., Sage, J. T., Debrunner, P. G. & Hager, L. P. (1984) *Biochemistry* 23, 4743-4754.
- Sheats, J. E., Armstrong, W. H., Beer, R. H., Czernuszewicz, R. S., Dismukes, G. C., Lippard, S. J., Petrouleas, V., Rheingold, A. L. & Stubbe, J. (1987) *J. Am. Chem. Soc.* 1, 1, 1.
- Sjöberg, B.-M., Eklund, H., Fuchs, J. A., Carlson, J., Standart, N. M., Ruderman, J. V., Bray, S. J. & Hunt, T. (1985) *FEBS Lett.* 183, 99-102.
- Sjöberg, B.-M. & Gräslund, A. (1983) *Adv. Inorg. Biochem.* 5, 87-110.
- Sjöberg, B.-M., Gräslund, A., Sanders-Loehr, J. & Loehr, T. M. (1980) *Biochem. Biophys. Res. Comm.* 94, 793-799.

- Sjöberg, B.-M., Karlsson, M. & Jörnvall, H. (1987) *J. Biol. Chem.* 262, 9736-9743.
- Sjöberg, B.-M., Loehr, T. M. & Sanders-Loehr, J. (1982) *Biochemistry* 21, 96-102.
- Sjöberg, B.-M., Reichard, P., Gräslund, A. & Ehrenberg, A. (1977) *J. Biol. Chem.* 252, 536-541.
- Stubbe, J. (1990a) *J. Biol. Chem.* 265, 5329-5332.
- Stubbe, J. (1990b) *Adv. Enzymol. Relat. Areas Mol. Biol.* 63, 349-417.
- Stubbe, J. (1991) *Curr. Opin. Struct. Biol.* 1, 788-795.
- Stubbe, J., Ackles, D., Segal, R. & Blakley, R. L. (1981) *J. Biol. Chem.* 256, 4843-4846.
- Stubbe, J., Ator, J. & Krenitsky, T. (1983) *J. Biol. Chem.* 258, 1625-1630.
- Stubbe, J. & van der Donk, W. A. (1995) *Chemistry and Biology* 2, 793-801.
- Sturgeon, B. E., Burdi, D., Chen, S., Huynh, B. H., Stubbe, J. & Hoffman, B. M. (1996) *J. Am. Chem. Soc.* Submitted.,
- Sun, X. Y., Eliasson, R., Pontis, E., Andersson, J., Buist, G., Sjöberg, B.-M. & Reichard, P. (1995) *J. Biol. Chem.* 270, 2443-2446.
- Swarts, J. C., Aquino, M. A. S., Han, J.-Y., Lam, K.-Y. & Sykes, G. (1995) *Biochim. et Biophysica Acta* 1247, 215-224.
- Thelander, L. (1973) *J. Biol. Chem.* 248, 4591-4601.
- Thelander, L. & Gräslund, A. (1994) "Ribonucleotide Reductase in Mammalian Systems." *Metal Ions in Biological Systems.* 109-129.
- Thelander, L. & Reichard, P. (1979) *Annu. Rev. Biochem.* 48, 133-158.
- Thelander, M., Gräslund, A. & Thelander, L. (1985) *J. Biol. Chem.* 260, 2737-2741.
- True, A. E., Scarrow, R. C., Randall, C. R., Holz, R. C. & Que, L., Jr. (1993) *J. Am. Chem. Soc.* 115, 4246-4255.
- Uhlen, U. & Eklund, H. (1994) *Nature* 270, 533-539.

Vincent, J. B., Oliver-Lilley, G. L. & Averill, B. A. (1990) *Chem. Rev.* 90, 1447-1467.

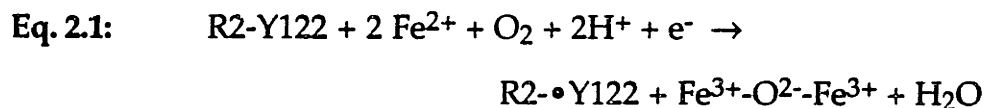
Wilkins, P. C. & Wilkins, R. G. (1987) *Coord. Chem. Rev.* 79, 195-214.

Willing, A., Follman, H. & Auling, G. (1988) *Eur. J. Biochem.* 178, 603-611.

Woodland, M. P., Patil, D. S., Cammack, R. & Dalton, H. (1986) *Biochim. Biophys. Acta* 873, 237-242.

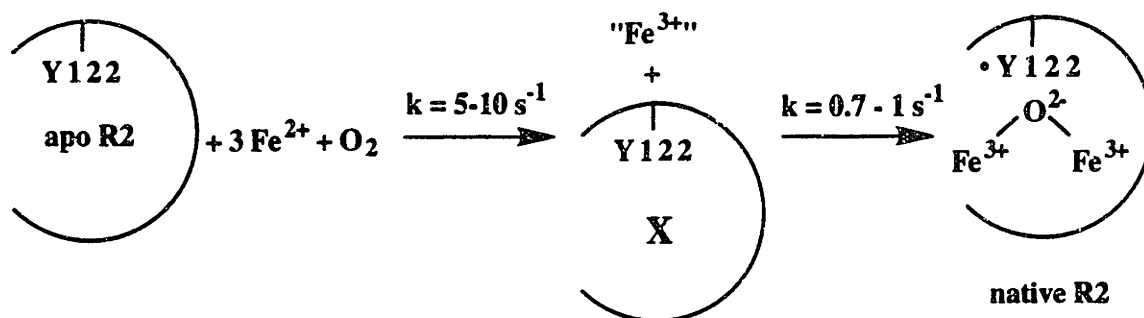
**Chapter 2: Reconstitution of Native R2 from Ferrous R2 and O₂
under Excess Fe²⁺ Conditions**

The tyrosyl radical-diferric cluster cofactor in the R2 subunit of *E. coli* ribonucleotide reductase self-assembles when the apo form of R2 is mixed with Fe²⁺ and O₂. In previous work, kinetic and spectroscopic evidence allowed us to propose a mechanism for this reconstitution reaction (Scheme 1.3) (Bollinger *et al.*, 1991a; Bollinger *et al.*, 1991b; Bollinger *et al.*, 1994b). A key feature of this hypothesis is a partitioning into two pathways, with a different intermediate generating •Y122 in each pathway. It was proposed that the partition ratio between the pathways is determined by the Fe²⁺/R2 ratio, which determines the availability of the fourth reducing equivalent that is required to balance the four-electron reduction of O₂ (Eq. 2.1). When the extra electron is readily available (from excess Fe²⁺) to rapidly convert I into II (Scheme 1.3), the kinetics simplify to Scheme 2.1, in which an iron cluster intermediate, X, accumulates with a k_{obs} of 5 - 10 s⁻¹, and decays concomitantly with formation of •Y122 and diferric cluster with a k_{obs} of 0.7 - 1 s⁻¹.



In the main focus of this work, the complementary spectroscopic methods of stopped-flow absorption (SF-Abs), rapid freeze-quench EPR (RFQ-EPR), and rapid freeze-quench Mössbauer (RFQ-Möss) spectroscopies have been used to characterize the kinetics of the cofactor assembly when pre-formed Fe(II)-R2 complex is mixed with O₂ under excess Fe²⁺ conditions. By using these methods, rate constants for decay of X and for formation of the cofactor have been independently measured. The results of these experiments suggest that X generates •Y122 with a k_{obs} of 0.7 - 1.0 s⁻¹ and that X is the precursor to the product diferric cluster. Thus, these results

Scheme 2.1: Proposed minimal mechanism for the reaction at 5 °C of apo R2, O₂, and excess Fe²⁺. The broken circle represents only one of the two monomers of apo R2.



provide further support for the mechanism proposed for the cofactor assembly in the reaction of apo R2, O₂ and excess Fe²⁺ (Scheme 2.1) (Bollinger, 1992; Bollinger *et al.*, 1994b). Identical experiments were also carried out on a mutant R2 subunit in which the oxidizable Y122 was replaced by with the less easily oxidized residue, phenylalanine (F). The results suggest the X exhibits increased lifetimes in R2-Y122F, providing additional evidence that this species is responsible for •Y122 production in R2-wt.

In addition, the results described in this chapter indicate that formation of the intermediate X is much faster in the reaction of Fe(II)-R2 with O₂ (k_{obs} of 60 - 80 s⁻¹) than in the reaction of apo R2 with Fe²⁺ and O₂ (k_{obs} of 5 - 10 s⁻¹). This observation implies that the rate-limiting step in the formation of X in the apo R2 reaction occurs before binding of Fe²⁺, and offers support for the hypothesis that a slow conformational change occurs in apo R2 to allow for entry of Fe²⁺ into the cofactor site (Bollinger, 1992; Bollinger *et al.*, 1994b). Furthermore, these experiments have allowed detection of a species which is not associated with any of the previously defined components, and preliminary kinetic data suggest that it may be a new intermediate in the assembly process. Mössbauer data suggest that this species may

be similar to the peroxo-diiron(III) intermediate ($\text{MMOH}_{\text{peroxo}}$) observed in the reaction of diferrous methane monooxygenase hydroxylase from *M. capsulatus* (Bath) with O_2 (Liu *et al.*, 1994; Liu *et al.*, 1995a). The temporal behavior of this putative peroxo-diiron(III) intermediate also suggests that it may be the precursor that leads to the intermediate X.

Another issue that is addressed from the experiments described in this chapter is the source of the fourth electron required for cofactor assembly (Eq. 2.1). While the requirement for a fourth electron and the ability of Fe^{2+} to provide it were previously shown by Elgren *et al.* (Elgren *et al.*, 1991) and Bollinger *et al.* (Bollinger *et al.*, 1991a) for *E. coli* R2 and by Ochiai *et al.* (Ochiai *et al.*, 1990) for mouse R2, the mechanism by which this electron is delivered remains unclear. All three groups measured a Fe^{2+} /tyrosyl radical stoichiometry of ≈ 3 and concluded that oxidation of a third Fe^{2+} provides the fourth electron required to balance the four-electron reduction of O_2 (Eq. 2.1). Elgren *et al.* examined the reconstituted *E. coli* R2 by EPR and Mössbauer spectroscopies and found that $> 92\%$ of the added Fe had been incorporated into diferric clusters. Since previous studies have shown that added Fe^{3+} is not incorporated by R2 into diferric cluster (Pettersson *et al.*, 1980), Elgren *et al.* reasoned that electron transfer between R2 monomers must occur, allowing Fe^{2+} bound in the cofactor site of one R2 monomer to supply the fourth reducing equivalent to the iron cluster in another monomer (Elgren *et al.*, 1991). In contrast, Ochiai *et al.* reported an EPR signal at $g = 4.3$ which is indicative of mononuclear Fe^{3+} ion, and proposed that a third binding site for Fe^{2+} exists in mouse R2 to facilitate delivery of the fourth electron (Ochiai *et al.*, 1990). While the broad signal at $g = 4.3$ provide a serious obstacle to precise quantitative evaluation of the data, this hypothesis is consistent with the results of Bollinger *et al.* that a fast-relaxing ferric species is produced concomitantly with formation of X in the reaction of apo R2 with excess Fe^{2+} at 5°C (Bollinger *et al.*, 1994b). However, the amount of

fast-relaxing ferric species observed can account for only to 50% of the "fourth" electron required for cofactor assembly. This result thus suggest that a second mechanism exists for delivery of this electron by Fe^{2+} (Bollinger *et al.*, 1994b). In the experiments described in this chapter, the reaction of Fe(II)-R2 with O_2 was examined by EPR and Mössbauer spectroscopies for the formation of Fe^{3+} species which correlates in time with the accumulation of X. The experiments described in this chapter indicate that the fast-relaxing ferric species can only account for a fraction of the electrons required for formation of X. These experiments further reveal that several additional oxidized iron species were generated in the reconstitution reaction. The possible mechanistic significance of these observations is discussed below.

Experimental Procedures

Materials and Methods

Sephadex G-25, Sephadex G-50, QAE-Sephadex, ferrozine, and Fe atomic absorption standard were purchased from Sigma. DEAE-Biogel A was purchased from BioRad. S-300 was purchased from Pharmacia. Natural abundance (^{56}Fe) iron wire was purchased from Baker. ^{57}Fe (95.1 atom%) metal was purchased from Advanced Materials and Technology. 2-Methyl butane (reagent grade) was purchased from Aldrich. All other chemicals were of the highest purity commercially available. Suprasil quartz EPR samples tubes (O.D. 4 mm, I.D. 2.4 mm, 7 in. long) for RFQ-EPR experiments were obtained from Wilmad Glass Company.

The $^{56}\text{Fe}^{2+}$ stock solution was prepared by dissolution of $\text{FeSO}_4 \cdot 7\text{H}_2\text{O}$ in a 2.5-5.0 mN H_2SO_4 solution. The concentration of Fe^{2+} was determined using the ferriin chelator, ferrozine (Massey, 1957; Stookey, 1970; Salowe, 1987). A typical assay contained 30 μL 10 mM ferrozine, 30 μL saturated ammonium acetate, and 2 - 15 nmol of Fe^{2+} in a final volume of 760 μL . A $\epsilon_{562} = 27900 \text{ M}^{-1}\text{cm}^{-1}$ was used for

the calculation of $[\text{Fe}^{2+}]$ (Stookey, 1970). Assays were carried out in the absence of ascorbate in order to determine $[\text{Fe}^{2+}]$, and with ascorbate (2 mM) to determine total $[\text{Fe}]$ ($[\text{Fe}^{2+}] + [\text{Fe}^{3+}]$). The $^{57}\text{Fe}^{2+}$ stock solutions for the Mössbauer experiments were prepared by anaerobic dissolution of ^{57}Fe metal in 2 N H_2SO_4 (Bollinger, 1992). The resulting concentrated Fe^{2+} stock was diluted with H_2O or with dilute H_2SO_4 in order to give the desired Fe^{2+} concentration in 3 - 6 mN H_2SO_4 .

UV-visible absorption spectra were recorded on an HP-8452A Diode Array Spectrometer maintained at constant temperature with a Brinkmann Instruments Lauda K-2/R circulating water bath. SDS/PAGE was performed as described by Laemmli (1970) R2 subunit activity was assayed by following NADPH oxidation spectrophotometrically in an assay containing 50 mM HEPES (pH 7.6), 15 mM MgSO_4 , 1 mM EDTA, 1.6 mM ATP, 1 mM CDP, 0.16 mM NADPH, 20 μM thioredoxin, 0.5 μM thioredoxin reductase, 2 μM R1, and 0.1 - 0.2 μM R2 in a final volume of 400 μL (Salowe, 1987).

Kinetic modeling was performed using HopKIMSIM, a Macintosh version of Barshop and Freiden's kinetic simulation program, KINSIM (Barshop *et al.*, 1983). Non-linear regression analysis of the EPR and Mössbauer kinetic data was carried out with the Git and Gear programs of Dr R. J. McKinney and Dr. F. J. Wiegert, Central Research and Development Department, E. I. du Pont de Nemours and Co.

Purification of E. coli R2

R2-wt was isolated from 100 g of N6405/pSPS2 as previously reported (Bollinger *et al.*, 1994b), but with minor modifications. All steps in the purification were performed at 5 °C. Frozen wet cell paste (100 g) was suspended in 500 mL of 50 mM Tris-HCl at pH 7.6 (at 5 °C), containing 5% glycerol (hereafter referred to as Tris buffer). Phenylmethylsulfonylfluoride (PMSF) was added to 500 μM , and the cell suspension was passed through a French pressure cell at 12 - 14,000 psi to rupture

the bacteria. To the cell lysate was added 0.4 g $\text{Fe}(\text{NH}_4\text{SO}_4)_2$ and 0.4 g sodium ascorbate freshly dissolved in a small volume (<10 ml) of the Tris buffer. The crude lysate was stirred for several minutes, and then centrifuged at 14,000 x g for 20 min. The supernatant was brought to 1% in streptomycin sulfate by the addition of 0.2 volumes of a 5.5% (w/v) solution of streptomycin sulfate in the Tris buffer over 10 min, with stirring. This solution was stirred for an additional 10 min, and then centrifuged at 14,000 x g for 20 min. The supernatant was brought to 60% saturation in $(\text{NH}_4)_2\text{SO}_4$ by addition of the solid (390 g/L), over 20 min, with stirring. This solution was stirred for an additional 30 min, and then centrifuged at 14,000 x g for 20 min. The pellet was redissolved in ~80 mL of the Tris buffer containing 500 μM PMSF. This solution was centrifuged at 14,000 x g for 10 min to pellet any remaining undissolved material, and was desalted through a Sephadex G-25 column (6.5 x 60 cm) equilibrated in the Tris buffer. The fractions containing protein (typically 800 mL) were pooled and diluted with an equal volume of the Tris buffer. This solution was brought to 500 μM in PMSF, and then loaded on a DEAE-Biogel A column (6.5 x 25 cm) equilibrated in the Tris buffer. After the sample was loaded, the column was washed with 1.5 column volumes of the Tris buffer containing 500 μM PMSF, followed by 1.6 column volumes of the Tris buffer containing 110 mM NaCl and 500 μM PMSF. R2 was then eluted from the column with the Tris buffer containing 140 mM NaCl and 500 μM PMSF. Fractions containing R2 (as judged by the A_{410} , dropline / A_{280} ratio) were pooled (700-800 mL), and the pool was diluted with an equal volume of the Tris buffer with 500 μM PMSF. The solution was loaded onto a QAE-Sephadex column (5 x 18 cm) equilibrated in the Tris buffer containing 70 mM NaCl. This column was washed with 2.5 volumes of the Tris buffer containing 225 mM NaCl and 500 μM PMSF. R2 was then eluted from the column with the Tris buffer containing 300 mM NaCl and 500 μM PMSF. Fractions containing R2 (typically 400 - 500 mL) were pooled and concentrated to 6 - 8 mL in an Amicon Diaflow Ultrafilter

equipped with a PM-30 or with a YM-30 membrane. A solution, which generally contained 500 - 600 mg of R2, was loaded onto a S-300 column (2.5 x 110 cm) equilibrated in the Tris buffer. (At this point PMSF was no longer required.) The column was eluted at 0.5 ml/min. Fractions (10 mL) which contained R2 were pooled, and the pool was concentrated by ultrafiltration to a final [R2] of >60 mg/ml, as judged by the absorbance at 280 nm (assuming $\epsilon_{280} = 131 \text{ mM}^{-1}\text{cm}^{-1}$). The protein was frozen in liquid N₂ and stored at -80 °C. Isolation of R2-wt in this manner typically yielded 1 g of >95% pure (as assessed by SDS-PAGE and Commassie blue staining) protein from 100 g of wet N6405/pSPS2 cell paste. The protein typically had a specific activity of 7000 - 8000 U/mg.

Protein R2-Y122F was isolated from 100 g K38/pTB2-Y122F using a similar procedure. Isolation of R2-Y122F from these cells gave 600-800 mg of > 95% pure R2-Y122F from 100 g of wet cell paste.

The apo form of R2-wt and R2-Y122F were prepared from native R2 as previously described (Atkin *et al.*, 1973; Salowe, 1987). The concentration of apo R2 was determined by absorbance at 280 nm (assuming $\epsilon_{280} = 120 \text{ mM}^{-1}\text{cm}^{-1}$) (Thelander, 1973).

Stopped-flow Absorption Spectroscopy

Stopped-flow experiments were carried out on an Applied Photophysics DX.17MV Sequential Stopped-Flow Spectrofluorimeter maintained at constant temperature with a Brinkmann Instruments Lauda K2R circulating water bath. The concentration of •Y122 was determined from A₄₁₀, dropline from the UV-visible absorption spectrum as described previously (Bollinger *et al.*, 1994b).

EPR Spectroscopy

X-band EPR spectra at temperature below 40 K were recorded on either a Brüker Model ESP 300 equipped with a Oxford Instrument ESR 900 continuous flow cryostat, or a Brüker ER 200D-SRC spectrometer equipped with an Oxford Instruments ESR 910 continuous flow cryostat. X-band EPR spectra were also recorded at 100 K on a Brüker Model ESP 300 spectrometer maintained at constant temperature with a Brüker ER4111VT variable temperature controller. Detailed experimental conditions were described in the figure legends.

Analysis of the EPR spectra acquired on the Brüker ER 200D-SRC spectrometer was carried out using programs written in the laboratory of Prof. Huynh at Emory University. Analysis of the EPR spectra acquired on the Brüker Model ESP 300 spectrometer was carried out using KaleidaGraph by Abelbeck Software. The relative quantities of X and •Y122 present in each spectrum was determined as described previously (Bollinger *et al.*, 1994b). The reference sample for X was prepared by mixing 0.14 mM apo R2-Y122F in Ar-saturated 100 mM HEPES buffer (pH 7.7) with an equal volume of air-saturated 1.0 mM Fe²⁺ stock in 5 mM HNO₃ at 5 °C and the reaction mixture was freeze-quenched at 0.27 s (Ravi *et al.*, 1994). Two different samples were used as references for •Y122. The first is the 60 s time-point of the reaction of Fe(II)-R2-wt (Fe²⁺/R2 = 5) with O₂. As shown in the SF-Abs studies described below, this sample contains 1.2 •Y122 per R2. The second is the 60 s time-point of the reaction of apo R2-wt with 5 Fe²⁺ and O₂ (Bollinger *et al.*, 1994b). The •Y122/R2 ratio in this sample was shown to be 1.2 ± 0.1 from previous studies (Bollinger *et al.*, 1994b). These two samples show identical EPR spectra.

Mössbauer Spectroscopy

Mössbauer spectra were recorded in the laboratory of Prof. B. H. Huynh at Emory University on a weak-field Mössbauer spectrometer equipped with a Janis

8DT variable-temperature cryostat and operated in a constant acceleration mode in a transmission geometry. The zero velocity of the Mössbauer spectra refers to the centroid of the room temperature spectrum of a metallic iron foil. All Mössbauer spectra were acquired at 4.2 K with a magnetic field of 50 mT applied parallel to the γ -beam. Analysis of the Mössbauer spectra of the freeze-quenched samples to determine the quantities of the intermediate X, diferric cluster and other iron-containing species in the reaction was carried out in the laboratory of Prof. Huynh as described previously (Bollinger *et al.*, 1994b). The programs compute the total area under the absorption spectrum (which is proportional to the quantity of ^{57}Fe present in the sample) and allows a theoretical or experimental reference spectrum to be superimposed upon and then subtracted from the original spectrum. The known, total quantity of ^{57}Fe present in the sample served as an internal standard, which allowed the absolute quantity of a given component of the reaction (ferrous R2, X or the diferric cluster) to be calculated from the fraction of ^{57}Fe in that component. Experimental reference spectra for X, diferric cluster, fast-relaxing ferric species, ferrous-R2, and $^{57}\text{Fe}^{2+}$ in HEPES buffer were prepared as described previously¹ (Bollinger *et al.*, 1994b). As mentioned previously, recent studies have resulted in a simulation of X which is in very good agreement with the experimental data (Sturgeon *et al.*, 1996). Therefore, a theoretical spectrum for X was generated using the new parameters (Table 1.2) and this reference spectrum was also used for the current analysis. The analysis carried out in Prof. Huynh's laboratory was also repeated in our laboratory.

¹The reference spectra for X, ferrous R2 and diferric cluster used in the initial analysis of the time-course samples in this study were acquired over a velocity scale of -7 to 7 mm/s (Bollinger 1992). For reasons that will become obvious, the reference spectra have been reanalyzed using a velocity scale of -14 to 14 mm/s. With the new reference spectra, better agreement between theory and the data described in this chapter is obtained.

Reaction of Fe(II)-R2 with O₂ as Monitored by Stopped-Flow Absorption Spectroscopy

Reagents for the SF-Abs experiments were prepared as described below. An aliquot of the apo R2 stock (1.0 - 1.5 mM) was placed in a septa-capped 5-mL pear-shaped flask. The flask was connected to a vacuum line and a source of humidified Ar and the flasks were briefly evacuated. After several seconds, the vessels were refilled with humidified Ar. This vacuum/Ar cycle was repeated 2 times, and then the solutions were incubated on ice, with stirring, for 15-20 min. The routine of 3 cycles of pump/Ar purge followed by incubation on ice was repeated 5-7 times over a period of 1 - 2 h. The Fe²⁺ stock (10 - 17 mM Fe²⁺ in 5 mN H₂SO₄) was deoxygenated using the same procedure. A solution of 100 mM HEPES (pH 7.6) was deoxygenated by bubbling Ar through the solution at 5 °C for > 2 h. A concentrated dithionite solution (50 - 100 mM) was made by transferring the deoxygenated HEPES buffer via cannula to a septa-capped, argon-purged flask containing solid sodium dithionite. An aliquot of this dithionite solution was transferred via cannula to a septa-capped flask containing deoxygenated 100 mM HEPES (pH 7.6) to make a 200 - 400 μM dithionite solution. An O₂-saturated HEPES buffer (100 mM, pH 7.6) was prepared by bubbling O₂ through the solution for ~ 2 h at 5 °C. The O₂-saturated buffer contains ~1.6 mM of dissolved O₂ at 5 °C (Hitchman, 1978).

For anaerobic stopped-flow experiments, the complete flow circuit of the stopped-flow instrument including reagent reservoirs, drive syringes, stopping syringe and sample flow lines were purged thoroughly with a solution of 100-500 mM sodium dithionite in 100 mM HEPES buffer (pH 7.6) at least 12 h before the experiment. Argon gas was bubbled through the thermostat medium (at 5 °C) in the circulating water bath for ~ 2 h prior to and throughout the experiment. Shortly before the experiment, 1 gm of sodium dithionite was dissolved in 5 - 10 mL of 100 mM HEPES buffer (pH 7.6) and the solution was added to the thermostat medium.

Just before introducing the reagents to the stopped-flow instrument, the complete flow circuit was purged thoroughly with Ar-saturated buffer (100 mM HEPES, pH 7.6). In a typical stopped-flow experiment, the reaction of Fe(II)-R2 with O₂ was initiated by mixing (at 5 °C) equal volumes of an Ar-saturated solution containing 140 - 600 μM apo R2 and 5 molar equivalents of Fe²⁺ in 100 mM HEPES (pH 7.6) and an O₂-saturated solution of 100 mM HEPES (pH 7.6).

Calibration of Rapid Freeze-Quench Apparatus

The rapid freeze-quench method involves mixing two (or more) reactants rapidly and efficiently, allowing the reaction to proceed for a desired length of time (the time required for the mixture to pass through an aging hose of appropriate volume), freeze-quenching the reaction mixture by spraying it into isopentane cooled to -140 °C, and packing the resulting ice crystals into a receptacle appropriate for spectroscopic analysis. The reaction time is thus determined by the flow rate, the volume of the aging hose, the time elapsed after the reaction mixture escapes the nozzle until it contacts the cold isopentane, and the time elapsed after the reaction mixture contacts the cold isopentane until it is cooled to the temperature at which no further reaction occurs (quenching time). In a previous study (Bollinger, 1992), it was established that a ram velocity of 1 cm/s gave ice crystals with suitable packing properties for the RFQ-EPR and RFQ-Möss experiments. Therefore, a ram velocity of 1 cm/s was used for our experiments. The quenching time can vary from one reaction system to another (Ballou & Palmer, 1974), and is difficult to determine. For most reactions, the quenching time is ~10 ms.

The volume of the aging hose was determined experimentally, as follows. The entire aging hose consists of the mixer, connecting hose (hereafter referred to as reaction hose), and the spray nozzle. In these experiments, the volumes of the mixer (1.6 μL) and the nozzle (1 μL) were assumed to be those quoted by the

manufacturer. The volume of each reaction hose was determined experimentally by one of two methods. In one case, the empty hose is connected to a drive syringe filled with water. The ram unit was programmed for a given displacement, actuated, and the water expelled from the hose was collected in an Eppendorf tube. The volume of the hose was then calculated from the difference between the weight of the water expelled by the drive syringe and the weight of the water collected in the tube. In the second case, the water in the drive syringe was replaced with a solution of [³²P]-ATP. The volume of the aging hose was calculated as the difference between the amount of radioactivity expelled by the drive syringe for a given displacement and the amount of radioactivity collected in the tube.

As demonstrated below, the reactions of interest in this chapter are considerably faster than those in our previous studies of the R2 reconstitution reaction (Bollinger *et al.*, 1994a; Bollinger *et al.*, 1994b). In the previous studies, it was clear that the volumes of the mixer and the nozzle were small compared to the volume of the smallest reaction hose used, and they were therefore neglected. For more rapid reactions, it becomes increasingly important to include the volumes of the mixer and the nozzle in the determination of the aging time. It is also critical to minimize the time elapsed after the reaction mixture escapes the nozzle until it contacts the cold isopentane during freeze-quenching. A distance of 1 cm between the spray nozzle and the cold isopentane in the sampling apparatus can result in addition of ~ 0.003 s to the reaction age.

Table 2.1 summarizes the volume determinations for the aging hoses and the corresponding reaction times for a 1 cm/s ram velocity. The reaction time for each aging hose was calculated from the volumes of the mixer (1.6 μ L), the aging hose, and the nozzle (1 μ L), with the addition of the estimated time elapsed after the reaction mixture escapes the nozzle until it contacts the cold isopentane (0.002 s),

Table 2.1: Measured volumes of the rapid freeze-quench aging hoses and the corresponding reaction times for a ram velocity of 1 cm/s. The combined volume expelled by the two drive syringes was found to be 660 μL for a 1 cm displacement of the ram drive.

Aging Hose No.	Volume (μL)	Reaction Time (ms)
6.4	8.0 ± 0.2	28
8.0	8.9 ± 0.2	29
10.0	11 ± 1	33
12.5	14 ± 2	37
16.0	17 ± 2	42
20	21 ± 3	48
25	24 ± 3	52
32	31 ± 4	63
40	35 ± 2	69
50	41 ± 2	78
64	49 ± 2	90
80	62 ± 3	110
125	94 ± 4	158
160	118 ± 6	195
250	175 ± 9	281
320	219 ± 13	348
400	281 ± 16	442
500	326 ± 7	510

and a quenching time of 0.010 s.

Reaction of Fe(II)-R2 with O₂ as Monitored by RFQ-EPR and RFQ-Möss Spectroscopies

The RFQ-EPR and RFQ-Möss samples were prepared by the rapid freeze-quench method as previously described (Bray, 1961; Ballou & Palmer, 1974; Ravi *et al.*, 1994). EPR samples were prepared by mixing (at 5 °C) an Ar-saturated solution containing 400 µM apo R2, 2.0 mM Fe²⁺ in 100 mM HEPES buffer (pH 7.6) with an equal volume of an O₂-saturated HEPES buffer (pH 7.6) and the samples were freeze-quenched at various reaction times. Unless otherwise stated, Mössbauer samples were prepared by mixing an Ar-saturated solution containing 600 µM apo R2, 3.0 mM Fe²⁺ in 100 mM HEPES buffer (pH 7.6) with an equal volume of an O₂-saturated HEPES buffer (pH 7.6) at 5 °C and the samples were freeze-quenched at various reaction times.

The stock solutions for the rapid freeze-quench experiments were prepared as follows. An aliquot of apo R2 (1.0 - 1.5 mM) was made anaerobic using the procedure described above. The Fe²⁺ solution (~15 mM) and the 100 mM HEPES buffer (pH 7.6) were deoxygenated as described below. The solutions (5 - 10 mL) were placed in separate 25 mL pear-shaped flasks. The flasks were connected to a vacuum line and a source of humidified Ar. The solutions were frozen with liquid N₂. The flasks were then briefly evacuated and the frozen solutions were allowed to thaw under static vacuum. After the solutions had thawed, the vessels were refilled with humidified Ar. This freeze-pump-Ar purge cycle was repeated for at least 5 times over a period of 1 - 2 h. The solution was gently stirred throughout the procedure to ensure equilibration.

The Fe(II)-R2 sample was prepared in an anaerobic chamber, before loading into the drive syringe of the rapid freeze-quench instrument. The flasks containing

the O₂-free solutions of apo R2, Fe²⁺, and HEPES buffer were transferred into the anaerobic chamber. Inside the anaerobic chamber, an aliquot of buffer was first mixed with an aliquot of Fe²⁺ in a 5-mL pear-shaped flask, followed by addition of apo R2. The solution was swirled carefully to ensure good mixing. This Fe(II)-R2 sample was then drawn into a drive syringe. The open end of the loaded syringe was capped with a small septum before the syringe was removed from the anaerobic chamber and transferred to the ram unit.

The RFQ-EPR and RFQ-Möss samples were prepared in the laboratory of Prof. D. Edmondson as previously described (Bollinger, 1992), or in our laboratory in the same fashion, with minor modifications. An Update Instrument System 1000 Chemical/Freeze Quench Apparatus, in conjunction with an Update Instrument isopentane bath was used. The bath holds ~ 8 L isopentane and was maintained at between -140 and -150 °C by periodically adding liquid N₂ to the outer bath. A copper-constant thermocouple is used to monitor the temperature of the isopentane.

Determination of the Packing Factor for the RFQ-EPR Experiments

In the RFQ-EPR experiments, the reaction mixture is sprayed into cold isopentane contained in a RFQ-EPR tube, and the ice crystals are packed firmly into the bottom of the EPR tube with a packer constructed from a stainless-steel rod. One of the problems associated with this method is the considerably large variability in the packing of the sample. It has been found that samples prepared by the RFQ-EPR method typically have about 0.5 - 0.7 of the EPR signal density of samples frozen manually (Ballou, 1978) because of the isopentane trapped in the packed crystalline samples. With practice, precision of packing is about ±5 - 10 %, while precision of spin quantitation by EPR spectroscopy is typically about ±5 - 10 %. These factors

constitute the most significant uncertainties in quantitative analysis of the RFQ-EPR samples.

The packing factor depends on at least two factors: the intrinsic properties of the sample and the operator. The uncertainty in the overall packing factor associated with the operator was determined experimentally, as follows. RFQ-EPR samples were prepared by mixing a solution containing 1.0 mM CuSO₄, 2.0 M NaClO₄, 0.010 M HCl, and 20% (v/v) glycerol (Malmström *et al.*, 1970) with an equal volume of water, and the mixture was freeze-quenched. The "operator packing factor" was determined by comparing the EPR signal density of the freeze-quenched samples with one that was frozen manually, and it was found to be 0.65 ± 0.07 for the experiments described in this chapter.

The packing factor can also vary from one reaction system to another. Depending on the intrinsic properties of the reaction mixture, the ice crystals in each sample may aggregate to different extents, and thus trap different amounts of isopentane. Assuming that the packing factor is the same for all the samples of a given reaction, the packing factor associated with the reconstitution reaction of R2-wt can be determined as follows. The EPR spectrum of the reconstitution reaction at completion was acquired. The sample was then thawed by submerging the EPR tube in a cold water bath (~ 0 °C). Due to its hydrophobicity and lower density compared to water, the isopentane trapped in the freeze-quench sample rose to the top when the sample was thawed. The EPR tube was tapped gently to ensure that all the aqueous sample was collected at the bottom of the EPR tube. The sample was refrozen by submerging the EPR tube slowly into liquid N₂. The EPR spectrum of the sample after thawing was acquired. The packing factor was calculated according to Eq. 2.2, where I_{thawed} is the EPR signal density of the sample before thawing, and I_{thawed} is the EPR signal density of the sample after the thaw/refreezing procedure.

The packing factor determined by this method for the R2 reconstitution reaction is 0.7 ± 0.1 .

$$\text{Eq. 2.2:} \quad \text{Packing factor} = \frac{I_{\text{unthawed}}}{I_{\text{thawed}}}$$

Results

Reaction of Fe(II)-R2-wt with O₂ as Monitored by SF-Abs Spectroscopy

When Fe(II)-R2-wt is mixed at 5 °C with an equal volume of an O₂-saturated solution of 100 mM HEPES (pH 7.6), development of the absorption spectrum characteristic of •Y122 is complete within 10 s. Time-resolved spectra (330 - 650 nm) of the reaction indicate that a broad absorption band centered at around 365 nm rapidly develops before formation of •Y122 (Fig. 2.1). About 50 % of the final absorption at 365 nm has developed 0.04 s after mixing, while no •Y122 (as judged by A_{410, dropline}) is yet observable. As shown in our previous work, the iron-containing intermediate X exhibits a broad band centered around 365 nm. These results thus suggest that X accumulates in the reaction of Fe(II)-R2 with O₂. In contrast to the apo R2 reaction, however, the A₃₆₅-versus-time trace in the Fe(II)-R2-wt reaction exhibits no initial lag phase (Fig. 2.2). Furthermore, formation of X (as judged by absorbance at 365 nm) is initially faster in the Fe(II)-R2 reaction than that observed in the apo R2 reaction. Therefore, an accordant interpretation of the data is that the lag phase observed in the reconstitution of apo R2 most likely reflects a slow step before formation of Fe(II)-R2.

The kinetics of •Y122 formation in the reconstitution of Fe(II)-R2-wt are also consistent with the above deductions. As shown in Fig. 2.3, the formation of •Y122 shows a significantly shorter lag (~0.04 s) than that observed in the reconstitution of apo R2. The A_{410,dropline}-versus-time trace of the reaction (Fig. 2.4) illustrates that, after a short lag phase, formation of •Y122 is first order. Non-linear least

Table 2.2: Summary of least-squares fits of a first-order process to the region between 0.05 - 5.0 s of the A_{410} , dropline-versus-time traces of the reaction of Fe(II)-R2-wt with O_2 under excess Fe^{2+} conditions.

Expt.	[apo R2] (μM)	[Fe^{2+}] (μM)	k_{obs} (s^{-1})	($\bullet Y122/R2$) $_{\infty}$
1 ^a	79	490	0.87	1.10 ± 0.05
2 ^a	80	504	0.88	1.04 ± 0.05
3	300	1500	0.80	1.04 ± 0.05
4	300	1500	0.83	1.2 ± 0.05

^aIn some of the early anaerobic experiments, dithionite ($\sim 420 \mu M$) was included in the buffer to minimize O_2 -contamination of the Fe(II)-R2 sample. Six separate experiments, with the results of 3 - 5 individual trials suggest that a low level of dithionite ($< 500 \mu M$) has no adverse effect on $\bullet Y122$ production

squares fitting of the region of this trace between 0.050 and 5.0 s to the equation for a first-order process gives a k_{obs} of $0.85 \pm 0.05 s^{-1}$ (Table 2.2). The magnitude of A_{410} , dropline at completion (< 10 s) observed in four separate experiments is consistent with a $\bullet Y122/R2$ ratio of 1.1 ± 0.1 . Previous studies have shown that the $\bullet Y122$ formation in the reconstitution of apo R2 occurs with apparent first order rate constants of $0.7 - 1 s^{-1}$ and the $\bullet Y122/R2$ at completion is 1.2 ± 0.1 (Bollinger *et al.*, 1991a; Bollinger *et al.*, 1994b). It thus appears that the oxidation of Y122 by X is not affected by pre-forming diferrous R2 before exposure to O_2 . The reaction of Fe(II)-R2 with O_2 , thus, differs from the reaction of apo R2 with O_2 only in the steps leading up to the formation of X and not in the subsequent formation of $\bullet Y122$.

Fig. 2.1: Development of the absorption spectrum of the cofactor upon mixing Fe(II)-R2-wt with O₂ under excess Fe²⁺ conditions (Fe²⁺/R2 = 5). The reaction conditions (after mixing) were: 300 μM R2-wt, 1.5 mM Fe²⁺, 1 mM O₂, 100 mM HEPES, pH 7.6, 5 °C. The spectra were taken 0.002, 0.010, 0.040, 0.200, 1.50 and 8.0 s after mixing.

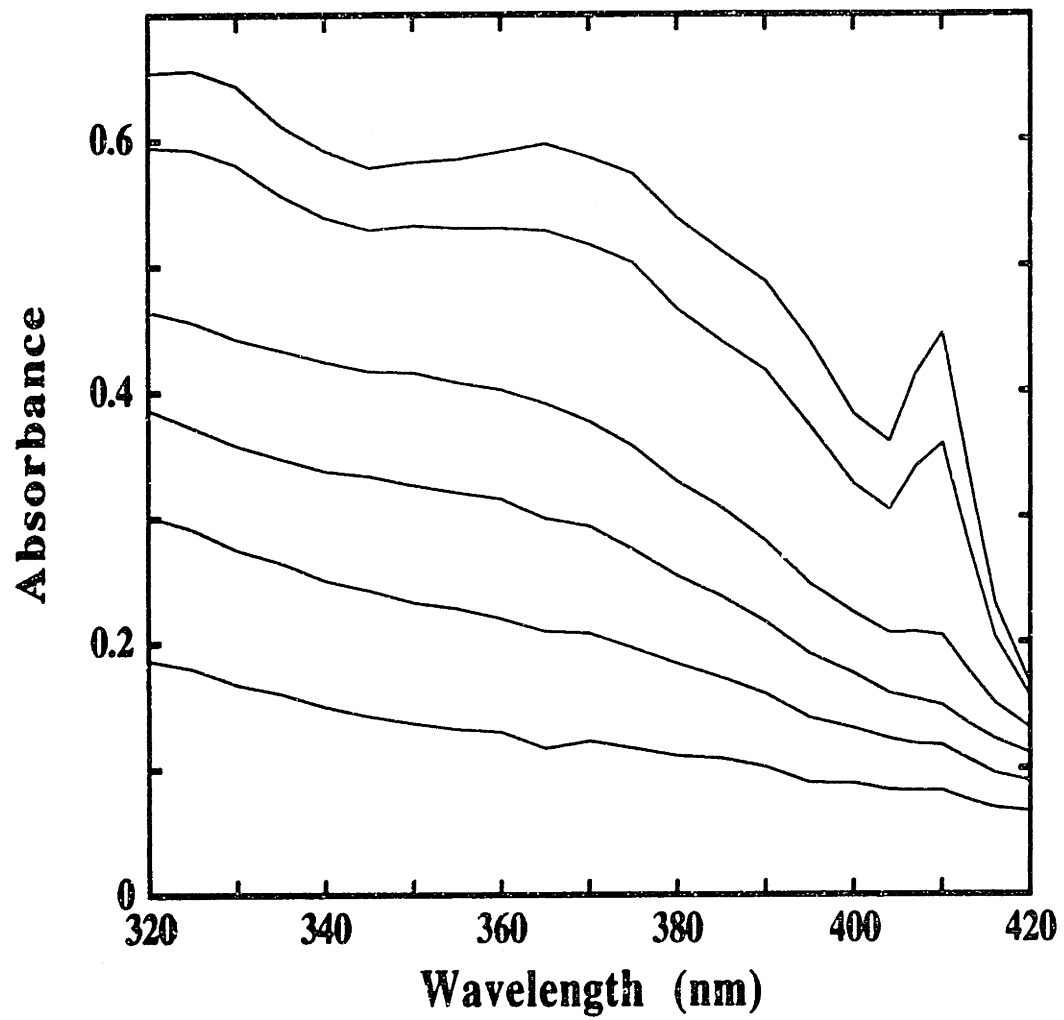


Fig. 2.2: A_{365} -versus-time trace in the reaction of Fe(II)-R2-wt with O_2 compared to that in the reaction of apo R2-wt with Fe^{2+} and O_2 . The reaction conditions (after mixing) were: 300 μ M R2-wt, 1.5 mM Fe^{2+} , 1 mM O_2 , 100 mM HEPES, pH 7.6, 5 $^{\circ}$ C. Each trace represents the average of 3 - 4 trials.

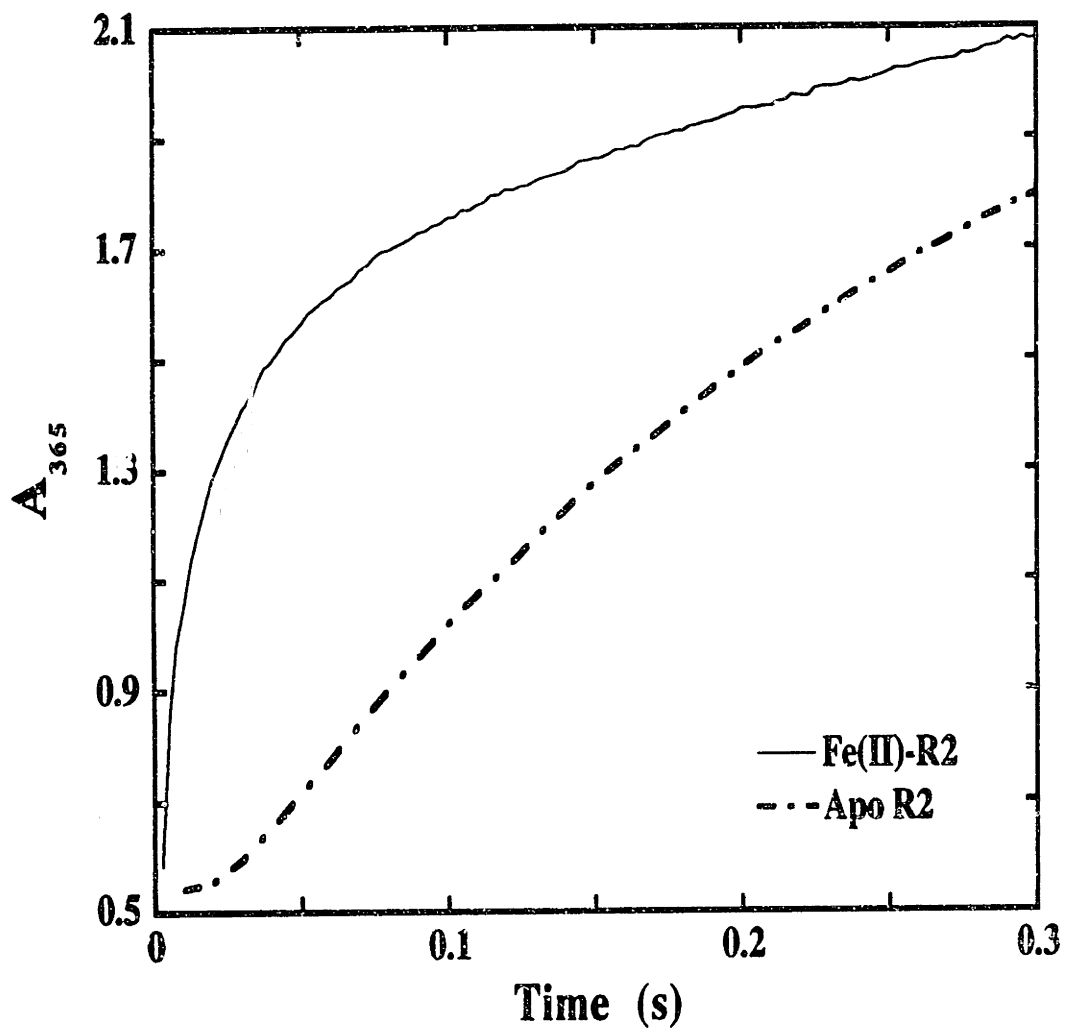


Fig. 2.3: Formation of $\bullet Y122$ in the reaction of Fe(II)-R2-wt with O_2 compared to that in the reaction of apo R2-wt with Fe^{2+} and O_2 . The reaction conditions (after mixing) were: 300 μM R2-wt, 1.5 mM Fe^{2+} , 1 mM O_2 , 100 mM HEPES, pH 7.6, 5 $^\circ C$. Each trace was constructed from the averages of 3 - 4 trials at each wavelength.

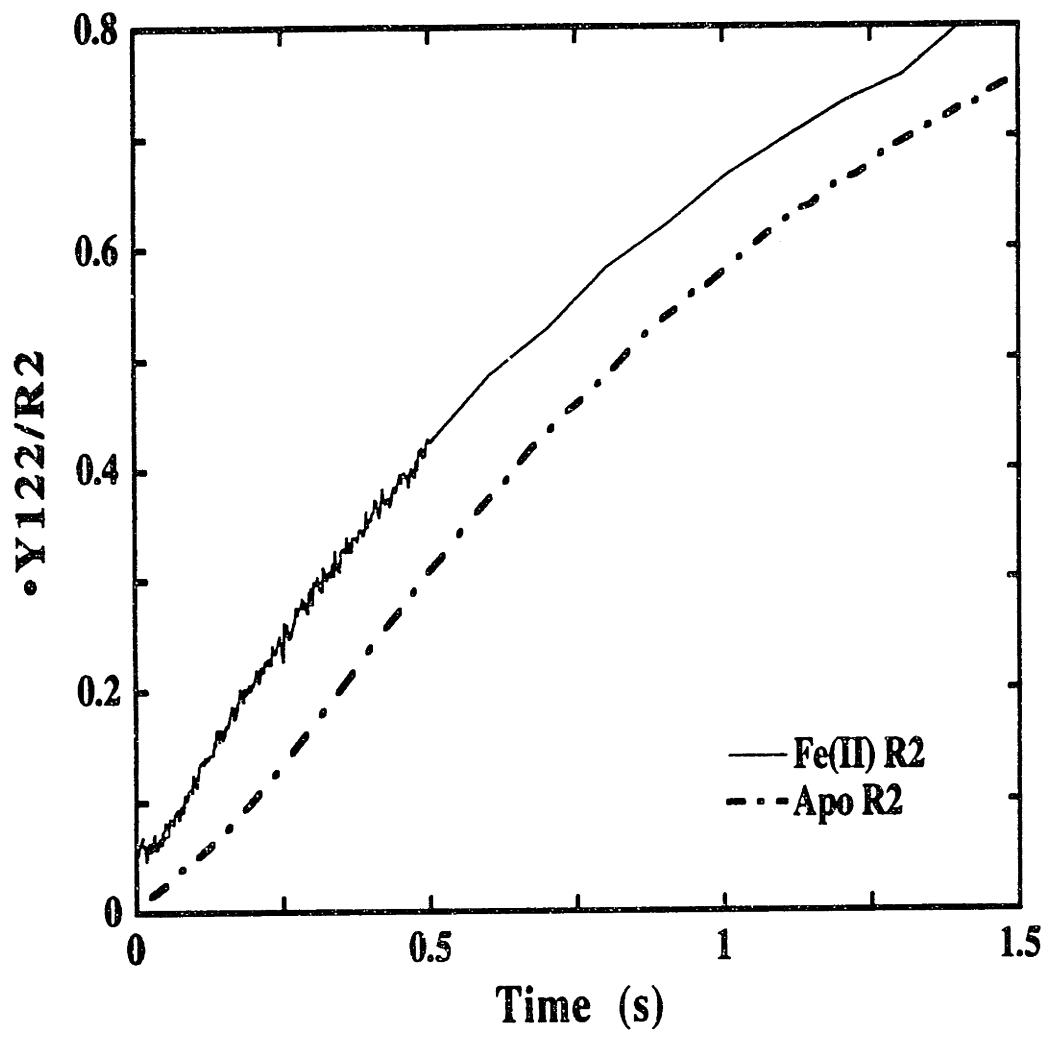
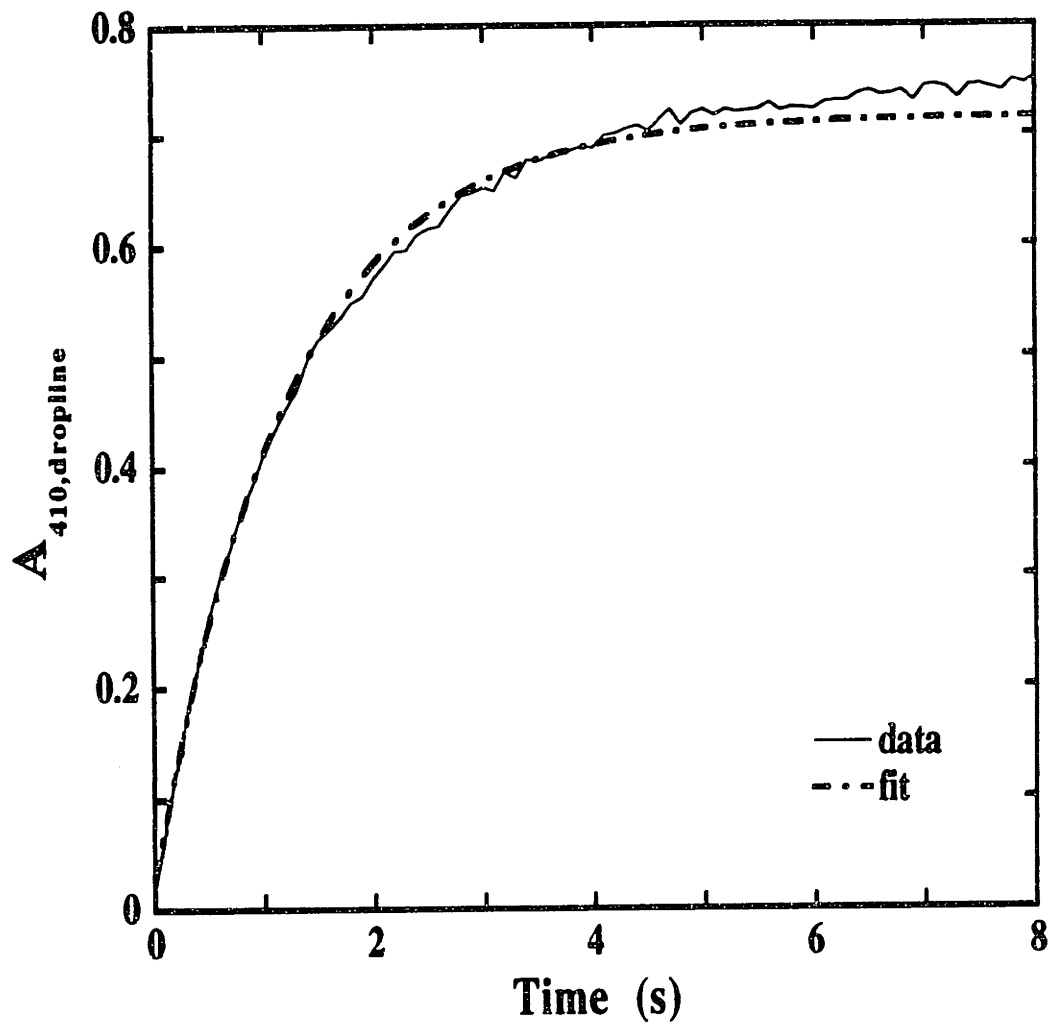
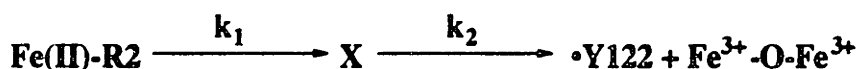


Fig. 2.4: A_{410} , dropline-versus-time trace in the reaction of Fe(II)-R2-wt with O_2 . The reaction conditions (after mixing) were: 300 μ M R2-wt, 1.5 mM Fe^{2+} , 1 mM O_2 , 100 mM HEPES, pH 7.6, 5 °C. The experimental trace represents the average of 3 trials. The theoretical trace is obtained by fitting a first-order process to 0.050 - 5.00 s of the experimental trace, and corresponds to a k_{obs} of 0.83 s^{-1} .



In order to obtain a rate constant for the events leading to formation of \bullet Y122, the $A_{410, \text{dropline}}$ -versus-time trace was analyzed according to the simple kinetic model of two consecutive, first-order process (Scheme 2.2) (Bollinger *et al.*, 1994b). Eq. 2.3 gives the $A_{410, \text{dropline}}$ as a function of time ($A_{410, \text{dropline}}(t)$) for the kinetic model shown in Scheme 2.2. Fitting the 0.0-5.0 s regions of traces from the experiments in Table 2.2 to Eq. 2.3, gives a rate constant (k_1) of 60 - 80 s^{-1} for the formation of X, and a rate constant (k_2) of $0.83 \pm 0.05 \text{ s}^{-1}$ for its decay and the concomitant formation of \bullet Y122. Fig. 2.4 shows the theoretical curve along with the experimental data. As shown previously by Bollinger *et al.*, similar analysis of the apo R2 reaction gives a k_1 of 5 - 10 s^{-1} and a k_2 of 0.7 - 1.0 s^{-1} . These results are consistent with the inference made from Fig. 2.2 that the \bullet Y122-generating intermediate forms more rapidly in the reconstitution from Fe(II)-R2 than in the reconstitution from apo R2.

Scheme 2.2:



Eq. 2.3:

$$A_{410, \text{dropline}}(t) = [\text{Y122}\bullet]_{\infty} \epsilon_{410, \text{dropline}} \left(1 + \frac{k_1 \exp(-k_2 t) - k_2 \exp(-k_1 t)}{k_2 - k_1} \right)$$

Eq. 2.4: $A_t = A_{\infty} + \alpha \exp(-k_1 t) + (A_0 - A_{\infty} - \alpha) \exp(-k_2 t)$

Eq. 2.5: $\alpha = \frac{[(\epsilon_B - \epsilon_A)k_1 + (\epsilon_A - \epsilon_C)k_2]}{(k_2 - k_1)} [A]_0$

In a further attempt to determine values for k_1 and k_2 , the A_{365} -versus-time traces were also analyzed according to the kinetic model of Scheme 2.2. The

absorbance as a function of time for a reaction involving two sequential, first-order processes (Scheme 2.2) is given by Eq. 2.4 (Espenson, 1981), where A_t is the absorbance at any time t , A_0 is the absorbance at $t = 0$, A_∞ is the absorbance at $t = \infty$, and α is related to the molar absorptivities of species A, B, C (ϵ_A , ϵ_B , ϵ_C , respectively), the rate constants k_1 and k_2 , and the concentration of species A at $t = 0$, $[A]_0$, (Eq. 2.5). As shown in Table 2.3, the rate constants calculated vary with the fit-range used, indicating that the model is insufficient to account for the data. When k_2 is held fixed at 0.85 s^{-1} (the mean value calculated for $\bullet\text{Y122}$ formation), a value of 23 s^{-1} is calculated for k_1 . As shown in Fig. 2.5, in the rapid rise phase of the A_{365} -versus-time trace, the theoretical trace lags behind the experimental trace, suggesting that the values of k_1 obtained in the fit may be underestimates of the true values. Decreasing the fit-range below 3.0 s biases both k_1 and k_2 towards greater values and results in increasingly better fit for the rapid rise phase and increasingly poor fits for the slower rise phase(s) (data not shown). Thus, the data are poorly fit according to the oversimplified kinetic model of Scheme 2.2.

Reaction of Fe(II)-R2-Y122F with O₂ as Monitored by SF-Abs Spectroscopy

As with the R2-wt reaction, when Fe(II)-R2-Y122F ($\text{Fe}^{2+}/\text{R2} = 5$) is mixed at 5 °C with O₂, the 365 nm broad absorption band characteristic of X rapidly accumulates (Fig. 2.6) before formation of the diferric cluster. Analysis of the A_{365} -versus-time trace according to Scheme 2.2 was carried out. The data are fairly well fit according to the simple kinetic model of Scheme 2.2, and the analysis gives a k_1 of 6.5 s^{-1} and a k_2 of 0.20 s^{-1} . Fig. 2.6 shows the fit along with the experimental data. In previous studies, the 0 - 30 s region of the A_{365} -versus-time trace for the reaction of apo R2-Y122F with excess Fe^{2+} and O₂ was analyzed according to Scheme 2.2 and the analysis gives a k_1 of 2.6-2.9 s^{-1} , and a k_2 of 0.12-0.19 s^{-1} (Bollinger, 1992). These results also suggest that formation of X in the Fe(II)-R2-Y122F reaction is faster than

Fig. 2.5: A_{365} -versus-time trace in the reaction of Fe(II)-R2-wt with O_2 . The reaction conditions (after mixing) were: 300 μ M R2-wt, 1.5 mM Fe^{2+} , 1 mM O_2 , 100 mM HEPES, pH 7.6, 5 $^{\circ}$ C. The experimental trace represents the average of 3 trials. The theoretical trace is obtained by fitting two sequential, first-order processes to 0.001 - 5.00 s of the experimental trace in which k_2 was fixed at 0.85 s^{-1} and k_1 was allowed to vary.

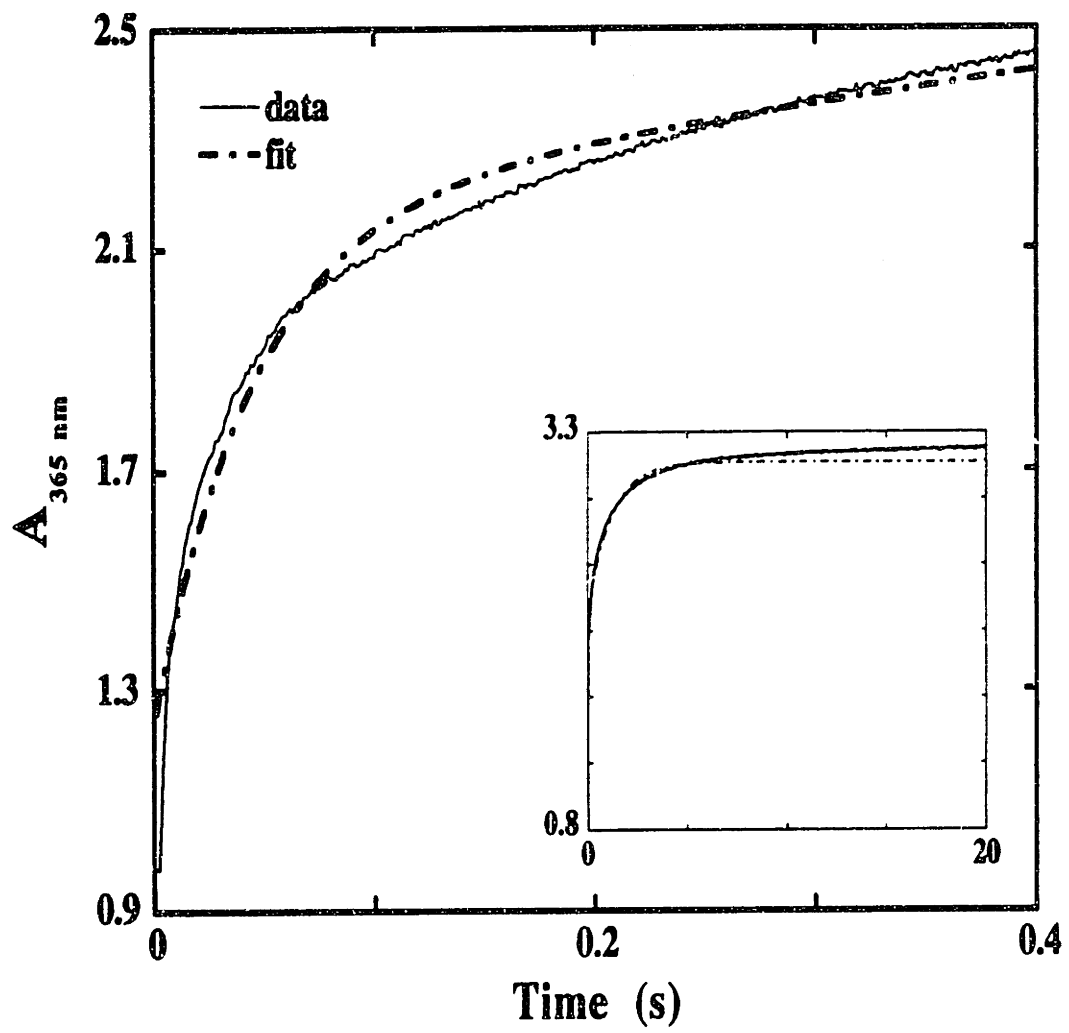


Fig. 2.6: A_{365} -versus-time trace in the reaction of Fe(II)-R2-Y122F ($\text{Fe}^{2+}/\text{R2} = 5$) with O_2 . The reaction conditions (after mixing) were: 300 μM R2-Y122F, 1.5 mM Fe^{2+} , 1 mM O_2 , 100 mM HEPES, pH 7.6, 5 °C. The experimental trace represents the average of 3 trials. The theoretical trace is obtained by fitting two sequential, first-order processes to 0.001 - 5.00 s of the experimental trace and corresponds to k_1 of 6.5 s^{-1} and k_2 of 0.20 s^{-1} .

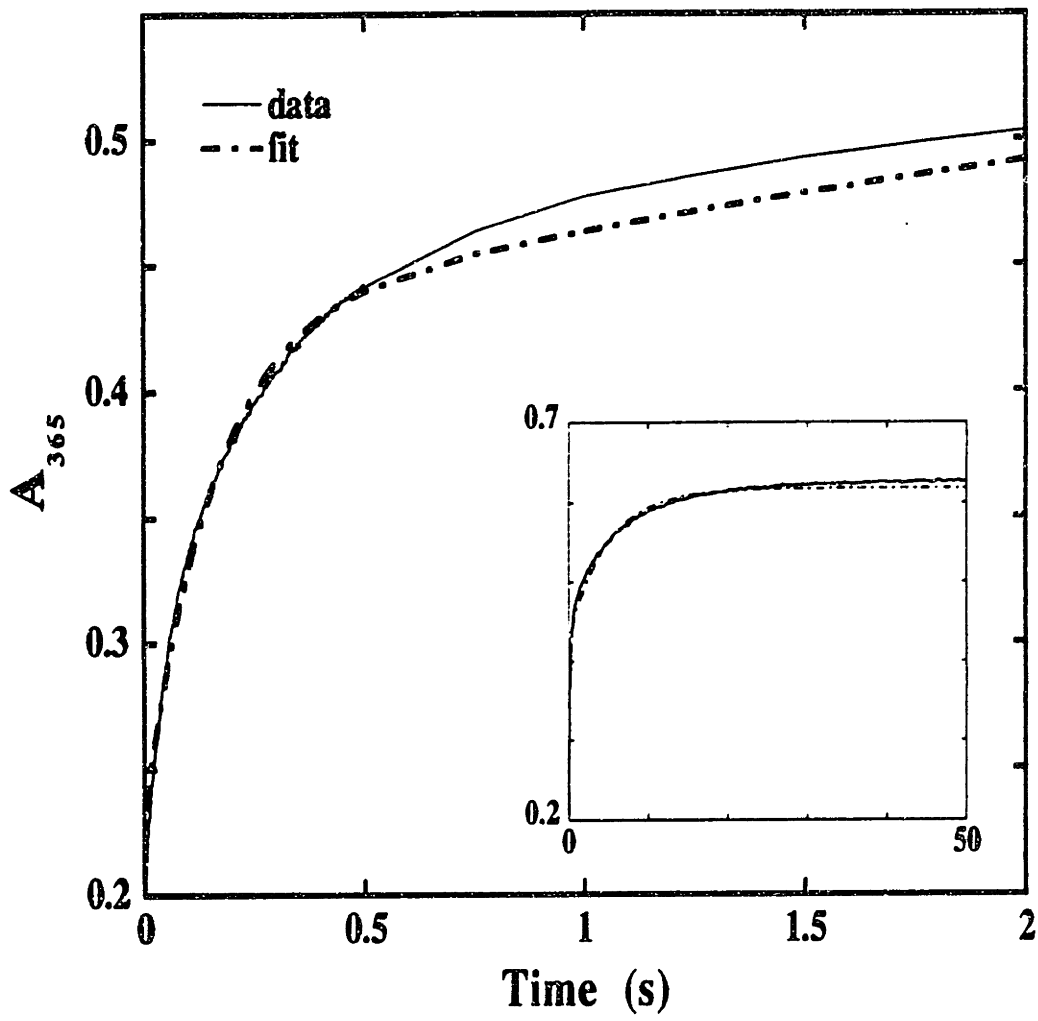


Table 2.3: Summary of least-squares fit to Scheme 2.2 of the A_{365} -versus-time traces from the reaction of Fe(II)-R2-wt with O_2 .

Expt.	Fit-range (s)	k_1 (s ⁻¹)	k_2 (s ⁻¹)
1	0.002 - 0.500	41	2.8
	0.002 - 1.02	35	1.9
	0.003 - 3.02	31	1.3
	0.003 - 20.0	34	0.99
2	0.002 - 0.500	46	2.6
	0.002 - 1.02	42	2.1
	0.003 - 3.02	35	1.5
3	0.002 - 0.500	64	3.7
	0.002 - 1.02	57	2.9
	0.003 - 3.02	41	1.7
	0.001 - 5.02	23	0.85
4	0.002 - 0.500	67	3.6
	0.002 - 1.00	58	2.8
	0.002 - 3.00	45	1.7
	0.002 - 5.00	20	0.9
	0.002 - 20.0	25	0.95

that in the apo R2-R2-Y122F by a factor of approximately 2. In contrast, the rate constant for conversion of X into the diferric cluster in the Fe(II)-R2-Y122F reaction is identical (within experimental variation) to that in the apo R2-Y122F reaction.

Reaction of Fe(II)-R2 -wt with O₂ as Monitored by RFQ-EPR Spectroscopy

The reaction at 5 °C of Fe(II)-R2-wt with O₂ was also monitored by EPR spectroscopy. The results confirm that X is rapidly formed in this reaction. Time-resolved spectra are shown in Fig. 2.7. At early time-points, the spectra are dominated by the isotropic, $g = 2.00$ signal of X. Over time, the doublet signal characteristic of •Y122 appears while the signal of X decays. The EPR spectrum at completion of reaction is characteristic of •Y122. When the reaction was carried out with ⁵⁷Fe²⁺ (Fig. 2.8), the ⁵⁷Fe hyperfine couplings are identical to that observed previously (Bollinger, 1992).

As demonstrated previously by Bollinger *et al.*, analysis of the spectrum at each time-point allowed for accurate quantitation as a function of time of the quantities of X and •Y122 (Table 2.4). This quantitation allowed rate constants for formation and decay of X and for the formation of •Y122 to be determined. At all times during the reaction, the spectrum can be accounted for as the sum of the spectra of X and •Y122. Using the relative quantities of the two species estimated for each time-point, along with the double integrated intensity for each spectrum, the absolute quantities of X and of •Y122 in each sample can be determined. As shown in Table 2.4, X accumulates rapidly, reaches its maximum value at ~0.032 s, and begins to decay after 0.059 s. After an initial lag, quantities of •Y122 rise smoothly. The •Y122/R2 ratio at 60 s (completion of reaction) is 1.2 ± 0.1 , which is in good agreement with the SF-Abs results.

Over the entire time-course, the quantities of •Y122 measured by EPR correlate well with the measured quantities of •Y122 based on the SF-Abs data (Fig. 2.9). At very short reaction time ($t > 50$ ms) the quantity of •Y122 measured by EPR appears only slightly higher than those measured by SF-Abs, probably due to small amount of residual O₂ in the Fe(II)-R2-wt sample. Non-linear least squares fitting of

Fig. 2.7: Time-course of the reaction of Fe(II)-R2-wt ($\text{Fe}^{2+}/\text{R2} = 5$) with O_2 as monitored by EPR spectroscopy. The reaction conditions (after mixing) were: 200 μM R2-wt, 1.0 mM Fe^{2+} , 1 mM O_2 , 100 mM HEPES, pH 7.6, 5 $^\circ\text{C}$. The reaction was quenched (A) at 0.025 s, (B) at 0.093 s, (C) at 0.46 s, (D) at 0.74 s, and (E) at 60 s. The spectra were acquired at 20 K with a microwave power of 1 μW , a frequency of 9.43 GHz, a modulation frequency of 100 kHz, a modulation amplitude of 4 G, a time constant of 200 ms, a scan time of 200 s, and a receiver gain of 4×10^4 .

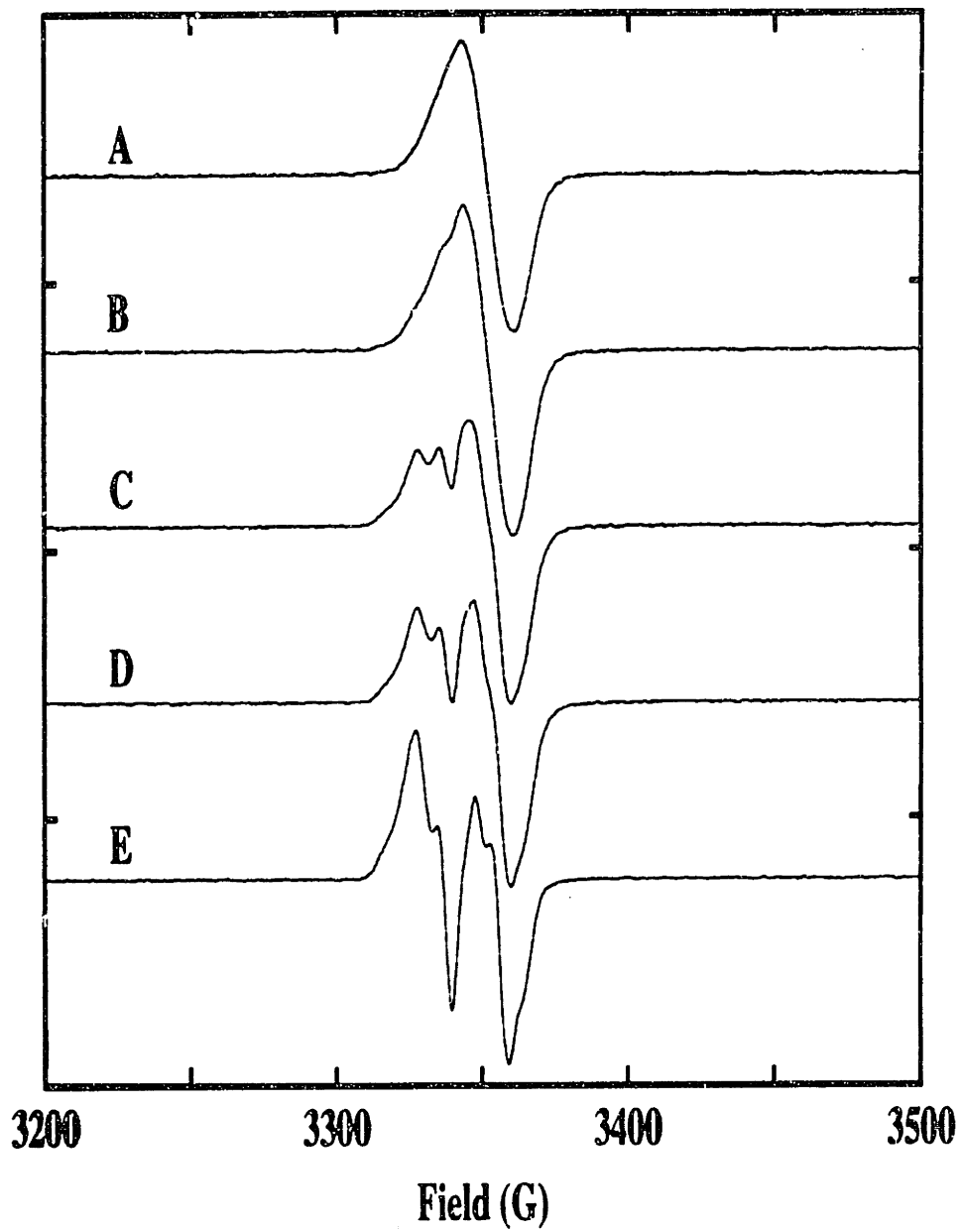


Fig. 2.8: EPR spectra of the reaction of Fe(II)-R2-wt with O₂ quenched at 0.044 s. The reaction conditions (after mixing) were: 200 μM R2-wt, 1 mM O₂, 100 mM HEPES, pH 7.6, 5 °C, and (A) 1.0 mM ⁵⁶Fe²⁺, or (B) 1.0 mM ⁵⁷Fe²⁺. The spectra were acquired at 20 K with a microwave power of 1 μW, a frequency of 9.43 GHz, a modulation frequency of 100 kHz, a modulation amplitude of 4 G, a time constant of 200 ms, a scan time of 200 s, and a receiver gain of 4 × 10⁴.

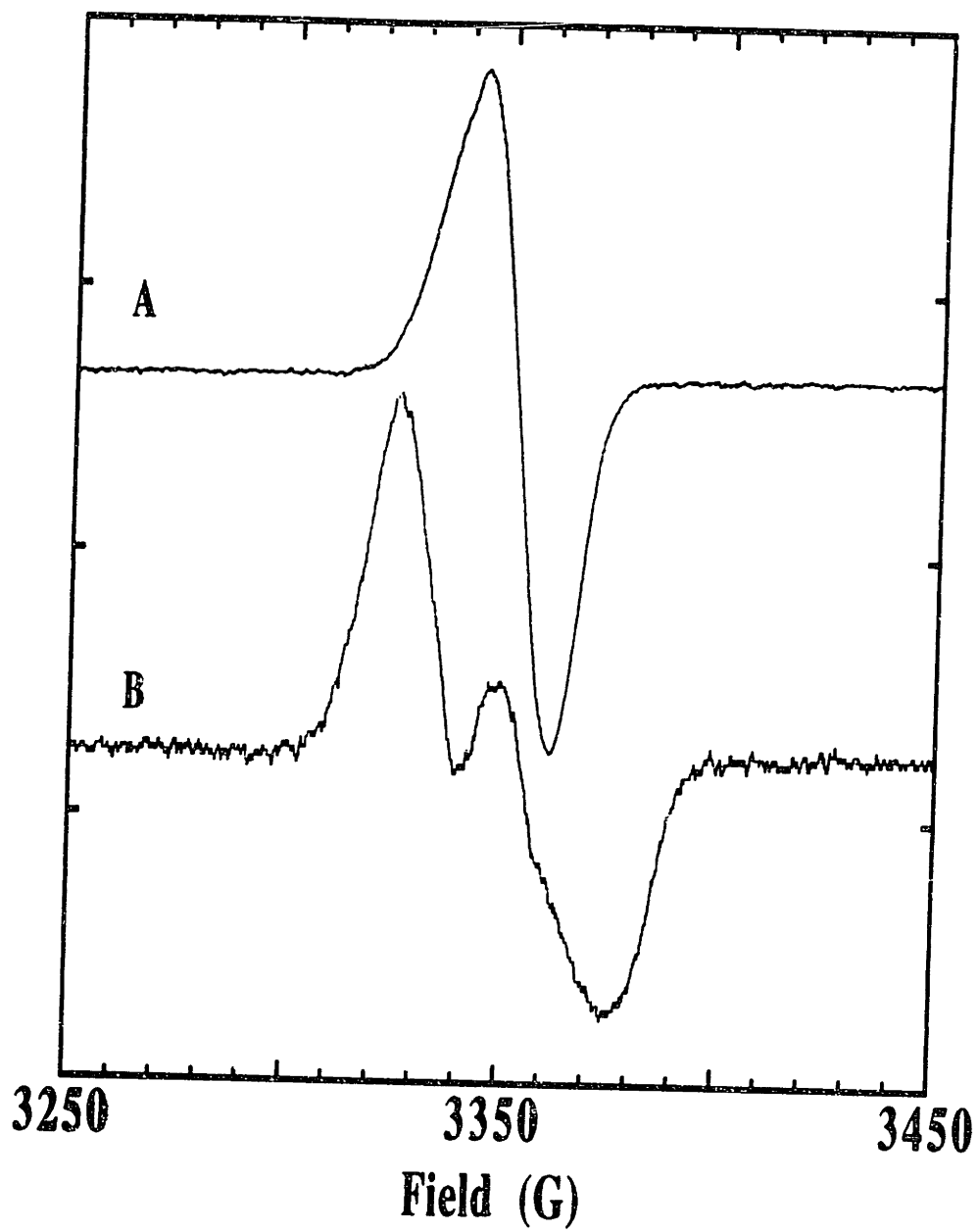


Fig. 2.9: Kinetics of formation of X and •Y122 in the reaction of Fe(II)-R2-wt with O₂. The quantities of X and •Y122 are from the EPR data in Table 2.4. The trace for •Y122 is from the SF-Abs experiment in Fig. 2.3. The reaction conditions for the EPR experiment are identical to those in Fig. 2.7.

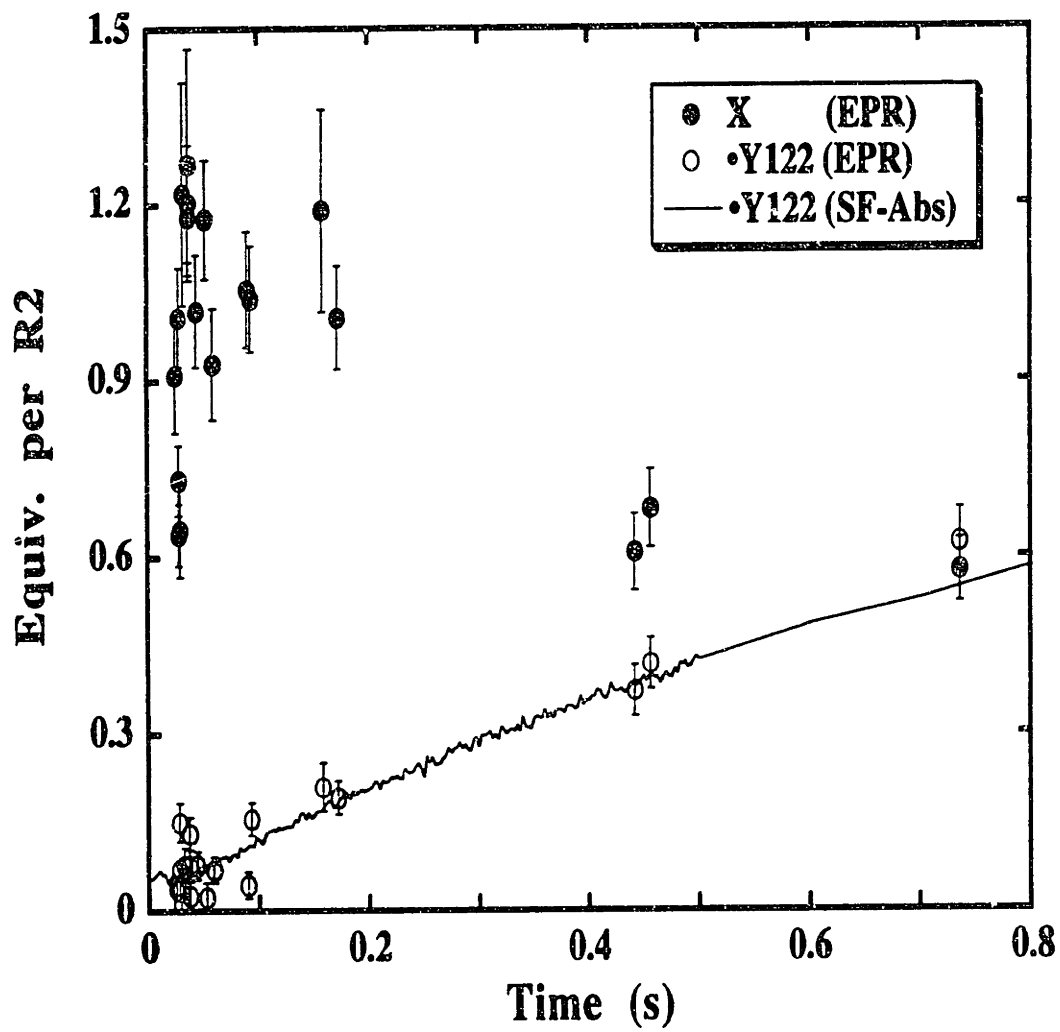


Table 2.4: Summary of the analysis for the EPR spectra from the reaction of Fe(II)-R2-wt with O₂ under excess Fe²⁺ conditions.

Expt.	Time (s)	% X	% •Y122	Spin/R2	X/R2	•Y122/R2
1 ¹	0.025	96 ± 2	4 ± 2	0.95 ± 0.1	0.91 ± 0.10	0.04 ± 0.02
	0.032	94 ± 2	6 ± 2	1.3 ± 0.2	1.2 ± 0.19	0.08 ± 0.03
	0.044	93 ± 2	7 ± 2	1.1 ± 0.1	1.0 ± 0.10	0.08 ± 0.02
	0.059	93 ± 2	7 ± 2	1.0 ± 0.1	0.93 ± 0.10	0.07 ± 0.02
	0.093	87 ± 2	13 ± 2	1.2 ± 0.1	1.0 ± 0.09	0.16 ± 0.03
	0.172	84 ± 2	16 ± 2	1.2 ± 0.1	1.0 ± 0.09	0.19 ± 0.03
	0.456	62 ± 2	38 ± 2	1.1 ± 0.1	0.68 ± 0.07	0.42 ± 0.04
	0.736	48 ± 2	52 ± 2	1.2 ± 0.1	0.58 ± 0.05	0.62 ± 0.06
	60	0	100	1.1 ± 0.1	0	1.2 ± 0.1
2 ²	0.028	98 ± 2	2 ± 2	0.66 ± 0.08	0.65 ± 0.08	0.01 ± 0.01
	0.037	98 ± 2	2 ± 2	1.3 ± 0.2	1.3 ± 0.20	0.03 ± 0.03
	0.052	98 ± 2	2 ± 2	1.2 ± 0.1	1.2 ± 0.10	0.02 ± 0.02
	0.090	96 ± 2	4 ± 2	1.1 ± 0.1	1.1 ± 0.10	0.04 ± 0.02
	0.158	85 ± 2	15 ± 2	1.4 ± 0.2	1.2 ± 0.17	0.21 ± 0.04
	0.442	62 ± 2	38 ± 2	0.98 ± 0.1	0.61 ± 0.07	0.37 ± 0.04
	0.742	41 ± 2	59 ± 2	-	-	-
	60	0	100	1.2 ± 0.1	0	1.2 ± 0.1
	3	0.028	95 ± 2	5 ± 2	0.77 ± 0.06	0.73 ± 0.06
0.028		87 ± 2	13 ± 2	1.2 ± 0.1	1.0 ± 0.08	0.15 ± 0.03
0.028		90 ± 2	10 ± 2	0.71 ± 0.06	0.64 ± 0.05	0.07 ± 0.02
0.037		90 ± 2	10 ± 2	1.3 ± 0.1	1.2 ± 0.1	0.13 ± 0.03
0.037		94 ± 2	6 ± 2	1.3 ± 0.1	1.2 ± 0.1	0.08 ± 0.03
60		0	100	1.2 ± 0.1	0	1.2 ± 0.1

¹Total spin per R2 was calculated assuming a packing factor of 0.67.

²Total spin per R2 was calculated assuming a packing factor of 0.65.

the equation for a first order growth to the 0.05 - 60 s region of the EPR time-course of •Y122 (Fig. 2.10) gives a k_{obs} of $0.95 \pm 0.1 \text{ s}^{-1}$. Fitting the 0.05 - 60 s region of the EPR time-course of X to a first-order process gives a k_{obs} of $1.0 \pm 0.1 \text{ s}^{-1}$ (Fig. 2.11). These results are consistent with the SF-Abs data and suggest that X decays to give rise to •Y122.

In a further attempt to assess the validity of Scheme 2.2 and to determine values for k_1 and k_2 , the measured quantities of X and •Y122 were analyzed simultaneously. Fitting the measured quantities of X and •Y122 to the kinetic model of Scheme 2.2 gives a k_{obs} of 60 - 80 s^{-1} for formation of X, and a k_{obs} of 1.0 s^{-1} for decay of X and concomitant formation of •Y122 (Fig. 2.12). The theoretical curve agrees reasonably well with the experimental data. These results are in good agreement with the SF-Abs data which suggest that the intermediate X generates •Y122 with a k_{obs} of 0.8 - 0.9 s^{-1} .

Reaction of Fe(II)-R2-Y122F with O₂ as Monitored by RFQ-EPR Spectroscopy

As with R2-wt, when Fe(II)-R2-Y122F is mixed with O₂ at 5 °C, the sharp isotropic $g = 2.00$ singlet characteristic of X develops. Between reaction time of 0.037 to 1.04 s, the lineshape of the spectrum does not change with time (data not shown), indicating that X is the only EPR active species in the reaction. Spin quantitation as a function of time for the reaction suggests that X exhibits the increased lifetime in R2-Y122F as predicted for the •Y122-generating intermediate in R2-wt (Fig. 2.13). Table 2.5 indicates that the amount of X in the R2-Y122F reaction rises continuously from 0.03 to 0.28 s, at which point, spin quantitation indicates that 0.7 equiv. of X per R2 is present. In contrast, the amount of X in the R2-wt reaction reaches its maximum (~ 1.2 equiv.) at ~ 0.03 s.

Fig. 2.10: Non-linear least-squares fitting of the measured quantity of $^{\bullet}\text{Y122}$ as a function of time in the reaction of Fe(II)-R2-wt with O_2 . The theoretical curve was obtained by fitting a first-order process to the 0.05 - 60 s region of the experimental data, and corresponds to a k_{obs} of $0.95 \pm 0.1 \text{ s}^{-1}$.

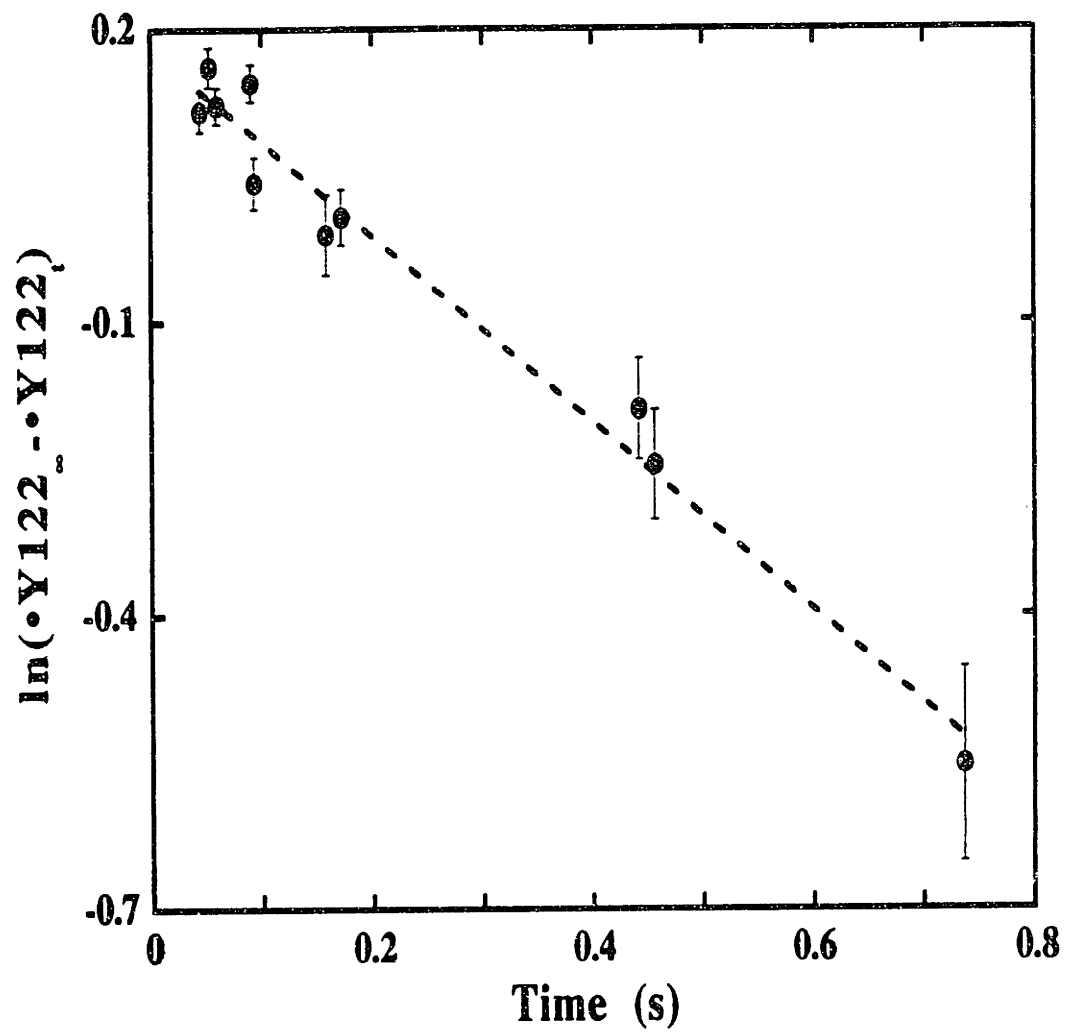


Fig. 2.11: Non-linear least-squares fitting of the measured quantity of X as a function of time in the reaction of Fe(II)-R2-wt with O₂. The theoretical curve was obtained by fitting a first-order process to the 0.05 - 60.0 s region of the experimental data, and corresponds to a k_{obs} of $1.0 \pm 0.1 \text{ s}^{-1}$.

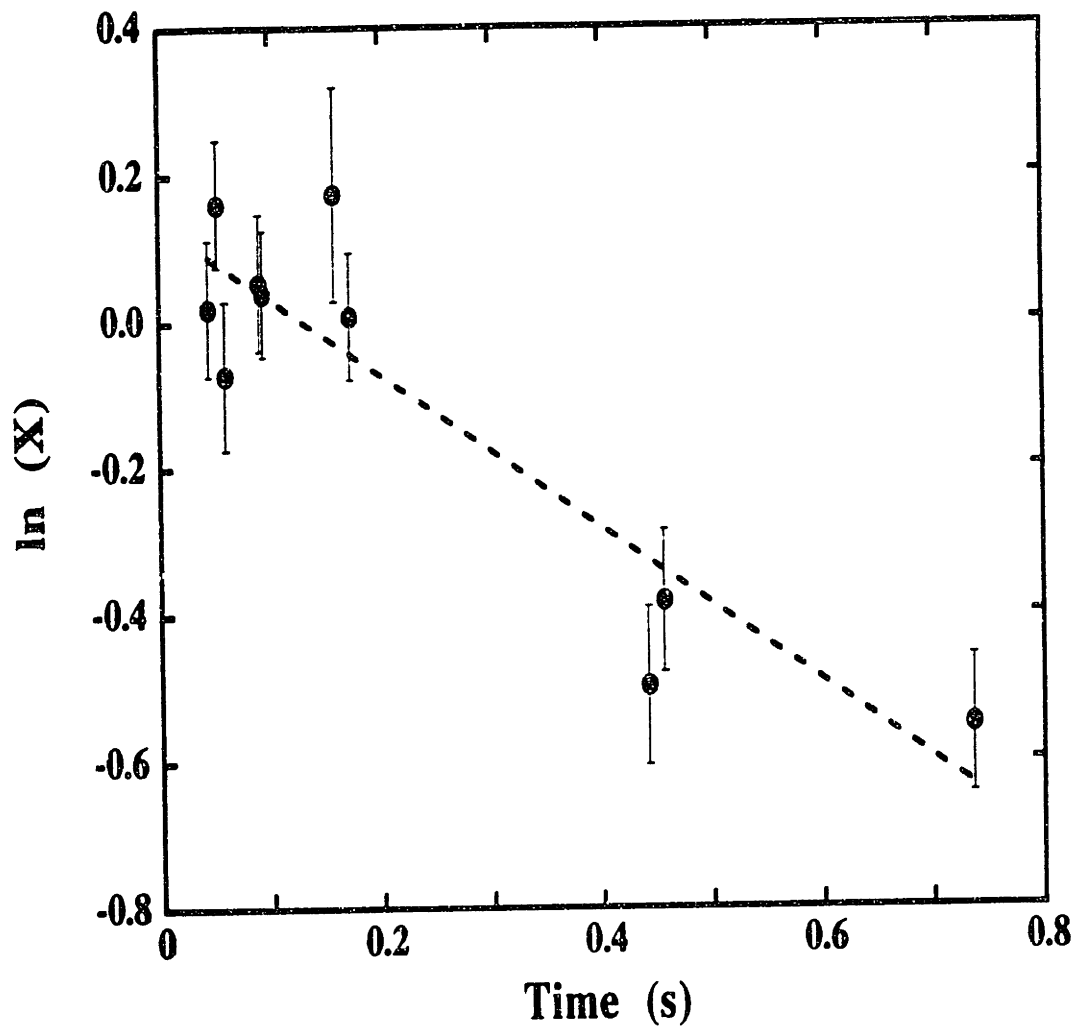


Fig. 2.12: Non-linear least-squares fitting of the measured quantity of X as a function of time to two sequential, first-order processes, with a k_1 of 60 s^{-1} and a k_2 of 1.0 s^{-1} . The reaction conditions are identical to those in Fig. 2.7.

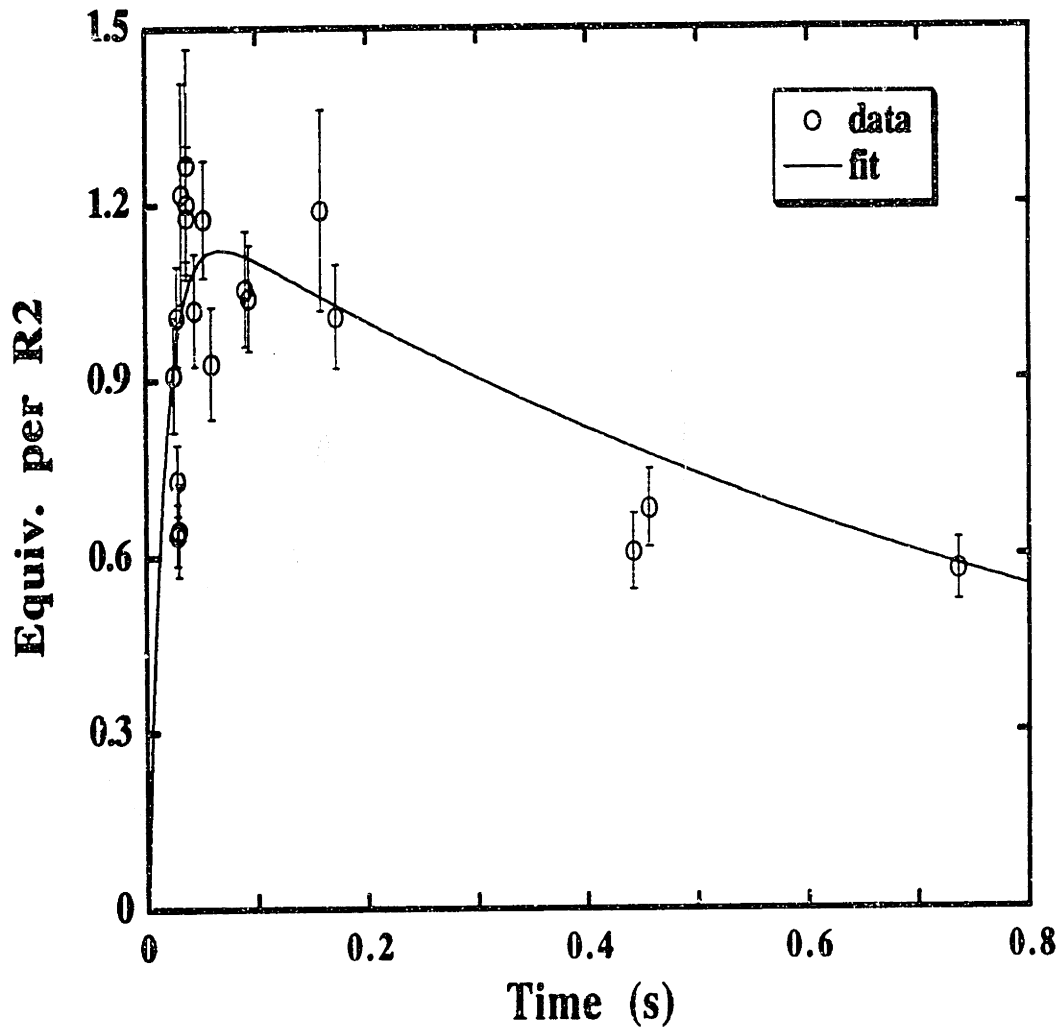


Fig. 2.13: Measured quantity of X as a function of time in the reaction of Fe(II)-R2-Y122F with O₂ under excess Fe²⁺ conditions as monitored by EPR spectroscopy. The reaction conditions (after mixing) were: 200 μM R2-wt, 1.0 mM Fe²⁺, 1.0 mM O₂, 100 mM HEPES, pH 7.6, 5 °C. The spectra were acquired at 20 K with a microwave power of 1 μW, a frequency of 9.47 GHz, a modulation frequency of 100 kHz, a modulation amplitude of 4 G, a time constant of 160 ms, a scan time of 170 s, and a receiver gain of 4 x 10⁴.

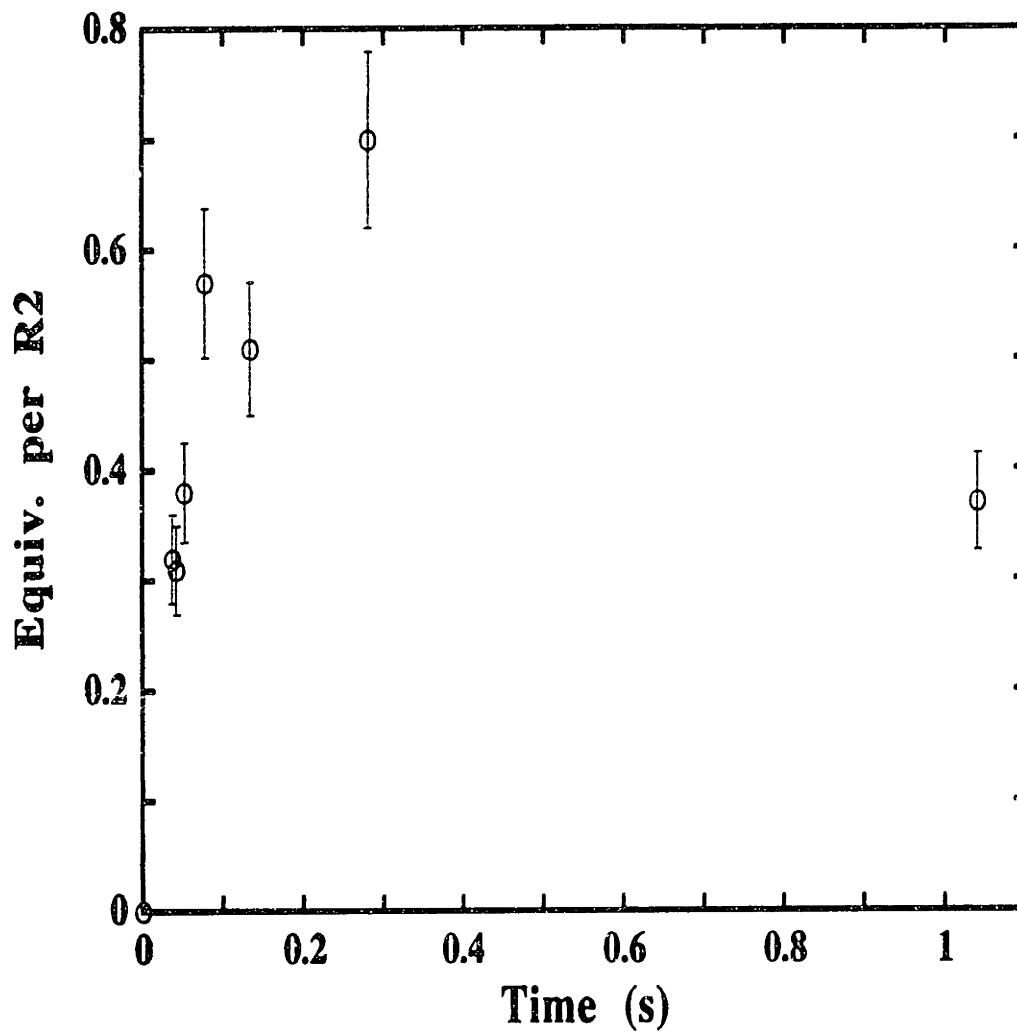


Table 2.5: Quantitation of X in the time-resolved EPR spectra of the reaction of Fe(II)-R2-Y122F with O₂ under excess Fe²⁺ conditions. Total spin was calculated assuming a packing factor of 0.67.

Reaction Time (s)	Equiv. X
0.037	0.32 ± 0.03
0.042	0.31 ± 0.03
0.052	0.38 ± 0.04
0.078	0.57 ± 0.06
0.134	0.51 ± 0.05
0.281	0.70 ± 0.07
1.04	0.37 ± 0.04

Mössbauer Time-course of the Reaction of Fe(II)-R2-wt with O₂

As demonstrated previously by Bollinger *et al.*, RFQ-Möss spectroscopy provides an additional method to monitor the reconstitution reaction (Bollinger, 1992; Bollinger *et al.*, 1994a; Bollinger *et al.*, 1994b). With the spectra of Fig. 2.14 as references, RFQ-Möss spectroscopy was used to monitor the time-course of the reaction of Fe(II)-R2-wt with O₂ (Fig. 2.15). In the first time-point taken (0.028 s, Fig. 2.15A), the spectrum is dominated by the features of X (see below for quantitation). At this time-point, a significant quantity of unreacted Fe²⁺ ion still remains, while only a very small quantity of the diferric cluster is apparent. With increasing reaction time, the contribution from Fe²⁺ ion decreases, while that from diferric cluster increases (Fig. 2.15B and C). Finally, at completion of the reaction (Fig. 2.15D), the features of the diferric cluster dominate the spectrum.

Table 2.6: Parameters for the reference spectra used in the quantitative analysis of the Mössbauer spectra of the time-course samples.

Species	Site	δ (mm/s)	ΔE_Q (mm/s)	$A/g_n\beta_n$ (T)	η
ferrous R2 ^a	1	1.31 ± 0.03	3.24 ± 0.06	-	-
	2	1.20 ± 0.03	2.92 ± 0.06	-	-
diferric R2 ^a	1	0.54 ± 0.03	1.64 ± 0.06	-	-
	2	0.45 ± 0.03	2.41 ± 0.06	-	-
X ^b	1	0.56 ± 0.03	-0.90 ± 0.10	-53.0, -51.6, -52.3	0.5 ± 0.2
	2	0.26 ± 0.04	-0.60 ± 0.10	+19.6, +26.3, +26.3	2.7 ± 0.3
fast-relaxing ferric species ^a		0.56 ± 0.03	0.95 ± 0.03	-	-
putative peroxo-diiron (III) species ^c		0.66 ± 0.03	1.51 ± 0.06	-	-
putative ferryl species ^c		0.09 ± 0.03	0.60 ± 0.06	-	-

^aparameters from Bollinger et al. (Bollinger, 1992)

^bparameters from Sturgeon et al. (Sturgeon *et al.*, 1996)

^csimulation of the data

Quantitation of X and the Diferric Cluster as Functions of Time

Using the reference spectra in Fig. 2.14, X and the diferric cluster can be quantitated as functions of time from the Mössbauer spectra of the time-course samples. Table 2.7 summarizes the quantities of the two species determined for each time-point in the reaction of Fe(II)-R2-wt ($Fe^{2+}/R2 = 5$) at 5 °C with O₂, and Fig. 2.16 shows a plot of the data. The measure quantities of X from the EPR data were included for comparison. As shown in Fig. 2.16, X accumulates to 1.1 ± 0.1

Fig. 2.14 Experimental reference spectra for ferrous-R2 (A), the diferric cluster(B), and the diiron intermediate X (C, outer spectrum). Preparation of the samples used to acquire these spectra was described previously by Bollinger *et al.* (1992). The inner spectrum of C is a theoretical spectrum for X generated using the parameters reported by Sturgeon *et al.* (1996) The parameters for these spectra are also shown in Table 2.6.

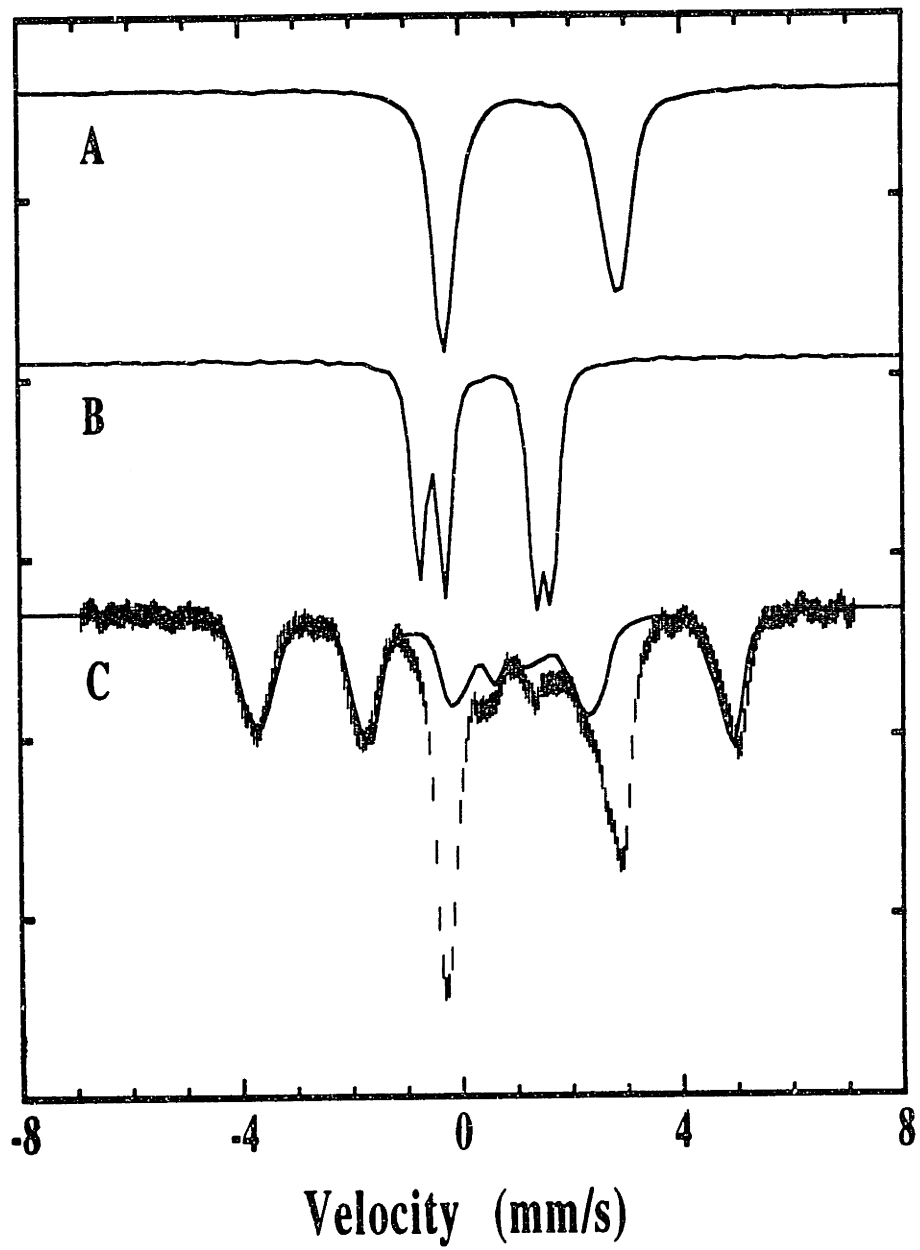


Fig. 2.15: Time-course of the reaction of Fe(II)-R2-wt with O₂ as monitored by Mössbauer spectroscopy. The reaction conditions (after mixing) were: 300 μM R2-wt, 1.5 mM Fe²⁺, 1 mM O₂, 100 mM HEPES, pH 7.6, 5 °C. The reaction was quenched (A) at 0.028 s, (B) at 0.052 s, (C) at 0.64 s, (D) at 14 min. The experimental spectra were acquired at 4.2 K with a magnetic field of 50 mT applied parallel to the γ-beam. The solid line plotted over the data in A is the reference spectrum for ferrous-R2 (Bollinger, 1992). It is scaled to 30 % of the integrated intensity of the experimental spectrum and corresponds to 1.5 equiv. of Fe²⁺ per R2 subunit. The solid line plotted just above the data in A is the reference spectrum of X scaled to 44 % of the intensity of the experimental spectrum and corresponds to 1.1 equiv. of X per R2. In B and C, the solid line above the data is the reference spectrum of the X (1.2 equiv. in B and 0.50 equiv. in C). The line plotted over the data in B is the reference spectrum of ferrous-R2 (1.1 equiv. Fe²⁺). The line plotted over the data in C is the reference spectrum of diferric cluster (0.95 equiv.). In D, the solid line over the data is the reference spectrum of the diferric cluster (1.53 equiv.). The reference spectrum for X is a simulation based on the parameters reported by Sturgeon *et al.* (Table 2.6) (Sturgeon *et al.*, 1996). The reference spectra for ferrous-R2 and the diferric cluster were acquired on samples prepared by Bollinger *et al.* (Bollinger, 1992).

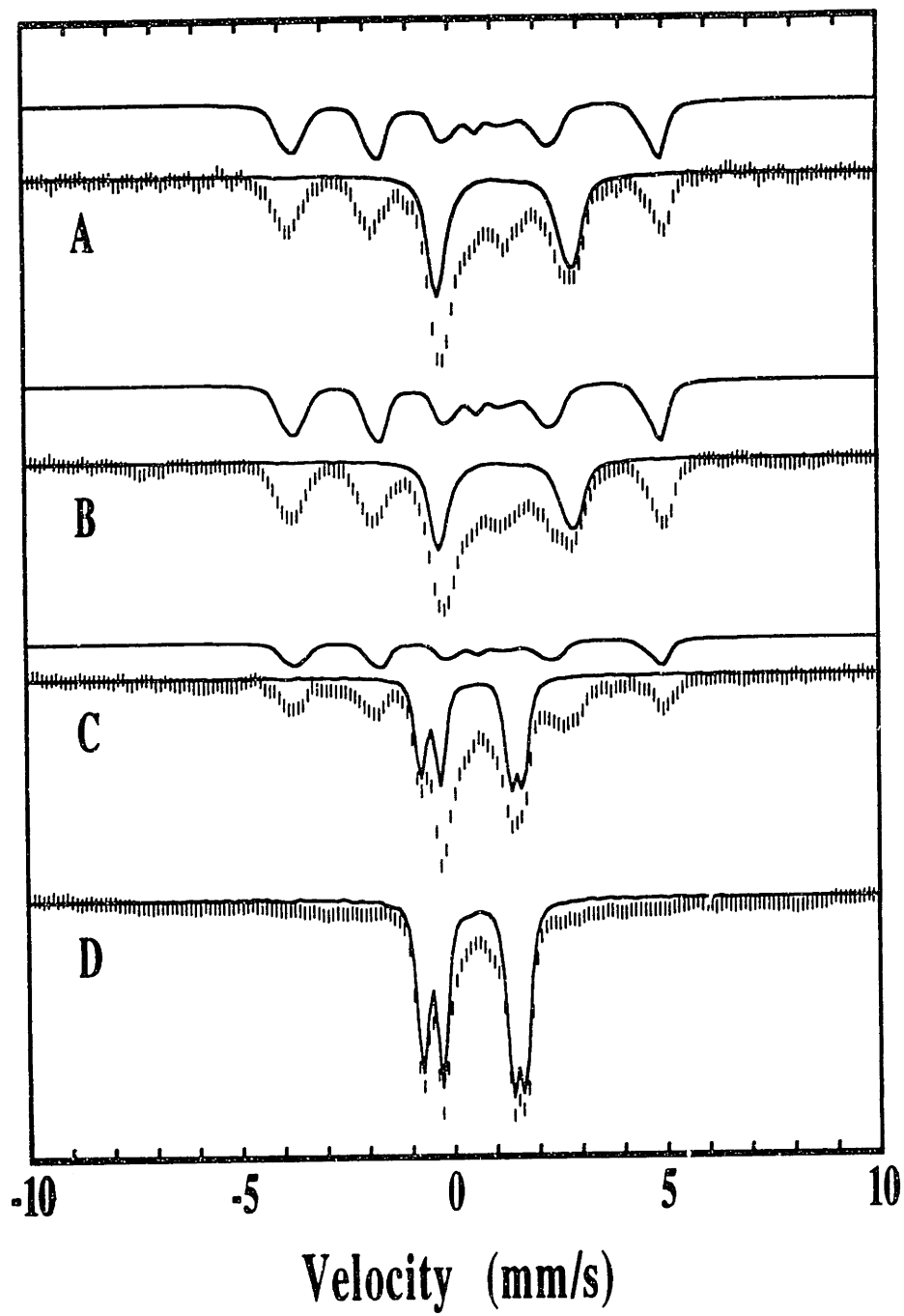


Fig. 2.16: Time-course of X in the reaction of Fe(II)-R2-wt with O₂ as monitored by RFQ-Mössbauer spectroscopy. The measured quantities of X of the corresponding EPR experiment are included for comparison. The reaction conditions for the Mössbauer experiment are identical to those in Fig. 2.15. The data for the EPR experiment are from Fig. 2.7.

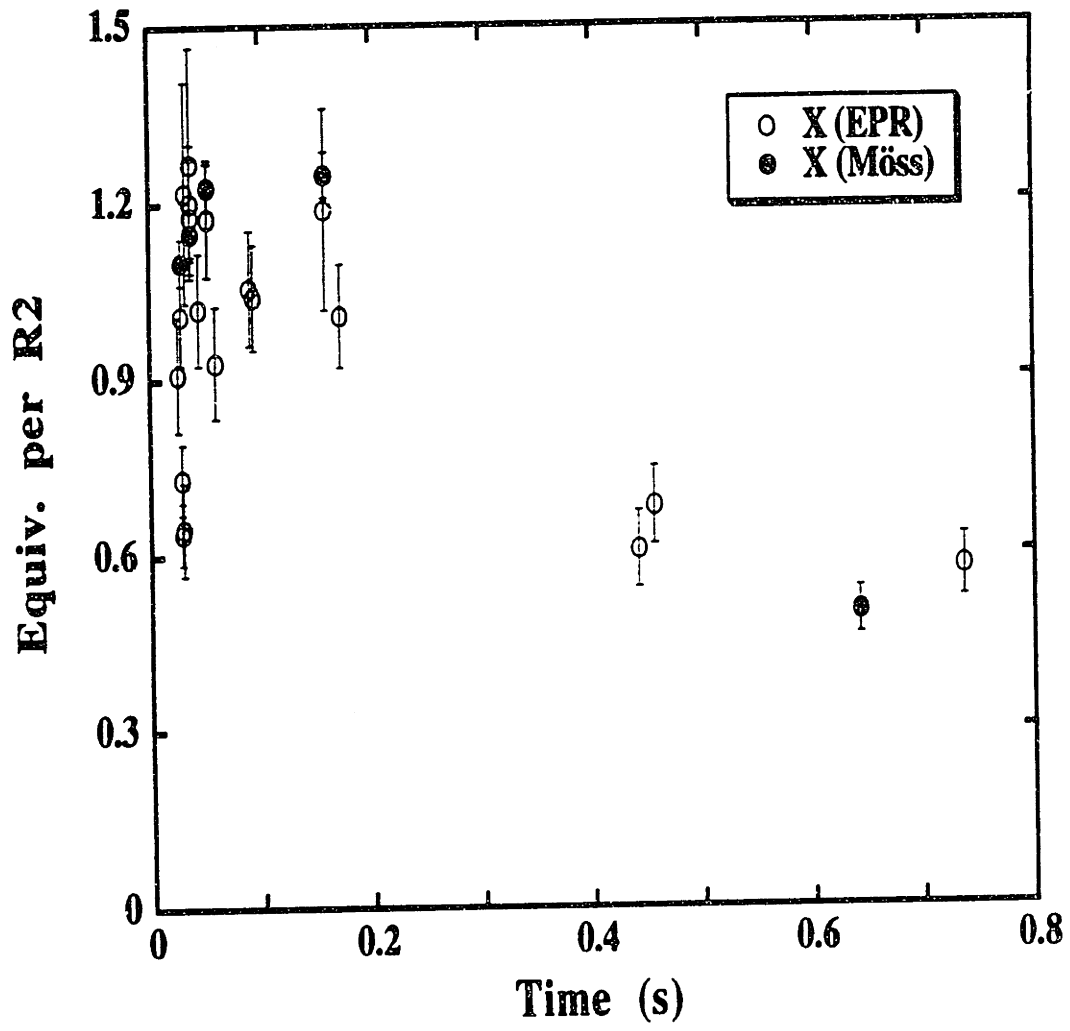


Table 2.7: Quantitative analysis of the Mössbauer spectra of the reaction of Fe(II)-R2 (5 Fe²⁺ / R2) with O₂.

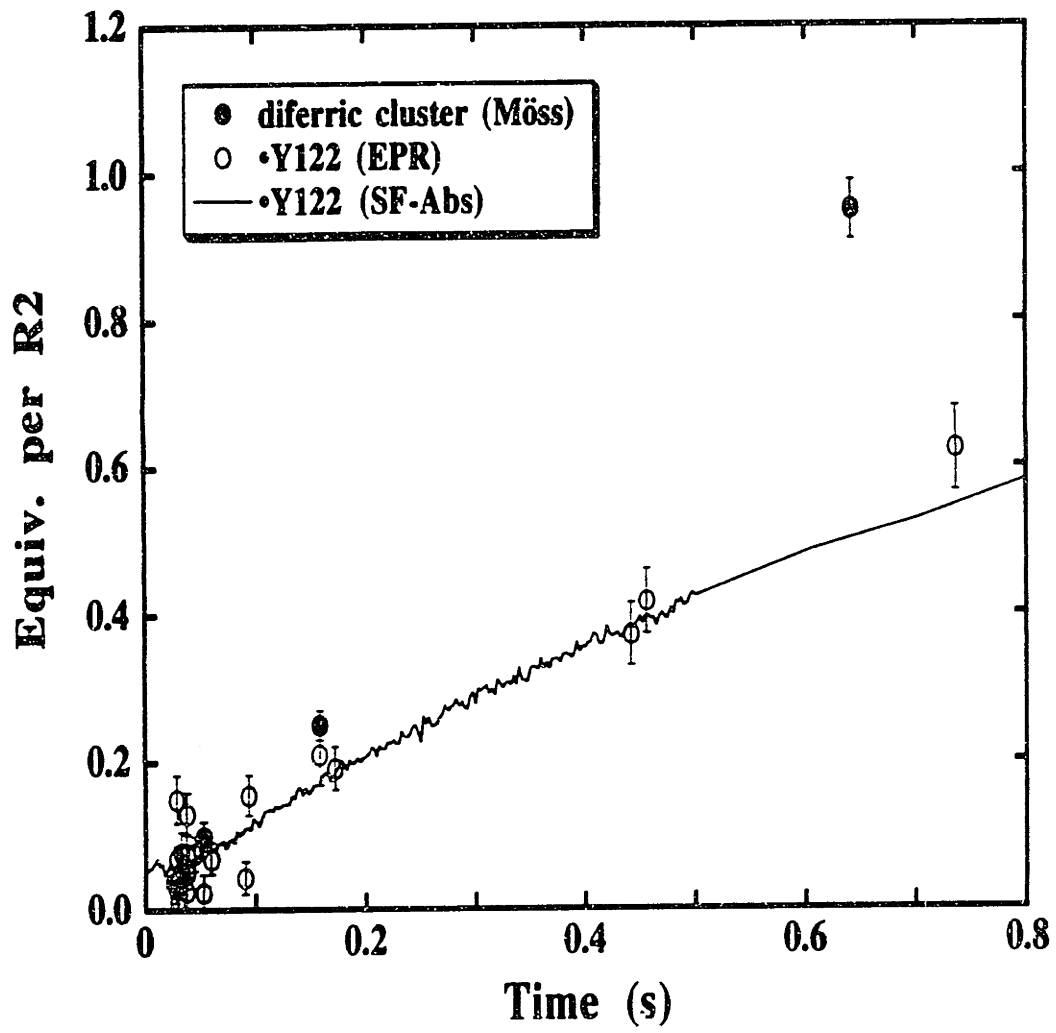
Reaction Time (s)	Equiv. Fe ²⁺	Equiv. diferric cluster	Equiv. X	Equiv. Fast-relaxng Fe ³⁺	Equiv. Peroxo Species	Equiv. Ferryl species	Equiv. High-spin Fe ³⁺	Equiv. Possible Fe ³⁺ Species
0.028	1.5 ± 0.04	< 0.07	1.10 ± 0.04	< 0.2	0.23 ± 0.02	0.35 ± 0.05	0	0.25 ± 0.08
0.037	1.5 ± 0.08	< 0.07	1.15 ± 0.04	0.15 ± 0.05	0.15 ± 0.02	0.25 ± 0.05	0.25 ± 0.04	0.10 ± 0.08
0.052	1.1 ± 0.08	0.10 ± 0.02	1.23 ± 0.04	0.35 ± 0.05	< 0.1	0.25 ± 0.05	0.30 ± 0.08	0.10 ± 0.08
0.158	0.86 ± 0.04	0.25 ± 0.02	1.25 ± 0.04	0.50 ± 0.05	0	0.25 ± 0.05	0.10 ± 0.04	0.60 ± 0.16
0.642	0.50 ± 0.08	0.95 ± 0.04	0.50 ± 0.04	0.50 ± 0.05	0	0.25 ± 0.05	< 0.10	0.60 ± 0.16
10.5	0.40 ± 0.04	1.15 ± 0.04	0.30 ± 0.04	0.45 ± 0.05	0	0.25 ± 0.05	< 0.10	0.75 ± 0.16
60.5	0.30 ± 0.04	1.30 ± 0.04	0.17 ± 0.04	0.45 ± 0.05	0	0.20 ± 0.05	0.20 ± 0.04	0.85 ± 0.16
840	0.14 ± 0.04	1.53 ± 0.04	0	0.40 ± 0.05	0	0.15 ± 0.05	< 0.10	1.2 ± 0.16

equiv. per R2 in the first time-point taken (0.028 s) and then begins to decay appreciably after 0.16 s. The quantity of the diferric cluster increases with time. Over the entire time-course, the quantities of X measured by Mössbauer spectroscopy correlate (within experimental uncertainty) with the quantities of X measured by EPR spectroscopy (Fig. 2.16). At the early time-points (0 - 0.2 s), the measured quantities of diferric cluster agree with the quantity of •Y122 measured by EPR spectroscopy, suggesting that these two species are generated concomitantly (Fig. 2.17). With increasing reaction time, however, the measured quantities of the diferric cluster become significantly larger than those of •Y122. At 0.64 s, the Mössbauer data indicate that 0.95 ± 0.04 equiv. of diferric cluster are present, while the SF-Abs data indicate that 0.50 ± 0.04 equiv. of •Y122 is present (Fig. 2.17). Furthermore, the EPR data indicate that only 0.62 ± 0.06 equiv. of •Y122 is present at 0.74 s (Table 2.4). In fact, in the four Mössbauer samples that span 0.64 s to 14 min, the measured quantities of diferric cluster (Table 2.7) are significantly greater than the measured quantities of •Y122 (Table 2.4). As mentioned above, the SF-Abs data indicate that the formation of •Y122 is completed in 10 s and that 1.2 equiv. of •Y122 per R2 are formed at this time-point. In contrast, the quantities of diferric cluster increase continuously from 0.95 equiv. at 0.64 s to 1.53 equiv. at 14 min (Table 2.7). These results, thus, suggest that 0.2 - 0.3 equiv. of X is converted to diferric cluster without oxidizing Y122 to •Y122.

Quantitation of the Fast-Relaxing Ferric Species

Previous studies by Bollinger et al. have shown that a stable or slowly decaying fast-relaxing ferric species is produced concomitantly with X (Bollinger *et al.*, 1994b). It was proposed that this Fe^{3+} species represents the product of the donation of the fourth electron by Fe^{2+} required for the formation of X. Therefore, the Mössbauer spectra of the time-course samples were examined carefully for the

Fig. 2.17: Time-course of the diferric cluster in the reaction of Fe(II)-R2-wt with O₂ as monitored by RFQ-Mössbauer spectroscopy. The measured quantities of •Y122 of the corresponding EPR experiment are included for comparison. The reaction conditions for the Mössbauer experiment are identical to those in Fig. 2.15. The data for the EPR experiment are from Fig. 2.7.



presence of the putative fast-relaxing ferric species. To create the inner spectra of Fig. 2.18, the reference spectra of ferrous-R2, X, and the diferric cluster were summed in ratios appropriate to approximate the amount of these species in the experimental spectrum (Table 2.7). Fig. 2.18 clearly shows that additional features are present in the 0 - 2 mm/s region of the spectrum. To estimate the quantity of the putative fast-relaxing species present in each of the time-course samples, the hypothetical spectrum (solid line above the data in Fig. 2.18) for a quadrupole doublet with $\delta = 0.56$ and $\Delta E_Q = 0.95$ (Bollinger, 1992; Bollinger *et al.*, 1994b) was compared to the experimental spectra. Using this hypothetical spectrum, the quantity of the putative fast-relaxing ferric species present in the time-course samples was determined. The quantitation of this species is summarized in Table 2.7. In the first time-point taken (0.028 s), < 0.2 equiv. of the putative fast-relaxing ferric species is present. With increasing reaction time, the measured quantity of the fast-relaxing ferric species rises and accumulates to $\sim 0.4 - 0.5$ equiv. Fe^{3+} per R2 upon completion of the reaction. Fitting the measured quantities of this species to the equation for a first-order process gives a k_{obs} of 22 s^{-1} (Fig. 2.19), which is significantly greater than the k_{obs} (7.3 s^{-1}) in the reaction of apo R2 with excess Fe^{2+} (Bollinger, 1992; Bollinger *et al.*, 1994b). The results summarized in Table 2.7, however, suggest that the putative fast-relaxing species is not a major component of the reaction. In the 0.028 s time-point, < 0.2 equiv. of the putative fast-relaxing ferric species is present, even though 1.1 ± 0.1 equiv. of X has already accumulated. These results imply that this ferric species accumulates to $< 20\%$ of the quantity which would be expected if it arises from delivery of an electron from Fe^{2+} ion to generate X.

Analysis of the Mössbauer Time-course for Additional Components

Examination of the Mössbauer time-course also reveals additional features that are not associated with any of the previously defined components. An attempt to illustrate this observation is shown in Fig. 2.20 and Fig. 2.21. The inner spectrum of Fig. 2.20 is generated by summing the reference spectra of ferrous-R2, X, the diferric cluster and the fast-relaxing ferric species in ratios which approximate the amount of these species in the experimental spectrum (Table 2.7). Fig. 2.20 clearly shows additional features in the 1 - 2 mm/s region of the spectrum. Because the features contribute a small fraction of the integrated intensity of any given spectrum, it is not possible to unambiguously define the spectra of these additional components. Nevertheless, analysis of the entire time-course has allowed Prof. Huynh to deduce hypothetical spectra for three additional components. Perhaps the most interesting of these is a partially resolved peak centered at approximately 1.2 mm/s. Assuming that the resolved peak is the high energy line of a quadruple doublet, and assuming that the low energy line is obscured by the low energy line of the ferrous ion spectrum, a hypothetical spectrum was generated with $\delta = 0.66$ and $\Delta E_Q = 1.51$ mm/s (Fig. 2.20). If this hypothetical spectrum is representative of the unknown species, these parameters would identify it as similar to the peroxo-diiron intermediate ($\text{MMOH}_{\text{peroxo}}$) observed in the catalytic cycle of methane monooxygenase hydroxylase from *M. capsulatus* (Bath). Again, assuming that the hypothetical spectrum of Fig. 2.20 is accurate, the species accumulates to 0.23 equiv. per R2 in the first time-point taken (0.028 s). The resolved peak at ~ 1.5 mm/s is only prominent in the first time-point of the reaction (0.028 s) and decays rapidly with increasing reaction time. The possible mechanistic significance of these observations is discussed below.

In addition, a feature at ~ 0.0 mm/s is apparent in the spectra of several time-course samples. This feature appears as a shoulder on the low energy line of the

Fig. 2.18: Quantitation of the putative fast-relaxing ferric species. The experimental spectrum is of the 0.028 s time-point in Fig. 2.15. The inner spectrum is the sum of the spectra of ferrous-R2, diferric cluster and X, in proportions indicated in Table 2.7. The solid line plotted above the data is the hypothetical reference spectrum for the fast-relaxing ferric species scaled to 4 % of the total intensity of the experimental spectrum. The parameters used to generate the reference spectra are given Table 2.6.

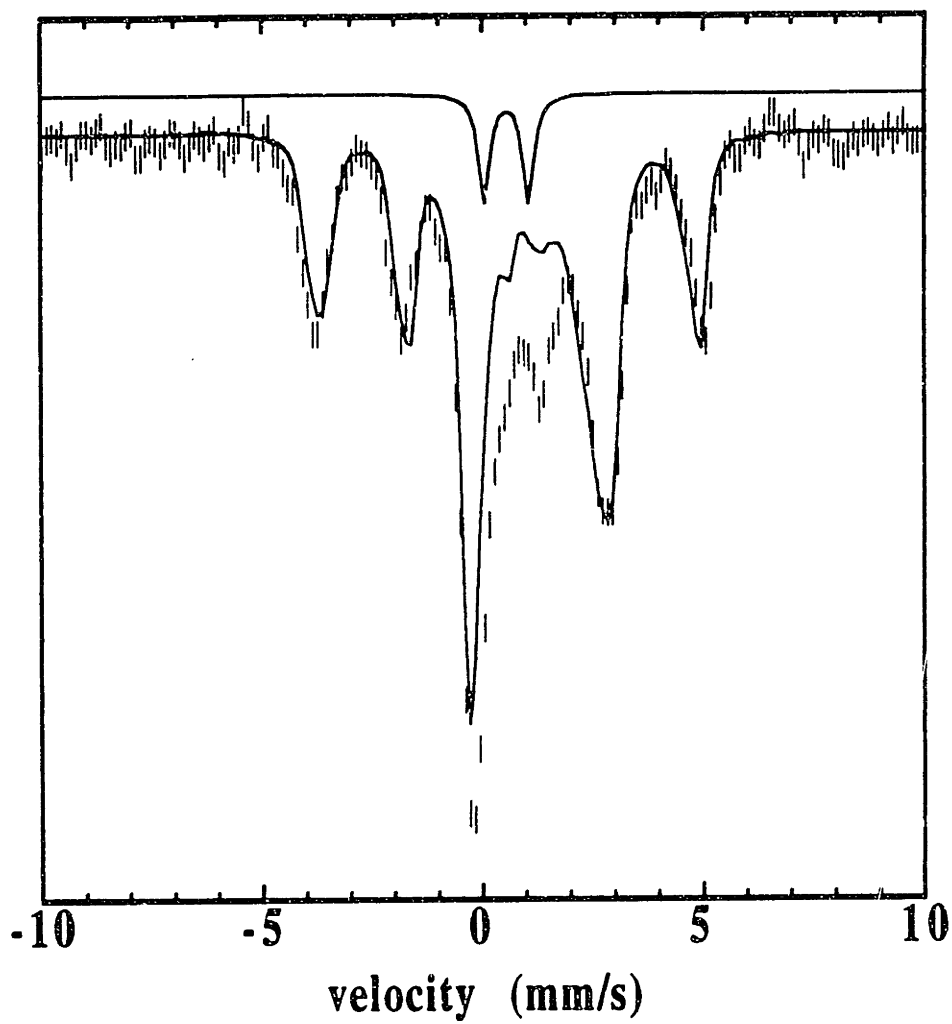


Fig. 2.19: Least-squares fitting of the measured quantity of the fast-relaxing ferric species as a function of time to the equation of a first-order process with a rate constant of 22 s^{-1} . The reaction conditions are identical to those in Fig. 2.15.

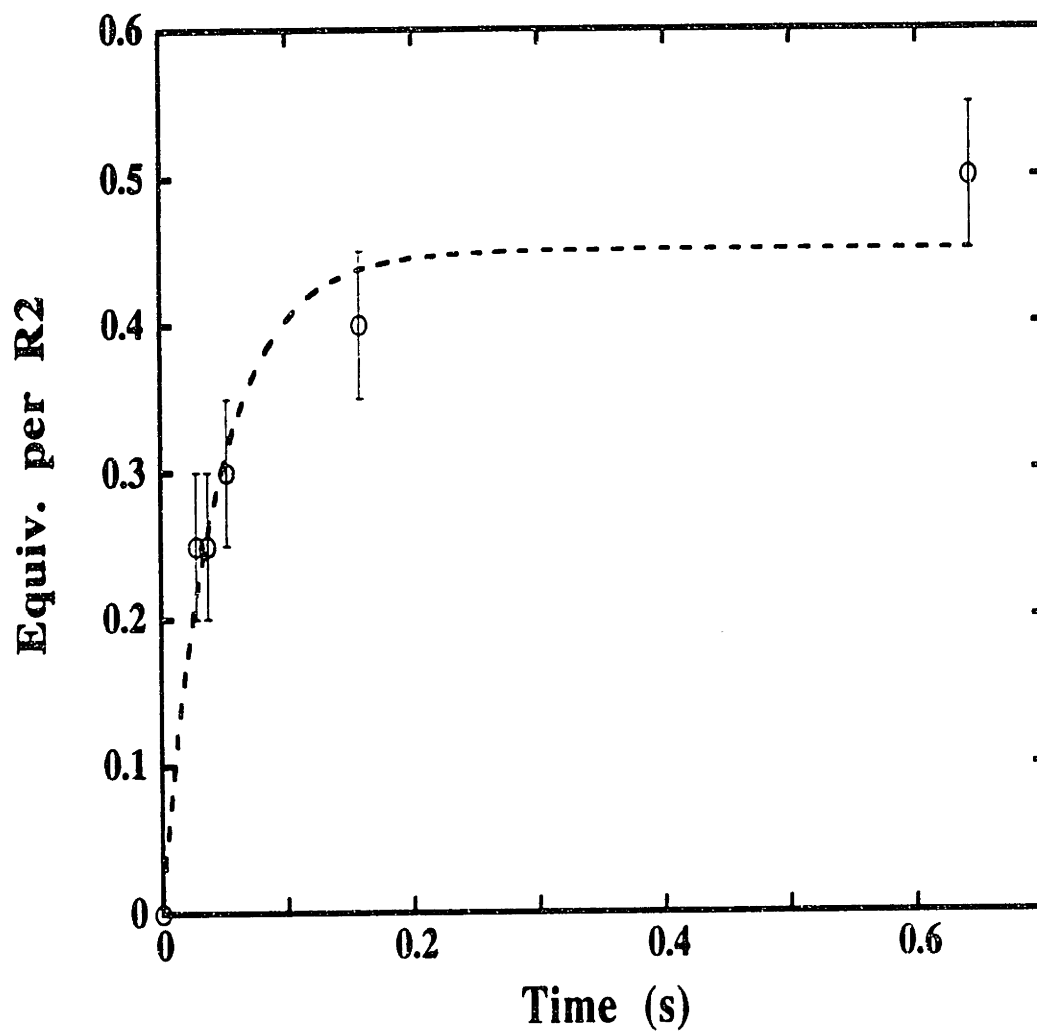


Fig. 2.20: Mössbauer spectrum showing a partially resolved peak at approximately 1.2 mm/s in the 0.028 s time-point of the reaction shown in Fig. 2.15. The inner spectrum is the sum of the spectra of ferrous-R2, diferric cluster, X and the fast-relaxing ferric species, in proportions indicated in Table 2.7. The solid line plotted above the data is the hypothetical reference spectrum for the putative peroxo-diiron (III) species scaled to 9 % of the total intensity of the experimental spectrum. The parameters used to generate the reference spectra are given in Table 2.6.

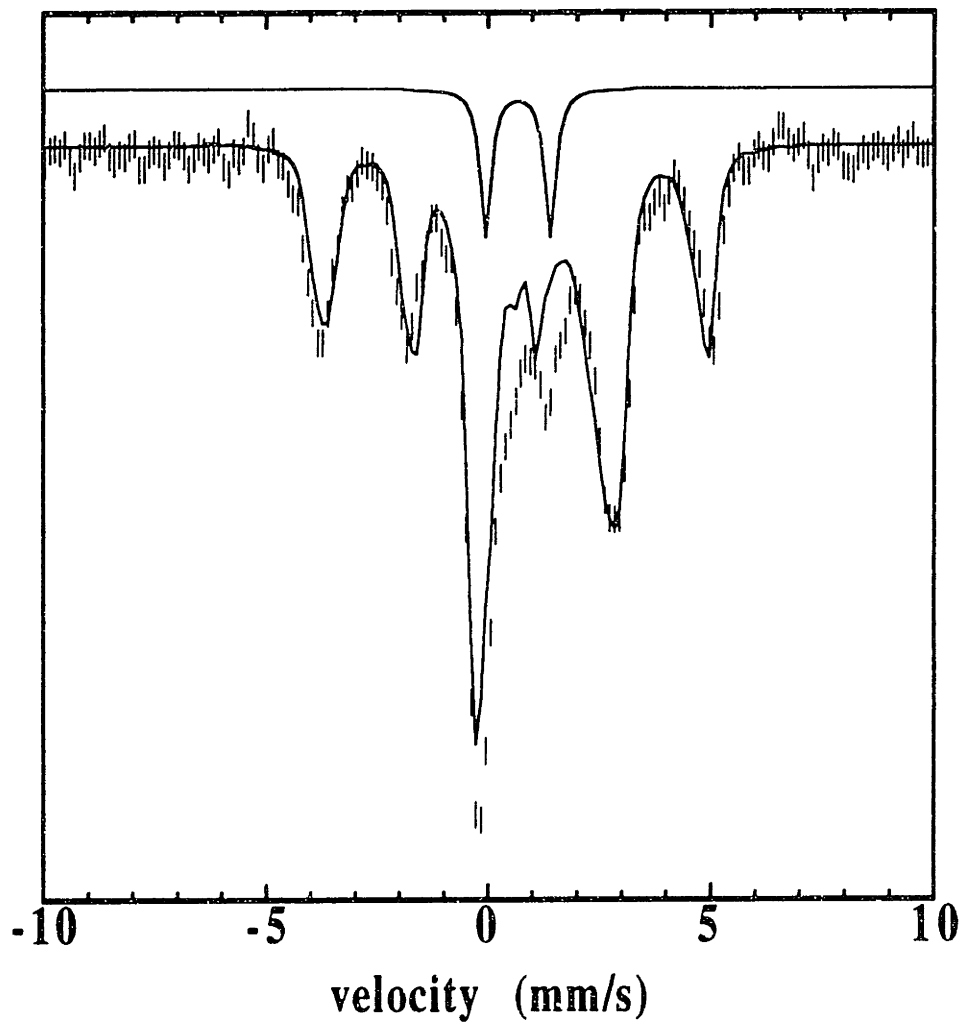
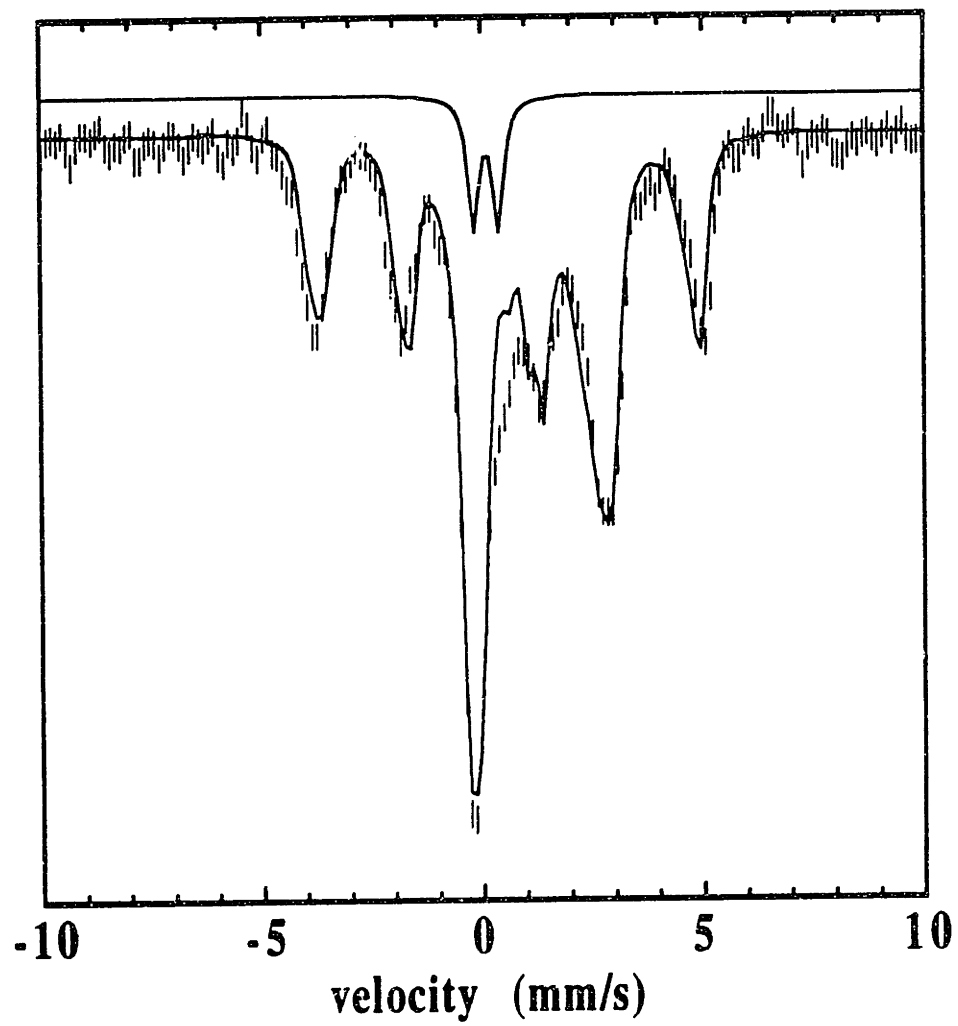


Fig. 2.21: Mössbauer spectrum showing a partially resolved peak at approximately 0.02 mm/s in the 0.028 s time-point of the reaction shown in Fig. 2.15. The inner spectrum is the summation of the spectra of ferrous-R2, diferric cluster, X, fast-relaxing ferric species and the putative peroxo-diiron(III) species, in proportions indicated in Table 2.7. The solid line plotted above the data is the hypothetical reference spectrum for the putative ferryl species scaled to 7 % of the total intensity of the experimental spectrum. The parameters used to generate the reference spectrum are given in Table 2.6.



ferrous ion doublet (Fig. 2.21). A hypothetical spectrum for this feature was generated with Mössbauer parameters ($\delta = 0.09$ and $\Delta E_Q = 0.65$ mm/s) which are characteristic of ferryl (Fe(IV)) species (Schulz *et al.*, 1984; Leising *et al.*, 1991). Using this hypothetical spectrum, the putative ferryl species was quantitated as a function of reaction time and the quantitation is summarized in Table 2.7. The analysis suggests that this species is present throughout the reaction (~ 0.3 equiv. per R2), and the quantity varies only slightly with time.

Since the time-resolved quantitation of the fast-relaxing ferric species indicated that this species, at best, can only account for $< 20\%$ of the reducing equivalents required to generate X, the Mössbauer spectra of the time-course were examined carefully for the presence of features of other Fe³⁺ species which correlate in time with accumulation of X. No such feature ($< 5\%$ of total iron) could be discerned in the first time-point, even though up to 1.1 ± 0.1 equiv. of X has accumulated (Fig. 2.22A). In the later time-points, weak features that are associated with high-spin ferric species become visible (indicated by the arrow in Fig. 2.22B). The line shapes of these features, however, change somewhat with time. With increasing time, these features become obscured by development of some very broad features (Fig. 2.22C). A hypothetical spectrum for these broad features is obtained by subtraction of the known components from the experimental spectrum of the 14 min time-point (Fig. 2.22C). At present, definitive characterization of these broad species has not been achieved, but they appear to be paramagnetic in nature and may arise from a mixture of Fe(III)-containing species. Using the hypothetical spectrum in Fig. 2.22C, the quantities of this "possible ferric species" in the time-course samples are estimated, and the results are summarized in Table 2.7. Assuming that the hypothetical spectrum of Fig. 2.22C is correct, then the broad species would account for 1.25 equiv. of Fe³⁺ per R2 at completion of reaction (Table 2.7), which

may ultimately account for a portion of the extra electrons required for cofactor assembly. The possible mechanistic significance of these results is discussed below.

Table 2.6 summarizes the parameters of the reference spectra used for analysis of the Mössbauer spectra of the time-course samples. Again, it should be emphasized that the hypothetical spectra shown in Fig. 2.20, Fig. 2.21, and Fig. 2.22 may not accurately represent the spectra of the real components. Nevertheless, by using these reference spectra, together with those in Fig. 2.14, the spectrum of each time-point during the reaction can be accounted for. Table 2.7 summarizes this analysis, an example for the result of this analysis is shown in Fig. 2.23².

Discussions

As shown previously by Bollinger *et al.*, the kinetics of the reaction of apo R2, O₂ and excess Fe²⁺ are consistent with the mechanism shown in Scheme 2.1 (Bollinger *et al.*, 1994b). Scheme 2.1 accounts for all the data on this reaction in terms of two sequential, first-order processes. When apo R2-wt is mixed with excess Fe²⁺ and O₂, an intermediate X accumulates ($k_{\text{obs}} = 5 - 10 \text{ s}^{-1}$) and is subsequently reduced by one electron to give a •Y122 and diferric cluster ($k_{\text{obs}} = 0.7 - 1.0 \text{ s}^{-1}$). The experiments described in this chapter have provided additional evidence for the proposed mechanism, and allow additional mechanistic details of the reaction to be filled in. Drawing on the observation that the reaction kinetics are independent of the absolute concentrations of apo R2, Fe²⁺, and O₂, Bollinger *et al.* reasoned that the **rate-limiting step** in the formation of X cannot be the bimolecular association of

²In an attempt to quantitate the ferric products in the reaction of Fe(II)-R2 with O₂ under excess Fe²⁺ conditions, the Mössbauer spectra of the time-course samples in this study (Table 2.7) were acquired over a velocity scale of -14 to 14 mm/s. As shown in Fig. 2.18, 2.20 and 2.22, the hypothetical spectra in the initial analysis show imperfect agreement with the experimental data. The small difference in line-width is due to the fact that the reference spectra for X, ferrous R2 and diferric cluster used in the initial analysis were acquired over a velocity scale of -7 to 7 mm/s. Very recently, the reference spectra were reanalyzed using the wider velocity scale. With these newly acquired reference spectra, very good agreement between experiment and theory is obtained. The results of the most recent analysis are summarized in Table 2.7, and Fig. 2.23 demonstrates the goodness of fit of the most current analysis.

Fig. 2.22: Mössbauer spectra showing features of the possible "ferric" species which accumulate in the reaction of Fe(II)-R2-wt with O₂ under excess Fe²⁺ conditions. The spectra are (A) of the 0.028 s time-point, (B) of the 0.052 s time-point, and (C) of the 14 min time-points of the reaction in Fig. 2.15. The arrow in B indicates the feature which is associated with high-spin ferric ion. The solid line plotted over the data in C is the hypothetical reference spectrum for the "possible ferric species" scaled to 24 % of the total intensity of the experimental spectrum.

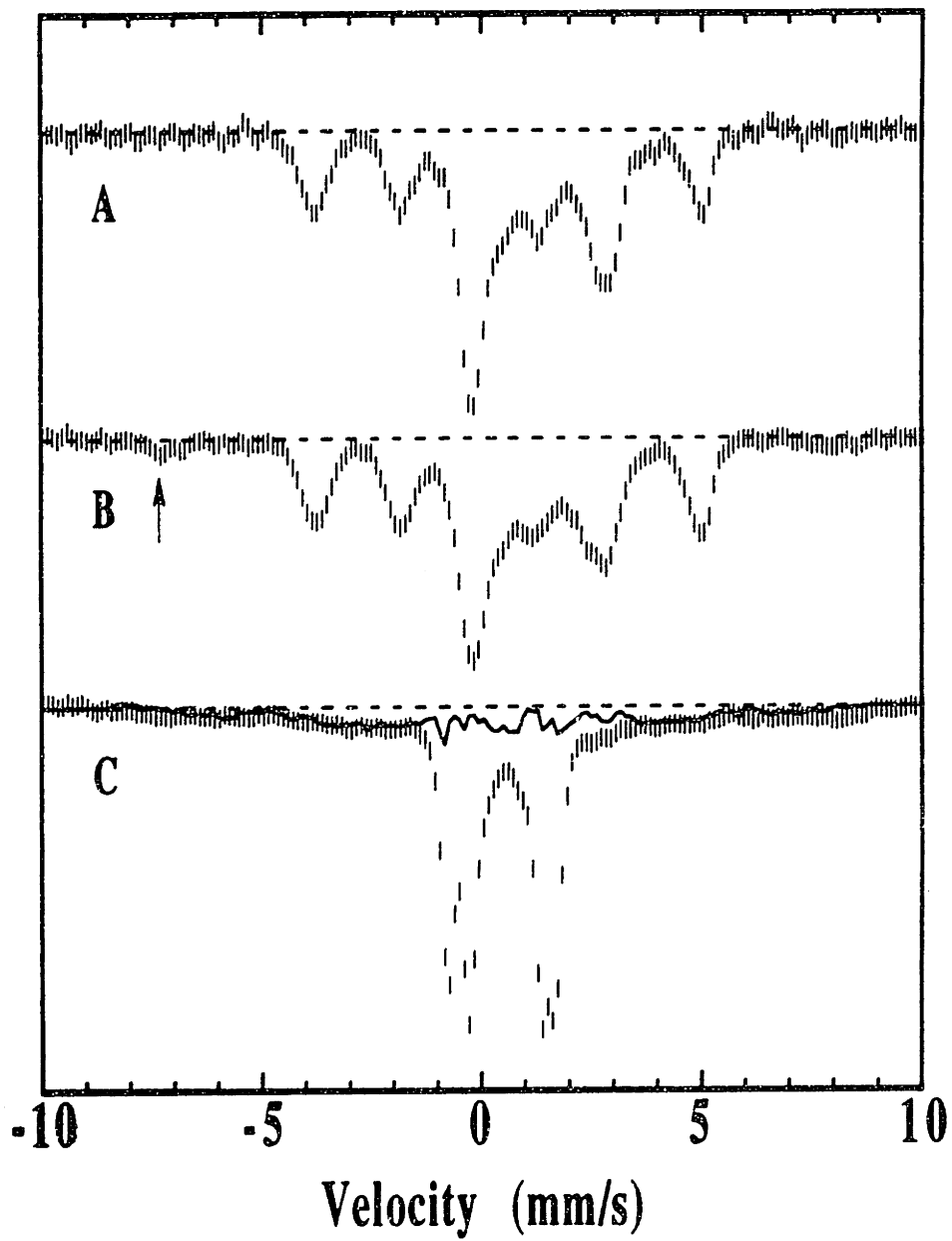
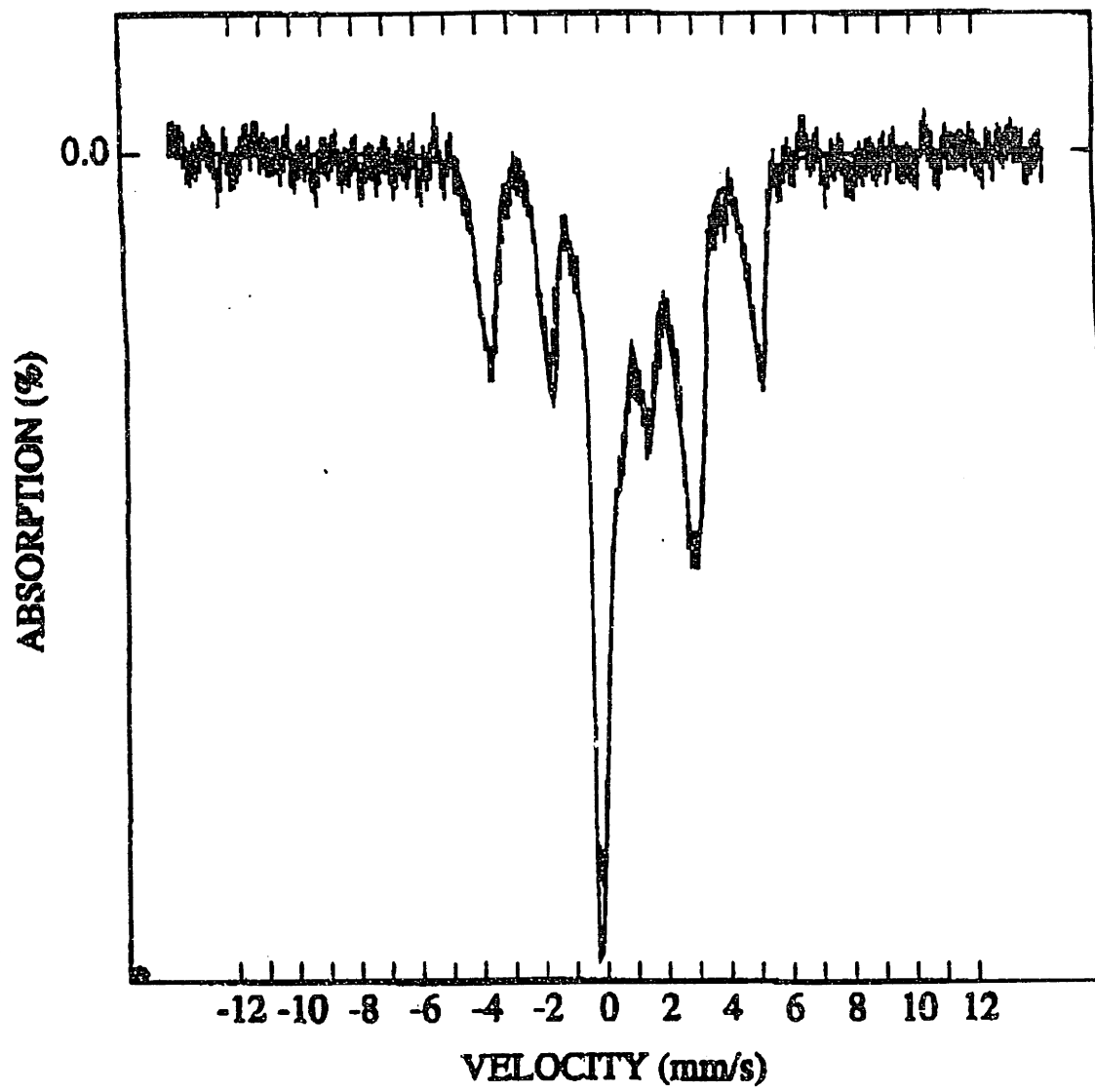
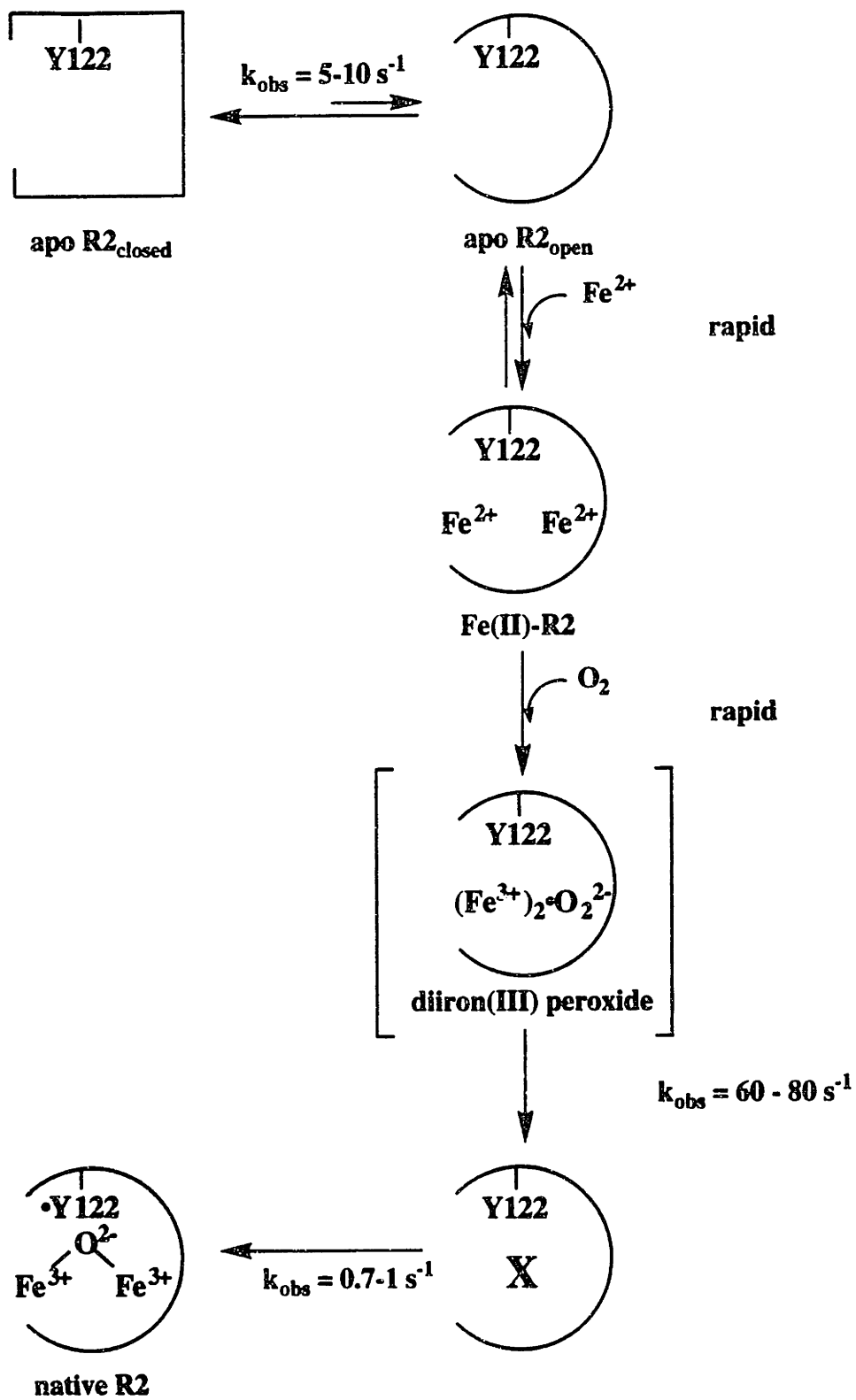


Fig. 2.23: Mössbauer spectrum demonstrating the goodness of fit of the most current analysis. The experimental spectrum is of the 0.028 s time-point of the reaction shown in Fig. 2.15. The theoretical spectrum (solid line) is the summation of the spectra of the various components in proportions indicated in Table 2.7.



Scheme 2.3: Schematic mechanism for the excess Fe^{2+} reaction elaborated to reflect the conformational change which occurs prior to formation of diferrous-R2.



Fe²⁺ and apo R2 or that of O₂ and ferrous-R2. It is therefore likely that the first-order rate constant of 5 - 10 s⁻¹ reflects a conformational change of apo R2 required for Fe²⁺ and/or O₂ binding. In Scheme 2.3, the mechanism proposed for the excess Fe²⁺ reaction is expanded to reflect the possibility that a conformational change in apo R2 occurs to allow entry of Fe²⁺ into the cofactor site. The results described in this chapter can readily be interpreted with the mechanism in Scheme 2.3. When Fe(II)-R2-wt (Fe²⁺/R2 = 5) is mixed with O₂, the stopped-flow data indicate that formation of X is much faster in the Fe(II)-R2 reaction than that in the apo R2 reaction. This observation is also reflected in the EPR data and the Mössbauer data. The k_{obs} for formation of X as determined by EPR spectroscopy (60 - 80 s⁻¹) is in agreement the k_{obs} deduced from the A₄₁₀, dropline-versus-time trace.

In addition to showing that the intermediate X is generated rapidly in the Fe(II)-R2 reaction, the experiments described in this chapter demonstrate that X generates •Y122. The decay of the EPR singlet due to X and the development of the doublet characteristic of •Y122 correspond temporally with the development of the UV/vis absorption spectrum characteristic of the product cofactor. The rate constant for decay of X and for formation of •Y122 as determined by EPR (k_{obs} = 1 s⁻¹) is in agreement with the rate constant for formation of •Y122 (k_{obs} = 0.85 ± 0.05 s⁻¹) determined from the stopped-flow data. The Mössbauer results are also quantitatively consistent with the EPR data and provide additional evidence for the mechanism proposed for the excess Fe²⁺ reaction. Finally, the EPR results indicate that decay of X is slower in R2-Y122F than in R2-wt, which is consistent with the hypothesis that X is the •Y122-generating species in R2-wt. Thus, the SF-Abs, RFQ-EPR and RFQ-Möss data together provide strong support for the major features of this mechanism in Scheme 2.3.

While the results described in this chapter are consistent with the proposed mechanism, more definitive interpretation of these results would be facilitated by more precise EPR spin quantitation. As shown in Fig. 2.12, the quantitative agreement of the EPR results with the simple three-component model in Scheme 2.2 is, at best, fair. More accurate spin quantitation as a function of time of both X and •Y122 may provide stronger evidence for the conclusion that X generates •Y122. As shown in Table 2.4 and Fig. 2.12, the values obtained in the EPR experiments show substantial scatter. One reason for this scatter may be related to heterogeneity in the packing of the rapid freeze-quench samples. As mentioned above, the uncertainties associated with EPR spin quantitation of freeze-quench samples can be $\pm 10 - 15\%$. Furthermore, the observation of a small amount of •Y122 (0.04 - 0.07 equiv.) in the EPR spectrum of the first few time-points taken (0.025 s - 0.028 s) suggest that a small amount of O₂ contamination in the Fe(II)-R2 sample might have contributed to the scatter in the EPR data. The kinetic analysis of the EPR data is also limited by the fact that only a few time-points (0.025 - 0.028 s) have been taken in the rise phase of X. With our current RFQ instrumentation, and without increasing the ram speed (1 cm/s), the smallest sampling time is 0.025 s. The formation of X in the experiments in this chapter, however, is sufficiently rapid that the rise phase appears to be completed after 0.030 s (Table 2.4). An important objective of future efforts should be to solve these experimental problems which have precluded detailed kinetic analysis of the EPR data.

More accurate spin quantitation as a function of time would also allow certain predictions based on the Mössbauer and the SF-Abs data to be tested experimentally. For example, the Mössbauer data indicate that 1.5 equiv. of diferric cluster is formed at the end of the reaction (Table 2.7), a value which is significantly greater than the amount of •Y122 formed as determined from the SF-Abs data (Table 2.2). This result suggests that a portion of X is converted to the diferric cluster

without generating a •Y122. At present, the reason for this behavior is not obvious. It is, however, important to note that thus far studies examining the R2 cofactor assembly under a number of different conditions have all reported a •Y122/R2 ratio that is smaller than the Fe/R2 ratio (Lynch *et al.*, 1989; Elgren *et al.*, 1991; Bollinger, 1992). Using EPR spectroscopy for quantitation of the tyrosyl radical and inductively coupled plasma emission spectroscopy for quantification of Fe³⁺, Lynch *et al.* determined that 1.9 diferric cluster and 1.3 - 1.4 •Y122 were present in R2 in crude extract (Lynch *et al.*, 1989). In a separate study, Elgren *et al.* examined the reconstituted R2 and determined by EPR and Mössbauer spectroscopies a diferric cluster/R2 ratio of 1.9 ± 0.2 and a •Y122/R2 ratio of 1.0 ± 0.07 (Elgren *et al.*, 1991). Using EPR spectroscopy for quantitation of •Y122 and several methods for quantitation of the iron content, Bollinger *et al.* determined a diferric cluster/R2 ratio of 1.4 ± 0.2 and a •Y122/R2 ratio of 1.2 ± 0.1 (Bollinger, 1992; Bollinger *et al.*, 1994b). The reason for the differences between these results is not clear, but they have been attributed, in part, to differences in experimental protocol (Bollinger, 1992). Despite the differences between these results, in all these cases, the amount of diferric cluster exceeds that of •Y122. The fact that the quantity of the diferric cluster exceeds the quantity of •Y122 in each of these studies and in the experiment described in this chapter support the notion that a portion of the diferric cluster is generated without concomitant formation of •Y122. More accurate quantitation of X and •Y122 by EPR might provide more definitive evidence for this hypothesis and might allow details of this hypothesis to be filled in.

New Features of Current R2 Reconstitution Mechanism

As stated above, the SF-Abs, RFQ-EPR and RFQ-Möss data together strongly suggest that the first-order rate constant of $5 - 10 \text{ s}^{-1}$ in Scheme 2.1 represents a slow conformational change which occurs before formation of Fe(II)-R2. The nature of

the postulated conformational change in apo R2 warrants discussion. The crystallographic studies of apo R2, ferrous-R2, and met R2 suggest that the structures of these different forms of the protein are essentially identical, differing only at the cofactor sites (Nordlund *et al.*, 1990; Aberg, 1993; Nordlund & Eklund, 1993; Regnstrom *et al.*, 1994; Nordlund *et al.*, 1995). The cluster-binding site of R2 is buried in the protein: the shortest distance between the cofactor site and the protein surface is 10 Å. Comparison of the met R2 and the apo R2 structure reveal no channel in these structures between the protein surface and the buried cluster-binding site (Aberg, 1993; Nordlund & Eklund, 1993). It is thus reasonable to propose that formation of Fe(II)-R2 may require a conformational change in the apo R2 to allow for access of Fe²⁺ to the cluster-binding site and that this conformational change may be rate-limiting in the conversion of apo R2 to X. Interpreting the crystal structure of the diferrous form of a R2-S211A mutant, Aberg *et al.* have implicated Y209 as a candidate to be involved in conformational change to expose the ligand residues to the solvent during cofactor assembly (Aberg, 1993). In support of this possibility, the authors shows that the hydroxyl group of Y209 moves 2 Å to open up a channel from the surface down to the cluster binding site. Alternatively, such a conformation change might involve subtle but crucial changes in the cluster-binding site to allow for iron binding. The x-ray crystallographic data of apo R2 and met R2 indicate that all the carboxyl side chains of the cluster-binding site of apo R2 change their conformation somewhat and fill the vacancy created by the removal of the iron ions (Aberg, 1993; Aberg *et al.*, 1993). Comparison of Fig. 1.8 and Fig. 1.6 clearly reveals that extensive rearrangements of the carboxylate ligands, with formation of new hydrogen bonds and cleavage of existing hydrogen bonds, must occur in the transition from apo R2 to Fe(II)-R2 (Aberg, 1993; Aberg *et al.*, 1993).

In addition to revealing a rate-limiting conformational change in the reconstitution reaction, the experiments described in this chapter have also allowed

for identification and quantitation of additional components of the reaction. The Mössbauer experiment show that an iron species ($\delta = 0.66$ and $\Delta E_Q = 1.51$ mm/s), which is distinct both from X and from the diferric cluster, is produced very rapidly and decay completely within ~ 50 ms of reaction time. Preliminary results indicate that this species has Mössbauer parameters very similar to those of the diiron(III) peroxide intermediate ($\text{MMOH}_{\text{peroxo}}$) in the reaction of O_2 with the diferrous form of methane monooxygenase hydroxylase (MMOH) from *M. capsulatus* (Bath) (Liu *et al.*, 1994). On the basis of the structural similarities of the diiron sites in R2 and MMOH, the possibility of a common mechanism for oxygen activation by the diferrous cluster in R2 and in MMOH has been suggested. Thus, the experiments described in this chapter have provided the first indication of a peroxo diiron(III) intermediate in the R2 reconstitution reaction. The time-dependent behavior of this species also suggest that it may be a precursor of X. It should, however, be emphasized that, because the features associated with this new species are only partially resolved, and because the features contribute only a small fraction of the experimental spectrum, definitive characterization of this species has not yet been achieved. Nevertheless, preliminary stopped-flow absorption data have provided support for this assertion. Stopped-flow absorption spectroscopic traces of the reaction of reduced MMOH with O_2 reveal a broad band for the diiron(III) peroxide intermediate with $\lambda \sim 600 - 660$ nm ($\epsilon_{625} \sim 1500 \text{ M}^{-1} \text{ cm}^{-1}$). The early spectra of the R2 reaction also appear to exhibit a weak transient absorption band in the region of 600 nm. As shown in Fig. 2.24, the 0.0 - 0.040 s region of the A_{605} -versus-time trace in the reaction of Fe(II)-R2-wt with O_2 shows a rise-fall behavior, which may be indicative of formation and decay of a transient species. An objective of future work will be to ascertain whether this species is associated with a diiron(III) peroxide species and to determine whether this species is the precursor of X.

Implications for Mechanism of Delivery of the "Fourth Electron"

As discussed above, a key issue in the study of the reconstitution reaction is the delivery of the fourth electron. The studies of Ochiai *et al.*, Elgren *et al.*, and Bollinger *et al.* all indicated that oxidation of a third Fe^{2+} ion provides the fourth electron when no other reductant is present. Since X is oxidized by one electron to the diferric cluster, and since it obtains this electron by oxidizing Y122, it would imply that 1 equiv. of Fe^{3+} must accumulate per equiv. of X produced. Previous studies with apo R2 have indicated that a stable or slowly decaying fast relaxing ferric species is produced concomitantly with X and this species can account for 50 % of the fourth electron required for cofactor assembly (Bollinger *et al.*, 1994b). It was thus proposed that this fast-relaxing ferric species may represent at least part of the Fe^{3+} product(s) which is formed when Fe^{2+} donates the extra electron during formation of X.

The Mössbauer results described in this chapter, however, indicate that the mechanism by which the fourth electron is delivered may be different in the Fe(II)-R2 reaction. More importantly, these data suggest that there are multiple sources for the fourth electron. An attempt to illustrate this observation is shown in Table 2.8. Table 2.8 shows that, in the first time-point taken (0.028 s), less than 0.2 equiv. of fast-relaxing ferric species is observed even though 1.1 ± 0.1 equiv. of X has accumulated. Thus, the fast-relaxing ferric species can, at best, account for 20 % of the reducing equivalents required for generation of X at this time-point. Furthermore, if it is assumed that all of the diferric cluster which is produced (1.53 ± 0.06 equiv.) results from reduction of X, then the maximum quantity of the fast-relaxing ferric species (0.40 equiv.) accounts for less than one third of the total quantity of X produced (Table 2.8). Since the fast-relaxing ferric species accounts for only a small fraction of the extra electron required, it is reasonable to expect that an additional ferric species might be present.

Fig. 2.24: A_{605} -versus-time trace in the reaction of Fe(II)-R2-wt with O_2 . The reaction conditions (after mixing) were: 80 μ M R2-wt, 504 μ M Fe^{2+} , 1 mM O_2 , 100 mM HEPES, pH 7.6, 5 °C. The experimental trace represents the average of 3 trials.

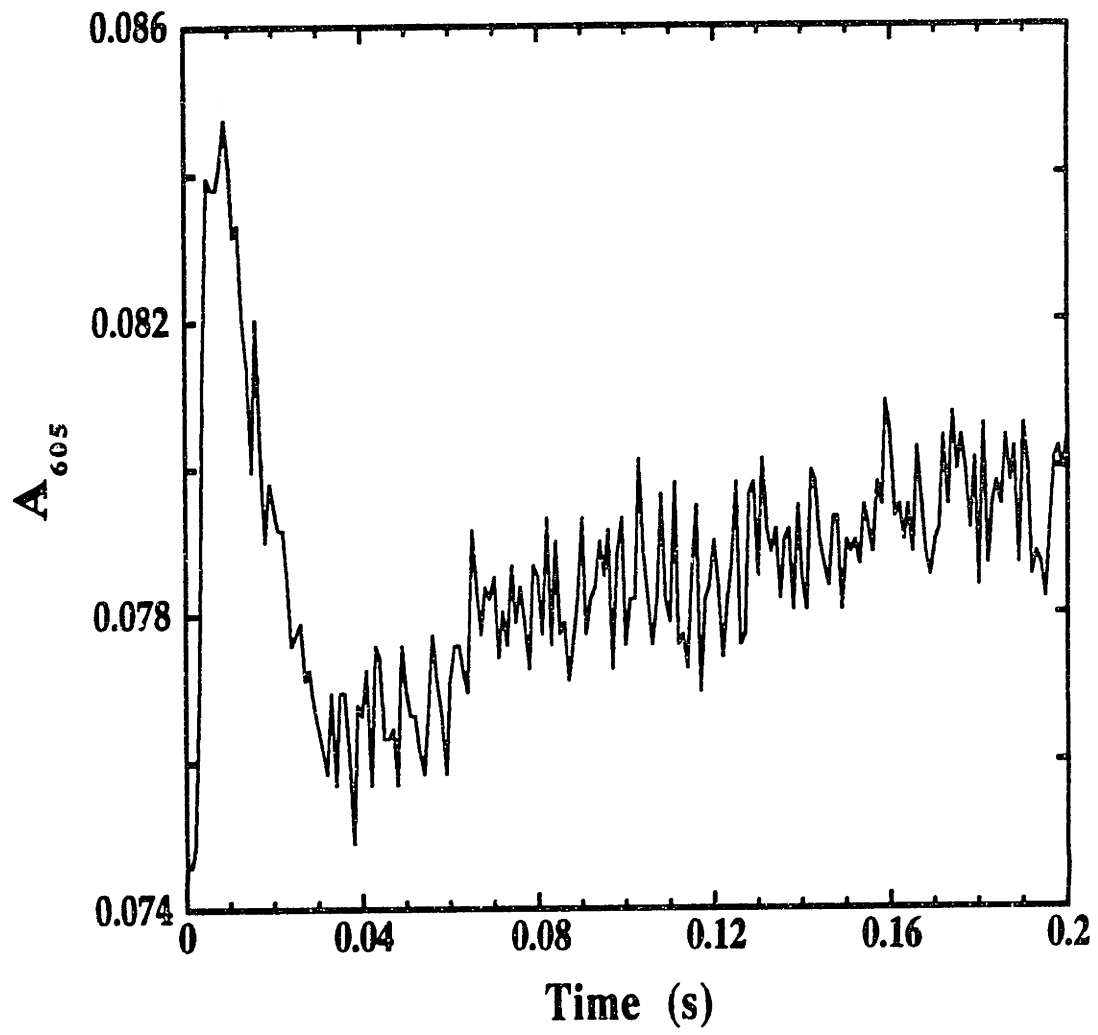


Table 2.8: Electron counting for selected time-points in the reaction of Fe(II)-R2-wt with O₂ under excess Fe²⁺ conditions. The data are from the experiment in Table 2.7

Reaction Time (s)	Equiv. X	Equiv. diferric cluster	Equiv. Fast-relaxing Fe ³⁺	Equiv. High-spin Fe ³⁺	Equiv. Possible Fe ³⁺ Species	Equiv. Ferryl species	Sum ^a
0.028	1.10 ± 0.04	< 0.07	< 0.2	0	0.25 ± 0.08	0.35 ± 0.05	1.15 ± 0.1
0.037	1.15 ± 0.04	< 0.07	0.15 ± 0.05	0.25 ± 0.04	0.10 ± 0.08	0.25 ± 0.05	1.00 ± 0.1
0.052	1.23 ± 0.04	0.10 ± 0.02	0.35 ± 0.05	0.30 ± 0.08	0.10 ± 0.08	0.25 ± 0.05	1.25 ± 0.1
840	0	1.53 ± 0.04	0.40 ± 0.05	< 0.10	1.2 ± 0.16	0.15 ± 0.05	1.85 ± 0.2

^aSum of reducing equivalents provided in the formation of the fast-relaxing ferric species, the high-spin ferric species, the possible ferric species and the putative ferryl species. It was assumed that one electron equiv. is provided for every equiv. of ferric species generated, and two electron equiv. are provided for every equiv. of ferryl species generated.

Since it has been shown that significant quantities of mononuclear Fe^{3+} ion are produced in the reconstitution of mouse R2 (Ochiai *et al.*, 1990), the possibility that mononuclear Fe^{3+} ion is formed in the reaction of Fe(II)-R2 with O_2 has also been carefully examined. As shown In Table 2.7, no appreciable amount of mononuclear Fe^{3+} species was detected in the Mössbauer spectrum of the first time-point taken (0.028 s). In the later time-points, however, the spectra clearly indicate additional features which are associated with high-spin mononuclear Fe^{3+} ion. With increasing time, these features become obscure by development of some very broad features. The reference spectrum for the broad features, which was deduced by analysis of the 14 min time-point, appears to exhibit large hyperfine splitting. At present, definitive characterization of the broad species has not yet been achieved, but one possible interpretation is that the very broad features represent a mixture of ferric species. If this interpretation is correct, then these species would account for 1.25 equiv. of Fe^{3+} per R2 at completion of reaction (Table 2.8). This interpretation, however, would still fail to account for the 1.1 equiv. of electrons required for formation of X at the 0.028 s time-point (Table 2.8).

As stated above, insufficient amounts of an Fe^{3+} species are produced early in the reaction to account for the early production of X. These results thus suggest that either we have failed to identify an Fe^{3+} containing species, or that a species other than Fe^{3+} is produced in the delivery of the extra reducing equivalent. However, it seems unlikely that the fourth electrons come from a source other than Fe^{2+} , as this occurrence would generate an additional radical which might be detectable by EPR spectroscopy. The EPR data described in this chapter clearly show that at all times the $g = 2.00$ region of the spectrum can be accounted for by the summation of the spectra of X and $\bullet\text{Y122}$. It is thus unlikely that the fourth electron is provided by oxidation of a protein residue. It is, therefore, tempting to speculate that the putative Fe(IV) species observed by Mössbauer spectroscopy may account for the

missing electrons. As shown in Table 2.8, the putative Fe(IV) species accumulates rapidly to ~ 0.35 equiv. in the first time-point (0.028 s). If it is assumed that two electrons are provided by oxidation of Fe(II) to Fe(IV), then the quantitation of the putative Fe(IV) species would account for an additional 0.7 equiv. of electrons required for formation of X at 0.028 s. Furthermore, inspection of Table 2.8 reveals that, at each of the time-points taken, the sum of the fast-relaxing ferric species, the high-spin ferric species and the putative ferryl species can account for the total quantities of X and diferric cluster produced. This observation thus suggests that there might be multiple sources for the fourth electron required for cofactor assembly. However, while this interpretation provides an account for almost all of the required electrons, additional experiments are required to know if this hypothesis is plausible. As discussed above, it is not possible to unambiguously define the spectral features shown in Fig. 2.20 and Fig. 2.21. The temporal behavior of the species shown in Fig. 2.21 also provides argument against its containing Fe(IV), as a ferryl species would not be expected to persist for 60 s. The mechanism by which this putative ferryl species is formed is also unclear. An objective of future work will be to determine the identities and the possible mechanistic roles of these species.

The observation of multiple species in the Mössbauer spectra of the time-course samples have also allowed an apparently anomalous observation to be rationalized. As shown in Fig. 2.5, the 365 nm absorbance data are poorly fit according to the oversimplified kinetic model of Scheme 2.2. One possible explanation for this discrepancy is related to the fact that more diferric cluster than •Y122 is formed in the reaction. As mentioned above, the Mössbauer data indicate that ~ 0.3 equiv. of X is converted to the diferric cluster without generating •Y122. This result might be expected to complicate kinetic analysis of the A_{365} -versus-time trace. It is also reasonable to expect that some of the iron-containing species

observed in the Mössbauer spectra may also contribute to the absorbance in the 365 nm region of the UV/vis spectrum. In this case, the kinetic behavior at 365 nm would be expected to be more complex than the model in Scheme 2.2.

References

- Aberg, A. (1993) Ph. D. Thesis, Stockholm University.
- Atkin, C. L., Thelander, L., Reichard, P. & Lang, G. (1973) *J. Biol. Chem.* 248, 7464-7472.
- Ballou, D. P. (1978) *Methods in Enzymol.* 54, 85-93.
- Ballou, D. P. & Palmer, G. (1974) *Anal. Chem.* 46, 1248.
- Barshop, B. A., Wrenn, R. F. & Frieden, C. (1983) *Anal. Biochem.* 130, 134-145.
- Bollinger, J. M., Jr. (1992) Ph. D. Thesis, Massachusetts Institute of Technology.
- Bollinger, J. M., Jr., Edmondson, D. E., Huynh, B. H., Filley, J., Norton, J. R. & Stubbe, J. (1991a) *Science* 253, 292-298.
- Bollinger, J. M., Jr., Stubbe, J., Huynh, B. H. & Edmondson, D. E. (1991b) *J. Am. Chem. Soc.* 113, 6289-6291.
- Bollinger, J. M., Jr., Tong, W. H., Ravi, N., B. H., Edmondson, D. E. & Stubbe, J. (1994a) *J. Am. Chem. Soc.* 116, 8024-8032.
- Bollinger, J. M., Jr., Tong, W. H., Ravi, N., Huynh, B. H., Edmondson, D. E. & Stubbe, J. (1994b) *J. Am. Chem. Soc.* 116, 8015-8023.
- Bray, R. C. (1961) *Biochem. J.* 81, 189.
- Elgren, T. E., Lynch, J. B., Juarez-Garcia, C., Münck, E., Sjöberg, B.-M. & Que, L., Jr. (1991) *J. Biol. Chem.* 266, 19265-19268.
- Espenson, J. H. (1981) *Chemical Kinetics and Reaction Mechanisms*. McGraw-Hill, New York.

- Hitchman, M. L. (1978) *Measurement of Dissolved Oxygen*. Wiley, New York.
- Laemmli, U. K. (1970) 227, 280.
- Leising, R. A., Brennan, B. A., Que, L., Jr., Fox, B. G. & Münck, E. (1991) *J. Am. Chem. Soc.* 113, 3988-3990.
- Liu, K. E., Valentine, A. M., Qiu, D., Edmondson, D. E., Appelman, E. H., Spiro, T. G. & Lippard, S. J. (1995a) *J. Am. Chem. Soc.* 117, 4997-4998.
- Liu, K. E., Wang, D., Huynh, B. H., Edmondson, D. E., Salifoglou, A. & Lippard, S. J. (1994) *J. Am. Chem. Soc.* 116, 7465-7466.
- Lynch, J. B., Juarez-García, C., Münck, E. & Que, L., Jr. (1989) *J. Biol. Chem.* 264, 8091-8096.
- Malmström, B., Reinhammar, B. & Vänngård, T. (1970) *Biochim. Biophys. Acta* 205, 48.
- Massey, V. (1957) *J. Biol. Chem.* 229, 763-770.
- Nordlund, P. (1990) Ph.D. Thesis, Swedish University of Agricultural Sciences.
- Nordlund, P. & Eklund, H. (1993) *J. Mol. Biol.* 232, 123-164.
- Nordlund, P., Eklund, H., Åberg, A. & deMare, D. (1995) "Abstracts of Papers." 209th National Meeting of the American Chemical Society.
- Nordlund, P., Sjöberg, B. M. & Eklund, H. (1990) *Nature* 345, 593-598.
- Ochiai, E.-I., Mann, G. J., Gräslund, A. & Thelander, L. (1990) *J. Biol. Chem.* 265, 15758-15761.
- Petersson, L., Gräslund, A., Ehrenberg, A., Sjöberg, B.-M. & Reichard, P. (1980) *J. Biol. Chem.* 255, 6706-6712.
- Ravi, N., Bollinger, J. M., Jr., Tong, W. H., Ravi, N., B. H., Edmondson, D. E. & Stubbe, J. (1994) *J. Am. Chem. Soc.* 116, 8007-8014.

Regnstrom, K., Aberg, A., Ormo, M., Sehline, M. & Sjöberg, B.-M. (1994) *J. Biol. Chem.* 269, 6355-6361.

Salowe, S. P. (1987) Ph. D. Thesis, University of Wisconsin.

Schulz, C. E., Rutter, R., Sage, J. T., Debrunner, P. G. & Hager, L. P. (1984) *Biochemistry* 23, 4743-4754.

Stookey, L. L. (1970) *Anal. Chem.* 42, 779-781.

Sturgeon, B. E., Burdi, D., Chen, S., Huynh, B. H., Stubbe, J. & Hoffman, B. M. (1996) *J. Am. Chem. Soc.* Submitted.

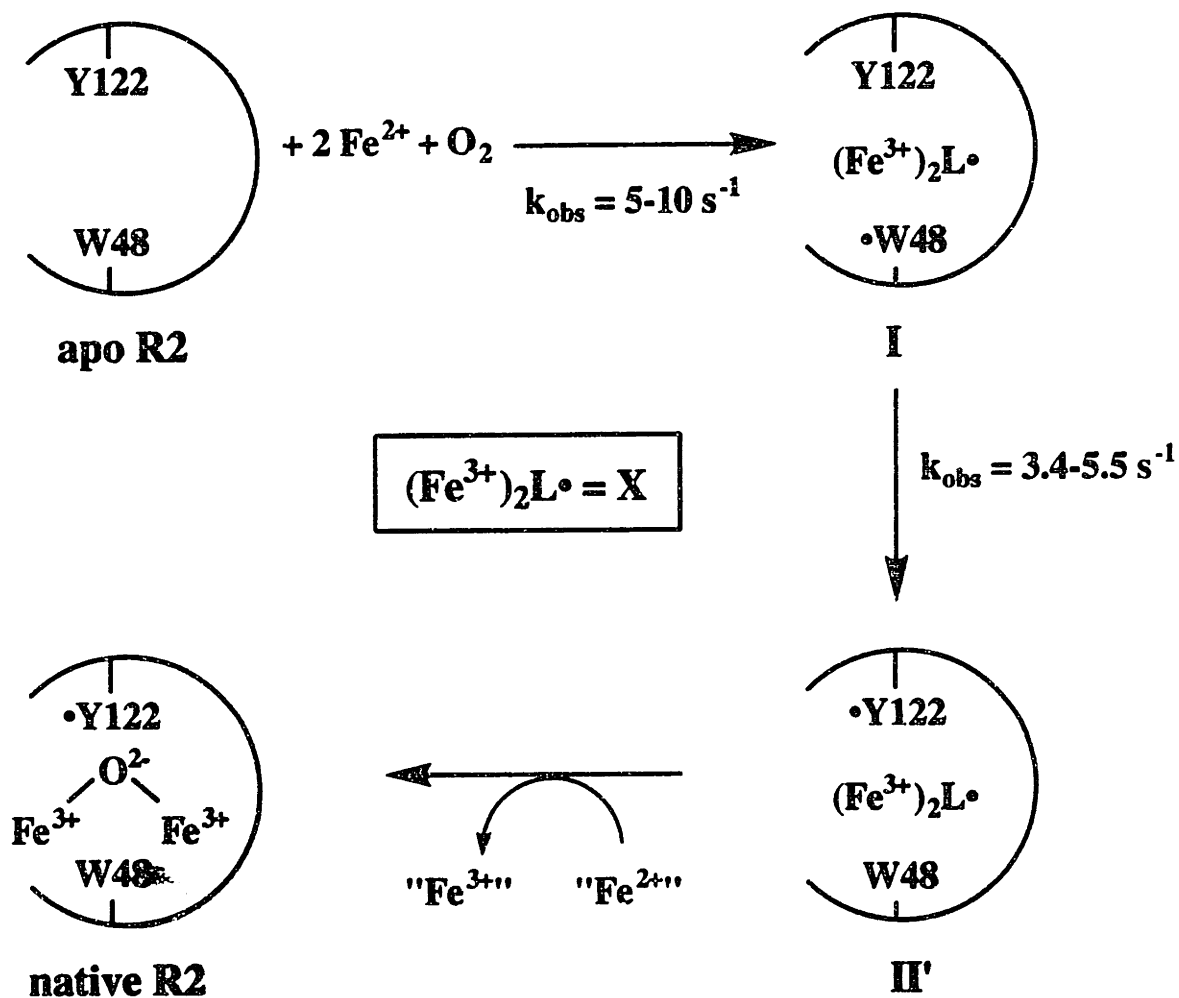
Thelander, L. (1973) *J. Biol. Chem.* 248, 4591-4601.

**Chapter 3: Reconstitution of Native R2 under
Limiting Fe²⁺ Conditions**

The results of Chapter 2 demonstrate that pre-forming the Fe(II)-R2 complex before exposure to O₂ provides a very useful probe for the reconstitution mechanism. In the work that is described in this chapter, we have extended this approach to further characterize the limiting Fe²⁺ pathway (Scheme 3.1). Previously, the reaction of apo R2 with 2.3 molar equivalents of Fe²⁺ has been studied in detail using a combination of SF-Abs, RFQ-EPR and RFQ-Möss spectroscopies (Bollinger *et al.*, 1994b). These studies showed that the limiting Fe²⁺ reaction differ markedly both kinetically and spectroscopically from the excess Fe²⁺ reaction. In addition to X, a transient species with a broad absorption feature at 560 nm was detected in the limiting Fe²⁺ reaction, and it was concluded that the 560 nm absorbing species is responsible for oxidizing Y122 to •Y122. On the basis of its UV/visible absorption characteristics, as well as structural and functional analogies to the •W191⁺ in compound I of cytochrome c peroxidase, the 560 nm-absorbing species was proposed to be a tryptophan radical cation (•W48⁺). In support of this hypothesis, the EPR time-course of the reaction showed a transient species with broad features at g = 2, which correlated temporally with the 560 nm absorbance. While this hypothesis provides an attractive explanation for the data, the kinetic complexity of the reaction and the lack of time-resolved quantitation of the intermediates makes it impossible to conclude with certainty the mechanism of the limiting Fe²⁺ reaction, and additional experiments are required to assess the validity of the proposed mechanism shown in Scheme 3.1.

In the experiments that are described in this chapter, the reaction of Fe(II)-R2 complex with O₂ under limiting Fe²⁺ conditions was followed by SF-Abs, RFQ-EPR and RFQ-Möss spectroscopies. The results indicate that formation of X in the reaction of Fe(II)-R2 (2.3 Fe²⁺/R2) with O₂ is much faster than that in the reaction of

Scheme 3.1: Schematic representation for the mechanism proposed in our previous work for the reaction of apo R2-wt at 5 °C with O₂ and limiting Fe²⁺ (Bollinger *et al.*, 1994b).



apo R2 with 2.3 Fe²⁺ and O₂. These results thus provide further support for the idea that was put forth earlier that one of the slow steps in the reaction of apo R2 with Fe²⁺ is a conformational change in the protein to allow entry of Fe²⁺ into the cofactor-binding site. In agreement with our previous work, the kinetic and spectroscopic characteristics of the reconstitution reaction depend markedly on the initial ratio of Fe²⁺/R2. The 560 nm transient absorption is observed under limiting Fe²⁺ conditions and is not observed in the presence of excess Fe²⁺ or ascorbate. Comparison of the *k*_{obs} for the decay of the 560 nm species and the *k*_{obs} for formation of •Y122, however, indicates that the 560 nm-absorbing species does not generate •Y122. Furthermore, the EPR spectrum of this reaction quenched at 0.46 s shows a substantial amount of the broad *g* ~ 2 features, even though the decay of the 560 nm absorption band is completed at this time-point. Thus, under these conditions, the broad EPR signal is not correlated with the 560 nm-absorbing species. This assertion is also supported by the EPR data of the reaction of apo R2 with limiting Fe²⁺ in ²H₂O. These results show that only X and •Y122 are present in the EPR spectra. No broad EPR features were observed, even though the 560 nm transient absorption is still observable. These results provide further evidence that the EPR broad features and the 560 nm absorbance are not correlated.

Experimental Procedures

Materials

Apo R2-wt and apo R2-Y122F were prepared as described in Chapter 2. ²H₂O (99%) was purchased from Aldrich.

Reaction of Fe(II)-R2 (2.3 Fe²⁺/R2) with O₂ as Monitored by SF-Abs, RFQ-EPR and RFQ-Möss Spectroscopies

The reaction of Fe(II)-R2 (Fe²⁺/R2 = 2.3) with O₂ was monitored by SF-Abs, RFQ-EPR and RFQ-Möss spectroscopies. With the exception of the difference in the Fe²⁺/R2 ratio, these experiments were carried out as described in Chapter 2. Detailed experimental conditions were described in the figure legends. X-band EPR spectra were recorded at 20 K on a Brüker Model ESP 300 equipped with an Oxford Instrument ESR 900 continuous flow cryostat, or at 100 K with a Brüker ER4111VT variable temperature controller. Alternatively, EPR spectra were recorded at 20 K on a Brüker ER 200D-SRC spectrometer equipped with an Oxford Instruments ESR 910 continuous flow cryostat. Mössbauer spectra were acquired at 4.2 K with a magnetic field of 50 mT applied parallel to the γ -beam. The EPR and the Mössbauer spectra were analyzed as described in Chapter 2.

Is the Species Trapped by the Rapid Freeze-quench Method Chemically Competent to Generate the Native Cofactor?

The reaction of Fe(II)-R2 (2.3 Fe²⁺/R2) with O₂ was quenched at 0.059 s and the EPR spectrum acquired. The sample was then thawed by submerging the EPR tube in a ice water bath. After the sample was completely thawed (~ 2 min), it was incubated at 0°C for an additional 3 min. The EPR tube was tapped gently to ensure that all the aqueous samples collect at the bottom of the EPR tube and the isopentane layer was at the top. The sample was then refrozen by submerging the EPR tube slowly into liquid N₂. The EPR spectrum of this sample was acquired and was compared with the first spectrum taken.

Time-Course of the Reaction of apo R2 -wt with 2.3 Fe²⁺ and O₂ as Monitored by SF-Abs, RFQ-EPR and RFQ-Möss Spectroscopies

In these experiments, 600 μM apo R2-wt in O₂-saturated 100 mM HEPES (pH 7.7) was mixed at 5 ± 1 °C with 1.38 mM Fe²⁺ in O₂-saturated 5 mN H₂SO₄, and the reaction was monitored by SF-Abs, RFQ-EPR and RFQ-Möss spectroscopies as described previously (Bollinger *et al.*, 1994a; Bollinger *et al.*, 1994b). The amount of •Y122 as a function of time was determined from the A₄₁₀, dropline-versus-time trace acquired with the Applied Photophysics Spectrofluorimeter as described previously. The amount of X was determined by analysis of the Mössbauer spectra. The concentration of total EPR active species was determined by comparison of the EPR intensity in the $g = 2$ region with two different standards. The first standard contained 1.00 mM CuSO₄, 2.0 M NaClO₄, 0.010 M HCl and 20 % (v/v) glycerol (Malmström *et al.*, 1970). The second standard contained a R2 sample that contained 1.2 equiv. of •Y122 per R2.

Temperature dependence of the reaction of apo R2-wt with limiting Fe²⁺ was also examined using SF-Abs spectroscopy. Detailed experimental conditions were described in the figure legends. A typical experiment involves mixing equal volumes of a solution containing 146 μM apo R2, 100 mM HEPES (air-saturated) buffered at pH 7.7 and a solution of 340 μM Fe²⁺ in 5 mN H₂SO₄ (air-saturated), at various temperatures between 5 and 25 °C. Identical experiments were also carried out with a mutant protein R2-Y122F.

Time-Course of the Reaction of Apo R2 with O₂ and Fe²⁺ in ²H₂O as Monitored by SF-Abs, and RFQ-EPR Spectroscopies

The Fe²⁺ stock solutions were prepared by dissolution of ⁵⁶Fe metal in 4 mN ²H₂SO₄. A HEPES buffer in ²H₂O was prepared by first lyophilizing 50 mL of 100 mM HEPES pH 7.7 to dryness, and then dissolving the lyophilized sample in 50 mL

of $^2\text{H}_2\text{O}$ at 5 °C. Aliquots of a 10 M NaOH solution was added to the HEPES buffer until the pH meter read 7.3. The resulting buffer contained 100 mM HEPES in $^2\text{H}_2\text{O}$ (> 98%) at pD 7.7 (Glasoe & Long, 1960). The protein solution was prepared by adding 100 μL of 1.4 mM apo R2-wt to a 2 mL solution of the HEPES/ $^2\text{H}_2\text{O}$ buffer. The resulting solution was concentrated using a Centricon-30 concentrator, and then diluted to 2 mL with the HEPES/ $^2\text{H}_2\text{O}$. The concentration/dilution cycle was repeated 3 times. The SF-Abs experiments were carried out by mixing at 5 °C equal volumes of a solution containing 60 μM apo R2, 100 mM HEPES/ $^2\text{H}_2\text{O}$ (air-saturated) buffered at pD 7.7 and a solution of Fe^{2+} in 5 mN $^2\text{H}_2\text{SO}_4$ (air-saturated). The RFQ-EPR samples were prepared as described previously (Ravi *et al.*, 1994; Bollinger *et al.*, 1994a; Bollinger *et al.*, 1994b). In the EPR experiments, 400 μM apo R2 in O_2 -saturated 100 mM HEPES/ $^2\text{H}_2\text{O}$ (pD 7.7) was mixed at 5 ± 1 °C with 930 μM Fe^{2+} in O_2 -saturated 5 mN $^2\text{H}_2\text{SO}_4$, and the reaction mixtures were freeze quenched at time-points between 0.070 - 180 s.

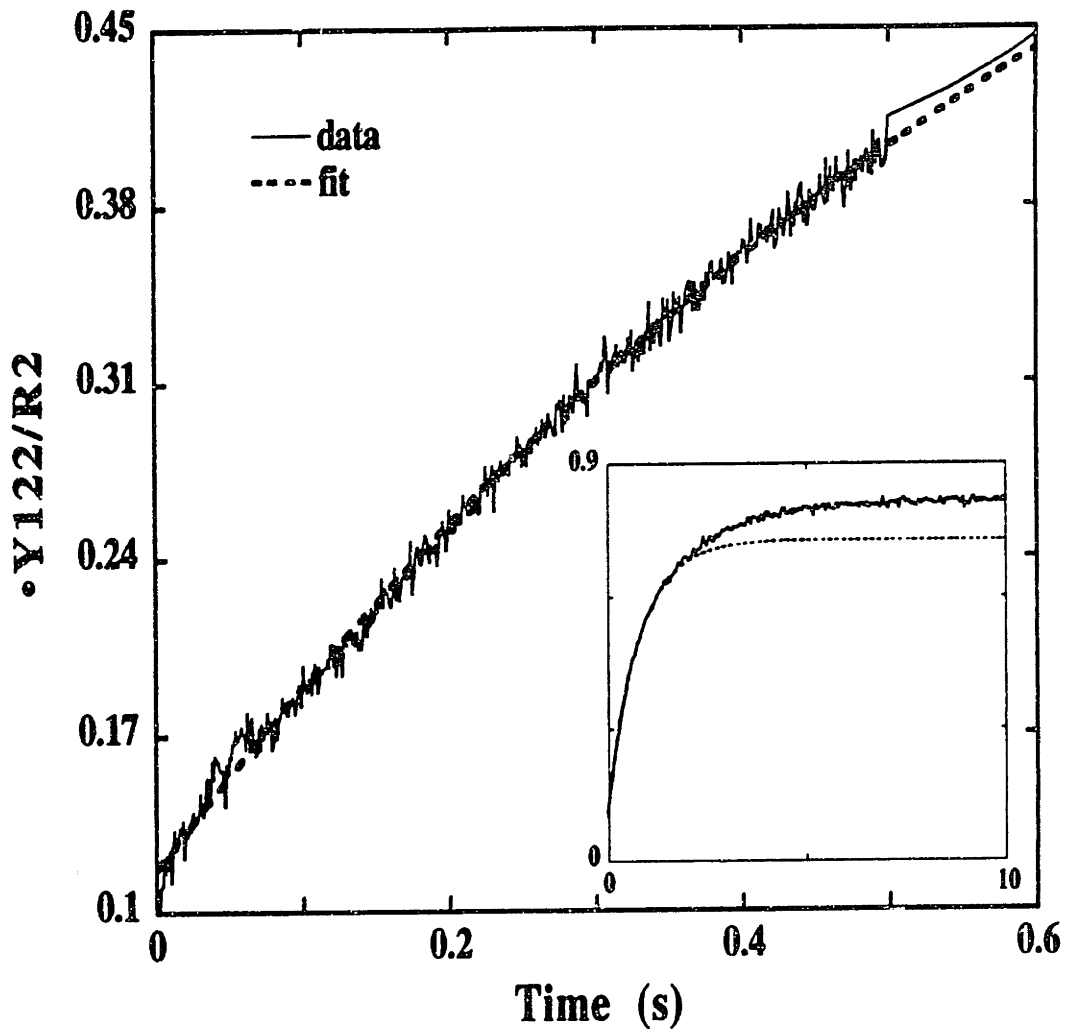
Results

Reaction of Fe(II)-R2-wt ($\text{Fe}^{2+}/\text{R2} = 2.3$) with O_2 as Monitored by SF-Abs Spectroscopy

When the Fe(II)-R2 complex, prepared with 2.3 molar equivalents of Fe^{2+} per R2, is mixed with O_2 , the reaction exhibits kinetic behavior different from that in the excess Fe^{2+} reaction. Unlike the reaction carried out with excess Fe^{2+} , there is no observable lag in the formation of $\bullet\text{Y122}$ in the limiting Fe^{2+} reaction (Fig. 3.1). The quantity of $\bullet\text{Y122}$ reaches its maximum value in ~ 8 s, at which point, the A_{410} dropline indicates a $\bullet\text{Y122}/\text{R2}$ ratio of 0.8 ± 0.08 .

In order to obtain the rate constants for the formation of $\bullet\text{Y122}$, non-linear least squares fitting of the A_{410} dropline-versus-time traces was carried out. Fitting the equation for a first-order process to the trace in Fig. 3.1 between 0.002 and

Fig. 3.1: Formation of •Y122 in the reaction of Fe(II)-R2-wt with O₂ under limiting Fe²⁺ conditions as monitored by SF-Abs spectroscopy. The reaction conditions (after mixing) were: 69 μM R2-wt, 161 μM Fe²⁺, 1 mM O₂, 50 μM dithionite, 100 mM HEPES, pH 7.6, 5 °C. The experimental trace represents the average of 3 trials. The theoretical trace is obtained by fitting a first-order process to 0.00 - 1.80 s of the experimental trace, and corresponds to a k_{obs} of 1.3 s⁻¹.



1.8 s gives a k_{obs} of 1.3 s^{-1} (Fig. 3.1). The theoretical trace and the experimental trace agree quite well for the first 2 s (85 % of total absorbance change), but deviate somewhat thereafter. These results suggest that rate of formation of $\bullet\text{Y122}$ in the reaction of Fe(II)-R2 ($2.3 \text{ Fe}^{2+}/\text{R2}$) with O_2 is quite similar to that in the reaction carried out with excess Fe^{2+} ($k_{\text{obs}} = 0.8 \text{ s}^{-1}$).

The 560 nm transient observed in the reaction of apo R2 with limiting Fe^{2+} was also observed in the reaction of Fe(II)-R2 complex with O_2 under limiting Fe^{2+} conditions (Fig. 3.2A). As shown in Chapter 2, this feature was not observed in the reaction carried out with excess Fe^{2+} . Nor was it observed when the reaction is carried out with limiting Fe^{2+} and 2.5 mM ascorbate (Fig. 3.2B). These results, thus, suggest that excess reductant can suppress the formation of the transient species. Table 3.1 summarizes the least squares fits of the A_{560} -versus-time traces to the general equation (Eq. 3.1) for a reaction involving two consecutive, first-order processes shown in Scheme 3.2 (Espenson, 1981), where A corresponds to the Fe^{2+} -R2 complex and B corresponds to the 560 nm-absorbing species. The kinetics of this transient can be very well described with a k_1 of $120\text{-}133 \text{ s}^{-1}$ and a k_2 of $15\text{-}23 \text{ s}^{-1}$ (Fig. 3.3). In contrast, the A_{560} -versus-time traces in the reaction of apo R2 with limiting Fe^{2+} and O_2 are poorly fit to the kinetic model of Scheme 3.2 (Bollinger *et al.*, 1994b).

Scheme 3.2:



Eq. 3.1: $A_t = A_\infty + \alpha \exp(-k_1 t) + (A_0 - A_\infty - \alpha) \exp(-k_2 t)$

Eq. 3.2: $\alpha = \frac{[(\epsilon_B - \epsilon_A)k_1 + (\epsilon_A - \epsilon_C)k_2]}{(k_2 - k_1)} [A]_0$

Table 3.1: Summary of least-squares fits to Eq. 3.1 of the A₅₆₀-versus-time traces from the reaction of Fe(II)-R2-wt (Fe²⁺/R2 = 2.3 - 2.4) with O₂.

Expt.	[Apo R2] (μM)	[Fe ²⁺] (μM)	Fit-range (s)	k ₁ (s ⁻¹)	k ₂ (s ⁻¹)
1	69	161	0.003 - 0.150	119	23
			0.003 - 0.300	130	21
2	73	176	0.003 - 0.150	132	16
			0.003 - 0.300	127	17
			0.001 - 8.02	132	15
3	300	690	0.003 - 0.300	133	16

When apo R2-wt is mixed with limiting Fe²⁺, the decay of the 560 nm absorbing transient appeared to correlate temporally with the formation of •Y122 in the initial part of the reaction (Bollinger *et al.*, 1994b). This observation led to the proposal that this transient species generates •Y122. However, in the Fe(II)-R2 reaction, the rate of decay of the 560 nm absorbing species (16-23 s⁻¹) is > 10 fold greater than the rate of formation of •Y122 (~ 1.3 s⁻¹). These results indicate that the 560 nm absorbing species is not directly involved in generating •Y122 under these conditions.

The 560 nm species appears and disappears at sufficiently rapid rates that it could give rise to a second intermediate which in turn could generate •Y122 (Scheme 3.3). Kinetic modeling, however, ruled out this possibility. Fig. 3.4 illustrates the scenario in which the 560 nm absorbing species generates a second intermediate with a rate constant of 16 s⁻¹ and this second intermediate generates

Fig. 3.2: A_{560} -versus-time trace in the reaction of Fe(II)-R2-wt with O_2 under limiting Fe^{2+} conditions. The reaction conditions (after mixing) were: 73 μM R2-wt, 176 μM Fe^{2+} , 1 mM O_2 , 50 μM dithionite, 100 mM HEPES, pH 7.6, 5 °C and (A) no ascorbate, or (B) 2.5 mM ascorbate. The experimental trace represents the average of 3 trials.

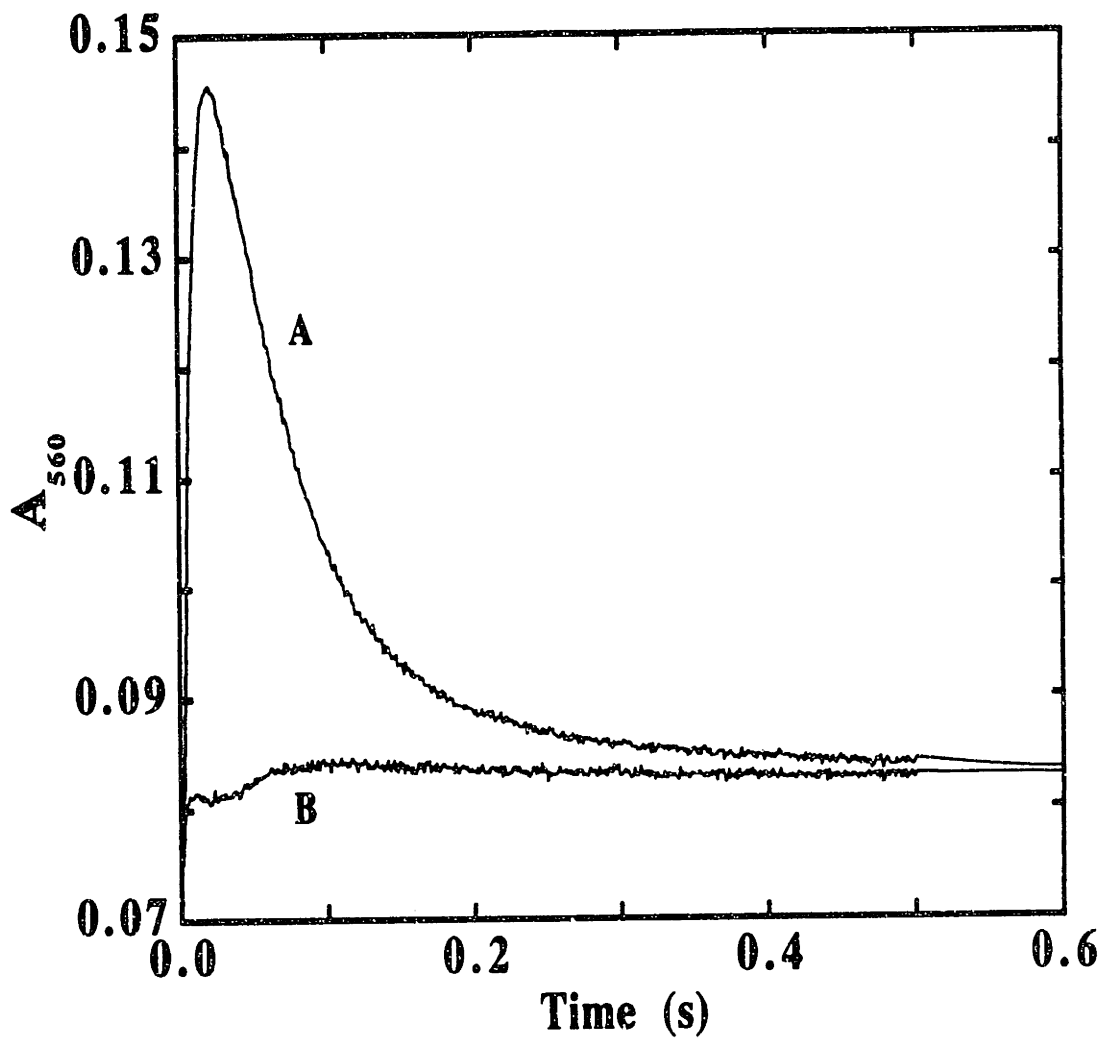


Fig. 3.5: A_{560} -versus-time trace in the reaction of Fe(II)-R2-wt with O_2 under limiting Fe^{2+} conditions. The reaction conditions (after mixing) were: 300 μM R2-wt, 690 μM Fe^{2+} , 1 mM O_2 , 100 mM HEPES, pH 7.6, 5 °C. The experimental trace represents the average of 3 trials. The theoretical trace is obtained by fitting two sequential, first-order processes to the 0.00 - 0.30 s region of the experimental trace, and corresponds to a k_1 of 133 s^{-1} and a k_2 of 16 s^{-1} .

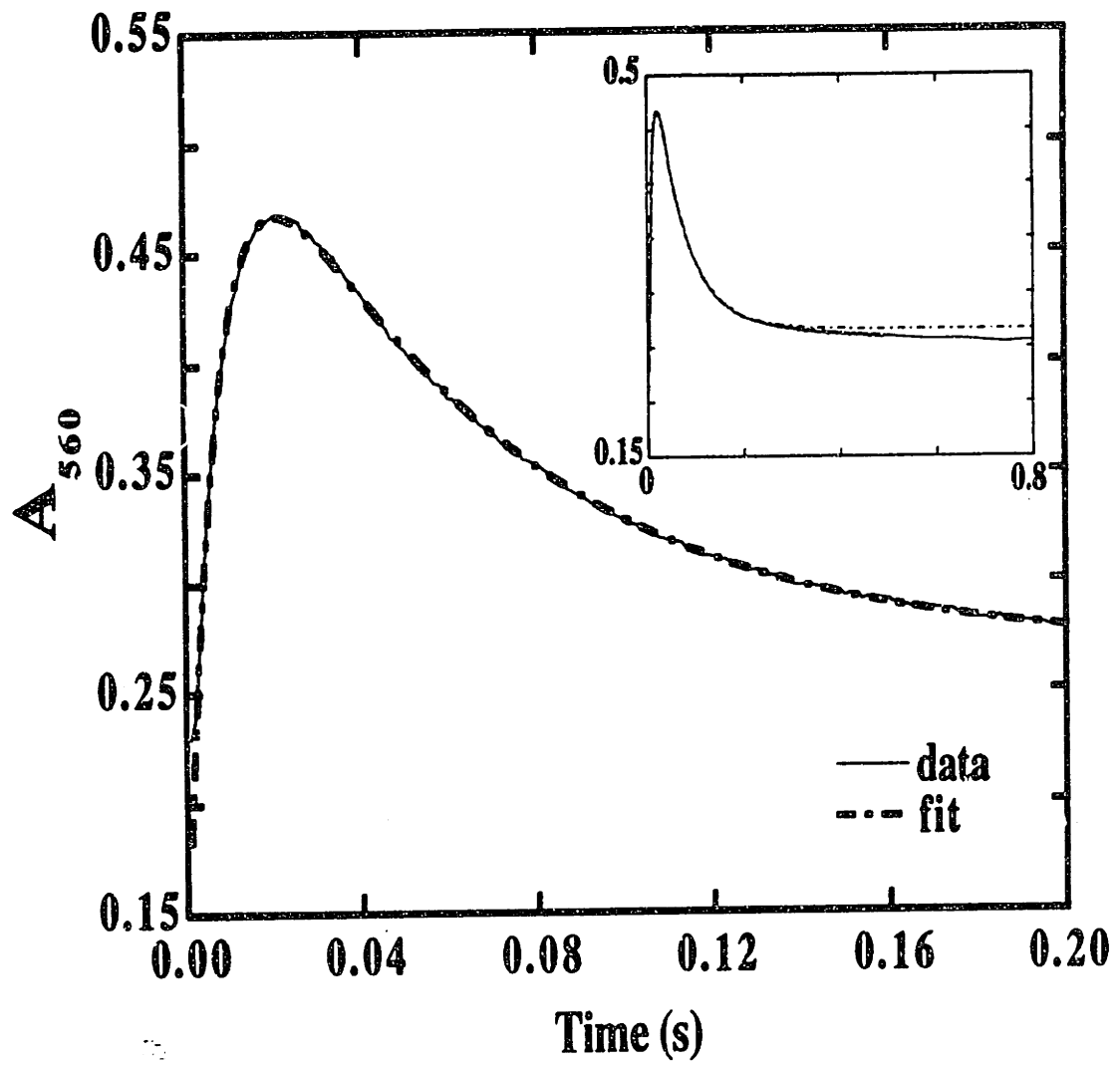
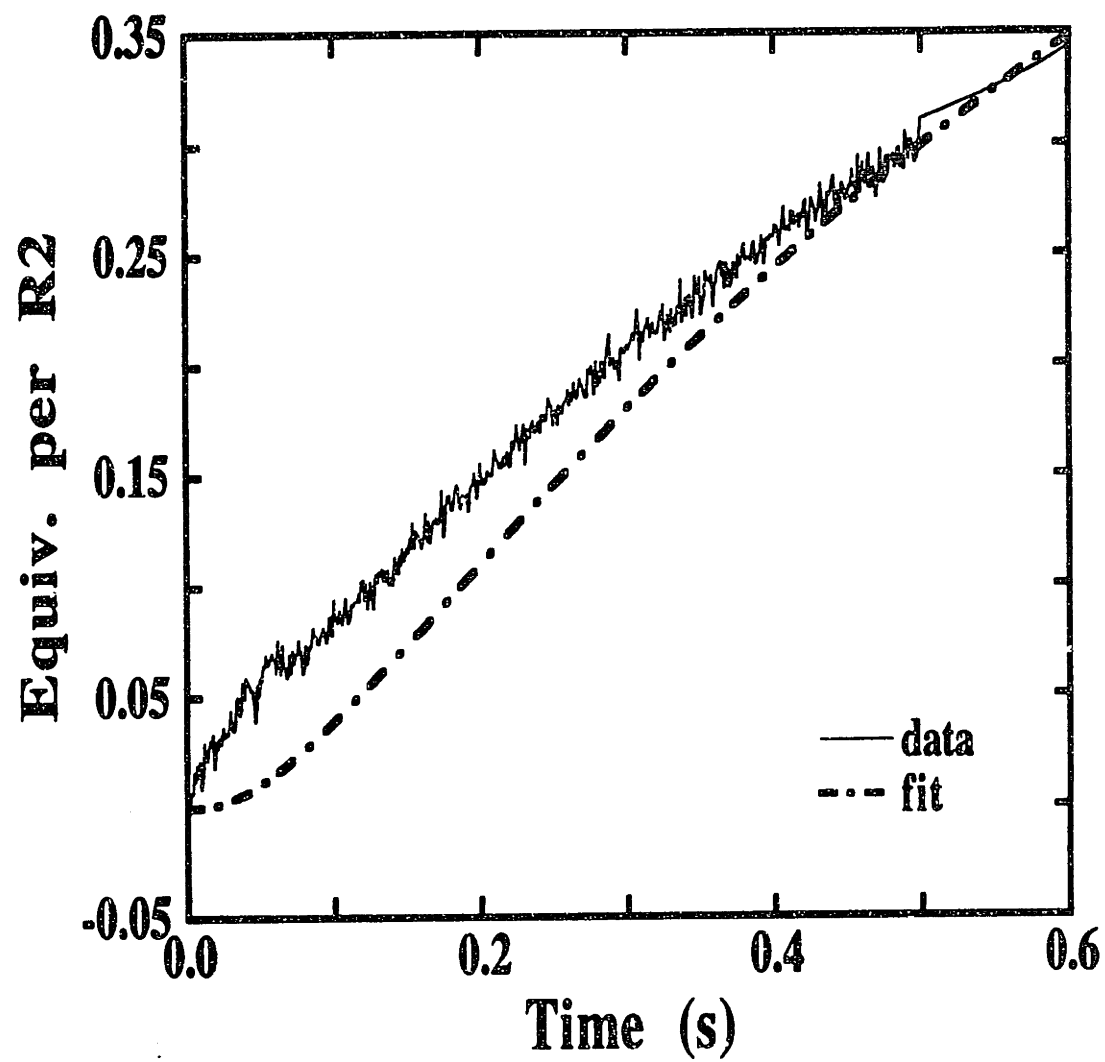
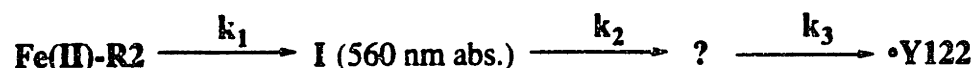


Fig. 3.4: Formation of \bullet Y122 in the reaction of Fe(II)-R2-wt with O₂ under limiting Fe²⁺ conditions. The reaction conditions were identical to those in Fig. 3.1. The theoretical trace describes formation of \bullet Y122 according to the kinetic model in Scheme 3.3, with $k_1 = 133 \text{ s}^{-1}$, $k_2 = 16 \text{ s}^{-1}$, and $k_3 = 1.3 \text{ s}^{-1}$.



•Y122 with a rate constant of 1.3 s^{-1} . In this scenario, formation of •Y122 exhibits a pronounced lag phase (Fig. 3.4). The experimental data, however, deviates markedly from the hypothetical curve and exhibits no lag phase. Thus, the model in Scheme 3.3 cannot account for the data.

Scheme 3.3:



Reaction of Fe(II)-R2-wt ($\text{Fe}^{2+}/\text{R2} = 2.3$) with O_2 as Monitored by RFQ-EPR Spectroscopy

The development of the EPR spectra in the limiting Fe^{2+} reaction (Fig. 3.5) is much more complex than that in the excess Fe^{2+} reaction. As with the excess Fe^{2+} reaction, the intermediate X forms rapidly, and at increasingly longer reaction times the spectra show increasing contribution from •Y122 and decreasing contribution from X. However, a significant amount of additional signals, with features broader than those of X and •Y122, are apparent in the $g = 2$ region in the spectra.

Table 3.2 summarizes the results of the double integration of the EPR spectra of the time-course samples. As with the excess Fe^{2+} reaction, the values determined for most samples agree well (within experimental errors) with the values obtained for the 60 s sample (completion of reaction). Even at the first time-point, 0.8 ± 0.2 equiv. of EPR active species (X, •Y122 and broad features) has accumulated. These results indicate that the reaction of Fe(II)-R2 ($2.3 \text{ Fe}^{2+}/\text{R2}$) with O_2 is significantly faster than the reaction of apo R2 with 2.3 Fe^{2+} and O_2 .

Furthermore, comparison of the EPR and the SF-Abs data suggests that the broad EPR signal and the 560 nm absorption band are not temporally correlated in the reaction of Fe(II)-R2 ($2.3 \text{ Fe}^{2+}/\text{R2}$) with O_2 . Inspection of the EPR spectra of the

Table 3.2: Summary of analysis of the EPR spectra from the reaction of Fe(II)-R2-wt (2.3 Fe²⁺/R2) with O₂. The ratio of spin/R2 was calculated by comparing the EPR intensity of each time-point to the 60 s time point which contains 0.8 •Y122/R2.

Time (s)	Spin/R2
0.025	0.79 ± 0.09
0.032	0.73 ± 0.08
0.044	0.91 ± 0.10
0.059	0.81 ± 0.09
0.093	0.91 ± 0.10
0.17	0.74 ± 0.09
0.46	0.91 ± 0.10
0.74	0.56 ± 0.07
60	(0.80)

0.46 s and the 0.74 s time-points (Fig. 3.5D and E) reveals a substantial amount of the broad features. The stopped-flow data, however, indicate that the decay of the 560 nm transient is already completed at these time-points (Fig. 3.3). These observations are in contradiction with the proposal that these two signals are correlated with a common •WH⁺ (Bollinger *et al.*, 1994b).

Control for Rapid Freeze-Quenching of R2

To ascertain that the species observed by the RFQ-EPR method represent true intermediate(s) in the reaction, a control was performed in which a RFQ-EPR sample was thawed and allowed to react at 0 °C. Fig. 3.6A shows the EPR spectrum

Fig. 3.5: Time-course of the reaction of Fe(II)-R2-wt with O₂ as monitored by EPR spectroscopy. Fe(II)-R2 (400 μM) prepared with 2.3 Fe²⁺/R2 in anaerobic 100 mM HEPES (pH 7.6) was mixed at 5 °C with an equal volume of O₂-saturated 100 mM HEPES (pH 7.6). The reaction was quenched (A) at 0.025 s, (B) at 0.093 s, (C) at 0.46 s, (D) at 0.74 s, and (E) at 60 s. The spectra were acquired at 20 K with a microwave power of 1 μW, a frequency of 9.43 GHz, a modulation frequency of 100 kHz, a modulation amplitude of 4 G, a time constant of 200 ms, a scan time of 200 s, and a receiver gain of 4 × 10⁴.

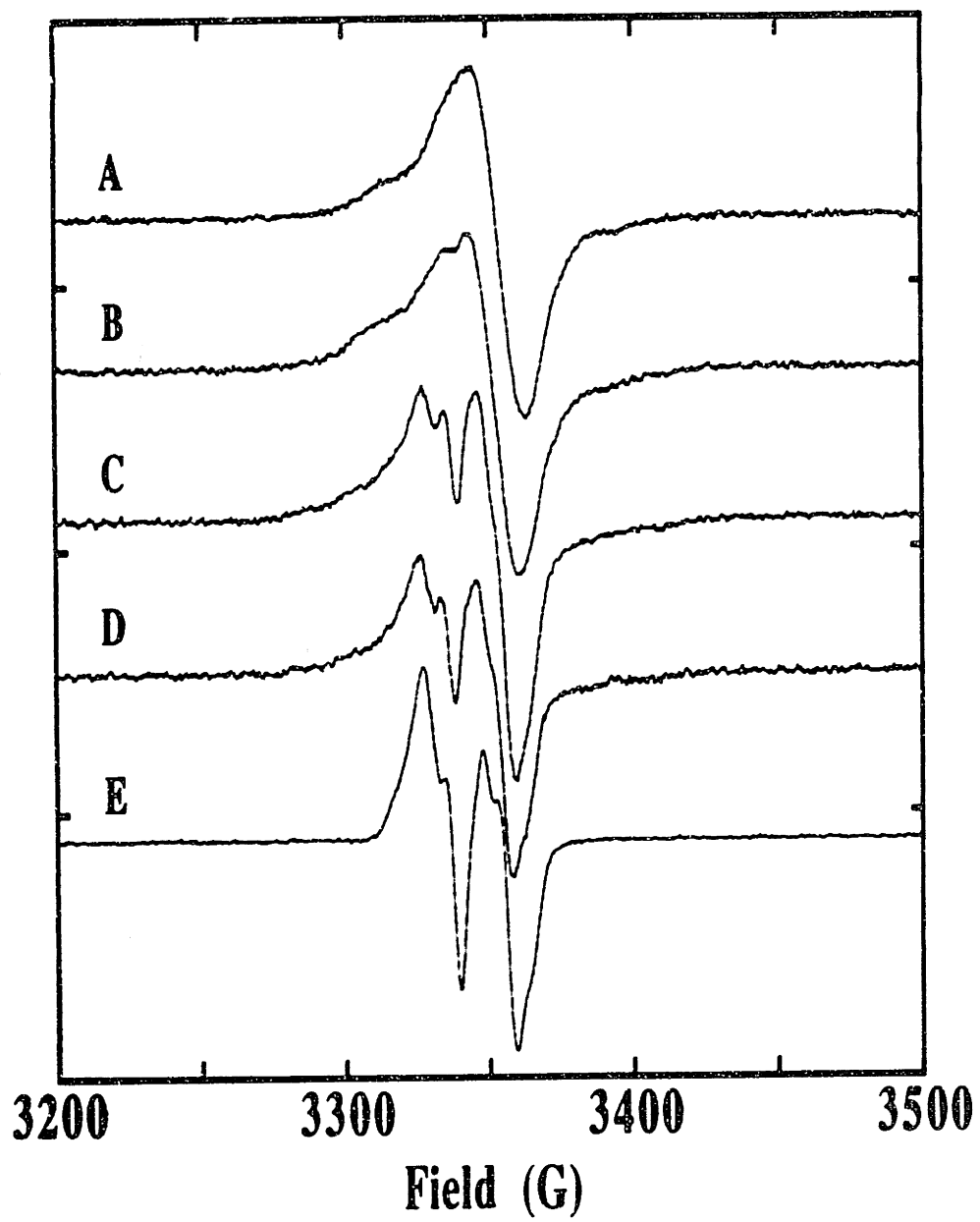
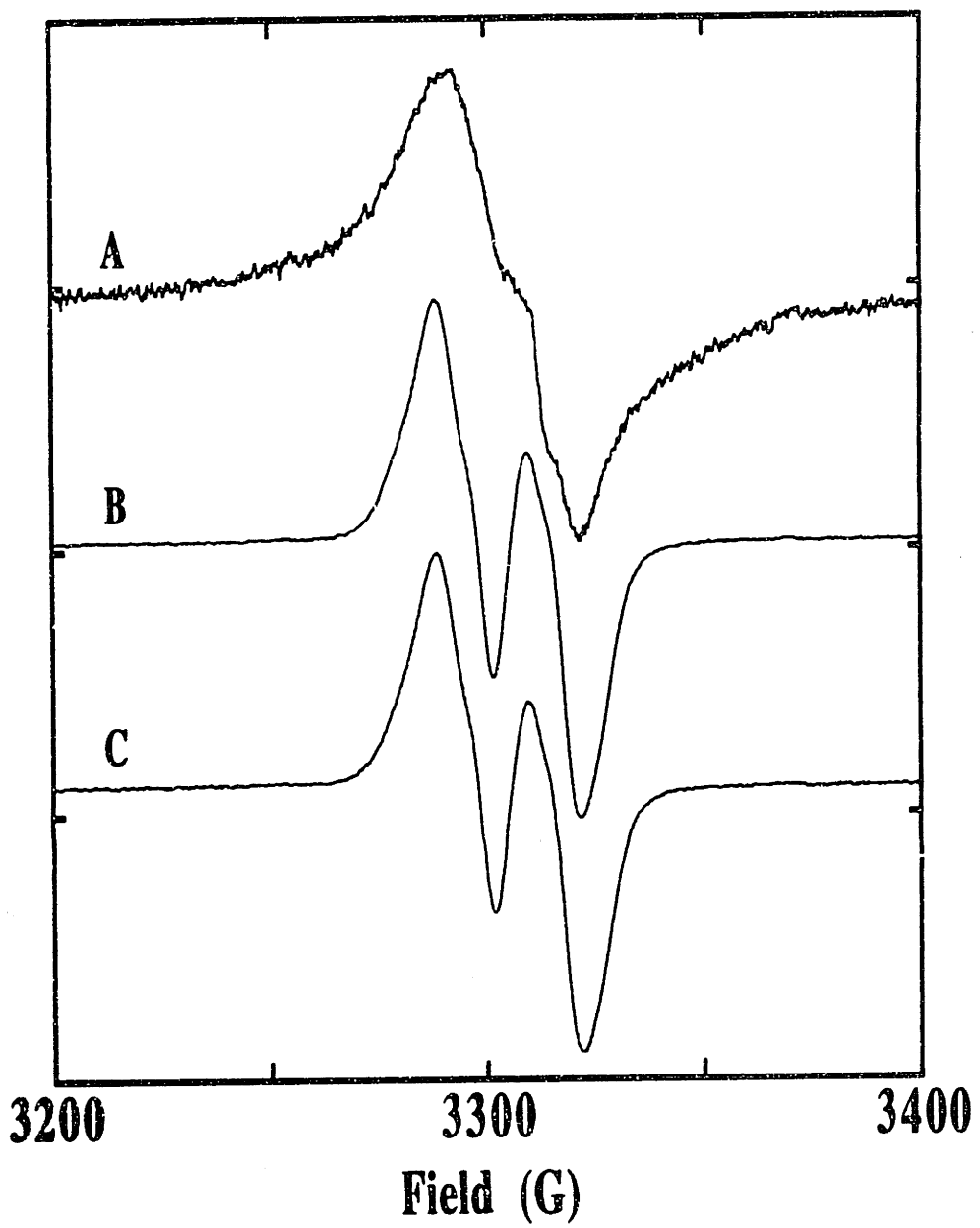


Fig. 3.6: EPR spectra of the reaction of Fe(II)-R2-wt ($\text{Fe}^{2+}/\text{R2} = 2.3$) with O_2 quenched at 0.059 s before (A) and after (B) the sample was thawed. The reaction conditions (after mixing) were: 200 μM R2-wt, 690 μM Fe^{2+} , 1 mM O_2 , 100 mM HEPES, pH 7.6, 5 °C. C is the EPR spectrum of the 60 s sample after it has been thawed and refrozen. The spectra were acquired at 100 K with a microwave power of 1 μW , a frequency of 9.27 GHz, a modulation frequency of 100 kHz, a modulation amplitude of 4 G, a time constant of 160 ms, a scan time of 160 s, and a receiver gain of 4×10^4 .



of the 0.059 s sample before thawing and the double-integrated intensity indicates that 0.91 ± 0.1 equiv. of spin per R2 is present. As shown in Fig. 3.6B, the EPR spectrum of the thawed sample is identical to the spectrum of a sample quenched at 60 s that contain only \bullet Y122 (Fig. 3.6C). Spin quantitation indicates that, after thawing, the sample contains 0.89 ± 0.1 equiv. of spin per R2. These results suggest that the EPR active species in the Fig. 3.6A is entirely converted into \bullet Y122.

Reaction of Fe(II)-R2-wt with O₂ in the Presence of Ascorbate as Monitored by SF-Abs and RFQ-EPR Spectroscopies

As mentioned above, no 560 nm transient is observed when Fe(II)-R2-wt ($2.4 \text{ Fe}^{2+}/\text{R2}$) is mixed with O₂-saturated HEPES buffer containing ascorbate (Fig. 3.2). The A₄₁₀, dropline-versus-time curve of the reaction of Fe(II)-R2-wt ($3 \text{ Fe}^{2+}/\text{R2}$) with O₂ in the presence of ascorbate illustrates that, after a small lag phase (~ 0.05 s), formation of \bullet Y122 is first-order (Fig. 3.7). Non-linear least squares fitting of the equation for a first order process to the region between 0.05 and 5.0 s gives a k_{obs} of 0.81 s^{-1} . The magnitude of A_{410,dropline} at completion (< 10 s) observed is consistent with a \bullet Y122/R2 ratio of 1.1. These results indicate that the reaction of Fe(II)-R2 in the presence of ascorbate is very similar to the excess Fe²⁺ reaction. Previous studies have already demonstrated that the reaction of apo R2-wt with limiting Fe²⁺ and ascorbate is similar to the reaction with excess Fe²⁺. As with apo R2-wt, the results of the Fe(II)-R2 reactions are consistent with the model in which ascorbate can serve to donate the required fourth electron in the place of excess Fe²⁺.

The EPR time-course of the reaction of Fe(II)-R2-wt ($3 \text{ Fe}^{2+}/\text{R2}$) with O₂ in the presence of ascorbate (Fig. 3.8) is also very similar to that of the excess Fe²⁺ reaction. The spectra of the samples quenched in the first 40 ms show almost exclusively X. (A small amount of \bullet Y122, accounting for $\sim 3 - 4\%$ of EPR intensity, is present, probably due to a low level of O₂ contamination in the Fe(II)-R2 sample.)

At longer reaction times, the spectra show increasing contribution from $\bullet Y122$ and decreasing contribution from X (Table 3.3). As with the excess Fe^{2+} reaction, at all times, the spectrum can be accounted for as the sum of the spectra of X and $\bullet Y122$, suggesting that X and $\bullet Y122$ are the only EPR active species present.

Quantitative Analysis of the Reaction of Apo R2 with Limiting Fe^{2+}

The model in Scheme 3.1 makes predictions that can be experimentally tested. If the proposed mechanism for the limiting Fe^{2+} pathway is correct, the spin quantitation of the time-course samples should reflect the presence of the putative $\bullet W48^+$. From the A_{560} -versus-time trace and the ϵ_{560} of tryptophan cation radicals ($\bullet WH^+$) reported in the literature, it is possible to estimate the amount of the 560 nm species accumulated at t_{max} . As illustrated in Fig. 3.9, the absorbance change from $t = 0$ to $t = t_{max}$ provides an estimate for the upper limit of the amount of 560 nm absorbing species formed, whereas the absorbance change from $t = t_{max}$ to $t = \infty$ provides the lower limit. Assuming an ϵ_{560} of $3000 M^{-1}cm^{-1}$ for a tryptophan cation radical (Solar *et al.*, 1991), this analysis would imply that 0.18 - 0.36 equiv. of the 560 nm absorbing species is present at $t_{max} = 0.18$ s in the reaction of apo R2-wt with limiting Fe^{2+} . As shown in Table 3.4 and Fig. 3.10, the Mössbauer data of the 0.18 s time-point indicates that 0.51 ± 0.05 equiv. of X is present, while the A_{410} , dropline-versus-time trace indicates that 0.09 equiv. of $\bullet Y122$ is present. If the model in Scheme 3.1 is correct, these results imply that a total of 0.78 - 0.96 equiv. of EPR active species (X + $\bullet Y122$ + $\bullet WH^+$) is present at this time. The EPR spectrum, however, indicates that only 0.69 ± 0.08 equiv. of total radical is present (Fig. 3.10). Therefore, the EPR and stopped-flow data appear to be inconsistent with the model in Scheme 3.1, and suggest that 560 nm absorption feature is not a $\bullet WH^+$.

Fig. 3.7: Formation of \bullet Y122 in the reaction of Fe(II)-R2 ($\text{Fe}^{2+}/\text{R2} = 3$) with O_2 in the presence of ascorbate as monitored by SF-Abs spectroscopy. The reaction conditions (after mixing) were: 296 μM R2-wt, 895 μM Fe^{2+} , 2.5 mM ascorbate, 1 mM O_2 , 100 mM HEPES, pH 7.6, 5 $^\circ\text{C}$. Each trace was constructed from the averages of 3 - 4 trials. The theoretical trace is obtained by fitting a first-order process to 0.05 - 5.0 s of the experimental trace, and corresponds to a k_{obs} of 0.81 s^{-1} .

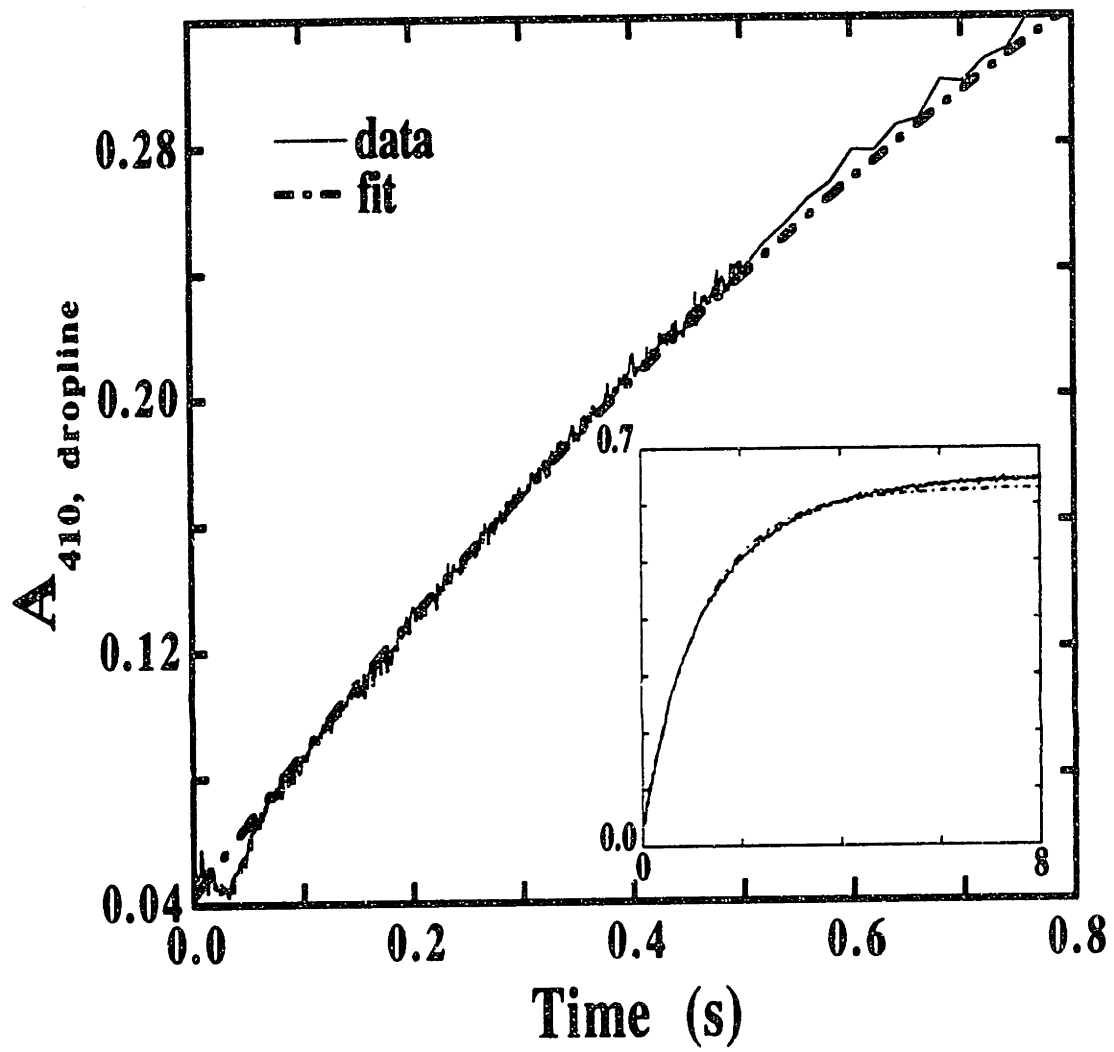


Fig. 3.8: Time-course of the reaction of Fe(II)-R2 ($\text{Fe}^{2+}/\text{R2} = 3$) with O_2 in the presence of ascorbate as monitored by EPR spectroscopy. The reaction conditions (after mixing) were: 200 μM R2-wt, 605 μM Fe^{2+} , 1 mM O_2 , 2.5 mM ascorbate, 100 mM HEPES, pH 7.6, 5 °C. The reaction was quenched (A) at 0.025, (B) at 0.093, (C) at 0.46, (D) at 0.74, and (E) at 60 s. The spectra were acquired at 20 K with a microwave power of 1 μW , a frequency of 9.43 GHz, a modulation frequency of 100 kHz, a modulation amplitude of 4 G, a time constant of 200 ms, a scan time of 200 s, and a receiver gain of 4×10^4 .

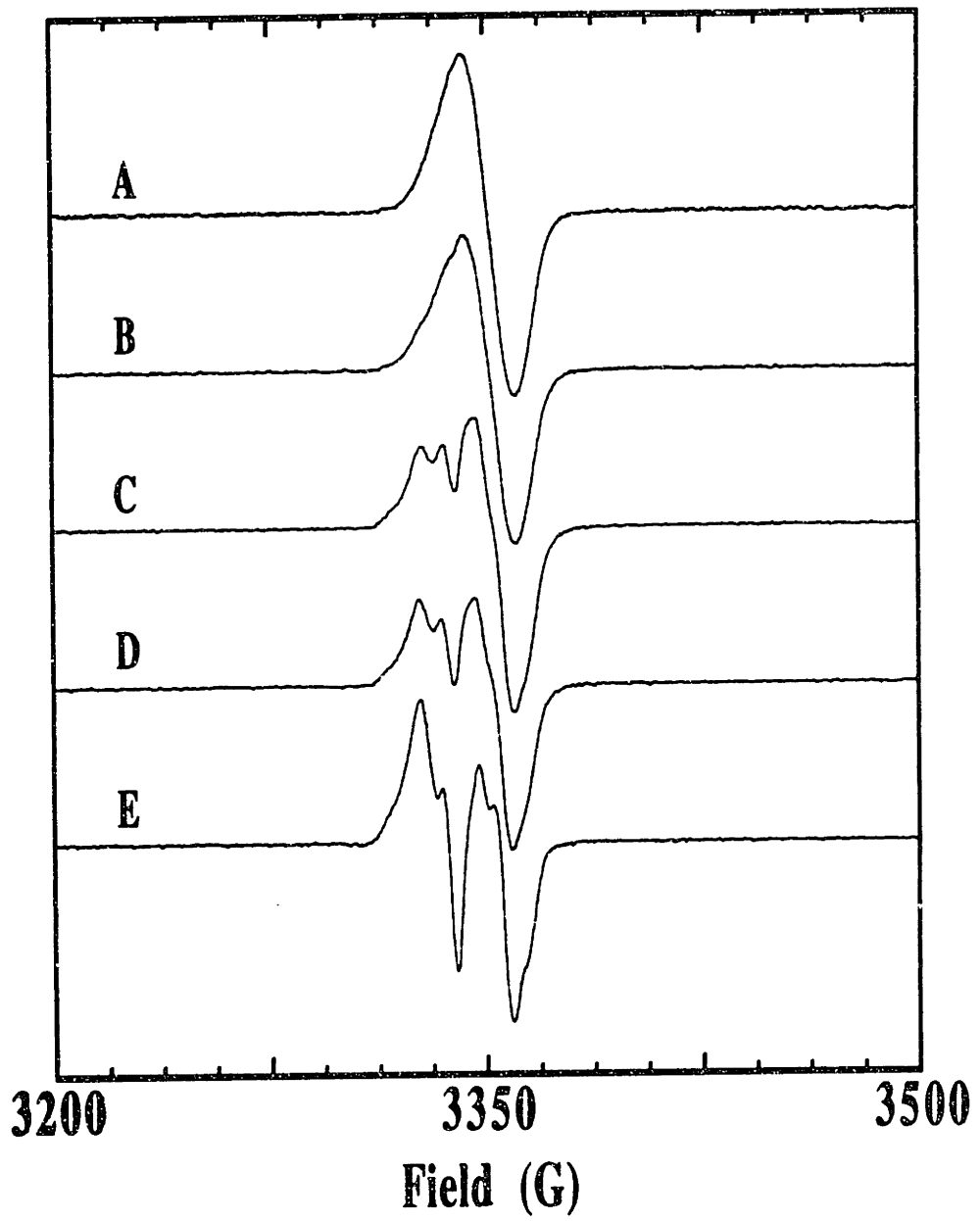


Fig. 3.9: Demonstration of how the amount of the 560 nm-absorbing transient species is estimated from the A_{560} -versus-time trace of the reaction of apo R2-wt with limiting Fe^{2+} and O_2 . $\Delta A_{560, \text{max}}$ is defined as the absorbance change at 560 nm from $t = 0$ to $t = t_{\text{max}}$, while $\Delta A_{560, \text{min}}$ is defined as the absorbance change between $t = t_{\text{max}}$ to $t = \infty$.

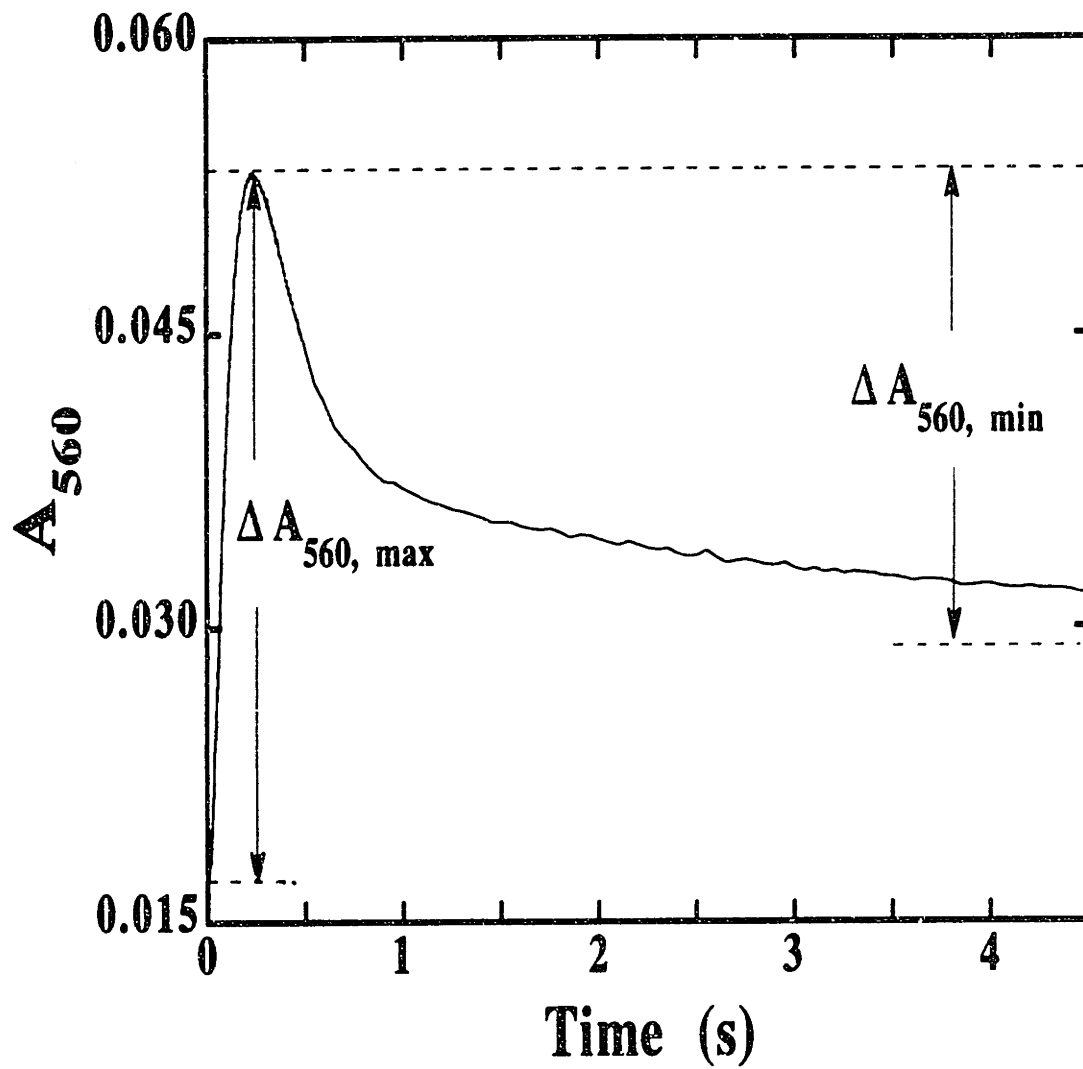


Fig. 3.10: Comparison of the measured quantities of X and •Y122 with the measured quantity of EPR-active species in the $g = 2$ region in the reaction of apo R2-wt with limiting Fe^{2+} . The amount of total spin in the $g = 2$ region are taken from Table 3.4. The amount of X was from the Mössbauer data. The •Y122 data was obtained from the stopped-flow experiments.

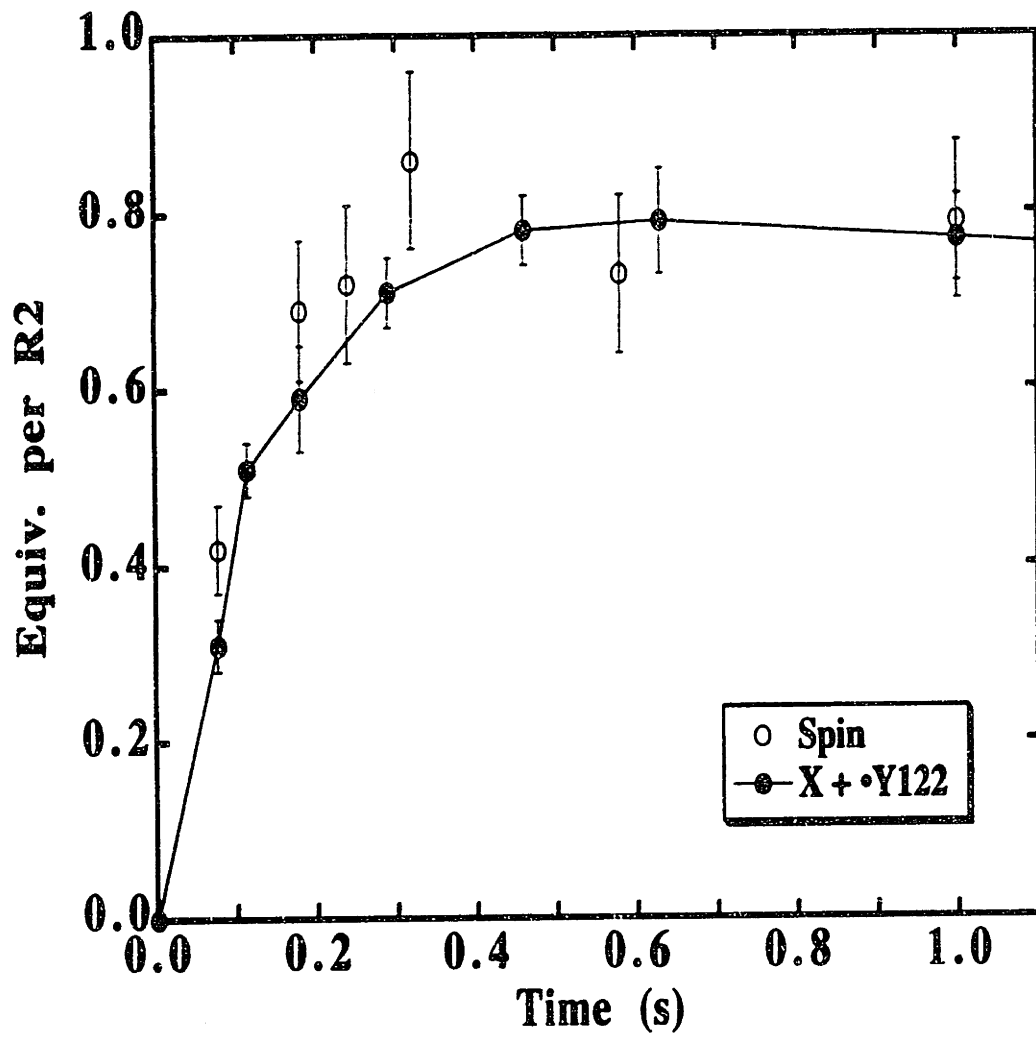


Table 3.3: Summary of the analysis of the EPR spectra from the reaction of Fe(II)-R2-wt (3 Fe²⁺/R2) with O₂ in the presence of ascorbate.

Time (s)	% X	% •Y122	Spin/R2	X/R2	•Y122/R2
0.025	97 ± 2	3 ± 2	1.0 ± 0.1	0.97 ± 0.1	0.03 ± 0.02
0.032	97 ± 2	3 ± 2	1.0 ± 0.1	0.97 ± 0.1	0.03 ± 0.02
0.044	96 ± 2	4 ± 2	1.1 ± 0.1	1.1 ± 0.1	0.04 ± 0.02
0.059	95 ± 2	5 ± 2	1.1 ± 0.1	1.0 ± 0.1	0.05 ± 0.02
0.093	-	-	1.0 ± 0.1	-	-
0.172	85 ± 2	15 ± 2	1.1 ± 0.1	0.93 ± 0.09	0.17 ± 0.03
0.46	60 ± 2	40 ± 2	1.0 ± 0.1	0.60 ± 0.06	0.40 ± 0.04
0.74	46 ± 2	46 ± 2	1.0 ± 0.1	0.46 ± 0.05	0.46 ± 0.05
60	0	100	1.1 ± 0.1	0	1.1 ± 0.1

¹Total spin per R2 was calculated assuming a packing factor of 0.67.

Reaction of Apo R2 with Fe²⁺ in ²H₂O as Monitored by SF-Abs Spectroscopy

Since at least two protons are required for the reconstitution reaction, the effect of replacing the solvent-exchangeable protons with deuterons was investigated. Stopped-flow results indicate that ²H₂O substitution has a substantial effect on the reaction of apo R2-wt with limiting Fe²⁺. In ²H₂O, the formation of •Y122 is slower than that observed in ¹H₂O. The A_{410,dropline}-versus-time trace of the reaction (Fig. 3.11) illustrates that formation of •Y122 in ²H₂O exhibits a significantly longer lag phase than that in ¹H₂O. Surprisingly, after a long lag phase, •Y122 formation is approximately first-order, and the reaction is completed in ~ 10 s. At completion, 0.61 ± 0.1 •Y122 per R2 (from two separate experiments) are present. When the lag phase is excluded from the fit-range, fitting of the experimental trace

Table 3.4: Summary of total spin quantitation at various time-points in the reaction of apo R2-wt with limiting Fe²⁺.

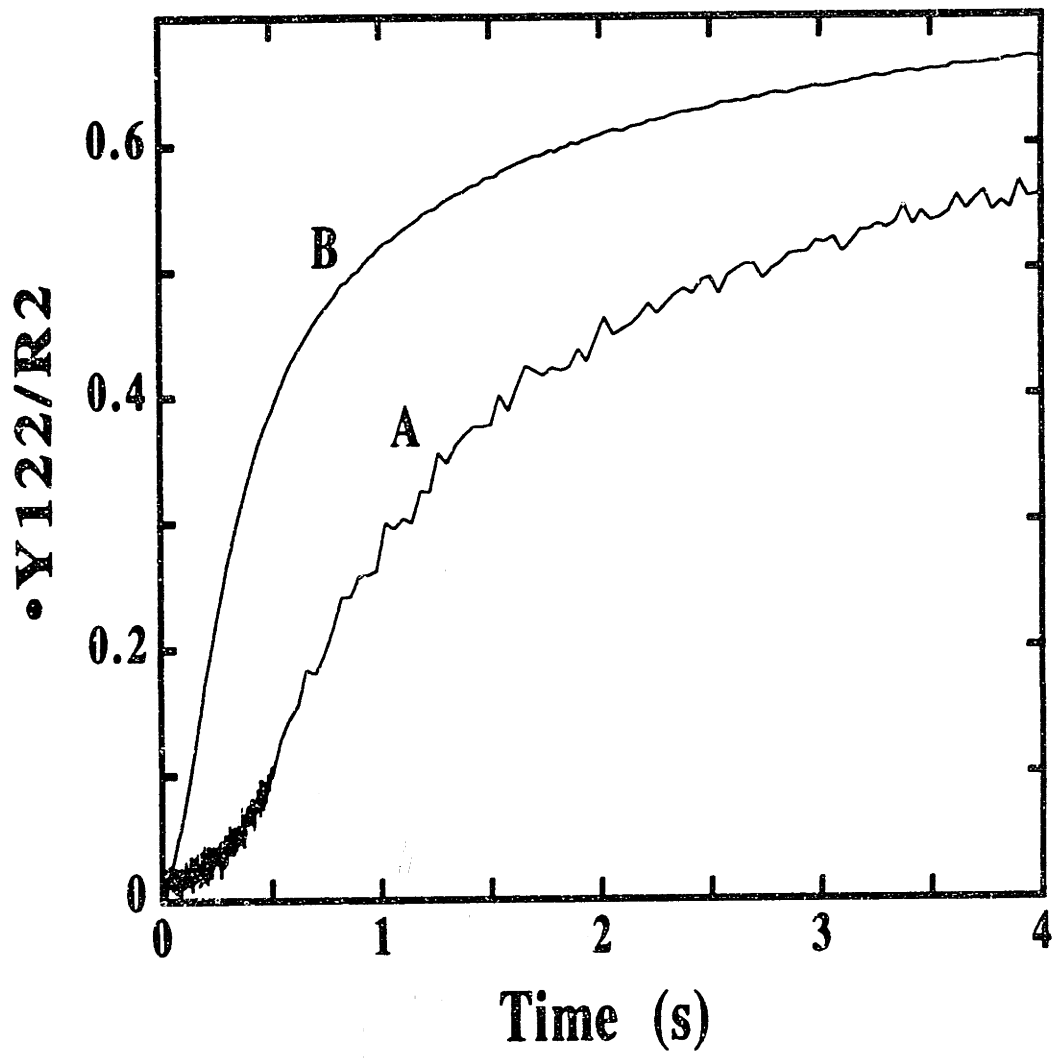
Time (s)	Spin/R2 ^a	X/R2 ^b	•Y122/R2 ^c	(X+•Y122)/R2
0.077	0.42 ± 0.05	0.29 ± 0.03	0.022	0.31 ± 0.03
0.114	-	0.46 ± 0.03	0.046	0.51 ± 0.03
0.18	0.69 ± 0.08	0.51 ± 0.05	0.089	0.59 ± 0.06
0.24	0.72 ± 0.09	-	0.16	-
0.29	-	0.51 ± 0.03	0.21	0.71 ± 0.04
0.32	0.86 ± 0.10	-	0.23	-
0.46	-	0.46 ± 0.03	0.32	0.78 ± 0.04
0.58	0.73 ± 0.09	-	0.37	-
0.63	-	0.39 ± 0.05	0.40	0.79 ± 0.06
1.0	0.79 ± 0.09	0.29 ± 0.03	0.48	0.77 ± 0.05
1.8	-	0.17 ± 0.03	0.55	0.72 ± 0.05
3.0	-	0.14 ± 0.05	0.61	0.75 ± 0.07
5.0	-	0.09 ± 0.05	0.64	0.73 ± 0.07
10	0.70 ± 0.09	-	0.68	-
60	-	<0.06	0.76	0.82 ± 0.07
180	0.71 ± 0.08	-	-	-

^aTotal spin per R2 was determined by EPR spectroscopy. assuming a packing factor of 0.7 ± 0.1.

^bQuantitation by Mössbauer spectroscopy.

^cAssessed by A410, dropline.

Fig. 3.11: A_{410} , dropline-versus-time trace in the reaction of apo R2-wt with limiting Fe^{2+} in 2H_2O (A) and in 1H_2O (B). The reaction conditions (after mixing) were: (A) 28 μM R2-wt, 63 μM Fe^{2+} , 100 mM HEPES (air-saturated), pD 7.6, 5 $^{\circ}C$; or (B) 54 μM R2-wt, 124 μM Fe^{2+} , 100 mM HEPES (air-saturated), pH 7.6, 5 $^{\circ}C$. The experimental traces were constructed from the averages of three trials at each wavelengths. The traces were scaled to reflect differences in protein concentrations.



to the equation of a first order process gives a k_{obs} of 0.75 s^{-1} (Fig. 3.12). In contrast, the formation of $\bullet\text{Y122}$ in $^1\text{H}_2\text{O}$ exhibits multiphasic kinetic behavior (Bollinger *et al.*, 1994b). In $^1\text{H}_2\text{O}$, the limiting Fe^{2+} reaction requires 60 - 120 μs to reach completion, at which point $0.8 \pm 0.1 \bullet\text{Y122}$ per R2 are present. The 560 nm transient is also observed in the limiting Fe^{2+} reaction carried out in $^2\text{H}_2\text{O}$ (Fig. 3.13). The formation and decay of the 560 nm transient in $^2\text{H}_2\text{O}$ is much slower than that in $^1\text{H}_2\text{O}$. In $^1\text{H}_2\text{O}$, the t_{max} is $\sim 0.2 \text{ s}$, while the t_{max} in the $^2\text{H}_2\text{O}$ is $\sim 0.8 \text{ s}$.

The reaction of apo R2-wt with excess Fe^{2+} is likewise affected by $^2\text{H}_2\text{O}$, although to a lesser extent than the limiting Fe^{2+} reaction. Fig. 3.14 illustrates that formation of $\bullet\text{Y122}$ in $^2\text{H}_2\text{O}$ exhibits a longer lag phase ($\sim 0.4 \text{ s}$) than that in $^1\text{H}_2\text{O}$. After the lag phase, formation of $\bullet\text{Y122}$ is approximately first order. Non-linear least squares fitting of the equation for a first order process to the region of this curve between 0.50 and 5.0 s gives an observed first-order rate constant of 0.37 s^{-1} . Thus, formation of $\bullet\text{Y122}$ is approximately 2 fold slower in $^2\text{H}_2\text{O}$ than that in H_2O . The magnitude of $A_{410, \text{dropline}}$ at completion (20 s) observed is consistent with a $\bullet\text{Y122}/\text{R2}$ ratio of 1.1 ± 0.1 , which is identical that in $^1\text{H}_2\text{O}$.

Reaction of Apo R2-wt with limiting Fe^{2+} in $^2\text{H}_2\text{O}$ as Monitored by RFQ-EPR Spectroscopy

To further characterize the limiting Fe^{2+} reaction in $^2\text{H}_2\text{O}$, the reaction was monitored by EPR spectroscopy. Molecular orbital calculations by Kim *et al.* (Kim *et al.*, 1993) using the Hückel-McLachlin technique suggested that the spin density of $\bullet\text{WH}^+$ is localized primarily at the C(2) and C(3) positions, and that the spin density is minimal (0.04) at the indole N position. These results predict that the spectrum of a $\bullet\text{WH}^+$ would only be affected slightly by the presence of $^2\text{H}_2\text{O}$. On the other hand, our previous work had shown that the EPR spectrum of X generated in $^2\text{H}_2\text{O}$ shows significant narrowing, probably due to coupling to at least one solvent-exchangeable

H nucleus (Bollinger, 1992). If the broad signal is associated with a $\bullet\text{WH}^+$, this signal would likely be better resolved in $^2\text{H}_2\text{O}$. Fig. 3.15 shows the EPR time-course of the reaction of apo R2 with limiting Fe^{2+} in $^2\text{H}_2\text{O}$. The EPR time-course of the reaction in $^1\text{H}_2\text{O}$ is included for comparison (Fig. 3.16).

When the reaction is carried out in $^2\text{H}_2\text{O}$, X is the only EPR active species detected in the 0.14 s time-point. At longer reaction time, the spectra show increasing contributions from $\bullet\text{Y122}$ and decreasing contributions from X. Surprisingly, at all times during the reaction, the spectrum can be accounted for as the sum of the spectra of X and $\bullet\text{Y122}$ (Table 3.5). Fig. 3.17 demonstrates that at 0.84 s no broad features were observed, even though Fig. 3.13 shows that the 560 nm absorbing species reaches its maximum at this time-point. The theoretical spectra in Fig. 3.17 are generated by summation of the reference spectra for X (62 %) and $\bullet\text{Y122}$ (38 %) in proportions to approximate the line-shape of the experimental spectra. As shown in Fig. 3.17, the simulation reproduces both the absorption spectrum and the first-derivative spectrum of the 0.84 s time-point extremely well. This analysis, thus, strongly suggest that the broad EPR features observed is not correlated with the 560 nm absorption band.

Although the analysis shown in Fig. 3.17 provide strong support that no broad features are detected in the limiting Fe^{2+} reaction carried out in $^2\text{H}_2\text{O}$, we have considered the possibility that the species which give rise to the broad EPR features might have accumulated to a lesser extent in $^2\text{H}_2\text{O}$ such that it becomes indistinguishable in the EPR spectra. Inspection of Fig. 3.13 reveals that the A_{560} -versus-time trace of the reaction in $^2\text{H}_2\text{O}$ fails to reach as great a maximum absorbance as the trace obtained in $^1\text{H}_2\text{O}$. Comparison of the two traces in Fig. 3.13 suggest that the 560 nm-absorbing species in $^2\text{H}_2\text{O}$ accumulates to roughly 30 - 50 % of that in $^1\text{H}_2\text{O}$. If it is assumed that the 560 nm-absorption band and the broad EPR features are associated with a common $\bullet\text{WH}^+$, the amount of the broad EPR features

Fig. 3.12: Non-linear regression analysis of A_{410} , dropline-versus-time trace in Fig. 3.11A. The theoretical curve was obtained by fitting a first-order process to 0.50-6.0 s of the experimental trace. It corresponds to a k_{obs} of 0.75 s^{-1} .

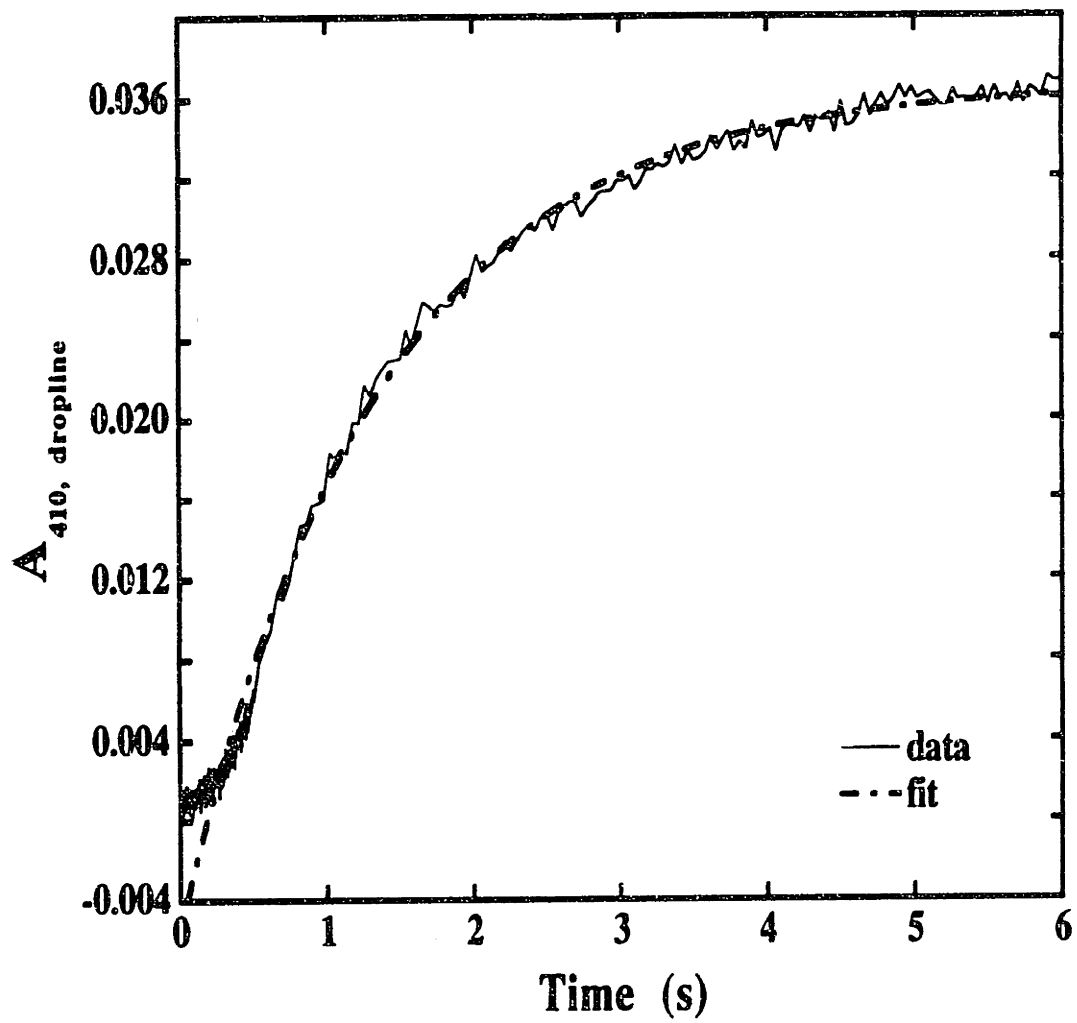


Fig. 3.13: A_{560} -versus-time trace in the reaction of apo R2-wt with limiting Fe^{2+} in 2H_2O (A) and in 1H_2O (B). The reaction conditions (after mixing) were: (A) 28 μM R2-wt, 63 μM Fe^{2+} , 100 mM HEPES (air-saturated), pD 7.6, 5 $^{\circ}C$; or (B) 54 μM R2-wt, 124 μM Fe^{2+} , 100 mM HEPES (air-saturated), pH 7.6, 5 $^{\circ}C$. The experimental traces were constructed from the averages of three trials. The traces were scaled to reflect differences in protein concentrations.

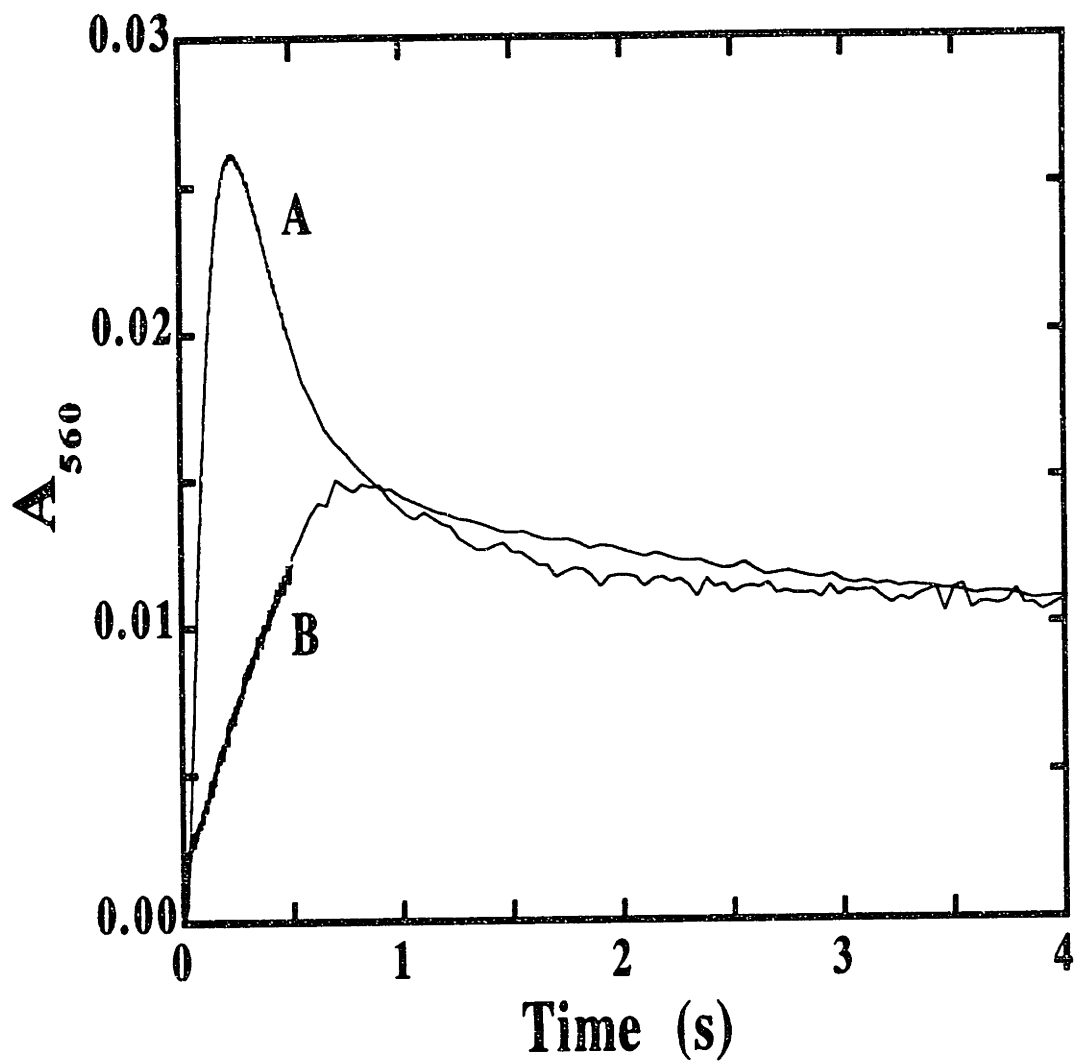


Fig. 3.14: Formation of \bullet Y122 in the reaction of apo R2-wt with excess Fe^{2+} in $^2\text{H}_2\text{O}$ (A) and in $^1\text{H}_2\text{O}$ (B). The reaction conditions (after mixing) were: (A) 28 μM R2-wt, 140 μM Fe^{2+} , 100 mM HEPES (air-saturated), pD 7.6, 5 $^\circ\text{C}$; or (B) 295 μM R2-wt, 1.47 mM Fe^{2+} , 100 mM HEPES (air-saturated), pH 7.6, 5 $^\circ\text{C}$. The experimental traces were constructed from the averages of three trials.

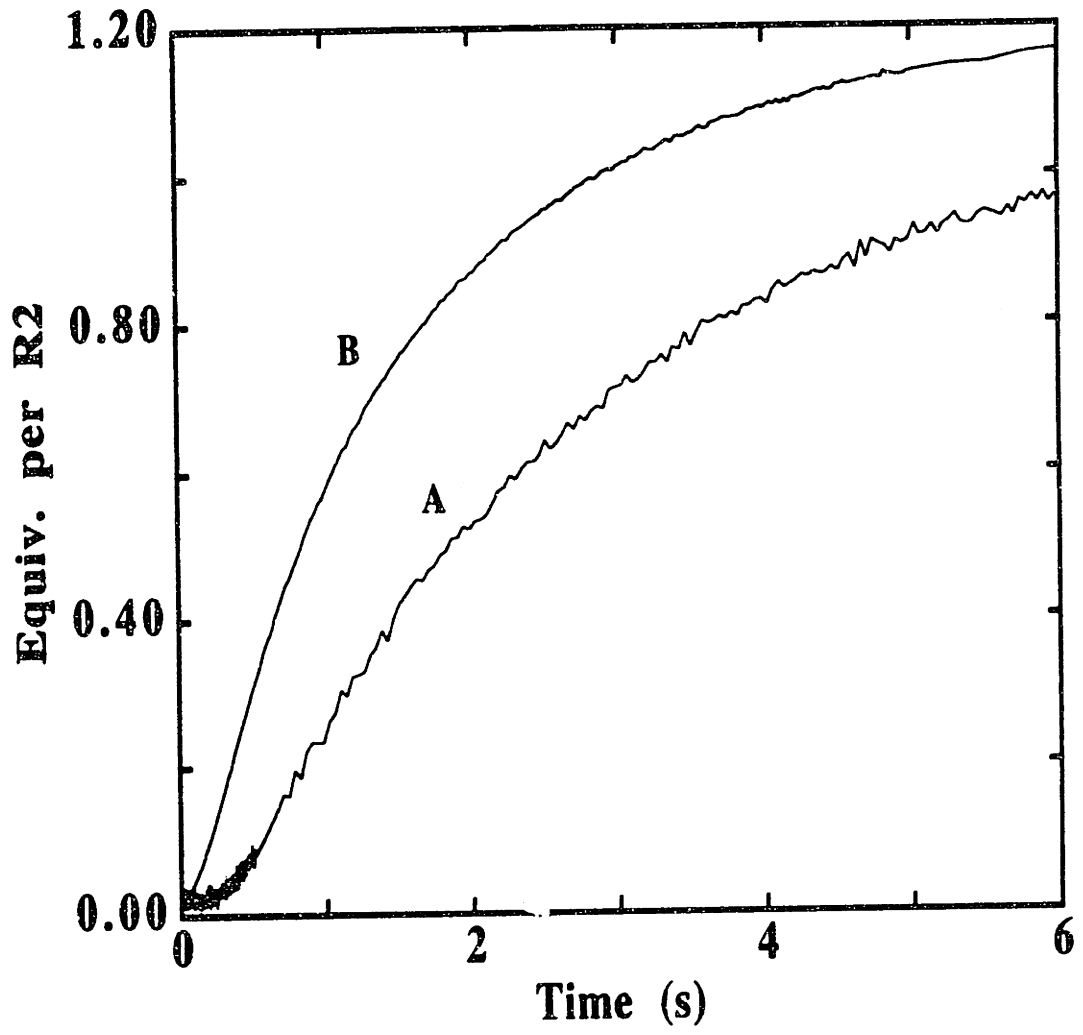


Fig. 3.15: Time-course of the reaction of apo R2-wt with limiting Fe²⁺ in ²H₂O as monitored by EPR spectroscopy. The reaction conditions (after mixing) were: 200 μM R2-wt, 461 μM Fe²⁺, 100 mM HEPES (air-saturated), pD 7.6, 5 °C; The reaction was quenched (A) at 0.090 s, (B) at 0.35 s, (C) at 0.84 s, (D) at 1.74 s, and (E) at 5 min. The spectra were acquired at 20 K with a microwave power of 1 μW, a frequency of 9.47 GHz, a modulation frequency of 100 kHz, a modulation amplitude of 4 G, a time constant of 160 ms, a scan time of 170 s, and a receiver gain of 4 × 10⁴.

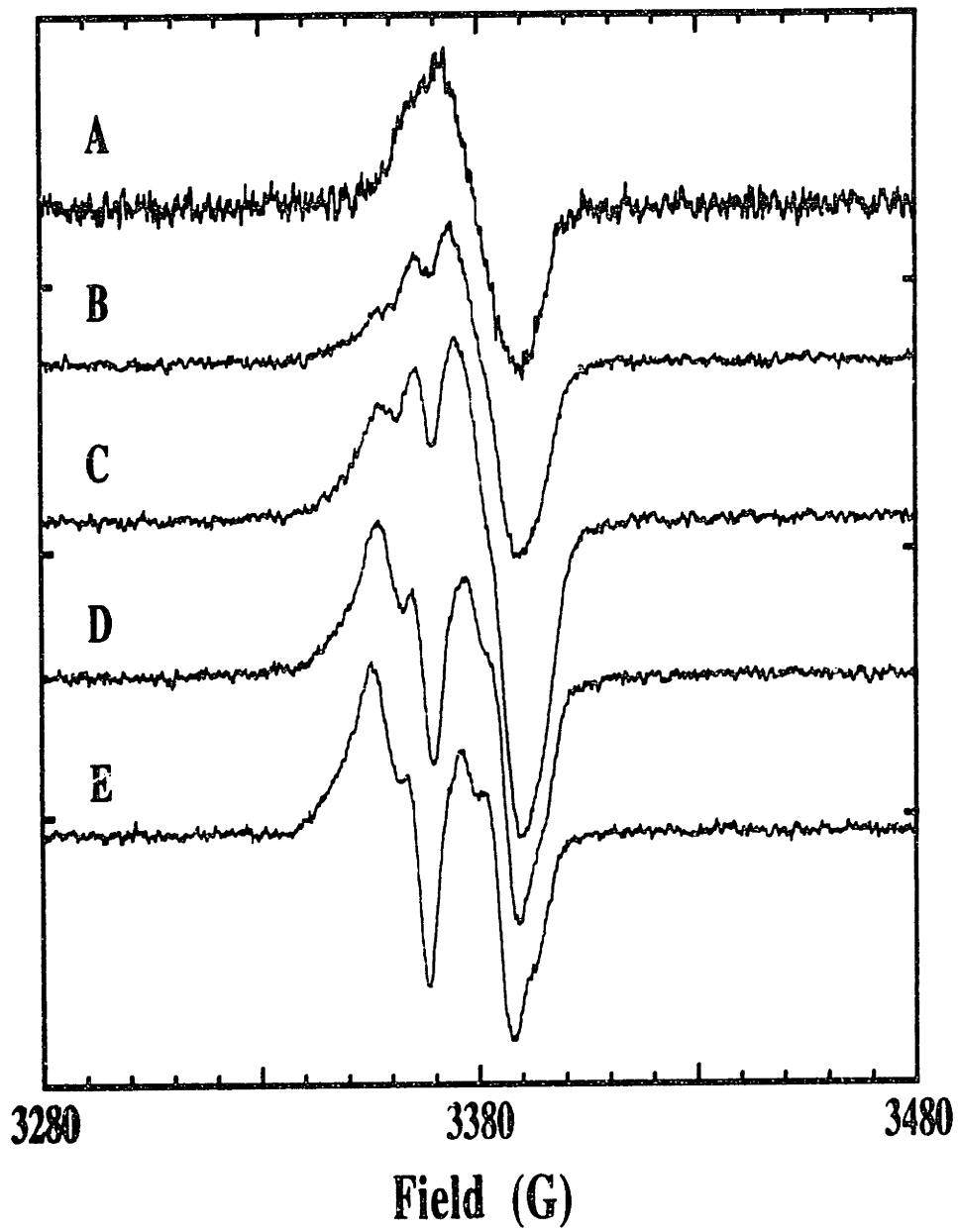


Fig. 3.16: Time-course of the reaction of apo R2-wt with O₂ in ¹H₂O as monitored by EPR spectroscopy. The reaction conditions (after mixing) were: 300 μM R2-wt, 690 μM Fe²⁺, 100 mM HEPES, pH 7.6, 5 °C; The reaction was quenched (A) at 0.077 s, (B) at 0.18 s, (C) at 0.31 s, (D) at 1.0 s, and (E) at 180 s. The spectra were acquired at 20 K with a microwave power of 1 μW, a frequency of 9.43 GHz, a modulation frequency of 100 kHz, a modulation amplitude of 4 G, a time constant of 200 ms, a scan time of 200 s, and a receiver gain of 4 x 10⁴.

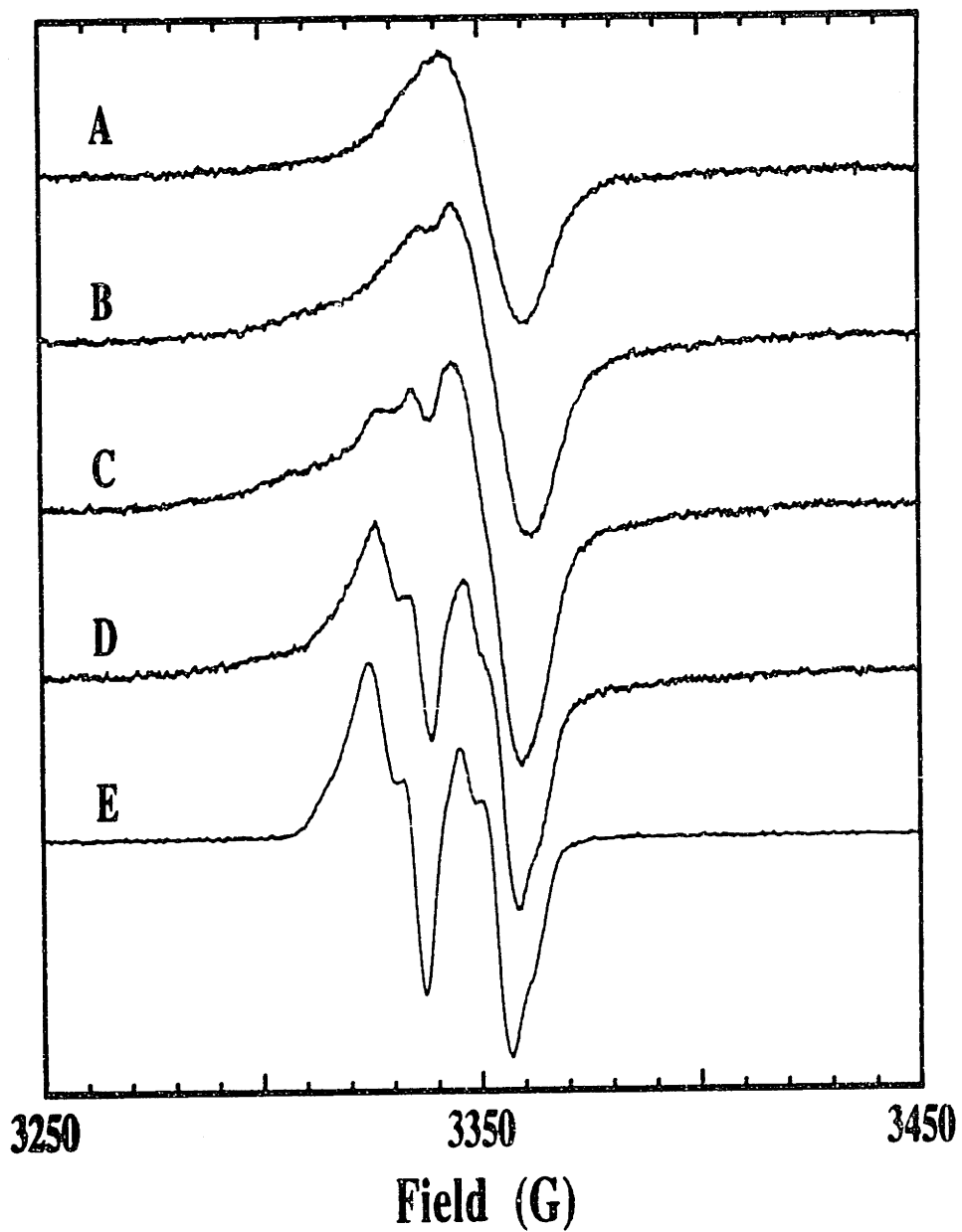


Fig. 3.17: An example of the deconvolution of the EPR spectrum from the reaction of apo R2-wt with limiting Fe^{2+} in $^2\text{H}_2\text{O}$. The experimental spectrum in **A** is the absorption spectrum of the 0.84 s time-point of the experiment depicted in Fig. 3.15. **B** is the more standard derivative presentation of the same spectrum. The theoretical spectrum was obtained by summation of the reference spectra of **X** and $\bullet\text{Y122}$ in a ratio of 62:38 (**X**: $\bullet\text{Y122}$). (The reference spectrum for $\bullet\text{Y122}$ is of the 60 s time-point of the same reaction. The reference spectrum for **X** was generated by allowing the reaction of apo R2-Y122F with excess Fe^{2+} in $^2\text{H}_2\text{O}$ to react for 0.22 s at 5 °C before the reaction was freeze-quenched. The reaction conditions (after mixing) were: 70 μM R2-Y122F, 520 μM Fe^{2+} , 100 mM HEPES (air-saturated), pD 7.6 and 5 °C.)

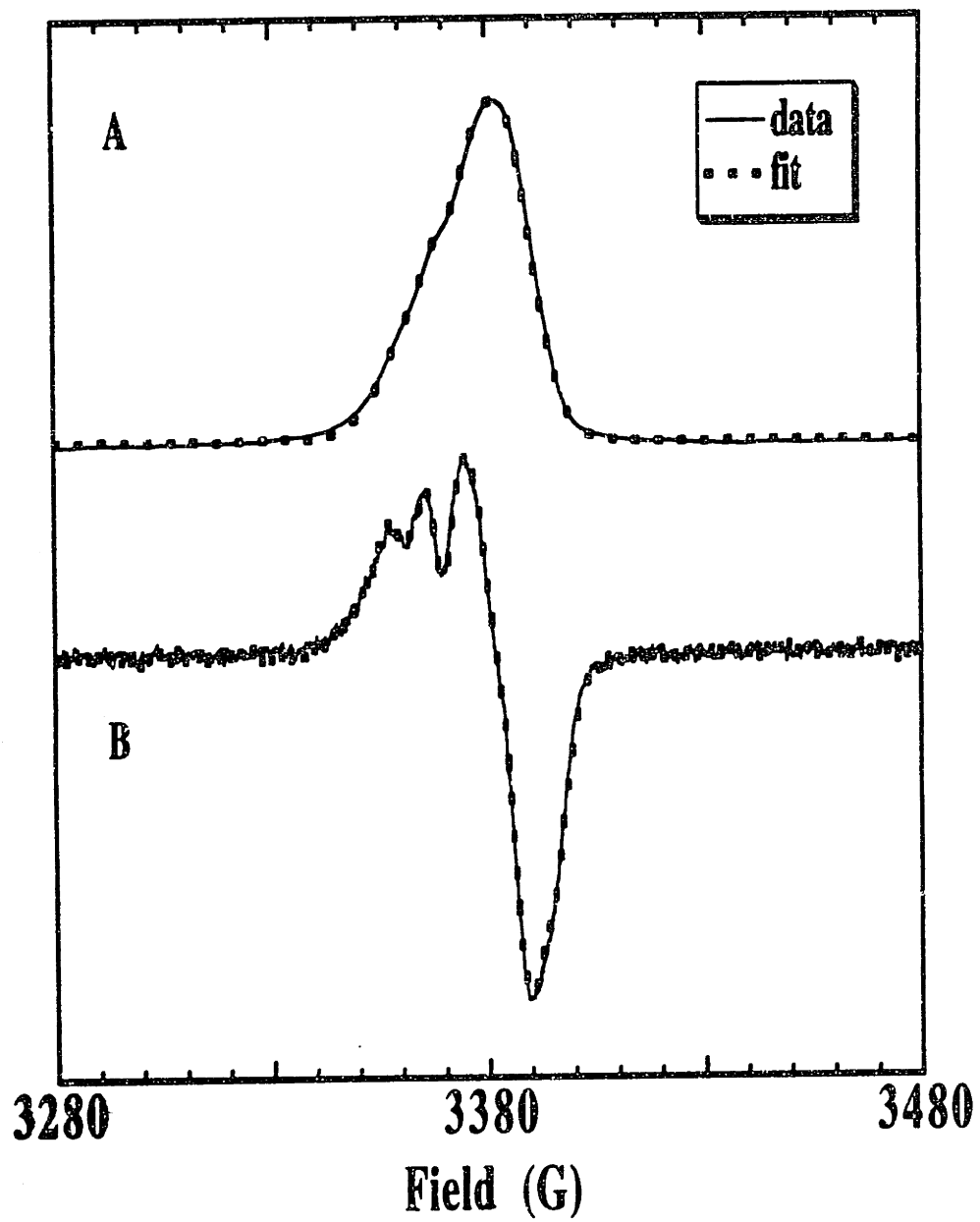


Table 3.5: Summary of total spin quantitation at various time-points in the reaction of apo R2-wt with limiting Fe²⁺ in ²H₂O. Total spin per R2 was calculated assuming a packing factor of 0.7 ± 0.1.

Time (s)	Spin/R2	% X	% •Y122	X/R2	•Y122/R2
0.091	0.19 ± 0.02	100	-	0.19	-
0.19	0.47 ± 0.06	67 ± 1	33 ± 1	0.31	0.16
0.35	0.48 ± 0.06	76 ± 1	24 ± 1	0.36	0.12
0.44	0.56 ± 0.07	73 ± 1	27 ± 1	0.41	0.15
0.84	0.80 ± 0.07	62 ± 1	38 ± 1	0.49	0.31
1.44	0.89 ± 0.07	42 ± 1	58 ± 1	0.37	0.52
1.74	0.70 ± 0.08	24 ± 1	76 ± 1	0.17	0.53
300	0.62 ± 0.07	-	100	-	0.62

might be less in the ²H₂O reaction than that in ¹H₂O reaction.

In order to explore the possibility that the amount of the broad EPR features in the ²H₂O reaction may be below detection limit, we attempted to fit the experimental spectrum in Fig. 3.17 with a hypothetical spectrum for the broad EPR features (Fig. 3.18) to estimate the lower limit of detection for this species. The hypothetical spectrum¹ for the broad EPR features shown in Fig. 3.18 was obtained

¹ Generation of the hypothetical spectrum of the broad EPR features in Fig. 3.18 is complicated by the complexity of the experimental spectra and by the errors in subtraction. Thus, the inner part of the spectrum in Fig. 3.18 - where the spectra of X and •Y122 had been subtracted away - may not reflect the spectrum of the real component. The part of the spectrum which falls outside the summed spectra of X and •Y122 (as indicated by the square brackets in Fig. 3.18), however, should reflect contribution from only a third EPR-active species.

by subtracting away the spectra of X and of •Y122 from the experimental spectra of the reaction of apo R2-wt with limiting Fe²⁺ (Bollinger, 1992). In the reaction of apo R2-wt with limiting Fe²⁺, it was estimated that ~50 % of the intensity of the experimental spectrum is associated with the broad EPR features (Bollinger, 1992). Since formations of both X and the 560 nm-absorbing-species are roughly 2 - 3 fold slower in ²H₂O than in ¹H₂O, if the assumption that the 560 nm-absorbing species is associated with the broad EPR features is correct, it might be expected that the broad EPR features would contribute approximately 25 - 50 % of the total intensity of the experimental spectrum. Using the reference spectra for X and •Y122 and using the hypothetical spectrum for the broad EPR features shown in Fig. 3.18, we constructed a series of summation spectra with different ratios of X, •Y122 and the broad features, and compared these summation spectra to the experimental spectrum in Fig. 3.17. The outer spectra in Fig. 3.19A and 3.19B are the summation spectra if the broad EPR features contributes 25 or 50 % of the total intensity of the experimental spectrum of the 0.84 s time-point (inner spectra of Fig. 3.19A and 3.19B), and it is clear that these summation spectra are significantly different from that of the experimental spectrum. In contrast, Fig. 3.17 shows that the simulation using only the spectra of X and •Y122 can reproduce the experimental spectra extremely well. The experimental spectrum in Fig. 3.17A has an absorption envelop of the same width as the summed spectra of X and •Y122. This result indicates that no significant amount of the broad features (Fig. 3.18) is present in the experimental spectrum of Fig. 3.17. This analysis was also carried out the other time-points of the same experiment, and the results suggest that these is very little, if any, broad EPR features present in the EPR spectra of the ²H₂O reaction.

Fig. 3.18: Hypothetical spectrum for the broad EPR features which accumulate in the reaction of apo R2 with limiting Fe²⁺. This spectrum is obtained by subtracting away the spectra for X and •Y122 from the experimental spectrum of the 0.15 s time-point of the reaction of apo R2-wt with limiting Fe²⁺ (Bollinger, 1992). The square brackets indicate the features that fall outside the summed spectra of X and •Y122, and these features are associated solely with the additional EPR-active species.

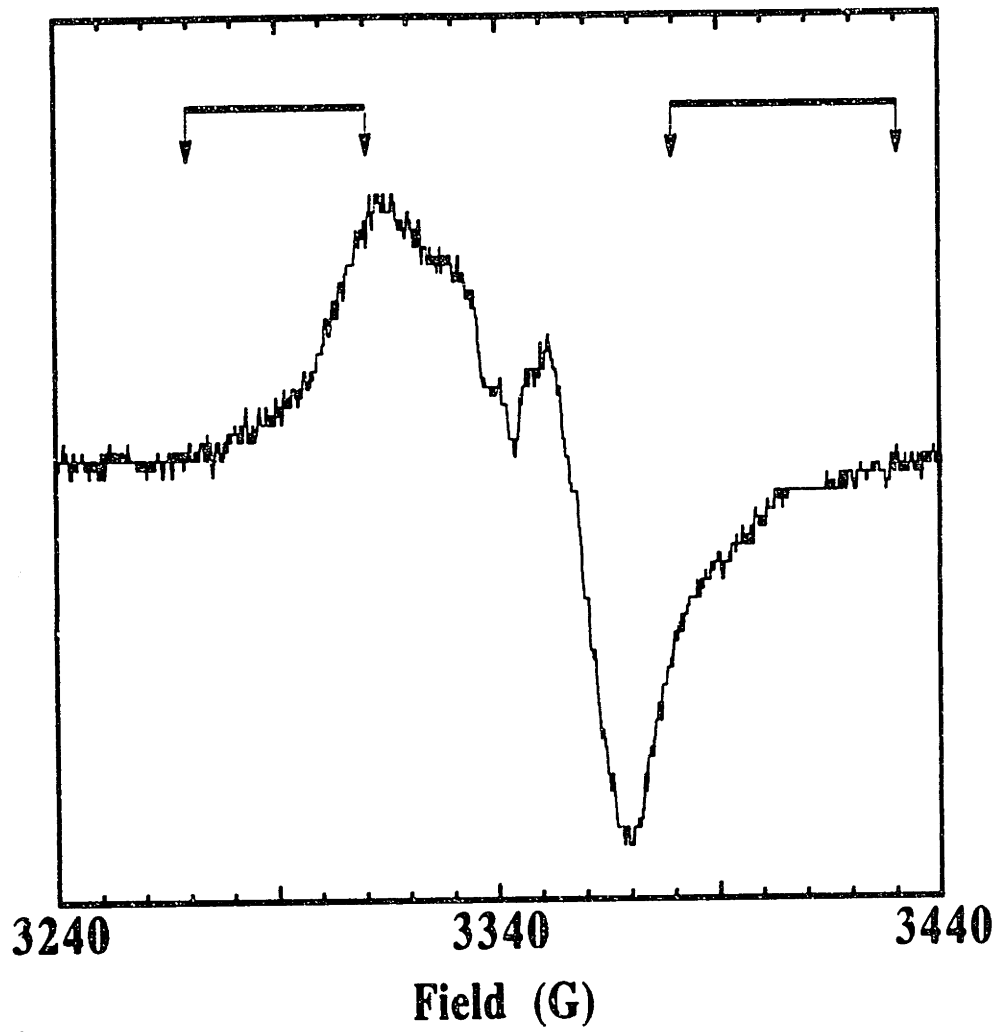
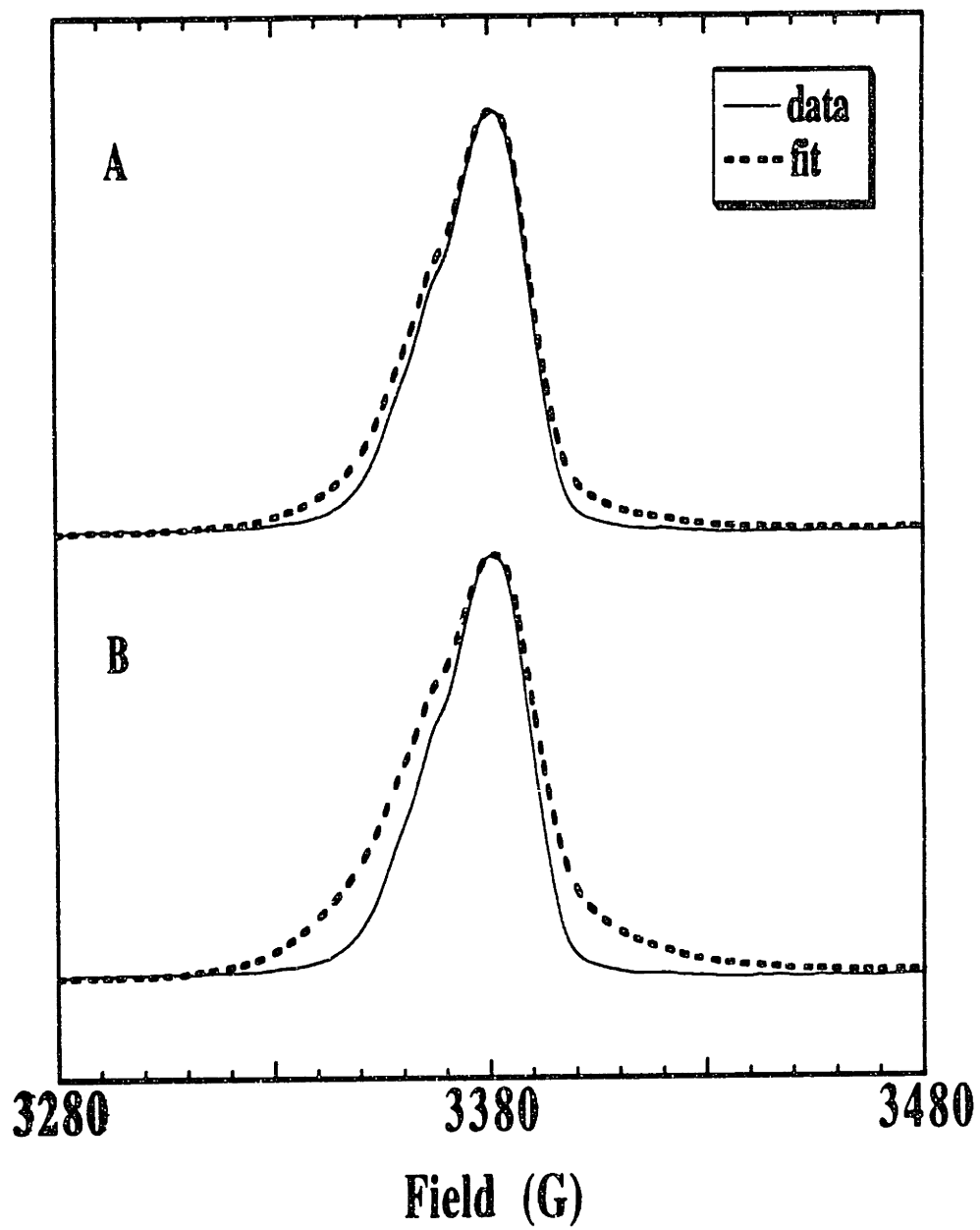


Fig. 3.19: Analysis of the experiment depicted in Fig. 3.15 to show that no significant amount of the broad EPR features accumulates in the reaction of apo R2-wt with limiting Fe^{2+} in $^2\text{H}_2\text{O}$. The inner spectra of **A** and **B** are the spectrum of the 0.84 s sample from the experiment depicted in Fig. 3.15. The outer spectrum of **A** is a hypothetical spectrum generated by adding the spectrum of the broad EPR features (Fig. 3.18) and the experimental spectrum in Fig. 3.15C in a ratio of 25:75. The outer spectrum of **B** is a hypothetical spectrum generated by adding the spectrum of the broad EPR features and the experimental spectrum in a ratio of 50:50.



Temperature Dependence of the Reconstitution Reaction from Apo R2-wt with Limiting Fe²⁺ as Monitored by SF-Abs Spectroscopy

Recently, using stopped flow and freeze-quench EPR, Sahlin *et al.* demonstrated the formation of several transient free radical species in the reconstitution of R2-Y122F at room temperature (Sahlin *et al.*, 1994; Sahlin *et al.*, 1995). One of the species observed with room temperature EPR spectroscopy is a singlet-like signal. This signal forms with a rate constant of 7 s^{-1} and decays with a rate constant of 0.35 s^{-1} . The amount of this EPR singlet depends markedly on the initial ratio of $\text{Fe}^{2+}/\text{R2}$, and reaches its maximum value at a $\text{Fe}^{2+}/\text{R2}$ ratio of 2. Increasing the $\text{Fe}^{2+}/\text{R2}$ ratio to 4 reduces the amount of the singlet accumulated. At a $\text{Fe}^{2+}/\text{R2}$ ratio of 10, the singlet was not observed. Since the 560 nm absorbing species we observed shows a similar dependence on the $\text{Fe}^{2+}/\text{R2}$ ratio, the possibility that these two species are correlated has also been examined.

The argument for a correlation of these two species must first demonstrate that the 560 nm transient is also observed at room temperature and that it exhibits kinetic behavior identical to those of singlet EPR signal. As shown in Fig. 3.20 and Fig. 3.21, the 560 nm transient exhibits a significant dependence on temperature in both the reconstitution of R2-wt and that of R2-Y122F. When the reaction of apo R2-wt (or R2-Y122F) with 2.3 molar equivalents of Fe^{2+} is carried out at $15 \text{ }^{\circ}\text{C}$, the transient is still observed, but the amplitudes of the rise and fall are decreased markedly with respect to the reaction carried out at $5 \text{ }^{\circ}\text{C}$. At $20 \text{ }^{\circ}\text{C}$ or $25 \text{ }^{\circ}\text{C}$, no significant absorption at 560 nm is observed. In order to estimate the rate constants for formation and decay of the 560 nm transient, non-linear least squares analysis of the A_{560} -versus-time traces was carried out. The results are summarized in Table 3.6. At $15 \text{ }^{\circ}\text{C}$, the transient species in R2-wt forms with a rate constant of $\sim 18 \text{ s}^{-1}$ and decays with a rate constant of $\sim 3 \text{ s}^{-1}$ (Fig. 3.22). At $15 \text{ }^{\circ}\text{C}$, the transient species in R2-Y122F forms with a rate constant of $13\text{-}17 \text{ s}^{-1}$ and decays with a rate constant of

Table 3.6: Summary of analysis of the A_{560} -versus-time traces from the reaction of apo R2 with limiting Fe^{2+} at different temperatures.

Protein	Temp. (°C)	k_1 (s ⁻¹)	k_2 (s ⁻¹)
apo R2-wt	5	5.4 - 7.2	6.7 - 6.9
	10	11.5 - 13.9	6.5 - 6.7
	15	17.4 - 18.0	2.9 - 3.1
apo R2-Y122F	5	2.9	2.7
	10	4.4 - 7.0	1.8 - 3.0
	15	14 - 17	0.85 - 2.1

0.8 - 2.0 s⁻¹ (Fig. 3.23). As expected, both the formation and the decay of the 560 nm transient occur with greater rate constants with increasing temperature. More importantly, the rate constants at 15 °C are significantly different from those reported for the room temperature EPR singlet. These results, thus, indicate that the 560 nm transient is not correlated with the EPR singlet observed by room temperature EPR spectroscopy.

The production of •Y122 at 25 °C was also examined by SF-Abs spectroscopy. After an initial lag, formation of •Y122 at 25 °C in the reaction of apo R2 with limiting Fe^{2+} is well described by a first-order process with a k_{obs} of 2.9 s⁻¹ (Fig. 3.24). The A_{410} dropline at completion indicates that 0.6 equiv. of •Y122 is generated. These results stood in contrast with the results for the same reaction at 5 °C, which indicates complex kinetics for •Y122 production (Bollinger *et al.*, 1994b).

Fig. 3.20: Effect of temperature on the A_{560} -versus-time trace in the reaction of apo R2-wt with limiting Fe^{2+} . The reaction conditions (after mixing) were: 66.6 μ M R2-wt, 153 μ M Fe^{2+} , 100 mM HEPES (air-saturated), pH 7.6. The experimental trace was constructed from the averages of three trials.

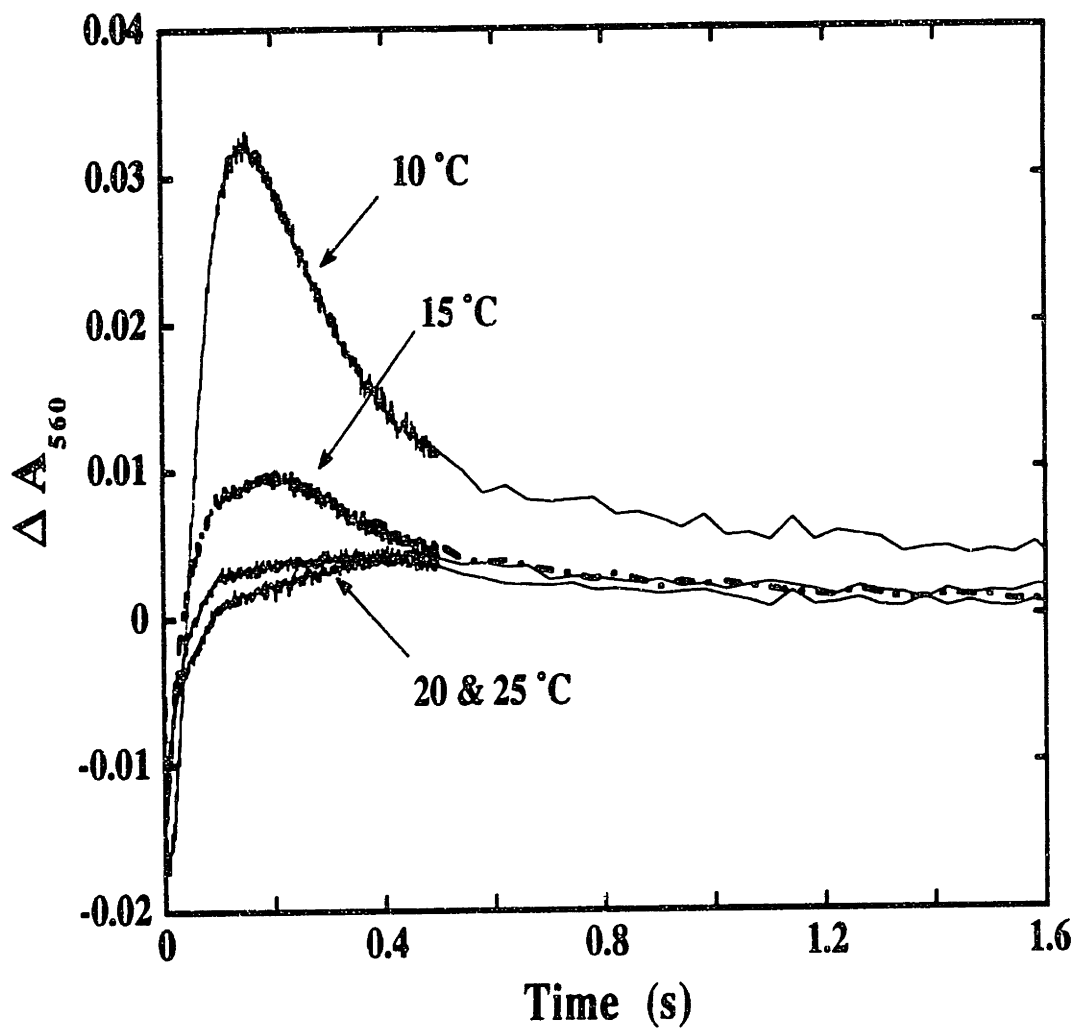


Fig. 3.21: Effect of temperature on the A_{560} -versus-time trace in the reaction of apo R2-Y122F with limiting Fe^{2+} . The reaction conditions (after mixing) were: 73 μM R2-wt, 170 μM Fe^{2+} , 100 mM HEPES (air-saturated), pH 7.6. The experimental trace was constructed from the averages of three trials.

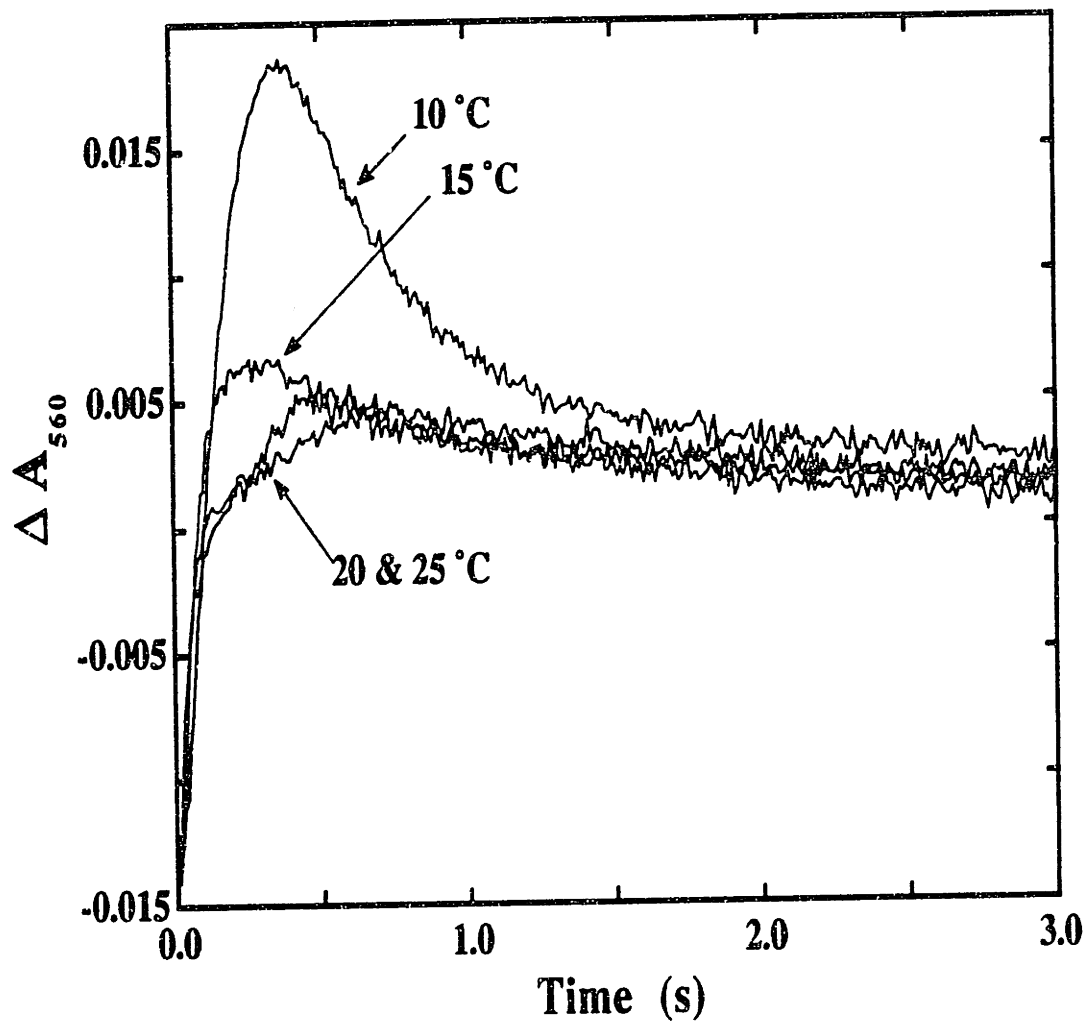


Fig. 3.22: A_{560} -versus-time trace in the reaction of apo R2-wt with limiting Fe^{2+} at 15 °C. The reaction conditions (after mixing) were: 66.6 μM R2-wt, 153 μM Fe^{2+} , 100 mM HEPES (air-saturated), pH 7.6, 15 °C. The experimental trace was constructed from the averages of three trials. The theoretical curve was obtained by fitting an equation for two sequential, first-order processes to 0.0 - 2.0 s of the experimental trace. It corresponds to a k_1 of 18 s^{-1} and a k_2 of 2.9 s^{-1} .

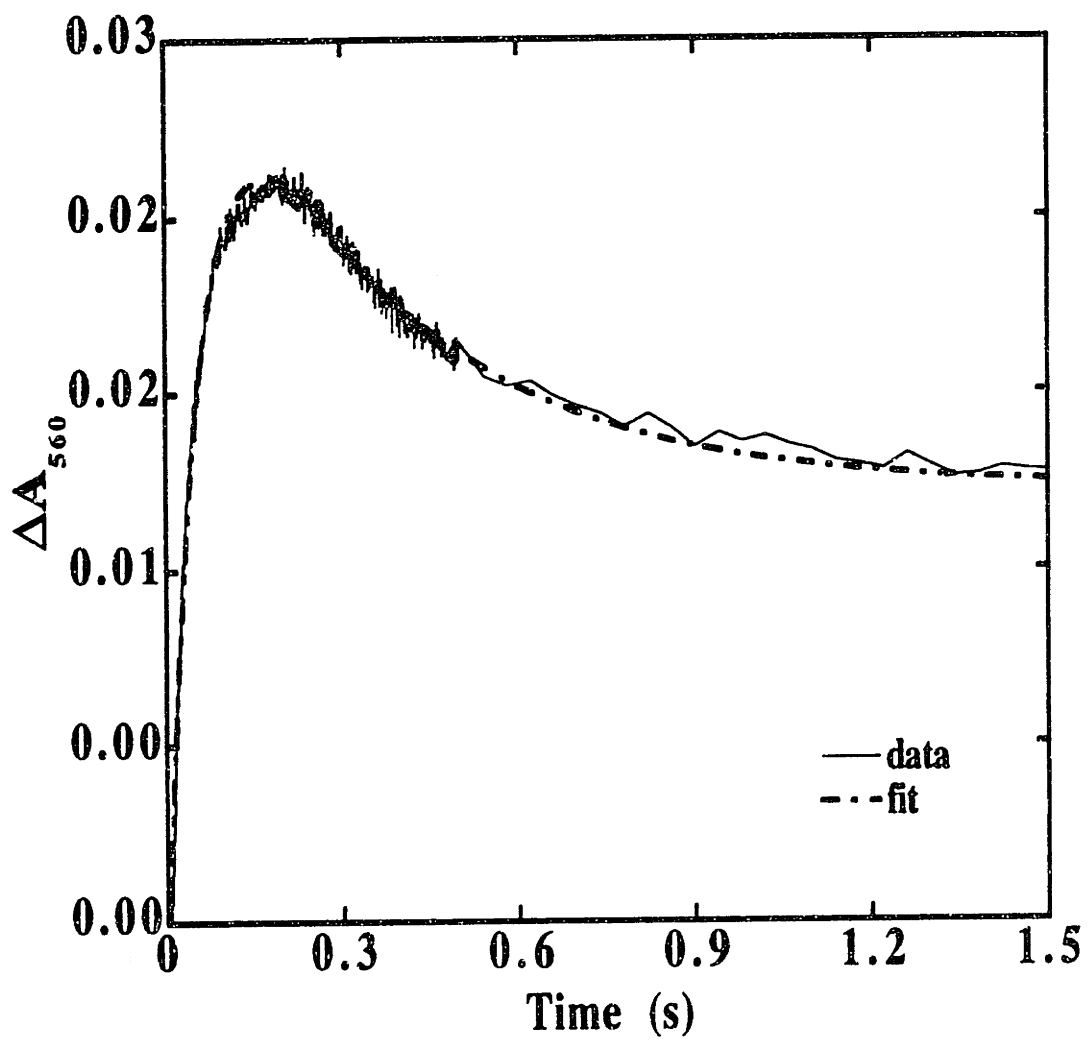


Fig. 3.23: A_{560} -versus-time trace in the reaction of apo R2-Y122F with limiting Fe^{2+} at 15 °C. The reaction conditions (after mixing) were: 73 μM R2-wt, 170 μM Fe^{2+} , 100 mM HEPES (air-saturated), pH 7.6, 15 °C. The experimental trace was constructed from the averages of three trials. The theoretical curve was obtained by fitting an equation for two sequential, first-order processes to 0.00 - 2.0 s of the experimental trace. It corresponds to a k_1 of 17 s^{-1} and a k_2 of 0.85 s^{-1} .

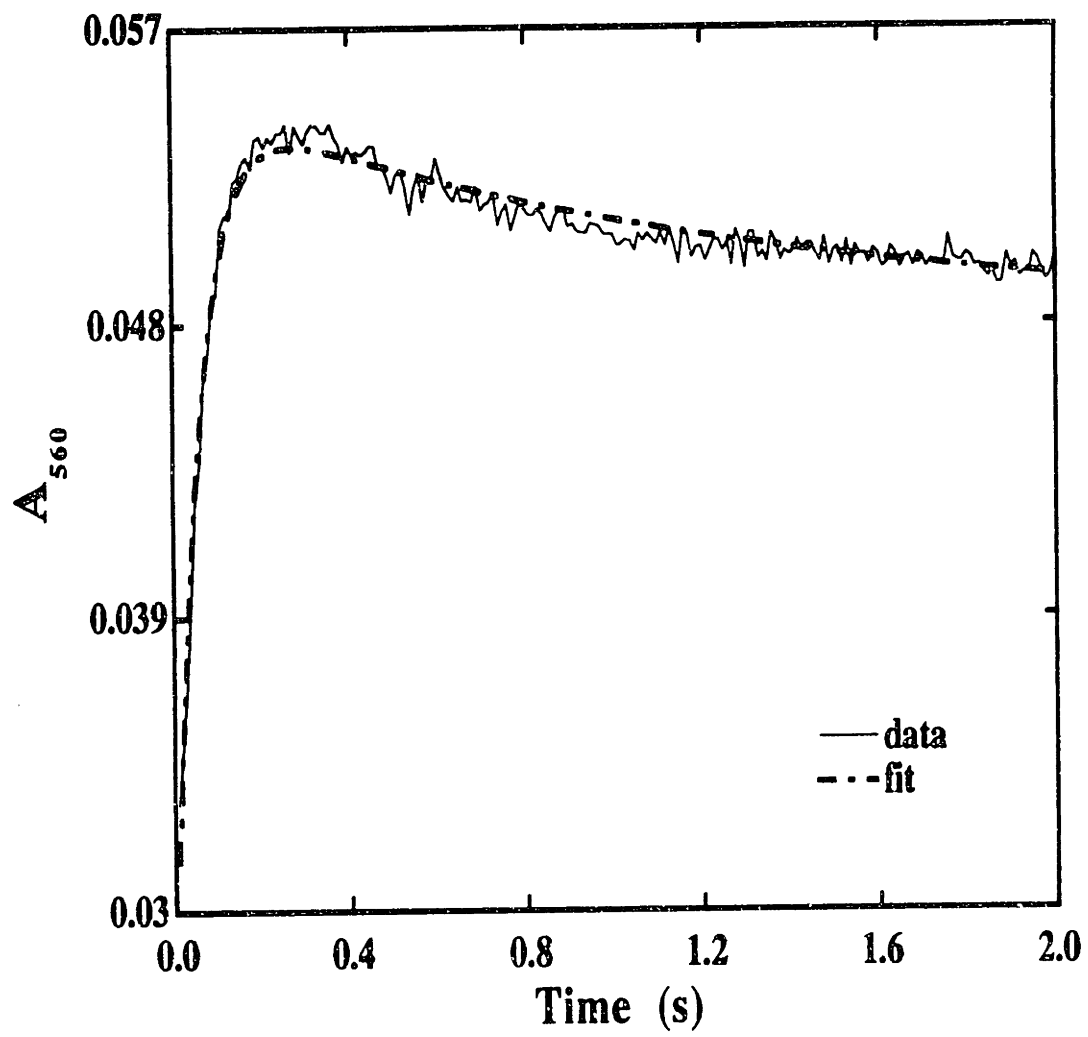
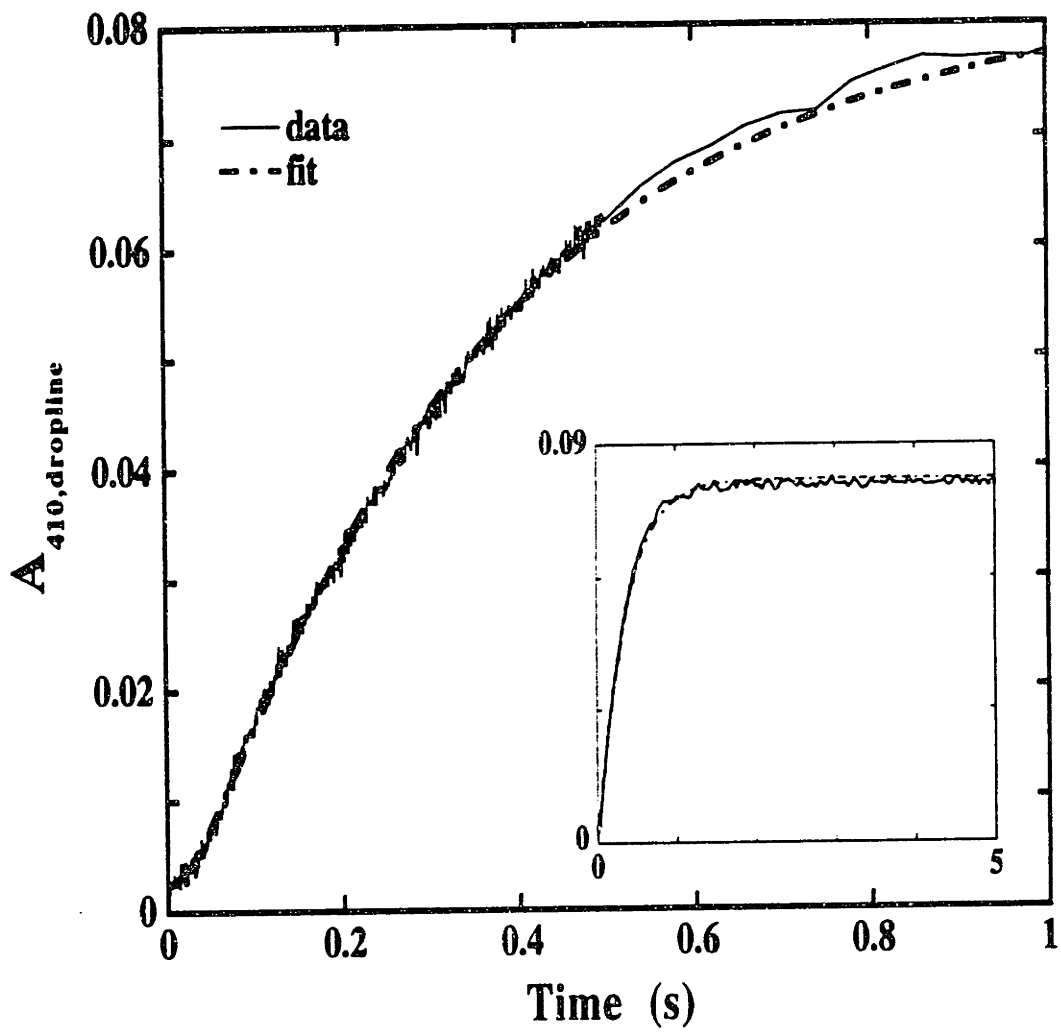


Fig. 3.24: A_{410} , dropline-versus-time trace in the reaction of apo R2-wt with limiting Fe^{2+} at 25 °C. The reaction conditions (after mixing) were: 67 μM R2-wt, 153 μM Fe^{2+} , 100 mM HEPES (air-saturated), pH 7.6, 25 °C. The experimental trace was constructed from the averages of three trials at each wavelengths. The theoretical curve was obtained by fitting a first-order process to 0.00 - 2.0 s of the experimental trace. It corresponds to a k_{obs} of 2.9 s^{-1} .



Discussion

Mechanism of the Reconstitution Reaction under Limiting Fe²⁺ condition

As demonstrated in the preceding chapter, the kinetics of the reaction of Fe(II)-R2 with O₂ under excess Fe²⁺ conditions can be accommodated by the proposed mechanism for the reaction of apo R2, O₂ and excess Fe²⁺ (Scheme 1.3). The results of this chapter, however, provide arguments for a different mechanism for the formation of •Y122 in the reaction of Fe(II)-R2 with O₂ under limiting Fe²⁺ conditions than that proposed for the reaction of apo R2 with O₂ and limiting Fe²⁺ (Scheme 1.3). Two lines of evidence provide support for this assertion. First, the SF-Abs data indicates that the decay of the putative •WH⁺ (as judged by 560 nm absorption band) is almost 10 fold faster than the formation of •Y122. This observation indicates that this 560 nm-absorbing species cannot be the •Y122-generating intermediate in the Fe(II)-R2 reaction.

Second, several experiments described in this chapter strongly implicates that the 560 nm-absorbing species is not correlated with a •WH⁺. One of the major arguments for the previous assignment of the 560 nm absorption band to a •WH⁺ is related to the observation of a transient EPR-active species with broad features at $g = 2$, which correlated temporally with the 560 nm absorbance. It was thus proposed that the 560 nm-absorbing species may be EPR-active. The experiments described in this chapter, however, indicates an inconsistency with this conclusion. Fig. 3.8C shows that a substantial amount of the EPR broad features is present in the 0.46 s sample in the reaction of Fe(II)-R2 (2.3 Fe²⁺/R2) with O₂, even though the decay of the 560 nm absorbance is already completed at this time (Fig. 3.3). This observation is ultimately taken as evidence against the previous correlation of the 560 nm absorption band with the broad EPR features. Furthermore, quantitative analysis presented in this chapter, indicates that the total EPR-active species throughout the time-course of the reaction of apo R2-wt with limiting Fe²⁺ is consistently less than

the amount predicted by the model in Scheme 3.1. More importantly, the total spin as a function of time agrees (within experimental error) with the sum of the measured quantity of X and \bullet Y122 as functions of time. This result, thus, suggest that the broad EPR features in Fig. 3.8 might be associated with X and not with the 560 nm-absorbing species.

Further argument against the correlation of the 560 nm absorption band with the broad EPR features was provided by the experiments carried out in $^2\text{H}_2\text{O}$. As mentioned above, the EPR time-course of the reaction of apo R2 with limiting Fe^{2+} in $^2\text{H}_2\text{O}$, which shows that only X and \bullet Y122 are present. No broad EPR features were observed, even though the 560 nm transient absorption is still observable in the time-resolved absorption spectra. These results, taken together, strongly suggest that the EPR broad features and the 560 nm absorbance are not correlated. In fact, despite careful examination under a variety of EPR conditions (4 - 100 K), no evidence was found to support that the 560 nm-absorbing species is EPR-active. If the 560 nm absorbing species is, in fact, not a radical species, it would provide a strong argument against the proposal that this species functions as an electron conduit to generate \bullet Y122 from Y122. The possible identity of the 560 nm-absorbing species is discussed below.

With the 560 nm absorbing species ruled out, the most likely candidate for the species responsible for generation of \bullet Y122 is X. Two observations have led to the reconsideration of the role of X in generating \bullet Y122 in the limiting Fe^{2+} reaction. First, the results in this chapter suggest that the k_{obs} for formation of \bullet Y122 in the reaction of Fe(II)-R2 with O_2 under limiting Fe^{2+} conditions ($k_{\text{obs}} \sim 1.3 \text{ s}^{-1}$) may not be significantly different from that of the excess Fe^{2+} reaction ($k_{\text{obs}} \sim 0.8 \text{ s}^{-1}$). One interpretation is that formation of \bullet Y122 in both the excess and the limiting Fe^{2+} reactions proceeds through the same intermediate X. A time-resolved quantitation

of X in the reaction of Fe(II)-R2 with O₂ under limiting Fe²⁺ conditions by Mössbauer spectroscopy may provide more definitive evidence for this hypothesis.

Furthermore, the EPR study on the limiting Fe²⁺ reaction carried out in ²H₂O also suggests that X may be responsible for generating •Y122 under these conditions. At all times during the reaction, the spectrum can be accounted for as the sum of the spectra of X and •Y122 (Table 3.5). Thus, X is the only observable radical intermediate in this reaction and the best candidate for generating •Y122. Unfortunately, detailed kinetic description of the ²H₂O reaction has not been successful. These analysis indicate that the simple kinetic model of two consecutive, first-order processes (Scheme 3.2, in which B corresponds to X) is not of sufficient complexity to describe the ²H₂O reaction (data not shown). Additional experiments are required to provide more definitive evidence for the hypothesis that X generates •Y122 in the ²H₂O reaction. In Chapter 4, the possibility that X generates •Y122 in the reaction of Fe(II)-R2 with O₂ under limiting Fe²⁺ conditions is further investigated using a Mn-quench experiment and a EDTA-quench experiment. The results of these experiments provide strong kinetic evidence that X can generate •Y122 in the reaction of Fe(II)-R2 with O₂ under limiting Fe²⁺ conditions. The results described in Chapter 4 also allow the kinetic complexity of the limiting Fe²⁺ reaction to be rationalized. It should be emphasized that none of the results of this work provide direct evidence against the hypothesis put forth previously that the 560 nm-absorbing species generate •Y122 in the reaction of apo R2 with limiting Fe²⁺. Nevertheless, the results reported herein indicate that the mechanism in Scheme 3.1 is, at best, operational under a very narrow set of conditions.

Identity of the Broad EPR g ~ 2 Features

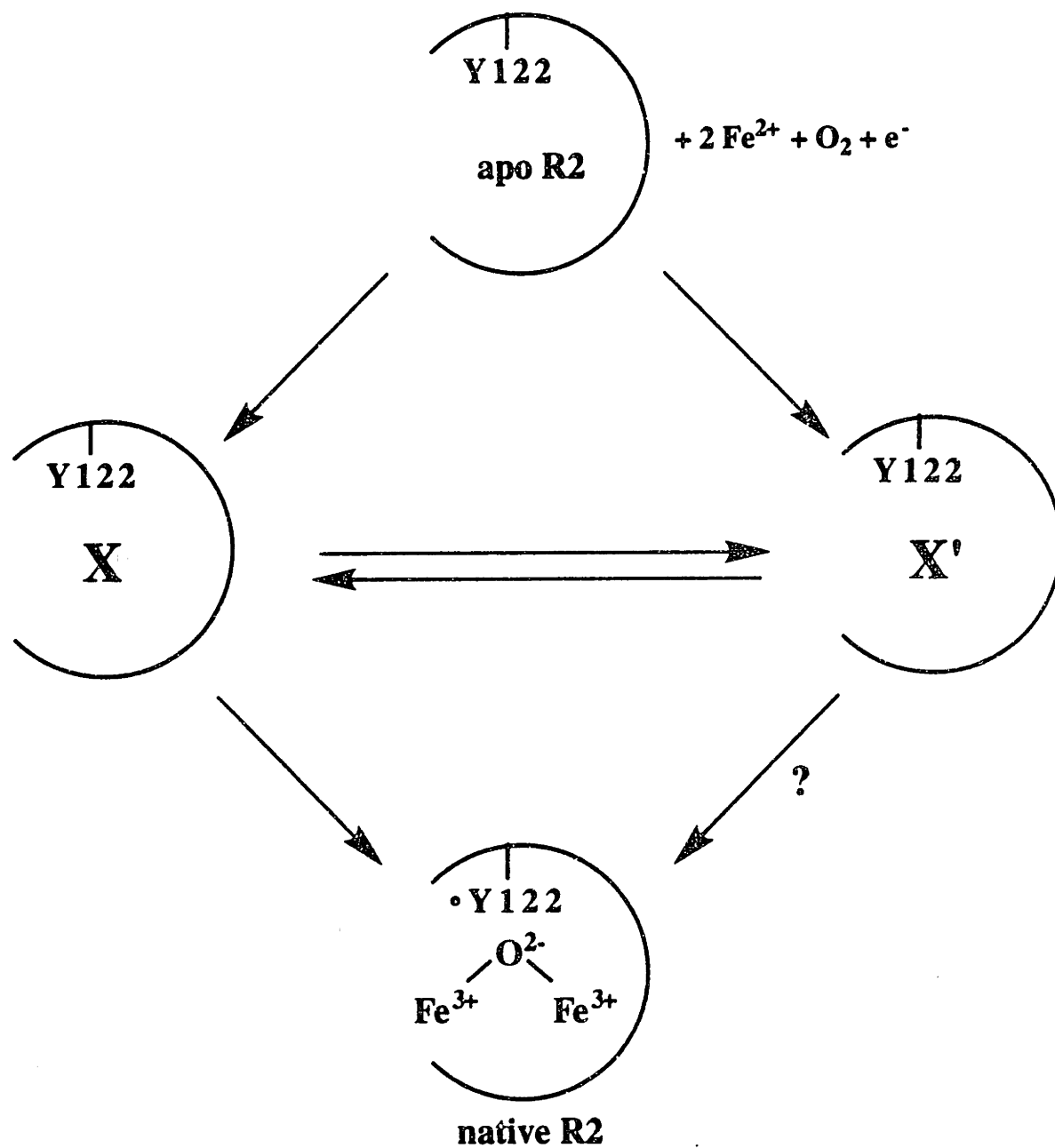
The observation that the broad EPR g = 2 signal does not correlate with the 560 nm absorption band strongly suggests that the species that give rise to the broad

EPR signal is not a $\bullet\text{WH}^+$. Interestingly, the spin quantitation data in this chapter suggest that the broad EPR features might be associated with an alternate form of X (hereby denoted X'). Despite the substantial amount of the broad EPR signal observed in Fig 3. 16, Fig. 3.10 shows that the total spin agree (within experimental error) with the sum of the amount of X (measured by Mössbauer spectroscopy) and that of $\bullet\text{Y122}$ (measured by SF-Abs spectroscopy). These results, thus, suggest that the broad EPR signal may represent a different form of X, (or X').

If this interpretation is correct, X and X' have different EPR line shapes but have indistinguishable Mössbauer spectra. The reason for this behavior is not obvious, but it is possible that the difference in EPR line shape could arise from different conformers involving X and X'. The difference in the protein conformation around the iron cluster necessary to cause the observed broadening in the EPR spectrum may not be enough to perturb the Mössbauer spectrum of X.

In Scheme 3.4, the mechanism proposed for the reconstitution reaction under limiting Fe^{2+} conditions is expanded to reflect the possibility that the formation of the native cofactor is preceded by an equilibrium between X and X'. This scheme may also provide some explanation for the kinetic complexity of the limiting Fe^{2+} reaction. As shown in Fig. 3.11, the formation of $\bullet\text{Y122}$ exhibits surprisingly simple kinetics in $^2\text{H}_2\text{O}$ than that in $^1\text{H}_2\text{O}$. Associated with this change in kinetic behavior is the absence of the broad features in the EPR spectra (Fig. 3.15). The kinetic and spectroscopy differences between the reaction carried out in $^2\text{H}_2\text{O}$ and the reaction in $^1\text{H}_2\text{O}$ can be rationalized according to Scheme 3.4. In $^1\text{H}_2\text{O}$ and under limiting Fe^{2+} conditions, the equilibrium favors a mixture of X and X' which results in the complex kinetics in the $\bullet\text{Y122}$ production (Bollinger, 1992; Bollinger *et al.*, 1994b) In $^2\text{H}_2\text{O}$, a shift of the equilibrium towards X may simplify the kinetics of the reaction. Preliminary results indicate that this "equilibrium between X and X'" might be very sensitive to changes of pH and temperature, since the kinetics of

Scheme 3.4: Mechanism for the limiting Fe^{2+} reaction expanded to reflect the possibility that R2 cofactor assembly is preceded by an equilibrium between X and X'.



•Y122 formation (Fig. 3.24) and the amount of the broad EPR signal (data not shown) depends markedly on the experimental conditions. If confirmed, these observations might provide a useful probe for future study of reconstitution reaction under limiting Fe^{2+} conditions.

Identity of the 560 nm Absorbing Species

One final aspect of the limiting Fe^{2+} reaction that warrants some further discussion is the identity of the 560 nm-absorbing species. Although the results of this work suggest that the species is not a • WH^+ , it is unclear whether the species has mechanistic significance. Without proper identification of the species, it is not possible to determine the amount of this transient species accumulated. Nevertheless, assuming a ϵ_{560} of $3000 \text{ M}^{-1}\text{cm}^{-1}$, the species would accumulate to 0.1-0.3 equivalents per R2. We are currently considering three possibilities for the species which gives rise to the transient absorption band at 560 nm. First, as stated above, we have examined the possibility that the 560 nm absorbing species is associated with the singlet-like EPR feature observed using room temperature rapid-flow EPR spectroscopy in the reaction of apo R2-Y122F with 2 equiv. of Fe^{2+} (Sahlin *et al.*, 1995). Kinetic study of this signal suggested that it was produced with a rate constant of 7 s^{-1} and decayed with a rate constant of 0.35 s^{-1} . Our kinetic study of the temperature dependence of the limiting Fe^{2+} reaction indicates, however, that at temperature $\geq 20 \text{ }^\circ\text{C}$, no 560 nm transient absorbance is observed. Hence, it is unlikely that the 560 nm absorption band is associated with the EPR singlet observed Sahlin *et al.* (Sahlin *et al.*, 1995). Furthermore, despite careful examination of the reconstitution reaction by EPR spectroscopy under a variety of conditions, no evidence was found to suggest that the 560 nm-absorbing species is EPR-active.

Second, it is possible that the 560 nm transient may be associated with a diferric peroxide species as was originally proposed. Previous observation that no

spectral features in the Mössbauer spectra correlated in time with the 560 nm transient have implicated that the transient does not arise from a Fe-containing intermediate. However, it is possible that one-electron reduction of the putative ferric peroxide intermediate can occur subsequent to freeze-quenching, such that this species was not detected by the RFQ method. Electron transfer has been measured in proteins at temperature as low as -140 °C. In this interpretation, the putative ferric peroxide species is reduced by one electron at 16 s^{-1} with concomitant formation of a second intermediate (presumably X), which in turn oxidizes Y122 to $\bullet\text{Y122}$ at $\sim 1.3 \text{ s}^{-1}$. However, iterative simulation of this model indicates that a significant lag phase ($\sim 0.05 \text{ s}$) in $\bullet\text{Y122}$ would be expected. As mentioned above, no lag phase ($\sim 0.005 \text{ s}$) was observed in the formation of $\bullet\text{Y122}$ in the limiting Fe^{2+} reaction. Thus, this model also cannot account for the data.

Third, the 560 nm feature may arise from a ferric to tyrosinate charge-transfer band. Interestingly, a Fe(III)-tyrosinate complex with $\lambda_{\text{max}} = 550 \text{ nm}$ has been shown to be a transient precursor of polynuclear iron cluster formation in ferritin (Rose, 1980; Thelander & Gräslund, 1994). It is possible that the ferric product generated in delivery of the extra reducing equivalent required for formation of X may be coordinated transiently to a tyrosine residue on R2. Interpreting the crystal structure of met R2-wt and that of the reduced form of a R2-S211A mutant protein, Aberg *et al.* have shown that the hydroxyl group of Y209 moves 2 \AA to open up a channel from the surface down to the cluster binding site (Aberg, 1993). It is interesting to speculate that the 560 nm absorbing species may arise from transient formation of a Fe(III)-Y209 complex. In support of this possibility, the 60 s time-point of the reaction of apo R2 with 2.3 Fe^{2+} exhibits weak features of the type which are associated with "adventitiously bound" high-spin ferric ion. Neither the magnetic spectrum characteristic of the high-spin ferric ion nor the transient 560 nm species is observed in the excess Fe^{2+} reaction. It is possible that the "Fe(III)-

tyrosinate" is not generated in the excess Fe^{2+} reaction or that it may be rapidly reduced in the presence of excess reductant.

References

- Aberg, A. (1993) Ph. D. Thesis, Stockholm University.
- Bollinger, J. M., Jr. (1992) Ph. D. Thesis, Massachusetts Institute of Technology.
- Bollinger, J. M., Jr., Tong, W. H., Ravi, N., Huynh, B. H., Edmondson, D. E. & Stubbe, J. (1994a) *J. Am. Chem. Soc.* 116, 8015-8023.
- Bollinger, J. M., Jr., Tong, W. H., Ravi, N., B. H., Edmondson, D. E. & Stubbe, J. (1994b) *J. Am. Chem. Soc.* 116, 8024-8032.
- Espenson, J. H. (1981) *Chemical Kinetics and Reaction Mechanisms*. McGraw-Hill, New York.
- Glusoe, P. K. & Long, F. A. (1960) *J. Phys. Chem.* 64, 188.
- Kim, S.-T., Sancar, A., Essenmacher, C. & Babcock, G. T. (1993) *Proc. Natl. Acad. Sci. USA* 90, 8023-8027.
- Malmström, B., Reinhammar, B. & Vänngård, T. (1970) *Biochim. Biophys. Acta* 205, 48.
- Ravi, N., Bollinger, J. M., Jr., Tong, W. H., Ravi, N., B. H., Edmondson, D. E. & Stubbe, J. (1994) *J. Am. Chem. Soc.* 116, 8007-8014.
- Rose, I. A. (1980) *Methods Enzymol.* 64, 47-59.
- Sahlin, M., Lassmann, G., Pötsch, S., Sjöberg, B.-M. & Gräslund, A. (1995) *J. Biol. Chem.* 270, 12361-12372.
- Sahlin, M., Lassmann, G., Pötsch, S., Slaby, A., Sjöberg, B.-M. & Gräslund, A. (1994) *J. Biol. Chem.* 269, 11699-11702.
- Solar, S., Getoff, N., Surdhar, P. S., Armstrong, D. A. & Singh, A. (1991) *J. Phys. Chem.* 95, 3639-3643.

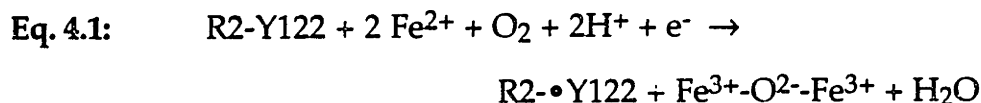
Thelander, L. & Gräslund, A. (1994) "Ribonucleotide Reductase in Mammalian Systems." *Metal Ions in Biological Systems*. 109-129.

**Chapter 4: Probing the Binding Interactions
Between R2 and Fe²⁺**

The results of Chapter 2 and 3, in conjunction with previous studies by Bollinger, *et al.* (Bollinger *et al.*, 1994a; Bollinger *et al.*, 1994b), show that the reconstitution of R2 with sub-stoichiometric amounts of Fe^{2+} exhibits much more complex kinetic behavior than the reaction in the presence of excess Fe^{2+} . One possible explanation for these results is that the addition of less than 4 equiv. of Fe^{2+} to apo R2 results in multiple forms of Fe^{2+} -R2 complexes. Scheme 4.1 illustrates the statistical complexities of a mixture of apo R2 with less than 4 equiv. of Fe^{2+} . The scheme shows that a number of Fe^{2+} -R2 complexes with different states of iron site occupancy can be generated under these conditions, and the distribution of Fe^{2+} in the various complexes is defined by the relative accessibility of the different binding sites. All of these species are in equilibrium with the free Fe^{2+} in solution, and they must be accounted for in any attempt to describe the kinetics of the reconstitution reaction. Thus, it is possible that the complex kinetic behavior is at least in part a reflection of the dissociation and reallocation of Fe^{2+} until a "competent Fe^{2+} -R2 complex" is formed, which can then react with O_2 in a productive manner.

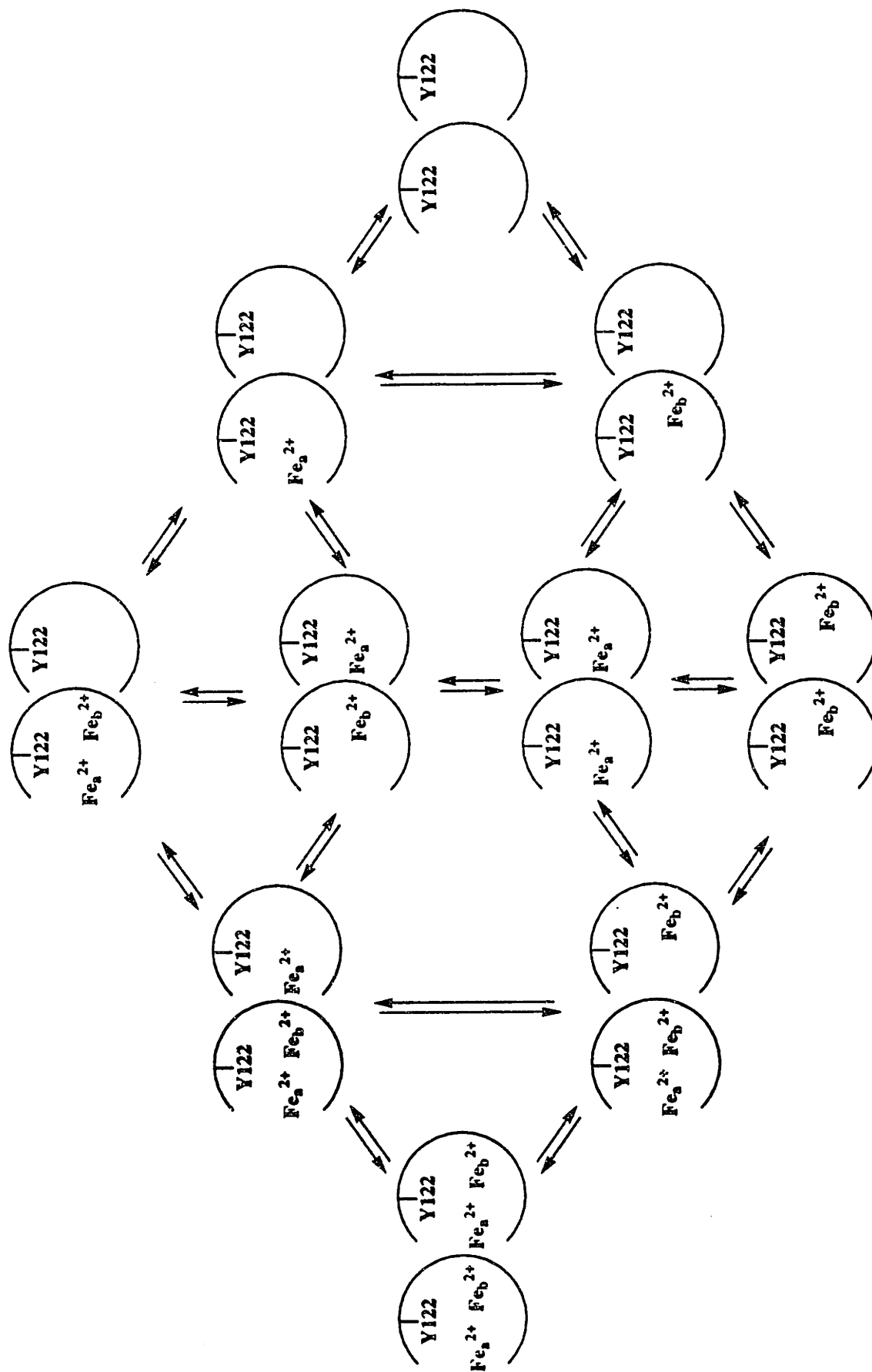
The kinetics of the reaction is further complicated by the fact that Fe^{2+} is not only a building block of the product cluster, but can also serve as an electron donor required for cofactor assembly. As indicated in Eq.4.1, in addition to the three reducing equivalents provided by oxidation of Y122 to $\bullet\text{Y122}$ and oxidation of two Fe^{2+} ions to the diferric cluster, a fourth electron is required for cofactor assembly. Several studies have indicated that both Fe^{2+} and ascorbate are capable of providing this fourth electron (Ochiai *et al.*, 1990; Elgren *et al.*, 1991; Bollinger *et al.*, 1991a; Bollinger *et al.*, 1994a). The studies by Bollinger *et al.* (Bollinger *et al.*, 1994a; Bollinger *et al.*, 1994b) and the experiments described in Chapter 2 and 3 have further shown that delivery of the fourth electron required for cofactor assembly

depends markedly on the initial $\text{Fe}^{2+}/\text{R2}$ ratio, and on whether the Fe(II)-R2 complex is allowed to pre-form before exposure to O_2 . These results, together with the observation that the reaction kinetics show no dependence on the absolute concentration of Fe^{2+} (Bollinger, 1992), suggest that the Fe^{2+} ion which donates the fourth electron is bound by R2. To date, the data are ambiguous as to whether this Fe^{2+} is bound in the cofactor site of the opposite monomer or in an as yet undefined "third" binding site (Ochiai *et al.*, 1990; Elgren *et al.*, 1991; Ochiai *et al.*, 1991; Bollinger *et al.*, 1994a). It is reasonable to expect that the state of this third Fe^{2+} (the donor of the fourth electron) would affect the overall reaction kinetics. Finally, the proposal of a third Fe^{2+} -binding site in R2 may also imply an even more complex distribution of Fe^{2+} in the equilibrium mixture of apo R2 and Fe^{2+} (Scheme 4.2).

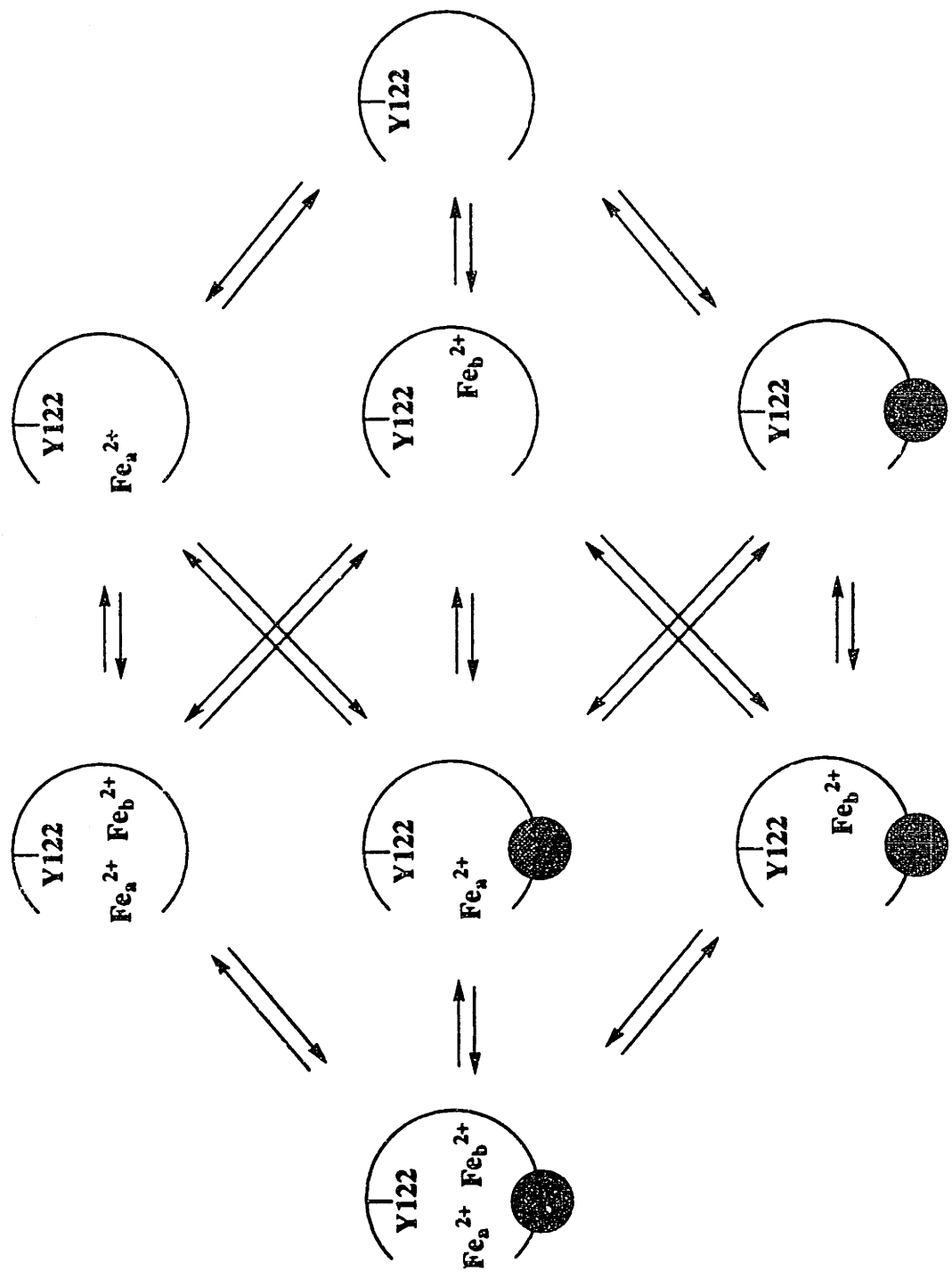


In this chapter, several experiments were designed to probe both the equilibrium and the dynamic aspects of the interactions between Fe^{2+} and apo R2. These experiments were carried out with the expectation that they may facilitate interpretation of the kinetic data described in Chapters 2 and 3, and provide further insight into the reaction mechanism. The results described in this chapter have led to some important general conclusions. First, the kinetic data on the reaction of Fe(II)-R2 ($\text{Fe}^{2+}/\text{R2} = 1$) with O_2 have provided evidence that mixing of apo R2 with 1 equiv. of Fe^{2+} results in predominantly mononuclear Fe^{2+} binding. Furthermore, the kinetic data on the release of Fe^{2+} at different $\text{Fe}^{2+}/\text{R2}$ ratios indicate that addition of 2.3 or 3.4 equiv. of Fe^{2+} to apo R2 results in a mixture of Fe^{2+} -R2 complexes with different states of iron site occupancy. These results are in

Scheme 4.1: Schematic representation of the Fe^{2+} -R2 complexes which might be present in the equilibrium mixture of apo R2 and Fe^{2+} under anaerobic conditions for the case of two metal-binding sites in each R2 monomer. For clarity, only some of the interconversions are indicated in this scheme.



Scheme 4.2: Schematic representation of the Fe^{2+} -R2 complexes which might be in the equilibrium mixture of apo R2 and Fe^{2+} under anaerobic conditions for the case of three metal-binding sites in each R2 monomer. In this scenario, up to 36 different forms of the Fe^{2+} -R2 dimer complexes might be present. For clarity, only one monomer (broken circle) is shown.



contradiction to the previous hypothesis by Elgren *et al.* that binding of Fe^{2+} by R2 is "highly cooperative" (Elgren *et al.*, 1991).

In addition, experiments in this chapter have allowed the reaction of the competent Fe^{2+} -R2 complexes with O_2 to be monitored without the interference due to improper binding. The Mn^{2+} -quench experiments described in this chapter have taken advantage of the ability of Mn^{2+} to compete for the Fe^{2+} -binding sites in R2. This approach has allowed trapping of any non-competent Fe^{2+} -R2 complex. Using a similar logic, a EDTA-quench experiment has been designed to chelate any free Fe^{2+} , thus preventing further reaction with the non-competent Fe^{2+} -R2 complexes. On the basis of the results described in this chapter, a simple model is presented to describe the statistical distribution of the various Fe^{2+} -R2 complexes in the anaerobic equilibrium mixture of apo R2 with less than 4 molar equivalents of Fe^{2+} . This model is ultimately taken as an argument against the hypothesis that addition of Fe^{2+} to apo R2 results exclusively in dinuclear Fe^{2+} binding (Fontecave *et al.*, 1990b; Elgren *et al.*, 1991). Finally, the time-courses of $\bullet\text{Y122}$ production in the Mn^{2+} - and EDTA-quench experiments have provided kinetic evidence that X can generate $\bullet\text{Y122}$ in the reaction of Fe(II)-R2 with O_2 under limiting Fe^{2+} conditions. These results are consistent with the results described in Chapter 3 which indicates that the 560 nm-absorbing species is not responsible for generation of $\bullet\text{Y122}$ in this reaction. The mechanistic implications of these results will be discussed.

A final issue which has been addressed in this chapter is the sequence of events that lead to formation of X. The results of the pulse/chase experiment described in this chapter indicate a rate constant of $\sim 4 \text{ s}^{-1}$ for the formation of the competent Fe^{2+} -R2 complex. The observation that the rate constant of $\sim 4 \text{ s}^{-1}$ is close to the rate constant of $5 - 10 \text{ s}^{-1}$ for the formation of X in the reaction of apo R2 with excess Fe^{2+} (Scheme 2.1) suggest that the rate-limiting step in the formation of X occurs before formation of the competent Fe^{2+} -R2 complex. These results are

entirely consistent with those in Chapter 2 and 3 which show that the formation of X is much faster in the reaction of Fe(II)-R2 with O₂ ($k_{\text{obs}} = 60 - 80 \text{ s}^{-1}$) than in the reaction of apo R2 with Fe²⁺ and O₂ ($k_{\text{obs}} = 5 - 10 \text{ s}^{-1}$). Taken together, these results have provided further support for the proposal that a conformational change is required in apo R2 to allow entry of Fe²⁺ into the cofactor binding site.

Theory

One of the major focuses of this chapter is to probe the nature of the "competent Fe²⁺-R2 complex" and the equilibria that characterize the interaction of apo R2 and Fe²⁺ under anaerobic conditions. Here, we define the competent Fe²⁺-R2 complex as a Fe²⁺-R2 complex in which the bound Fe²⁺ does not have to dissociate and reassociate with R2 before entering into productive reaction upon binding of O₂. In this definition, the competent Fe²⁺-R2 complex has to fulfill at least two requirements. First, the competent Fe²⁺-R2 complex must have two Fe²⁺ ions (i.e., a diferrous cluster) bound in the cofactor site. Second, the fourth electron required for cofactor assembly must be readily available. As shown previously, in the absence of an alternative reductant, Fe²⁺ is capable of providing this fourth electron. Thus, it is reasonable to expect that a competent Fe²⁺-R2 might have three Fe²⁺ ions bound. As discussed below, the state of this third Fe²⁺ has been a center of debate in several studies. Several experiments described in this chapter have been designed in an attempt to address this issue. A brief discussion of the rationale and the design of these experiments are presented here.

The first issue that will be addressed in this study is related to the possibility of high cooperativity in the binding of Fe²⁺ by R2. The observations that the final •Y122/R2 ratio of the reaction is independent of the ratio of Fe²⁺/apo R2 has led to the proposal that addition of Fe²⁺ to apo R2 results exclusively in formation of the competent Fe²⁺-R2 complex (infinite cooperativity) (Elgren *et al.*, 1991). However,

this proposal is inconsistent with the finding that, in the reaction of apo R2 with 1 equiv. of Fe^{2+} , formation of $\bullet\text{Y122}$ is much slower overall than in the limiting Fe^{2+} or the excess Fe^{2+} reactions (Bollinger, 1992). The results of Bollinger, *et al.*, instead, suggested that mixing apo R2 with 1 equiv. of Fe^{2+} results in a mixture of different Fe^{2+} -R2 complexes with different states of iron-site occupancy. The slowing of the reaction and the complex kinetics might be a reflection of slow rearrangement of Fe^{2+} bound in mononuclear fashion until a productive Fe^{2+} -R2 complex is achieved.

The issue of cooperativity in Fe^{2+} -binding can be tested experimentally. If the proposal of preferential formation of diferrous R2 is correct, the release of Fe^{2+} would exhibit identical kinetic behaviors whether the initial Fe^{2+} /R2 ratio is 1, 2.3, or 3.4. The observation of distinctly different off-rates at different Fe^{2+} /R2 ratios would argue strongly for the case of multiple forms of Fe^{2+} -R2 complexes in the equilibrium mixture of apo R2 with sub-stoichiometric amounts of Fe^{2+} . The results presented in this chapter show that the release of Fe^{2+} from $\text{Fe}(\text{II})$ -R2 exhibits different kinetic behavior at different Fe^{2+} /R2 ratios, strongly suggesting that multiple binding modes exist in the equilibrium mixture of apo R2 and sub-stoichiometric amounts of Fe^{2+} . These results thus provide an argument against the previous hypothesis that Fe^{2+} -binding is highly cooperative (Elgren *et al.*, 1991).

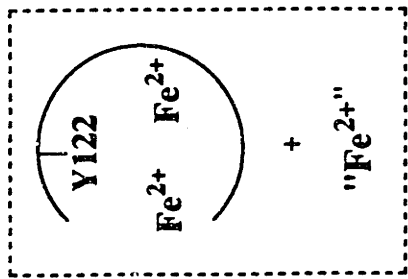
In an attempt to distinguish among the various modes of Fe^{2+} -binding, a Mn^{2+} -quench experiment has been developed. The experimental design is illustrated in Scheme 4.3 and Fig. 4.1. The ability of Mn^{2+} to compete with Fe^{2+} for the natural Fe^{2+} -binding sites in R2 has been established previously by EPR spectroscopy and x-ray crystallography (Atta *et al.*, 1992). These studies indicated that no tyrosyl radical is generated when apo R2 is mixed with 4 equiv. of Mn^{2+} . Instead, two relatively stable dimanganese(II) centers are formed. In the Mn-quench experiment, an anaerobic equilibrium mixture of apo R2 and Fe^{2+} (Fe^{2+} /R2 = 1, 2.3,

or 3.4) is mixed with O_2 and a large excess of Mn^{2+} . The formation of $\bullet Y_{122}$ production in this reaction is followed by stopped-flow absorption (SF-Abs) spectroscopy. Provided that reaction with O_2 is much faster than release of the Fe^{2+} bound by R2, only R2 with all the Fe^{2+} properly bound will react with O_2 to form $\bullet Y_{122}$ (Scheme 4.3). The addition of large excess of Mn^{2+} would essentially trap any non-competent Fe^{2+} -R2 complex by binding to the vacant metal-binding sites and prevent further reaction to generate $\bullet Y_{122}$. Thus the $\bullet Y_{122}/R2$ at completion in this Mn^{2+} -quench experiment may reflect the amount of competent Fe^{2+} -R2 complex in the anaerobic equilibrium mixture of apo R2 and Fe^{2+} .

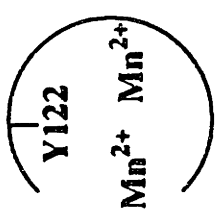
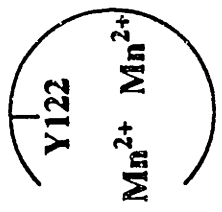
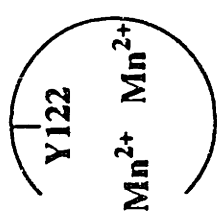
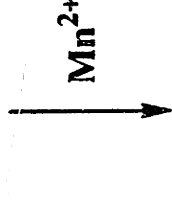
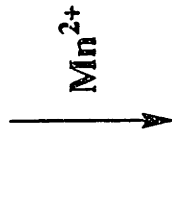
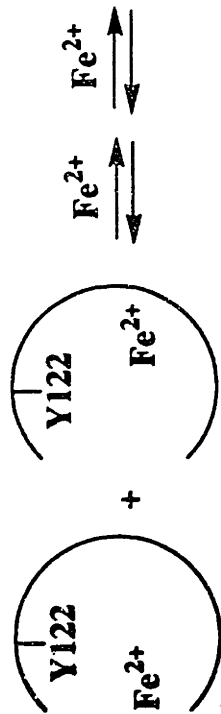
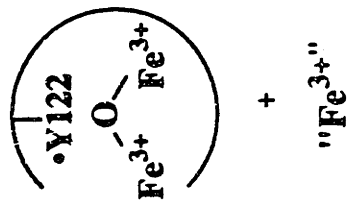
Identical experiments were also carried out using EDTA instead of Mn^{2+} . In concept, the EDTA-quench experiment is very similar to the Mn^{2+} -quench experiment. As shown in Scheme 4.4, when an equilibrium mixture of apo R2 and Fe^{2+} is mixed with O_2 and large excess of EDTA, only the competent Fe^{2+} -R2 complexes will react with O_2 to form $\bullet Y_{122}$. The addition of EDTA will trap any free Fe^{2+} and prevent further reaction of any non-competent Fe^{2+} -R2 complex to form $\bullet Y_{122}$. Evidence will be presented that these experiments have allowed determination of the amount of competent Fe^{2+} -R2 complexes in an equilibrium mixture of apo R2 and Fe^{2+} . These results also provide evidence against the proposal that binding of Fe^{2+} by apo R2 is highly cooperative (Fontecave *et al.*, 1990b; Elgren *et al.*, 1991; Atta *et al.*, 1992). More importantly, these experiments have provided the unique opportunity to view exclusively the reaction of the competent Fe^{2+} -R2 complexes with O_2 , without the complexities introduced by improper binding. The results of these experiments indicate that formation of $\bullet Y_{122}$, when $Fe^{2+}/R2 = 2.3$ and in the presence of Mn^{2+} or EDTA, proceeds with a rate constant identical with that observed in the excess Fe^{2+} reaction. These results, thus, suggest that an essential factor distinguishing the limiting Fe^{2+} and the excess Fe^{2+} reaction might be the effect of different binding modes.

Scheme 4.3: Illustration of the manner in which addition of excess Mn^{2+} to the reconstitution reaction mixtures can inhibit the formation of $\bullet\text{Y122}$ from the non-competent Fe^{2+} -R2 complexes. The broken circle representing R2 refers to one monomer of the dimer. No implication is intended with regard to the identity of the " Fe^{2+} " which donates the fourth electron required for cofactor assembly. This approach is also applicable to the case of three metal-binding sites in each R2 monomer (Scheme 4.2). In that case, only R2 monomer with three Fe^{2+} ions bound will react with O_2 to form $\bullet\text{Y122}$.

Competent Fe^{2+} -R2
Complex



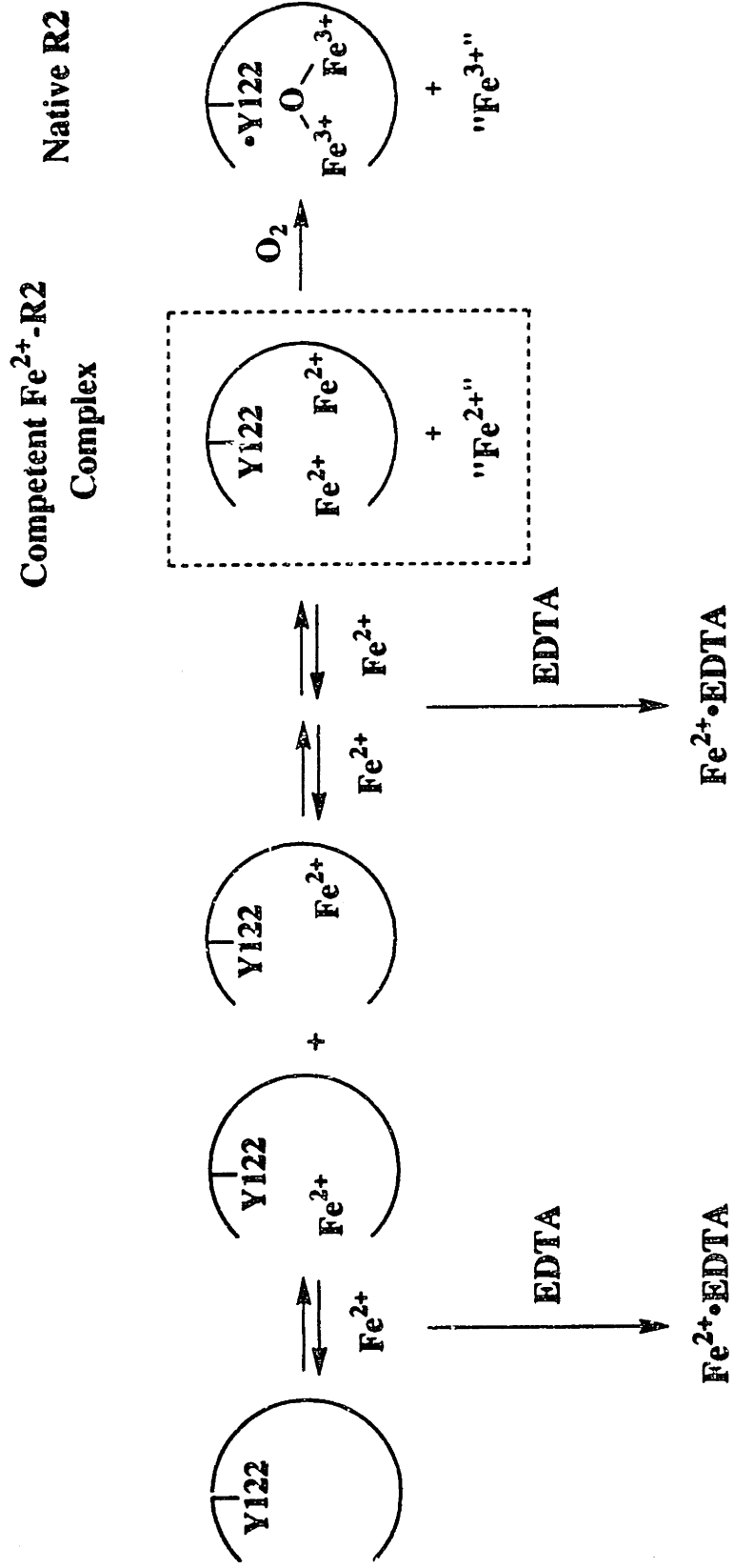
Native R2



No •Y122 formation

No •Y122 formation No •Y122 formation

Scheme 4.4: Illustration of the manner in which addition of excess EDTA to the reconstitution reaction mixtures can inhibit the formation of •Y122 from the non-competent Fe²⁺-R2 complexes. No implication is intended with regard to the identity of the "Fe²⁺" which donates the fourth electron required for cofactor assembly. This approach is also applicable to the case of three metal-binding sites in each R2 monomer (Scheme 4.2). In that case, only R2 monomer with three Fe²⁺ ions bound will react with O₂ to form •Y122.



No $\cdot\text{Y122}$ formation

No $\cdot\text{Y122}$ formation

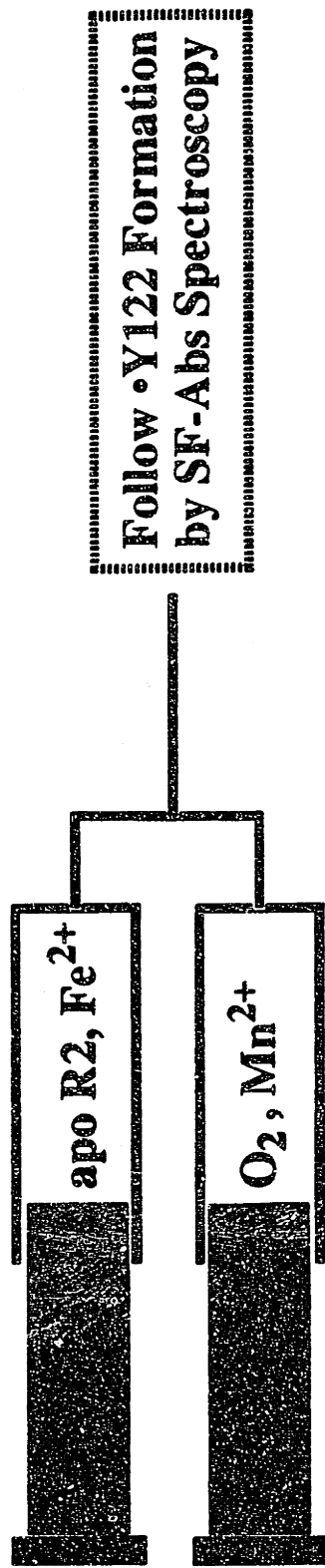


Fig. 4.1: Experimental design for the Mn²⁺-quench experiment.

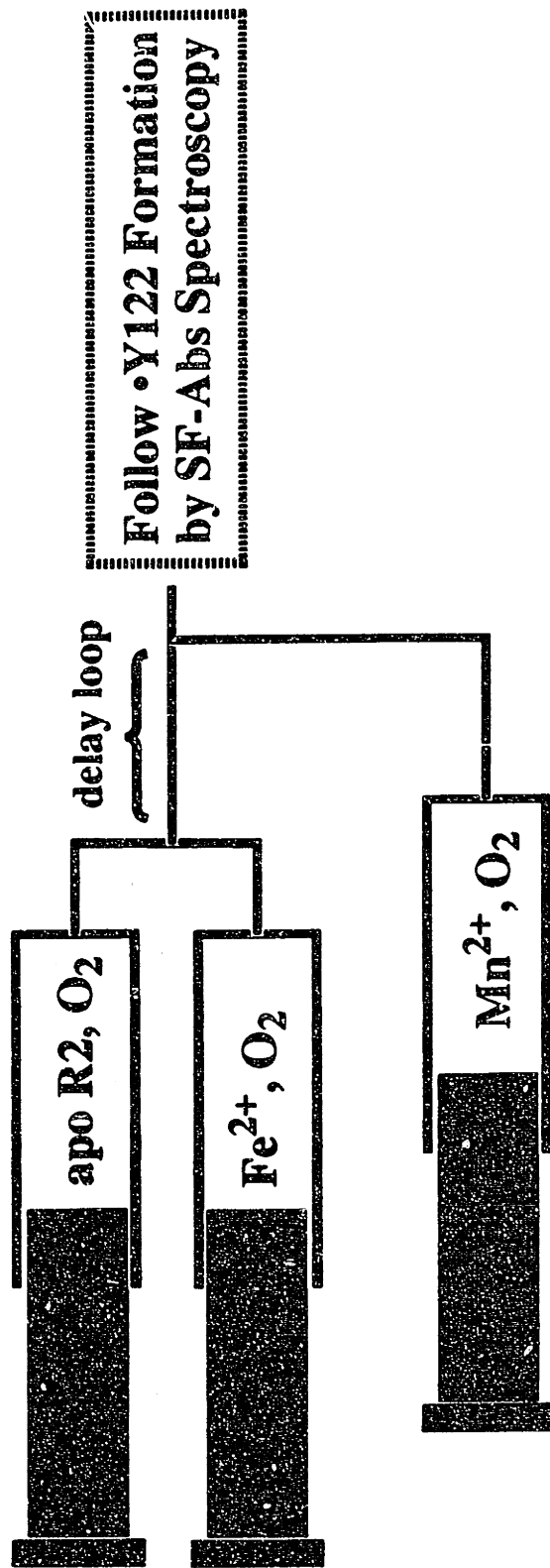


Fig. 4.2: Experimental design for the Mn²⁺ pulse/chase experiment.

Another issue that may be addressed from the Mn^{2+} - and EDTA-quench experiments is the number of Fe^{2+} -binding sites in R2. In studying the reconstitution of mouse R2, Ochiai, *et al.* found by EPR spectroscopy a significant quantity of mononuclear Fe^{3+} ion at completion of the reaction, and proposed that an additional (lower affinity) Fe^{2+} binding site exists in R2 specifically to facilitate delivery of the fourth electron required for cofactor assembly (Ochiai *et al.*, 1990). This observation is consistent with the results of Bollinger, *et al.* which indicated that a significant quantity of a fast-relaxing ferric species is produced concomitantly with the formation of the intermediate iron cluster, X (Bollinger *et al.*, 1994a). In Scheme 4.2, the schematic representation of the equilibrium mixture of apo R2 and Fe^{2+} is expanded to reflect the possibility that a third Fe^{2+} -binding site exists in R2. The results of Ochiai, *et al.* (1990) and those of Bollinger, *et al.*, (1994a) however, contrast with the results of Elgren, *et al.* (1991). Using Mössbauer spectroscopy, Elgren *et al.* showed that > 92 % of the added Fe^{2+} is incorporated into diferric clusters at completion of the reaction (Elgren *et al.*, 1991). On the basis of these results, Elgren, *et al.* proposed that electron transfer among R2 monomers must occur, allowing Fe^{2+} bound in one monomer to supply the fourth electron to a different R2 monomer without producing mononuclear Fe^{3+} . The experiments described in this chapter have provided new insight into the possibility of a third Fe^{2+} -binding site in R2 and the possibility of electron transfer between monomers in a R2 dimer. As discussed below, the different mechanisms mentioned above have statistical features that are distinct from one another. Therefore, in an attempt to distinguish between these different proposals, the statistical distribution of Fe^{2+} in each scenario is calculated and compared to the results of the Mn^{2+} - and EDTA-quench experiments.

Finally, the Mn^{2+} -quench approach has been expanded in order to measure the rate of formation of the competent Fe^{2+} -R2 complex. Previous studies by

Bollinger, *et al.* have led to the proposal that the first-order, 5 - 10 s⁻¹ step observed in the reaction of apo R2 with Fe²⁺ and O₂ reflects a conformational change in apo R2 to allow for entry of Fe²⁺ (Bollinger *et al.*, 1994a). If this hypothesis is correct, it would imply a rate constant of 5 - 10 s⁻¹ for formation of the competent Fe²⁺-R2 complex. In an attempt to measure the rate of formation of the competent Fe²⁺-R2 complex, a pulse/chase experiment has been carried out (Fig. 4.2). In this experiment, apo R2 was first mixed with 5 equiv. of Fe²⁺ and excess O₂. After a short period, the reaction mixture in the delay loop was mixed with a large excess of Mn²⁺ and the formation of •Y122 was monitored by SF-Abs spectroscopy. As shown in Scheme 4.3, only the competent Fe²⁺-R2 complex and the subsequent reaction intermediates would react productively to form •Y122. Any preceding reaction intermediates would be trapped by Mn²⁺ and prevented from reaction further to form •Y122. Thus, the •Y122/R2 at completion of the reaction would be a function of [competent Fe²⁺-R2] formed at the time when O₂ and Mn²⁺ are added. In other words, plotting the •Y122/R2 against the delay time provides a measure of [competent Fe²⁺-R2] as a function of time. The results of the pulse/chase experiment show that formation of the competent Fe²⁺-R2 complex fits to a first-order process with a rate constant of 4 s⁻¹.

Experimental Procedures

Materials

Apo R2-wt was prepared as described in Chapter 2. Ferrozine was purchased from Sigma (St. Louis, MO). MnCl₂ was purchased from Mallinckrodt Inc.

Reaction of Fe(II)-R2 (1 Fe²⁺/R2) with O₂ as Monitored by SF-Abs Spectroscopy

The reaction of Fe(II)-R2 (Fe²⁺/R2 = 1) with O₂ was monitored by SF-Abs spectroscopy. With the exception of the difference in the Fe²⁺/R2 ratio, these

experiments were carried out as described in Chapter 2. Detailed experimental conditions are described in the figure legends. In a typical experiment, the reaction of Fe(II)-R2 with O₂ was initiated by mixing at 5 °C an Ar-saturated solution containing 140 - 600 μM apo R2 and 1 molar equivalents of Fe²⁺ in 100 mM HEPES (pH 7.6) with equal volume of an O₂-saturated solution of 100 mM HEPES (pH 7.6), and the formation of •Y122 formation was monitored by A₄₁₀, dropline as previously described.

Dissociation of Fe²⁺ from Fe(II)-R2 Complex

The release of Fe²⁺ from Fe²⁺-R2 complex was monitored by mixing at 5 °C a Fe(II)-R2 sample (60 - 100 μM R2, Fe²⁺/R2 = 1, 2.3 or 3.4) in O₂-free 100 mM HEPES (pH 7.6) containing 190 - 220 μM dithionite¹ with an equal volume of a solution containing 60 mM ferrozine in O₂-free 100 mM HEPES (pH 7.6). Formation of the Fe²⁺-ferrozine complex (Miller *et al.*, 1988; Erman *et al.*, 1989; Miller *et al.*, 1992). was monitored at 562 nm ($\epsilon_{562} = 27900 \text{ M}^{-1}\text{cm}^{-1}$) using an Applied Photophysics DX.17MV Sequential Stopped-Flow Spectrofluorimeter.

Reaction of Fe(II)-R2 with O₂ in the Presence of Mn²⁺ and EDTA

In the Mn²⁺ quench experiments, equal volumes of an O₂-free solution of Fe(II)-R2 (60 - 100 μM R2, Fe²⁺/R2 = 1.0, 2.3 or 3.4) in 100 mM HEPES (pH 7.6) and an O₂-saturated solution of 250 mM Mn²⁺ in 100 mM HEPES (pH 7.6) were mixed at 5 °C and the reaction was followed by SF-Abs spectroscopy. The formation of •Y122 was monitored by following the A₄₁₀, dropline as a function of time (Bollinger *et al.*, 1994a). The Fe(II)-R2 sample was prepared as described in Chapter 2. The Mn²⁺

¹In some of the early anaerobic experiments, dithionite was included in the buffer to minimize O₂ contamination of the Fe(II)-R2 samples. Six separate experiments, with the results of 3 - 5 individual traces averaged in each experiment, suggest that a low level of dithionite (< 500 μM) has no adverse effect on the •Y122 production.

stock solution was prepared by dissolution of MnCl_2 in H_2O or HEPES buffer to make a 500 mM stock solution. Shortly before the SF-Abs experiment, the concentrated Mn^{2+} stock was diluted with O_2 -saturated HEPES buffer in order to give the desired Mn^{2+} concentration in 100 mM HEPES buffer (pH 7.6).

In the EDTA quench experiments, equal volumes of an O_2 -free solution of Fe(II)-R2 (60 - 100 μM R2, $\text{Fe}^{2+}/\text{R2} = 1.0, 2.3$ or 3.4) in 100 mM HEPES (pH 7.6) and an O_2 -saturated solution of 250 mM EDTA in 100 mM HEPES (pH 7.6) were mixed at 5 °C and the formation of $\bullet\text{Y122}$ was followed by SF-Abs spectroscopy.

Mn²⁺ Pulse/chase Experiment

A dual-mixing stopped-flow experiment was carried out in which a solution of apo R2-wt (101 μM) in 100 mM HEPES (air-saturated, pH 7.6) was mixed at 5 °C with an equal volume of 507 μM Fe^{2+} in 5 mM H_2SO_4 (air-saturated) and 10 mM ascorbate. The reaction was allowed to proceed for varying lengths of time (delay time), and was then mixed rapidly with an equal volume of a chase solution containing 25 mM Mn^{2+} in 100 mM HEPES (pH 7.6, air-saturated). The formation of $\bullet\text{Y122}$ after addition of Mn^{2+} was monitored by A_{410} , dropline as previously described.

Results

Reaction of Fe(II)-R2-wt ($\text{Fe}^{2+}/\text{R2} = 1$) with O_2 as Monitored by SF-Abs Spectroscopy

Previous studies by Bollinger have shown that the reaction of apo R2 with excess O_2 and 1 equiv. of Fe^{2+} is slow, and exhibits complex kinetic behavior (Bollinger, 1992). This kinetic complexity was proposed to be a reflection of the slow release of Fe^{2+} from monoferrous R2. Reassociation of the free Fe^{2+} with another molecule of R2 ultimately forms a competent Fe^{2+} -R2 complex which can then react with O_2 to form native R2. In order to test this hypothesis, the reaction of Fe(II)-R2 with O_2 when $\text{Fe}^{2+}/\text{R2} = 1$ has been examined. When Fe(II)-R2 (1 $\text{Fe}^{2+}/\text{R2}$) is mixed

with O_2 , the reaction requires more than 180 s to reach completion, at which time the A_{410} dropline indicates an $Fe^{2+}/\bullet Y122$ ratio of 3.0 ± 0.03 . Fig. 4.3 illustrates that the formation of $\bullet Y122$ in the reaction with an $Fe^{2+}/R2$ ratio of 1 is much slower than that in the reaction with an $Fe^{2+}/R2$ of 2.3. Interestingly, non-linear least squares fitting indicates that the formation $\bullet Y122$ fits well to a first-order process with a rate constant of $0.031\ s^{-1}$ (Fig. 4.4).

To address the possibility that the marked slowing of the reaction with 1 $Fe^{2+}/R2$ might be the result of the limited availability of the fourth electron, the reaction was also carried out in the presence of ascorbate. The ability of ascorbate to donate the required fourth electron in place of Fe^{2+} has been established previously (Bollinger, 1992). As shown in Fig. 4.5, in the presence of ascorbate, $\bullet Y122$ formation is still much slower than that in the reaction with 2.3 $Fe^{2+}/R2$. Thus, limited availability of the reducing equivalent is not the determining factor for the very slow formation of $\bullet Y122$ in the 1 $Fe^{2+}/R2$ reaction. One scenario consistent with these data is that mixing apo R2 with 1 equiv. of Fe^{2+} results in predominantly mononuclear Fe^{2+} binding, such that the essential factor determining the rate of $\bullet Y122$ formation in this reaction is related to the rate at which Fe^{2+} is released from monoferrous R2 and associates with another R2 molecule to form the competent Fe^{2+} -R2 complex.

Dissociation of Fe^{2+} from $Fe(II)$ -R2

The marked slowing and the first-order kinetic behavior of the reaction of $Fe(II)$ -R2 with O_2 when $Fe^{2+}/R2 = 1$ suggest that the rate-determining step in this reaction might be the dissociation of Fe^{2+} from monoferrous R2. In order to test this hypothesis, the k_{off} of Fe^{2+} from the Fe^{2+} -R2 complexes was examined using a Fe^{2+} -chelator, ferrozine (Miller *et al.*, 1988; Erman *et al.*, 1989; Miller *et al.*, 1992). The release of Fe^{2+} from Fe^{2+} -R2 complex was monitored by mixing at 5 °C an Ar-

saturated solution of Fe(II)-R2 sample ($\text{Fe}^{2+}/\text{R2} = 1, 2.3$ or 3.4) with an equal volume of an Ar-saturated solution containing 60 mM ferrozine in 100 mM HEPES (pH 7.6). A control was carried out in which a solution of 100 μM Fe^{2+} in Ar-saturated 100 mM HEPES buffer (pH 7.6) is mixed at 5 °C with equal volume of an Ar-saturated solution of 20 mM ferrozine in 100 mM HEPES (pH 7.6). The A_{562} -versus-time trace of this reaction indicates that the reaction of ferrozine with free Fe^{2+} under these conditions is completed in 8 ms. Fitting the experimental trace to a first-order process gives a k_{obs} of $460 \pm 20 \text{ s}^{-1}$. As illustrated below, the formation of Fe^{2+} -ferrozine complex in the presence of R2 appears to be much slower than that in the absence of R2. Therefore, it is reasonable to assume that the A_{562} -versus-time trace of the reaction of Fe(II)-R2 with ferrozine reflects of the release of Fe^{2+} bound by R2.

When Fe(II)-R2 ($1 \text{ Fe}^{2+}/\text{R2}$) is mixed at 5 °C with ferrozine, the A_{562} -versus-time trace indicates that Fe^{2+} release requires $> 200 \text{ s}$ to reach completion (Fig. 4.6). Table 4.1 summarizes the kinetic analysis of the A_{562} -versus-time trace from the reaction of Fe(II)-R2 with ferrozine at three different $\text{Fe}^{2+}/\text{R2}$ ratios. When Fe(II)-R2 ($\text{Fe}^{2+}/\text{R2} = 1$) is mixed with ferrozine, non-linear least square analysis indicates that the A_{562} -versus-time trace of this reaction fits reasonably well to a first-order process with a k_{obs} of 0.045 s^{-1} (Fig. 4.6). The shape of the experimental trace can be more accurately reproduced by fitting the data to the sum of two exponentials (Eq. 4.2, $n = 2$) with exponential terms (P_n) of 0.064 s^{-1} and 0.024 s^{-1} (Fig. 4.7), suggesting that more than one class of Fe^{2+} -binding sites might be present.

The proposal by Elgren *et al.* (1991) that mixing apo R2 with Fe^{2+} results in exclusively the competent Fe^{2+} -R2 complexes implies that the kinetics of Fe^{2+} release would not change with different $\text{Fe}^{2+}/\text{R2}$ ratios. Fig. 4.8, however, indicates that the release of Fe^{2+} exhibits more complex kinetics in the reaction with an $\text{Fe}^{2+}/\text{R2}$ ratio of 2.3 than that with an $\text{Fe}^{2+}/\text{R2}$ ratio of 1 (Fig. 4.7). The shape of the

Fig. 4.3: A_{410} , dropline-versus-time traces in the reaction of O_2 with (A) Fe(II)-R2 (2.3 $Fe^{2+}/R2$), and of (B) Fe(II)-R2 (1 $Fe^{2+}/R2$). The reaction conditions (after mixing) were: (A) 69 μM R2-wt, 159 μM Fe^{2+} , 1 mM O_2 , 100 mM HEPES, pH 7.6, 5 $^{\circ}C$, and (B) 300 μM R2-wt, 301 μM Fe^{2+} , 1 mM O_2 , 100 mM HEPES, pH 7.6, 5 $^{\circ}C$. The absorbance changes were scaled to reflect difference in protein concentrations.

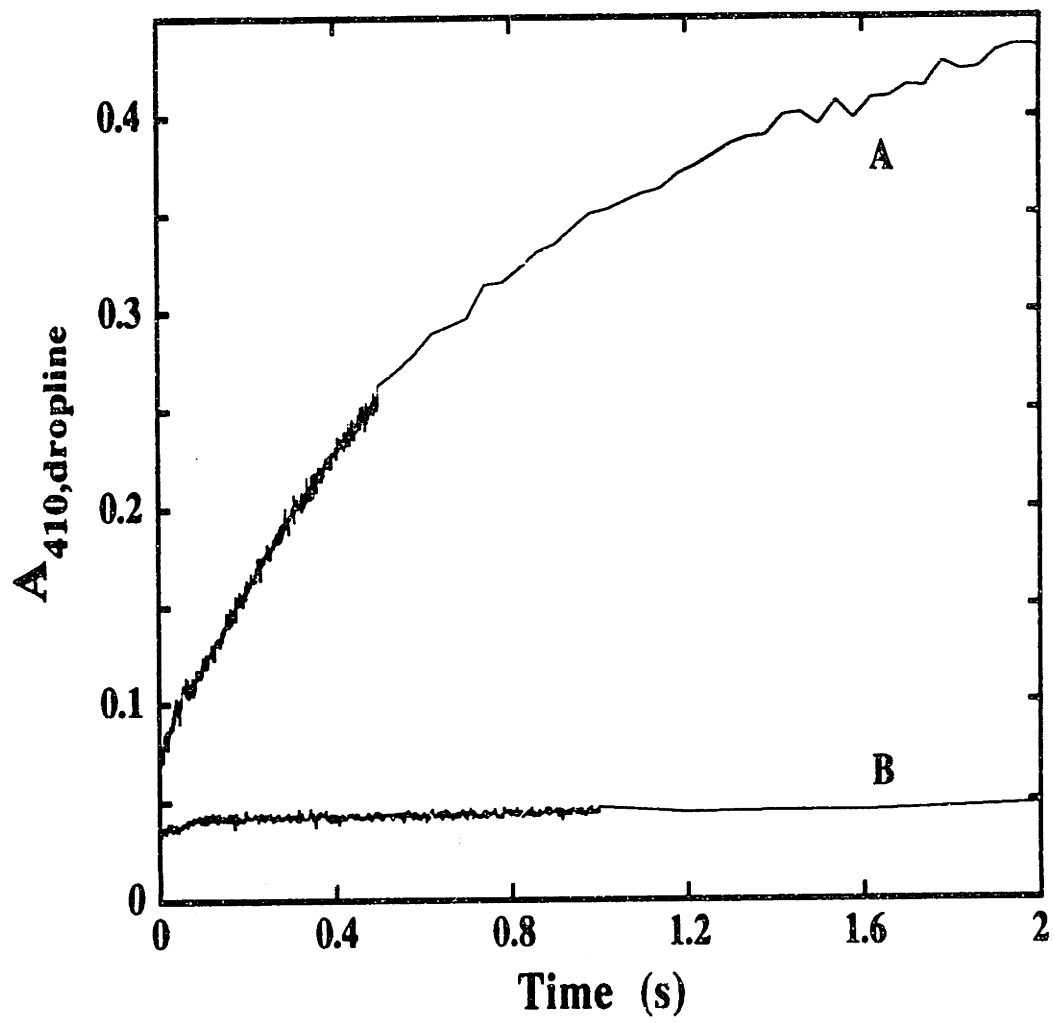


Fig. 4.4: Formation of \bullet Y122 in the reaction of Fe(II)-R2 with O₂ when Fe²⁺/R2 = 1. The reaction conditions (after mixing) were: 300 μ M R2-wt, 300 μ M Fe²⁺, 1 mM O₂, 100 mM HEPES, pH 7.6, 5 °C. The experimental trace represents the average of 3 trials. The theoretical trace is obtained by fitting a first-order process to 0.0 - 100 s of the experimental trace, and corresponds to a k_{obs} of 0.031 s⁻¹.

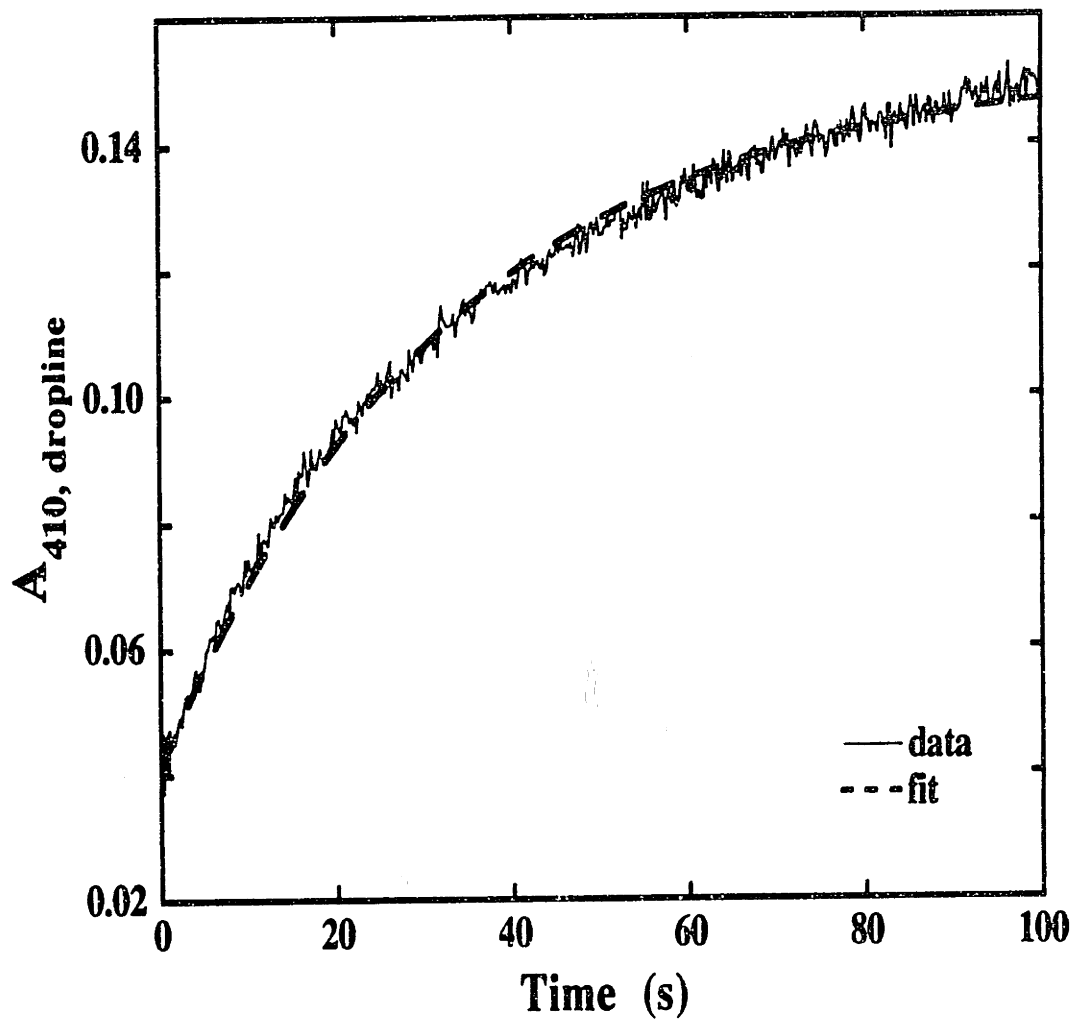


Fig. 4.5: A_{410} , dropline-versus-time traces in the reaction of Fe(II)-R2 (2.3 Fe²⁺/R2) with O₂ (A), compared with that of Fe(II)-R2 (1 Fe²⁺/R2) with O₂ in the presence of ascorbate (B). The reaction conditions (after mixing) were: (A) 69 μM R2-wt, 159 μM Fe²⁺, 1 mM O₂, 100 mM HEPES, pH 7.6, 5 °C, and (B) 300 μM R2-wt, 300 μM Fe²⁺, 1.25 mM ascorbate, 1 mM O₂, 100 mM HEPES, pH 7.6, 5 °C. The absorbance changes were normalized to reflect difference in protein concentrations.

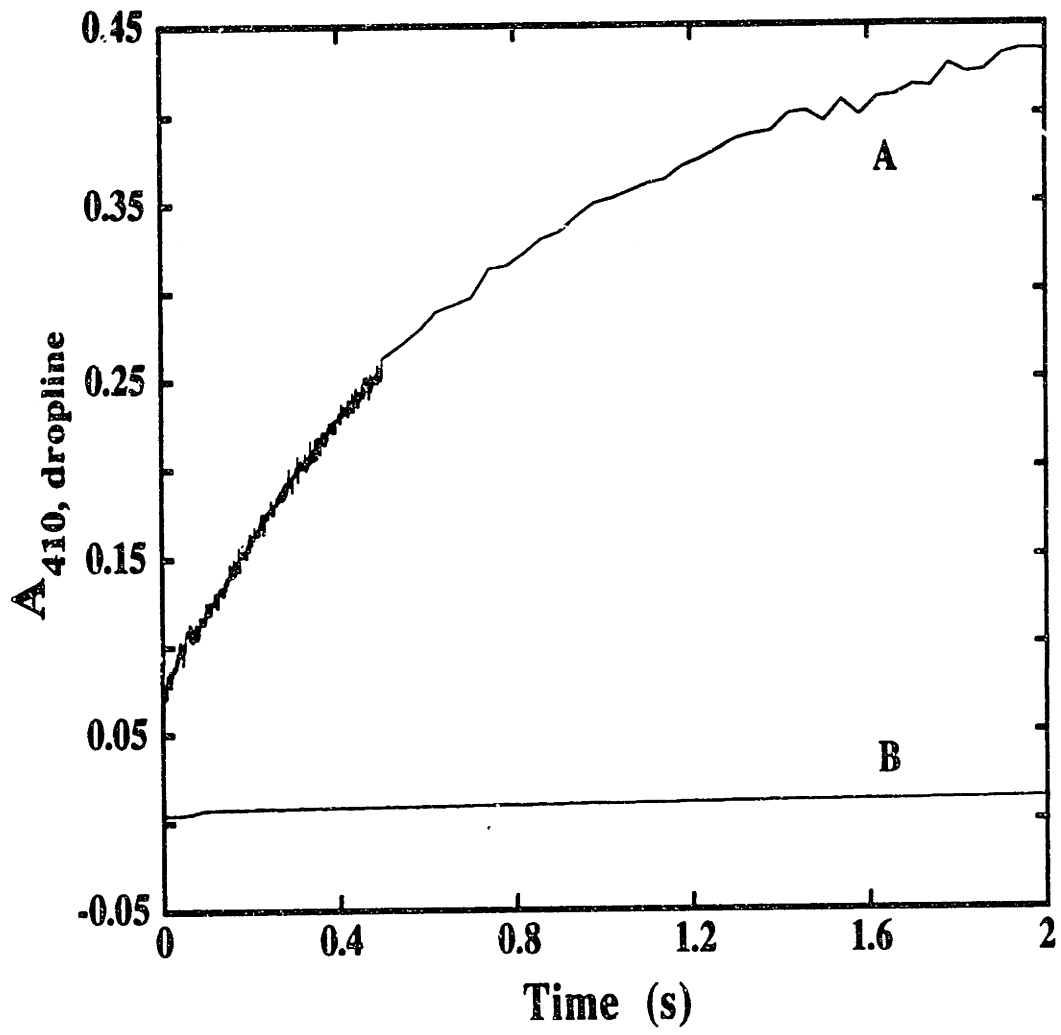


Fig. 4.6: A_{562} -versus-time trace upon mixing Fe(II)-R2-wt with ferrozine when $\text{Fe}^{2+}/\text{R2} = 1$. The reaction conditions (after mixing) were: 60 μM R2-wt, 60 μM Fe^{2+} , 97 μM dithionite, 100 mM HEPES, pH 7.6, 5 °C. The experimental trace represents the average of 4 trials. The theoretical trace is obtained by fitting a first-order process to the 0.00 - 200 s region of the experimental trace, and corresponds to a k_{obs} of 0.045 s^{-1} .

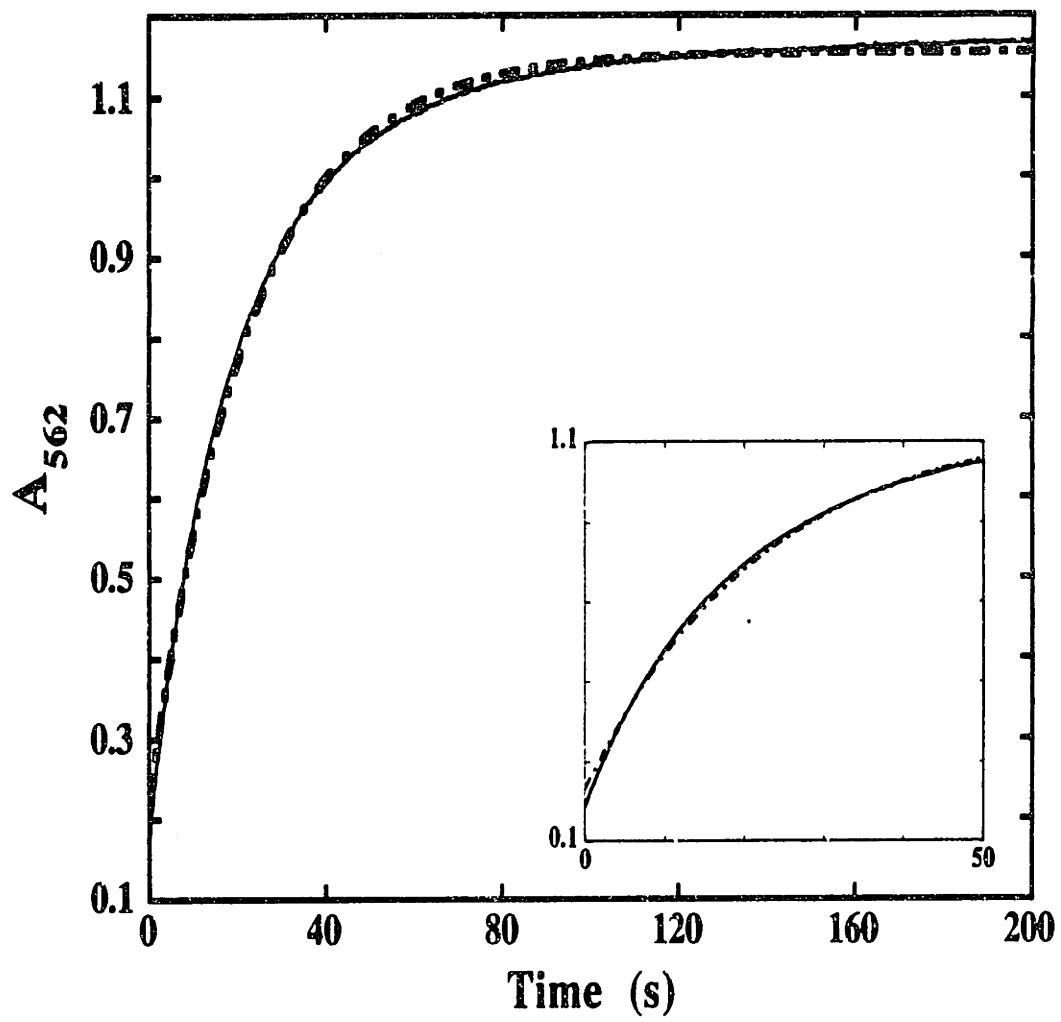


Fig. 4.7: A_{562} -versus-time trace in the reaction of Fe(II)-R2-wt with ferrozine when $\text{Fe}^{2+} / \text{R2} = 1$. The reaction conditions (after mixing) were: 60 μM R2-wt, 60 μM Fe^{2+} , 97 μM dithionite, 100 mM HEPES, pH 7.6, 5 $^{\circ}\text{C}$. The experimental trace represents the average of 4 trials. The theoretical trace is obtained by fitting two exponentials to the 0.0 - 200 s region of the experimental trace, and corresponds to rate constants of 0.064 s^{-1} and 0.024 s^{-1} .

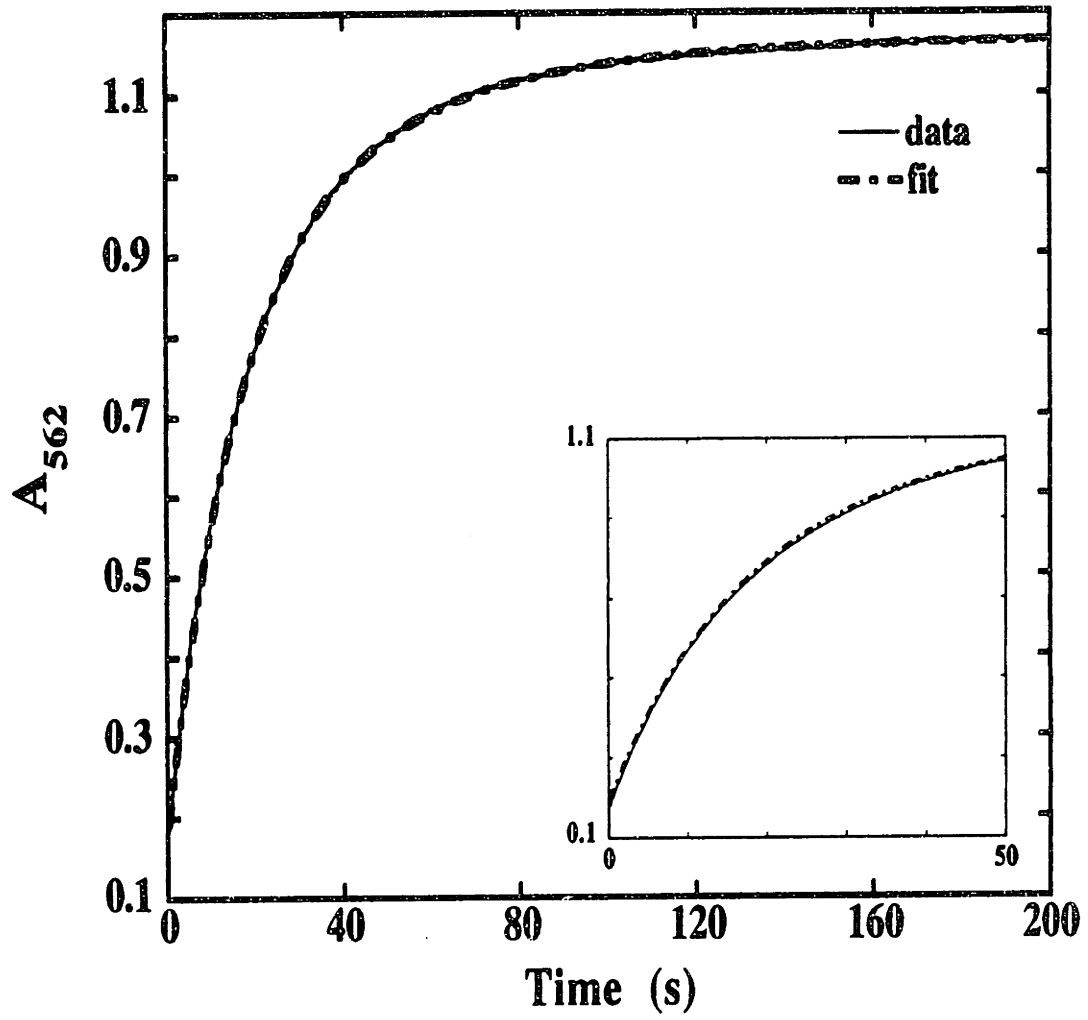


Fig. 4.8: A_{562} -versus-time trace in the reaction of Fe(II)-R2-wt with ferrozine when $\text{Fe}^{2+} / \text{R2} = 2.3$. The reaction conditions (after mixing) were: 100 μM R2-wt, 230 μM Fe^{2+} , 90 μM dithionite, 100 mM HEPES, pH 7.6, 5 $^{\circ}\text{C}$. The experimental trace represents the average of 4 trials. The theoretical trace is obtained by fitting three exponentials to the 0.0 - 200 s region of the experimental trace, and corresponds to rate constants of 1.1 s^{-1} , 0.14 s^{-1} and 0.033 s^{-1} .

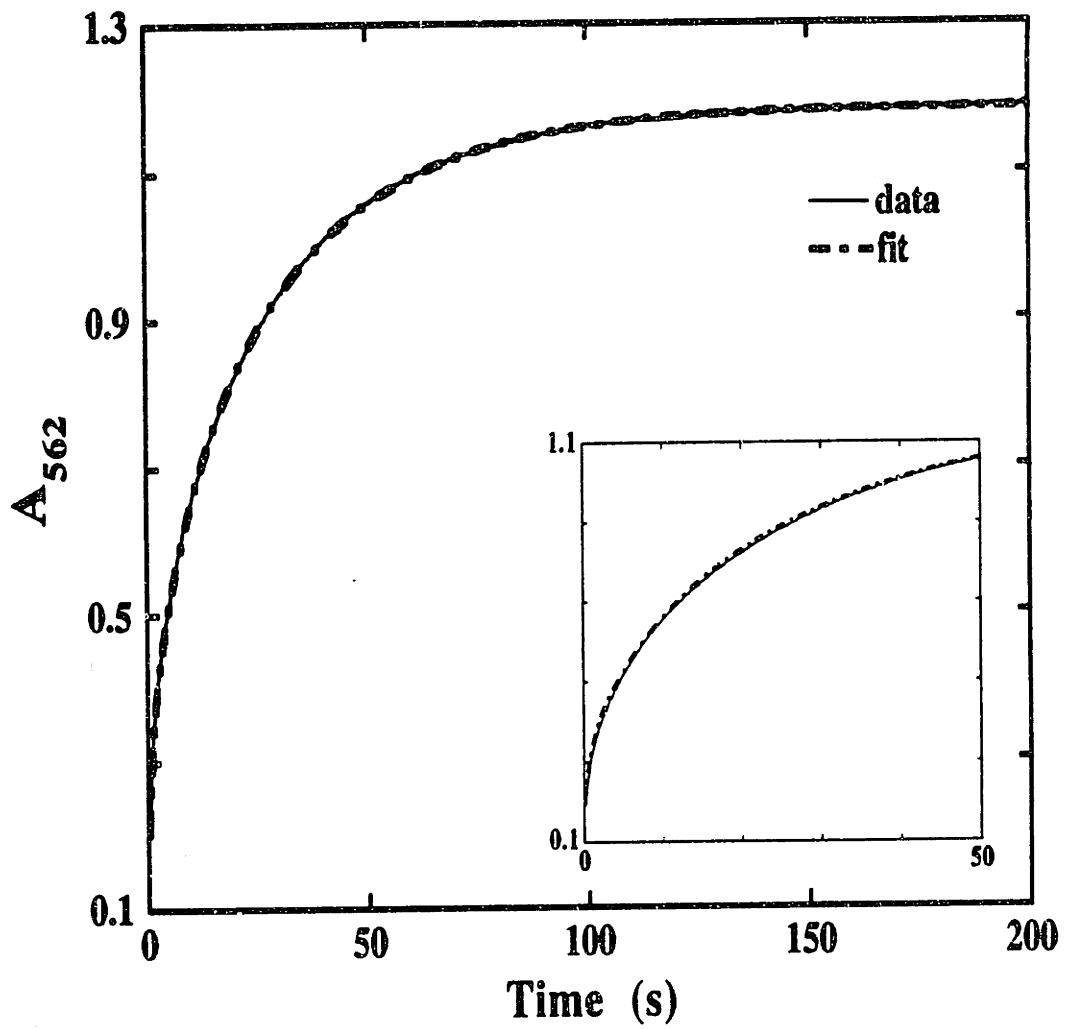


Fig. 4.9: A_{562} -versus-time trace in the reaction of Fe(II)-R2-wt with ferrozine when $\text{Fe}^{2+} / \text{R2} = 3.4$. The reaction conditions (after mixing) were: 95 μM R2-wt, 322 μM Fe^{2+} , 110 μM dithionite, 100 mM HEPES, pH 7.6, 5 °C. The experimental trace represents the average of 4 trials. The theoretical trace is obtained by fitting three exponentials to the 0.1 - 200 s region of the experimental trace, and corresponds to rate constants of 0.91 s^{-1} , 0.14 s^{-1} and 0.027 s^{-1} .

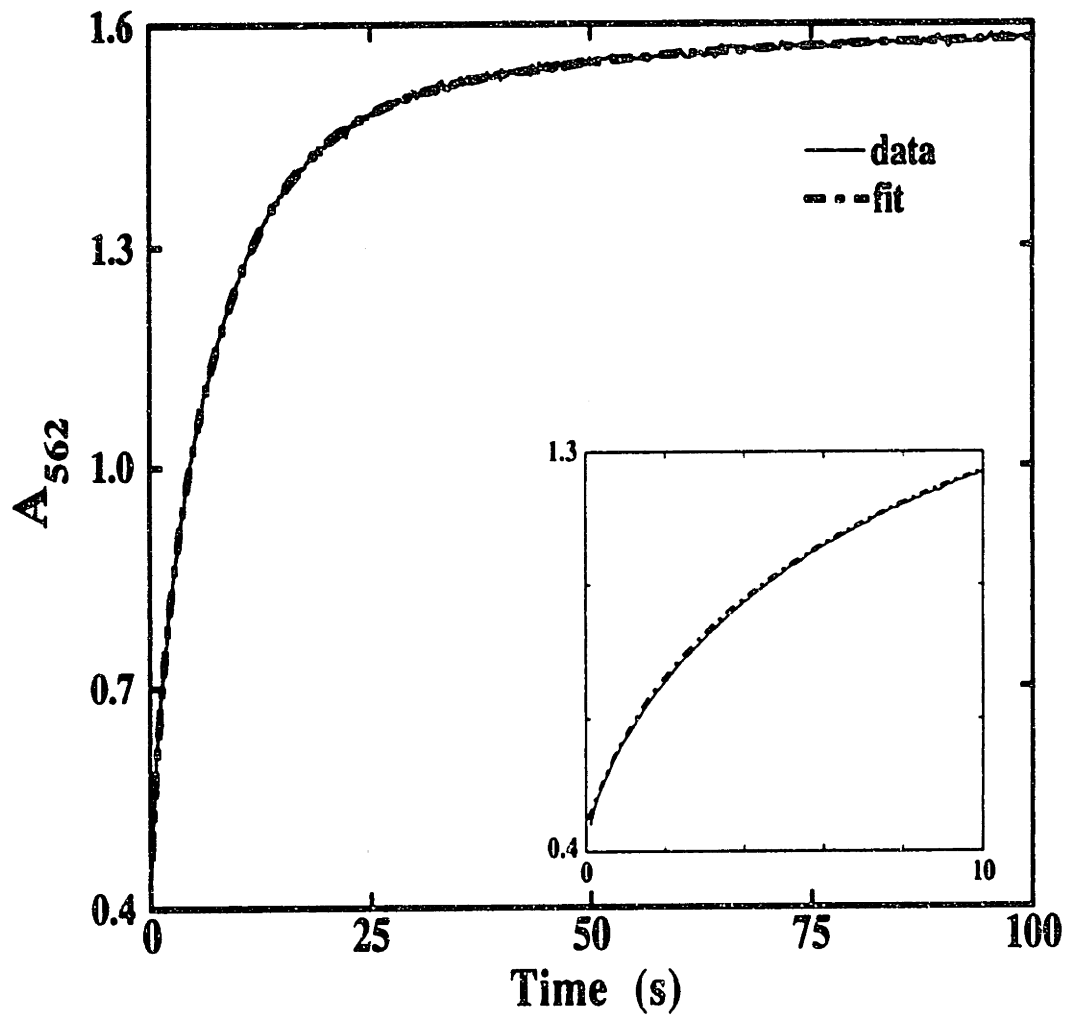


Table 4.1: Summary of least-squares fits to Eq. 4.1 of the A_{562} -versus-time traces from the reaction of Fe(II)-R2 with ferrozine.

$\text{Fe}^{2+}/\text{R2}$	Fit-range (s)	n	Amp _n	P_n (s ⁻¹)
1.0	0.0 - 200	1	95 %	0.045
		2	68 %	0.064
			32 %	0.024
2.3	0.0 - 200	3	15%	1.1
			20 %	0.14
			66 %	0.033
3.4	0.1 - 200	3	14%	0.91
			71 %	0.14
			14 %	0.027

$$\text{Eq. 4.2 : } A_{562} = \text{Amp}_1 \cdot \exp(-P_1 t) + \text{Amp}_2 \cdot \exp(-P_2 t) + \dots + \text{Amp}_n \cdot \exp(-P_n t)$$

where $n = 1, 2, 3 \dots$

experimental trace can be reproduced by fitting the data to the sum of three exponentials with exponential terms of 1.1 s^{-1} , 0.14 s^{-1} and 0.033 s^{-1} (Fig. 4.8). With an $\text{Fe}^{2+}/\text{R2}$ ratio of 3.4, the A_{562} -versus-time trace can be described by the sum of three exponentials with exponential terms of 0.91 s^{-1} , 0.14 s^{-1} and 0.027 s^{-1} (Fig. 4.9). The exponential terms obtained from the reaction with $\text{Fe}^{2+}/\text{R2}$ ratio of 3.4 are close to those obtained from the reaction with an $\text{Fe}^{2+}/\text{R2}$ ratio of 2.3, although the amplitude terms associated with each exponential terms are different in the two

cases (Table 4.1). The difference in the amplitude terms may be a reflection of the statistical distributions of the different Fe^{2+} -R2 complexes present in the reaction mixture (Scheme 4.1 or 4.2) at different $\text{Fe}^{2+}/\text{R2}$ ratios.

It is also possible to quantitate the amount of Fe^{2+} bound to R2 from the A_{562} -versus-time trace of these experiments. As mentioned above, the reaction in the control experiment is completed in 8 ms, while the reaction in the presence of R2 requires > 200 s. Therefore, the ΔA_{562} in the presence of R2 from $t = 8$ ms to $t = \infty$ should be proportional to the concentration of Fe^{2+} bound by R2 ($[\text{Fe}^{2+}]_{\text{bound}}$). As shown in Table 4.2, under the experimental conditions examined, 93 - 97 % of the Fe^{2+} present are bound by R2. This result establishes that all the Fe^{2+} in the Fe(II)-R2 sample are complexed with R2 in the experiments described in Chapter 2 and 3.

Table 4.2: Summary of quantitation of Fe^{2+} bound by R2 in the Fe(II)-R2 sample.

$[\text{Fe}^{2+}]$ (μM)	[Apo R2] (μM)	$[\text{Fe}^{2+}]_{\text{bound}}/[\text{Fe}^{2+}]_{\text{total}}$
60	60	$97 \pm 5 \%$
100	230	$93 \pm 5 \%$
95	322	$97 \pm 5 \%$

Reaction of Fe(II)-R2 with O_2 in the Presence of Mn^{2+} or EDTA

The observation of distinctly different kinetics in the release of bound Fe^{2+} at different $\text{Fe}^{2+}/\text{R2}$ ratios suggests that there are multiple forms of Fe^{2+} -R2 complex in the equilibrium mixture of apo R2 and Fe^{2+} . In an attempt to distinguish between the different binding modes, the reactions of Fe(II)-R2 with O_2 in the presence of

Mn²⁺ or EDTA were examined. As shown in Scheme 4.3 and 4.4, these experiments provide a method to quantitate the amount of the competent Fe²⁺-R2 complexes in which all the Fe²⁺ ions required for the cofactor assembly are bound properly. Table 4.3 shows the •Y122/R2 at completion when the reaction of Fe(II)-R2 with O₂ is carried out in the presence of Mn²⁺ or EDTA. In the three cases examined, the •Y122/R2 ratios in the presence of Mn²⁺ are close to the •Y122/R2 ratios in the presence of EDTA, but differ significantly from those in the normal reconstitution reaction when Mn²⁺ and EDTA are absent. In the case with an Fe²⁺/R2 ratio of 1, the •Y122/R2 ratio in the presence of Mn²⁺ is 0.054 ± 0.03, which is close to the ratio of 0.023 ± 0.03 from an identical reaction quenched with EDTA instead of Mn²⁺. These results can be contrasted with the •Y122/R2 ratio in the normal reaction (•Y122/R2 = 0.39 ± 0.03). A lower •Y122/R2 ratio in the presence of Mn²⁺ and EDTA was also observed in the reactions with Fe²⁺/R2 ratios of 2.3 and 3.4. These results indicate that both Mn²⁺ and EDTA can depress the •Y122 yield by allowing only the competent Fe²⁺-R2 complex to react further to form •Y122. The fact that the two different methods of quenching - one by trapping R2 molecules with a vacant metal-binding site, the other by trapping free Fe²⁺ in solution - give very similar results strongly suggest that these results represent true estimates of the amount of the competent Fe²⁺-R2 complex.

The kinetics of •Y122 formation in the presence of Mn²⁺ or EDTA have also been examined. Table 4.4 summarizes the results of the least squares fits of the A₄₁₀, dropline-versus-time traces of the experiments in Table 4.3. Fig. 4.10 to 4.13 show that in all four cases, formation of •Y122 is first-order with a k_{obs} of 0.8 ± 0.1. More importantly, these rate constants are identical to the k_{obs} for formation of •Y122 in the excess Fe²⁺ reaction (0.85 ± 0.05 s⁻¹). These results strongly suggest that, in the presence of Mn²⁺ or EDTA, only the competent Fe²⁺-R2 complex reacts to form •Y122. The mechanistic implications of these results will be discussed.

Table 4.3: Summary of $\bullet Y_{122}/R_2$ ratio at completion in the reaction Fe(II)-R₂ with O₂ in the presence of EDTA or Mn²⁺.

Fe ²⁺ /R ₂	O ₂	O ₂ + EDTA	O ₂ + Mn ²⁺
1.0	0.39 ± 0.03	0.023 ± 0.03	0.054 ± 0.03
2.3	0.75 ± 0.05	0.47 ± 0.03	0.42 ± 0.03
3.4	1.06 ± 0.09	0.82 ± 0.05	0.70 ± 0.05

Table 4.4: Summary of least-squares fits of the A₄₁₀, dropline-versus-time traces to a first-order process from the reaction of Fe(II)-R₂ with O₂ in the presence of Mn²⁺ or EDTA.

Fe ²⁺ /R ₂	Inhibitor	Fit-range (s)	k _{obs} (s ⁻¹)	($\bullet Y_{122}/R_2$) _∞
2.3	Mn ²⁺	0.02 - 5.0	0.68	0.42 ± 0.03
	EDTA	0.02 - 5.0	0.87	0.47 ± 0.03
3.4	Mn ²⁺	0.01 - 10.0	0.81	0.70 ± 0.05
	EDTA	0.01 - 10.0	0.70	0.82 ± 0.05

These results may also provide further insight to the manner by which Fe²⁺ donates the fourth electron required for cofactor assembly. Consider the reaction of Fe(II)-R₂ (Fe²⁺/R₂ = 2.3) with O₂ in the presence of Mn²⁺. The fourth reducing equivalent required for cofactor assembly in this reaction can be provided by a Fe²⁺ bound in the form of monoferrous R₂. Alternatively, it can come from a free Fe²⁺

Fig. 4.10: A_{410} , dropline-versus-time traces in the reaction of Fe(II)-R2-wt with O_2 when $Fe^{2+}/R2 = 2.3$ and in the presence of Mn^{2+} . The reaction conditions (after mixing) were: 100 μM R2-wt, 230 μM Fe^{2+} , 90 μM dithionite, 125 mM Mn^{2+} , 100 mM HEPES, pH 7.6, 5 °C. The experimental trace represents the average of 3 trials. The theoretical trace is obtained by fitting a first-order process to the 0.02 - 5.0 s region of the experimental trace, and corresponds to a k_{obs} of 0.68 s^{-1} .

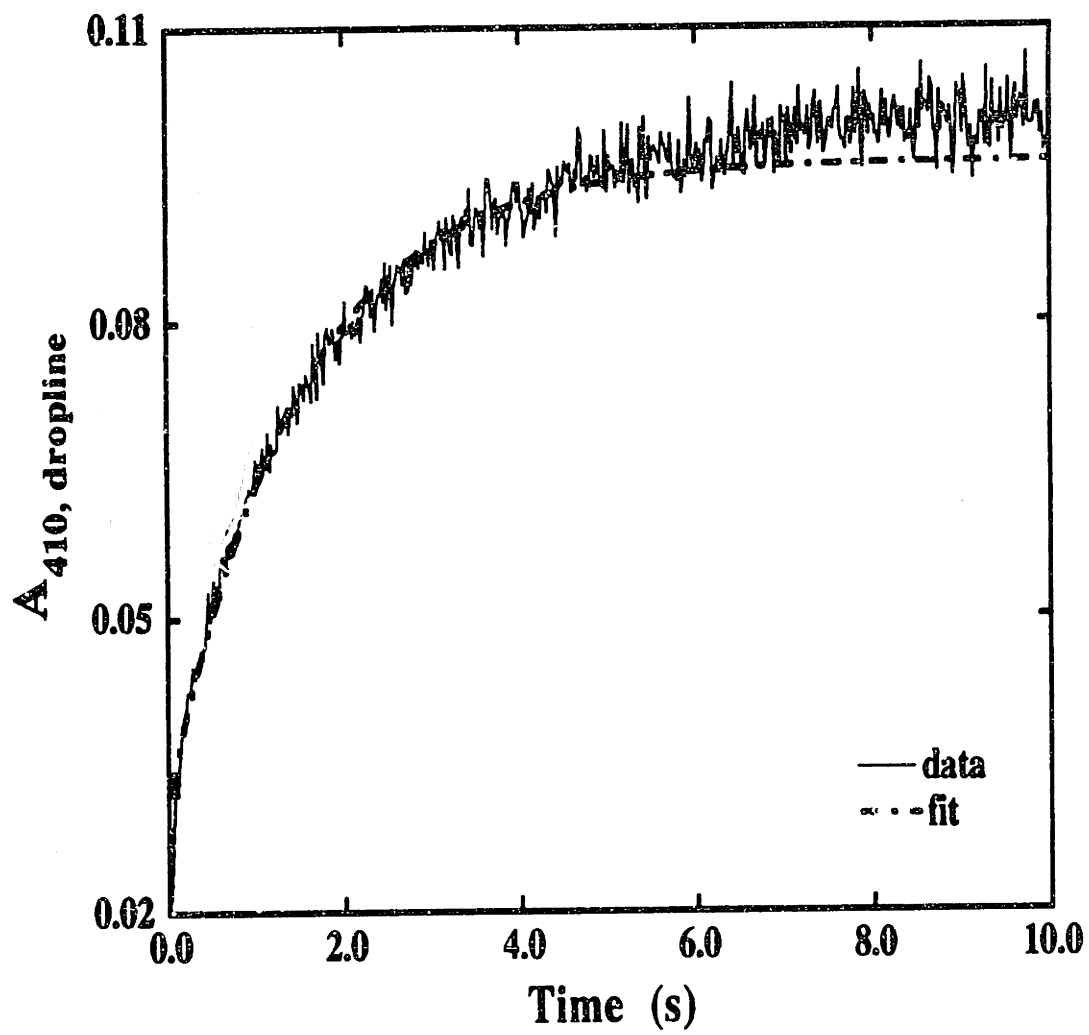


Fig. 4.11: A_{410} , dropline-versus-time traces in the reaction of Fe(II)-R2-wt with O_2 when $Fe^{2+}/R2 = 3.4$ and in the presence of Mn^{2+} . The reaction conditions (after mixing) were: 95 μM R2-wt, 322 μM Fe^{2+} , 110 μM dithionite, 125 mM Mn^{2+} , 100 mM HEPES, pH 7.6, 5 °C. The experimental trace represents the average of 3 trials. The theoretical trace is obtained by fitting a first-order process to the 0.01 - 10.0 s region of the experimental trace, and corresponds to a k_{obs} of 0.81 s^{-1} .

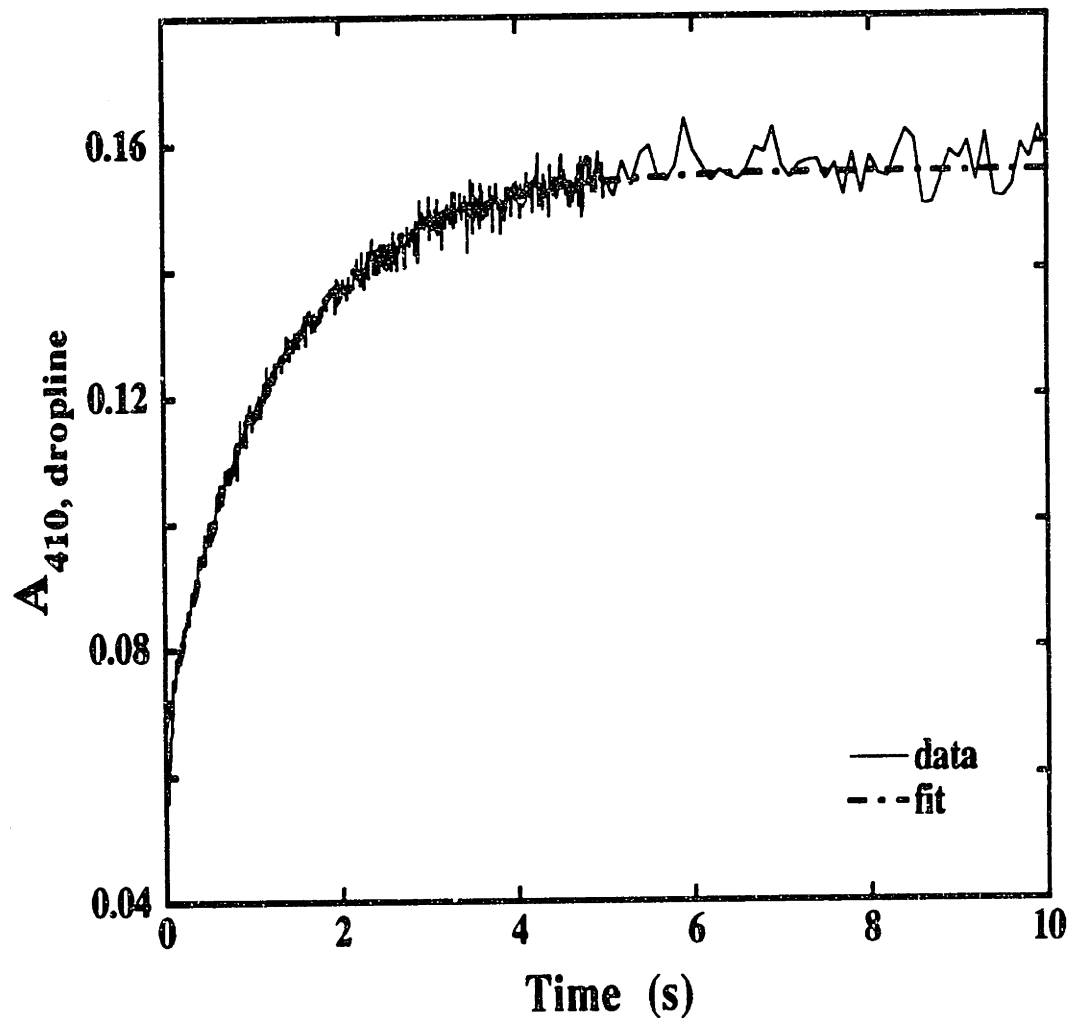


Fig. 4.12: A_{410} , dropline-versus-time traces in the reaction of Fe(II)-R2-wt with O_2 when $Fe^{2+}/R2 = 2.3$ and in the presence of EDTA. The reaction conditions (after mixing) were: 100 μM R2-wt, 230 μM Fe^{2+} , 90 μM dithionite, 125 mM EDTA, 100 mM HEPES, pH 7.6, 5 $^{\circ}C$. The experimental trace represents the average of 3 trials. The theoretical trace is obtained by fitting a first-order process to the 0.02 - 5.0 s region of the experimental trace, and corresponds to a k_{obs} of 0.87 s^{-1} .

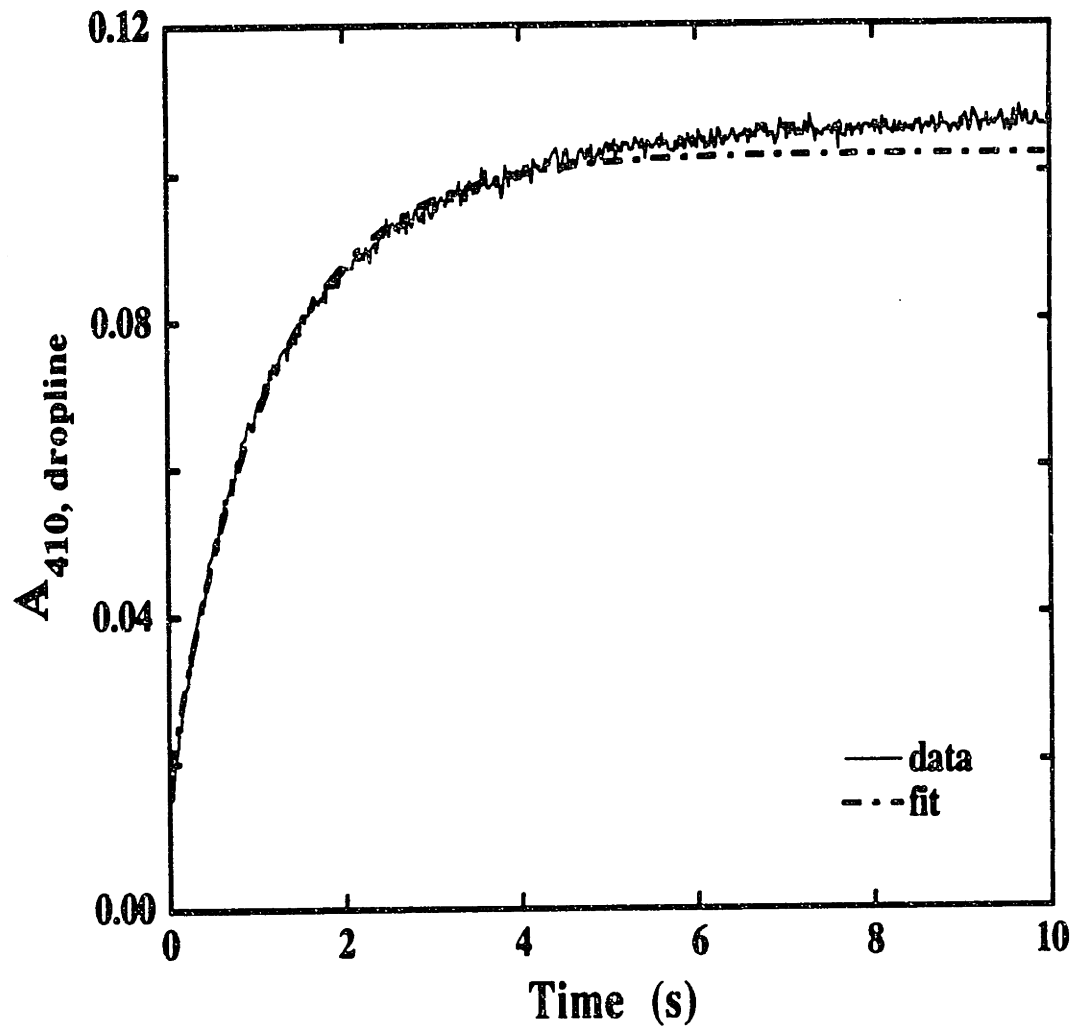
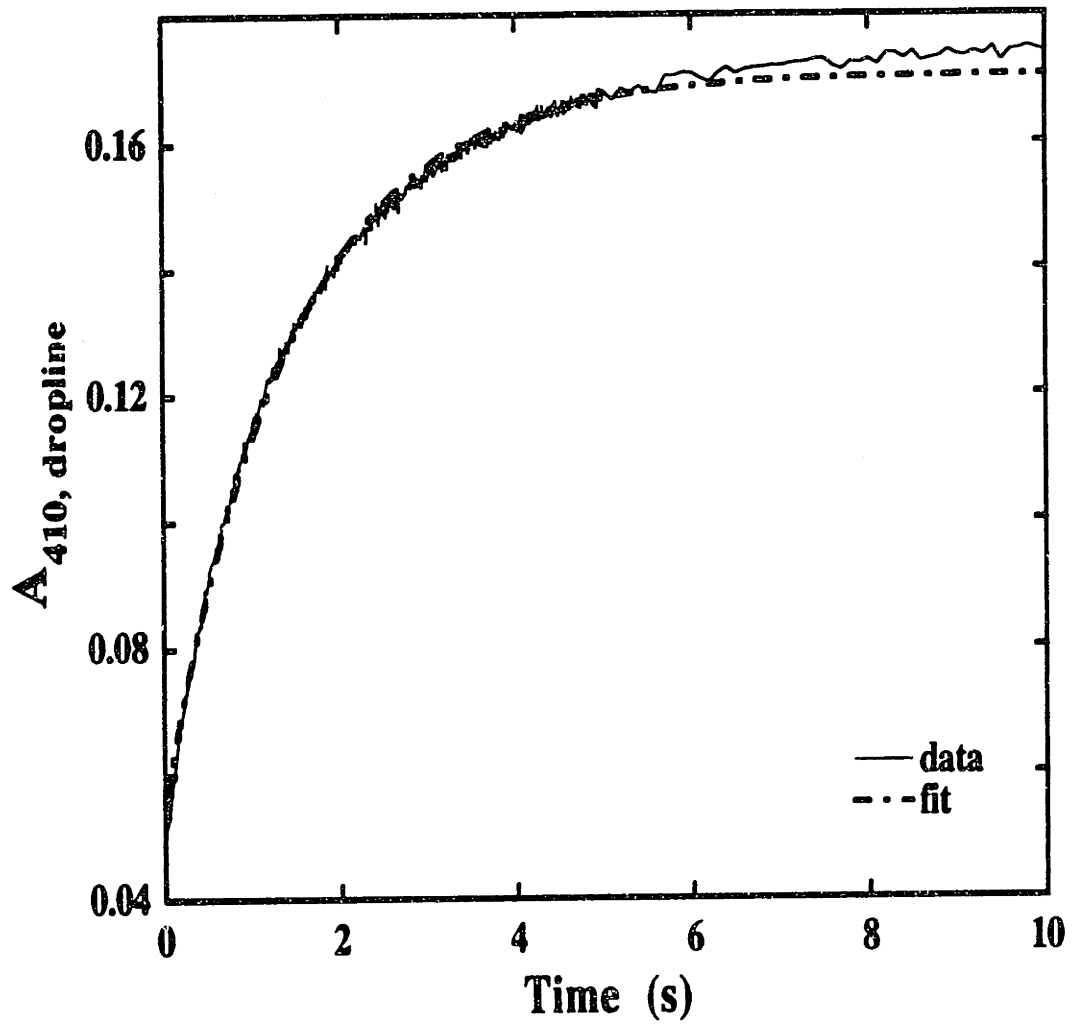


Fig. 4.13: A_{410} , dropline-versus-time traces in the reaction of Fe(II)-R2-wt with O_2 when $Fe^{2+}/R2 = 3.4$ and in the presence of EDTA. The reaction conditions (after mixing) were: 95 μM R2-wt, 322 μM Fe^{2+} , 110 μM dithionite, 125 mM Mn^{2+} , 100 mM HEPES, pH 7.6, 5 °C. The experimental trace represents the average of 3 trials. The theoretical trace is obtained by fitting a first-order process to the 0.01 - 10.0 s region of the experimental trace, and corresponds to a k_{obs} of 0.70 s^{-1} .



in solution. However, the results indicated in Table 4.2 indicate that essentially all Fe^{2+} are bound. If electron transfer can occur only from a free Fe^{2+} , then the formation of $\bullet\text{Y122}$ in this reaction would be limited by the dissociation rate of monoferrous R2 ($k_{\text{obs}} = 0.03 - 0.04 \text{ s}^{-1}$). This is clearly in contradiction with the experimental results which indicate that $\bullet\text{Y122}$ is generated with a k_{obs} of $\sim 0.8 \text{ s}^{-1}$ (Table 4.4). Taken together, these results suggest that the Fe^{2+} which donates the fourth electron in this experiment is bound by R2. The state of this Fe^{2+} will be discussed further below.

Mn²⁺ Pulse/chase Experiment

As demonstrated above, Mn^{2+} can provide a useful tool to determine the amount of the competent Fe^{2+} -R2 present in the equilibrium mixture of apo R2 and Fe^{2+} . However, the Mn^{2+} -quench experiments described above provide no kinetic information on the formation of this species. In an attempt to measure the rate of formation of the competent Fe^{2+} -R2 complex, a pulse/chase experiment was carried out (Fig. 4.2). In this experiment, apo R2 was first mixed with 5 equiv. of Fe^{2+} and excess O_2 . After a short period (delay time), the reaction mixture is mixed with a large excess of Mn^{2+} and the formation of $\bullet\text{Y122}$ is monitored by SF-Abs spectroscopy. The reaction was carried out in the presence of excess Fe^{2+} and ascorbate such that the delivery of the fourth electron will not be inhibited by addition of Mn^{2+} .

As shown in Table 4.5, addition of Mn^{2+} to the reconstitution reaction mixture at early time-points depresses the formation of $\bullet\text{Y122}$. Addition of Mn^{2+} 20 ms after mixing apo R2 with 5 equiv. of Fe^{2+} results in a final $\bullet\text{Y122}/\text{R2}$ ratio of 0.29 ± 0.08 . With increasing delay times, the $\bullet\text{Y122}/\text{R2}$ ratio increases, indicating that the reconstitution reaction becomes refractory to addition of Mn^{2+} . When apo R2 is

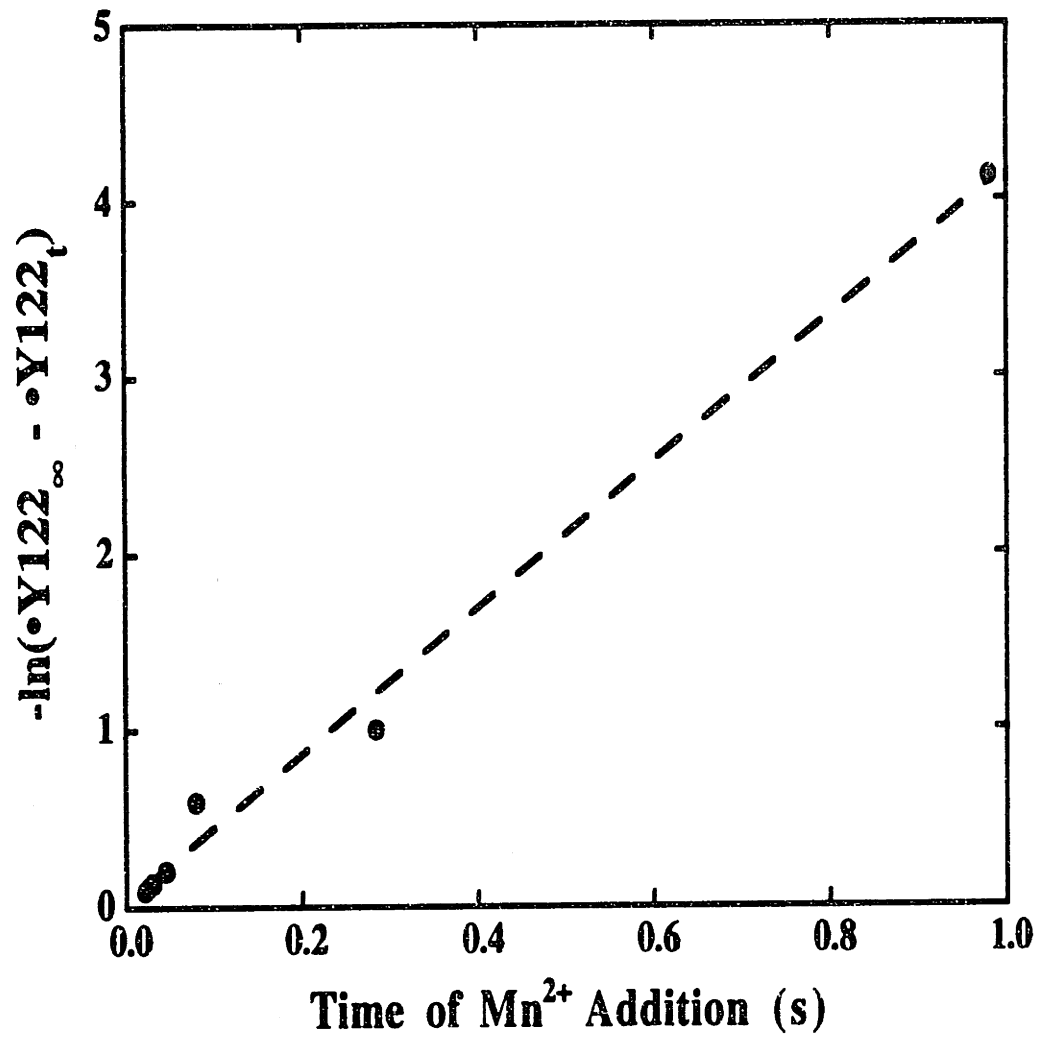
Table 4.5: Summary of $\bullet Y122/R2$ ratio at completion in the pulse/chase experiment.

Time of Mn^{2+} Addition (s)	$(\bullet Y122/R2)_{\infty}$
0.021	0.29 ± 0.04
0.025	0.31 ± 0.04
0.030	0.33 ± 0.04
0.045	0.39 ± 0.05
0.079	0.65 ± 0.08
0.284	0.83 ± 0.1
0.481	0.92 ± 0.1
0.98	1.18 ± 0.1

allowed to react with excess Fe^{2+} for > 1 s, addition of Mn^{2+} appears to have no effect on $\bullet Y122$ yield.

As shown in Scheme 4.3, formation of $\bullet Y122$ may depend on several steps, but Mn^{2+} -quenching depends only on the steps up to and including the first irreversible step toward product formation. Since it has been shown that the reaction of O_2 with the diferrous cluster is rapid (see Chapter 2), it is reasonable to assume that the only steps in the reaction pathway that are sensitive to addition to Mn^{2+} are the ones that occur prior to formation of the competent Fe^{2+} -R2 complex (Scheme 4.3). Thus, the rate at which the reconstitution reaction becomes insensitive to addition of Mn^{2+} is related to the rate of formation of the competent Fe^{2+} -R2 complex. As shown in Fig. 4.14, the reconstitution reaction becomes insensitive to the addition of Mn^{2+} with first-order kinetics ($k_{obs} 4 \pm 1 s^{-1}$).

Fig. 4.14: \bullet Y122 yield as a function of delay time in the pulse/chase experiment. The reaction conditions (after mixing) were: 25 μ M R2-wt, 127 μ M Fe²⁺, 2.5 mM ascorbate, 12.5 mM Mn²⁺, 100 mM HEPES, pH 7.6, 5 °C. The experimental data are summarized in Table 4.5. The theoretical trace is obtained by fitting a first-order process to the experimental data, and corresponds to a k_{obs} of 4 s⁻¹.



suggesting that the rate-determining step in the formation of the competent Fe^{2+} -R2 complex is a first-order process with a k_{obs} of $4 \pm 1 \text{ s}^{-1}$. These results are consistent with previous study by Bollinger *et al.* (Bollinger *et al.*, 1994a) and the results in Chapter 2 which suggest that the rate determining step in formation of X from apo R2 is a conformational change with a k_{obs} of $5 - 10 \text{ s}^{-1}$.

It should also be noted that a "burst" of $\bullet\text{Y122}$ was observed in the pseudo-first-order plot in Fig. 4.14. As shown in Fig. 4.15, extrapolation of the pseudo-first-order plot in Fig. 4.14 to zero time indicates a $\bullet\text{Y122}/\text{R2}$ ratio of 0.23. The possible reason for this "burst" will be discussed.

Discussion

Implications for Binding of Fe^{2+} by Apo R2

Based on the finding that the $\bullet\text{Y122}/\text{R2}$ ratio of the reconstitution reaction is largely independent of the ratio of $\text{Fe}^{2+}/\text{apo R2}$ and the finding that the majority of Fe^{2+} added is ultimately incorporated into diferric cluster, it had been proposed by several authors that addition of Fe^{2+} to apo R2 results exclusively in dinuclear Fe^{2+} binding (Fontecave *et al.*, 1990b; Elgren *et al.*, 1991; Atta *et al.*, 1992). However, as stated above, this proposal is inconsistent with the finding that formation of $\bullet\text{Y122}$ is much slower in the reaction of apo R2 with 1 equiv. of Fe^{2+} than that in the reaction with 2.3 equiv. of Fe^{2+} (Bollinger, 1992).

The results in this chapter provide further arguments against the proposal that the binding of Fe^{2+} by apo R2 is highly cooperative. As indicated in Fig. 4.3, the formation of $\bullet\text{Y122}$ in the reaction of Fe(II)-R2 ($\text{Fe}^{2+}/\text{R2} = 1$) with O_2 is much slower than that in the reaction with an $\text{Fe}^{2+}/\text{R2}$ ratio of 2.3. More importantly, the rate of formation of $\bullet\text{Y122}$ in the reaction with 1 $\text{Fe}^{2+}/\text{R2}$ is first-order with a k_{obs} of 0.031 s^{-1} . This rate constant is close to the rate constants determined for release of Fe^{2+} in the reaction with $\text{Fe}^{2+}/\text{R2}$ ratio of 1 (0.064 and 0.024 s^{-1}). Taken together, these

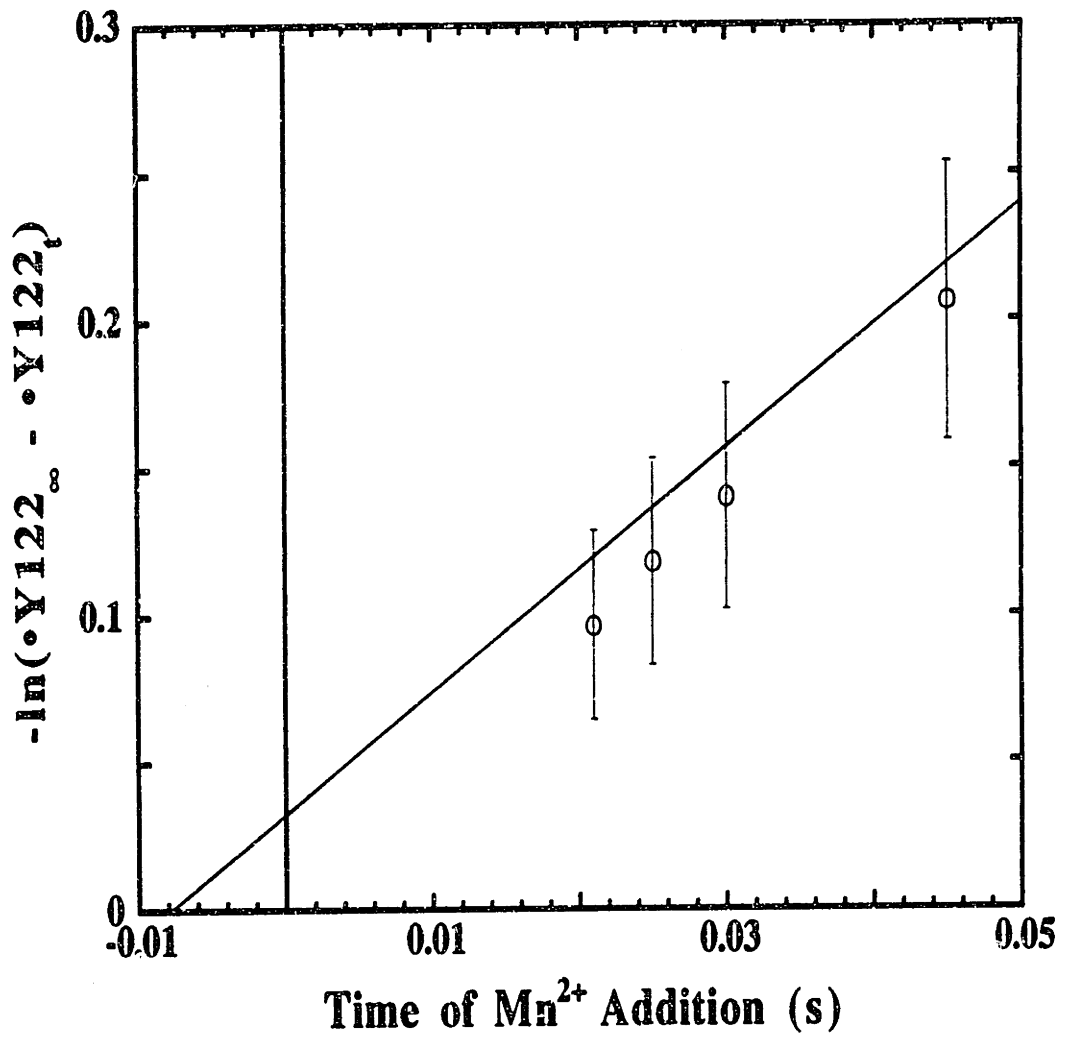
results are most consistent with the model in which mixing of apo R2 with 1 equiv. of Fe^{2+} results in predominantly mononuclear binding. Thus, the rate determining step in the formation of $\bullet\text{Y122}$ in the reaction of Fe(II)-R2 ($\text{Fe}^{2+}/\text{R2} = 1$) with O_2 is the release of Fe^{2+} bound in the nonproductive monoferrous R2. The subsequent steps - association of Fe^{2+} with another R2 to ultimately form a competent $\text{Fe}^{2+}\text{-R2}$ complex, and reaction of the competent complex with O_2 - are more rapid. Furthermore, the observation that the release of Fe^{2+} exhibits different kinetic behaviors at different $\text{Fe}^{2+}/\text{R2}$ ratios also provide strong argument against the idea that has been put forth that binding of Fe^{2+} to apo R2 is "highly cooperative".

The Mn^{2+} and EDTA-quench experiments have also provided insight into the question of cooperativity in the R2-Fe^{2+} binding interactions. The $\bullet\text{Y122}/\text{R2}$ ratios at completion in these experiments provide an estimate of the amount of $\text{Fe}^{2+}\text{-R2}$ in an equilibrium mixture of apo R2 with Fe^{2+} that is *competent* to generate $\bullet\text{Y122}$. The observation that the $\bullet\text{Y122}/\text{R2}$ ratios in the presence of Mn^{2+} or EDTA are consistently lower than the $\bullet\text{Y122}/\text{R2}$ ratio in the normal reaction (Table 4.3) argue strongly against the proposal that the binding of Fe^{2+} by apo R2 is highly cooperative.

Implications for Mechanism of the R2 Reconstitution Reaction

An essential feature of the previously proposed mechanism for the reaction of apo R2 with Fe^{2+} and O_2 is the proposed partitioning of the intermediate I which contains a 560 nm-absorbing species and the intermediate iron cluster, X (Scheme 1.3) (Bollinger *et al.*, 1994a; Bollinger *et al.*, 1994b). On the basis of its UV/vis absorption characteristics, as well as structural and functional analogies to the $\bullet\text{W191}^+$ in compound I of cytochrome c peroxidase, the 560 nm absorbing species was proposed to be a tryptophan radical cation ($\bullet\text{WH}^+$) (Bollinger *et al.*, 1994b). However, the results in Chapter 3 indicate that the 560 nm-absorbing species is not

Fig. 4.15: Extrapolation of the pseudo-first-order curve in Fig. 4.14 to show the "burst" of •Y122 formation in the pulse/chase experiment.



responsible for generating \bullet Y122 in the reaction of Fe(II)-R2 with O₂ under limiting Fe²⁺ conditions. The SF-Abs data indicate that the decay of the 560 nm absorption transient is >10 fold faster than the \bullet Y122 production. Furthermore, the EPR results indicate that the 560 nm- absorbing species is not a tryptophan cation radical. In fact, no EPR features can be discerned which correlate temporally with the 560 nm absorption transient. This result suggests that the transient is not a radical. Were the 560 nm absorbing species not a radical species, it would provide a strong argument against the proposal that this species functions as an electron conduit to oxidize Y122 to \bullet Y122.

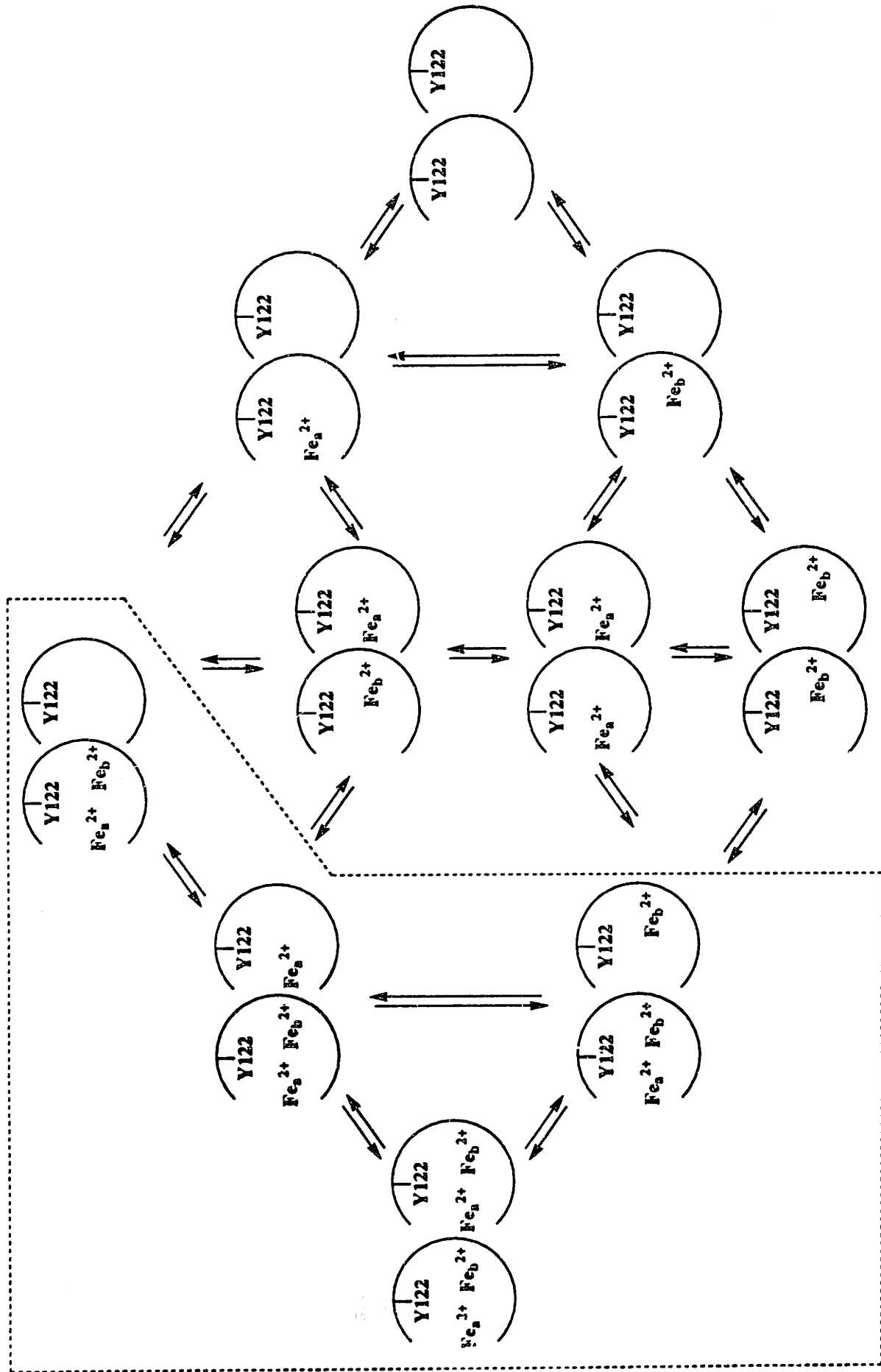
While the kinetic analysis in Chapter 3 indicates that the 560 nm-absorbing species is not the \bullet Y122-generating species in the reaction of Fe(II)-R2 with O₂ when the Fe²⁺/R2 ratio is 2.3, no decision can be reached as to whether X can be generating \bullet Y122 in this reaction. Unfortunately, the kinetic complexity of this reaction has made it very difficult to demonstrate the kinetic competence of this intermediate. Another significant result presented in this chapter is the use of the Mn²⁺- and EDTA-quench experiments to provide kinetic evidence that X can generate \bullet Y122 under limiting Fe²⁺ conditions. As stated above, the Mn²⁺- and EDTA-quench experiments have provided the unique opportunity to view the reaction of only the competent Fe²⁺-R2 complex without the complications due to improper binding. In the presence of Mn²⁺ or EDTA, the formation of \bullet Y122 in the reaction of Fe(II)-R2 (Fe²⁺/R2 = 2.3) exhibits less complex kinetics than that in the normal reconstitution reaction. Analysis of the A₄₁₀, dropline-versus-time traces indicates that the formation of \bullet Y122 is first-order with a k_{obs} of $\sim 0.8 \text{ s}^{-1}$. This rate constant is identical with the k_{obs} of \bullet Y122 formation in the reaction of Fe(II)-R2 with O₂ under excess Fe²⁺ conditions. This correlation strongly suggest that formation of \bullet Y122 in both cases proceed through the same intermediate, X.

The complete mechanistic hypothesis which results from this chapter and the two preceding chapters is shown in Scheme 4.5. Mixing apo R2 ($> 60 \mu\text{M}$) with excess Fe^{2+} under anaerobic conditions results in formation of the diferrous clusters. Upon mixing with O_2 , these diferrous cluster react rapidly, accepting an electron from a third Fe^{2+} (or ascorbate) to generate X ($k_{\text{obs}} = 60 - 80 \text{ s}^{-1}$), which then accepts an electron from Y122 ($k_{\text{obs}} = 0.7 - 1.0 \text{ s}^{-1}$) to generate the product native R2. This hypothesis is consistent with the results in Chapter 2 and the previous studies by Bollinger, *et al.* (Bollinger *et al.*, 1994a) which showed that the kinetics of the excess Fe^{2+} reaction can be described by a simple three-component kinetic mechanism shown in Scheme 2.1. The kinetic complexity of the limiting Fe^{2+} reactions can be rationalized by proposing that when apo R2 is mixed with sub-stoichiometric amount of Fe^{2+} , multiple forms of Fe^{2+} -R2 complex are generated. Upon mixing with O_2 , only the competent Fe^{2+} -R2 complex reacts in a manner analogous to the mechanism proposed for the excess Fe^{2+} reaction, generating $\bullet\text{Y122}$ with a k_{obs} of 0.8 s^{-1} . Reallocation of Fe^{2+} bound in non-competent fashion to form a competent Fe^{2+} -R2 complex is required to allow all added Fe^{2+} to react productively. Thus, the overall complex kinetics might be in part a reflection of the slow dissociation of Fe^{2+} from monoferrous R2 and reassociation with another molecule of R2, until a competent Fe^{2+} -R2 complex is achieved, after which reaction with O_2 leads to formation of X, which ultimately generates $\bullet\text{Y122}$ and diferric cluster.

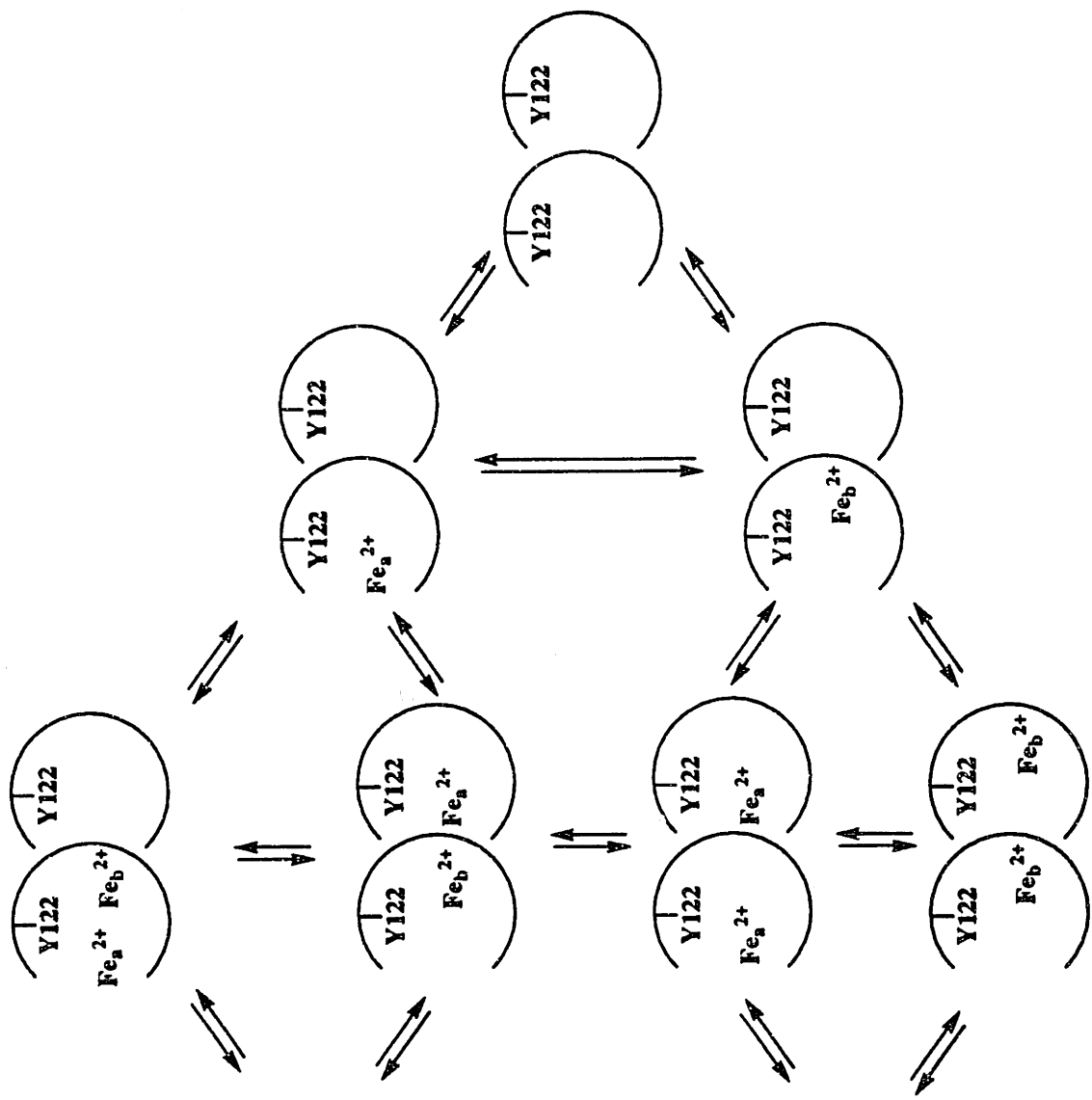
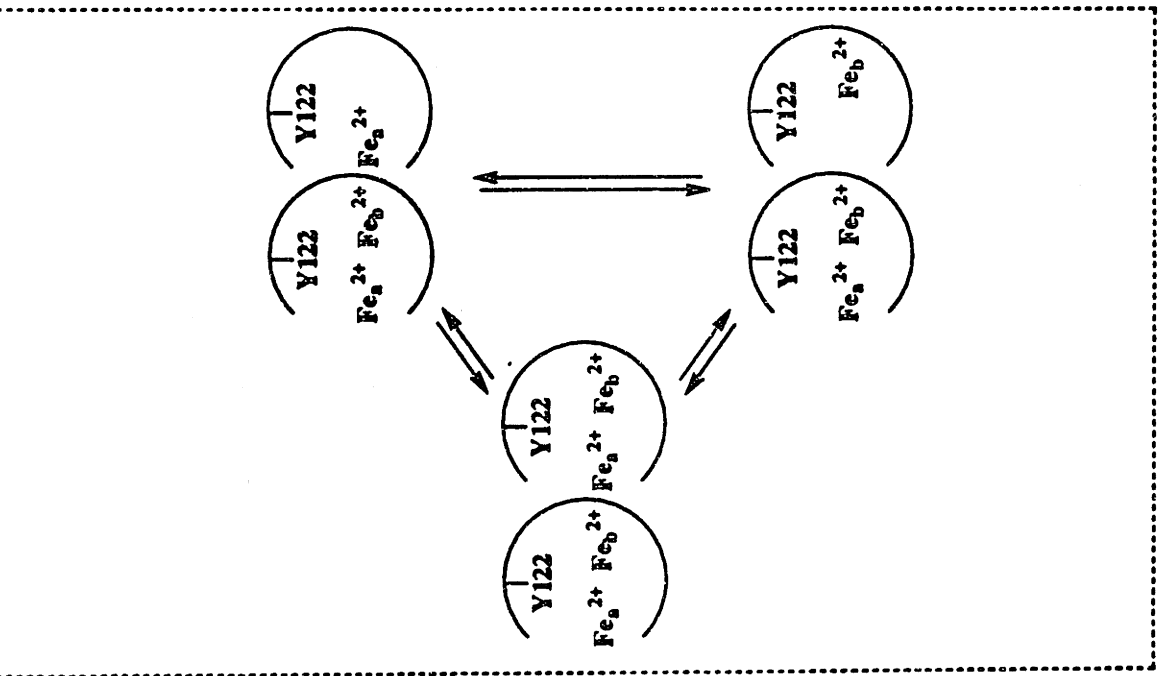
Another issue which might be addressed by the results of the Mn^{2+} - and EDTA-quench experiments is the manner in which Fe^{2+} donates the fourth electron required for cofactor assembly. As discussed previously in Chapter 2, the studies of Elgren *et al.* and Bollinger *et al.* have provided conflicting results in terms of the state of the "third Fe^{2+} " which donate the fourth electron (Elgren *et al.*, 1991; Bollinger *et al.*, 1994a). Schemes 4.6 to 4.8 illustrate how the Mn^{2+} - and EDTA-quench experiments may aid in distinguishing among several possible mechanisms

Scheme 4.5: Schematic representation of the mechanism proposed for the reaction of Fe(II)-R2 with O₂. For clarity, only one monomer of the R2 dimer is shown. The steps that are visible in the reaction of Fe(II)-R2 with O₂ are indicated by a dashed box.

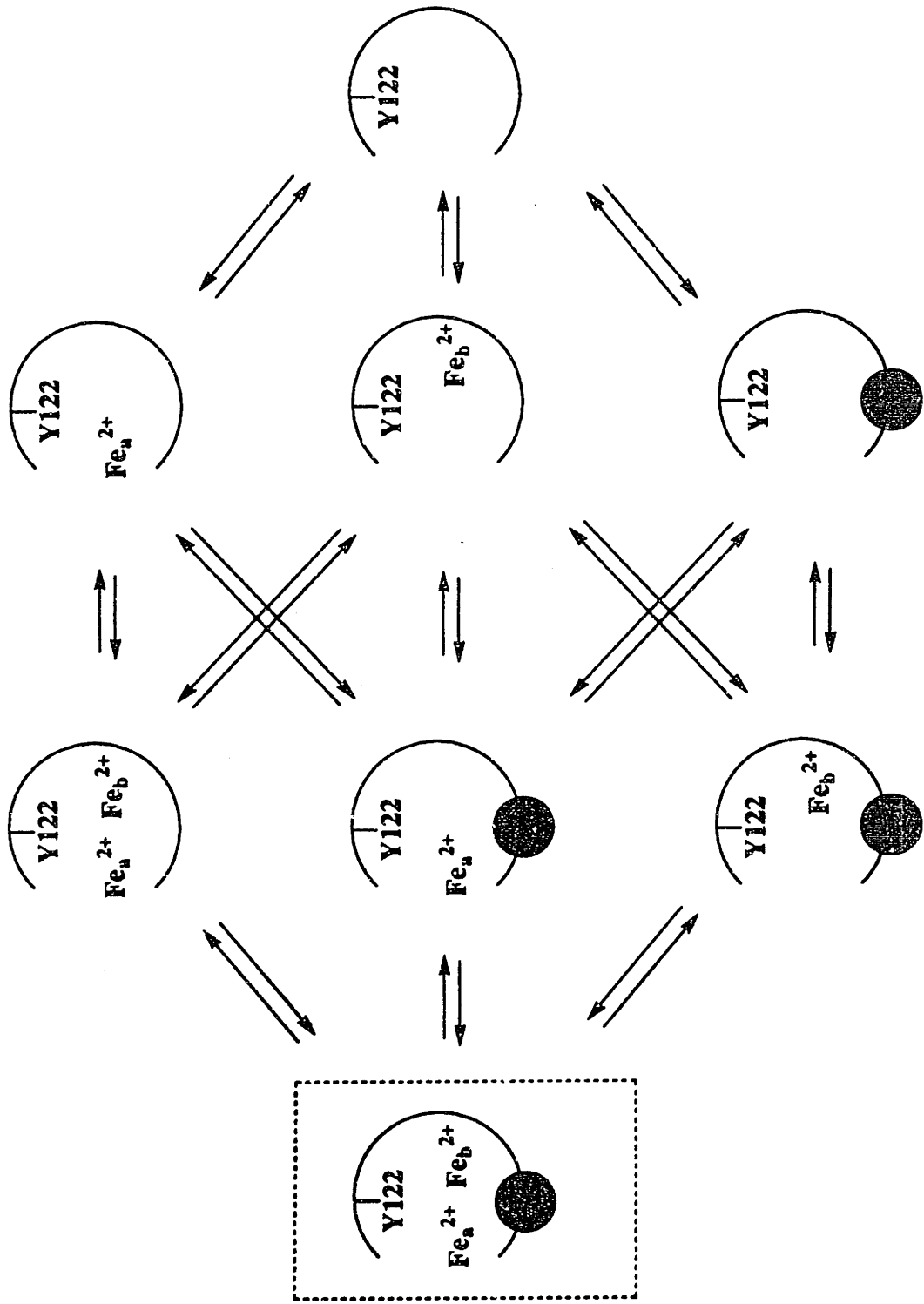
Scheme 4.6: The scenario in which any R2 with a diferrous cluster in the cofactor site would not be affected by addition of Mn^{2+} or EDTA and would proceed to generate $\bullet Y122$. In this scenario, four different Fe^{2+} -R2 complexes are considered to be competent to generate $\bullet Y122$. This scheme is the same as Scheme 4.1, with the competent Fe^{2+} -R2 complexes enclosed by a dashed box.



Scheme 4.7: The scenario in which there are two Fe^{2+} -binding sites on each R2 monomer and that only R2 dimer with at least three Fe^{2+} bound can form $\bullet\text{Y122}$ in the presence of Mn^{2+} or EDTA. The competent Fe^{2+} -R2 complexes are enclosed by a dashed box.



Scheme 4.8: The scenario in which each R2 monomer contains three Fe²⁺-binding sites. In this scenario, only R2 with all three Fe²⁺-binding sites filled will react to form •Y122 in the presence of Mn²⁺ or EDTA. This scheme is the same as Scheme 4.2, with the competent Fe²⁺-R2 complex enclosed by a dashed box.



In the first scenario, any Fe^{2+} -R2 complex with at least one diferrous cluster is proposed to be *competent*. Scheme 4.6 illustrates this scenario in which any R2 with a diferrous cluster would not be affected by addition of Mn^{2+} or EDTA and would proceed to generate $\bullet\text{Y122}$ at completion of the reaction. As indicated, in this scenario, four different forms of Fe^{2+} -R2 complexes are competent to generate $\bullet\text{Y122}$. It is recognized that one of these complexes has only two Fe^{2+} per R2 dimer. Thus, in the absence of an alternative reductant, the fourth electron required for cofactor assembly in this species would have to be supplied by a third Fe^{2+} that is not bound on the same R2 dimer.

Alternatively, one may consider that a competent Fe^{2+} -R2 requires at least three bound Fe^{2+} ions. In Scheme 4.7, the model in Scheme 4.6 is modified to reflect the possibility that a competent Fe^{2+} -R2 complex requires at least three Fe^{2+} bound per R2 dimer. In this scenario, the competent Fe^{2+} -R2 complex contains at least one diferrous cluster, and at least one Fe^{2+} bound in the cofactor site in the opposite monomer. An important implication of this scenario is that electron transfer can occur between two paired monomers to facilitate cofactor assembly.

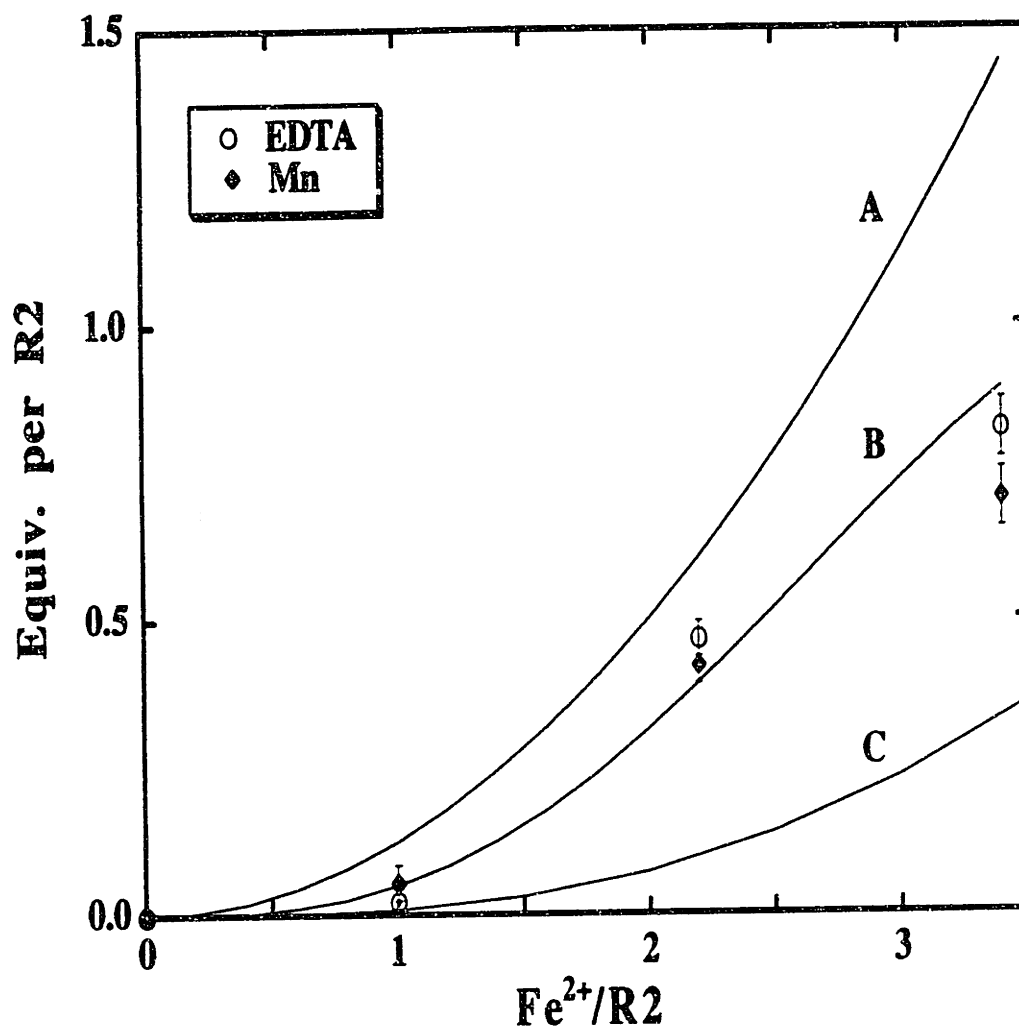
A third scenario which warrants consideration is one in which each R2 monomer contains three Fe^{2+} -binding sites. In this scenario, only R2 with all three Fe^{2+} -binding sites filled will react to form $\bullet\text{Y122}$ upon mixing with O_2 in the presence of Mn^{2+} or EDTA (Scheme 4.8).

For each mechanism (Scheme 4.6 to 4.8), the amount of competent Fe^{2+} -R2 complexes present will have a characteristic dependence on the Fe^{2+} /R2 ratio. Therefore, these three mechanisms might be resolved by calculating the amount of the competent Fe^{2+} -R2 complexes for each case and comparing them with the results of the Mn^{2+} - and EDTA-quench experiments. Fig. 4.16 shows the calculated amount of the competent Fe^{2+} -R2 complexes as a function of Fe^{2+} /R2 ratio for the three scenarios in Scheme 4.6 to 4.8. For first approximation, it was assumed that all

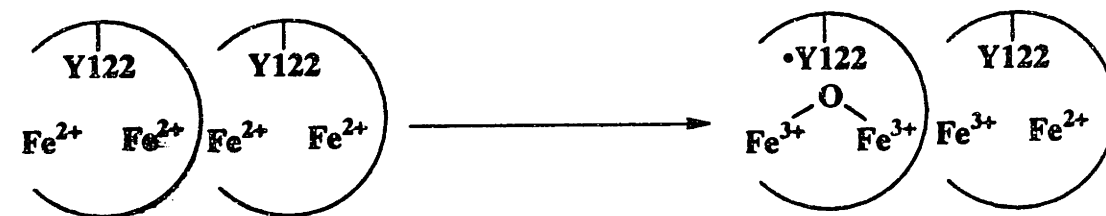
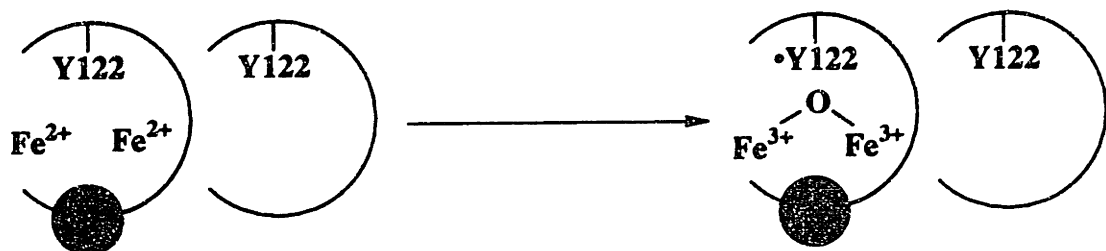
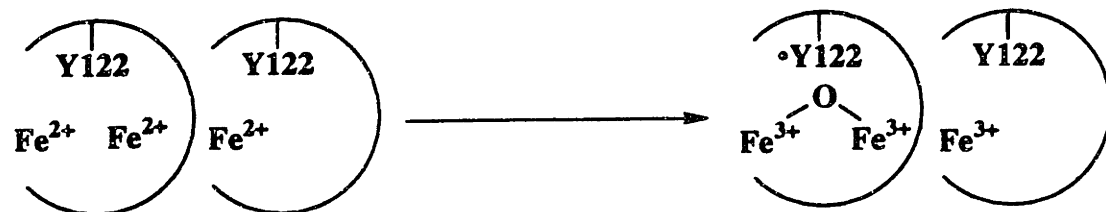
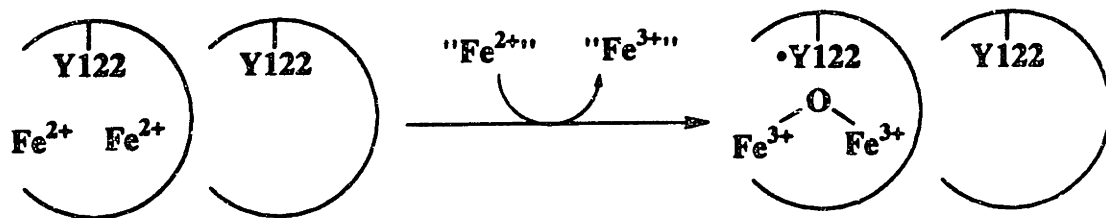
the Fe^{2+} -binding sites have identical affinities and that there is no cooperativity in Fe^{2+} -binding. The results of the Mn^{2+} - and EDTA-quench experiments are included for comparison. Fig. 4.16 shows that, of the three scenarios considered, the experimental results are most consistent with the one depicted in Scheme 4.7 in which Fe^{2+} bound in the cluster binding site of one monomer provides the fourth electron to the assembling cofactor in the other monomer. If this interpretation is correct, then it may imply that electron transfer can occur between paired R2 monomers.

It should, however, be emphasized that this analytical analysis does not eliminate the possibility that a third site exists in R2 with a lower affinity for Fe^{2+} than those in the cluster binding site. It is possible that in the presence of excess Fe^{2+} , this third site is also saturated and the Fe^{2+} bound in this site can also deliver the fourth electron required for cofactor assembly. In fact, this interpretation may also allow an apparently anomalous observation to be rationalized. Previous Mössbauer studies on the reaction of apo R2-wt with excess Fe^{2+} have suggested that a fast relaxing ferric species is produced concomitantly with X (Bollinger *et al.*, 1994a). It was proposed that this ferric species may represent the product of donation of the fourth electron by Fe^{2+} required for formation of X. However, although the species forms in a kinetically competent fashion, it accumulates only to about one-half the quantity which would be expected. The simplest interpretation is that there may be multiple sources for the fourth electron, and that the putative fast-relaxing ferric species may be produced in only a fraction of the events in which X is produced. These results could be rationalized according to Scheme 4.9. As indicated, a number of Fe^{2+} -R2 complexes can be generated when apo R2 is mixed with Fe^{2+} . Once a diferrous cluster is formed, it can react with O_2 , and both Fe^{2+} in solution and Fe^{2+} bound in a number of different manners may compete to provide the fourth electron (Scheme 4.9). In this scenario, a number of

Fig. 4.16: Theoretical plots of $\bullet\text{Y122}/\text{R2}$ ratio at completion of reaction versus $\text{Fe}^{2+}/\text{R2}$ ratio for the different scenarios in Scheme 4.6 (A), Scheme 4.7 (B) and Scheme 4.8 (C). The hypothetical plots are generated by a Monte Carlo simulation of the binding of Fe^{2+} to R2 (see Appendix 3). The results of the Mn^{2+} - and EDTA-quench experiments were included for comparison.



Scheme 4.9: Illustration of the manners in which a number of different Fe³⁺ products may be generated in the delivery of the fourth electron for cofactor assembly.



different Fe^{3+} product might be generated. This hypothesis is consistent with the results of Chapter 2 and the results of Bollinger, *et al.* (Bollinger, 1992; Bollinger *et al.*, 1994b). which show that a number of Fe^{3+} product are generated in the reconstitution reaction.

The speculative nature of the above discussion reveals the current state of knowledge regarding the delivery of the fourth electron to the assembling cluster. The main point of the statistical analysis is that the Mn^{2+} - and EDTA-quench experiments are consistent with the model in which Fe^{2+} bound in the one monomer can provide the fourth electron for cofactor assembly in the opposite monomer. Additional experiments to determine the number of Fe^{2+} -binding sites and the infinities of these binding-sites would be required to confirm these results.

The Sequence of Events Leading to Formation of the intermediate iron cluster, X

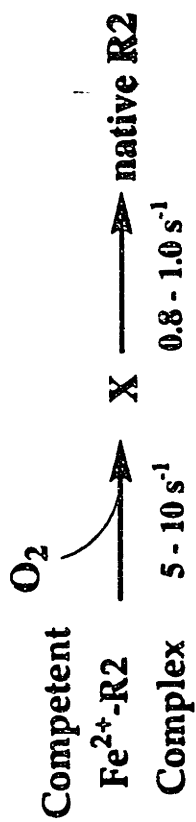
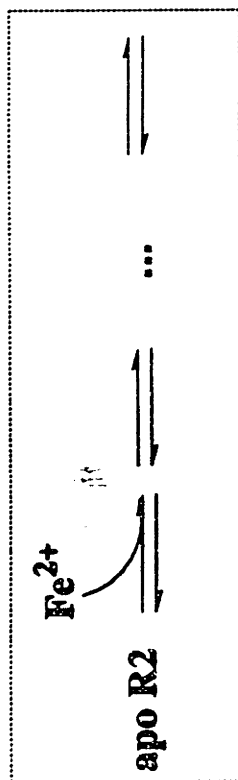
Previous studies by Bollinger, *et al.* indicated a first-order rate constant of 5 - 10 s^{-1} for the formation of X from the reaction of apo R2 with excess Fe^{2+} (Bollinger *et al.*, 1994). The observation that this rate constant is invariant over a 15-fold difference in concentration of apo R2 had led to the proposal that this first-order rate constant reflects a rate-limiting conformational change of apo R2 to allow for binding of Fe^{2+} and/or O_2 (Bollinger *et al.*, 1994a) . This hypothesis is supported by the results presented in Chapter 2. When Fe(II)-R2 ($\text{Fe}^{2+}/\text{R2} = 5$) is allowed to pre-form before mixing with O_2 , the formation of X is greatly accelerated ($k_{\text{obs}} = 60 - 80 \text{ s}^{-1}$), suggesting that the 5 - 10 s^{-1} step occurs prior to formation of the diferrous cluster. In order to further assess this hypothesis, a pulse/chase experiment has been carried out to determine the rate of formation of the competent Fe^{2+} -R2 complex. If the hypothesis of a rate-limiting conformation change in apo R2 is correct, it would predict that the formation of the competent Fe^{2+} -R2 complex would have a first-order rate constant of $\sim 5 - 10 \text{ s}^{-1}$.

Scheme 4.10 illustrates how the pulse/chase experiment can aid in differentiating among these reaction mechanisms. For each mechanism, the production of •Y122 will have a characteristic dependence on the delay time which can be diagnostic. Consider the scenario in which a step after binding of Fe²⁺ and O₂ is first-order and has a rate constant of 5 - 10 s⁻¹ (Scheme 4.10A). In this case, since the slow step occurs after formation of diferrous cluster, the production of •Y122 would become insensitive to the addition of Mn²⁺ at a rate much faster than 5 - 10 s⁻¹. Furthermore, the model predicts that the A₄₁₀, dropline-versus-time trace would always exhibit an initial lag phase corresponding to a first-order, 5 - 10 s⁻¹ process. Alternatively, a slow conformation change may occur before binding of any Fe²⁺ (Scheme 4.10C). Since the first-order, 5 - 10 s⁻¹ step occurs prior to formation of the competent Fe²⁺-R₂, it would be invisible in the pulse/chase experiment. In other word, the A₄₁₀, dropline-versus-time trace would not exhibit the lag phase corresponding to the 5 - 10 s⁻¹ step. Furthermore, in this scenario, the production of •Y122 would become insensitive to the addition of Mn²⁺ with a first-order rate constant of ~ 5 - 10 s⁻¹. A third scenario is depicted Scheme 4.10B, in which the first-order, 5 - 10 s⁻¹ step reflects ligand rearrangement before coordination of O₂. Since the formation of X is significantly faster in the reaction of Fe(II)-R₂ with O₂ than that in the reaction of apo R₂ with Fe²⁺ and O₂, the model in Scheme 4.10B requires that the competent Fe²⁺-R₂ complex is thermodynamically more favorable. This model would predict that, the production of •Y122 would become insensitive to the addition of Mn²⁺ in a complex kinetic manner.

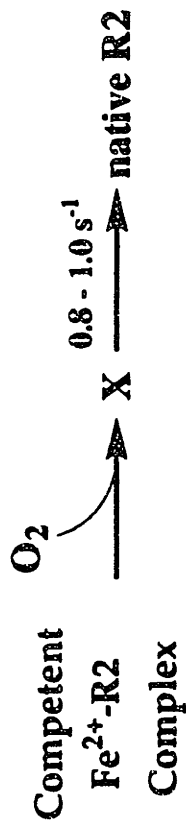
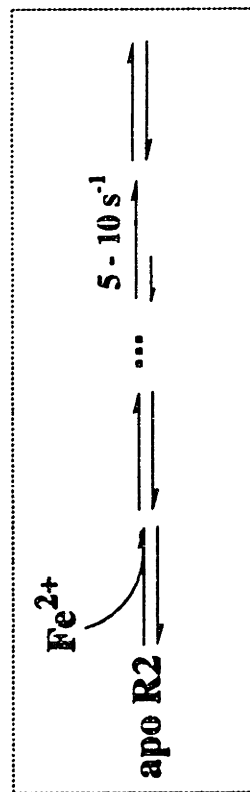
As shown in Fig. 4.14, the production of •Y122 becomes insensitive to the addition of Mn²⁺ with a first-order rate constant of $4 \pm 1 \text{ s}^{-1}$. Furthermore, the formation of •Y122 exhibits a significantly smaller lag in the presence of Mn²⁺ than that in the normal reaction (Fig. 4.17). These results, in conjunction with the results of Chapter 2, are most consistent with the scenario depicted in Scheme 4.10C in

Scheme 4.10: (A) The scenario in which a first-order, $5 - 10 \text{ s}^{-1}$ step occurs subsequent to Fe^{2+} and O_2 binding. (B) The scenario in which a slow conformational change occurs in diferrous R2 before binding of O_2 . (C) The scenario in which the rate-limiting step in the formation of from apo R2, Fe^{2+} and O_2 is a conformation change in apo R2 to allow for entry of Fe^{2+} . The boxes indicate the reaction steps that might be sensitive to addition of Mn^{2+} or EDTA.

(A)



(B)



(C)

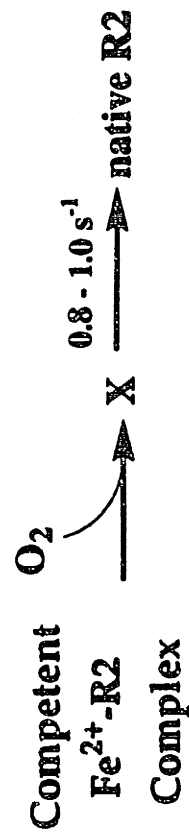
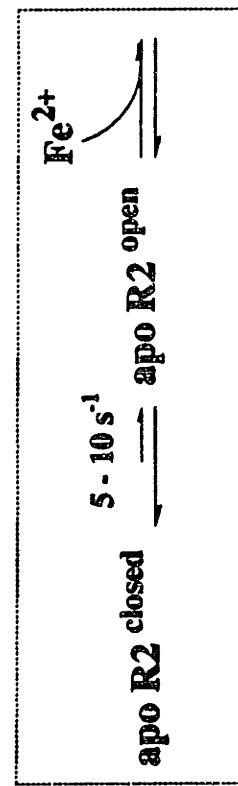
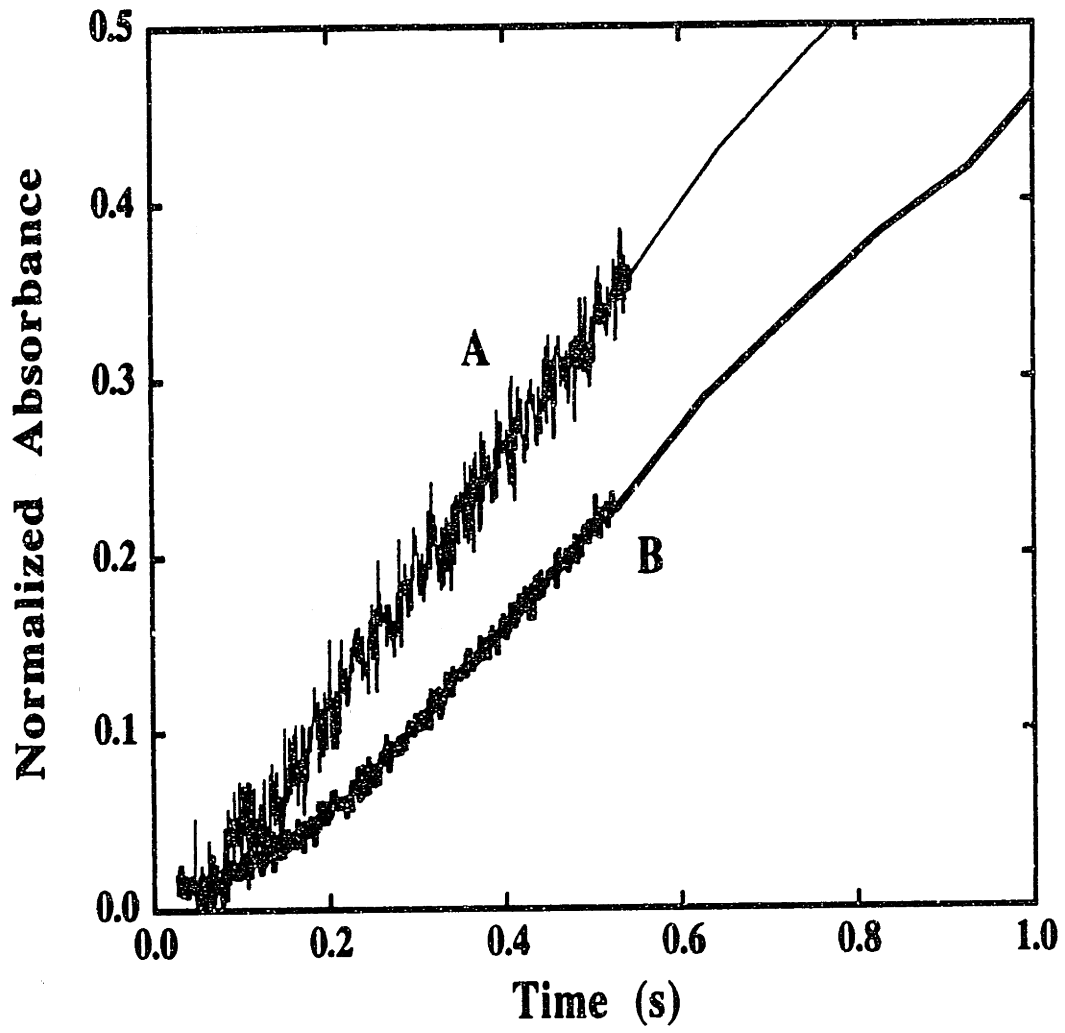


Fig. 4.17: A_{410} , dropline-versus-time trace when Mn^{2+} is added 45 ms after the reaction of apo R2 with excess Fe^{2+} is initiated (A). The reaction conditions were identical with those in Fig. 4.14. Trace B is the control in which 100 mM HEPES (pH 7.6) was added 28 ms after the reaction of apo R2 with excess Fe^{2+} is initiated.



which a conformational change in apo R2 occurs before binding of Fe²⁺. This hypothesis is consistent with the fact that the available x-ray crystallographic data on R2 thus far have failed to reveal any channel by which Fe²⁺ can access the cluster-binding site, which is >10 Å from the nearest surface (Nordlund & Eklund, 1993).

One final issue that has not been addressed thus far concerns the apparent *burst* of •Y122 formation in the pulse/chase experiment. As shown in Table 4.5, when Mn²⁺ is added to the reconstitution reaction at 0.021 s, a final •Y122/R2 ratio of 0.29 is obtained. This ratio is ~ 25% that of the final •Y122/R2 ratio obtained in the absence of Mn²⁺. Furthermore, extrapolation of the pseudo-first-order plot in Fig. 4.14 to zero time indicates a •Y122/R2 ratio of 0.23 (Fig. 4.15). The reason for this "burst" is not obvious, and we are currently considering two possible explanations for this observation. First, the "burst" can be merely a reflection of a systematic error in the pulse/chase experiment. As shown in Fig. 4.15, the pseudo-first-order plot has an x-intercept of -0.008 s. One interpretation is that the 0.008 s reflects the dead-time for the instrument in this experiment. For a normal stopped-flow experiment (as shown in Fig. 4.1), a dead-time of ~ 0.003 s is generally accepted. It is possible that the dual-mixing set-up (as shown Fig. 4.2) required for the pulse/chase experiment may have a longer dead-time. Alternatively, the burst could be a reflection of the equilibrium between two different apo R2 conformers. As mentioned in Chapter 2, the kinetic data is consistent with the proposal that a conformational change occurs in apo R2 to allow for entry of Fe²⁺. It is implied in Scheme 4.5 that the equilibrium favors apoR2_{closed}. However, it is certainly possible that some apo R2_{open} exists in the sample. The presence of a small amount of apo R2_{open} in the pulse/chase experiment could account for the observation of a burst of •Y122 formation. To speculate further, the fact that the rate of formation of X in the reaction of apo R2 with excess Fe²⁺ ($k_{obs} = 5 - 10 \text{ s}^{-1}$) is slightly faster than the rate of formation of the competent Fe²⁺-R2 complex ($k_{obs} = 4 \text{ s}^{-1}$) can be rationalized according to Scheme 4.5.

The presence of a small amount of apo R2_{open} in the reaction of apo R2 with excess Fe²⁺ could reduce the lag phase in the A₄₁₀, dropline-versus-time trace of the reaction. In this scenario, the rate of formation of X deduced from this trace would appear faster than the real rate of conversion of apo R2_{closed} to apo R2_{open}. However, this rationale is extremely speculative, and insufficient analysis has been carried out to know if it is plausible. Furthermore, additional experiments are required to assess whether the burst illustrated in Fig. 4.15 is real.

References

- Atta, M., Nordlund, P., Åberg, A., Eklund, H. & Fontecave, M. (1992) *J. Biol. Chem.* 267, 20682-20688.
- Bollinger, J. M., Jr. (1992) Ph. D. Thesis, Massachusetts Institute of Technology.
- Bollinger, J. M., Jr., Edmondson, D. E., Huynh, B. H., Filley, J., Norton, J. R. & Stubbe, J. (1991a) *Science* 253, 292-298.
- Bollinger, J. M., Jr., Tong, W. H., Ravi, N., Huynh, B. H., Edmondson, D. E. & Stubbe, J. (1994a) *J. Am. Chem. Soc.* 116, 8015-8023.
- Bollinger, J. M., Jr., Tong, W. H., Ravi, N., B. H., Edmondson, D. E. & Stubbe, J. (1994b) *J. Am. Chem. Soc.* 116, 8024-8032.
- Elgren, T. E., Lynch, J. B., Juarez-Garcia, C., Münck, E., Sjöberg, B.-M. & Que, L., Jr. (1991) *J. Biol. Chem.* 266, 19265-19268.
- Erman, J. E., Vitello, L. B., Mauro, J. M. & Kraut, J. (1989) *Biochemistry* 28, 7992-7995.
- Fontecave, M., Gerez, C., Mansuy, D. & Reichard, P. (1990b) *J. Biol. Chem.* 265, 10919-10924.
- Miller, M. A., Bandypadhyay, D., Mauro, J. M., Traylor, T. G. & Kraut, J. (1992) *Biochemistry* 31, 2780-2797.

Miller, M. A., Haqqard, J. T., Mauro, J. M., Edwards, S. L., Simmons, P. C., Tollin, G. & Kraut, J. (1988) *Biochemistry* 27, 9081-9088.

Nordlund, P. & Eklund, H. (1993) *J. Mol. Biol.* 232, 123-164.

Ochiai, E.-I., Mann, G. J., Gräslund, A. & Thelander, L. (1990) *J. Biol. Chem.* 265, 15758-15761.

Ochiai, E.-I., Swierczynski, S. L., Gräslund, A. & Thelander, L. (1991) *J. Inorg. Biochem.* 43, 531.

**Appendix 1: Reconstitution of R2-Y122F from Apo R2-Y122F,
Fe²⁺ and O₂ as Monitored by SF-Abs, RFQ-EPR,
and RFQ-Möss Spectroscopies**

In the experiments described in this chapter, mechanistic studies were carried out on a mutant R2 subunit, R2-Y122F, in which the oxidizable Y122 was replaced by site-directed mutagenesis with the less easily oxidized residue, F. Many of the results herein were previously published in two separate papers, and served as the support for the proposed mechanism in Scheme 1.3 (Bollinger *et al.*, 1994a; Bollinger *et al.*, 1994b). These earlier studies suggested that the reaction of apo R2-Y122F with Fe^{2+} and O_2 results in formation of the μ -oxo-diferric cluster via a mechanism similar to that of the wild-type protein. When apo R2-Y122F is mixed with Fe^{2+} and O_2 , an intermediate I accumulates which contains X and a putative $\bullet\text{W48}^+$ (Scheme 1.3). In the presence of excess reductant (Pathway B), I is rapidly reduced by one electron to give a second intermediate II, which is subsequently reduced by one electron to give the native cofactor. When reducing equivalents are not readily available, decay of the putative $\bullet\text{W48}^+$ in I is sufficiently slowed that it accumulates. In subsequent steps, I is reduced by one electron to give II'. One electron reduction of II' converts the intermediate iron species into the diferric cluster.

The experiments described in this chapter have provided further support for the proposed mechanism for the reaction carried out in the presence of excess Fe^{2+} . The EPR and Mössbauer data clearly demonstrate that the intermediate X exhibits an increased lifetime in R2-Y122F, as expected for a species that is responsible for oxidizing Y122 to $\bullet\text{Y122}$ in the wild-type protein. Associated with the slower decay of X is a slower formation of the diferric cluster. These results are entirely consistent with the proposal that X is the precursor of the diferric cluster. Furthermore, these experiments have

shown that the fast-relaxing ferric species also accumulates in the reaction of R2-Y122F, with a rate constant identical to the k_{obs} for formation of X. This is consistent with the proposal that the fast-relaxing ferric species is the ferric product generated in the donation of an electron from Fe^{2+} to convert I to II.

Another interesting result relates to a transient absorption feature at 410 nm that was first observed by Bollinger *et al.* in the reaction of apo R2-Y122F protein with limiting Fe^{2+} (Bollinger *et al.*, 1991a). It was proposed that, in the absence of the oxidizable Y122 residue, Y356 can cycle between an oxidized, radical form and its normal, reduced form to deliver the reducing equivalents required for formation of the diferric cluster. Residue Y356 in R2 has also been proposed to be an intermediary in electron transfer between the R1-R2 subunits during catalytic turnover (Nordlund, 1990). This conserved residue is located in the C-terminal region of the R2 subunit, which has been shown to be a major determinant in the subunit interaction between R1 and R2 (Sjöberg *et al.*, 1987; Climent *et al.*, 1991). When R2-Y356 is replaced by with an alanine residue, the mutant R2 is catalytically inactive, even though it has affinity for R1 which is essentially identical to that of R2-wt (Climent *et al.*, 1992). In this chapter, stopped-flow studies of two site-directed mutants, R2-Y356F and R2-Y122F/Y356F, together with protein cross-linking studies, have provided support for the proposal that the transient absorption feature at 410 nm is associated with a $\bullet Y356$ (Bollinger *et al.*, 1991a).

While this work was in progress, Sahlin and coworkers were also studying the reconstitution reactions of R2-Y122F and two double mutants R2-Y122F/Y356A and R2-Y122F/ $\Delta 30C$ (Sahlin *et al.*, 1995). The R2-Y122F/ $\Delta 30C$ mutant is a truncated chain in which the last 30 C-terminal residues, including the conserved Y356 residue, is missing. In these studies, apo R2 (50 or 100 μM) in air-saturated 50 mM Tris, pH 7.6 was mixed at 25 °C

with an equal volume of an anaerobic solution of $\text{Fe}(\text{NH}_4)_2(\text{SO}_4)_2$ (0.05 - 1.0 mM) in 50 mM Tris pH 7.6, and the reaction was monitored by SF-Abs, continuous-flow-EPR and RFQ-EPR spectroscopies. Six EPR active species were observed, and it was suggested that these species may represent radical intermediates in the reconstitution reaction and/or intermediates in the electron transfer between R1 and R2 subunits during turnover. One of these transient species exhibits a singlet EPR signal at 77K. The EPR line-shape, the saturation behavior, and its kinetic behavior suggest that it is X. This conclusion is confirmed by the Mössbauer results described in this chapter, which show that X also forms in the reaction of apo R2-Y122F with excess Fe^{2+} at 25 °C.

The study of Sahlin *et al.* has also provided evidence for a number of protein radicals (Bollinger *et al.*, 1991a). EPR studies on R2-Y122F grown on perdeuterated tryptophan has identified a tryptophan radical that is weakly coupled to the iron cluster (component II). Quantitation of component II, which is characterized by a quartet signal at 77 K, indicated that 0.1 equiv. of this species has accumulated at the 6 s time-point. The decay of the species was rather slow and was not completed until 10 min after mixing. A second transient tryptophan radical was observed using stopped-flow EPR experiments at room temperature applied in conjunction with deuterated tryptophan labeling. This doublet EPR signal did not start to accumulate until 10 s after mixing, and it reached its maximum intensity approximately 2 min after mixing. In addition to the tryptophan radicals, Sahlin *et al.* also observed a transient absorption feature by stopped-flow absorption spectroscopy, which is characteristic of a tyrosyl radical. Site-directed mutagenesis studies suggested that this radical resides on the Y356 residue, since neither R2-Y122F/Y356A nor R2-Y122F/ Δ 30C exhibits the transient

absorption feature. The implications of these findings on the reconstitution mechanism and the catalytic turnover will be discussed in conjunction with the results presented in this chapter.

Experimental Procedures

Materials

Natural abundance (^{56}Fe) iron wire was purchased from Baker (Phillipsburg, NJ). ^{57}Fe was purchased from Advanced Materials and Technology (New York, NY). Ferrozine and Fe atomic absorption standard were purchased from Sigma (St. Louis, MO). 2-Methyl butane (reagent grade) was purchased from Aldrich (Milwaukee, WI). All other materials were purchased in the highest purity available.

Protein R2-Y122F was isolated from 100 g overproducing strain K38/pTB2-Y122F as described in Chapter 2. Isolation of R2-Y122F from these cells gave 600 - 800 mg pure R2. The apo form of R2-Y122F was prepared from the native R2 as previously described (Atkin *et al.*, 1973; Salowe, 1987). The concentration of apo R2-Y122F was determined by absorbance at 280 nm (assuming $\epsilon_{280}=120 \text{ mM}^{-1}\text{cm}^{-1}$).

Reaction of apo R2-Y122F with O₂ and Fe²⁺ as Monitored by SF-Abs, RFQ-EPR, and RFQ-Möss Spectroscopies

As shown in previous studies, the kinetic behavior of the reconstitution reaction depends markedly on the initial ratio of $\text{Fe}^{2+}/\text{R2}$ present in the reaction mixture (Bollinger *et al.*, 1994a; Bollinger *et al.*, 1994b; Sahlin *et al.*, 1995) In this study, the reconstitution reaction was carried out at two different $\text{Fe}^{2+}/\text{R2}$ ratios. In the "limiting Fe^{2+} " experiments, the $\text{Fe}^{2+}/\text{R2}$ ratio is 2.1 - 2.4, whereas in the "excess Fe^{2+} " experiments, the $\text{Fe}^{2+}/\text{R2}$ ratio is

5. The detailed conditions employed in each experiment are described in the figure legends. SF-Abs experiments were carried out on an Applied Photophysics (Leatherhead, UK) DX.17MV sequential stopped-flow spectrofluorimeter. The temperature was maintained at 5 °C with a Lauda K-2/R circulating water bath (Brinkmann Instruments). In these experiments, apo R2-Y122F (25 - 300 μ M) in 100 mM HEPES (pH 7.7) was mixed with an equal volume of a solution of $\text{FeSO}_4 \cdot 7\text{H}_2\text{O}$ in 4 - 6 mN H_2SO_4 , and the reaction was monitored at wavelengths between 320 and 560 nm.

Samples were prepared for EPR and Mössbauer analysis by mixing equal volumes of apo R2-Y122F (300 μ M) in O_2 -saturated 100 mM HEPES buffer (pH 7.7) and a solution containing 2.3 or 5 molar equivalents of Fe^{2+} in 4 - 6 mN H_2SO_4 . The reaction mixture was freeze-quenched at various reaction times as described previously (Bray, 1961; Ballou & Palmer, 1974; Ravi *et al.*, 1994). EPR spectra were acquired on a Brüker ER 200D-SRC spectrometer equipped with an Oxford Instruments ESP 910 continuous flow cryostat, or on a Brüker Model ESP 300 equipped with an Oxford Instrument ESR 900 continuous flow cryostat. Analysis of EPR spectra was carried out with programs written in the laboratory of Prof. B. H. Huynh at Emory University. Mössbauer spectra were recorded and analyzed in the laboratory of Prof. B. H. Huynh. The analysis was repeated independently in our laboratory. Mathematical modeling was performed using HopKIMSIM, a Macintosh version of Barshop and Freiden's kinetic simulation program, KINSIM (Barshop *et al.*, 1983). Non-linear regression analysis on the EPR and Mössbauer kinetic data was carried out with the Git and Gear programs of Dr. R. J. McKinney and Dr. F. J. Wiegert, Central Research and Development Department, E. I. du Pont de Nemours and Co.

Results

Reaction of Apo R2-Y122F with Excess Fe²⁺ and O₂ as Monitored by SF-Abs Spectroscopy

When apo R2-Y122F is mixed with excess Fe²⁺ at 5 °C, a broad absorption band that is centered near 365 nm and characteristic of the intermediate X develops (Fig. A.1.1). In the 0.46 s spectrum, ~40 % of the final absorbance at 365 nm has developed, while the 325 nm shoulder characteristic of the diferric cluster is still undetectable, suggesting that X accumulates before formation of the product cluster. With increasing reaction time, the spectrum of the diferric cluster develops (as judged by the appearance of the more intense 360 nm and 325 nm bands).

In an attempt to estimate the rate constants for the formation and decay of X, the A₃₆₅-versus-time traces were analyzed according to the kinetic model of Scheme A.1.1. As shown in Fig. A.1.2, after a very small lag (< 0.040 s), the absorbance at 365 nm rises smoothly. The data fit well to the simple kinetic model, and suggest that X accumulates with a rate constant of 2.7 s⁻¹, and is reduced to diferric cluster with a rate constant of 0.16 s⁻¹. When the time-dependent absorption spectra were fit to the kinetic model of two sequential, first-order processes using a multi-component, multi-variate analysis method (Applied Photophysics Global Analysis), a k₁ of 2.5 s⁻¹ and a k₂ of 0.14 s⁻¹ are obtained. A similar analysis of the R2-wt reaction gives a k₁ of 3.9 s⁻¹ and a k₂ of 0.49 s⁻¹ (Bollinger *et al.*, 1994a), indicating that decay of X is slower in the mutant protein.

Scheme A.1.1:

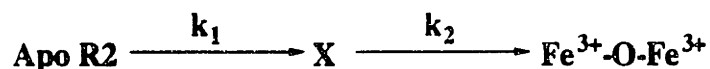


Fig. A.1.1: Development of the absorption spectrum of the diferric cluster upon mixing apo R2-Y122F with O₂ and excess Fe²⁺. The reaction conditions (after mixing) were: 50 μM apo R2-Y122F, 254 μM Fe²⁺, 50 mM HEPES (air saturated), pH 7.6, 5 °C. The spectra were constructed from the absorbance-versus-time traces acquired at multiple wavelengths on the Applied Photophysics spectrofluorimeter and were taken at 0.010, 0.20, 0.46, 3.0, 12 and 102 s after mixing.

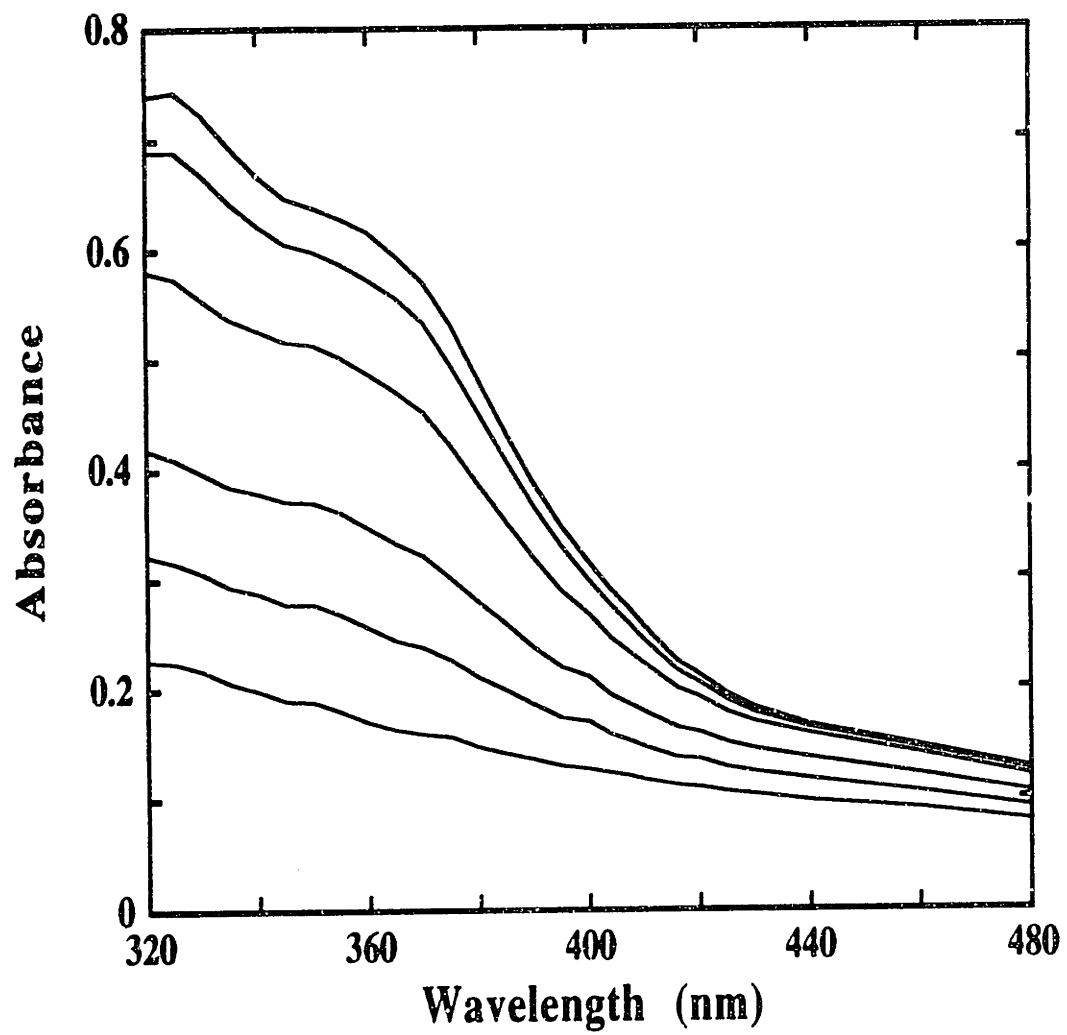
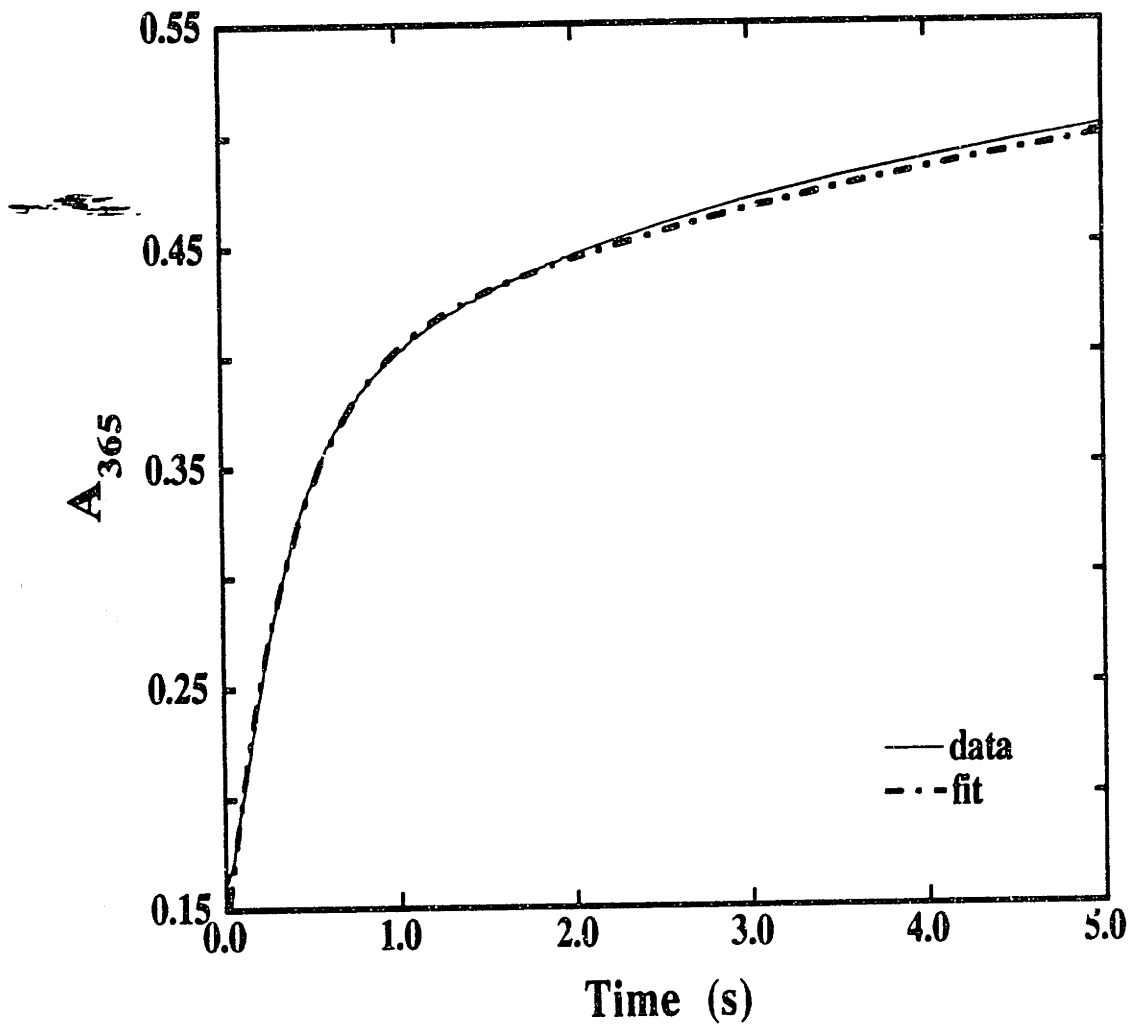


Fig. A.1.2: A_{365} -versus-time trace in the reaction of apo R2-Y122F with excess Fe^{2+} . The reaction conditions were: 50 μM apo R2-Y122F, 255 μM Fe^{2+} , 50 mM HEPES (air-saturated), pH 7.6, 5 °C. The experimental trace represents the average of 3 trials. The theoretical trace was obtained by fitting two sequential, first-order processes to the 0.040 - 40.0 s region of the experimental trace, and corresponds to a k_1 of 2.7 s^{-1} and a k_2 of 0.16 s^{-1} .



Quantitation of X and the Diferric Cluster in the Excess Fe²⁺ Reaction by Mössbauer Spectroscopy

The time-dependent Mössbauer spectra of the reaction of apo R2-Y122F with excess Fe²⁺ and O₂ clearly demonstrate the formation of the intermediate X. In the first time-point taken (0.077 s, Fig. A.1.3A), the spectrum is dominated by unreacted ferrous ion. Only a very small amount of X has accumulated, and no diferric cluster is yet detectable. With increasing reaction time (0.63 s and 5.0 s, Fig. A.1.3B and Fig. A.1.3C respectively), the relative contributions from Fe²⁺, while the contribution from the diferric cluster increases. Finally, at completion of the reaction (60 s, Fig. A.1.3D), the spectrum is dominated by the diferric cluster.

The measured quantities of X and the diferric cluster are summarized in Table A.1.1. The amount of X presents in the reaction increases with time, reaches its maximum value (~ 1.0 equiv.) at around 0.6 s. and then decays slowly. After an apparent initial lag phase, the amount of diferric cluster rises with time (Fig. A.1.4). The ratio of diferric cluster/R2 at completion (1.38 ± 0.08) is in good agreement with that in R2-wt (Bollinger *et al.*, 1994a).

The Mössbauer time-courses of X and the diferric cluster suggest that decay of X and formation of diferric cluster are concomitant processes. Fitting the decay of X in R2-Y122F gives an apparent first-order rate constant of 0.11 s^{-1} (Fig. A.1.5), which is close to the apparent rate of formation of the diferric cluster (0.2 s^{-1}) (Fig. A.1.4). Fitting the measured quantities of X and diferric cluster as functions of time to the kinetic model in Scheme A.1.1, however, clearly indicates that the 3-component model is of insufficient complexity to account for the data. The theoretical curve in Fig. A.1.6 is obtained by fitting

Table A.1.1: Summary of the analysis of the Mössbauer spectra from the reaction of apo R2-Y122F with excess Fe²⁺ at 5 °C.

Reaction Time (s)	Equiv. X	Equiv. Diferric Cluster	Equiv. Fast-Relaxing Fe ³⁺
0.077	0.40 ± 0.1	0	0.08 ± 0.05
0.18	0.65 ± 0.1	0	0.20 ± 0.05
0.24	0.73 ± 0.1	0.05 ± 0.03	0.25 ± 0.05
0.32	0.83 ± 0.05	0.10 ± 0.05	0.3 ± 0.08
0.46	0.95 ± 0.05	0.14 ± 0.04	0.45 ± 0.1
0.63	1.02 ± 0.05	0.23 ± 0.04	0.50 ± 0.1
1.0	0.98 ± 0.05	0.33 ± 0.04	0.50 ± 0.1
5.0	0.58 ± 0.05	0.85 ± 0.05	0.45 ± 0.1
10	0.38 ± 0.08	1.23 ± 0.06	0.40 ± 0.1
60	0	1.38 ± 0.08	0.40 ± 0.1

the Mössbauer data to the model in Scheme A.1.1 with a k_1 of 3.7 s^{-1} and a k_2 of 0.20 s^{-1} . The measured quantity of X does not rise and fall as sharply as the theoretical curve. The theoretical curve for formation of diferric cluster also lags behind the experimental data. This deviation of the data from the simple model of two sequential, first-order processes is not unexpected, since the normal electron donor, Y122, is absent. It is entirely possible that the intermediate X may accept an electron from a number of different donors in R2-Y122F. This interpretation is supported by the results of Sahlin *et al.* (1995)

~~Fig. A.1.3~~

Fig. A.1.3: Mössbauer time-course of the reaction of apo R2-Y122F with excess Fe²⁺. The reaction conditions were: 300 μM apo R2-Y122F, 1.5 mM Fe²⁺, 50 mM HEPES (O₂-saturated), pH 7.6, 5 °C. The reaction was quenched (A) at 0.077 s, (B) at 0.63 s, (C) at 5.0 s, or (D) at 60 s.

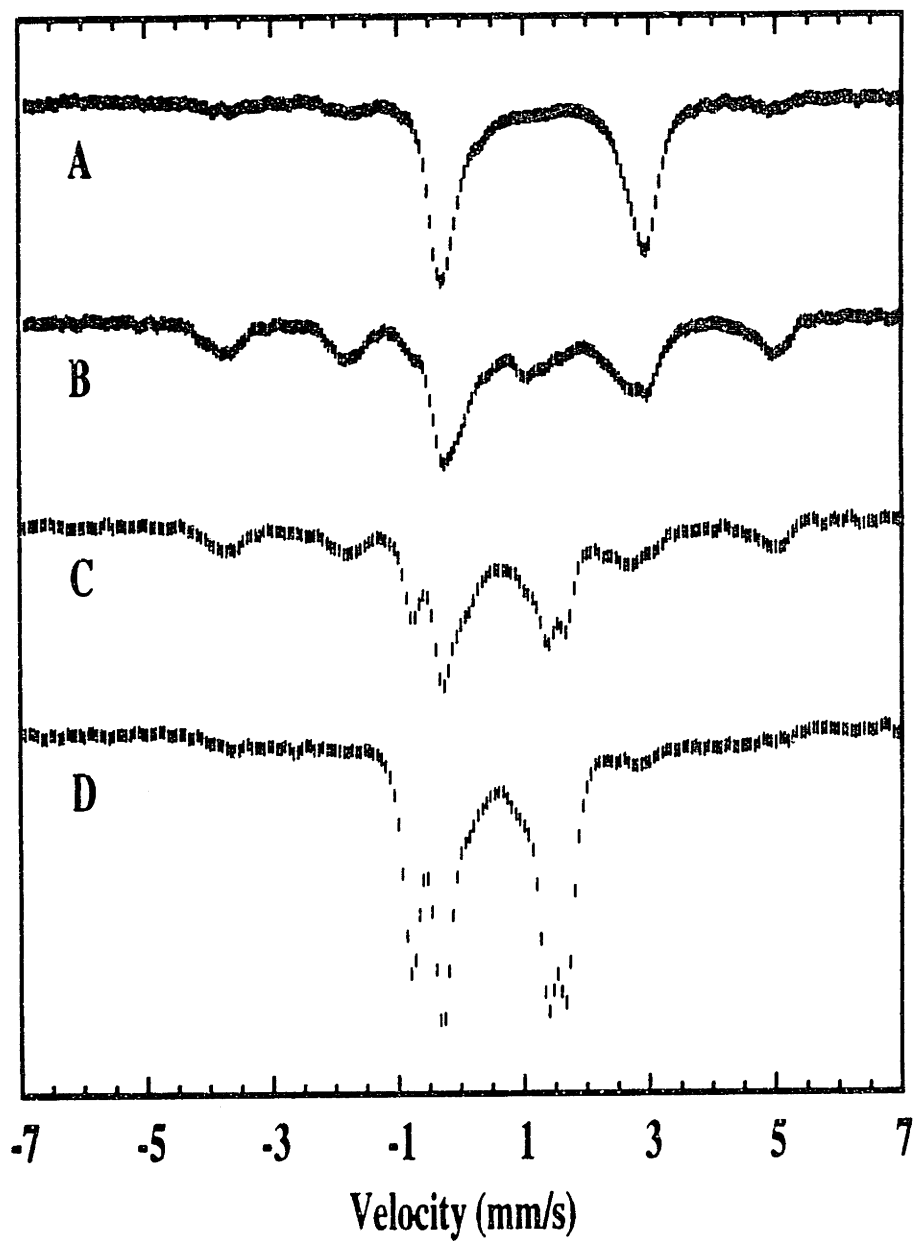


Fig. A.1.4: Formation of the diferric cluster in the reaction of apo R2-Y122F with excess Fe^{2+} as monitored by RFQ-Möss spectroscopy. The reaction conditions were identical to those in Fig. A.1.3. The theoretical trace is obtained by fitting a first-order process to the 0.22 - 60 s region of the experimental trace, and corresponds to a k_{obs} of 0.2 s^{-1} .

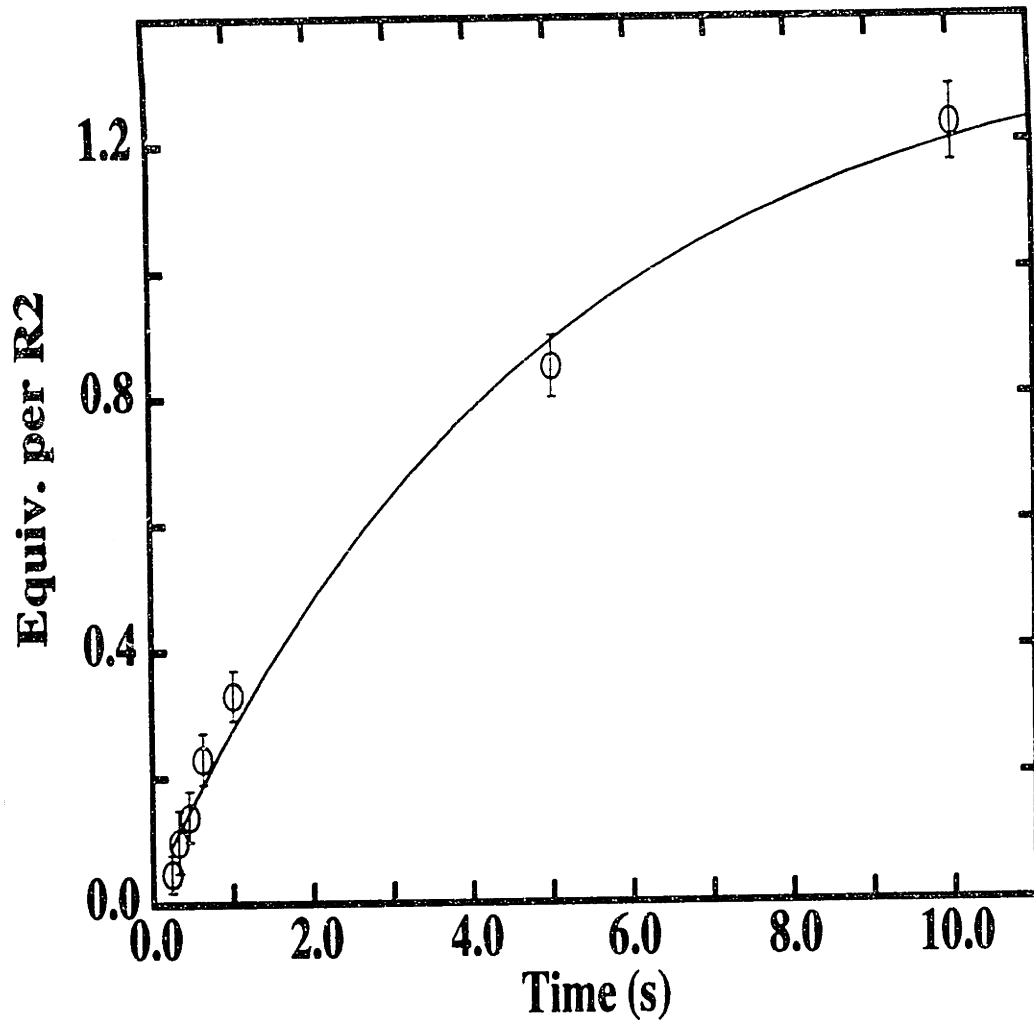
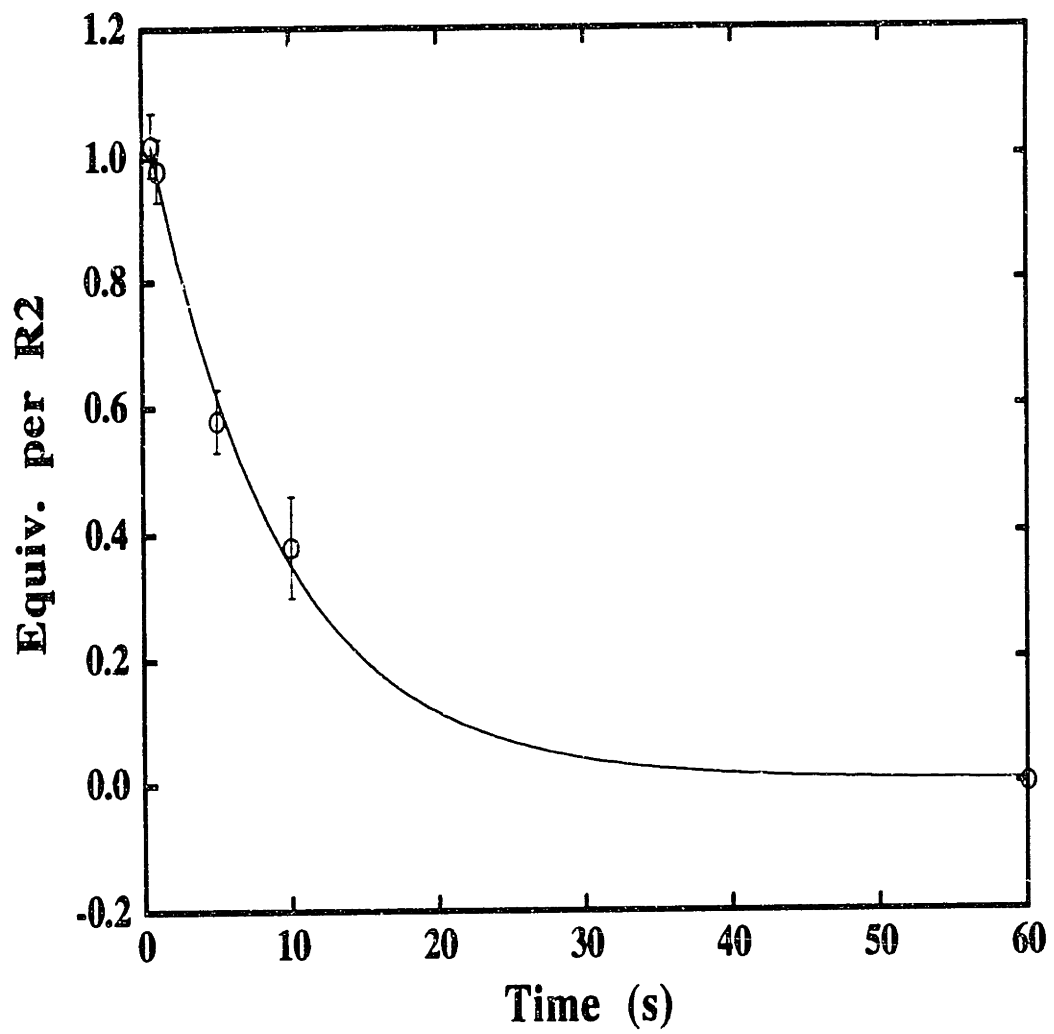


Fig. A.1.5: Decay of X in the reaction of apo R2-Y122F with excess Fe²⁺ as monitored by RFQ-Möss spectroscopy. The reaction conditions were identical to those in Fig. A.1.3. The theoretical trace is obtained by fitting a first-order process to the 1.0 - 60 s region of the experimental trace, and corresponds to a k_{obs} of 0.11 s⁻¹.




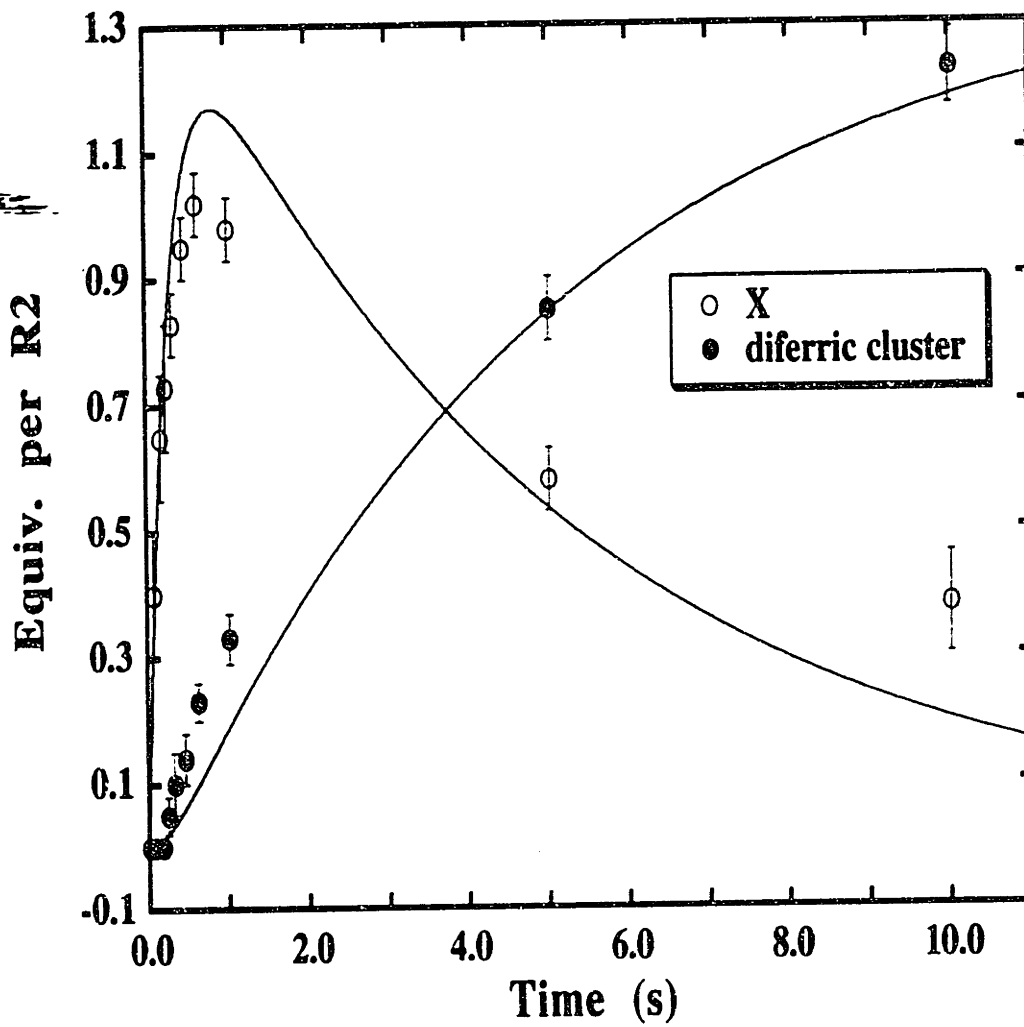


Fig. A.1.6: Non-linear least square fitting of the kinetic model of Scheme A.1.1 to the measured quantities of X and the diferric cluster as functions of time. The quantities of X and the diferric cluster are from Table A.1.1, The theoretical curves correspond to a k_1 of 3.7 s^{-1} , a k_2 of 0.2 s^{-1} , and a final diferric cluster/R2 ratio of 1.38.



which indicated that multiple EPR-active species were formed in the reaction of apo R2-Y122F with 4 Fe²⁺ at room temperature. Inspection of the EPR spectrum of the reaction of apo R2-Y122F with 5 Fe²⁺ at 5 °C quenched at 60 s reveals a small amount of EPR active species in the $g = 2$ region (Fig. A.1.7). In addition to a singlet signal which resembles X, there are multiple broader features which are not present in the earlier time-points. Spin quantitation of this spectrum suggests that there are only ~0.07 equiv. of EPR active species present. Thus, it is possible that small amount of one or more radical species are also generated in the long time-points in the reaction of apo R2-Y122F with 5 Fe²⁺ at 5 °C. The implication of these findings are discussed below.

Despite the apparent kinetic complexity of the reaction of R2-Y122F, it is possible to gain some insights to the mechanism of cofactor assembly through qualitative comparison of the R2-Y122F data with the R2-wt data. Both the SF-Abs data and the RFQ-Möss data suggest that the decay of X is slower in R2-Y122F than in R2-wt. Table A.1.2 and Fig. A.1.8 summarizes the time-course of X in the reaction of apo R2-Y122F compared to that of apo R2-wt. In the mutant protein, the t_{\max} of X is between 0.6 and 1.0 s, while the t_{\max} of X in R2-wt is between 0.22 and 0.31 s. Furthermore, as shown in Fig. A.1.8, the decay of X in R2-wt is almost completed at 3 s, while the decay of X is less than 50% completed at the 5 s time-point in R2-Y122F. Kinetic analysis of the apo R2-wt reaction suggests that X accumulates with a rate constant of 4 - 10 s⁻¹ and decays with a rate constant of 0.7-1.0 s⁻¹ to form diferric cluster. As mentioned above, decay of X in the apo R2-Y122F reaction occurs with a k_{obs} of roughly 0.1 s⁻¹. Associated with an increased lifetime of X is a marked slowing of diferric cluster formation in R2-Y122F (Fig. A.1.9). Taken together, these results are entirely consistent with the proposed model for the

Table A.1.2: Measured quantities of X in the reaction of apo R2-Y122F with excess Fe²⁺ compared to those in the reaction of apo R2-wt with excess Fe²⁺ at 5 °C.

Reaction Time (s)	Apo R2-Y122F	Reaction Time (s)	Apo R2-wt
0.077	0.40 ± 0.1	0.077	0.53 ± 0.11
0.18	0.65 ± 0.1	0.18	0.84 ± 0.10
0.24	0.73 ± 0.1	0.24	0.88 ± 0.07
0.32	0.83 ± 0.05	0.33	0.98 ± 0.09
0.46	0.95 ± 0.05	0.456	0.83 ± 0.07
0.63	1.02 ± 0.05	0.65	0.68 ± 0.09
1.0	0.98 ± 0.05	1.0	0.55 ± 0.09
--	--	1.5	0.38 ± 0.06
--	--	3.0	0.08 ± 0.03
5.0	0.58 ± 0.05	5.0	<0.08
10	0.38 ± 0.08	--	<0.04
60	0	60	<0.04

reconstitution of native R2-wt (Scheme 1.3). In the absence of Y122, conversion of X to diferric cluster would be expected to be slower.

Analysis of the Mössbauer Time -course for Additional Components

Previous studies on R2-wt have suggested that a stable or slowly decaying fast relaxing ferric species is produced concomitantly with X (Bollinger *et al.*, 1994a). It was proposed that this ferric species may represent




Fig. A.1.7: EPR spectrum of the reaction of apo R2-Y122F with excess Fe²⁺ quenched at 60 s (A). The reaction conditions were (after mixing): 300 μM apo R2-Y122F, 1.5 mM Fe²⁺, 50 mM HEPES (O₂-saturated), pH 7.6, 5 °C. The spectra were acquired at 20 K with a microwave power of 100 μW, a frequency of 9.43 GHz, a modulation frequency of 100 kHz, a modulation amplitude of 4 G, a time constant of 200 ms, a scan time of 200 s, and a receiver gain of 4 × 10⁴. The reference spectrum of X was included in B for comparison.

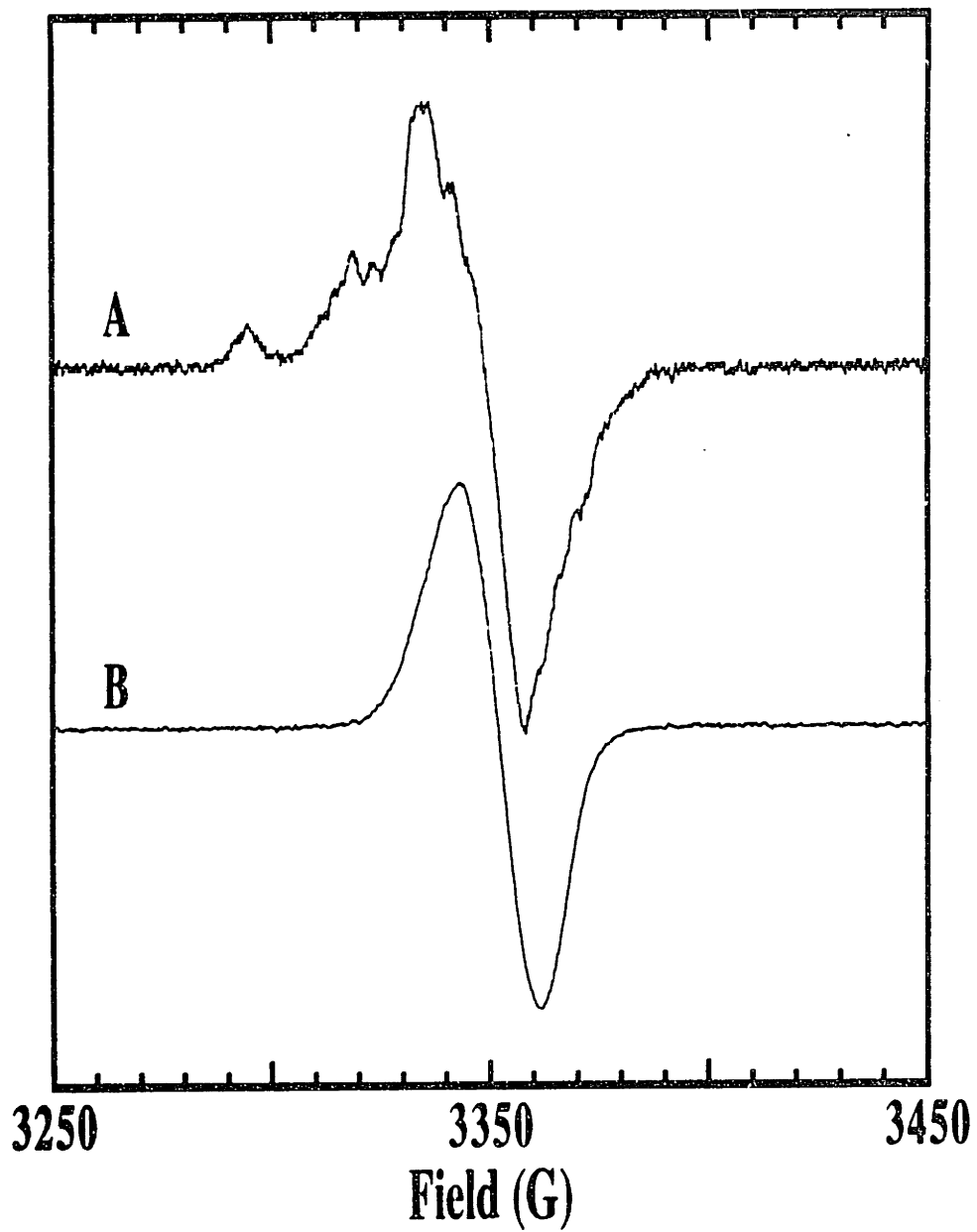


Fig. A.1.8: Mössbauer time-course of X in the reaction of apo R2-Y122F with excess Fe²⁺ compared with that of apo R2-wt under the same conditions. The reaction conditions (after mixing) were: 300 μM apo R2-wt or apo R2-Y122F, 1.5 mM Fe²⁺, 50 mM HEPES, pH 7.6, 5 °C.

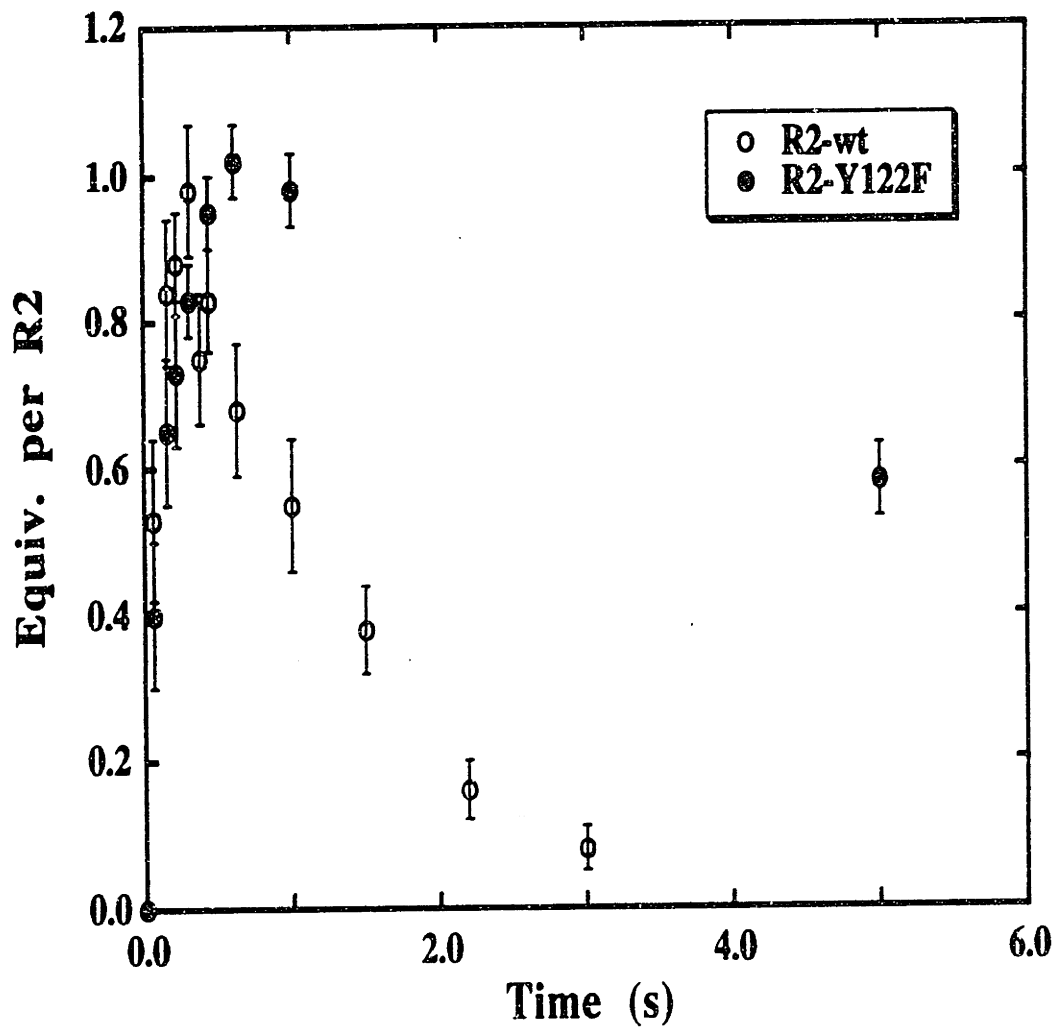
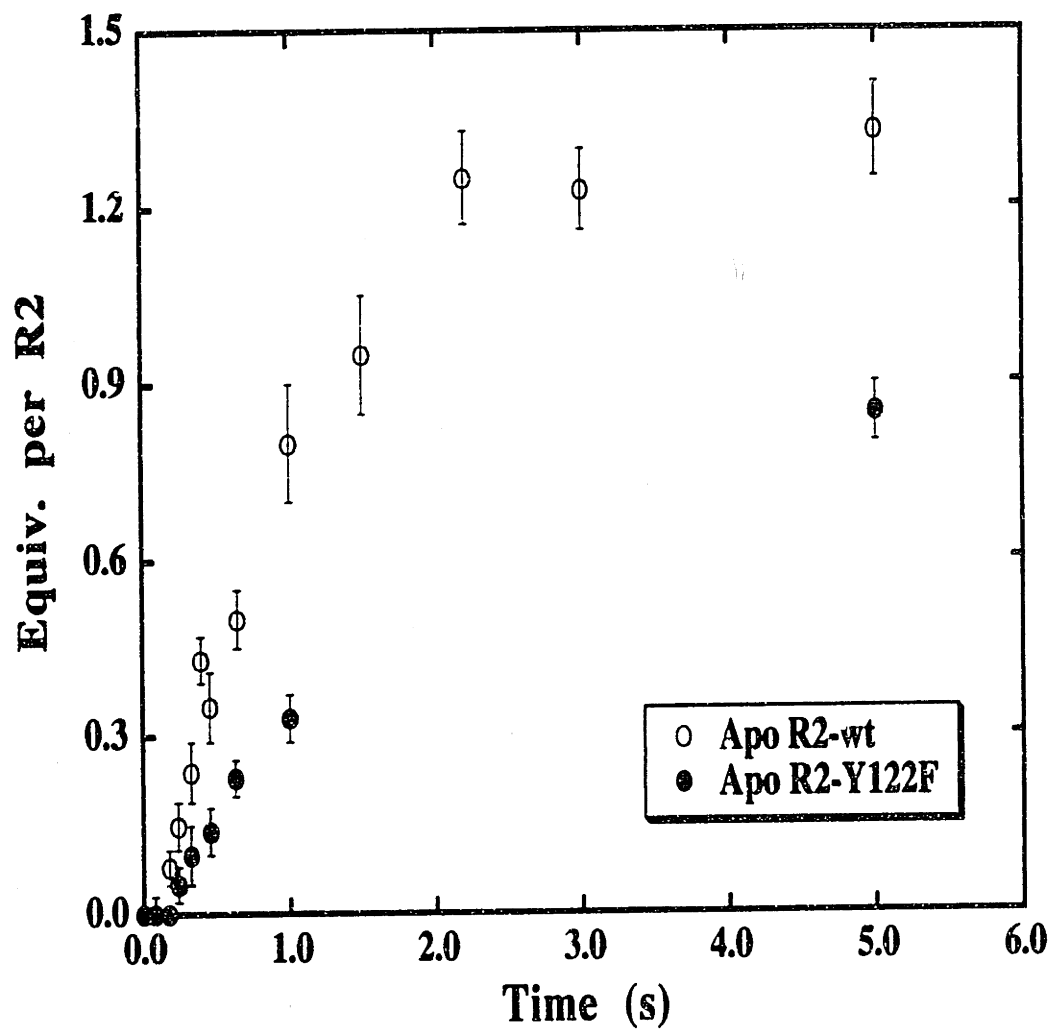


Fig. A.1.9: Mössbauer time-course of the diferric cluster in the reaction of apo R2-Y122F with excess Fe^{2+} compared with that of apo R2-wt under the same conditions. The reaction conditions (after mixing) were: 300 μM R2-wt or R2-Y122F, 1.5 mM Fe^{2+} , 50 mM HEPES, pH 7.6, 5 °C.



the product of donation of the fourth electron by Fe^{2+} required for formation of X. This putative fast-relaxing ferric species is also produced in the reaction of apo R2-Y122F with excess Fe^{2+} . As shown in Table A.1.1, the measured quantity of the fast-relaxing ferric species increases with time and accumulates to ~0.5 equiv. between 0.4 - 0.6 s, and does not appear to decay significantly within 60 s. Consistent with differences in temporal behavior of X in R2-v t and in R2-Y122F, formation of the fast-relaxing ferric species also appears to be ~2 fold slower in R2-Y122F than in R2-wt. Fitting the measured quantities of this species as a function of time to the equation for a first-order process gives a rate constant of 3.6 s^{-1} (Fig. A.1.10). These observations again suggest that the putative fast-relaxing Fe^{3+} species is produced when a Fe^{2+} donates an electron to generate X (Scheme 1.3).

Reaction of Apo R2-Y122F with Excess Fe^{2+} and O_2 as at 25 °C as Monitored by RFQ-Möss Spectroscopy

When apo R2-Y122F is mixed with excess Fe^{2+} at 25 °C, both X and the fast-relaxing species are observed (Fig. A.1.11). At the 0.18 s time-point, 0.63 equiv. of X has accumulated (Table A.1.3). At this time, 0.50 equiv. of fast-relaxing species and 0.23 equiv. of diferric cluster are also present. Comparison of the data in Table A.1.1 and Table A.1.3 suggests that the reaction is faster at 25 °C than at 5 °C. Finally, at completion of the reaction (60 s), the spectrum indicates that X has decayed completely and that 1.38 equiv. of the diferric cluster are present.

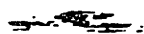


Fig. A.1.10: Formation of the fast-relaxing ferric species in the reaction of apo R2-Y122F with excess Fe^{2+} compared with that of apo R2-wt under the same conditions. The reaction conditions (after mixing) were: 300 μM R2-wt or R2-Y122F, 1.5 mM Fe^{2+} , 50 mM HEPES, pH 7.6, 5 °C. The theoretical trace is obtained by fitting a first-order process to the data from the R2-Y122F reaction, and corresponds to a k_{obs} of 3.6 s^{-1} and a final fast-relaxing ferric species/R2 ratio of 0.5.

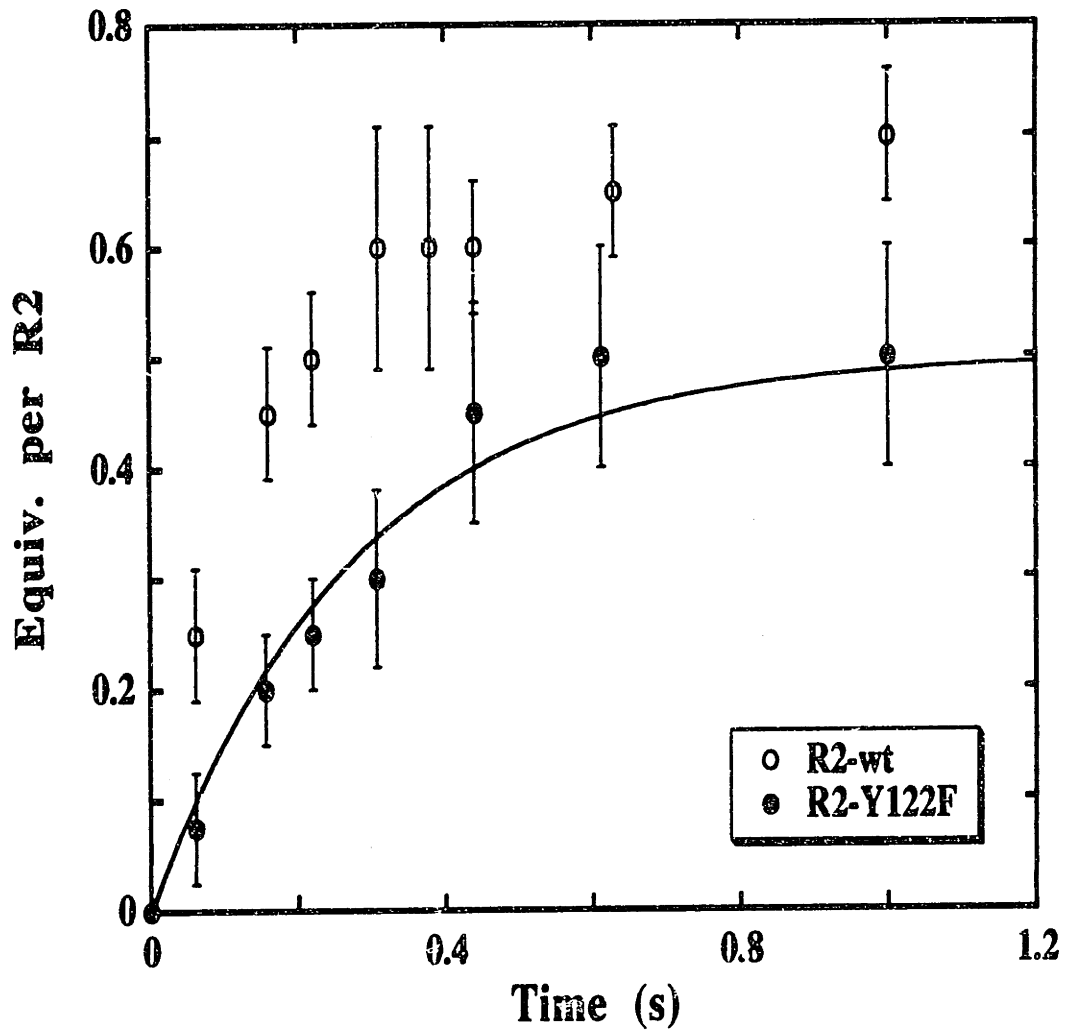


Fig. A.1.11: Mössbauer spectrum showing the accumulation of X in the reaction of apo R2-Y122F with excess Fe²⁺ at 25 °C. The reaction conditions (after mixing) were: 300 μM apo R2-Y122F, 1.5 mM Fe²⁺, 50 mM HEPES (O₂-saturated), pH 7.6, 25 °C. The reaction was quenched (A) at 0.18 s, (B) at 0.33 s, or (C) at 60.0 s.

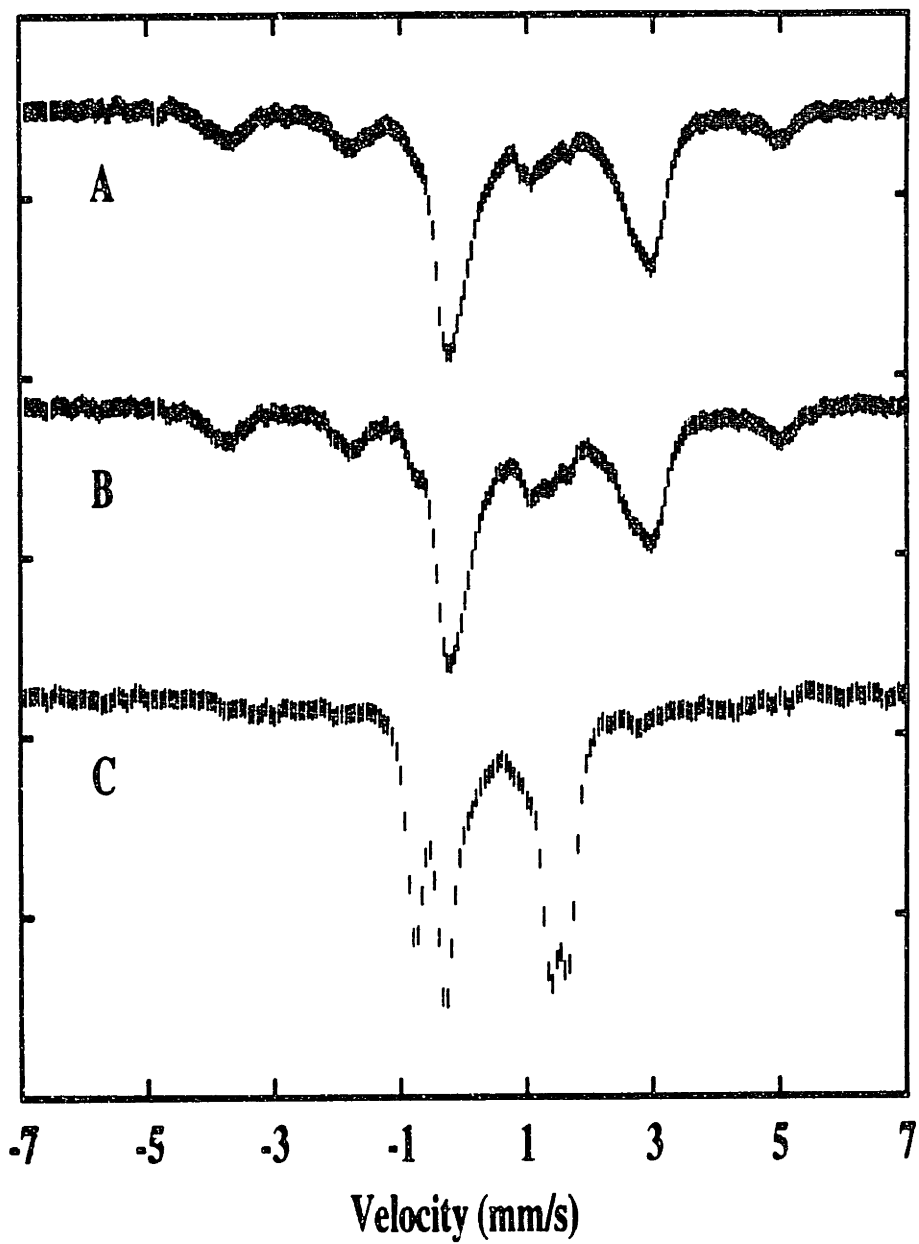


Table A.1.3: Summary of the analysis of the Mössbauer spectra from the reaction of apo R2-Y122F with excess Fe²⁺ at 25 °C.

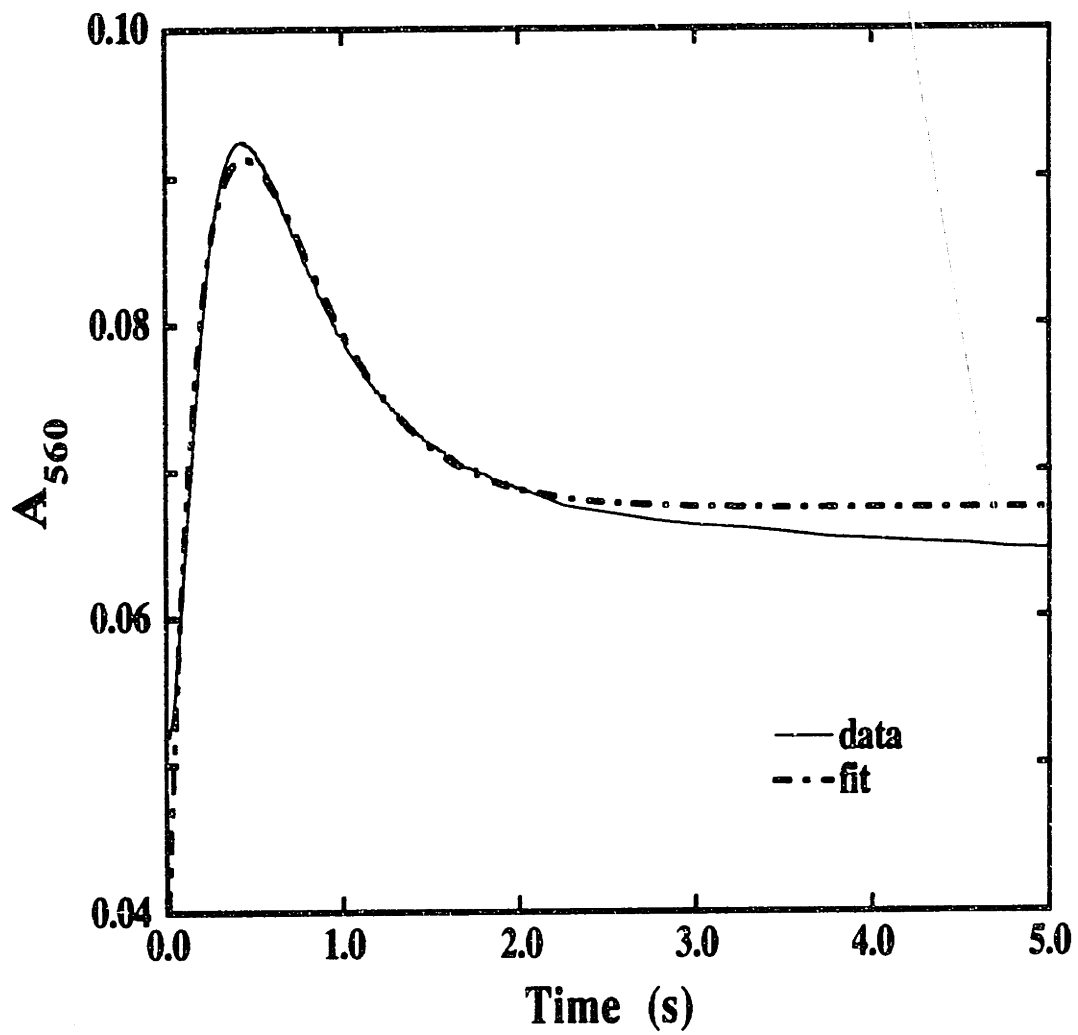
Reaction Time (s)	Equiv. X	Equiv. Diferric Cluster	Equiv. Fast-Relaxing Fe ³⁺
0.18	0.63 ± 0.1	0.23 ± 0.03	0.5 ± 0.1
0.33	0.63 ± 0.1	0.35 ± 0.03	0.55 ± 0.1
60	0	1.38 ± 0.08	0.4 ± 0.1

Reaction of Apo R2-Y122F with Limiting Fe²⁺ and O₂ as Monitored by Abs-SF Spectroscopy

Initial studies of the reaction of apo R2-wt (or apo R2-Y122F) with limiting Fe²⁺ demonstrated the formation of a transient 560 nm-absorbing species. It was proposed that this 560 nm transient is a •W48⁺ which effects the one-electron oxidation of Y122 to •Y122 under limiting Fe²⁺ conditions. The initial survey experiments were carried out with an Applied Photophysics RX.1000 Rapid Kinetics Spectrometer Accessory in conjunction with a Hewlett Packard 8452A Diode Array Spectrometer, which has a rather long and variable dead-time (estimated to be 0.10-0.25 s). In order to obtain better time resolution and dead-time reproducibility, identical experiments were carried out with an Applied Photophysics DX.17MV Sequential Stopped-Flow Spectrofluorimeter.

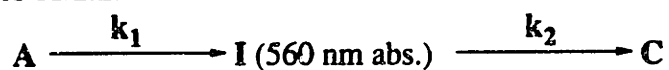
When apo R2-Y122F is mixed rapidly with 2.3 molar equivalents of Fe²⁺, the 560 nm-absorbing species accumulates (Fig. A.1.12). Fitting the A₅₆₀-versus-time curve to two sequential, first-order processes (Scheme A.1.2) gives a value of 3.2 s⁻¹ for one rate constant and a value of 2.8 s⁻¹ for the

Fig. A.1.12: A_{560} -versus-time trace in the reaction of apo R2-Y122F with limiting Fe^{2+} . The reaction conditions were: 51 μM apo R2-Y122F, 119 μM Fe^{2+} , 50 mM HEPES (air-saturated), pH 7.6, 5 °C. The experimental trace represents the average of 3 trials. The theoretical trace was obtained by fitting two sequential, first-order processes to the 0.040 - 3.0 s region of the experimental trace, and corresponds to a k_1 of 3.2 s^{-1} and a k_2 of 2.8 s^{-1} .



second rate constant (Bollinger, 1992; Bollinger *et al.*, 1994b) The transient species reaches maximum intensity at ~0.44 s, which is significantly greater than the t_{\max} of the 560 transient in R2-wt (0.16-0.18 s).

Scheme A.1.2:



As stated above, it has been proposed in several studies that a transient tyrosyl radical is generated in the reaction of apo R2-Y122F with limiting Fe^{2+} (Sahlin *et al.*, 1994; Pulver *et al.*, 1995; Sahlin *et al.*, 1995). The $A_{410, \text{dropline}}$ versus-time trace provides support for this assertion (Fig. A.1.13). When apo R2-Y122F is mixed with limiting Fe^{2+} , $A_{410, \text{dropline}}$ rises with time initially, reaches its maximum value at 1.2 - 1.4 s, and then decays more slowly. Fitting the equation for a first-order reaction to the decay phase of the curve gives a k_{obs} of 0.05 s^{-1} . Assuming that the $\epsilon_{410, \text{dropline}}$ of this tyrosyl radical is identical to that of $\bullet\text{Y122}$, the magnitude of $A_{410, \text{dropline}}$ at t_{\max} indicates that 0.04 tyrosyl radical are present. Interestingly, recent studies on a R2-Y122F/Y356F double mutant indicates that the 410 nm transient observed in R2-Y122F is not observed in the double mutant, suggesting that the putative tyrosyl radical does not form in R2-Y122F/Y356F. The simplest interpretation of these results is that the transient tyrosyl radical observed in the reaction of apo R2-Y122F with limiting Fe^{2+} resides on residue Y356.

EPR Time-Course of the Reaction of Apo R2-Y122F with Limiting Fe^{2+}

Fig. A.1.14 shows the EPR time-course of the reaction of apo R2-Y122F with limiting Fe^{2+} and O_2 at 5 °C. The EPR spectra show the sharp, isotropic, $g = 2.00$ singlet, characteristic of the intermediate X, indicating that X forms in

Fig. A.1.13: A_{410} , dropline-versus-time trace used to assess the formation of tyrosyl radical in the reaction of apo R2-Y122F with limiting Fe^{2+} . The reaction conditions were: 51 μM apo R2-Y122F, 119 μM Fe^{2+} , 50 mM HEPES (air-saturated), pH 7.6, 5 °C. The experimental trace was constructed from the averages of three trials at each wavelength.

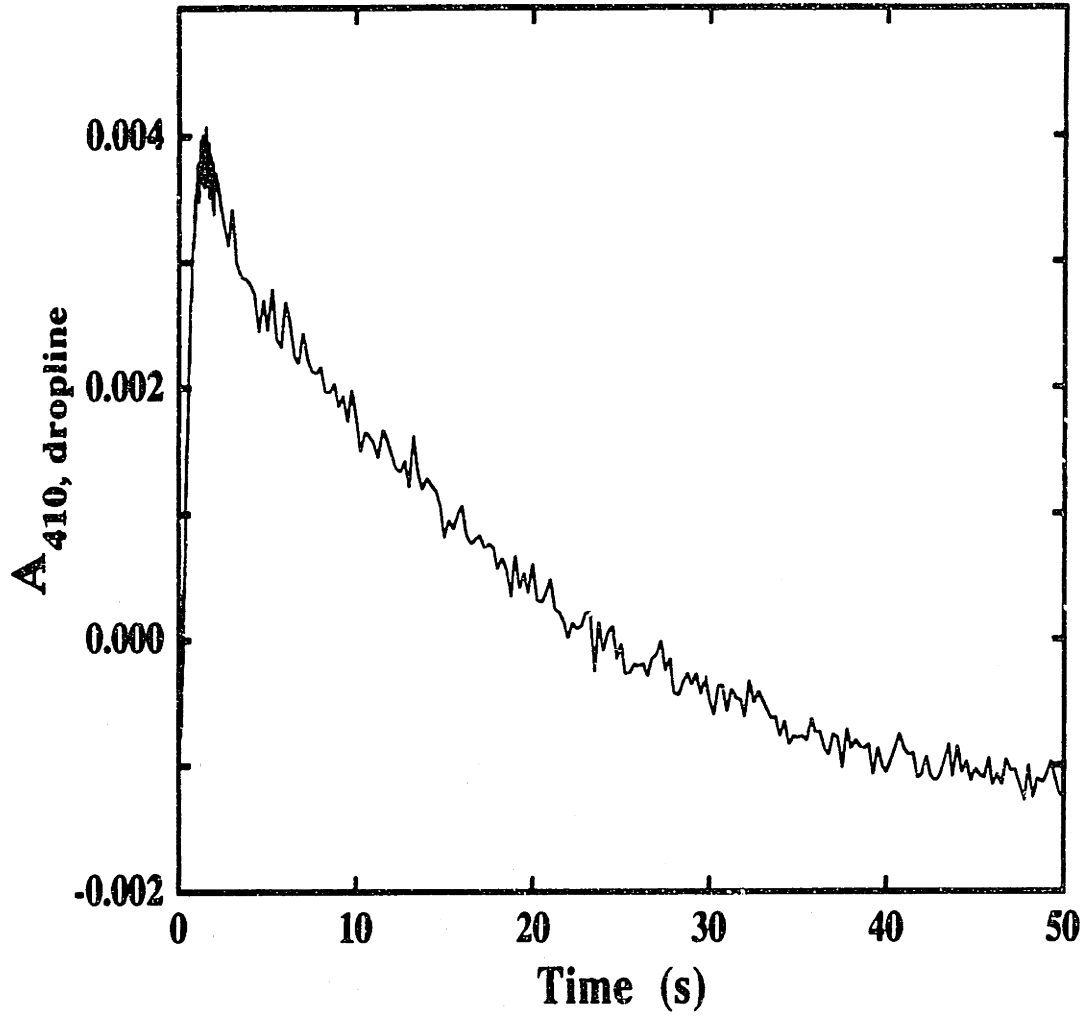
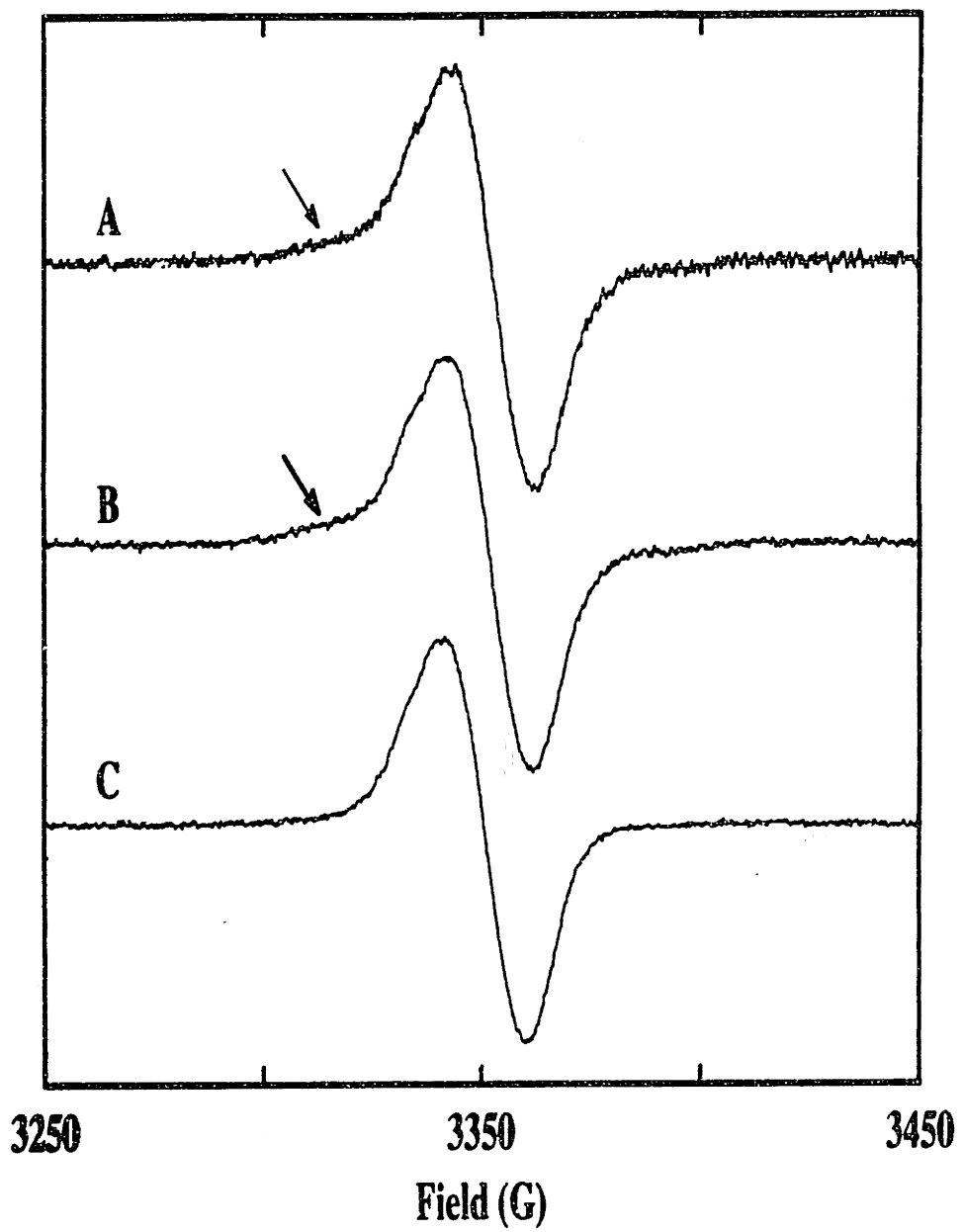


Fig. A.1.14: EPR time-course of the reaction of apo R2-Y122F with limiting Fe²⁺. The reaction conditions were: 300 μM apo R2-Y122F, 1.38 mM Fe²⁺, 50 mM HEPES (O₂-saturated), pH 7.6, 5 °C. The outer (experimental) spectra of **A**, **B**, and **C** are the spectra of the reaction quenched at 0.077 s, 0.31 s, and 1.0 s respectively. The inner spectrum in **A-C** is the reference spectrum for **X**. The spectra were acquired at 20 K with a microwave power of 1 μW, a frequency of 9.43 GHz, a modulation frequency of 100 kHz, a modulation amplitude of 4 G, a time constant of 200 ms, a scan time of 200 s, and a receiver gain of 4 × 10⁴.



this reaction (Bollinger *et al.*, 1994b). As with R2-wt, the EPR spectra show substantial amount of additional broad features in the $g = 2$ region.

Quantitative Analysis of the Reaction of Apo R2 -Y122F with Limiting Fe²⁺

The model in Scheme 1.3 requires that the spin quantitation of the limiting Fe²⁺ reaction should reflect the sum of X and •W48⁺ present at any particular time-point. In order to test this model, we set out to estimate the amount of the putative •W48⁺ present from the stopped-flow data and compare the total spin predicted by the model in Scheme 1.3 with the EPR data.

In estimating the amount of the putative •W48⁺ present at any given time-point, no assumptions were made on the rate constants or the mechanism. Only the absorption change at 560 nm was taken into consideration. From the A₅₆₀-versus-time trace (Fig. A.1.12) and the ϵ_{560} of tryptophan cation radicals (•WH⁺) reported in the literature, it should be possible to estimate the amount of the putative •W48⁺ accumulated in the limiting Fe²⁺ reaction. As discussed in Chapter 3, the absorbance change at 560 nm from $t = 0$ to $t = t_{\max}$ provides an estimate for the upper limit of the amount of 560 nm-absorbing species formed (Fig. 3.9), whereas the absorbance change at 560 nm from $t = t_{\max}$ to $t = \infty$ provides the lower limit. Assuming an ϵ_{560} for •WH⁺ of 3000 M⁻¹cm⁻¹ (Solar *et al.*, 1991), this analysis would imply that 0.16 - 0.30 equiv. of the 560 nm-absorbing species is present at t_{\max} (~0.44 s) in the reaction of apo R2-Y122F with limiting Fe²⁺. As shown in Table A.1.4, the Mössbauer spectrum of the 0.46 s time-point indicates that 0.75 ± 0.05 equiv. of X is present. If it is assumed that all the spin in the $g = 2.00$ region of the EPR spectra results from the sum of the spectra of X and •W48⁺, then it would imply that 0.92 to 1.1 equiv. of spin should be present at

Table A.1.4: Summary of the analysis of the EPR and the Mössbauer spectra from the reaction of apo R2-Y122F with limiting Fe²⁺. The amount of EPR active species in each sample was determined by double integration of the g = 2.00 region of the EPR first derivative spectrum, assuming a packing factor of 0.7 ± 0.1. The measured quantity of X was obtained from analysis of the Mössbauer spectrum.

Time (s)	Spin/R2	X/R2
0.077	0.39 ± 0.06	0.33
0.18	0.69 ± 0.13	-
0.25	0.73 ± 0.10	0.60
0.33	0.69 ± 0.10	-
0.46	0.69 ± 0.10	0.72, 0.78
0.58	-	0.74
1.0	0.88 ± 0.13	-
3.0	0.40 ± 0.06	

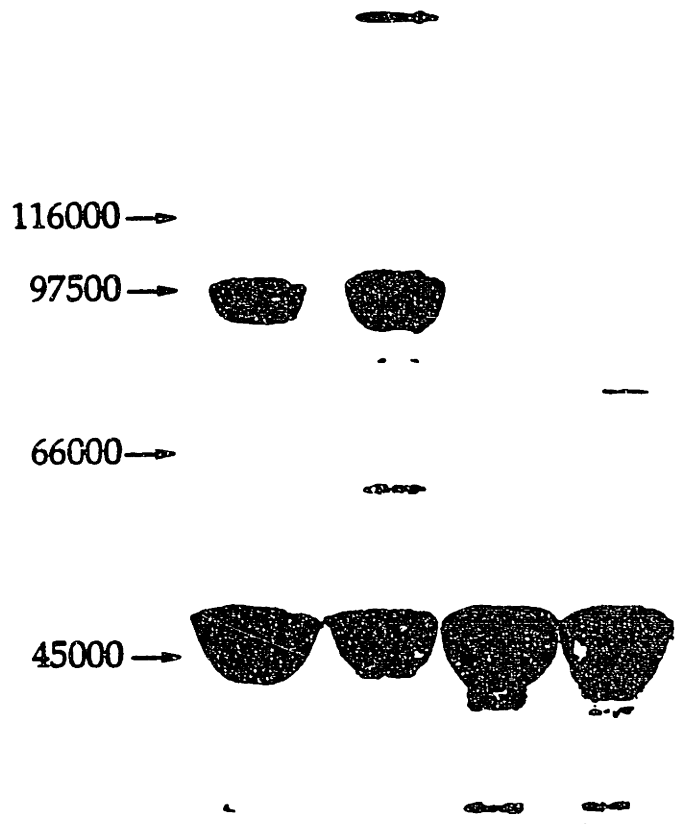
this time. The EPR data, however, indicates that only 0.69 ± 0.10 equiv. of total radical is present at the 0.46 s time-point (Table A.1.4). Thus, these results indicate a discrepancy between the EPR data and the proposed mechanism (Scheme 1.3). The mechanistic implications of these results are discussed below.

Reaction of apo R2-Y122F with Limiting Fe²⁺ is Accompanied by Cross-linking

As shown previously by Bollinger *et al* (Bollinger *et al.*, 1991a), a transient absorbance at 410 nm, which resembles the spectrum of a tyrosyl radical, is observed in the reaction of apo R2-Y122F with limiting Fe²⁺. This transient absorbance was not observed in the reaction with excess Fe²⁺ or in the reaction with limiting Fe²⁺ and ascorbate. These observations suggest that an unstable radical is generated from another tyrosine residue in R2 when reductant is limiting (Bollinger *et al.*, 1991a). The formation of intramolecular dityrosine cross-linkages, presumably resulting from the coupling of Y residues, has been demonstrated in the reaction of metmyoglobin with peroxide (Tew & Ortiz de Montellano, 1988). A similar mechanism involving surface Y radicals has been proposed to account for the cross-linking of cytochrome c peroxidase (CCP) which occurs when the ferrous enzyme reacts with O₂ in the absence of substrates (Miller *et al.*, 1992). To determine whether the formation of transient radical species in the limiting Fe²⁺ reactions also causes an intermolecular cross-linking reaction, the products of the reactions were analyzed by SDS gel electrophoresis. As shown in Fig. A.1.15, only one major band was observed in each of the excess Fe²⁺ reactions. These bands have migratory properties identical to that of native R2. Interestingly, when a very concentrated sample (1 mM) of apo R2-wt (or apo R2-Y122F) reacts with limiting Fe²⁺, the SDS-PAGE gel of the reaction mixtures shows that part of the R2 present initially is converted to bands corresponding to the dimeric forms of the protein and suggests that protein-protein cross-linking occurs in these reactions. Cross-linking was only observed at high protein concentrations. Reactions carried out at 50 μM protein concentrations show no cross-linking (data not shown).

Fig. A.1.15: The products of the reaction of apo R2-Y122F with Fe²⁺ as analyzed by SDS gel electrophoresis. From left to right: 1: reaction of 1 mM apo R2-wt with limiting Fe²⁺; 2: reaction of 1 mM apo R2-Y122F with limiting Fe²⁺; 3: reaction of 1 mM apo R2-wt with excess Fe²⁺; 4: reaction of 1 mM apo R2-Y122F with excess Fe²⁺.

apo R2-wt + 2.3 Fe
apo R2-Y122F + 2.3 Fe
apo R2-wt + 5 Fe
apo R2-Y122F + 5 Fe



Sequence information, NMR, crystallographic, and biochemical studies all indicate that Y356 is on the surface of R2 and this conserved residue has been proposed to be involved in electron transfer between the R1 and R2 subunits during catalytic turnover (Climent *et al.*, 1992; Nordlund & Eklund, 1993). It has also been proposed that the transient absorbance at 410 nm observed in the reaction of apo R2-Y122F with limiting Fe²⁺ corresponds to transient formation of a •Y356 (Pulver *et al.*, 1995). This residue is therefore a ~~good~~ candidate for the site of cross-linking observed in the reaction of apo R2-Y122F with limiting Fe²⁺. To address the possible role of Y356 during catalytic turnover and during assembly of the R2 cofactor, two mutants, R2-Y356F and R2-Y122F/Y356F were examined. The transient absorption at 410 nm was not observed in the reaction of apo R2-Y122F/Y356F double mutant with limiting Fe²⁺ (Burdi *et al.*,). These results are in accord with a recently published report which showed the absence of the transient absorption at 410 nm in the reaction of apo R2-Y122F/Y356A (Sahlin *et al.*, 1995). Furthermore, there is no indication of any cross-linking in the reaction of apo R2-Y356F and in the reaction of apo R2-Y122F/Y356F under both excess and limiting Fe²⁺ conditions (data not shown). These results are consistent with the hypothesis that the transient tyrosyl radical observed in the reaction of R2-Y122F with limiting Fe²⁺ resides on the Y356 residue.

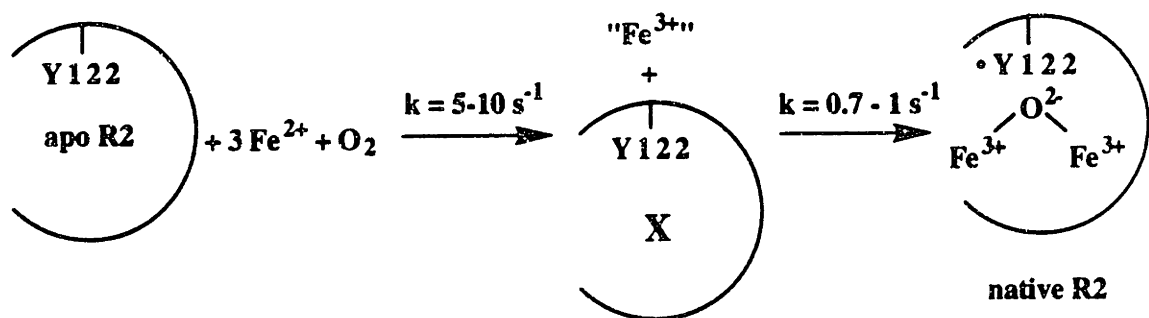
Discussion

Mechanism for the Reaction of Apo R2-Y122F with Excess Fe²⁺ and O₂

Previous studies on the reaction of apo R2-wt with Fe²⁺ and O₂ by Bollinger *et al.* have provided spectroscopic and kinetic evidence for the

proposed mechanism shown in Scheme 1.3 (Bollinger *et al.*, 1994a; Bollinger *et al.*, 1994b; Ravi *et al.*, 1994). When apo R2-wt is mixed with excess Fe^{2+} and O_2 , an intermediate I (which contains X and the putative $\bullet\text{W48}^+$) forms and is rapidly reduced by one electron to give a second intermediate II. In a subsequent step, II decays to give $\bullet\text{Y122}$ and diferric cluster. Because conversion of I to II is significantly faster than formation of I, I is kinetically invisible and pathway B in Scheme 1.3 can be reduced to Scheme A.1.3. The data are consistent with a minimal mechanism involving two sequential first-order processes, in which X accumulates ($k_{\text{obs}} = 5 - 10 \text{ s}^{-1}$), and decays concomitantly with formation of $\bullet\text{Y122}$ and the diferric cluster ($k_{\text{obs}} = 0.7 - 1 \text{ s}^{-1}$).

Scheme A.1.3:



The results described in this chapter provide further support with this mechanism. The SF-Abs results suggest that, in the reaction of apo R2-Y122F with excess Fe^{2+} and O_2 , X accumulates prior to formation of the diferric cluster. These results are supported by the Mössbauer data which suggest that X is a precursor to the diferric cluster. More importantly, the data show that both the decay of X and the formation of diferric cluster are significantly slower in the mutant protein than in R2-wt. The increased lifetime of the

intermediate **X** in the mutant protein provides additional evidence that it generates \bullet Y122 in the reaction of apo R2-wt with excess Fe^{2+} .

Another aspect of the reconstitution mechanism on which the data of this chapter may shed light is the source of the fourth electron required for cofactor assembly. It was proposed that, in the reaction of apo R2-wt with excess Fe^{2+} , donation of an electron from Fe^{2+} to convert I to II gives rise to the fast-relaxing ferric species. However, although the species forms in a kinetically competent fashion, it accumulates only to about one-half the quantity which would be expected if it arises from conversion of I to II. A possible explanation for this discrepancy is that the fast-relaxing ferric species may not be related to delivery of the fourth electron, in which case the correspondence of its rate of formation with that of **X** would be coincidental. However, the same correspondence observed in R2-wt reaction is also observed in the reconstitution of R2-Y122F. The experiments described in this chapter indicate that, in the reaction of apo R2-Y122F with excess Fe^{2+} at 5 °C, the ferric species also accumulates with a rate constant identical to that for formation of **X**. Interestingly, this species also accumulates to about 0.4 - 0.5 equiv. per R2, which is only slightly less than the amount of the species observed in the reaction of R2-wt. The simplest interpretation is that there may be multiple sources for the fourth electron, and that the putative fast-relaxing ferric species may be produced in only a fraction of the events in which **X** is produced. However, we have thus far failed to observe another kinetically competent species to account for the missing 0.7 - 1.0 equiv. of electrons required for conversion of I to II.

Qualitatively speaking, the reaction of apo R2-Y122F with excess Fe^{2+} is consistent with the mechanism proposed for that of R2-wt. However, as stated above, the R2-Y122F reaction exhibits more complex kinetic behavior

than the R2-wt reaction. While the R2-wt reaction can be well described with Scheme A.1.1, the simple model of two consecutive, first-order processes is of insufficient complexity to describe the R2-Y122F reaction (Fig. A.1.6). The most likely explanation for these results is that when the oxidizable Y122 residue is absent, the intermediate X can accept an electron from multiple electron donors. An examination of the crystal structure of R2 indicates a number of aromatic residues (W48, W107, W111) within 4 - 8 Å of the cofactor site which can potentially deliver a reducing equivalent to X. Oxidation of these residues is consistent with the recent study of Sahlin *et al.* (1995) which showed six transient EPR active species in the reaction of apo R2-Y122F with Fe²⁺ at 25 °C. At least two of these species are convincingly identified, by specific deuteration of the protein, as tryptophan radicals (Sahlin *et al.*, 1995). Furthermore, previous study by Bollinger *et al.* have led to the proposal that a transient •Y356 is generated during the reaction of apo R2-Y122F with limiting Fe²⁺ (Bollinger *et al.*, 1991a). This hypothesis is supported by the findings of Burdi *et al.* (1995) and Sahlin *et al.* (1995) that the 410 nm absorption feature is not observed in the mutant protein R2-Y122F/Y356A. Taken together, these results suggest that there may be multiple pathways in R2-Y122F for delivery of the fourth electron required for formation of the diferric cluster.

It is also conceivable that new structural constraints exist in the mutant protein which results in its complex kinetic behavior. The fact that substitution a Y122 with a F results in slower rate of formation of X, the fast-relaxing species, and the 560 nm-absorbing species leads to several interesting questions. From the X-ray crystal structures of the R2 subunits (Nordlund & Eklund, 1993), it is clear that long-range electron transfer to deliver reducing equivalents into the buried cofactor site is probably required during the

reconstitution reaction. The current concept of long-range electron transfer proposes a specific pathway connecting the donor and the acceptor, which is determined by the structure of the protein (Winkler & Gray, 1992; Wuttke *et al.*, 1992). X-ray crystallographic studies suggest that Y122 is part of an intricate hydrogen-bonding network in apo R2-wt (Aberg *et al.*, 1993). Alteration of this residue may result in subtle changes in the cofactor site and defective orientation for the normal electron transfer pathway.

On the other hand, direct participation of Y122 in the early steps of the reconstitution reaction remains an intriguing possibility. ENDOR (Bender *et al.*, 1989) and resonance Raman (Backes *et al.*, 1989) studies on R2 indicate that \bullet Y122 is a neutral radical. During cofactor assembly, deprotonation of Y122 must occur. Perturbations of the hydrogen bonding network and the multiple proton transfer processes involved could have a substantial effect on the overall kinetics of the reconstitution reaction. That the hydrogen bonding network and the proton transfer process(es) may play important roles in the overall kinetic mechanism is also supported by the results of Chapter 3 which show that multiple steps in the reconstitution reaction are sensitive to deuterium substitution of the solvent-exchangeable protons. The A_{410} , dropline-versus-time trace of the reaction of apo R2-wt with excess Fe^{2+} in 2H_2O exhibits a significantly longer lag (Fig. 3.____). The subsequent rise phase is also significantly slower than that in 1H_2O . Preliminary results indicate that the reconstitution reaction is also very sensitive to changes in pH.

Mechanism for the Reaction of Apo R2-Y122F with Limiting Fe^{2+} and O_2

As stated above, the experiments described in this chapter have provided support for the mechanism proposed for the reaction of apo R2-

Y122F with excess Fe^{2+} . The data on the limiting Fe^{2+} reaction, however, reveals an apparent inconsistency with the model in Scheme 1.3. The EPR results indicate that the measured quantities of total EPR active species presented at early time-points are consistently lower than the estimated value based on the stopped-flow data. This observation thus argues against the proposal of a $\bullet\text{W48}^+$ intermediate. We are currently considering three possibilities for this discrepancy. First, it should be emphasized that the uncertainties associated with EPR spin quantitation of freeze-quench samples can be $\pm 10\text{-}15\%$, as is evident in the results in this chapter as well as those in Chapter 2 and 3. An experimental error of $\pm 10\%$ in quantitative determinations is generally accepted in most EPR applications, which may be related to heterogeneity in the EPR tubes used, spectrometer stability, and/or poor temperature control in the EPR cryostat. Furthermore, the marriage of rapid freeze-quench techniques and EPR spin quantitation poses additional problems (Ballou, 1978). As mentioned in Chapter 2, a "packing factor" is included in the analysis of the EPR data. This factor, in part, corrects for the "dilution" of the reaction mixture by isopentane trapped in the crystalline sample. The packing factor also corrects for loose, uneven packing of the ice crystals in the EPR tubes. Ballou and Palmer determined a typical packing factor to be 0.5 - 0.7, and the precision of packing to be $\pm 5 - 10\%$ (Ballou & Palmer, 1974). In our experience, this factor varies between 0.6 to 0.8. These factors, considered together, may preclude meaningful quantitation of the 560 nm-absorbing species by RFQ-EPR techniques. However, while the difference between the calculated quantity and the measured quantity of EPR active species at any one time-point is less than the sum of the errors associated with these values, the fact that the theoretical quantity consistently exceeds the measured quantity of total EPR active species at each time-point in both R2-wt

and R2-Y122F suggests that the illustrated difference may be real. Furthermore, the analysis described above suggest that a substantial quantity of the 560 nm-absorbing species (50 - 75 μM spin, assuming a ϵ_{560} of 3000 $\text{M}^{-1}\text{cm}^{-1}$) should accumulate at t_{max} in the EPR experiment, a value that is well within the detection limit of EPR spectroscopy. If the hypothesis that the 560 nm absorption band is associated with a tryptophan cation radical is correct, the presence of this radical should be reflected in the EPR spin quantitation.

Second, the broad $g = 2$ features in the reaction of apo R2-Y122F with limiting Fe^{2+} may arise from multiple species. By subtracting away the spectrum of X, it was shown that the line shape of the resulting spectra changes somewhat with time (Bollinger, 1992) suggesting that the broad features arise from are multiple species. It is possible that dipolar interactions between some of these species may lead to further broadening of the spectrum, such that the real spectrum may have additional features which are unresolved. However, x-ray crystallographic data indicates that the distance between W48 and the nearest Fe in R2 is rather long (8 Å). It is, therefore, unlikely that the putative $\bullet\text{W48}^+$ would be broadened beyond detection.

Third, the data presented in Chapter 3 have shown that the broad EPR features at $g = 2.0$ and the 560 nm transient are not correlated under a number of conditions. When Fe(II)-R2 ($\text{Fe}^{2+}/\text{R2} = 2.3$) is mixed with O_2 , the EPR spectrum of the 0.44 s time-point shows substantial amount of the broad features (Fig. 3.____), even though the stopped-flow data indicates that the decay of the 560 nm-absorbing species is already completed at this time-point (Fig. 3.____). Furthermore, when the reaction of apo R2 with limiting Fe^{2+} is carried out in $^2\text{H}_2\text{O}$, the broad EPR signal is not detected, even though the 560 nm transient absorbance was still observable in the stopped-flow experiments. These results, together with the EPR data in this chapter, provide strong

argument against the hypothesis that the 560 nm absorption feature is associated with a \bullet W48⁺.

Implications on Electron Transfer Pathway during Cofactor Assembly and Catalytic Turnover

In studying the catalytic mechanism of *E. coli* RNR, it has become apparent that long range electron transfer has a particular functional importance in this enzyme. The available biochemical and crystallographical evidence supports the working hypothesis for the catalytic mechanism of *E. coli* RNR shown in Scheme 1.3 (Stubbe, 1990; Uhlin & Eklund, 1994). In this mechanism, a protein radical initiates turnover by abstracting the 3'-H atom from the ribose ring of the substrate (Stubbe, 1990). The participation of a protein radical in the reaction mechanism provides an explanation for the requirement for the tyrosyl radical in the R2 subunit. However, direct participation of the tyrosyl radical in 3'-H atom abstraction is unlikely, since, as mentioned, the cofactor is well buried in the R2 subunit (Nordlund & Eklund, 1993). A large conformational change would be required to bring the buried \bullet Y122 into proximity with the substrate (Nordlund *et al.*, 1990). Such a conformational change was deemed unlikely, as no observable changes in the spectroscopic properties of the R2 cofactor occur upon binding of R1 or upon turnover (Ehrenberg, 1988). It has been, therefore, proposed that turnover requires electron transfer from the R1 subunit to the tyrosyl radical in R2, thus, generating a transient C439 radical in R1 and a reduced Y122 in R2 (Mao *et al.*, 1992).

The recognition that electron transfer between R1 and R2 may be important in the catalytic mechanism of *E. coli* RNR has fueled efforts to identify residues near the R1 binding domain of R2 that might be involved in

an electron transfer pathway between the two subunits. Recently, several studies indicated that transient protein radicals are generated during the assembly of the R2 cofactor. Our earlier studies demonstrated occurrence of a transient absorption band characteristic of a tyrosyl radical during the reaction of apo R2-Y122F with 2.3 Fe²⁺ at 5 °C (Bollinger *et al.*, 1991a). Sahlin and coworkers reported that six radical species were detected in the reaction of apo R2-Y122F with Fe²⁺ (2 - 4 Fe²⁺/R2) at 25 °C (Sahlin *et al.*, 1995). It was proposed that these transient protein radicals may identify mechanistically important electron transfer pathway(s) in R2 (Sahlin *et al.*, 1995).

The experiments described in this chapter have provided further support that a •Y356 is generated during the reaction of apo R2-Y122F with limiting Fe²⁺. First, the transient absorption band observed in this reaction matches with those of a tyrosyl radical. Second, the fact that the transient absorption feature at 410 nm is not observed in the reaction of apo R2-Y122F/Y356F with limiting Fe²⁺ is entirely consistent with the hypothesis that this feature corresponds to a •Y356. Third, protein cross-linking was observed in the reaction of R2-Y122F with limiting Fe²⁺, which suggests that some surface residues were oxidized to amino acid radicals during this reaction. The fact that no cross-linking was observed when the reaction was carried out with R2-Y356F or R2-Y122F/Y356F provides strong evidence that the cross-linking occurs mainly through the conserved residue Y356 on the C-terminal end of the polypeptide. However, it is important to note that, thus far, there is no EPR evidence for this •Y356 from either our work or that of Sahlin *et al.* (1995). The reason for this discrepancy is not obvious, but one possible reason for the failure to observe this radical may be related to the fact that it accumulates to only a small amount (0.04 - 0.06 equiv. at ~ 1.2 s) such that it becomes masked by the other components in the EPR spectra.

On the basis of sequence information, NMR, crystallographic, and biochemical studies, this conserved Y356 residue was proposed to be involved in electron transfer between the R1 and R2 subunits during catalytic turnover (Climent *et al.*, 1992; Nordlund & Eklund, 1993). The results in this chapter provide evidence for the proposal that this residue can cycle between an oxidized, radical form and its normal, reduced form during reconstitution under limiting Fe^{2+} conditions. While it is interesting to speculate on the possible role of a $\bullet\text{Y356}$ in the electron process(es) during reconstitution and catalytic turnover, it should, however, be emphasized that the demonstration of a $\bullet\text{Y356}$ provides no direct evidence for its obligatory role in either of these physiological events. The evidence for a $\bullet\text{Y356}$ is strongest under conditions where the normal electron donor, i.e. Y122, is absent, or when the system is "starving for electrons", as in the limiting Fe^{2+} reactions. Stopped-flow studies indicate that reconstitution of the tyrosyl radical-diferric cluster cofactor in the mutant protein R2-Y356F proceeds in a manner very similar to that of R2-wt. Reaction of apo R2-Y356F with excess Fe^{2+} and O_2 gives rise to 1.2 equiv. of $\bullet\text{Y122}$, and the formation of $\bullet\text{Y122}$ is well described by a first-order rate constant of 0.7 s^{-1} (Burdi *et al.*,). When apo R2-Y356F is mixed rapidly with 2.3 equiv. of Fe^{2+} , the 560 nm-absorbing transient is observed, and the kinetics of this species are also remarkably similar to that in R2-wt. Furthermore, there is no evidence for the $\bullet\text{Y356}$ in the reaction of Fe(II)-R2 with O_2 under limiting Fe^{2+} conditions. Despite the fact that formation of X and the 560 nm-absorbing species are both much faster, neither the 410 nm transient absorption nor cross-linking are observed in the Fe(II)-R2 reaction. These results thus suggest that there may be alternative pathway(s) for delivering electrons into the developing cofactor which do not involve Y356.

Likewise, it is important to note that, thus far, there is no direct evidence that the tryptophan radicals observed by Sahlin *et al.* are mechanistically important (Sahlin *et al.*, 1995). As pointed out by Sahlin *et al.*, the temporal behavior of these species argued against a role for them in the normal reconstitution reaction (Sahlin *et al.*, 1995). With the exception of X and a singlet signal observed by continuous-flow-EPR spectroscopy at room temperature¹, the other three EPR active species observed by Sahlin *et al.* occur *after* the formation of the product diferric cluster. Two of the species (component I and II) were observed in the EPR spectra at 77 K after a 6-s reconstitution of apo R2-Y122F with 4 equiv. of Fe²⁺ at 25 °C (Sahlin *et al.*, 1995). Experiments using R2-Y122F with deuterated tryptophan indicated that component II is a tryptophan radical. Spin quantitation indicated that this tryptophan radical accumulates to 0.1 equiv. per R2 at the 6 s time-point and decays with a half-life of ~ 1.8 min. Component I in the EPR spectra at 77 K exhibits an axial signal with a g_{\parallel} of 2.036 and a g_{\perp} of 2.009. Spin quantitation indicated that 0.1 equiv. of component I per R2 is present at the 6 s time-point, and that it does not decay appreciably until after 10 s ($t_{1/2}$ ~ 7.5 min). In considering the species which gives rise to this axial signal, Sahlin *et al.* pointed out the similarities between the line-shape of component I and that of the signal observed for the tryptophan radical in cytochrome c peroxidase (CCP). These investigators, therefore, proposed that component I is a tryptophan radical, even though the signal in CCP was observable only at 4 K (Hoffman *et al.*, 1981; Houseman *et al.*, 1993). In addition to component I and II, a doublet signal observed in the continuous-flow-EPR experiments have been identified as a tryptophan radical by specific deuteration of the protein (Sahlin *et al.*, 1995). This signal becomes visible in the EPR spectra after 10 s

¹See Chapter 3 for a more detailed discussion of this singlet signal.

and reaches its maximum intensity at ~ 2 min. Recognizing that these species cannot be intermediates in R2 cofactor assembly - since they do not accumulate to any appreciable amount until after formation of the product diferric cluster is completed - Sahlin *et al.* proposed that these species identify the catalytically important electron transfer pathway(s) in R2 (Sahlin *et al.*, 1995). As mentioned above, extensive biochemical and structural studies have underscored the importance of long-range electron transfer during the reconstitution reaction and during nucleotide reduction (Stubbe, 1990; Uhlin & Eklund, 1994). It is, however, important to note that these protein radicals were observed under somewhat "anomalous" reconstitution conditions in which the normal electron donor, Y122, is absent and the reducing equivalents required for cofactor assembly are limited. At present, it is not clear whether these protein radicals represent intermediates during normal turnover or that they are mechanistically uninteresting side-products. Additional experiments are required to determine the possible role for these transient radical species.

References

- Aberg, A., Nordlund, P. & Eklund, H. (1993) *Nature* 361, 276-278.
- Atkin, C. L., Thelander, L., Reichard, P. & Lang, G. (1973) *J. Biol. Chem.* 248, 7464-7472.
- Backes, G., Loehr, T. M., Sjöberg, B.-M., Sahlin, M. & Sanders-Loehr, J. (1989) *Biochemistry* 28, 1923-1929.
- Ballou, D. P. (1978) *Methods in Enzymol.* 54, 85-93.
- Ballou, D. P. & Palmer, G. (1974) *Anal. Chem.* 46, 1248.
- Barshop, B. A., Wrenn, R. F. & Frieden, C. (1983) *Anal. Biochem.* 130, 134-145.

- Bender, C. J., Sahlin, M., Babcock, G. T., Barry, B. A., Chandrashekar, T. K., Salowe, S. P., Stubbe, J., Lindström, B., Petersson, L., Ehrenberg, A. & Sjöberg, B.-M. (1989) *J. Am. Chem. Soc.* 111, 8076-8083.
- Bollinger, J. M., Jr. (1992) Ph. D. Thesis, Massachusetts Institute of Technology.
- Bollinger, J. M., Jr., Edmondson, D. E., Huynh, B. H., Filley, J., Norton, J. R. & Stubbe, J. (1991a) *Science* 253, 292-298.
- Bollinger, J. M., Jr., Tong, W. H., Ravi, N., Huynh, B. H., Edmondson, D. E. & Stubbe, J. (1994a) *J. Am. Chem. Soc.* 116, 8015-8023.
- Bollinger, J. M., Jr., Tong, W. H., Ravi, N., B. H., Edmondson, D. E. & Stubbe, J. (1994b) *J. Am. Chem. Soc.* 116, 8024-8032.
- Bray, R. C. (1961) *Biochem. J.* 81, 189.
- Burdi, D., Daniel, R., Hunyh, B. H., Edmondson, D. & Stubbe, J., personal communication.
- Climent, I., Sjöberg, B.-M. & Huang, C. Y. (1992) *Biochemistry* 31, 4801-4807.
- Climent, I., Sjöberg, B.-M. & Huang, C. Y. (1991) *Biochemistry* 30, 5164-5171.
- Ehrenberg, A. (1988) *Chemica Scripta* 28A, 27-31.
- Hoffman, B. M., Roberts, J. E., Kang, C. H. & Margoliash, E. (1981) *J. Biol. Chem.* 256, 6556-6564.
- Houseman, A. L. P., Doan, P. E., Goodin, D. B. & Hoffman, B. M. (1993) *Biochemistry* 32, 4430-4443.
- Mao, S. S., Holler, T. P., Yu, G.-X., Bollinger, J. M., Jr., Booker, S., Johnston, M. I. & Stubbe, J. (1992) *Biochemistry* 31, 9733-9743.
- Miller, M. A., Bandypadhyay, D., Mauro, J. M., Traylor, T. G. & Kraut, J. (1992) *Biochemistry* 31, 2780-2797.

- Nordlund, P. (1990) Ph.D. Thesis, Swedish University of Agricultural Sciences.
- Nordlund, P. & Eklund, H. (1993) *J. Mol. Biol.* 232, 123-164.
- Nordlund, P., Sjöberg, B. M. & Eklund, H. (1990) *Nature* 345, 593-598.
- Pulver, S. C., Tong, W. H., Bollinger, J. M., Jr., Stubbe, J. & Solomon, E. I. (1995) *J. Am. Chem. Soc.* 117, 12664-12678.
- Ravi, N., Bollinger, J. M., Jr., Tong, W. H., Ravi, N., B. H., Edmondson, D. E. & Stubbe, J. (1994) *J. Am. Chem. Soc.* 116, 8007-8014.
- Sahlin, M., Lassmann, G., Pötsch, S., Sjöberg, B.-M. & Gräslund, A. (1995) *J. Biol. Chem.* 270, 12361-12372.
- Sahlin, M., Lassmann, G., Pötsch, S., Slaby, A., Sjöberg, B.-M. & Gräslund, A. (1994) *J. Biol. Chem.* 269, 11699-11702.
- Salowe, S. P. (1987) Ph. D. Thesis, University of Wisconsin.
- Sjöberg, B.-M., Karlsson, M. & Jörnvall, H. (1987) *J. Biol. Chem.* 262, 9736-9743.
- Solar, S., Getoff, N., Surdhar, P. S., Armstrong, D. A. & Singh, A. (1991) *J. Phys. Chem.* 95, 3639-3643.
- Stubbe, J. (1990) *Adv. Enzymol. Relat. Areas Mol. Biol.* 63, 349-417.
- Tew, D. & Ortiz de Montellano, P. R. (1988) *J. Biol. Chem.* 263, 17880-17886.
- Uhlen, U. & Eklund, H. (1994) *Nature* 270, 533-539.
- Winkler, J. R. & Gray, H. B. (1992) *Chemical Reviews* 92, 369-379.
- Wuttke, D. S., Bjerrum, M. J., Winkler, J. R. & Gray, H. B. (1992) *Science* 256, 1007-1009.

**Appendix 2: Characterization of Two Mutant Proteins,
R2-W48F and R2-W48Y**

A central feature in the mechanism of reconstitution proposed by Bollinger *et al.* is the participation of a •W48⁺ (Scheme 1.3). Interpreting the SF-Abs, RFQ-EPR and RFQ-Möss data, Bollinger *et al.* proposed that the 560 nm transient absorption band observed in the reaction of apo R2 with limiting Fe²⁺ is associated with a tryptophan radical cation, and that this species can generate •Y122 when the extra reducing equivalent is not readily available (Bollinger *et al.*, 1994a). Three lines of evidence were used to provide support for this hypothesis. First, the Mössbauer spectra of the limiting Fe²⁺ time-course samples were scrutinized for the presence of features that correlate in time with the 560 nm absorption band, and no such feature could be discerned. This result indicates that the species associated with the transient absorption band is not an iron-based intermediate. On the other hand, the EPR spectra of the early time-points exhibit some broad features in the $g = 2.00$ region which appears to be temporally correlated with the 560 nm absorption band. This result leads to the proposal that the 560 nm absorption band is associated with a protein radical.

Further support for this hypothesis was drawn from the proposed analogy between the intermediate I in R2 and an oxidized, reactive intermediate Compound I in a heme iron protein yeast cytochrome c peroxidase (CCP). CCP is a heme enzyme that catalyzes the peroxide-dependent oxidation of ferrous cytochrome c (Marnett *et al.*, 1986). Heterolytic decomposition of an enzyme bound peroxide equivalent in CCP gives an oxidized, reactive intermediate, compound I. Compound I harbors two oxidizing equivalents. In the case of yeast CCP, one of the oxidizing equivalents is stored as an oxyferryl (Fe(IV)) heme species, and a second is stored as an amino acid radical (Yonetani *et al.*, 1966; Langet *et al.*, 1976; Marnett *et al.*, 1986). The radical species exhibits an axially symmetric, $g = 2.0$ EPR signal and a broad visible absorption band centered near 570 nm (Coulson *et al.*, 1971; Hoet *et al.*

1983). Spectroscopic and rapid kinetic methods applied in conjunction with site-directed mutagenesis have provided strong evidence that the radical of CCP compound I results from one electron oxidation of W191 (Erman *et al.*, 1989; Scholes *et al.*, 1989; Sivaraja *et al.*, 1989). ENDOR measurements on CCP grown on perdeuterated tryptophan have provided convincing evidence that the Compound I radical is located at a tryptophan residue (Sivaraja *et al.*, 1989). The CCP-W191F mutant fails to exhibit the axial $g = 2.0$ EPR signal upon reaction with H_2O_2 (Scholes *et al.*, 1989), but instead, forms a transient porphyrin π -cation radical which is not observed in the unaltered protein (Erman *et al.*, 1989). The W191F mutation also greatly reduces the steady state rate at which ferrocyanochrome c is oxidized by the enzyme and the rate at which the $Fe(IV)=O$ form of the enzyme is reduced by ferrocyanochrome c (Mauro *et al.*, 1988). These and other data provide strong evidence that CCP compound I contains a $\bullet W191$ and that the residue W191 plays a key role in the electron transfer process from cytochrome c to the heme site of CCP (Erman *et al.*, 1989).

The crystal structure of CCP reveals that the W191 residue is linked by hydrogen bonding with D235 to the proximal histidine (H175) of the heme, suggesting that these residues are part of the electron transfer chain to the heme (Finze *et al.*, 1984). Interestingly, a similar hydrogen bonding network involving a conserved residue W48 in *E. coli* R2 has been pointed out by Nordlund and coworkers (Nordlund & Eklund, 1993). Residue W48 in *E. coli* R2 is linked to the iron cluster by a hydrogen bonding network involving H118 and D237, is near the putative R1-binding domain, and is completely conserved among all known R2 sequences. Interpreting the crystal structure of R2, Nordlund and coworkers have suggested that W48 may cycle between an oxidized, radical form and its normal, reduced form and be part of the long range electron transfer pathway between the R1 and R2 subunits during catalytic turnover (Nordlund & Eklund, 1993).

In order to investigate the possible role of W48 in the assembly of the cofactor of R2 and in the electron transfer pathway between the two subunits of *E. coli* ribonucleotide reductase, two R2 mutants, R2-W48F and R2-W48Y, were constructed. This chapter reports the construction and characterization of these mutants.

Experimental Procedures

Materials

Restriction enzymes and DNA modifying enzymes were purchased from New England Biolab, Gibco BRL, and Boehringer Mannheim. *E. coli* strain K38 containing the plasmid pGP1-2 was the generous gifts of Prof. S. Tabor at the Harvard Medical School. Ampicillin, lysozyme, ethidium bromine, ATP, ferrozine, and Fe atomic absorption standard were purchased from Sigma. ATP- γ ³²P (6000 Ci/mmol) was obtained from New England Nuclear. NickTM columns were from Pharmacia. Site directed mutagenesis kit was obtained from Amersham. Kanamycin was purchased from United States Biochemicals. The dsDNA cycle sequencing system, T4 DNA ligase, competent DH5 α and HM101 were purchased from Gibco BRL. TA CloningTM system was from Invitrogen. *E. coli* thioredoxin (TR) (specific activity 50 U/mg) and thioredoxin reductase (TRR) (specific activity 800 U/mg) were isolated from overproducing strains SK2981 (Lunn *et al.*, 1984) and K91/pMR14 (Russel & Model, 1985). DNA PCR primers were made at the MIT Biopolymers Laboratory, or Oligos *etc.*, Inc. of Wilsonville, OR. All other chemicals were of the highest purity commercially available.

Construction and Expression of nrdB-W48 mutants by the Eckstein Method

Site directed mutagenesis was also performed by the method of Taylor *et al.* (Tayloret *al.*, 1985; Nakamaye & Eckstein, 1986; Sayers *et al.*, 1988), according to the

instructions included in the Amersham kit. Degenerate primers for the construction of the R2 mutants (Table A.2.1) were designed from known sequence of pTB2 (Bollinger, 1992) which contain the coding sequence of R2 (Fig. A.2.1). Single stranded M13*nrdB* (Bollinger, 1992) which encodes R2-wt was isolated by a standard method, and was used, together with the appropriate mutant primer 1 or 2 (for W->F or W->Y mutation respectively), in construction of the R2 mutants.

Single stranded DNA was isolated from plaques obtained following mutagenesis. Mutants were identified by sequencing in the region containing the desired mutation site. DNA sequencing was performed by the dideoxy chain termination method of Sanger *et al.*, according to the instructions included in the United States Biochemicals sequencing kit.

The replicative forms of the M13*nrdB*-W48 mutants were isolated (from the plaques that were shown to contain the desired mutation) by a standard procedure. The 0.6 kilobase pair *EcoRI/KpnI* restriction fragment (which contains the first half of the *nrdB* coding sequence) was ligated into the parent vector pTB2 (which had been previously digested with *EcoRI* and *KpnI*) to yield pTB2-W48 mutants. The mutant proteins were overexpressed in a system developed for the expression of toxic genes (Tabor & Richardson, 1985) and used previously in this laboratory for the production of R2-Y122F (Bollinger, 1992; Bollinger *et al.*, 1994b). K38 cells containing pGP1-2 were transformed with pTB2-W48 mutant plasmids, and colonies resistant to ampicillin and kanamycin were shown by restriction analysis to contain the mutant plasmid. The sequence of the insert (~650 base pairs) was determined to verify that no other mutation have been introduced.

Expression of R2 was tested using the following procedure. A 5 mL overnight culture of each recombinant in enriched media with 50 µg/mL each of ampicillin

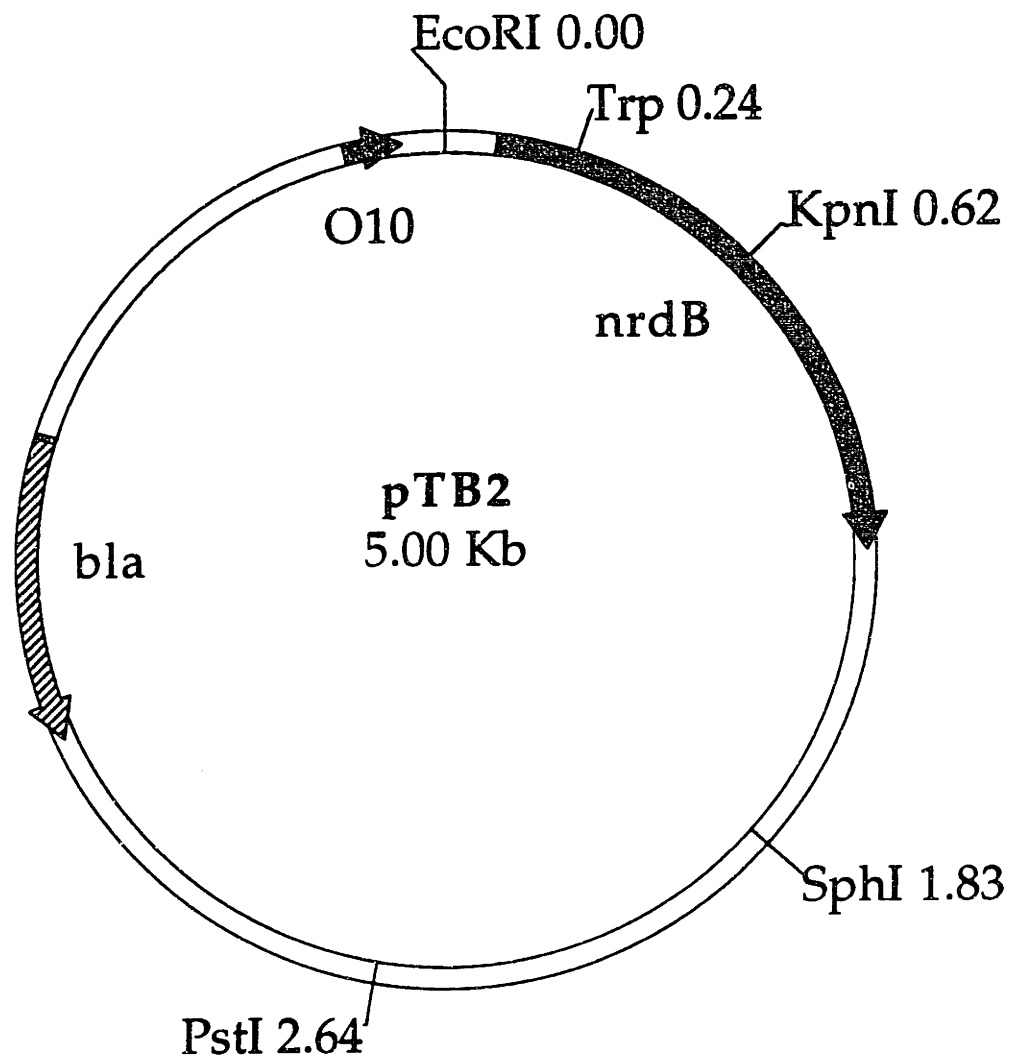


Fig. A.2.1: Schematic representation of the plasmid pTB2 that contains the coding sequence of R2 (*nrdB*).

Table A.2.1: Oligonucleotide primers used for mutagenesis by the Eckstein method.

Primer	Sequence ¹
1	5'-TCTTTCTTCT <u>TTT</u> CGTCCGGAAGAAGTTG-3'
2	5'-TCTTTCTTCT <u>TAC</u> CGTCCGGAAGAAGTTG-3'

¹Underlined bases represent mutation codons in primers 1 and 2.

and kanamycin was used to inoculate 100 mL of enriched media containing 50 µg/mL each of ampicillin and kanamycin. Growth at 30 °C was monitored until A₆₀₀ = 0.9-1.1, at which time a 1 mL aliquot was withdrawn and pelleted in a microcentrifuge (uninduced cell sample). The remainder of the culture was induced by transferring the culture to a 54 °C incubator. The temperature of the culture would reach 42 °C in 7-8 min. The culture was then transferred to a 42 °C incubator and heat induction was allowed to proceed at 42 °C for an additional 30 min. An aliquot of the induced cell sample was withdrawn and pelleted in a microcentrifuge. The remainder of the culture was allowed to grow at 37 °C for an additional 3 hours. Growth of the R2-W48 mutant after induction was monitored by withdrawing an aliquot of the culture at each hour and pelleting the aliquots using a microcentrifuge. Expression of the R2 mutant subunits was analyzed by SDS gel electrophoresis.

Purification of R2-W48F and R2-W48Y

The over-producing strains were grown in enriched medium (per liter of medium: 20 g tryptone, 10 g yeast extract, 5 g NaCl, 2 g glycerol, 50 mM potassium phosphate buffered at pH 7.2) at 30 °C to an OD₆₀₀ of 1.0-1.2, at which time expression of R2 was induced by heating the cells to 42 °C for 30 min. The cells were

grown at 37 °C for an additional 3 h, after which they were harvested by centrifugation. The yield in this fermentation was 2.5 g of wet cell paste/L of culture.

Protein R2-W48F was isolated from the overproducing strain K38/pTB2-W48F, using procedure previously described for R2-wt, with a few modifications. All steps in the purification were performed at 5 °C. Frozen wet cell paste (18.1 g) was suspended in 91 ml of 50 mM Tris (pH 7.6) containing 5% glycerol and 500 μ M PMSF (hereafter referred to as Tris buffer). The cell suspension was passed through a french pressure cell at 12 - 14,000 psi to rupture the bacteria. The crude lysate was stirred for several minutes, and then centrifuged at 14,000 x g for 20 min. The supernatant was brought to 1% in streptomycin sulfate by the addition (over 10 min., with stirring) of 0.2 volumes of a 5.5% (w/v) solution in the Tris buffer. This solution was stirred for an additional 15 min, and then centrifuged at 14,000 x g for 20 min. The supernatant was brought to 60% saturation in $(\text{NH}_4)_2\text{SO}_4$ (390 g/L), over 20 min, with stirring. This solution was stirred for an additional 30 min, and then centrifuged at 14,000 x g for 20 min. The pellet was redissolved in 10 ml of the Tris buffer. This solution was centrifuged at 14,000 x g for 10 min to pellet any remaining undissolved material, and was desalted through a G-25 Sephadex column (4 x 25 cm) equilibrated in the Tris buffer. The fractions containing protein (in 182 ml) were pooled and diluted with an equal volume of the Tris buffer. This solution was then loaded on a DEAE-Biogel A column (4 x 11 cm) equilibrated in the Tris buffer, and the column was washed with 1.5 column volumes of the Tris buffer. The column was then washed with 1.6 column volumes of the Tris buffer containing 110 mM NaCl. The R2 subunit was eluted from the column with Tris buffer containing 140 mM NaCl and 500 μ M PMSF. Fractions containing R2 were pooled (154 mL), and the pool was diluted with an equal volume of Tris buffer. PMSF was added to this solution to 500 μ M, and the solution was loaded onto a

QAE-Sephadex column (2.5 x 18 cm) equilibrated in the Tris buffer containing 70 mM NaCl. This column was washed with 2.5 volumes of the Tris buffer containing 225 mM NaCl. R2 was then eluted from the column with Tris buffer containing 300 mM NaCl. Fractions containing R2 (103 mL) were pooled and concentrated to ~1.8 mL in an Amicon Diaflow Ultrafilter equipped with a YM-30 membrane. The protein was frozen in liquid N₂ and stored at -80 °C. Isolation of R2-W48F in this manner yielded ~ 100 mg (judged by OD₂₈₀, using $\epsilon=120 \text{ mM}^{-1}\text{cm}^{-1}$) of > 90% pure (as assessed by SDS-PAGE and Comassie blue staining). Protein R2-W48Y was isolated from the overproducing strain K38/pTB2-W48Y using procedure described above, except that no iron or ascorbate was added in the beginning of the purification procedure.

Circular Dichroism Spectra of R2-W48F and R2-W48Y

Circular dichroism spectra were recorded at 5 °C on a Jason Model J500 spectropolarimeter using a 0.1-cm wavelength cell. A typical sample contained 5 μM R2 in 10 mM HEPES buffered at pH 7.6 at 5 °C.

Effects of R2-W48F and R2-W48Y on the Catalytic Activity of R2-wt

Wild-type R2 activity was assayed by following NADPH oxidation spectrophotometrically in the presence of apo R2-wt, R2-Y122F, R2-W48F and R2-W48Y (Salowe, 1987). A typical reaction contained, in a final volume of 400 μL , 50 mM HEPES buffer pH 7.6, 15 mM MgSO₄, 1 mM EDTA, 1.6 mM ATP, 1 mM CDP, 0.16 mM NADPH, 0.02 mM thioredoxin, 0.5 μM thioredoxin reductase, 0.11 μM R1, 0.22 μM R2-wt, and 0.22 - 1.1 μM inhibitor (Salowe, 1987)..

Iron Binding Properties of R2-W48F and R2-W48Y

Three sets of experiments were carried out to characterize the iron binding properties of the R2-W48 mutants. In the first set of experiments, the iron contents of the protein as purified were determined. Two different methods of extracting the iron from the protein were employed. An aliquot of the protein (5 - 10 nmol) was denatured by bringing the solution to 4.5% in trichloroacetic acid (Salowe, 1987). Alternatively, the iron in the protein was extracted by incubating the protein sample at 100 °C for 15 min with 2 M HCl (Lynch *et al.*, 1989). The sample was centrifuged to pellet the denatured protein and the supernatant was removed. The pellet was washed two times with 4.5% in trichloroacetic acid (or 2 N HCl depending on which extraction procedure was used) and the washes were combined with the supernatant. The iron content in the supernatant and the washes was determined by the ferrozine assay in the presence of ascorbate (Massey, 1957; Stookey, 1970; Salowe, 1987).. A typical assay contained 20 μL 10 mM ferrozine, 20 μL of 75 mM ascorbate, 160 μL of a saturated solution of ammonium acetate, and 2 - 15 nmol of Fe^{2+} in a final volume of 800 μL . An $\epsilon_{562} = 27900 \text{ M}^{-1}\text{cm}^{-1}$ was used for the calculation of $[\text{Fe}^{2+}]$ (Stookey, 1970)..

In an experiment designed to determine if the R2-W48 mutant proteins react with Fe^{2+} , a 400 μL aliquot of $\sim 250 \mu\text{M}$ R2-W48F (or R2-W48Y) in 50 mM HEPES buffer (pH 7.7) was placed in a cuvette and an absorption spectrum was recorded. An aliquot (50 μL) of 4.9 mM Fe^{2+} in 10 mM H_2SO_4 was added to the protein sample, with repeated mixing (by inversion) immediately after addition. The reaction was followed by acquiring spectrum of the resulting solution every 5 sec for 2 min using a Hewlett Packard 8452A Diode Array Spectrometer. The reaction of the mutant proteins with Fe^{2+} was also examined in the presence of ascorbate. A 400 μL aliquot of $\sim 250 \mu\text{M}$ protein in 50 mM HEPES buffer (pH 7.7) was placed in a cuvette and an absorption spectrum was recorded. Immediately before use, 1.5 mg of

FeSO₄·7H₂O and 1.8 - 2.0 mg of sodium ascorbate was dissolved in 1 mL of 100 mM HEPES buffer (pH 7.7). A 50 μL aliquot of this Fe/ascorbate solution was added to the protein solution in the cuvette, and an absorption spectrum of the resulting solution was acquired every 5 sec for 2 min. The iron content of the protein before and after treatment with the Fe/ascorbate solution was also determined using the acid extraction method and the ferrozine assay discussed above.

Another experiment was designed to test if the R2-W48 mutants react with Fe²⁺ under anaerobic conditions. The protein stock and the Fe²⁺ stock were deoxygenated separately using procedures described in Chapter 2. An aliquot of the O₂-free Fe²⁺ stock was added via cannula to the O₂-free protein sample such that the Fe²⁺/R2 ratio is 5. The reaction mixture was incubated at 4 °C for 30 min. A second aliquot of Fe²⁺ was added such that the final Fe²⁺/R2 was ~ 10. This was followed by incubation at 4 °C for an additional 30 min. The reaction mixture was then loaded onto an air-saturated G-25 column previously equilibrated in 100 mM HEPES buffer, pH 7.6, 5 °C. Fractions containing the protein (judged by A₂₈₀) were collected and the iron content was determined as described above by ferrozine assay after acid extraction.

Results

Preparation of R2-W48F and R2-W48Y

The Eckstein method was employed for the construction of the mutant protein R2-W48F and R2-W48Y. Dozens of white transformants were obtained following the mutagenesis procedure. Out of six of the white transformants obtained using primer 1, five showed the desired W→F mutation (TGG→TTT), and the remaining one showed wild-type sequence. Out of six of the white transformants obtained using primer 2, one showed wild-type sequence, one did not

yield sequence information, and the remaining four showed the desired W→Y mutation (TGG→TAC).

The K38/pTB2-W48 mutants were tested for induction of the recombinant proteins. As shown in Fig. A.2.2, synthesis of protein having approximately the predicted relative molecular mass (MW) is induced in the K38/pTB2-W48Y. Out of the three K38/pTB2-W48F recombinants tested, only one shows good expression of a protein having approximately the predicted relative molecular mass.

Characterizations of the R2-W48 Mutants

The integrity of each mutant was confirmed by DNA sequencing. Both mutants have the expected sequences. The mutant proteins were purified to > 90% homogeneity and both exhibited behaviors similar to R2-wt throughout each step of the purification. Surprisingly, the absorption spectrum of neither one of the purified mutant proteins has the distinctive UV-visible light spectrophotometric features of native R2 (data not shown).

To test if that the mutant proteins are properly folded, the CD spectra of R2-wt, R2-W48F and R2-W48Y were recorded. The spectra of all the protein are dominated by the α -helical structures (Fig. A.2.3). In general, the CD spectra suggest that the structures of the mutants are not drastically perturbed. The spectra of the mutants show only slightly more eclipticity than those of R2-wt and apo R2-wt. The small difference in the eclipticities of these proteins may merely reflect an overestimation of the protein concentrations. The protein concentrations were determined by absorbance at 280 nm. The ϵ_{280} of R2-wt and that of apo R2-wt were reported to be 130.5 and 120 $\text{mM}^{-1}\text{cm}^{-1}$ respectively (Thelander, 1973). In this study, the latter value is used to estimate the concentrations of the mutant proteins. The strong absorption of proteins at 280 nm is primarily due to tryptophan and tyrosine residues, and therefore vary with the content of these amino acids. The gene

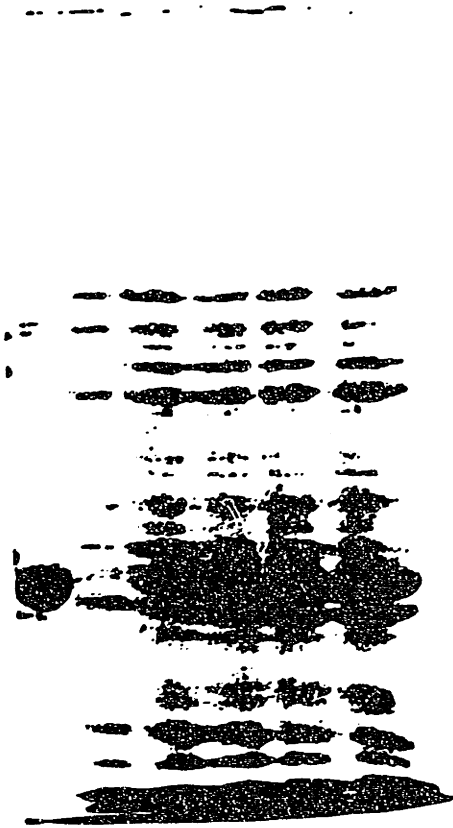
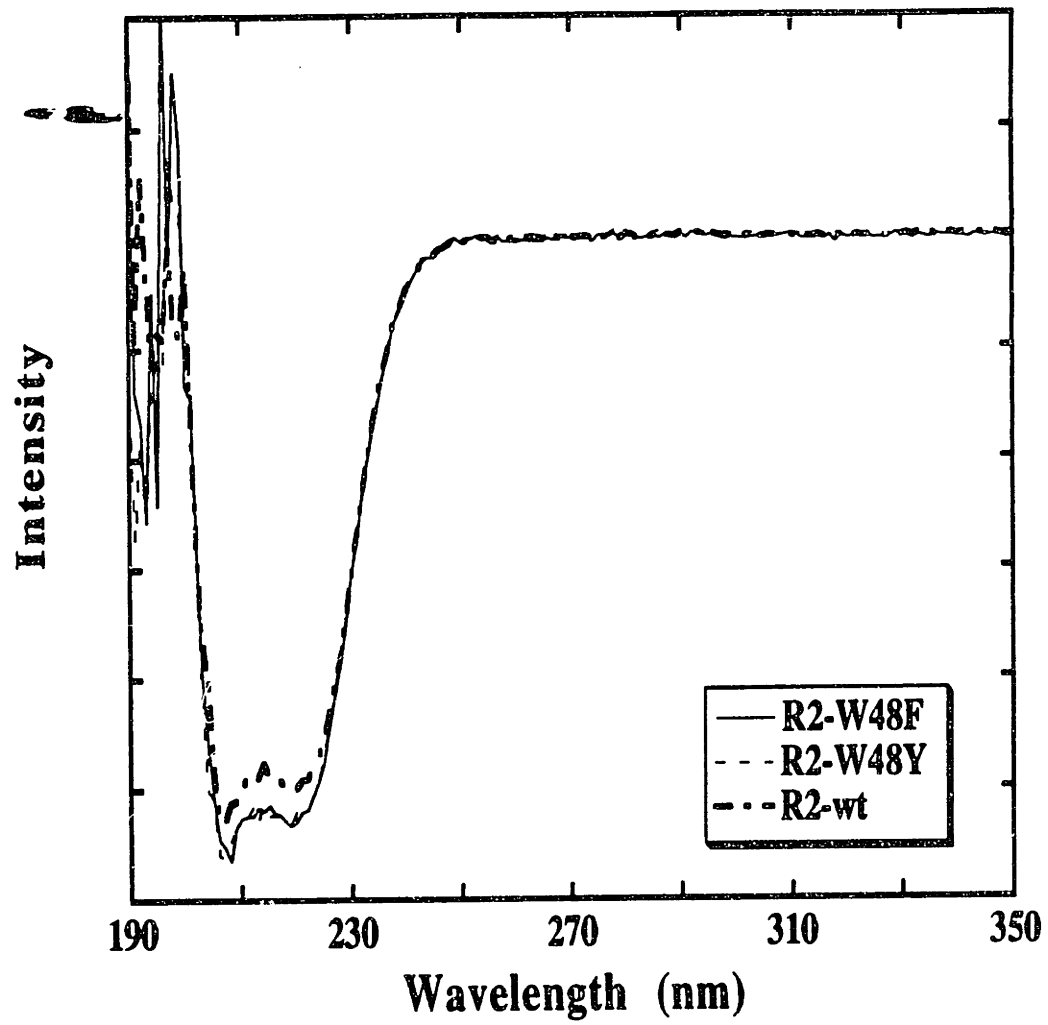


Fig. A.2.2: SDS gel showing heat-induced expression of R2-W48Y in K38/pTB2-W48Y. From left-to right: lane 1: R2; lane 2: K38/pTB2-W48Y before induction; lane 3: K38/pTB2-W48Y after 30 min incubation at 42 °C; lane 4 - 6: after 1, 2, and 3 hour incubation at 37 °C.

Fig. A.2.3: CD spectra of R2-W48F, R2-W48Y and R2-wt at 5 °C. Each sample contained 5 μ M R2 in 10 mM HEPES buffered at pH 7.6.



sequence of R2-wt indicates that the protein contains 7 tryptophan and 16 tyrosine residues per monomer. Taking the difference in the number of tryptophan residues between R2-wt and the mutants into account, the CD spectra of the mutants are almost identical to that of the R2-wt.

Reaction of R2- W48 Mutants with Fe²⁺ and O₂

As mentioned above, neither one of the purified mutant proteins shows the distinctive UV-visible light spectrophotometric features of native R2. Iron assays of the purified proteins indicate that there are only 0.8 equiv. iron per R2-W48F and 0.4 equiv. iron per R2-W48Y. When R2-W48F is mixed with Fe²⁺, the absorption features characteristic of the tyrosyl radical-diferric cluster cofactor are not observed (Fig. A.2.4). Instead, the UV/vis spectrum shows a broad absorption band below 500 nm due to auto oxidation of ferrous. When R2-W48F is mixed with Fe²⁺ in the presence of ascorbate, the spectrum shows a transient, broad feature centered at 540 nm which corresponds to the iron-ascorbate complex (Fig. A.2.5). Identical results were obtained with the R2-W48Y mutant. It is important to note that the transient absorption is not observed when apo R2-wt or ferrozine, a ferrous ion chelator, is mixed with Fe²⁺ in the presence of ascorbate (data not shown). These observations suggest that both apo R2-wt and ferrozine can scavenge Fe²⁺ sufficiently rapidly to compete with autooxidation of Fe²⁺ at neutral pH. In contrast, neither of the two W48 mutant proteins protect Fe²⁺ from autooxidation, suggesting that Fe²⁺ binding in these proteins is much slower than in R2-wt. Furthermore, treatment with Fe²⁺ (with or without ascorbate) does not appear to increase the iron content of the R2-W48 mutant proteins significantly. These result strongly suggest that the abilities of the protein to bind Fe²⁺ ions and to direct assembly of its tyrosyl radical-diferric cluster cofactor are somewhat impaired in the mutants.

Fig. A.2.4: Development of the absorption spectrum of R2-W48F upon mixing with an aliquot of Fe^{2+} in 10 mM H_2SO_4 . The reaction conditions were (A): 250 μM R2-W48F, 50 mM HEPES buffer (pH 7.7) in a final volume of 400 μL , (B) immediately after A was mixed with 50 μL of a solution containing 4.9 mM Fe^{2+} in 10 mM H_2SO_4 , or (C) 280 s after A was mixed with Fe^{2+} . The spectra were acquired on the HP8452A diode array apparatus at 22°C.

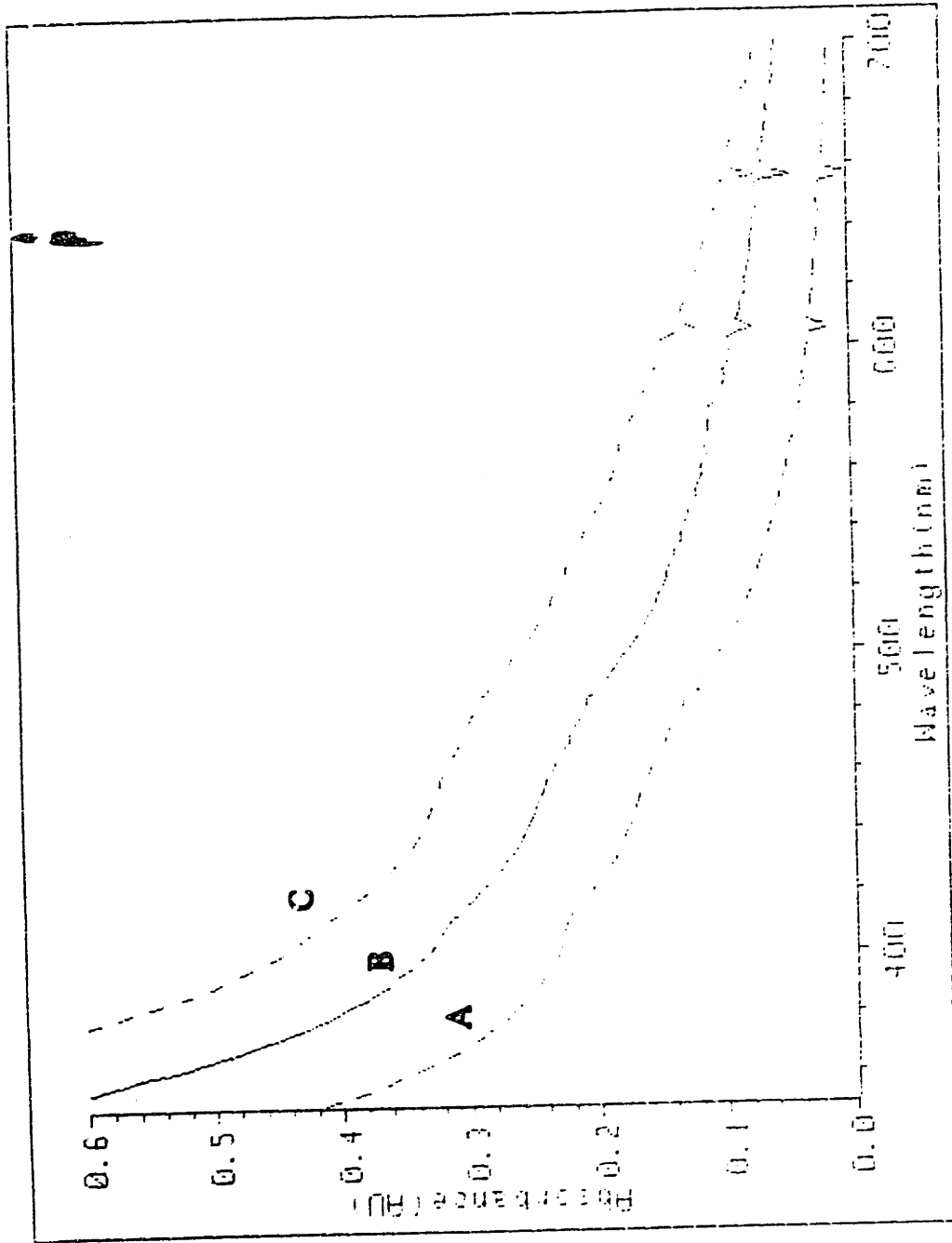
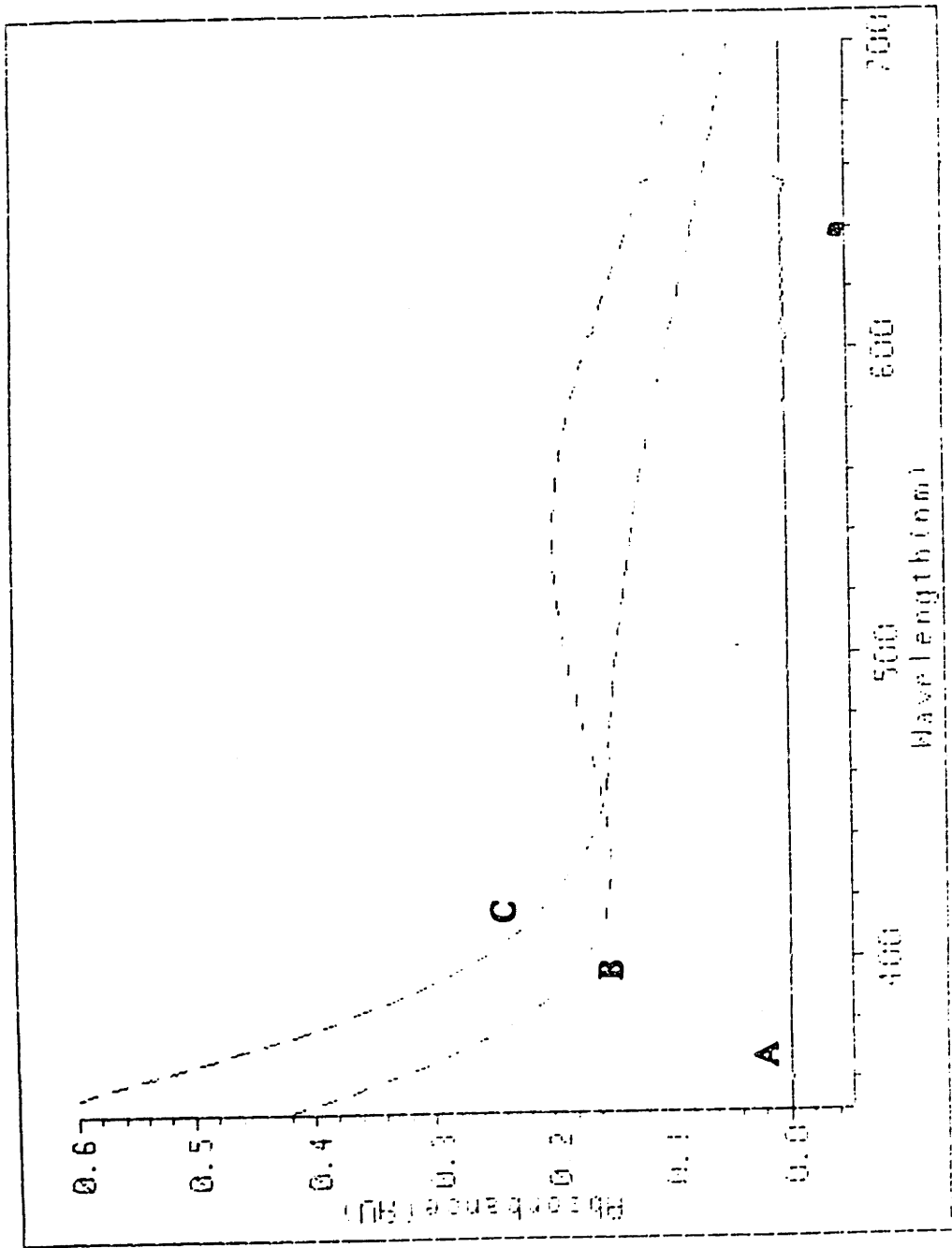


Fig. A.2.5: Development of the absorption spectrum of R2-W48F upon mixing with Fe^{2+} and ascorbate. The reaction conditions were (A): 250 μM R2-W48F, 50 mM HEPES buffer (pH 7.7) in a final volume of 400 μL , (B) immediately after A was mixed with 50 μL of a solution containing 4.9 mM Fe^{2+} and 9 mM ascorbate in 100 mM HEPES (pH 7.7), or (C) 280 s after A was mixed with Fe^{2+} and ascorbate. The spectra were acquired on the HP8452A diode array apparatus at 22°C.



Effects of R2-W48F and R2-W48Y on the Catalytic Activity of R2-wt

Wild-type R2 activity was determined by following NADPH oxidation spectrophotometrically in the presence of apo R2-wt, R2-Y122F, R2-W48F and R2-W48Y (Salowe, 1987). The results of these experiments, summarized in Table A.2.2, suggest that the two W48 mutants are not very efficient in inhibiting wild-type R2 activity. The R2-wt activity decreases by only ~7% when the R2-W48F/R2-wt ratio is 1. In contrast, the R2-wt activity decreases by ~ 50 % when the met R2-wt/R2-wt ratio is 1. These results suggest that the protein-protein interactions between the W48 mutants and the R1 subunit are somehow impaired by a single amino acid substitution.

Discussion

R2-W48F and R2-W48Y can be isolated to > 90% pure using the procedure for purifying R2-wt and R2-Y122F. SDS-PAGE analysis indicates that the mutant proteins have the predicted molecular weight. The CD spectrum of these mutant proteins appears to be almost identical to that of the wild-type protein. These results, taken together, suggest that the W48 mutants are not grossly different in structures from R2-wt. However, unlike R2-wt, addition of Fe^{2+} and ascorbate in the beginning of the purification procedure did not result in isolation of mutant proteins with stable cofactors. The absorption spectra of the purified mutant proteins have none of the distinctive UV-visible light spectrophotometric features of native R2 (data not shown). Iron assays of the purified proteins indicate that there are 0.8 and 0.4 iron per R2-W48F and R2-W48Y dimer respectively. Not surprisingly, no ribonucleotide reduction activities were observed in the mutants since the mutant proteins do not contain the essential tyrosyl radical-diferric cluster cofactor.

Table A.2.2: Summary of the effect of different forms of R2 on the interaction between R1 and R2-wt.

Inhibitor	R2-wt Activity	
	[Inhibitor] = 0.22 μ M	[Inhibitor] = 1.1 μ M
Met R2-wt	53%	19%
Apo R2-wt	92%	75%
R2-Y122F	62%	28%
R2-W48F	93%	79%
R2-W48Y	94%	68%
R2-Y356F	83%	29%
R2-Y122F/Y356F	86%	49%
Apo R2-Y356F	94%	70%
Apo R2-Y122F/Y356F	86%	64%

When the purified mutant proteins are mixed with excess Fe^{2+} , no development of the UV/visible features characteristic of the tyrosyl radical-diferric cluster cofactor is observed. Iron assays of the W48 mutants after incubation with excess Fe^{2+} and ascorbate indicate no further incorporation of iron into these proteins. Autooxidation of ferrous (assessed by the large absorption change below 500 nm) is not affected by the presence of the proteins, suggesting that neither R2-W48 mutants bind iron efficiently. These results suggest that modifications of the W48 residue may have impaired the assembly of the cofactor in the mutant proteins, either by inhibiting binding of Fe^{2+} or by impairing electron transfer required for cofactor assembly.

A final aspect of the W48 mutant proteins that warrants discussion is their ability, or lack thereof, to interact with the R1 subunit. Previously, met R2-wt and R2-Y122F were reported to be effective inhibitors of R2-wt catalytic activity, with K_i of 0.1 μM , comparable to the K_d for the R1-R2 complex (0.2 μM). These results indicate that the modifications in these proteins have little effects on the physical interactions between the R1 and R2 subunits during catalytic turnover. In contrast, the W48 mutants are much less effective in inhibiting the interaction between R1 and R2-wt during turnover. Surprisingly, in the course of this work, it was found that apo R2-wt is also much less effective in inhibiting R2-wt activity (Table A.2.2). In light of this, it is not surprising that R2-W48F and R2-W48Y are ineffective inhibitors of R2-wt, since both these proteins contain less than 1 equivalent of iron per dimer. It is not clear why the apo form of R2 is less effective than either the met R2 or the native R2 in interacting with the R1 subunit. The crystallographic studies of the apo R2 and the met R2 suggest that the structures are essentially identical, differing only at the cofactor sites (Aberg, 1993; Nordlund & Eklund, 1993). The CD spectra of apo R2-wt and met R2-wt are also identical. These results suggest that the static picture of a crystal structures is not sufficient to explain the dynamic interactions between various components in these macromolecules in solution.

References

- Aberg, A. (1993). Ph. D. Thesis, Stockholm University.
- Bollinger, J. M. (1992). Ph. D. Thesis, Massachusetts Institute of Technology.
- Bollinger, J. M., Jr., Tong, W. H., Ravi, N., B. H., Edmondson, D. E. & Stubbe, J. (1994a). *J. Am. Chem. Soc.* 116, 8024-8032.
- Bollinger, J. M., Jr., Tong, W. H., Ravi, N., Huynh, B. H., Edmondson, D. E. & Stubbe, J. (1994b). *J. Am. Chem. Soc.* 116, 8015-8023.

- Coulson, A. F. W., Erman, J. E. & Yonetani, T. (1971). *J. Biol. Chem.* 246, 917-924.
- Erman, J. E., Vitello, L. B., Mauro, J. M. & Kraut, J. (1989). *Biochemistry* 28, 7992-7995.
- Finzel, B. C., Poulos, T. L. & Kraut, J. (1984). *J. Biol. Chem.* 259, 13027-13036.
- Ho, P. S., Hoffman, B. M., Kang, C. H. & Margoliash, E. (1983). *J. Biol. Chem.* 258, 4356-4363.
- Lang, G., Saprtalian, K. & Yonetani, T. (1976). *Biochim. Biophys. Acta* 451, 250-258.
- Lunn, C. A., Kathju, S., Wallace, C., Kushner, S. & Pigiet, V. (1984). *J. Biol. Chem.* 259, 10469-10474.
- Lynch, J. B., Juarez-García, C., Münck, E. & Que, L., Jr. (1989). *J. Biol. Chem.* 264, 8091-8096.
- Marnett, L. J., Weller, P. & Battista, J. R. (1986). "Comparison of the Peroxidase Activity of Hemoproteins and Cytochrome P-450" in *Cytochrome P-450 Structure, Function and Biochemistry* (Ortiz de Montellano, ed.) Plenum Publishing Corp., London, 29-76.
- Massey, V. (1957). *J. Biol. Chem.* 229, 763-770.
- Mauro, J. M., Fishel, L. A., Hazzard, J. T., Meyer, T. E., Tollin, G., Cusanovich, M. A. & Kraut, J. (1988). *Biochemistry* 27, 6243-6256.
- Nakamaye, K. & Eckstein, F. (1986). *Nucl. Acids Res.* 14, 9679-9698.
- Nordlund, P. & Eklund, H. (1993). *J. Mol. Biol.* 232, 123-164.
- Russel, R. & Model, P. (1985). *J. Bacteriol.* 163, 238-242.
- Salowe, S. P. (1987). Ph. D. Thesis, University of Wisconsin.
- Sayers, J. R., Schmidt, W. & Eckstein, F. (1988). *Nucl. Acids Res.* 16, 791-802.
- Scholes, C. P., Liu, Y., Fishel, L. A., Farnum, M. F., Mauro, J. M. & Kraut, J. (1989). *Isr J. Chem.* 29, 83-92.
- Sivaraja, M., Goodin, D. B., Smith, M. & Hoffman, B. M. (1989). *Science* 245, 738-740

Stookey, L. L. (1970). *Anal. Chem.* 42, 779-781.

Tabor, S. & Richardson, C. (1985). *Proc. Natl. Acad. Sci. U.S.A.* 82, 1074-1078.

Taylor, J. W., Ott, J. & Eckstein, F. (1985). *Nucleic Acids Res.* 13, 8765-8785.

Thelander, L. (1973). *J. Biol. Chem.* 248, 4591-4601.

Yonetani, T., Schleyer, H. & Ehrenberg, A. (1966). *J. Biol. Chem.* 241, 3240-3243.



**Appendix 3: Simulation of the Statistical Distribution
of Fe²⁺ Bound to R2**

A computer program in Fortran was written to simulate the statistic distribution of Fe^{2+} in an anaerobic equilibrium mixture of apo R2 and Fe^{2+} . The program calculates the number of different Fe^{2+} -R2 complexes in equilibrium, as a function of Fe^{2+} /R2 ratio from 0.1 - 6.0. It was assumed that 1) all the Fe^{2+} are bound; 2) that each R2 dimer has at most six different Fe^{2+} -binding sites; 3) that each of the Fe^{2+} -binding site may have different affinity for Fe^{2+} ; 4) that Fe^{2+} -binding is a one-step formation, and 5) that there is no cooperativity in Fe^{2+} -binding.

```
*****  
C PROGRAM FE2_R2  
C Written by Alaine Young  
C Last modified : Dec 28, 1995  
C  
C This is a Monte Carlo simulation of the filling of FE2+ in R2.  
C It calculates the distribution of different reaction products,  
C in equilibrium, as a function of FE2+/R2 ratio for up to 1,000,000  
C R2 molecules, assuming all FE2+ are used. It is assumed that each  
C R2 has at most six different sites to be filled by FE2+.  
C Each of these site may have different affinity for FE2+. Other  
C assumptions include one step formation and no cooperativity.  
C  
C Notes on the random number generators used:  
C - RNDM from CERN Program Library is used for selecting the molecule  
R2 to  
C be filled.  
C - RAN2 taken from Numerical Recipes in Fortran, Second Edition, is  
used  
C for selecting the site to be filled.  
C  
C Complied with standard VAX/VMS FORTRAN compiler  
C Linked with KERNLIB.OLB of the CERN library
```

PROGRAM FE2_R2

IMPLICIT NONE

INTEGER*4 MAX_R2 ! Max number of R2 molecules
PARAMETER (MAX_R2 = 1000000)
INTEGER*4 NUMBER_FE ! Number of FE2+
INTEGER*4 NUMBER_R2 ! Number of R2
REAL*4 RATIO ! Ratio of FE2+/R2
REAL*4 LOW_LIMIT, UP_LIMIT ! Lower and upper limit for the
 ! range of ratios entered by user
REAL*4 MIN_RATIO, MAX_RATIO ! Lower and upper limit for
the
 ! range of ratios actually used by
 ! program
REAL*4 STEP_SIZE ! Step size for the range of ratios
 ! entered by user
INTEGER*4 NUM_STEPS ! Number of steps between
MIN_RATIO
 ! and MAX_RATIO with size STEP_SIZE
INTEGER*4 MAX_NUM_STEPS ! Maximum of steps allowed
PARAMETER (MAX_NUM_STEPS = 500)
INTEGER*4 NUM_LOOP ! Loop counter associated with
current
 ! ratio of FE2+/R2
INTEGER*4 ID_FE, ID_R2, ID_SITE ! Identifies which FE2+, R2, site
 ! respectively
INTEGER*4 NUM_FE_FILLED ! Number of FE2+ filled so far

INTEGER*4 MOLECULE(MAX_R2) ! Value labels the status of
different
 ! sites for each R2 molecule
INTEGER*4 SITE(6) ! Store vaule of each SITE used to
 ! label status of MOLECULE
INTEGER*4 CASE(0:63) ! Each case correspond to a

! permutation for filling the R2
! The value contains the number of
! for each permutaion.

REAL*4 A,B,C,D,E,F ! Relative affinities for different
! sites

REAL*4 X ! Random number between 0 and
! A+B+C+D+E+F

INTEGER*4 OCCUPIED ! 0 if site is not occupied

INTEGER*4 MAX_LOOP_R2 ! Maximum number of times a
selected

! FE2+ encounters an R2 molecule

INTEGER*4 FILLED_SITE_ENCOUNTERS ! Number of times a
selected FE2+

! encounter a filled site of an R2
! molecule which is not fully filled.

INTEGER*4 MAX_LOOP_SITE ! Maximum value allowed for
! FILLED_SITE_ENCOUNTERS

INTEGER*4 K,L

INTEGER*4 JUNK ! Number of Junk events, for debugging

REAL*4 TEMP

CHARACTER YESNO

LOGICAL WRITE_FILE ! True if user want to write to files

REAL*4 RANDOM ! Random number between 0 and 1

INTEGER*4 SEED ! Seed for RAN2

REAL*4 RAN2 ! Random number generator taken
! from Numerical Recipe

REAL*4 RNDM ! Random number generator from CERN
! library

EXTERNAL RNDM

DATA SITE /1,2,4,8,16,32/

C-----
C WRITE HEADER TO SCREEN ...
C-----

```
WRITE (6,*) ''  
  WRITE (6,*) ' ***** '  
WRITE (6,*) ' ****   PROGRAM FE2_R2   **** '  
WRITE (6,*) ' ****                       **** '  
WRITE (6,*) ' **** Last modified Dec 28, 1995 **** '  
  WRITE (6,*) ' ***** '  
WRITE (6,*) ''
```

C-----
C GET NUMBER OF R2 FROM USER ...
C-----

```
WRITE (6,*)  
& ' Please enter the number of R2 (max 1,000,000)'  
READ (6,*) NUMBER_R2  
IF ((NUMBER_R2.GT.MAX_R2).OR.(NUMBER_R2.LE.0)) THEN  
  WRITE (6,*) ' Number entered invalid, will use 1,000,000'  
  NUMBER_R2 = 1000000  
ENDIF
```

C-----
C SET MAXIMA TO VARIOUS LOOPS ...
C-----

```
MAX_LOOP_R2 = 100 * NUMBER_R2
```

C Note: Choice of MAX_LOOP_SITE should be less than MAX_LOOP_R2
MAX_LOOP_SITE = 100 * 6

C-----
C GET RANGE OF RATIOS OF F2+/R2 FROM USER ...
C-----

C Getting lower limit, upper limit

```
1  WRITE (6,*)
   & ' Please enter the lower and the upper limit of,
   & ' of the ratio FE2+/R2'
   WRITE (6,*)
   & ' Values entered must be between 0 and 6 exclusive)'
   READ (5,*) LOW_LIMIT, UP_LIMIT
   IF (LOW_LIMIT .GT. UP_LIMIT) THEN
     TEMP = LOW_LIMIT
     LOW_LIMIT = UP_LIMIT
     UP_LIMIT = TEMP
   END IF
   IF ((LOW_LIMIT .LE. 0) .OR. (UP_LIMIT .GE. 6)) THEN
     WRITE (6,*) ' !!! Invalid limits !!!'
     GO TO 1
   END IF
```

C If there is a range of ratios ...

```
IF (LOW_LIMIT .NE. UP_LIMIT) THEN
```

C Get step size

```
2  WRITE (6,*) ' Please enter step size'
   READ (5,*) STEP_SIZE
   IF (STEP_SIZE .EQ. 0) THEN
     WRITE (6,*) ' !!! Step size of zero is not allowed !!!'
     GO TO 2
   END IF
   NUM_STEPS = (UP_LIMIT - LOW_LIMIT)/STEP_SIZE
   IF (NUM_STEPS .EQ. 0) THEN
     STEP_SIZE = 0
     WRITE (6,*) ' !!! Step size is too big !!!'
     GO TO 2
   ELSE IF (NUM_STEPS .LT. 0) THEN
```

```

WRITE (6,*) ' !!! Invalid step size !!!'
GO TO 2
ELSE IF (NUM_STEPS .GT. MAX_NUM_STEPS) THEN
  NUM_STEPS = MAX_NUM_STEPS
  STEP_SIZE = (UP_LIMIT - LOW_LIMIT)/NUM_STEPS
  WRITE (6,*) ' !!! Step size is too small !!!'
  WRITE (6,*)
& ' !!! Will use step size of ', STEP_SIZE
END IF

```

C If there is only one ratio ...

```

ELSE
  NUM_STEPS = 0
  STEP_SIZE = 0
END IF

```

C Determine the minimum ratio and the max ratio ...

```

MIN_RATIO = LOW_LIMIT
MAX_RATIO = LOW_LIMIT + NUM_STEPS * STEP_SIZE

WRITE (6,*) ' '
WRITE (6,100) MIN_RATIO, MAX_RATIO, STEP_SIZE
WRITE (6,*) ' '

```

C-----
C GET RELATIVE AFFINITIVE STRENGTHS OF SITES A,B,C,D,E,F
C-----

```

WRITE (6,*)
& ' Please enter relative affinities of sites',
& ' A,B,C,D,E,F respectively'
WRITE (6,'(1X,A)')
& ' WARNING: Entering zero for any of the affinities',
& '      would introduce error in the calculation,',

```

```
&' EXCEPT when only 4 sites are used.',
&' When using only 4 sites, enter zero for',
&' both sites E and F.'
READ (5,*) A,B,C,D,E,F
```

```
C-----
C DETERMINE IF USER WANT TO WRITE DATA TO FILES ...
C-----
```

```
WRITE (6,*) ' Do you want to write data to files ? [Y]'
READ (5,'(A)',ERR=3) YESNO
IF ((YESNO.EQ.'N').OR.(YESNO.EQ.'n')) THEN
  WRITE_FILE = .FALSE.
ELSE
3  WRITE_FILE = .TRUE.
ENDIF
```

```
C-----
C GET SEED FOR RANDOM NUMBER GENERATOR RAN2
C-----
```

```
WRITE (6,*)
&' Please enter a large, arbitrary negative integer to start'
READ (5,*) SEED
```

```
C-----
C OPENNING OUTPUT FILES AND WRITE HEADER TO EACH FILE
C-----
```

```
IF (WRITE_FILE) THEN
  OPEN (10, FILE='FE2_R2.DAT',STATUS='NEW',ERR=998)
  OPEN (11, FILE='ONE_FE2.DAT',STATUS='NEW',ERR=998)
  OPEN (12, FILE='TWO_FE2_PT1.DAT',STATUS='NEW',ERR=998)
  OPEN (13, FILE='THREE_FE2_PT1.DAT',STATUS='NEW',ERR=998)
  OPEN (14, FILE='FOUR_FE2_PT1.DAT',STATUS='NEW',ERR=998)
  OPEN (15, FILE='FIVE_FE2.DAT',STATUS='NEW',ERR=998)
```

```
OPEN (22, FILE='TWO_FE2_PT2.DAT',STATUS='NEW',ERR=998)
OPEN (23, FILE='THREE_FE2_PT2.DAT',STATUS='NEW',ERR=998)
OPEN (24, FILE='FOUR_FE2_PT2.DAT',STATUS='NEW',ERR=998)
```

```
OPEN (32, FILE='TWO_FE2_PT3.DAT',STATUS='NEW',ERR=998)
OPEN (33, FILE='THREE_FE2_PT3.DAT',STATUS='NEW',ERR=998)
OPEN (34, FILE='FOUR_FE2_PT3.DAT',STATUS='NEW',ERR=998)
```

```
OPEN (50,
FILE='EMPTY_FULL_FE2.DAT',STATUS='NEW',ERR=998)
```

C ... Comprehensive data file ...

```
WRITE (10,100) MIN_RATIO, MAX_RATIO, STEP_SIZE
WRITE (10,*) ' Initial number of R2 =',NUMBER_R2
WRITE (10,*) ' Relative strengths of sites A, B, C, D, E, F '
WRITE (10,*) A,B,C,D,E,F
WRITE (10,*) ''
WRITE (10,*) ''
```

C ... Data file for one filled site ...

```
WRITE (11,100) MIN_RATIO, MAX_RATIO, STEP_SIZE
WRITE (11,*) ' Initial number of R2 =',NUMBER_R2
WRITE (11,*) ' Relative strengths of sites A, B, C, D, E, F '
WRITE (11,*) A,B,C,D,E,F
WRITE (11,*) ''
WRITE (11,*) ''
WRITE (11,301) 'FE2+/R2','A', 'B','C','D','E','F'
WRITE (11,*) ''
```

C ... Data file for two filled site ...

```
WRITE (12,100) MIN_RATIO, MAX_RATIO, STEP_SIZE
WRITE (12,*) ' Initial number of R2 =',NUMBER_R2
WRITE (12,*) ' Relative strengths of sites A, B, C, D, E, F '
WRITE (12,*) A,B,C,D,E,F
WRITE (12,*) ''
WRITE (12,*) ''
```

```
WRITE (12,301) 'FE2+/R2','A-B','A-C','A-D', 'B-C','B-D','C-D'  
WRITE (12,*) ''
```

```
WRITE (22,100) MIN_RATIO, MAX_RATIO, STEP_SIZE  
WRITE (22,*) ' Initial number of R2 =',NUMBER_R2  
WRITE (22,*) ' Relative strengths of sites A, B, C, D, E, F '  
WRITE (22,*) A,B,C,D,E,F  
WRITE (22,*) ''  
WRITE (22,*) ''  
WRITE (22,301) 'FE2+/R2','A-E','B-E','C-E','D-E'  
WRITE (22,*) ''
```

```
WRITE (32,100) MIN_RATIO, MAX_RATIO, STEP_SIZE  
WRITE (32,*) ' Initial number of R2 =',NUMBER_R2  
WRITE (32,*) ' Relative strengths of sites A, B, C, D, E, F '  
WRITE (32,*) A,B,C,D,E,F  
WRITE (32,*) ''  
WRITE (32,*) ''  
WRITE (32,301) 'FE2+/R2','A-F','B-F','C-F','D-F','E-F'  
WRITE (32,*) ''
```

C ... Data file for three filled site ...

```
WRITE (13,100) MIN_RATIO, MAX_RATIO, STEP_SIZE  
WRITE (13,*) ' Initial number of R2 =',NUMBER_R2  
WRITE (13,*) ' Relative strengths of sites A, B, C, D, E, F '  
WRITE (13,*) A,B,C,D,E,F  
WRITE (13,*) ''  
WRITE (13,*) ''  
WRITE (13,301) 'FE2+/R2','A-B-C','A-B-D','A-C-D','B-C-D',  
& 'A-B-E','A-B-F','A-C-E'  
WRITE (13,*) ''
```

```
WRITE (23,100) MIN_RATIO, MAX_RATIO, STEP_SIZE  
WRITE (23,*) ' Initial number of R2 =',NUMBER_R2  
WRITE (23,*) ' Relative strengths of sites A, B, C, D, E, F '  
WRITE (23,*) A,B,C,D,E,F
```

```

WRITE (23,*) ''
WRITE (23,*) ''
WRITE (23,301) 'FE2+/R2','A-C-F','A-D-E','A-D-F','A-E-F',
&           'B-C-E','B-C-F','B-D-E'
WRITE (23,*) ''

```

```

WRITE (33,100) MIN_RATIO, MAX_RATIO, STEP_SIZE
WRITE (33,*) ' Initial number of R2 =',NUMBER_R2
WRITE (33,*) ' Relative strengths of sites A, B, C, D, E, F '
WRITE (33,*) A,B,C,D,E,F
WRITE (33,*) ''
WRITE (33,*) ''
WRITE (33,301) 'FE2+/R2','B-D-F','B-E-F','C-D-E','C-D-F',
&           'C-E-F','D-E-F'
WRITE (33,*) ''

```

C ... Data file for four filled site ...

```

WRITE (14,100) MIN_RATIO, MAX_RATIO, STEP_SIZE
WRITE (14,*) ' Initial number of R2 =',NUMBER_R2
WRITE (14,*) ' Relative strengths of sites A, B, C, D, E, F '
WRITE (14,*) A,B,C,D,E,F
WRITE (14,*) ''
WRITE (14,*) ''
WRITE (14,301) 'FE2+/R2','A-B-C-D','A-B-C-E','A-B-C-F',
&           'A-B-D-E','A-B-D-F'
WRITE (14,*) ''

```

```

WRITE (24,100) MIN_RATIO, MAX_RATIO, STEP_SIZE
WRITE (24,*) ' Initial number of R2 =',NUMBER_R2
WRITE (24,*) ' Relative strengths of sites A, B, C, D, E, F '
WRITE (24,*) A,B,C,D,E,F
WRITE (24,*) ''
WRITE (24,*) ''
WRITE (24,301) 'FE2+/R2','A-B-E-F','A-C-D-E','A-C-D-F',
&           'A-C-E-F','A-D-E-F'
WRITE (24,*) ''

```

```

WRITE (34,100) MIN_RATIO, MAX_RATIO, STEP_SIZE
WRITE (34,*) ' Initial number of R2 =',NUMBER_R2
WRITE (34,*) ' Relative strengths of sites A, B, C, D, E, F '
WRITE (34,*) A,B,C,D,E,F
WRITE (34,*) ''
WRITE (34,*) ''
WRITE (34,301) 'FE2+/R2','B-C-D-E','B-C-D-F','B-C-E-F',
&
'B-D-E-F','C-D-E-F'
WRITE (34,*) ''

```

C ... Data file for five filled site ...

```

WRITE (15,100) MIN_RATIO, MAX_RATIO, STEP_SIZE
WRITE (15,*) ' Initial number of R2 =',NUMBER_R2
WRITE (15,*) ' Relative strengths of sites A, B, C, D, E, F '
WRITE (15,*) A,B,C,D,E,F
WRITE (15,*) ''
WRITE (15,*) ''
WRITE (15,301) 'FE2+/R2','A-B-C-D-E', 'A-B-C-D-F',
&
'A-B-C-E-F','A-B-D-E-F','A-C-D-E-F',
&
'B-C-D-E-F'
WRITE (15,*) ''

```

C ... Data file for empty R2 and full R2 ...

```

WRITE (50,100) MIN_RATIO, MAX_RATIO, STEP_SIZE
WRITE (50,*) ' Initial number of R2 =',NUMBER_R2
WRITE (50,*) ' Relative strengths of sites A, B, C, D, E, F '
WRITE (50,*) A,B,C,D,E,F
WRITE (50,*) ''
WRITE (50,*) ''
WRITE (50,301) 'FE2+/R2','NO FE2+', 'SIX FE2+'
WRITE (50,*) ''

```

ENDIF

C-----

C BEGIN SIMULATION ...

C INITIALIZATION

C _____
NUM_LOOP = 0

C BEGIN LOOPING FOR EACH RATIO ...

C _____

C Note: NUM_LOOP is incremented by 1 at the end before going back to the

C the statement below

10 CONTINUE

C Get ratio and the number of FE2+ for the current loop

RATIO = MIN_RATIO + NUM_LOOP*STEP_SIZE
NUMBER_FE = RATIO * NUMBER_R2

C Initialization

DO K = 1,MAX_R2
MOLECULE(K) = 0
END DO
NUM_FE_FILLED=0
FILLED_SITE_ENCOUNTERS = 0

C Write message to screen to indicate progress

WRITE (6,*) ' Now simulating for the ratio :', RATIO

C FOR EACH FE2+ ...

C _____
DO ID_FE = 1, NUMBER_FE

C FOR EACH R2 MOLECULE ENCOUTNERED ...

C _____

```
DO K = 1, MAX_LOOP_R2
```

```
C Get ID of R2 molecule encounter
```

```
  RANDOM = RNDM(K)
```

```
  ID_R2 = INT(RANDOM*(NUMBER_R2)) + 1
```

```
C Note: Since RANDOM is between 0 and 1 exclusively,
```

```
C   maximum value of RANDOM will be slightly less than 1.
```

```
C   maximum value of RANDOM*NUMBER_R2 will be slightly less  
than
```

```
C       NUMBER_R2
```

```
C   maximum value of INT(RANDOM*NUMBER_R2) will be truncated  
to
```

```
C       NUMBER_R2-1
```

```
C If the molecule chosen is not fully filled
```

```
  IF (MOLECULE(ID_R2).LT.63) THEN
```

```
C Get ID of site encounter base on site affinities
```

```
  RANDOM = RAN2(SEED)
```

```
  X = RANDOM*(A+B+C+D+E+F)
```

```
  IF (X.LE.A) THEN
```

```
    ID_SITE = 1
```

```
  ELSE IF (X.LE.A+B) THEN
```

```
    ID_SITE = 2
```

```
  ELSE IF (X.LE.A+B+C) THEN
```

```
    ID_SITE = 3
```

```
  ELSE IF (X.LE.A+B+C+D) THEN
```

```
    ID_SITE = 4
```

```
  ELSE IF (X.LE.A+B+C+D+E) THEN
```

```
    ID_SITE = 5
```

```
  ELSE
```

```
    ID_SITE = 6
```

```
  ENDIF
```

```
C Determine if site is occupied for the chosen molecule
```

OCCUPIED = IAND (MOLECULE(ID_R2),SITE(ID_SITE))

C If site chosen is not filled ...

IF (OCCUPIED.EQ.0) THEN

C ... marked site ID_SITE as filled in MOLECULE(ID_R2)

MOLECULE(ID_R2)=MOLECULE(ID_R2) + SITE(ID_SITE)

C ... set number of encounters of filled site to zero

FILLED_SITE_ENCOUNTERS = 0

C ... increment NUM_FE_FILLED

NUM_FE_FILLED = NUM_FE_FILLED + 1

C ... branch out of loop and try to fill the next FE2+

GO TO 40

C If site chosen is filled...

ELSE

C ... keep a record of how many times have tried to get an unfilled site

FILLED_SITE_ENCOUNTERS = FILLED_SITE_ENCOUNTERS +

1

C ... if FILLED_SITE_ENCOUNTERS is too large ...

C i.e. have tried too many times to get an unfilled site even though

C there are molecules that are not fully filled

IF (FILLED_SITE_ENCOUNTERS.GT.MAX_LOOP_SITE) THEN

C Write a info to screen

WRITE (6,*) ' *** Problem finding unfilled sites *** '

WRITE (6,*)

& ' Cannot fill FE2+ to R2 after ',FILLED_SITE_ENCOUNTERS

WRITE (6,*)

& ' encounters of R2 that is NOT fully filled'

WRITE (6,*)

```

& ' Number of FE2+ filled =', NUM_FE_FILLED

C ..... Stop futher simulations, do not try to fill any more FE2+
      GO TO 50
C ..... Done checking the number of times trying to get an unfilled site
      END IF

C Finish checking if site chosen is filled or not
      ENDIF

C Done with the case if molecule chosen is not fullied filled
      ENDIF

C DONE FOR EACH R2 MOLECULE ENCOUNTERED
C -----
      END DO

C Write information to screen
      WRITE (6,*) ' *** Problem finding R2 to fill *** '
      WRITE (6,*)
& ' Cannot fill FE2+ to R2 after ',MAX_LOOP_R2,' encounters'
      WRITE (6,*)
& ' Number of FE2+ filled =', NUM_FE_FILLED

C ..... Stop futher simulations, do not try to fill any more FE2+
      GO TO 50

40  CONTINUE

C DONE FOR EACH FE2+
C -----
      END DO

C This line would only be reach if every things go smoothly
      WRITE (6,*) ' Finish filling all FE2+ into R2'

```

C HISTOGRAMMING GOOD DATA ...

C -----

C Initialization

```
DO K = 0,63
  CASE(K)= 0
END DO
```

C Filling histograms

```
DO L = 1, NUMBER_R2
  K = MOLECULE(L)
  IF (K.GE.0 .AND. K.LE.63) THEN
    CASE(K) = CASE (K) + 1
  ELSE
    JUNK = JUNK + 1
  END IF
END DO
```

C WRITING DATA TO FILE ...

C -----

```
IF (WRITE_FILE) THEN
```

```
  WRITE (10,*) ' Ratio of FE2+/R2', RATIO
```

```
  DO K = 0,63
```

```
    WRITE (10,200) K, CASE(K)
```

```
  ENDDO
```

```
  WRITE (10,*) ' NUMBER JUNK EVENTS =', JUNK
```

```
  WRITE (10,*) ' -----'
```

```
  WRITE (11,300) RATIO, CASE(1), CASE(2), CASE(4), CASE(8),
```

```
&      CASE(16), CASE(32)
```

```
  WRITE (12,300) RATIO, CASE(3), CASE(5), CASE(9),
```

```
&      CASE(6), CASE(10), CASE(12)
```

```
  WRITE (22,300) RATIO, CASE(17), CASE(18), CASE(20),
```

```
&      CASE(24)
```

```
  WRITE (32,300) RATIO, CASE(33), CASE(34), CASE(36),
```

```
&      CASE(40), CASE(48)
```

```

WRITE (13,300) RATIO, CASE(7), CASE(11), CASE(13), CASE(14),
&          CASE(19), CASE(35), CASE(21)
WRITE (23,300) RATIO, CASE(37), CASE(25), CASE(41), CASE(49),
&          CASE(22), CASE(38), CASE(26)
WRITE (33,300) RATIO, CASE(42), CASE(50), CASE(28), CASE(44),
&          CASE(52), CASE(56)
WRITE (14,300) RATIO, CASE(15), CASE(23), CASE(39), CASE(27),
&          CASE(43)
WRITE (24,300) RATIO, CASE(51), CASE(29), CASE(45), CASE(53),
&          CASE(57)
WRITE (34,300) RATIO, CASE(30), CASE(46), CASE(54), CASE(58),
&          CASE(60)
WRITE (15,300) RATIO, CASE(31), CASE(47), CASE(55), CASE(59),
&          CASE(61), CASE(62)
WRITE (50,300) RATIO, CASE(0), CASE(63)

```

```
ELSE
```

```
C WRITING DATA TO SCREEN ...
```

```
C -----
```

```

WRITE (6,*) ' '
WRITE (6,*) ' Ratio of FE2+/R2', RATIO
DO K = 0,63
  WRITE (6,200) K, CASE(K)
ENDDO
WRITE (6,*) ' NUMBER JUNK EVENTS =', JUNK

```

```
ENDIF
```

```
C DONE FOR EACH RATIO
```

```
C -----
```

```
NUM_LOOP = NUM_LOOP + 1
```

C Repeat simulation for the next ratio if the max ratio has not been reached

```
    IF (NUM_LOOP .LE. NUM_STEPS) THEN  
      GO TO 10  
    ENDIF
```

C-----

C END SIMULATION

C-----

50 CONTINUE

```
    IF (WRITE_FILE) THEN
```

```
      CLOSE(10)
```

```
      CLOSE(11)
```

```
      CLOSE(12)
```

```
      CLOSE(13)
```

```
      CLOSE(14)
```

```
      CLOSE(15)
```

```
      CLOSE(22)
```

```
      CLOSE(23)
```

```
      CLOSE(24)
```

```
      CLOSE(32)
```

```
      CLOSE(33)
```

```
      CLOSE(34)
```

```
      CLOSE(50)
```

```
    ENDIF
```

```
    WRITE (6,*) ' '
```

```
      WRITE (6,*) ' **** Calculation finished ****'
```

```
    WRITE (6,*) ' '
```

```
100 FORMAT (' Requested ratio of FE2+/R2 ranges from',F10.5,  
& ' to ',F10.5/' in steps of ', F10.5)
```

```
200 FORMAT (' CASE(',I2,') : ',I10)
```

```
300 FORMAT (1X,(F9.5,1X),7(I9,1X))
```

```
301 FORMAT (1X,8(A9,1X))
```

```
999 STOP ' **** Have a nice day :) ****'  
998 STOP ' !!! Error opening output file !!!'
```

```
END
```

```
C
```

```
=====
```

```
C FUNCTION RAN 2
```

```
C Taken from Numerical Recipes in Fortran, 2nd Edition, by  
C William H. Press, Saul A. Teukolsky, William T. Vetterling,  
C and Brian P. Flannery, published by Cambridge University Press  
C (Page 272 to 273).
```

```
FUNCTION RAN2(idum)
```

```
IMPLICIT NONE
```

```
INTEGER*4
```

```
idum,IM1,IM2,IMM1,IA1,IA2,IQ1,IQ2,IR1,IR2,NTAB,NDIV
```

```
REAL*4 ran2,AM,EPS,RNMX
```

```
PARAMETER
```

```
(IM1=2147483563,IM2=2147483399,AM=1./IM1,IMM1=IM1-1,
```

```
* IA1=40014,IA2=40692,IQ1=53668,IQ2=52774,IR1=12211,
```

```
* IR2=3791,NTAB=32,NDIV=1+IMM1/NTAB,EPS=1.2E-7,RNMX=1.-
```

```
EPS)
```

```
C Long period (>2E18) random number generator of L'Ecuyer with Bays-  
Durham
```

```
C shuffle and added safeguards. Returns a uniform random deviate  
between
```

```
C 0.0 and 1.0 (exclusive of the endpoint values). Call with idum a negative
```

```
C integer to initialize; thereafter, do not alter idum between successive
```

```
C deviates in a sequence. RNMX should approximate the largest floating  
value
```

```
C that is less than 1.
```

```
INTEGER*4 idum2, j, k,iv(NTAB),iy
```

```
SAVE iv, iy, idum2
```

```
DATA idum2/123456789/, iv/NTAB*0/, iy/0/
```



```

if (idum.le.0) then          ! Initialize
  idum=max(-idum,1)         ! Be sure to prevent idum = 0
  idum2=idum
  do j=NTAB+8,1,-1         ! Load the shuffle table
                           ! (after 8 warm-ups).
    k=idum/IQ1
    idum=IA1*(idum-k*IQ1)-k*IR1
    if (idum.lt.0) idum=idum+IM1
    if (j.le.NTAB) iv(j)=idum
  end do
  iy=iv(1)
endif
k=idum/IQ1                  ! Start here when not initializing.
idum=IA1*(idum-k*IQ1)-k*IR1 ! Compute
idum=mod(IA1*idum,IM1)
                           ! without overflows by Schrage's
                           ! method.
  if (idum.lt.0) idum=idum+IM1
  k=idum2/IQ2
  idum2=IA2*(idum2-k*IQ2)-k*IR2 ! Compute
idum2=mod(IA2*idum2,IM2)
                           ! likewise.
  if (idum2.lt.0) idum2=idum2+IM2
  j=1+iy/NDIV              ! Will be in the range 1:NTAB
  iy=iv(j)-idum2          ! Here idum is shuffled, idum and
                           ! idum2 are combined to generate
                           ! output.
  iv(j)=idum
  if(iy.lt.1) iy=iy+IMM1
  ran2=min(AM*iy,RNMX)     ! Because users don't expect
                           ! endpoint values.

return
END

```

